



**HAL**  
open science

# Role of CD169 macrophages in cellular adaptive immune responses

Francois-Xavier Mauvais

► **To cite this version:**

Francois-Xavier Mauvais. Role of CD169 macrophages in cellular adaptive immune responses. Immunology. Université Sorbonne Paris Cité, 2016. English. NNT : 2016USPCB259 . tel-04515492

**HAL Id: tel-04515492**

**<https://theses.hal.science/tel-04515492v1>**

Submitted on 21 Mar 2024

**HAL** is a multi-disciplinary open access archive for the deposit and dissemination of scientific research documents, whether they are published or not. The documents may come from teaching and research institutions in France or abroad, or from public or private research centers.

L'archive ouverte pluridisciplinaire **HAL**, est destinée au dépôt et à la diffusion de documents scientifiques de niveau recherche, publiés ou non, émanant des établissements d'enseignement et de recherche français ou étrangers, des laboratoires publics ou privés.

# Université Paris Descartes

**Ecole doctorale Bio Sorbonne Paris Cité (BioSPC)**

*Laboratoire : INSERM-U1151 –Institut Necker-Enfants Malades (INEM)*

*Equipe de recherche : Présentation des antigènes : mécanismes et modulation par les récepteurs Toll-like (dirigée par le Pr. Peter van Endert)*

## **Rôle des macrophages CD169 dans les réponses immunitaires adaptatives cellulaires**

Par François-Xavier MAUVAIS

Thèse de doctorat d'Immunologie

Dirigée par Monsieur le Professeur Peter van Endert

Présentée et soutenue publiquement le 28 novembre 2016

Devant un jury composé de :

**Pr. Martin GUILLIAMS**, PhD

**Dr. Toby LAWRENCE**, PhD, DR

**Dr. Cédric AUFRAY**, PhD, CR

**Pr. Karl Sebastian LANG**, MD, PhD

**Pr. Peter VAN ENDERT**, MD, PU-PH

**Président et rapporteur**

Ghent University, Belgium

**Rapporteur**

Université d'Aix-Marseille, France

**Examineur**

Université Paris Descartes, France

**Examineur**

Duisburg-Essen University, Germany

**Directeur de Thèse**

Université Paris Descartes, France

**Résumé :** L'acquisition d'une immunité efficace contre les infections nécessite l'initiation de réponses immunitaires adaptatives, notamment l'activation et la différenciation de lymphocytes T (LT) spécifiques de motifs antigéniques dérivés des microbes. Cette étape cruciale doit être orchestrée de façon minutieuse pour prévenir le développement de maladies inflammatoires ou auto-immunes et de nombreux travaux attribuent un rôle important aux cellules dendritiques (CDs). Une de leurs caractéristiques majeure est de présenter efficacement des motifs antigéniques générés en leur sein à partir de protéines exogènes pour leur chargement sur les molécules du complexe majeur d'histocompatibilité de classe II (CMH-II) et du CMH-I au cours du processus de présentation croisée. En ce qui concerne cette dernière, il n'est cependant pas clair si d'autres cellules possèdent des capacités similaires. Par exemple, la capacité des macrophages CD169+ à présenter l'antigène aux lymphocytes T (LT) est controversée : alors qu'ils occupent une place critique dans le contrôle de certaines tumeurs par les LT CD8+ cytotoxiques stimulés dans les ganglions, ils ne joueraient qu'un rôle indirect en transférant l'antigène aux CDs dans la rate. La difficulté à les isoler *in vitro* et les étudier *in vitro* et *in vivo* constitue un obstacle majeur pour déterminer leur rôle précis dans les réponses immunitaires adaptatives. Les objectifs de ce travail sont de : préciser la contribution des macrophages CD169+ de la rate dans l'induction des réponses immunitaires adaptatives *in vivo*; identifier les facteurs moléculaires et cellulaires intervenant dans la régulation des réponses innées et adaptatives par les sous-types de phagocytes. En mettant au point une stratégie unique de purification combinant gradient de densité et tri par cytométrie en flux multiplexe, nous avons montré que les cellules CD169+ de la rate possèdent une signature moléculaire et protéique comparable aux macrophages tissulaires. Nous avons placé les macrophages CD169+ de la rate aux côtés des CDs, au rang des cellules dotées d'une grande efficacité de présentation croisée de l'antigène aux LT CD8+. Lorsqu'un antigène est dirigé vers les macrophages CD169+ de la rate *in vivo*, les LT CD8+ naïfs spécifiques forment des contacts étroits et prolongés avec ces cellules, se différencient en lymphocytes effecteurs et mémoires. En cherchant à comprendre les mécanismes en rapport avec leur capacité hautement efficace de présentation croisée, nous avons observé que les macrophages CD169+, au contraire des CDs, n'utilisent pas la voie cytosolique mais une voie vacuolaire unique pour générer des peptides antigéniques pour les molécules du CMH-I ; de même le profil trafic intracellulaire des molécules de CMH-I est unique au sein des macrophages CD169+. Finalement, ce travail suggère un rôle marginal d'un compartiment cellulaire pourtant présent au sein des macrophages CD169+, dont nous avons préalablement identifié et caractérisé le rôle important dans les CDs: les endosomes de régulation Rab14+. En régulant la maturation phagosomale, ces endosomes contrôlent les réponses immunitaires adaptatives mais aussi innées et inflammatoires dans les CDs. Au total ce travail bouleverse certaines des connaissances actuelles sur les acteurs régulant les réponses adaptatives par leur capacité à présenter les antigènes et propose une nouvelle voie efficace d'apprêtement des antigènes et de production de complexes entre des peptides issus d'antigènes internalisés et des molécules du CMH-I.

**Title:** Role of CD169 macrophages in cellular adaptive immune responses

**Abstract:** Protective immunity against infections requires the initiation of adaptive immune responses, including the generation of cytotoxic T lymphocytes specific of antigenic motifs expressed by microbes. These processes have to be tightly regulated to avoid the persistence of inflammation and the development of autoimmunity. In this context, dendritic cells play a major role and can efficiently present exogenous antigenic material for loading onto the major histocompatibility class II molecules (MHC-II), but also MHC-I molecules in a process referred to as cross-presentation. However, it is not clear if other phagocytes have similar capacities. For example, the ability of CD169+ macrophages to present antigens to T cells is controversial: in the lymph nodes they generate protective immunity against tumors by cross-presenting tumor derived antigens, whereas in the spleen they may act as an antigen transfer platform for cross-presenting dendritic cells. The crucial barrier to determining their precise role in adaptive immunity is the difficulty to isolate them. The objectives of this work are to: clarify the contribution of splenic CD169+ macrophages in inducing adaptive immune responses; identify the molecular and cellular factors involved in the regulation of innate and adaptive immunity by phagocyte subsets. By developing a unique strategy that combines density gradients and cell sorting by flow cytometry, we showed that CD169+ cells have a molecular and protein signatures close to macrophages. We place the splenic CD169+ macrophages together with dendritic cells, in a group of professional antigen presenting cells capable of efficient cross-presentation. Following antigen targeting to splenic CD169+ macrophages, specific naïve CD8+ T cells form long-standing contacts with macrophages resulting in their activation and differentiation into effector and memory cells. Surprisingly, we found that CD169+ macrophages exclusively use a unique vacuolar antigen cross-presentation pathway to generate antigenic peptides for loading onto MHC-I, at variance with dendritic cells. Similarly, the profile of MHC-I trafficking is unique in CD169+ macrophages. Finally, this work suggests a marginal role of the regulatory Rab14+ endosomes, which we have previously characterized as important in regulating cross-presentation by dendritic cells, by controlling inflammatory responses and phagosomal maturation.

**Mots clés :** macrophages CD169 ; cellules dendritiques ; endosome ; phagosome ; MHC-I ; immunité adaptative ; présentation croisée ; rate

**Keywords:** CD169 macrophages; dendritic cells; endosome; phagosome; MHC-I; adaptive immunity; antigen cross-presentation; spleen.

**« A la source de toute connaissance, il y a une idée, une pensée, puis l'expérience vient confirmer l'idée. »**

**« Les idées expérimentales ne sont point innées. Elles ne surgissent point spontanément, il leur faut une occasion ou un excitant extérieur, comme cela a lieu dans toutes les fonctions physiologiques. »**

**« C'est ce que nous pensons déjà connaître qui nous empêche souvent d'apprendre. »**

Claude Bernard. Introduction à l'étude de la médecine expérimentale (1865)

## Acknowledgements

*Je tiens à remercier très sincèrement et très chaleureusement les membres de mon Jury, le Docteur Cédric Auffray, le Professeur Martin Williams, le Professeur Karl Sebastian Lang et le Docteur Toby Lawrence, qui ont eu la gentillesse d'accepter d'évaluer mon travail et la patience de le lire et de le critiquer. C'est pour moi un véritable honneur et privilège de vous retrouver le jour de la soutenance et je tiens à immortaliser ma reconnaissance éternelle dans ce manuscrit.*

*Je tiens ensuite à remercier le Professeur Peter van Endert, particulièrement pour m'avoir accueilli depuis déjà de longues années dans son laboratoire et son équipe. Tu m'as beaucoup appris, plus que tu ne peux l'imaginer, pendant ses nombreuses années et j'ai toujours pu continuer sur ton soutien indéfectible, tes conseils cruciaux, ton expérience impressionnante. Plus que d'acquérir un raisonnement scientifique rigoureux, tout du moins je l'espère, tu m'as permis d'éveiller ma curiosité scientifique et de développer une ouverture d'esprit ; à mon sens ces trois éléments me serviront pour le reste de ma carrière et je t'en serai éternellement reconnaissant. Enfin, je te remercie très chaleureusement de m'avoir aidé à développer progressivement mes propres projets de recherche et j'espère que nous continuerons à travailler ensemble pendant encore de très nombreuses années.*

*Mes prochains remerciements sont pour le Docteur Yamina Hamel. Tu m'as montré ton soutien indéfectible, y compris dans les moments les plus difficiles, depuis de nombreuses années et très fortement contribué, de près ou de loin à mes différents projets scientifiques mais aussi médicaux et personnels depuis longtemps et par là-même à mes différents succès. Là aussi, je t'en serai éternellement reconnaissant et j'espère pouvoir te renvoyer l'ascenseur toutes les fois où tu en auras besoin...*

*Je tiens bien évidemment à remercier toutes les autres personnes qui ont contribué aux différents travaux présentés dans ce manuscrit mais aussi aux projets actuels ou à venir, tous aussi excitants les uns que les autres : le Docteur Loredana Saveanu, le Docteur Julien Diana, le Professeur Pascale de Lonlay, le Professeur Efstratios Stratikos, le Professeur Bertrand Knebelmann, le Professeur Roland Liblau, le Professeur Jean-Jacques Robert, le Docteur Olivia Boyer, le Professeur Rémi Salomon, le Professeur Emmanuel Gonzales, le Professeur Raja Brauner, le Professeur Luc Mouthon, le Docteur Irini Evnouchidou, le Docteur Gaël Menasche, Valérie Manceau, Emmanuelle Enée, Kathleen Dessaix, Lei Huang, Leslie Assouline, Meriem Garfa-Traore, Nicolas Goudin, Oliver Pellé, Michaël Dussiot, Corinne Cordier, Jérôme Mégret, Valentina Libri, Milena Hasan.*

*Je tiens ensuite à remercier particulièrement l'ensemble des membres de l'équipe de Peter van Endert, passés ou présents (je m'excuse pour ceux que j'aurais pu oublier) et qui ont bien sûr contribué aux succès et aux très bons et longs moments passés au laboratoire au cours de ces années : Nawel, Emmanuelle, Valérie, Sarah, Chloé, Julien, Irini, Loredana, Anastasia, Sebastian, Bénédicte, Clarissa, Michela, Luis, Myriam, Mira, Cézaire, Mirjana, Marie-Andrée, Roland, Emilie, Subash, Anne-Floor, Staëlle, Alicia.*

*Je remercie également l'ensemble des membres de l'équipe de Lucienne Chatenoud et Maria Leites de Moraes et de Jean Davoust et des membres de l'animalerie et de la laverie, avec une pensée particulière pour Anne-Perrine.*

*Je remercie l'ensemble de mes amis et tout particulièrement Nawel, Alexandre et Charlotte, Matthieu, Ricardo, Marvin, Kathleen, Angelina, Sonia, François.*

*Je remercie également tous mes collègues que j'ai pu rencontrer au cours de mes stages d'interne et qui m'ont énormément appris sur les plans médical et humain.*

*Je tiens enfin à remercier très sincèrement et du fond de mon coeur mes parents et mon frère pour leur soutien indéfectible dans tous mes projets et qui m'ont poussé jusqu'ici ; j'espère réussir à leur rendre la pareille...*

# TABLE OF CONTENTS

<b>Acknowledgements</b> .....	<b>4</b>
<b>Table of contents</b> .....	<b>5</b>
<b>List of abbreviations</b> .....	<b>6</b>
<b>List of illustrations</b> .....	<b>9</b>
<b>Introduction</b> .....	<b>10</b>
<b>Part I- Both the actors and functions of the immune system are heterogeneous and complex</b> .....	<b>10</b>
Chapter 1. Functions of immunity.....	10
Chapter 2. What are the actors of innate immunity? .....	11
Chapter 3. What are the actors of adaptive immunity?.....	27
<b>Part II- Communication and dynamics are two key features of immune responses</b> .....	<b>38</b>
Chapter 1. Inter-cellular communication between innate and adaptive immune cells is required for activation and regulation of adaptive immunity.....	38
Chapter 2. Innate and adaptive immunity is spatially and temporally dynamic.....	43
Chapter 3. Inter-cellular communication and dynamics of immune cells are influenced by the microenvironment. ....	47
Chapter 4. Concluding remarks .....	48
<b>Part III- Integration of exogenous signals by dendritic cells results in activation of adaptive immunity</b> .....	<b>49</b>
Chapter 1. Dendritic cell maturation is dependent on recognition of danger signals.. ....	49
Chapter 2. Antigenic material is actively internalized by phagocytes .....	51
Chapter 3. Antigenic material internalized is processed into peptides that will be presented to T lymphocytes after loading onto MHC molecules. ....	66
Chapter 4. Concluding remarks.....	86
<b>Part IV- CD169+ macrophages are tissue resident macrophages with unique functions and behaviors</b> .....	<b>88</b>
Chapter 1. What are the structure and the functions of the CD169 molecule?.. ....	88
Chapter 2. How are CD169 macrophage development and maintenance regulated? .....	90
Chapter 3. CD169+ macrophages play a crucial role of immune surveillance .....	91
Chapter 4. CD169+ cells can activate adaptive immune responses by antigen transfer or by antigen presentation to cognate cells.....	94
<b>Part V- High-dimensional technologies and analytic tools to unravel the complexity and the variability of immune responses</b> .....	<b>99</b>
Chapter 1. How to study immune responses in the lymphoid organs by multiplex technologies? .....	99
Chapter 2. How to study immune responses at the cellular level by multiplex technologies?.....	100
Chapter 3. How to study immune responses at the molecular level by multiplex technologies? .....	101
<b>Objectives</b> .....	<b>106</b>
<b>Experimental work</b> .....	<b>110</b>
<b>Conclusion and discussion</b> .....	<b>386</b>
<b>Bibliography</b> .....	<b>394</b>

## LIST OF ABBREVIATIONS

---

**AEP** Asparaginyl Endopeptidase  
**AMPK** AMP-activated protein kinase  
**AP** Adaptor Protein  
**Arp2/3** actin-related protein 2 and 3  
**ATP** adenosyl-triphosphate  
**ARF6** ADP-ribosylation factor 6 (ARF6)  
**β2m** beta-2-microglobulin  
**Bach2** BTB domain and CNC homolog 2  
**Batf** basic leucine zipper ATF-like transcription factor  
**BcR** B cell receptor  
**BDCA** Blood Dendritic Cell Antigen  
**BLIMP-1** B-Lymphocyte-Induced Maturation Protein-1  
**CBFB** core-binding factor beta subunit  
**CCL** Chemokine (C-C motif) ligand  
**CCR** C-C chemokine receptor type  
**CD** Cluster of Differentiation  
**cDC** conventional type dendritic cell  
**cdc42** cell division control protein 42 homolog  
**C/EBP** CCAAT-enhancer-binding proteins  
**CDP** common dendritic cell precursor  
**CLEC9A** C-type lectin domain family 9 member A  
**CLIP** class-II-associated invariant chain peptide  
**CMP** common monocyte progenitors  
**cMOP** committed progenitor with monocyte potential  
**CORVET** class C core vacuole/endosome tethering factor  
**CSF-1R** colony stimulating factor-1 receptor  
**CX3CR1** C-X3-C Motif Chemokine Receptor 1  
**CpG** cytidine-phosphate-guanosine  
**DCIR2** dendritic cell inhibitor receptor 2  
**DC-SIGN** DC-specific ICAM3-grabbing non-integrin  
**DEC-205** dendritic and epithelial cells, 205 kDa  
**DNA** Deoxyribonucleic acid  
**DRiPs** defective ribosomal products  
**EEA-1** early endosomal antigen 1  
**EOMES** Eomesodermin  
**ER** Endoplasmic Reticulum  
**ERAD** endoplasmic reticulum-associated degradation  
**ERAP** endoplasmic reticulum aminopeptidase  
**ERGIC** ER-Golgi intermediate compartment  
**ESCRT** endosomal sorting complexes required for transport  
**FACS** fluorescence-activated cell sorting  
**FcγR** Fc-gamma receptors  
**FITC** Fluorescein IsoThioCyanate  
**Flt3** Fms-like tyrosine kinase 3  
**Flt3-L** Flt3-ligand  
**Foxo1** Forkhead box protein O1  
**Foxp3** Forkhead box protein 3  
**GCN2** general control nonderepressible 2

**GDI** guanine nucleotide dissociation inhibitor  
**GDP** guanosyl-diphosphate  
**GEF** guanine nucleotide exchange factor  
**Gfi1** Growth Factor Independent 1 Transcription Repressor  
**GILT** gamma-interferon inducible lysosomal thiol reductase enzyme  
**GTP** guanosyl-triphosphate  
**GTPase** guanosine triphosphatase  
**HLA** human leukocyte antigen  
**HOPS** homotypic fusion and vacuole protein sorting  
**HSC** hematopoietic stem cell  
**Hsp** Heat shock protein  
**ICOS** Inducible T cell COStimulator  
**Id2** inhibitor DNA binding 2  
**IDE** Insulin-Degrading Enzyme  
**IFN** interferon  
**Ig** immunoglobulin  
**li** Invariant chain  
**IKK** I-kappa B kinase  
**IL** interleukin  
**iDC** Inflammatory dendritic cell  
**iTreg** induced-regulatory T cell  
**ILV** intra-luminal vesicle  
**IRAK** interleukin-1 receptor-associated kinase  
**IRAP** insulin-responsive aminopeptidase  
**IRF** interferon regulatory factor  
**ITAM** immunoreceptor tyrosine-based activation motif  
**ITIM** immunoreceptor tyrosine-based inhibition motif  
**KIF16b** Kinesin Family Member 16b  
**KLF-4** Kruppel-like factor 4  
**KLRG-1** Killer cell lectin-like receptor subfamily G member-1  
**Lamp** lysosome-associated membrane protein  
**LPS** lipopolysaccharide  
**MARCO** macrophage receptor with collagenous structure  
**MAPK** mitogen-activated protein kinase  
**MHC** major histocompatibility  
**MDP** monocyte/macrophage and dendritic cell progenitors  
**MIIC** MHC class II loading compartment  
**MPEC** memory-precursor effector cells  
**mRNA** messenger ribonucleic acid  
**mTOR** mammalian target of rapamycin  
**mTORC1** mammalian target of rapamycin complex 1  
**Myd88** Myeloid differentiation primary response protein 88  
**NFIL3** nuclear factor interleukin 3 regulated  
**NF-κB** nuclear-factor kappa B  
**NLRs** NOD-like receptors  
**NK** Natural Killer cells  
**Nod-like** nucleotide-binding oligomerization domain-like  
**OVA** ovalbumin  
**PAMP** pathogen-associated molecular pattern  
**pDC** plasmacytoid dendritic cell  
**PI3K** phosphatidylinositol 3-kinase  
**PI4K2A** Phosphatidylinositol 4-Kinase Type 2 Alpha



**PIKfyve** Phosphoinositide Kinase, FYVE-Type Zinc Finger Containing  
**PIP5K** phosphatidylinositol 4-phosphate 5-kinases  
**PRR** pattern-recognition receptor  
**PtdIns3P** phosphatidylinositol triphosphate  
**PtdIns3,5P2** phosphatidylinositol 3,5 bisphosphate  
**PtdIns4,5P2** phosphatidylinositol 4,5-bisphosphate  
**PtdIns3,4,5P3** phosphatidylinositol 3,4,5 trisphosphate  
**PtdIns4P** phosphatidylinositol-4-phosphate  
**qPCR** quantitative polymerase chain reaction  
**RIG-I** retinoic-acid-inducible gene I  
**RLRs** RIG-I-like receptors  
**ROR** Receptor-Related Orphan Receptor  
**RNA** ribonucleic acid  
**RBP-J** Recombination Signal Binding Protein For Immunoglobulin Kappa J Region  
**SFKs** Src-family tyrosine kinases  
**SIGN-R1** DC-SIGN-related protein 1  
**SNARE** soluble N-ethylmaleimide-sensitive factor attachment protein receptor  
**SNX** sorting nexin proteins  
**STAT** signal transducer and activator of transcription  
**Syks** spleen tyrosine kinases  
**TAP** transporter associated with antigen processing  
**TCF-1** T-cell factor 1  
**Tcm** central memory T cell  
**TFEB** Transcription Factor EB  
**T-bet** T-box expressed in T cells  
**TcR** T-cell receptor  
**Tem** effector memory T cell  
**Tfh** T follicular helper  
**TGN** trans-golgi network  
**Th** T helper  
**TIR** Toll-interleukin 1 receptor  
**TLR** toll-like receptor  
**TNF** tumor necrosis factor  
**TRAF6** TNF Receptor associated factor 6  
**TRAIL** TNF-related apoptosis-inducing ligand  
**Treg** regulatory T cell  
**TRIF** TIR- domain-containing adapter-inducing interferon- $\beta$   
**Trm** resident-memory T cell  
**UNC93B** unc-93 homolog B  
**UPR** unfolded protein response  
**VAMP** vesicle-associated membrane protein  
**V-ATPase** V-Adenosine TriPhosphatase  
**Vps** vacuolar protein sorting

## LIST OF ILLUSTRATIONS

---

- Figure 1.** A synthetic overview of the transcriptional development of dendritic cells (page 17)
- Figure 2.** Macrophage ontogeny and requirement on specific transcription factors (page 23)
- Figure 3.** A new proposition of classification for mononuclear phagocytes (page 26)
- Figure 4.** The three phases (expansion, contraction and stabilization) of an antigen-specific CD8 T cell responses following immunization (page 28)
- Figure 5.** Determinants for terminal-effector and memory T cell fate (page 35)
- Figure 6.** Modes of interaction between T cells and antigen-bearing dendritic cells (page 39)
- Figure 7.** Formation of the immunological synapse by TcR microclusters (page 42)
- Figure 8.** How subcapsular sinus macrophages influence the antigen presentation to follicular B cells in the lymph nodes (page 44)
- Figure 9.** TLR signaling in phagocytes (page 51)
- Figure 10.** Endosomal maturation (page 54)
- Figure 11.** Phagosome maturation (page 58)
- Figure 12.** Phagosome formation (page 61)
- Figure 13.** FcγR signaling leads to the phagocytosis of the microbe (page 62)
- Figure 14.** MHC-I endogenous (classical) antigen presentation (page 71)
- Figure 15.** The peptide loading complex dynamic (page 72)
- Figure 16.** MHC-II antigen presentation (page 76)
- Figure 17.** Antigen cross-presentation pathways in dendritic cells (page 82)
- Figure 18.** MHC-I recycling within the endocytic pathway (page 85)
- Figure 19.** Distribution and markers of macrophage subsets in the mouse spleen (page 95)
- Figure 20.** An example of workflow for a high-resolution analysis of macrophage activation (page 105)
- Table 1.** Origins, functions and transcription factors of tissue macrophages (page 24)
- Table 2.** Characterization of CD4+ helper and regulatory T cell subset functions (page 30)
- Table 3.** A brief overview of markers expressed by conventional memory T cell subsets in human and mouse (page 32)
- Table 4.** Markers used to delineate effector T cell subsets in mouse (page 34)

# INTRODUCTION

---

## PART I - BOTH THE ACTORS AND FUNCTIONS OF THE IMMUNE SYSTEM ARE HETEROGENEOUS AND COMPLEX

### **Chapter 1. Functions of immunity**

Immunity has been originally defined as the resistance to diseases, especially infectious diseases. Immunity involves a specific physiologic system, the immune system, and specific tissues, cells and molecules, the coordination of these components leading to the immune response. The most important physiologic functions of the immune system are to prevent infections and to eliminate established infections, as illustrated by the dramatic observation that individuals carrying defective immune responses are more prone to severe and life-threatening infectious settings (Picard, Al-Herz et al. 2015). Conversely, vaccination by stimulating immune responses against a particular microbe is the most effective process to protect individuals against infections. Vaccination is the unique example of a worldwide eradication of human disease in the context of smallpox vaccination (Tomori 2011). However, the importance of immunity goes far much beyond infectious diseases and is crucial for preventing or controlling tumor growth or spreading, as assessed by the encouraging results of strategies that manipulate the immune system (Mahoney, Rennert et al. 2015). Furthermore, immune responses contribute to the recognition and clearance of dead cells and in initiating tissue repair after injuries (Geissmann, Gordon et al. 2010). However, despite the large number of beneficial roles of the immune system, anomalies in the immune response lead to inflammatory diseases or to the recognition and destruction of self (autoimmunity). The immune response is also the main barrier to successful organ transplantation to treat organ failure.

The immune responses can be divided into two complementary and inter-dependent types of immunity: the innate and the adaptive immunity. The innate immunity represents a first line of defense, which is immediate and not specific. It consists of natural physical barriers (skin, mucosal tissues), molecules of the complement and a set of immune cells capable of attacking a foreign agent by phagocytosis or inflammatory response, the mononuclear phagocytes. Activation of the innate immune cells requires the recognition of a danger signal, referred to as a Pathogen Associated Molecular Pattern (PAMP) by a non-polymorphic receptor present

at the membrane of the cell, the Pattern-Recognition Receptor (PRR) (Iwasaki and Medzhitov 2015). By contrast, the adaptive immune response is of more recent appearance during evolution and is only present in vertebrates (Travis 2009). This second line of immunity takes at least four days to be recruited and activated. The two components of the adaptive immunity are the cellular and the humoral responses and adaptive immunity employs mechanisms much more elaborate and specific than the innate response; an important hallmark of adaptive immunity is the development of an immunological memory. To generate adaptive immune responses, the two cellular components, the B lymphocytes and the T lymphocytes need to recognize a specific motif derived from the pathogen, an antigenic epitope exposed by antigen presenting cells (mainly the mononuclear phagocytes) through the major histocompatibility (MHC) molecules, by specific antigen receptors, the BcR and the TcR, respectively (Iwasaki and Medzhitov 2015).

In the next pages, I will successively and briefly review and expose the key aspects of immunity that will be required for understanding the experimental works: the actors of innate and adaptive immune responses, how the dynamics of immune responses are dependent on an inter-communication between innate and adaptive immune cells, how these different cellular actors are regulated. Finally, I will also give an overview of the most recent technological tools that present a particular interest for studying immune responses under homeostatic and pathological settings.

## **Chapter 2. What are the actors of the innate immunity?**

Monocytes, macrophages and dendritic cells are the cellular members of the mononuclear phagocyte system and can be distinguished on the basis of their morphology, functions, origin and more recently by their gene-expression and protein-expression profiles. The term mononuclear phagocyte system was proposed in 1969 and initially comprised monocytes and macrophages derived from the bone marrow derived monocytes (van Furth, Cohn et al. 1972). Only four years later, R. Steinman and Cohn identified the third component of the system as a novel subset in lymphoid tissue distinguishable from macrophages and presenting with particular extensions reminiscent from the neuronal dendrites, the dendritic cells (Steinman and Cohn 1973). Next to the identification and the characterization of a high number of various macrophage and dendritic cell subsets, attention of immunologists has shifted to the identification of the factors involved and regulating their ontogeny. Furthermore, fundamental questions about the mononuclear phagocyte system remain still open and under investigation in the field: how do the different subsets relate between species? How is regulated the

phagocytosis? What are the mechanisms responsible for particle digestion? How do tissue macrophages maintain *in vivo*? What are the factors that dictate dendritic cell and macrophage functions? For monocytes, dendritic cells and macrophages I will try to compile crucial information to give an insight on how they are organized, how they are distinct one from each other and how their ontogeny and maintenance are orchestrated, with a particular focus on elements that are important and required for understanding the experimental work exposed in this manuscript.

### 1) Monocytes

Monocytes are short-lived mononuclear phagocytes and can be separated into two main subsets with specific signatures and functions, the patrolling monocytes and the inflammatory monocytes. Inflammatory (classical) monocytes express high Ly-6c and C-C chemokine receptor type 2 (CCR2) levels (Cluster of Differentiation (CD)14<sup>++</sup>CD16<sup>int/low</sup> in human) at the surface and under tissue injury they are attracted to the damaged tissue, and they extravasate through endothelium to the injury site (Wynn and Vannella 2016). They mainly contribute to the regulation of the inflammatory response at the resolution phase but can also differentiate into short-lived functional resident tissue macrophages promoting tissue repair (Wynn and Vannella 2016). Patrolling monocytes were first identified by the group of F. Geissmann as monocytes expressing low Ly-6C and CCR2 but high C-X3-C Motif Chemokine Receptor 1 (CX3CR1) levels (CD14<sup>dim</sup>CD16<sup>+</sup> in human) at the surface that contribute to the endothelium homeostasis under resting and inflammatory conditions (Auffray, Fogg et al. 2007, Carlin, Stamatiades et al. 2013). The roles of these non-classical monocytes may include: brain protection by removing amyloid beta (Michaud, Bellavance et al. 2013); regulation of vascular inflammation by contributing to both the initiation and progression phases (Thomas, Tacke et al. 2015); tumor surveillance by recruiting Natural Killer (NK) cells, as supported by the elegant study from the group of C.C. Hedrick (Hanna, Cekic et al. 2015), which showed that the depletion of circulating monocytes resulted in higher lung metastasis number and size.

Ontogeny of both monocyte subsets remains barely understood since no specific transcriptional factor has been linked to an impaired monocyte development solely (Tussiwand and Gautier 2015). Monocytes are detectable as soon as the multi-potent hematopoietic stem cell (HSC) progenitors have seeded the fetal liver; HSC progenitors differentiate into monocyte/macrophage and dendritic cell progenitors (MDPs) that cannot generate granulocytes. The fate of MDP is to give rise to either a common dendritic cell

precursor (CDP) or to common monocyte progenitors (CMP) (Tussiwand and Gautier 2015). High levels of the PU.1 transcription factor trigger the activation of the myeloid-specific factors such as Interferon Responsive Factor 8 (Irf8), Kruppel-like factor 4 (Klf4) and Erg1 and silence the key master transcription factors regulating other developmental pathways. PU.1 also promotes the surface expression of the colony stimulating factor-1 receptor (CSF-1R) on the MDP committed progenitors. Among the different candidates suggested, Irf8, Pu.1, Egr-1, Stat3, Gata2, Nur77, CCAAT-enhancer-binding proteins (C/EBP), Klf4, c-Maf, Csf-1R or retinoic acid receptors have been reported to be involved in monocyte development (Ginhoux and Jung 2014, Tussiwand and Gautier 2015). As described later, some of these factors are also involved in the dendritic cell development whereas other factors are required for macrophage development. All these transcription factors were found to be highly enriched in gene-expression analysis of a committed progenitor with monocyte potential cMOP (Hettinger, Richards et al. 2013, Anbazhagan, Duroux-Richard et al. 2014). Nonetheless, Nur77 seems to be crucial for patrolling monocytes and not inflammatory monocytes, since deficient animals for this factor totally lack of non-classical monocyte subset (Hanna, Carlin et al. 2011, Hilgendorf, Gerhardt et al. 2014).

## 2) Dendritic cells

Dendritic cells are a phagocyte subset specialized in processing and presenting antigen to cognate lymphocytes. Due to their migratory potential, dendritic cells have the unique function to bring captured antigens from the peripheral damaged tissues to the secondary lymphoid organs, resulting in the initiation of adaptive immune responses. Importantly, dendritic cells have been crucially implicated in the regulation of tolerance and immunological memory (Joffre, Segura et al. 2012). Dendritic cells are made of heterogeneous subsets that have been identified by variations in the surface protein expression as well as developmental particularities. Focusing on the lymphoid organs, two main dendritic cell subsets have been described under homeostatic conditions: the conventional and the plasmacytoid dendritic cells (pDCs). I will review the key features of mouse and human dendritic cell subset.

### Mouse dendritic cell subsets

Conventional dendritic cells. Two families of conventional dendritic cells have been identified in mouse, based on the surface expression of CD8 $\alpha$  or CD103 or CD24 and CD11b. CD8 $\alpha$ <sup>+</sup> dendritic cells are functionally specialized in cross-presentation (antigen presentation

of exogenous antigens by MHC-I molecules) of exogenous viral antigens, dead-cell associated antigens and soluble proteins (Bellone, Iezzi et al. 1997, Li, Davey et al. 2001, Pooley, Heath et al. 2001, Helft, Manicassamy et al. 2012). Additionally, CD8 $\alpha$ +CD103-dendritic cells also act as very efficient antigen presenting cells for exogenous glycolipids on CD1d to activate invariant NK-T cells, resulting in cytokine secretion (Arora, Baena et al. 2014). Contrasting with CD8 $\alpha$ + conventional dendritic cells, CD11b+ conventional dendritic cells are poorly efficient in cross-presenting these forms of antigen. However, recent reports suggest that CD11b+ conventional dendritic cells are more efficient cross-presenting cells than CD8 $\alpha$ + conventional dendritic cells in the context of larger particulate antigens such as yeast cells (Backer, van Leeuwen et al. 2008, Weimershaus, Maschalidi et al. 2012). Conversely, CD11b+ conventional dendritic cells are among the most efficient cells for MHC-II antigen presentation of soluble proteins to activate naïve CD4+ T cells and can produce large amounts of pro-inflammatory chemokines (Dudziak, Kamphorst et al. 2007). In mice, dendritic cells arise from CDP that express the hematopoietic cytokine receptor Fms-like tyrosine kinase 3 (Flt3) and give rise to pDCs or pre-conventional dendritic cells. The transcription factors PU.1, Growth Factor Independent 1 Transcription Repressor (Gfi1) and Core-Binding Factor, Beta Subunit (CBFb) control the development of the common dendritic cell lineage. Pre-conventional dendritic cells have been detected in the blood and develop further in tissue into the two subsets of conventional dendritic cells (Merad, Sathe et al. 2013). Development of CD8 $\alpha$ + conventional dendritic cells from the pre-dendritic cell progenitor is orchestrated by at least four transcriptional factors: inhibitor of Deoxyribonucleic acid (DNA) binding 2 (Id2), IRF8, basic leucine zipper ATF-like 3 transcription factor (BATF3) (Hildner, Edelson et al. 2008, Grajales-Reyes, Iwata et al. 2015) and the nuclear factor interleukin (IL) 3 regulated (NFIL3). CD11b+ conventional dendritic cells development is controlled by transcription factors including RelB, NOTCH 2, Recombination Signal Binding Protein For Immunoglobulin Kappa J Region (RBP-J), IRF2 and IRF4. During the whole life, conventional dendritic cells are continuously replenished from precursors in a FLT3-Ligand (FLT3-L) dependent manner, allowing their replacement despite their relatively short half-life of few (3-6) days.

Plasmacytoid dendritic cells. pDCs differ from conventional dendritic cell subsets by their morphology, phenotype and functions. The main role identified for pDCs and supported by a large number of independent studies is their massive type I interferon (IFN) production in response to viral infection (Cella, Jarrossay et al. 1999, Siegal, Kadowaki et al. 1999). This

function has been shown to be crucial for controlling infections by inducing adaptive immune responses (Honke, Shaabani et al. 2012). Next, pDCs might also act as antigen cross-presenting cells, although this capacity remains controversial (Sapozhnikov, Fischer et al. 2007, GeurtsvanKessel, Willart et al. 2008, Mouries, Moron et al. 2008, Kool, Geurtsvankessel et al. 2011). Regarding the factors required for pDC development, E2-2 has been identified as the key factor leading to its development (Cisse, Caton et al. 2008). Interestingly, E2-2 is promoted by the suppression of Id2, the transcription factor required for conventional dendritic cell development (Nagasawa, Schmidlin et al. 2008, Scott, Soen et al. 2016). Finally, half-life of pDCs seems to be longer than conventional dendritic cells.

*Inflammatory dendritic cells.* Inflammatory dendritic cells or monocyte-derived dendritic cells (iDCs) have been more recently identified under inflammatory conditions or during the course of infections. As indicated by their alternative nomenclature, iDCs originate from monocyte that infiltrate the damaged organs (Rotta, Edwards et al. 2003, Cheong, Matos et al. 2010). iDCs share similar expression for the main protein receptors that characterize conventional dendritic cell subsets with conventional dendritic cells, with the exception of CD64 that is specifically upregulated on iDCs (Langlet, Tamoutounour et al. 2012). To date, the functions and the regulation of iDCs are poorly understood.

### **Human dendritic cell subsets**

*Human dendritic cell classification.* Similar to mouse lymphoid organs, conventional dendritic cell and pDC subsets have been identified in human lymph nodes, spleen, tonsils and blood. Examination of their surface receptor pattern has allowed for the identification of three distinct antigens that are absent from rodents and that discriminate between the human subsets: Blood Dendritic Cell Antigen-1 (BDCA-1), BDCA-2 and BDCA-3 (Dzionek, Fuchs et al. 2000). Gene-expression and protein-expression analysis and comparison of murine and human dendritic cell subsets have given crucial information about how murine and dendritic cells are related. Thus, BDCA-1 subset is thought to be the human equivalent of murine CD8 $\alpha$ <sup>+</sup> conventional dendritic cell subset, BDCA-2 the equivalent of murine pDCs and BDCA-3 of murine CD8 $\alpha$ <sup>-</sup> conventional dendritic cell subset (Robbins, Walzer et al. 2008, Haniffa, Shin et al. 2012, Watchmaker, Lahl et al. 2014). Importantly in human, protein expression is not sufficient to identify and study the contribution of dendritic cells in pathological settings. Indeed, some markers currently used are not specific of a given dendritic cell subset, or their expression can vary during maturation or depending on the environment. BDCA-3 has found to be up-regulated in activated pDCs and BDCA-1 dendritic



cell subset whereas C-type lectin domain family 9 member A (CLEC9A) was downregulated rapidly during dendritic cell maturation (Dzionek, Fuchs et al. 2000, Chu, Ali et al. 2012, Schreiberl, Klinkenberg et al. 2012). Finally, iDCs have also been identified in inflamed tissues (Guttman-Yassky, Lowes et al. 2007, Segura, Touzot et al. 2013).

Ontogeny of human subsets. Only few reports have addressed human dendritic cell ontogeny. The existence of a constant replenishment of dendritic cell subsets from bone marrow precursors is supported by the loss of blood BDCA-1/2/3 subsets after cytotoxic therapies and by the replacement of dermal dendritic cell after HSC transplantation (Haniffa, Ginhoux et al. 2009, McGovern, Schlitzer et al. 2014). Factors required for the commitment of the putative progenitors into differentiated dendritic cells have been recently identified. FLT3-ligand facilitates the generation of most dendritic cell subsets: BDCA-1/2/3 subsets can be artificially derived *in vitro* by culturing hematopoietic progenitors with the cytokine; infusion of volunteers with FLT3-L increases the number of all blood dendritic cell subsets (Pulendran, Banchereau et al. 2000, Proietto, Mittag et al. 2012). Examination of the consequences of inherited mutations in transcription factors suspected to be involved allowed for the identification of two factors required for dendritic cell differentiation from a bone marrow derived progenitor, GATA2 and IRF8. Mutations in these genes resulted in a total lack of these blood dendritic cell subsets (Dickinson, Griffin et al. 2011, Hambleton, Salem et al. 2011). A committed dendritic cell progenitor has been recently identified in the bone marrow and the cord blood but was absent from adult blood or tonsils. *In vitro* culture of this committed progenitor resulted in the production of BDCA-1/2/3 subsets, and a pre-conventional dendritic cell intermediate as characterized in the bone marrow, tonsils and adult blood (Breton, Lee et al. 2015, Lee, Breton et al. 2015).

Functional specificities of human dendritic cell subsets. Contrary to mouse dendritic cells, under homeostatic conditions or sterile inflammation (induced by TLR activation), spleen, lymph node and tonsil BDCA-1 and BDCA-3 dendritic cells cross-present with a similar efficiency soluble antigens as well as endocytosed antigens targeted to an early endocytic compartment. One exception is the dead-cell associated antigens that are specifically cross-presented by BDCA-3 subset in blood (Cohn, Chatterjee et al. 2013). Regarding pDCs, a significant efficient cross-presentation of soluble antigen, viral antigen and antigen targeted to an early endocytic compartment was observed in blood, tonsils and lymph nodes (Hoeffel, Ripoche et al. 2007, Guillerme, Boisgerault et al. 2013, Tel, Schreiberl et al. 2013, Aspod, Leloup et al. 2014). Regarding *ex vivo* MHC-II antigen presentation by BDCA-1 and BDCA-

3 subsets, equal capacity of human conventional dendritic cells to polarize naïve CD4+ T cells toward Th1 has been observed in blood and lymph nodes both under homeostatic condition and exposure to microbes. In tissues such observations remain controversial and still an intense subject of debate (Durand and Segura 2015).

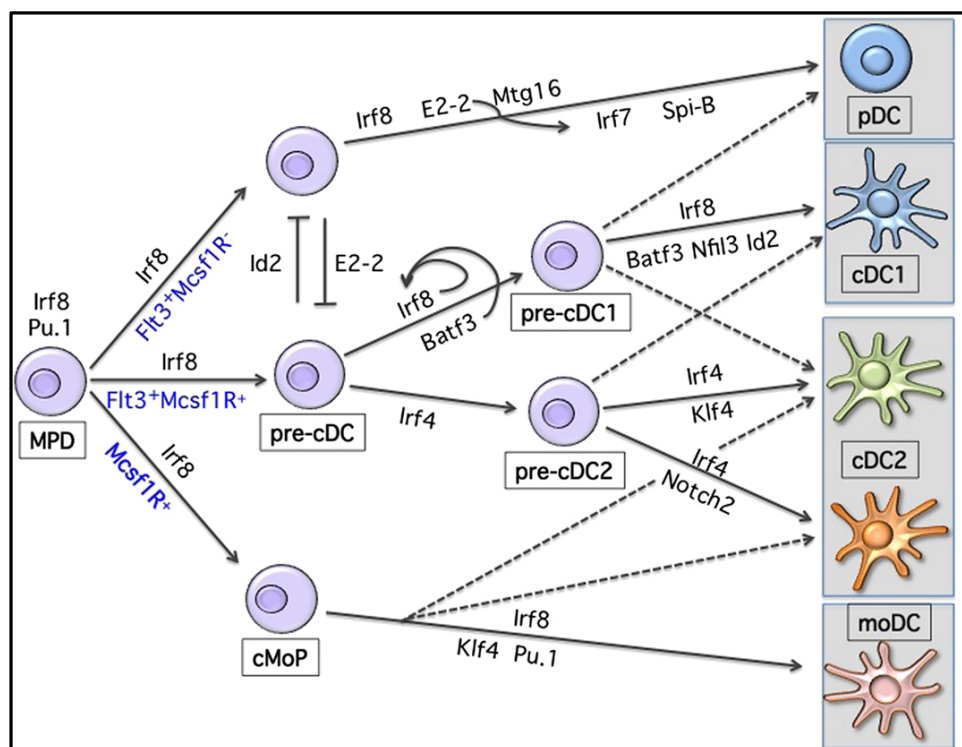


**Figure 1. A synthetic overview of the transcriptional development of dendritic cells (derived from (Tussiwand and Gautier 2015)).** Development of dendritic cells occurs from a Flt3-, Irf8-expressing hematopoietic progenitor and the progressive acquisition of one or more transcription factors will result in differentiation toward a specific dendritic cell subset.

### 3) Tissue macrophages

Macrophages are a mononuclear phagocyte subset specialized in the phagocytosis and neutralization of cell debris and pathogens (Geissmann, Gordon et al. 2010). Tissue macrophages are resident non-migratory cells that monitor and sense their local environment continuously. Regarding these general properties, macrophages differ from dendritic cells since the latter are specialized in initiating immune responses by presenting antigens to T lymphocytes after uptake by phagocytosis and endocytosis and migration to the tissue-draining lymph nodes (Geissmann, Gordon et al. 2010). As for dendritic cells tissue macrophages are equipped by a vast variety of PRRs including scavenger receptors, C-type lectin receptors, Toll-like receptors (TLRs) and retinoic acid-inducible gene 1 (RIG-I) receptors and nucleotide-binding oligomerization domain-like receptors (Nod-like receptors)

as well as adhesion molecules and cytokine receptors. Surface receptor patterns significantly vary from one tissue to another, indirectly supporting the concept of tissue specialization and of local adaptation and plasticity (Geissmann, Gordon et al. 2010). Clearance of cell debris and pathogens has been linked to their highly complex and developed late endosomal and lysosomal compartments that are equipped with critical protease and bactericidal activities. Furthermore, as dendritic cells, macrophages orchestrate and regulate inflammation by providing cytokines and chemokines, attracting and recruiting neutrophils, monocytes and lymphocytes. Finally, macrophages when challenged, secrete a lot of effector molecules that include metabolic and growth factors that may contribute to tissue repair and homeostasis (Geissmann, Gordon et al. 2010). Despite these common functions, tissue macrophages are heterogeneous populations as recently discovered by the examination of their gene expression profiles and epigenetic regulation. To date most of the factors regulating tissue specific features are unknown even if the current view strongly indicates the role of local environment.

I will review the key features of mouse and human macrophage subsets, their development and how they are maintained.

### **An overview of tissue-resident macrophage subsets**

*The liver.* The liver is mainly involved in the uptake and the storage of nutrients, aminoacids, sugars, lipids and vitamins. Next to its storage function the liver helps with the metabolic conversion and release into the blood and the bile and with the detoxification of chemicals (Kmiec 2001). To promote these functions, the liver is assisted by anatomical specificities including its particular blood circulation that makes it continuously exposed to food antigens, microbes and xenobiotics, because of blood irrigation by both the portal vein and the systemic arterial circulation. Interestingly, liver microcirculation includes a network of sinusoids made of a fenestrated layer of liver sinusoidal endothelial cells, that has been suggested to facilitate effective antigen capture and presentation (Racanelli and Rehermann 2006). The main liver resident macrophage population is the Kupffer cells with a predominant distribution in the periportal regions of the liver sinusoids (Racanelli and Rehermann 2006). Consistent with a macrophage population, Kupffer cells exhibit high phagocytic and lysosomal activities, strongly supporting their role of blood filter and in immune surveillance. They have been implicated in the clearance of blood-borne pathogens, of complement-opsonized particles, of cell debris and immune complexes. While in homeostatic settings they display a tolerogenic phenotype, they can trigger hepatocytes injury and damage under pathological conditions

(Racanelli and Rehermann 2006, Dixon, Barnes et al. 2013). As also observed in the spleen, Kupffer macrophages strongly contribute to the removal of senescent red cells that are either malformed or damaged (Willekens, Werre et al. 2005, Racanelli and Rehermann 2006). One of the mechanisms potentially involved in the phagocytosis of erythrocytes is the high expression of the CD163 scavenger receptor (Kristiansen, Graversen et al. 2001). Finally, they also participate in regulating lipid metabolism, this function being facilitated by the expression of specific receptors for lipoproteins (Racanelli and Rehermann 2006).

*Brain tissue macrophages (microglia, non-parenchymal macrophages)*. Microglia is a macrophage population that resides in the central nervous system parenchyma to complete two main functions including immune defense and homeostatic maintenance (Wake, Moorhouse et al. 2011). Supporting indirectly a role in the regulation of brain tissue function and viability, the acute ablation of adult microglia using a CSF-1 receptor kinase inhibitor in the central nervous system leads to the rapid and massive replenishment by newly-differentiated macrophages, presumably due to the infiltration by bone marrow derived cells that can enter through brain blood barrier disruption (Elmore, Najafi et al. 2014). Numerous mechanisms have been identified that may be used by microglia to regulate neuroglia integrity. During embryogenesis and post-natal period, microglia actively phagocytoses cell debris and synaptic material to perform neuronal pruning (Schafer, Lehrman et al. 2012, Kierdorf, Erny et al. 2013). Elimination of this process can be obtained through a CX3CR1 deficiency and leads to impaired functional brain connectivity and disturbance in social behavior in adult mice (Sierra, Encinas et al. 2010, Paolicelli, Bolasco et al. 2011, Zhan, Paolicelli et al. 2014). Microglia has been also linked to the formation of learning-induced spines in the motor cortex by secreting brain-derived neurotrophic factors. Interestingly, there is also evidence for a regulation of microglia by neuroglial cells. Neurons can fuel the renewal and maintenance of microglia by promoting the secretion of IL-34 that is a known ligand for CSF-1R. They were also shown to silence their function under inflammation by secreting Transforming Growth Factor-beta TGF- $\beta$  (Greter, Lelios et al. 2012, Wang, Szretter et al. 2012).

Non-parenchymal macrophages are made of perivascular, meningeal and choroid plexus macrophages that have been associated to the local immunosurveillance against local inflammation, neurotropic virus or brain tumors. Contrary to the microglia, non-parenchymal macrophages highly exchange with the blood circulation and myeloid cells (Prinz and Priller 2014).

The lung. The lung is a vital respiratory organ that regulates gas exchanges between the environment and the blood circulation. Due to its function, airways are constantly in direct contact with microbes, allergens and pollutants. A lung integrity is required to support its physiologic respiratory function so that the organ has to tightly equilibrate immune defense to protect from pathogenic infections and to limit susceptibility to allergic airway inflammation (Herold, Gabrielli et al. 2013). Two main populations have been identified to promote acute immune responses responsible for either tolerance or protective immunity: the alveolar macrophages and the CD103<sup>+</sup> and CD11b<sup>+</sup> conventional dendritic cell subsets (Guilliams, Lambrecht et al. 2013, Gollwitzer, Saglani et al. 2014). Alveolar macrophages are distributed among the alveoli of healthy airways and interact with alveolar epithelial cells through CD200 and TGF- $\beta$  signaling to ensure a tolerogenic phenotype (Morris, Huang et al. 2003, Snelgrove, Goulding et al. 2008). Alveolar macrophages are also in direct contact with surfactant-associated antigens derived from microbes, cell debris and allergens expressed by lung epithelial cells, promoting their neutralization without activating inflammatory gene program (Forbes and Haczku 2010). Reinforcing the role of surfactant in the regulation of the alveolar macrophage activation state, mice deprived from surfactant exhibit a chronic airway inflammation. In other words, the alveolar macrophages are required to clear surfactant by their phagocytic activity, the latter being supervised by the transcription factor BTB Domain And CNC Homolog 2 (Bach2) (Nakamura, Ebina-Shibuya et al. 2013). Lack of this transcription factor is responsible for the development of a pulmonary alveolar proteinosis. Alveolar macrophages also phagocytose respiratory bacteria and promote type I IFN in the context of respiratory viral infections (Goritzka, Makris et al. 2015). Finally, the alveolar macrophages are also involved in the termination of inflammation, presumably due to their homeostatic highly-tolerogenic phenotype (Tate, Pickett et al. 2010).

The splenic resident macrophage populations. The spleen is a secondary lymphoid organ that initiates and regulates adaptive immune responses against blood-borne self and foreign antigens. Contrary to the lymph nodes, the spleen is totally devoid of connections with the lymphoid circulation so that it is totally dependent on the systemic blood circulation (den Haan and Kraal 2012). Spleen homeostatic functions include the clearance of cells debris and senescent red cells and also the recognition and the control of blood microbial infections. To serve these functions, the spleen is divided into three main anatomical compartments, the red pulp and the white pulp zones separated and connected with a marginal zone (den Haan and Kraal 2012). Resident macrophages with specific roles can be found into the three regions.

Red pulp macrophages are specialized in iron metabolism and express a protein machinery dedicated to the support of all the recycling phases, including the engulfment of end-of-life red cells, the uptake of hemoglobin and heme breakdown and iron export (Ganz 2012). As for Kupffer cells in the liver, CD163 scavenger receptor is highly expressed at the cell surface and facilitates endocytosis of hemoglobin-haptoglobin complexes released by dying red cells (Kristiansen, Graversen et al. 2001). In addition to CD163, red pulp macrophages express high levels of F4/80 and mannose receptor at the surface and low or undetectable levels of CD11b, CD11c and intermediate levels of MHC-II molecules (den Haan and Kraal 2012). White pulp macrophages include the tingible body macrophages and other macrophage populations that have been poorly studied to date. The tingible body macrophages are located in the germinal center of B cell follicles and contribute to the removal and phosphatidyl-serine expressing apoptotic B lymphocytes that arise during the germinal center reaction (den Haan and Kraal 2012). The expression of specific receptors such as the Milk fat globule-EGF factor 8 (MFG-E8) directly supports this function since animals deficient for MFG-E8 develop autoimmune manifestations and a defect in apoptotic B cell removal (Hanayama, Tanaka et al. 2004). The marginal zone of the spleen is a transitional area at the interface between the red pulp and the white pulp regions. In this particular zone, systemic blood flow slows down, promoting the exposure of microbes or apoptotic cells to the two distinct residing marginal zone macrophage populations: the outer marginal zone macrophages and the metallophilic marginal zone macrophages (den Haan and Kraal 2012). Supporting a role for the removal of cell debris, the selective depletion of marginal zone macrophages leads to the accumulation of apoptotic cell debris in the other regions resulting in the development of severe autoimmunity (Miyake, Asano et al. 2007, McGaha, Chen et al. 2011). Marginal zone macrophages express a specific set of PRRs, such as macrophage receptor with collagenous structure (MARCO) and human dendritic cell-specific intercellular adhesion molecule (ICAM)-3-grabbing non-integrin-related protein 1 (DC-SIGN-related protein 1 (SIGN-R1)) that both contribute to the trapping and the clearance of microbial pathogens (Geijtenbeek, Groot et al. 2002). Marginal zone macrophages also interact with marginal zone B cells and this B cell subset influences both the maintenance and the retention of marginal zone macrophages by the secretion of chemokines such as Chemokine (C-C motif) ligand-19 (CCL19) and CCL21 and of lymphotoxin (Mackay, Majeau et al. 1997, Ato, Nakano et al. 2004, Nolte, Arens et al. 2004). In turn, MARCO expression has been implicated in the retention of marginal zone B cells (Karlsson, Guinamard et al. 2003) and SIGN-R1 in influencing Immunoglobulin M (IgM) responses to polysaccharides (Koppel, Litjens et al. 2008). Metallophilic macrophages form

an inner ring of macrophages adjacent to the white pulp and are characterized by the high expression of CD169 involved in the recognition of sialylated pathogens (den Haan and Kraal 2012). Metallophilic macrophages are close to the B cell follicles and are influenced by factors secreted by follicular B cells. Due to this specificity and work on the lymph node CD169<sup>+</sup> counterpart, metallophilic macrophages might transfer antigen to B cells for deposition on follicular dendritic cells (Junt, Moseman et al. 2007, Phan, Grigorova et al. 2007). Metallophilic macrophages have been also suggested to activate T cell adaptive immunity by transferring antigens to cross-presenting dendritic cells (Backer, Schwandt et al. 2010). Finally, both populations have been shown to fuel inflammatory responses via type I IFNs after a viral challenge (Eloranta and Alm 1999).

### **Tissue macrophage ontogeny**

Similar to dendritic cells tissue resident macrophage origin and development are a current topic of investigation. Initial examination of tissue macrophage ontogeny was performed by the groups of F. Geissmann and M. Merad, which focused on the development of brain microglia, and identified a yolk sac progenitor with a capacity of fueling developing embryo and self-renewing during adulthood (Ginhoux, Greter et al. 2010, Schulz, Gomez Perdiguero et al. 2012). Mechanistically this progenitor was characterized as Myb-independent and PU.1-dependent (Schulz, Gomez Perdiguero et al. 2012). In the same time other groups identified an alternative and fetal liver monocyte-derived progenitor for lung alveolar macrophages and Langerhans cells (Ginhoux, Greter et al. 2010). The group of F. Geissmann has recently proposed an original and elegant scenario that might explain the complex embryonic development and adult renewal of tissue resident macrophages: during development, a yolk sac erythro-myeloid progenitor arises, distinct from HSCs and colonizes the liver to differentiate into fetal monocytes, monocytes, granulocytes and macrophages (Gomez Perdiguero, Klapproth et al. 2015). Erythro-myeloid progenitors will generate microglia and participate to the liver Kupffer macrophages and Langerhans cells (Hoeffel, Wang et al. 2012, Gomez Perdiguero, Klapproth et al. 2015). This postulate was challenged by another study that demonstrated the role of fetal HSCs in promoting most of tissue-resident macrophages with the exception of microglia and non-parenchymal brain macrophages (Sheng, Ruedl et al. 2015). To conclude, whatever the precise progenitor involves, the literature strongly supports the role of embryonic progenitors and macrophages in tissue-resident macrophage populations and in their self-renewal during adulthood. However, complementary experiments from this study suggested a contribution for adult bone marrow HSC-derived monocytes during

adulthood in renewing tissue macrophages. The latter observation is supported by several studies that showed that: blood circulating monocytes give rise to fully functional heart macrophages during injury (Epelman, Lavine et al. 2014, Molawi, Wolf et al. 2014), to lung alveolar macrophages (Guilliams, De Kleer et al. 2013), to liver Kupffer macrophages (Scott, Zheng et al. 2016), to choroid plexus brain macrophages (Goldmann, Wieghofer et al. 2016); and that under inflammation setting inflammatory monocytes can differentiate into tissue resident macrophages before being eliminated with the resolution of inflammation (Gautier, Ivanov et al. 2013). Recent studies by the group of M. Guilliams also support the contribution of different progenitors during life to maintain tissue-resident macrophages homeostasis: after birth alveolar macrophages can be renewed by yolk sac macrophages, fetal liver monocytes and bone marrow HSC-monocytes that colonize an empty niche but not from differentiated resident macrophages from another organ (van de Laar, Saelens et al. 2016). Importantly, newly differentiated macrophages from the three progenitors displayed similar gene and protein signature and functionality to “natural” alveolar macrophages (van de Laar, Saelens et al. 2016).

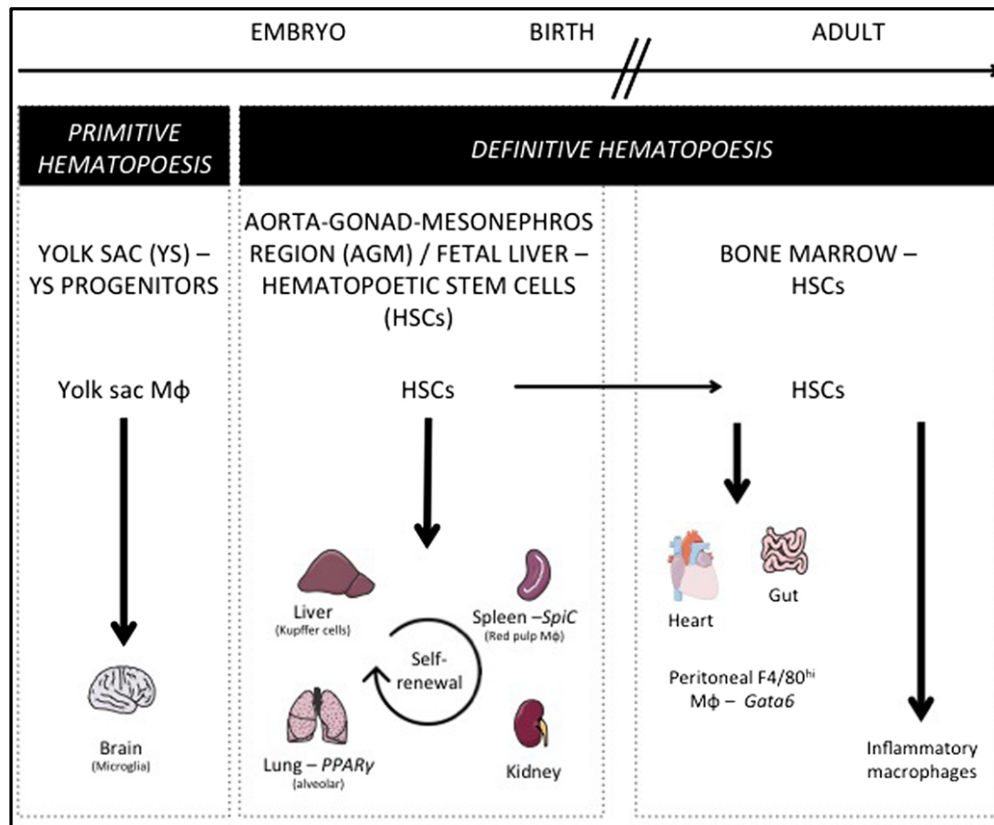


**Figure 2. Macrophage ontogeny and requirement on specific transcription factors (derived from (Tussiwand and Gautier 2015)).** During embryogenesis, yolk sac progenitors only give rise to microglia. Most tissue-resident macrophages develop before birth and derive



from early hematopoietic stem cells (HSC). After birth and in the adult mouse, alveolar, splenic, liver macrophages maintain their pool by self-renewal, while heart macrophages need a constant replenishment from bone marrow HSC. Also are depicted the transcription factors specifically controlling some of the resident macrophage populations.

### **Transcription factors required for development and maintenance of macrophages**

*Transcription factors involved in macrophage development.* Three inter-dependent factors have been identified to promote the macrophage development and the depletion or inhibition of these factors when viable led to a lack of detection of tissue-resident macrophages: runt-related transcription factor 1 (RUNX1), high levels of PU.1 and the Csf-1r (Tussiwand and Gautier 2015).

*Transcription factors involved in macrophage maintenance.* A few number of transcription factors can promote the maintenance of specific macrophage population in tissues: as examples, Spi-C is required for the maintenance of splenic red pulp macrophages whereas outer marginal zone and metallophilic splenic macrophages are both dependent on the transcription factor Liver-X-Receptor  $\alpha$  (LXR $\alpha$ ). Furthermore, PPAR $\gamma$  is required for the maintenance of lung alveolar macrophages, either by influencing the local environment or by a direct intrinsic effect on macrophages (Tussiwand and Gautier 2015).

**Table 1. Origins, functions and transcription factors of tissue macrophages**

<b>Tissue</b>	<b>Cell Type</b>	<b>Origin</b>	<b>Functions</b>	<b>Transcription factor/tissue</b>
<b>CNS</b>	Microglia	YS	Immunosurveillance Brain development, synaptic pruning, clearance of cell debris	CD200, CX3CL1, TGF- $\beta$
<b>CNS</b>	Non-parenchymal macrophages	HSC	Immunosurveillance	NA
<b>Liver</b>	Kupffer cells	YS	Immunosurveillance Metabolism, detoxification, iron recycling	NA
<b>Lung</b>	Alveolar macrophages	YS/HSC	Immune surveillance, clearance of surfactant	Surfactant, CSF-2, CD200
<b>Lymph nodes</b>	Subcapsular sinus macrophages	NA	Cross-presentation, uptake of opsonized antigens and transfer to B cell follicles	NA
<b>Lymph nodes</b>	Medullary macrophages	NA	Antigen capture, removal of apoptotic	NA

			granulocytes	
<b>Spleen</b>	Outer marginal zone macrophages	NA	Immune surveillance, tolerance to apoptotic debris, antigen transfer to B cells	LXR $\alpha$
<b>Spleen</b>	Metallophilic macrophages	NA	Immune surveillance, antigen transfer to DC	LXR $\alpha$
<b>Spleen</b>	Red pulp macrophages	YS>HSC	Iron recycling, immunosurveillance	Heme/Spi-C

CNS: central nervous system; HSC: hematopoietic stem cell; NA: not assessed; YS: yolk-sac

#### 4) A new nomenclature to facilitate the examination of phagocyte populations.

With the recent technological developments, a large set of macrophage and dendritic cell populations have been described in both human and mouse, with a particular phenotype and specific functions. However, in the same time this has induced confusion in naming some mononuclear phagocyte subsets, with critical implications in the interpretation of the literature. An additional level of confusion has also been brought by the fact that some of the protein markers currently used in flow cytometry panels may be specific of dendritic cell or of macrophage subsets depending on the tissue considered. In the context of the recent advances on the monocyte, dendritic cell and macrophage ontogeny, international experts have recently proposed a unified nomenclature for mononuclear phagocytes based on their ontogeny, with additional insight given by the location, the phenotype and the function (Guilliams, Ginhoux et al. 2014). Importantly, this proposition has been recently at least partly validated by a publication that proposed a high-dimensional and standardized examination of dendritic cell subsets from different species (Guilliams, Dutertre et al. 2016). As an example, dendritic cells are defined as FLT3-L dependent hematopoietic cells and can be further divided into conventional dendritic cells and pDCs because pDCs are dependent on E2-2 for their development. Among conventional dendritic cells, conventional type 1 dendritic cells (cDC1s) and conventional type 2 dendritic cells (cDC2s) are identified by their respective dependency on BATF3 and IRF4. By incremented with the level two of the classification, the location (spleen, lymph node) and the specific phenotype (CD103+, CD207+) the name of the subset considered will be completed following the nomenclature.

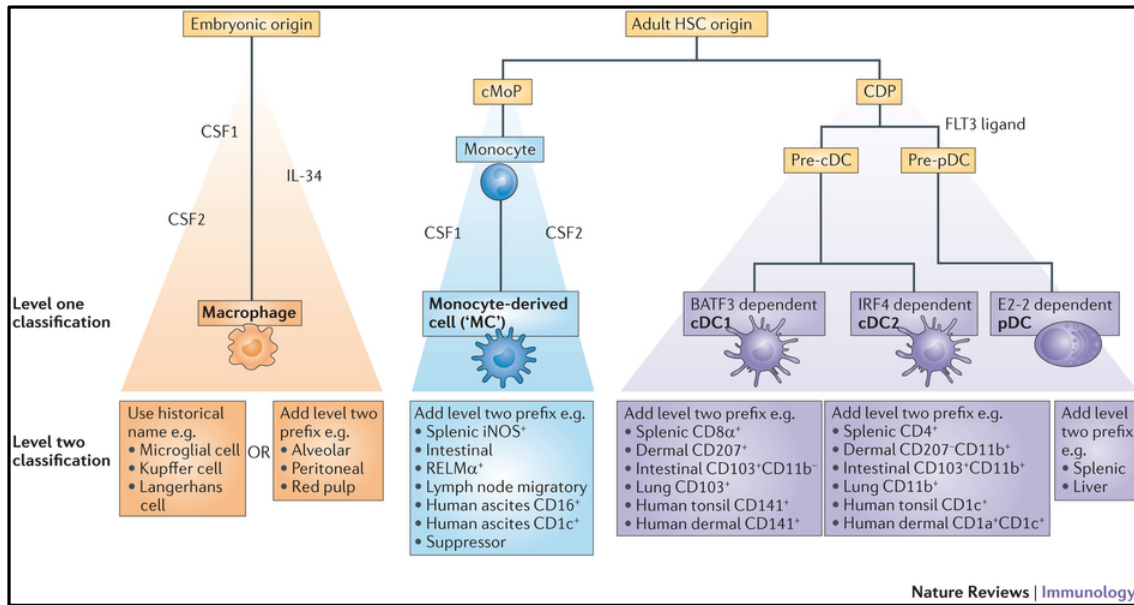


**Figure 3. A new proposition of classification for mononuclear phagocytes (derived from (Guilliams, Ginhoux et al. 2014)).** BATF3, basic leucine zipper transcriptional factor ATF-like 3; classical type 1 DCs (cDC1s); cMoP, common monocyte progenitor; CSF1, colony-stimulating factor 1; CSF2, colony-stimulating factor 2; FLT3, FMS-like tyrosine kinase 3; HSC, hematopoietic stem cell; IL-34, interleukin-34; iNOS, inducible nitric oxide synthase; IRF4, interferon-regulatory factor 4; MC: monocyte-derived cell ; pDCs : plasmacytoid dendritic cells ; RELM $\alpha$ , resistin-like molecule- $\alpha$ .

### 5) Concluding remarks.

As exposed above, the mononuclear phagocyte system is involved in key functions of both innate and adaptive immunity: they can initiate and regulate inflammatory responses, they contribute to tissue homeostasis and in the case of dendritic cells they can activate adaptive immunity by processing the exogenous material into antigenic peptides for their presentation onto MHC-I and MHC-II molecules. Both dendritic cells and macrophages are plastic cells that are influenced by signals present in their local microenvironment. While the transcription factors and the signals required for the development of dendritic cell subsets are similar, they differ for tissue macrophage subsets from one organ to another. An important insight has been recently made regarding dendritic cell and macrophage ontogeny, with the identification of the progenitors required for most of dendritic cell and macrophage subsets, yet some of them remain unknown. The recent advances on ontogeny together with the use of recent multiplex high-dimensional technologies have allowed to propose and validate a classification for dendritic cell and macrophage subsets.

### **Chapter 3. What are the actors of the adaptive immunity?**

As previously mentioned, the adaptive immune responses involve specific cellular and molecular actors including: T and B lymphocytes and antibodies. Contrasting with innate immune responses, adaptive immunity takes several days to be initiated but is specific to the pathogen. The specificity is driven by the recognition by the specific surface receptors present on B (BcR) and T (TcR) lymphocytes of motifs derived from self or foreign antigens. Another important key feature of adaptive immunity is the generation of specific memory responses: in the case of a second contact with the same antigen, specific adaptive immune responses take place more rapidly (few hours) and are more robust. I will illustrate how lymphocyte subsets are heterogeneous regarding their differentiation, their nature and their functional properties focusing on T lymphocytes, since some of the key aspects will be important for understanding and discussing the experimental results. Regarding other aspects of T cell biology, B lymphocytes and other lymphoid subsets, one can refer to recent reviews that provide a large insight about their nature, origin and functions (Papamichail, Perez et al. 2004, LeBien and Tedder 2008, DiLillo, Horikawa et al. 2011, Stritesky, Jameson et al. 2012, Dzhagalov, Chen et al. 2013, Spits, Artis et al. 2013, Eberl, Di Santo et al. 2015, Kim, Lynch et al. 2015, Vallentin, Barlogis et al. 2015, Fillatreau 2016, Huntington, Carpentier et al. 2016, Vivier, van de Pavert et al. 2016).

#### **1) An overview of T lymphocytes**

CD8<sup>+</sup> and CD4<sup>+</sup> T lymphocytes are characterized by the expression at the surface of a T cell receptor that is made of either  $\alpha\beta$  or  $\gamma\delta$  heterodimer chains. T lymphocytes not only induce protective immunity by exerting cytotoxic functions but also regulate innate and adaptive immune responses. Contrary to other hematopoietic cells that are produced in the bone marrow, the thymus promotes the development of T lymphocytes, from where naïve T lymphocytes exit to colonize peripheral tissues. During acute infections or vaccinations, naïve T cells are activated and differentiate into effector T cells over the course of 7 to 20 days. The full process of naïve T cell differentiation is assisted by robust proliferation, transcriptional and metabolic reprogramming and the acquisition of cardinal features of effector T lymphocyte phenotype: dramatic numerical expansion among the pool of bulk T cells; acquisition of effector functions and altered tissue homing. Next to the peak of expansion with the resolution of inflammation and the removal of antigen the vast majority of effector T cells die, with the exception of a particular subset that will persist over time to fuel the

memory T cell pool. Transition to the memory T cell pool is accompanied by the repression of the activation program of effector T cells. Interestingly upon a second encounter, these memory T cells are rapidly mobilized to the injured tissue and massively reactivate effector functions. Besides this antigen-dependent property, memory T cells exhibit self-renewal antigen-independent potentiality, thought to be driven by IL-7 and IL-15. Complicating our view of memory T cell development, several mouse and human memory T cell subsets have been identified, yet how do they relate and what are their specific properties and functions remain still debated. Importantly upon persistent antigen exposure or inflammatory environment, as this is the case in cancer, auto-immunity and chronic viral infections, memory T cell differentiation is impaired, resulting in a shift toward an altered differentiation status called exhausted T cells. Cardinal features of T cell exhaustion include gradual loss of effector functions, sustained up-regulation and segregation of inhibitory receptors, altered expression and use of transcription factors, metabolic alterations and loss of self-renewal capacity (Chang, Wherry et al. 2014).

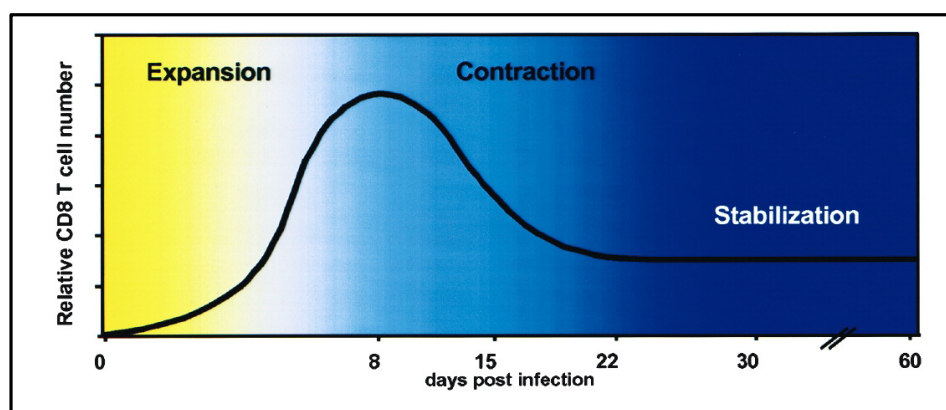


**Figure 4. The three phases (expansion, contraction and stabilization) of an antigen-specific CD8<sup>+</sup> T cell responses following immunization (derived from (Kaech, Hemby et al. 2002))**

## 2) Naïve-to-effector T cell differentiation, a plastic tightly regulated process

Naïve T cell activation and proliferation promote their differentiation into effector T cells. Effector T cells are highly heterogeneous as supported by the high diversity and plasticity observed for CD4<sup>+</sup> T cells (Murphy and Reiner 2002). Upon the influence of the environment, a naïve CD4<sup>+</sup> T cell can give rise to various effector subsets including T helper cell subset Th1, Th2, Th17, Th9, Th22, Th25 or follicular helper T (T<sub>fh</sub>) cells and the induced regulatory T cell population (iTreg) (Zhu, Yamane et al. 2010). In the CD4<sup>+</sup> compartment,

the current models support that transcription program required for Th subset differentiation is engaged and activated upon extrinsic stimuli. Th1 subset is defined by its capacity to produce IFN- $\gamma$  and naïve-to-Th1 polarization requires IL-12, type I IFNs, signal transducer and activator of transcription 4 (STAT4) and STAT1 activity and is partly dependent on T-box expressed in T cells (T-bet) expression (Szabo, Kim et al. 2000, Amsen, Spilianakis et al. 2009). Upon exposure to IL-12 and type I IFNs, STAT4 and STAT1 activation, respectively, facilitate chromatin accessibility and remodeling to the enhancer regions of Th1 gene program allowing for the subsequent T-bet recruitment and commitment to Th1 lineage, in the same time that other polarizing-gene programs are repressed (Fiorentino, Bond et al. 1989, Sundrud, Grill et al. 2003, Lee, Kim et al. 2006, Wilson, Rowell et al. 2009). Th2 subset is defined by its lack of IFN- $\gamma$  production and its high capacity to secrete IL-4. In a mechanism similar to Th1 subset, exposure to IL-4, STAT-5 or STAT-6 activity and engagement of the transcription factor GATA-3 are required for naïve-to-Th2 polarization (Sundrud, Grill et al. 2003, Lee, Kim et al. 2006, Ho, Tai et al. 2009, Wilson, Rowell et al. 2009). Th17 subset secretes IL-17 isoforms and during the naïve-to-Th17 polarization, IL-6 and IL-23 activate STAT-3 to promote the recruitment and activation of the nuclear receptors Receptor-Related Orphan Receptor- $\alpha$  (ROR $\alpha$ ) and ROR $\gamma$ T (Yang, Pappu et al. 2008, Korn, Bettelli et al. 2009); additional factors might be required such as BATF, IRF4, aryl hydrocarbon receptor both their precise roles remain to be fully investigated and understood (Lee, Mukasa et al. 2009). iTreg secrete TGF- $\beta$  or IL-10 and express cytotoxic granules; commitment toward iTreg requires IL-2 and upon binding to its receptor, STAT-5 activates and binds to the forkhead box P3 (FOXP3) gene to produce Foxp3 protein, that in turn promotes regulatory T cells (Treg) and represses other Th-polarizing programs (Lee, Mukasa et al. 2009). Th9 share a similar program than Th2 but a high concentration of TGF- $\beta$  forces the maturation towards Th9, in a BATF-dependent manner (Veldhoen, Uyttenhove et al. 2008). Th22 cells are related to Th17 cells and are promoted by IL-6 and Tumor Necrosis Factor-alpha (TNF- $\alpha$ ), which induce the activation of STAT-3 and the expression of aryl hydrocarbon (Pickert, Neufert et al. 2009). Th25 are induced by Act1 and probably derived from Th2 (Swaidani, Bulek et al. 2011). Tfh polarization requires the activation of STAT-3 and depends on the transcription factor MAF. Tfh subset promotes B cell class-switching for Ig production and guides B cells into germinal centers. IL-6 and STAT-3 as well as Inducible T cell COStimulator (ICOS) activation, initiate the transcription of the transcription factor MAF. OX-40/CD137 ligation is

also required (King 2009). The functions of CD4<sup>+</sup> regulatory and helper T cell subsets are summarized in the **table 2**.

**Table 2. Characterization of CD4<sup>+</sup> helper and regulatory T cell subset functions (derived from (Caza and Landas 2015))**

Th Subset	Effector cytokines	Functions
<b>Th1</b>	IFN- $\gamma$ , IL-2, TNF- $\alpha$	Cell-mediated immunity, delayed-type hypersensitivity, clearance of intracellular pathogens and tumor cells, B cell class-switching to IgG2a
<b>Th2</b>	IL-4, IL-5, IL-10, IL-13	Humoral immunity, clearance of extracellular bacteria and worms, B cell class-switching to IgE, allergic responses
<b>Th9</b>	IL-9, IL-10	Protection against parasitic worms/helminth infections
<b>Th17</b>	IL-17A, IL-17E, IL-17F, IL-6, IL-22, TNF- $\alpha$ , IL-10	Protection of mucosal surfaces, recruitment of neutrophils, clearance of <i>Mycobacterium tuberculosis</i> and <i>Klebsiella pneumonia</i>
<b>Th22</b>	IL-22, IL-13, FGF, CCL15, CCL17, TNF- $\alpha$	Mucosal immunity, prevention of microbial translocation across epithelial surfaces, promotes wound repair.
<b>Th25</b>	IL-25, IL-4, IL-5, IL-13	Mucosal immunity, stimulates non-lymphoid cells to produce IL-4, limits Th1 and Th17 induced in inflammation, CD4 <sup>+</sup> T cell memory (mouse)
<b>Tfh</b>	IL-21 OX40, ICOS	Helps B cells produce high affinity, class-switched antibodies, guides migration into germinal centers
<b>iTreg</b>	IL-10, TGF- $\beta$	Suppression of existing immune responses, maintains tolerance/protection against autoimmunity

CCL: CC chemokine ligand; FGF: fibroblast growth factor; ICOS: Inducible T-cell COStimulator; IFN: interferon; Ig: immunoglobulin; IL: interleukin; iTreg: induced regulatory T cells; Tfh: follicular helper T cells; Th: T helper; TNF: tumor necrosis factor.

Although such distinct subsets are not identified in the general physiological or pathological settings, effector functions may vary among effector CD8<sup>+</sup> T cells. For instance, effector T cells are heterogeneous in producing effector cytokines such as IL-2, TNF- $\alpha$  or IFN- $\gamma$  or chemokines and in co-producing these molecules. An additional level of heterogeneity in CD8<sup>+</sup> T cell subsets has been observed for the content in cytotoxic granules: some of them exhibit high levels of pre-formed ready-to-use perforin and granzymes whereas other require

their neosynthesis, degrees of co-expression may vary from one cell to each other (Seder, Darrah et al. 2008, Yuan, Gnjatic et al. 2008, Makedonas, Hutnick et al. 2010).

### **3) Differentiation effector-to-memory T cell subsets and T cell exhaustion**

#### **T cell memory**

Memory T cells are the effector T cells that escape apoptosis during the contraction phase and persist in either the secondary lymphoid organs in the case of central memory T cells or in the recently infected tissue in the case of effector memory T cells and tissue-resident memory T cells for long periods of time following the clearance of the cognate antigen that has been at the initiation of T cell activation (Ahmed and Gray 1996, Zinkernagel, Bachmann et al. 1996, Williams and Bevan 2007). As mentioned earlier, hallmarks of T cell memory are the evidence of prior expansion or activation, the persistence after the clearance of cognate antigen, an enhanced functional activity upon antigen re-exposure (Kaech and Wherry 2007). Regarding their gene-expression and protein-expression profiles as well as their functionality memory T cells are highly heterogeneous, which strongly contribute in limiting the accumulation of crucial clues about their ontogeny, maintenance and regulation (Chang, Wherry et al. 2014). To date, how do memory T cells are generated remains an unresolved question, yet it has been an intense subject of investigation.

At least four models of memory development and fate decisions have been proposed (Kaech and Wherry 2007). The current model postulates the existence of a memory precursor effector cell subset that are not fully mature memory T cells and require further differentiation to acquire the hallmarks of T cell memory (fate commitment with progressive differentiation) (Kaech and Wherry 2007). Furthermore, the effector T cell pool is heterogeneous and contains many short-lived effector cells (SLECs) that will mainly die after infection during the contraction phase, the remaining small fraction getting the potential to become long-lived memory T cells, referred to as memory-precursor effector cells (MPECs) (Gett, Sallusto et al. 2003, Chang, Palanivel et al. 2007). This model is currently preferred in the recent literature and proposes that MPECs are a plastic subset that can develop into SLECs in the case of strong stimulatory signals.



## Memory T cell subsets

As previously described, memory T cell subsets are highly heterogeneous with implications on their effector functions, tissue distribution and trafficking properties. Memory T cell subsets can be currently divided into at least four subtypes that are identified by some characteristic features: effector-memory (Tem), central memory (Tcm), tissue-resident memory (Trm), stem memory T cells (Chang, Wherry et al. 2014, Schenkel and Masopust 2014). After the contraction phase, the memory T cell pool is thought to slowly convert from a population of Tem to Tcm cells, that present less functional properties but a capacity of self-renewal. Tcm are defined by their expression of lymph node homing molecules (CCR7) and have the capacity to recirculate and patrol within the lymph nodes and the white pulp of the spleen, and to secrete IL-2 and proliferate upon TcR stimulation to generate in few days abundant effector T cells that migrate to the sites of infection. Tem recirculate between blood and non-secondary lymphoid organs, lack of secondary lymphoid organ homing molecules such as CD62L and CCR7, constitutively maintain effector-like functions that can act without requirement of a re-differentiation time. An additional subset has more recently been identified that arises from memory precursor cells during the effector phase and remains poisoned within the tissue, the tissue-resident memory T cells. Trm are permanently established *in situ*, do not have migratory capacities and totally lack of secondary lymphoid organs homing molecules, do express CD69, CD103, granzyme B, and low levels of CD122, Sphingosine-1-receptor 1 and Ly6-C (Schenkel and Masopust 2014).

**Table 3. A brief overview of markers expressed by conventional memory T cell subsets in human and mouse (derived from (Rosenblum, Way et al. 2016))**

Memory T cell subset	Mouse phenotype	Human phenotype
<b>Central memory</b>	CCR7 <sup>high</sup> , CD44 <sup>high</sup> , CD127 <sup>high</sup> , CD62L <sup>high</sup> , KLRG1 <sup>low</sup>	CD44 <sup>high</sup> , CD45RO <sup>high</sup> , CD45RA <sup>low</sup> , CD127 <sup>high</sup> and express high levels of IL-2 and intermediate levels of IFN $\gamma$ and TNF
<b>Effector Memory</b>	CCR7 <sup>low</sup> , CD44 <sup>high</sup> , CD127 <sup>high</sup> , CD62L <sup>low</sup> , KLRG1 <sup>high</sup>	CD44 <sup>high</sup> , CD45RO <sup>high</sup> , CD45RA <sup>low</sup> , CD127 <sup>high</sup> , CD62L <sup>low</sup> , express high levels of IFN $\gamma$ and TNF and express low levels of IL-2
<b>Tissue-resident memory</b>	CCR7 <sup>ow</sup> , CD69 <sup>high</sup> , CD103 <sup>high</sup> , KLRG1 <sup>low</sup>	CD45RO <sup>high</sup> , CD45RA <sup>low</sup> , CD69 <sup>high</sup> , and CD103 <sup>high</sup> and

		CD103 <sup>low</sup> subsets
<b>Stem cell memory</b>	CD44 <sup>high</sup> , CD62L <sup>high</sup> , CD95 <sup>high</sup> , CD122 <sup>high</sup> , SCA1 <sup>high</sup> , BCL-2 <sup>high</sup> , CD127 <sup>high</sup>	CD25 <sup>high</sup> , CD27 <sup>high</sup> , CD44 <sup>high</sup> , CD45RO <sup>high</sup> , CD45RA <sup>low</sup> , CCR7 <sup>low</sup> , FOXP3 <sup>high</sup> , CD62L <sup>low</sup> , CTLA4 <sup>high</sup> , CD127 <sup>low</sup> , ICOS <sup>high</sup> , BCL-2 <sup>high</sup> , Ki67 <sup>low</sup> and HLA-DR expression not defined

BCL-2: B-cell lymphoma-2; CCR7: CC chemokine receptor type 7; CTLA4: cytotoxic T-lymphocyte-associated protein 4; ICOS: Inducible T-cell Co-Stimulator; IFN: interferon; KLRG1: Killer cell lectin-like receptor subfamily G member 1; HLA: human leukocyte antigen; SCA1: Stem cells antigen-1.

### Determinants for terminal effector and memory T cell fate

The determinant of the cell fate decision in the current model is the magnitude of the overall strength of signal, which is a combination of antigen, co-stimulation and inflammation (Kaech and Wherry 2007). This last hypothesis is supported by the fate of single naive CD8<sup>+</sup> T cell transfer that can give rise to both effector and memory subsets, suggesting that one single CD8<sup>+</sup> T cell has the potentiality for different fates (Stemberger, Huster et al. 2007). Exogenous and endogenous signals have been associated with the fate of T cell protective effector and memory subsets during primary responses.

Examination of the endogenous factors governing activated T cell fates has allowed for the identification of at least seven categories that may influence T cell differentiation into effector-like and memory-like T cells. Endogenous factors that may promote effector-like T cell populations are a strong TcR strength (Tubo, Pagan et al. 2013), a high expression of IL-2R $\alpha$  (CD25) and Killer cell lectin-like receptor subfamily G member-1 (KLRG-1), a high expression of the transcription factors T-bet, Id2, B-Lymphocyte-Induced Maturation Protein-1 (BLIMP-1) and STAT4 (Pearce, Mullen et al. 2003, Intlekofer, Takemoto et al. 2005, Cannarile, Lind et al. 2006, Johnston, Poholek et al. 2009, Nurieva, Chung et al. 2009, Shin, Blackburn et al. 2009, Banerjee, Gordon et al. 2010, Cui, Liu et al. 2011), proximal daughter cell status among the asymmetric division process (Chang, Palanivel et al. 2007, Chang, Ciocca et al. 2011, King, Koehli et al. 2012), an open and on chromatin accessibility (Zediak, Johnnidis et al. 2011) and a glycolytic mammalian target of rapamycin (mTOR)-dependent metabolic status (Chi 2012). On the contrary, intrinsic factors more prone to the memory-like cell fate are a weak TcR strength, high expression of IL-7R and CXCR3, high levels of expression of transcriptional factors such as Id3, B-cell lymphoma-6 (Bcl-6), T-cell factor 1 (TCF-1), STAT3, Forkhead box protein O1 (Foxo1) and Eomesodermin (Eomes), a distal daughter cell status among the asymmetric division tree, a poised and off chromatin

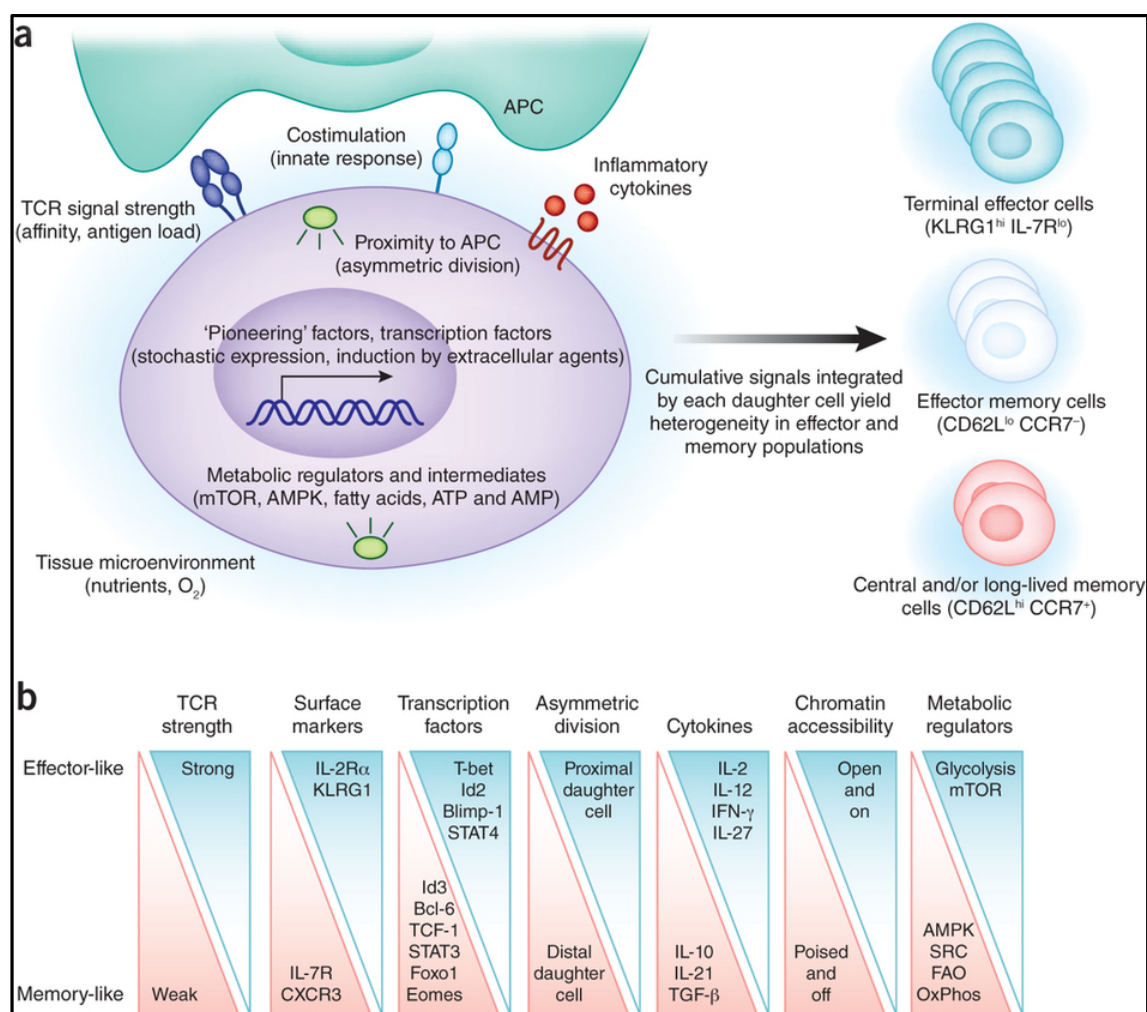
accessibility and a specific metabolic status that is AMP-activated protein kinase (AMPK) and SRC-dependent and uses fatty acid oxidation and mitochondrial oxidative phosphorylation (Chang, Wherry et al. 2014). Interestingly, intrinsic factors and notably transcription factors operate by pairs and in apparent opposing ways to foster terminal effector cells versus memory cells. For instance, induction of T-bet expression is higher under exposure to inflammatory stimuli linking inflammation to the expansion of terminally differentiated T cells that would reflect the need of effector functions during acute infection. Importantly, deleting T-bet expression induces a lack of KLRG-1<sup>high</sup> cells with little effect on memory-like CD127<sup>high</sup> cells (Chang, Wherry et al. 2014). On the contrary, Eomes, which is highly homologous to T-bet is thought to promote the expansion and the differentiation towards memory-like phenotype as assessed by the consequences of its genetic deletion (Banerjee, Gordon et al. 2010). Similar conclusions have been raised when analyzing the roles of the pair Id2 and Id3, and BLIMP-1 and Bcl-6 (Chang, Wherry et al. 2014). More than the presence or the absence of these transcriptional factors in T cells, it seems that the quantities or the gradual expression of these factors are required for the T cell fate. While mostly identified in CD8<sup>+</sup> T cells, such phenomena probably occur in the CD4<sup>+</sup> T cell compartment (Chang, Wherry et al. 2014).

Among exogenous signals, CD4<sup>+</sup> T cell help and IL-2 influence effector CD8<sup>+</sup> T cell expansion and the transition towards memory cells and their maintenance. Defective CD4<sup>+</sup> T cell help results in a Tem-like population with poor effector functions and that express TNF-related apoptosis-inducing ligand (TRAIL) (Janssen, Droin et al. 2005). IL-2 early secretion is required for robust memory T cell formation (Pepper, Pagan et al. 2011). IL-7 and IL-15 are crucial for antiviral memory responses and *in vitro* experiments support that the presence of these cytokines favor the differentiation toward memory T cell subsets; however, there is no clear evidence whether IL-7/IL-15 modulate T cell memory *in vivo* (van Leeuwen, Sprent et al. 2009). In addition, a large set of studies support a role for inflammation level in the regulation of effector and memory T cell differentiation (Williams and Bevan 2004, Virgin, Wherry et al. 2009, Lefrancois and Obar 2010, Xin, Masson et al. 2016) and a high level of inflammation may increase the SLEC/MPEC ratio, with a role for IL-12, IFN- $\gamma$  and type I IFNs.

**Table 4. Markers used to delineate effector T cell subsets in mouse (from (Plumlee, Obar et al. 2015))**

Effector T cell subset	Phenotype
Short-lived effector cells	CD127 <sup>low</sup> , KLRG1 <sup>high</sup>
Memory precursor effector cells	CD127 <sup>high</sup> , KLRG1 <sup>low</sup>
Early effector cells	CD127 <sup>low</sup> , KLRG1 <sup>low</sup>

KLRG1: Killer cell lectin-like receptor subfamily G member 1


**Figure 5. Determinants for terminal-effector and memory T cell fate (from (Chang, Wherry et al. 2014)).** (a) Many intrinsic and extrinsic factors can influence cell-fate specification following early T cell activation; for a detailed view, refer to the corresponding part or the manuscript. APC, antigen presenting cell. (b) Categories (top) and prominent examples of each category (below) of factors that can promote effector or memory T cells subsets; for a detailed view, please refer to the corresponding part of the manuscript. FAO, fatty acid oxidation; SRC, spare respiratory capacity; OxPhos, oxidative phosphorylation.

## T cell exhaustion

T cell exhaustion has been mainly identified and studied in the context of chronic viral infection and is thought to be influenced by antigen persistence over time as well as additional factors such as the lack of CD4 help and negative signals from the microenvironment, mainly cytokines or ligands. Duration of viral exposure has been correlated with the intensity of the exhausted phenotype in the context of lymphocytic choriomeningitis virus mouse infection (Blackburn, Crawford et al. 2010) or in human HIV-1 infection (Brooks, McGavern et al. 2006, Bucks, Norton et al. 2009, Angelosanto, Blackburn et al. 2012); supporting this hypothesis, removal of antigen only before a period of 2 weeks-exposure was sufficient to prevent the promotion of CD8<sup>+</sup> T cell exhaustion (Brooks, McGavern et al. 2006, Angelosanto, Blackburn et al. 2012). Prolonged and high level expression of inhibitory receptors at the cell surface is a common feature of exhausted T cells. Among the variety of putative inhibitory receptors, Programmed cell death 1 (PD-1) and (PD-1)-related signaling pathway has been tightly incriminated in T cell exhaustion using complementary mechanisms: ectodomain competition by sequestering target receptors or ligands (Pentcheva-Hoang, Egen et al. 2004); modulation of intracellular mediators resulting in altered TcR signaling or impaired positive signaling from co-stimulatory molecules/receptor (Yokosuka, Takamatsu et al. 2012); by promoting an inhibitory transcriptional program (Quigley, Pereyra et al. 2010). Other inhibitory receptors and molecules include the lymphocyte activation gene 3 (LAG3) protein, CD244, T-cell immunoglobulin and mucin-domain containing-3 (TIM3) and cytotoxic T-lymphocyte-associated protein 4 (CTLA4) are generally co-expressed at the surface of exhausted T cells and may synergize to promote negative signals as this is the case for PD-1 and LAG3 or PD1 and CTLA4 (Blackburn, Shin et al. 2009). Directly reinforcing the crucial negative roles of these molecules, PD-1 or CTLA4 blockade using specific inhibitors or antibodies reverse T cell exhaustion and are under investigation in cancer clinical trials (Blackburn, Shin et al. 2009). Next to inhibitory receptors, T cell exhaustion is also influenced by soluble mediators. IL-10 is an immunosuppressive cytokine and IL-10/IL-10 receptor pathway and signaling have been associated with T cell exhaustion: blockade of IL-10 during chronic LCMV infection restores T cell function (Brooks, Trifilo et al. 2006, Ejrnaes, Filippi et al. 2006) and the IL-10 sources incriminated are dendritic cells and particular CD4<sup>+</sup> T cell subset that express BLIMP-1 (Parish, Marshall et al. 2014). Another suppressive cytokine, TGF- $\beta$  has also been incriminated in T cell exhaustion (Tinoco, Alcalde et al. 2009); expression of a dominant negative receptor in CD8<sup>+</sup> T cells by inhibiting TGF- $\beta$

signaling improved T cell function (Tinoco, Alcalde et al. 2009). Inflammatory cytokines such as type I IFN and type I IFN signaling have been involved in promoting T cell exhaustion (Curtsinger and Mescher 2010, Sandler, Bosinger et al. 2014).

#### **4) Concluding remarks**

T lymphocytes are crucial actors of cellular adaptive immunity. To activate, expand and differentiate into effector T cells, their antigen receptor, the TcR, has to recognize and bind to a specific peptide loaded onto MHC-I (CD8<sup>+</sup> T cells) or MHC-II (CD4<sup>+</sup> T cells). Among the pool of effector T cells, a small number memory precursor cells will give rise to memory T cell subsets, whereas the majority of the effector T cell pool will undergo massive apoptosis during the contraction phase. The differentiation of naïve T cells into effector and memory T cells is influenced by a large set of endogenous and exogenous factors such as the strength and the duration of TcR signaling, the presence of an inflammatory environment, the proximity to the antigen presenting cell, the balance between the transcription factors that are recruited, the metabolic status, epigenetics. The ultimate function of T cells is to promote a protective immunity against tumors or infections. Although the precise molecular mechanisms are not fully identified, recent evidence highlights the role of two effector subsets in generating robust and protective immunity against pathogen, the Tem and the Trm, by two complementary mechanisms: the production of cytotoxic molecules such as IFN- $\gamma$  or cytotoxic granules and the licensing of effectors of the innate immune system (Lauvau, Boutet et al. 2016).

## PART II - COMMUNICATION AND DYNAMICS ARE TWO KEY FEATURES OF ONGOING IMMUNE RESPONSES

### Chapter 1. Inter-cellular communication between innate and adaptive immune cells is required for activation and regulation of adaptive immunity

#### 1) T cell/dendritic cells communications

##### An overview of T cell/dendritic cell interactions

Because of the important literature suggesting the superiority of dendritic cells in priming T cells, how these two cells connect to communicate has been an intense subject of investigation. Interestingly, even in the absence of antigen, T cells are constantly motile in the lymph nodes and scan the surface of dendritic cells for the presence of their cognate antigen, in a process called crawling. During crawling, T cells remain in contact with dendritic cells for short-lasting periods of 3 to 5 minutes (Stoll, Delon et al. 2002, Bousso and Robey 2003). These transient contacts do not trigger TcR activation as assessed by the absence of calcium signaling in T cells (Asperti-Boursin, Real et al. 2007, Wei, Safrina et al. 2007). The important rate of contacts is largely influenced by the secretion of the chemo-attractant protein CCL3 by dendritic cells that binds to CCR5 expressed on naïve T cells (Castellino, Huang et al. 2006). Surprisingly, crawling as a mode of T cell/dendritic cell interactions has been also detected in the presence of the cognate antigen. However, these short-lasting interactions were associated to partial activation as assessed by the up-regulation of the early T cell activation antigen CD69, yet the outcome was T cell anergy (Mempel, Henrickson et al. 2004, Miller, Safrina et al. 2004, Hugues, Boissonnas et al. 2006, Miller, Brown et al. 2012). These transient contacts in the presence of antigen are probably mediated by the absence of dendritic cell maturation stimulus or a high precursor frequency of antigen-specific T cells. The presence of robust T cell activation has been associated *in vivo* with the occurrence of stable and long-term interactions between T cells and dendritic cells (Iezzi, Karjalainen et al. 1998, Schrum and Turka 2002, Huppa, Gleimer et al. 2003). The duration of the contacts varies from one model to another but was estimated to at least 6 hours (Celli, Lemaitre et al. 2007). *In vitro* evidence suggests that duration might reach 24 hours. Importantly, these contacts are associated with an increase in cytosolic calcium concentration (Skokos, Shakhar et al. 2007, Wei, Safrina et al. 2007). Another way for T cells to collect signals from antigen-bearing dendritic cells is the formation of swarms, consisting in enlarged T cells that display looping patterns in their movements and intermittent contacts with dendritic cells (Miller, Wei

et al. 2002, Miller, Safrina et al. 2004). A correlation of functional outcomes and patterns of contacts has been provided by independent studies using different models. Collectively, the available literature points out the requirement of stable contacts for the generation of robust effector cells as well as memory T cells whereas T cell tolerance occurs when only transient contacts are observed. Importantly, stable contacts and consequently effector functions were impaired when dendritic cells lacked of the adhesion molecule InterCellular Adhesion Molecule 1 (ICAM-1) (Scholer, Hugues et al. 2008). This observation supports the existence of an active molecular machinery that fuels the stable and long-lasting contacts between T cells and dendritic cells.

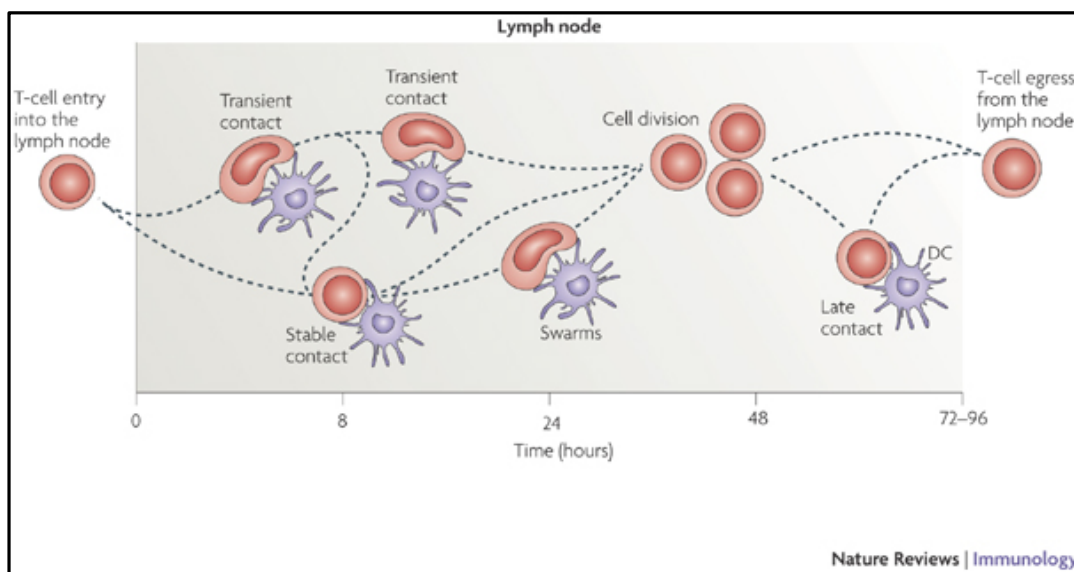


**Figure 6. Modes of interaction between T cells and antigen-bearing dendritic cells (derived from (Bousso 2008)).** Antigen recognition by T cells can occur through interactions with antigen-bearing dendritic cells that are short lasting, long lasting or in swarms.

### **A specific platform to facilitate the communication between T cells and antigen presenting cells, the immunological synapse**

A specific molecular platform that sustains these stable contacts and drives the signals from the dendritic cells to the T cells has been identified and extensively studied *in vitro*, the immunological synapse, yet its formation during *in vivo* stable interactions remains elusive. The immunological synapse is a specialized contact area that is formed between a T cell that is interacting with an antigen presenting cell and is composed of molecules important for establishing T cell adhesion and polarity (Benvenuti 2016, Niedergang, Di Bartolo et al. 2016). This structure is influenced by the cytoskeleton and transduces highly controlled secretory signals, allowing for instance the directed release of cytokines or lytic granules



towards the antigen presenting cell or the target cell. The initial event that gives rise to the immunological synapses is the binding of the TcRs to their ligands expressed at the surface of the antigen presenting cells (Lee, Holdorf et al. 2002, Crites, Padhan et al. 2014). This binding triggers the formation of hundreds of TcR microclusters accumulating at the center of the interface between the T lymphocyte and the antigen presenting cell upon stimulation (Campi, Varma et al. 2005, Yokosuka, Sakata-Sogawa et al. 2005, Varma, Campi et al. 2006) and is synchronized with the calcium response (Krummel, Sjaastad et al. 2000, Crites, Padhan et al. 2014). This TcR clustering phenomenon is accompanied by the recruitment of the Zeta Chain Of T Cell Receptor Associated Protein Kinase 70kDa (ZAP70) kinase and adaptor proteins required for T cell signaling. After TcR activation, TcR microclusters move towards a specific central zone of the immunological synapse called the central supra molecular activation cluster (c-SMAC) (Grakoui, Bromley et al. 1999). The c-SMAC exerts specific functions in the immunological synapse, including the promotion of cell adhesion between the T cell and the antigen presenting cell, by increasing the avidity for peptide-MHC complexes; the direction of the targeted secretion of cytotoxic granules and cytokines towards the antigen presenting cells; the provision of a platform that regulates the endocytosis and exocytosis of the TcR complex; the induction of co-stimulatory signals (Stinchcombe, Bossi et al. 2001, Huse, Lillemeier et al. 2006, Stinchcombe, Majorovits et al. 2006, Griffiths, Tsun et al. 2010, Huppa, Axmann et al. 2010, Choudhuri, Llodra et al. 2014). Generally, the c-SMAC segregates into two functional domains, a signaling domain through the TcR and a secretory domain, used for cytotoxic granule secretion onto target cells (Stinchcombe, Bossi et al. 2001, Griffiths, Tsun et al. 2010). In the signaling domain, endocytosis/exocytosis of the TcR is thought to negatively regulate T cell activation whereas the accumulation of the co-stimulatory molecule CD28 or CD40L positively influences the T cell fate by recruiting and activating crucial molecules such as protein kinase C (PKC) $\theta$  and CARD-containing MAGUK protein 1 (CARMA1). Also, negative molecules can accumulate to prevent or inhibit co-stimulation, by promoting the expression of inhibitory molecule CTLA-4 (Greenwald, Latchman et al. 2002, Yokosuka, Kobayashi et al. 2008, Kong, Yokosuka et al. 2011, Liang, Cucchetti et al. 2013). In the same time, on the antigen presenting cell, CD40 and CD80/CD86 are rapidly released to the membrane upon contact with the T cells.

After the TcR activation, the intercellular adhesion molecule Lymphocyte function-associated antigen 1 (LFA-1) is recruited to the periphery of the immunological synapse in an intact F-actin cytoskeleton-dependent manner and the TcR signals induce a specific LFA-1

conformational change that results in high affinity binding to its ligand, ICAM-1/ICAM-2/ICAM-3 (Comrie, Babich et al. 2015) on the antigen presenting cells, by an “inside-out” signaling, defining a peripheral zone in the immunological synapse, the p-SMAC (Grakoui, Bromley et al. 1999). Other molecules in the antigen presenting cell also rapidly accumulate to the p-SMAC supporting strong adhesion: semaphorins, plexins and neuropilins, or CD45 (Grakoui, Bromley et al. 1999).

### **T cell interactions with B cells and macrophages**

While mainly observed with dendritic cells, B cells were found to also form immunological synapse-like interactions with T cells, yet with some striking variations (Kabanova, Sanseviero et al. 2016). Formation of synapses between T cells and macrophages has also been observed occasionally, but might be less beneficial for T cell activation (Lee, Holdorf et al. 2002, Norbury, Malide et al. 2002, Hickman, Takeda et al. 2008). By analogy with the immunological synapse, the transient and short-term contacts have been identified *in vitro*, are referred to as “kinapses” and are associated with an impaired T cell activation; however, the mechanisms supporting the formation of kinapses are poorly understood (Moreau, Lemaitre et al. 2012).

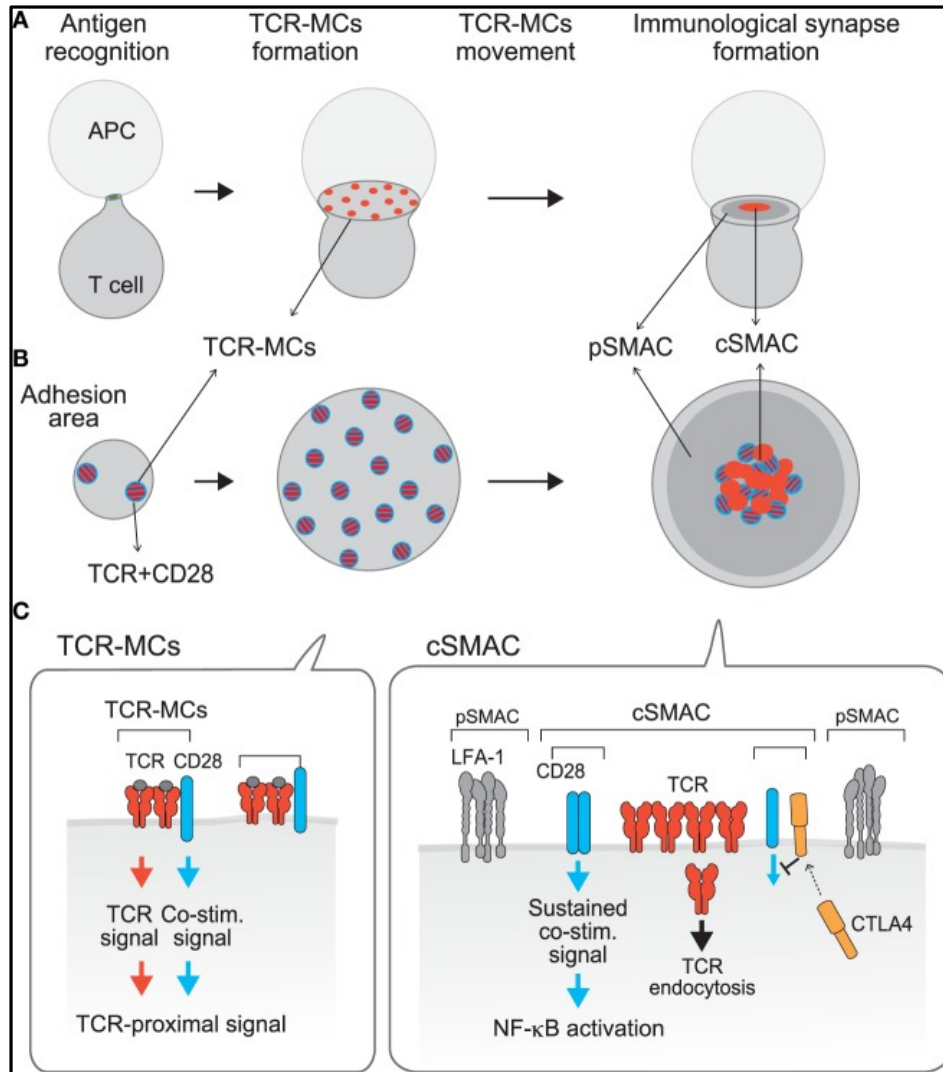


**Figure 7. Formation of the immunological synapse by TcR microclusters (derived from (Hashimoto-Tane and Saito 2016)).** (A) and (B) upon antigen recognition, T cells interact with the antigen presenting cell (APC) resulting in TcR-microclusters (MCs) at the interface with the APC. TcR–MCs contain TCRs (red) and the proximal signaling molecules as well as the CD28 co-stimulation receptor (blue), and induce the initial activation signal. TcR–MCs move toward the center of the interface to form the c-SMAC region. (C) It was noted that there is a CD3<sup>hi</sup> region (red) and a CD3<sup>lo</sup> region (mixture of red and blue) within the c-SMAC; the CD3<sup>hi</sup> region (red) within the c-SMAC may represent the site for TcR endocytosis/degradation for negative regulation, whereas in the CD3<sup>lo</sup> region (blue) co-stimulation molecules (CD28 and CTLA-4) are co-localized to induce a sustained co-stimulation signal (CD28) or inhibit co-stimulation signaling (CTLA-4).

## Chapter 2. Innate and adaptive immunity is spatially and temporally dynamic

### 1) Artificial T cell activation by antigen presenting cells *in vivo*

Pioneer works from the group of U.H. von Andrian have provided significant insights on the course of T cell activation *in vivo*. Using mostly *in vivo* live imaging of interactions between cognate T cells and peptide-loaded dendritic cells, the group of U.H. von Andrian observed that during the first 8 hours, contacts are mostly transient whereas a second phase of contact involves long-lasting and stable contacts (Mempel, Henrickson et al. 2004). However, using other artificial situations, independent studies observed that stable contacts might occur earlier (Bouso 2008). Whatever the kinetics of T cell arrest, this phenomenon is currently viewed as a prerequisite for productive T cell priming and is determined by a strong TcR signal (Bouso 2008). Different potential determinants for T cell arrest on dendritic cells have been identified including dendritic cell maturation status, strong T cell activation (by high amounts of peptides presented), a stochastic encounter between the “good” T cells on the “good” antigen presenting cells, with a higher probability of T cell arrest with time (Bouso and Robey 2003, Hugues, Boissonnas et al. 2006, Bouso 2008, Henrickson, Mempel et al. 2008, Scholer, Hugues et al. 2008). On a molecular basis, T cell arrest *in vivo* is linked to the presence of the adhesion molecules or integrins that are part of the *in vitro* synapse, since T cell arrest is impaired in the absence of adhesion molecules (Scholer, Hugues et al. 2008). The formation of cell kynapses has recently been proposed to favor an exploratory mode for naïve T cells (Moreau, Lemaitre et al. 2015).

### 2) Antigen transfer from macrophages to B cells promotes humoral responses

The groups of J.G. Cyster and U.H. von Andrian provided pioneer studies to decipher how efficient humoral responses are produced in the follicular zone. Previous experimental works identified that the follicular dendritic cells were the antigen presenting cells to the intra-follicular B cells (Allen, Okada et al. 2007). The group of U.H. von Andrian demonstrated that subscapular sinus macrophages were strictly required to generate efficient humoral responses against lymph-borne viruses, through a mechanism that involved the presentation of viral antigen to the cognate B cells that in turn migrated to the follicles (Junt, Moseman et al. 2007). A complementary work from the group of R.N. Germain allowed for the visualization of B lymphocytes/dendritic cell long-term interactions resulting in antigen acquisition by B cells from the antigen-bearing dendritic cells specifically in the high endothelial venule zones, suggesting the existence of alternative mechanisms (Qi, Egen et al. 2006). The group of J.G.

Cyster directly visualized immune complex/antigen transfer to the cognate migrating B cells and the antigen transport to the follicular dendritic cells (Suzuki, Grigorova et al. 2009). Importantly, they identified that this process is dependent on the presence of the complement receptor on subcapsular sinus macrophages (Phan, Grigorova et al. 2007). Further work from the group of J.G. Cyster demonstrated that antibody affinity maturation required the presence of subcapsular sinus macrophages and that they formed membrane processes to the germinal centers. Furthermore, non-cognate B cells relayed antigen opsonized from the macrophage surface to the germinal center fueling the affinity maturation process (Phan, Green et al. 2009). Such processes were recently extended to humoral anti-tumor responses. However, the latter study was challenged by the work from the group of M.J. Pittet that observed that melanoma-derived extracellular vesicles were trapped into the subcapsular sinus macrophages avoiding the entry of antigen into the lymph node cortex, their contact with B cells and the promotion of anti-tumor humoral responses (Pucci, Garris et al. 2016). To generate efficient long-term humoral responses, cooperation between antigen specific CD4+ T cells and B cells is required; in this context, the group of R.N. Germain has identified specific stable interactions between CD4+ T cells and cognate B cells but not antigen presenting dendritic cell, through the involvement of the signaling lymphocyte activation molecule-associated protein (Qi, Cannons et al. 2008, Cannons, Qi et al. 2010).

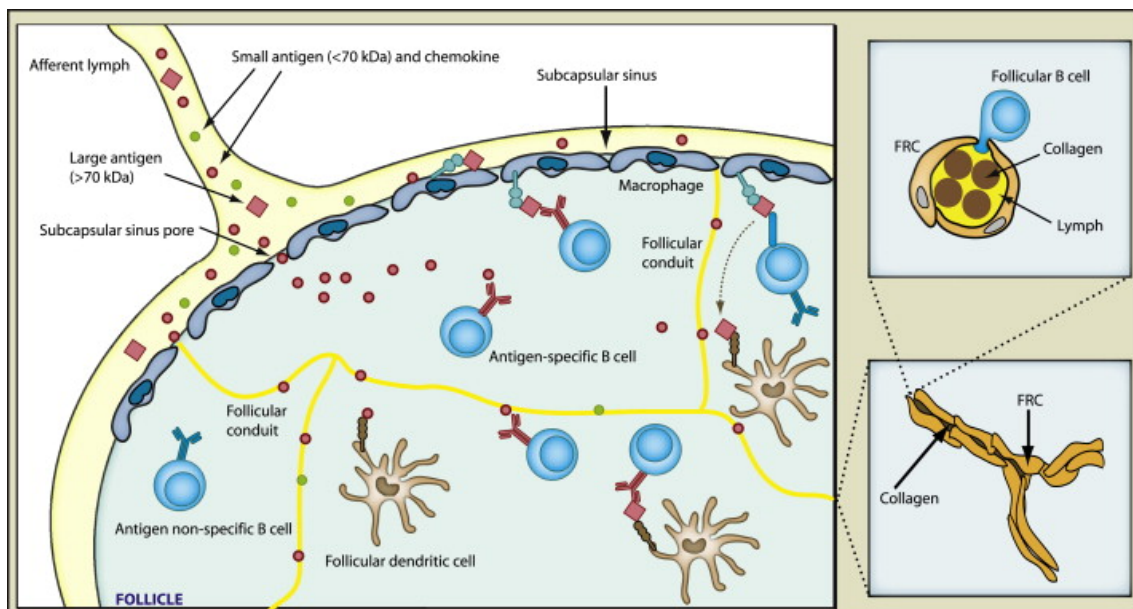


**Figure 8. How subcapsular sinus macrophages influence the antigen presentation to follicular B cells in the lymph nodes (derived from (Harwood and Batista 2009)).** On arrival, subcapsular sinus CD169+ macrophages prevent the passive and massive free diffusion of lymphatic fluid containing small antigens to the lymph node interior. Larger antigens are trapped by subcapsular sinus macrophages and can be directly presented to

antigen-specific B cells in the follicle or be transported by non-cognate B cells to follicular dendritic cells, in a complement-dependent manner. This transport may allow follicular dendritic cells to mediate antigen presentation to specific naive B cells.

Similar to the lymph nodes, a parallel mechanism was recently identified in the spleen, yet with some variations. Marginal zone B cells are a unique B cell subset with a pivotal role in mounting antibody responses against systemic pathogens. Marginal zone B cells mediate the delivery of opsonized antigens from the marginal zone to the follicle and recent studies provided indirect evidence that marginal zone B cells continuously exchange between the marginal zone and follicles (You, Myers et al. 2011). The group of J.G. Cyster has recently observed by live *in vivo* imaging microscopy that marginal zone B cells but not follicular B cells are dotted with motility and bi-directionally migrate between marginal zone and splenic follicles in a sphingosine-1-phosphate receptor-1-dependent manner, this process presumably being required for antigen transfer to follicular dendritic cells (Arnon, Horton et al. 2013). Recently, the expression of CD21 on marginal zone B cells was shown to regulate this antigen transport (Prokopec, Georgoudaki et al. 2016).

### 3) T cell/dendritic cell contacts during infection *in vivo*

Although important for dissecting spatio-temporal aspects of T cell/dendritic cell interactions associated with T cell fates, all the experimental highly controlled systems are a relatively poor source of information to decipher how T cells are *in fine* primed during pathogen infections. One would expect a specific pattern of spatio-temporal T cell/dendritic cell interaction associated to each pathogen, due to the unique combination of parameters that ultimately shapes the T cell/dendritic cell communication and that is unique for each pathogen. In the recent years, such studies were conducted. In mice infected by a subcutaneous infusion of vaccinia virus or vesicular stomatitis virus modified to express the model antigen Ovalbumin (OVA), viral particles were visualized among the lymph node subcapsular sinus zone, resulting in the accumulation of antigen specific T cells in the peripheral inter-follicular regions. Importantly, CD8<sup>+</sup> T cell/dendritic cell interactions were visualized in these peripheral inter-follicular regions and stable interactions were formed as soon as 6 hours post-infection (Hickman, Takeda et al. 2008). This totally contrasts with the T cell/dendritic cell interaction observed in the high-endothelial venules in the case of other modes of immunization. Further insight has been provided by a recent work from the group of R.N Germain. Using another virus modified to express OVA and a series of conditional depleting transgenic mouse model for cDC1 subset, they observed that two phases of priming

of CD8<sup>+</sup> and CD4<sup>+</sup> T cells by dendritic cells are observed in the lymph nodes with a spatial and temporal segregation. In the early phase of priming (few hours), CD4<sup>+</sup> and CD8<sup>+</sup> T cells were primed by different dendritic cell types whereas after few days, cDC1 dendritic cells were capable of co-presenting antigens to and activating T cells, providing a source of CD4<sup>+</sup> help for CD8<sup>+</sup> T cell priming (Eickhoff, Brewitz et al. 2015). In the context of another form of antigen, particulate antigens, the same group using a combination of imaging technologies including live multiphoton microscopy, histo-cytometry and whole-organ 3D imaging, has identified a population of resident cDC2 dendritic cells that scan the lymph close within the lymphatic sinuses, as being responsible for the priming of specific T cells (Gerner, Torabi-Parizi et al. 2015). However, the same group together with the group of F. Zavala has identified the cDC1 subset in the lymph nodes after subcutaneous immunization, as being responsible for the uptake of the malaria parasites, another particulate antigen, resulting in the subsequent priming of protective CD8<sup>+</sup> T cells (Radtke, Kastenmuller et al. 2015). Looking for an explanation of how the memory T cells exert their effector functions more rapidly than naïve T cells, the group of U.H. von Andrian has observed that memory T cells, but not naïve T cells are attracted to the site of initial infection in the lymph nodes, the subcapsular sinuses in a CXCR3-dependent manner where they recognize the infected subcapsular sinus macrophages. Importantly, no difference in terms of motility and interactive between naïve and memory T cells with deep cortex dendritic cells could be observed (Sung, Zhang et al. 2012).

#### **4) T cell priming during allograft rejection *in vivo***

In the context of allografts, one of the undesired outcomes is allograft rejection, which is mediated by innate immunity as well as alloreactive T cells. However, how the priming of alloreactive T cells occurs *in vivo* remains elusive. The group of P. Bousso has recently investigated the dynamics of immune responses supporting allograft rejection in a skin graft model. By live two-photon microscopy, the authors observed that the dermal migratory dendritic cells from the donor were rapidly replaced by a population of CD11b<sup>+</sup> mononuclear cells, responsible from donor antigen uptake and routing to host draining lymph nodes where they cross-primed alloreactive CD8<sup>+</sup> T cells (Celli, Albert et al. 2011).

### **Chapter 3. Inter-cellular communications and dynamics of immune cells are influenced by the microenvironment**

#### **1) Lessons from artificial experimental systems**

In artificial experimental systems signal TcR strength and induction of dendritic cell maturation are thought to be the main extrinsic determinant as assessed by the groups of P. Bousso (Garcia, Pradelli et al. 2007, Jusforgues-Saklani, Uhl et al. 2008) and S. Amigorena (Hugues, Boissonnas et al. 2006). However, exogenous signals are likely involved, although the precise mechanisms remain elusive, and include an inflammatory environment. Indeed, the group of S. Amigorena observed that infusing animals with LPS as an artificial inflammatory environment induce stable and long-standing contacts between CD8<sup>+</sup> T cells and antigen-bearing dendritic cells as compared to CD8<sup>+</sup> T cells and antigen-bearing dendritic cells alone (Hugues, Fetler et al. 2004). Similar findings were observed for CD4<sup>+</sup> T cells and dendritic cells when the model antigen was injected together with an alum-containing adjuvant cocktail (Miller, Hejazi et al. 2004). Finally, the group of R.N. Germain has very recently reported two elegant studies that identify a negative signal for T cell priming *in vivo* that contributes to prevent autoimmunity development. Using multiplex quantitative imaging technologies, the authors observed that Treg cells with highly suppressive capacities accumulate to form clusters with rare IL-2 positive T cells specific for self-antigen. The suppression mechanism was antigen specific as the abrogation of TcR by Treg cells disrupted Treg clusters and resulted in uncontrolled effector T cell responses (Kastenmuller, Gasteiger et al. 2011, Liu, Gerner et al. 2015).

#### **2) Lessons from infectious models**

A recent effort has been given to identify exogenous signals that shape the immune responses in more “physiological” pathological models. The group of P. Bousso has identified a few months ago a role for the subcapsular sinus macrophages in promoting T cell responses specific of the vaccinia Ankara virus in the lymph nodes (Sagoo, Garcia et al. 2016). The authors identified that after viral infection, inflammasome was highly recruited and activated specifically in subcapsular sinus macrophages, resulting in caspase-1-dependent cell death and cytokines release, and subsequent attraction of inflammatory cells to the site of the T cell priming, thereby promoting their higher activation. Altogether, these pioneer results shed the light on unexpected mechanisms that shape the ongoing adaptive immune responses. Whether



such mechanisms extend other infectious models or not remain to date elusive, but will probably be an intense subject of investigation in the future years.

#### **Chapter 4. Concluding remarks**

The current literature about how immune responses are orchestrated *in vivo* suggests that T cell priming requires inter-cellular communications with the antigen presenting cells and other innate or adaptive cellular actors. The signals identified as crucial for T cell priming are the TcR activation by peptide/MHC complexes, the maturation status of the antigen presenting cells, the level of inflammation in the local microenvironment. When adequate signals are present, T cells will cluster with antigen presenting cells and form transient and long-lasting contacts, presumably by forming an immunological synapse. In the context of viral and parasite infectious models, T cell priming seems to be very dynamic and depends on the type of pathogen, since various antigen presenting cells from different locations might be involved over time. T cell priming is also influenced by the presence of exogenous signals provided by environing innate or adaptive immune cells. The nature of the extrinsic signals might be positive, for example by the promotion of inflammation by macrophages, or negative by the activation of highly suppressive antigen-specific Treg cells. Although these studies are a massive source of knowledge about how the immune responses are orchestrated *in vivo*, the above described dynamics and regulatory mechanisms need to be confirmed in other models. As another limitation, these studies have been mostly conducted in the lymph nodes and it remains to identify if the collected results extend to the spleen or tertiary lymphoid organs, for instance.

## PART III - INTEGRATION OF EXOGENOUS SIGNALS BY DENDRITIC CELLS RESULTS IN ACTIVATION OF ADAPTIVE IMMUNITY

### **Chapter 1. Dendritic cell maturation is dependent on recognition of danger signals**

As mentioned earlier, a large set of the dynamics of the immune responses are regulated by the local milieu. Especially, phagocytes including dendritic cells and macrophages sense the local environment for danger signals, referred to as danger-associated molecular patterns that are recognized by membrane and cytosolic receptors: TLRs, NOD-like receptors and RIG-I-like receptors. Importantly, all these receptors upon binding to their ligand will signal within the cells and activate and regulate inflammatory programs, expression of co-stimulation and MHC molecules, as well as their migratory and internalization capacities.

#### **1) Description of the toll-like receptor family**

TLRs are type 1 transmembrane proteins involved in the recognition of PAMPs with ectodomains containing leucine-rich motifs that are necessary for the recognition of PAMPs and a TIR domain (Toll-interleukin 1 receptor) for the downstream transduction of the signal, resulting in the production of pro-inflammatory cytokines and type I IFNs to initiate the inflammatory response and are necessary for the elimination of pathogens (Kawai and Akira 2010). The nature of the PAMPs recognized by TLRs includes lipids, lipoproteins, proteins, nucleic acids derived from a large set of microbes. This recognition is achieved in different cellular compartments such as the plasma membrane, endosomes and lysosomes (Kawai and Akira 2010). Classically, TLRs can be divided into two subgroups based on their location: TLR1, TLR2, TLR4, TLR5, TLR6 and TLR11 are expressed at the plasma membrane and recognize lipids, lipoproteins and proteins from microbes whereas TLR3, TLR7, TLR8 and TLR9 are intracellular receptors mainly found in the endoplasmic reticulum (ER) and in the endocytic pathway, where they can recognize microbial and, in pathological settings, self-nucleic acids. As examples, I will briefly describe two TLRs, which have been studied during the experimental works, TLR4 and TLR9.

#### **Toll-like receptor 4**

TLR4 is involved in the recognition of membrane component of the gram-negative bacteria, the endotoxin or bacterial lipopolysaccharide (LPS). To bind LPS, TLR4 needs to interact together with an adaptor protein, MD2 (Kim, Park et al. 2007), resulting in the recruitment of adaptor proteins within the cells to trigger downstream signaling.

## **Toll-like receptor 9**

TLR9 recognizes unmethylated 2'-deoxyribo(cytidine-phosphate-guanosine) (CpG) DNA motifs that are frequently present in bacteria and viruses but are rare in mammalian cells, with the exception of mitochondrial DNA (Kawai and Akira 2010). TLR9 mainly resides in the ER in resting cells and rapidly traffics to the endocytic pathway upon binding to its ligand, in a process dependent on the ER-resident chaperon protein unc-93 homolog B UNC93B that can also bind to TLR3 and TLR7 (Kawai and Akira 2010). To be active and to signal, TLR9 needs to be cleaved by lysosomal proteases in endolysosomes, such as the cathepsins (Manoury 2011) or the leguminin (Sepulveda, Maschalidi et al. 2009).

## **Toll-like receptor 4 and 9 signaling**

All the TLRs, with the exception of TLR3, recruit the adaptor protein Myeloid differentiation primary response gene 88 (MyD88) for initiating intracellular signaling. TLR3 exclusively signals through the TIR- domain-containing adapter-inducing interferon- $\beta$  (TRIF)-dependent pathway, whereas TLR4 activates and requires both MyD88- and TRIF-dependent pathways to secrete inflammatory cytokines (Kumagai, Kumar et al. 2009). In the MyD88-dependent pathway, MyD88 recruits proteins from the interleukin-1 receptor-associated kinase (IRAK) and the TNF Receptor associated factor 6 (TRAF6), which in turn activate the kinase TAK1. TAK1 is responsible for the activation of the mitogen-activated protein kinase (MAPK) and of the nuclear-factor kappa B (NF- $\kappa$ B), through the activation of the complex I-kappa B kinase (IKK), as well as the IRF7 (Kumagai, Kumar et al. 2009). In the TRIF-dependent pathway, TRIF recruits the receptor-interacting protein 1 and TRAF6 to promote their activation, which in turn activate both IRF3 and IRF7. Finally, NF- $\kappa$ B translocates to the nucleus to stimulate the transcription of gene encoding for pro-inflammatory cytokines, whereas the IRF3 and 7 drive the transcription genes encoding for type I IFNs (Kumagai, Kumar et al. 2009).

### **2) Contribution of toll-like receptors in the regulation of dendritic cell functions**

TLRs, NOD-like receptors and RIG-I-like receptors are highly expressed in phagocytes, yet some striking differences have been noticed in their distribution among macrophage and dendritic cell subsets. The role of TLRs on the dendritic cells has been extensively studied, because TLR signaling can modify their capacity to present antigens through the MHC-I and the MHC-II pathways. Indeed, upon the recognition of PAMPs and TLR signaling, dendritic cells will undergo a maturation program that will strikingly modify their phenotypic and

functional properties. For instance, in addition to secrete inflammatory cytokines and type I IFNs, dendritic cells will up-regulate the expression of the co-stimulatory molecules on their surface, enhancing their ability to activate naïve T lymphocytes (Granucci, Ferrero et al. 1999). Additionally, MHC-I and MHC-II levels are up-regulated and antigen uptake and processing are strikingly increased during the first hours of stimulation (West, Wallin et al. 2004), before undergoing a strong reduction (Gil-Torregrosa, Lennon-Dumenil et al. 2004). TLR signaling in phagosomes modulates their own maturation, favoring antigen presentation (Blander and Medzhitov 2004, Nair-Gupta, Baccharini et al. 2014). Finally, maturing dendritic cells acquire the capacity to migrate from the injured tissue to the draining-lymph nodes where adaptive immunity will be initiated (Faure-Andre, Vargas et al. 2008).

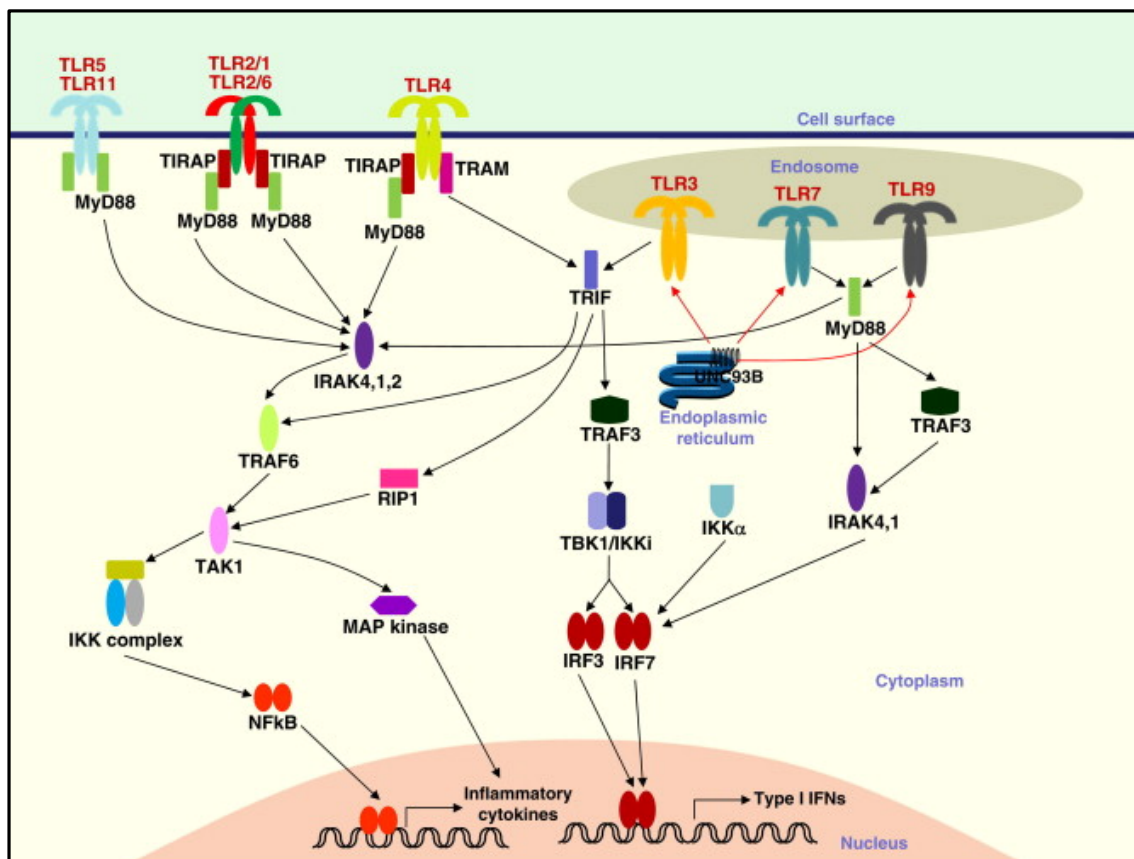


**Figure 9. TLR signaling in phagocytes (derived from (Kumagai, Kumar et al. 2009)).** For a detailed explanation, please refer to the manuscript.

## Chapter 2. Antigenic material is actively internalized by phagocytes

To be processed by the antigen presenting cells, antigenic material has to be internalized. To do so, antigen presenting cells can use different but complementary mechanisms of endocytosis, mainly pinocytosis and phagocytosis. Phagocytosis and pinocytosis are distinct by the size of the material internalized, generally >500 nm for phagocytosis. Pinocytosis

refers to the internalization of external fluids and may occur by four distinct mechanisms: macropinocytosis, clathrin-dependent endocytosis, caveolin-mediated endocytosis and dynamin-independent clathrin-independent endocytosis. The signals required for the resulting endosome formation differ depending on the type of pinocytosis. While clathrin-dependent endocytosis involves clathrin, dynamin, the adaptor protein 2 (AP-2) and the phosphatidylinositol 3-kinase (PI3K) activity, caveolin-dependent endocytosis involves cholesterol-rich membrane region, dynamin and caveolin, whereas macropinocytosis requires membrane ruffles and the small guanosine triphosphatase (GTPase) ADP-ribosylation factor 6 (ARF6). These general mechanistic requirements may vary depending on a given receptor (Liu and Shapiro 2003). I will give an overview on the processes that regulate both the formation and the maturation of endosomes and phagosomes, since they play a central role in the regulation of antigen presentation.

### **1) Endosome formation, maturation and resolution**

#### **Endosome system overview.**

Material internalized by endocytosis is generally targeted to degradation into the endolysosomes, through the endocytic process. The endocytosis can be simplified as a dynamic succession of endosome compartments/stages (early endosomes, multivesicular bodies, late endosomes and endolysosomes) that starts with the endosome formation and is followed by a maturation sequence (Huotari and Helenius 2011). Early endosomes are a key subcellular compartment among the endocytic pathway: they receive the incoming cargo and fluids, act as the main sorting station in the endocytic pathway, represent a potential signaling platform for endocytosed-receptors, and constitute the starting point for maturation toward the late endosomes. As the early endosome matures toward late endosomes and endolysosomes, striking modifications in protein and lipid membrane as well as in the endosomal lumen occur. Furthermore, protein cargos can detach from the maturing endosome membrane to be sorted into intra-luminal invaginations or vesicles (ILVs) of the early endosome membrane in order to generate free-cargo containing vesicles. ILVs accumulate and mature to form multivesicular bodies or endosomal carrier vesicles, the latter will eventually fusion with the late endosome (Huotari and Helenius 2011, Scott, Vacca et al. 2014). Late endosomes also serve as both a sorting and signaling platform. ILVs and their cargo are generally routed from late endosomes to the highly degradative lysosomes where they will be digested into small products (Huotari and Helenius 2011, Scott, Vacca et al. 2014). However, protein cargos including some housekeeping receptors might also be recycled back to the plasma membrane

by recycling endosomes or be routed toward the trans-golgi network (TGN) by retrograde protein transport. Recycling or retrograde transports are initiated at the early endosome stage but might occur at the late endosome stage, or in some cases even at the endolysosomal stage (Huotari and Helenius 2011, Scott, Vacca et al. 2014). The endocytosis involves fundamental concepts such as tethering, membrane docking and fusion, as well as membrane fission. All these events are tightly regulated by various molecules including the small GTPases of the Ras superfamily that recruit and activate effector enzymes or proteins mainly involved in the regulation of proteins and lipids related to the control of membrane traffic and cytoskeleton remodeling. GTPases are generally attached to membranes and alternate between an inactive GDP-bound form and an active GTP-bound form, capable of forming molecular complexes together with their recruited effectors (Huotari and Helenius 2011, Scott, Vacca et al. 2014). GTPases forms and activities are dependent on both activating regulators that are the Guanine-Nucleotide Exchange Factors (GEFs) and inhibitory regulators such as the guanine nucleotide dissociation inhibitors (GDIs). GTPase-activating proteins stimulate GTP hydrolysis whereas GDIs detach inactive GDP-bound proteins from endosome membranes (Huotari and Helenius 2011, Scott, Vacca et al. 2014). Importantly, endosome stages are defined by the preferential expression of specific small GTPases such as Rab5 on early endosomes, or Rab7 on late endosomes. More than defining the type of endosome structure, the small GTPases regulate the formation and the maturation of these endosomes, with the Rab5-to-Rab7 switch being strictly required to promote the transition from early to late endosomes. Additionally, membrane docking and homotypic fusion between similar endosome structures or heterotypic fusion between distinct endosome structures are observed during the phagosome maturation or the recycling and retrograde transport (Huotari and Helenius 2011, Scott, Vacca et al. 2014). These docking and fusion events generally involve specific transmembrane molecules, the Soluble N-ethylmaleimide-sensitive-factor Attachment protein Receptor (SNAREs). The complementary SNARE protein from the donor membrane (vesicle-SNARE or v-SNARE) binds to the target membrane (target-SNARE or t-SNARE) to catalyze the fusion process. Finally, at least two molecular complexes orchestrate the tethering, docking and fusion processes: the class C core vacuole/endosome tethering factor (CORVET) and the late endosomal/lysosomal homotypic fusion and vacuole protein sorting (HOPS) complexes. These two molecular complexes share a core of four proteins: vacuolar protein sorting 11 (Vps11), Vps16, Vps18 and Vps33 but differ in accessory subunits: Vps3 and Vps8 for CORVET: Vps39 and Vps41 for HOPS (Huotari and Helenius 2011, Scott, Vacca et al. 2014).

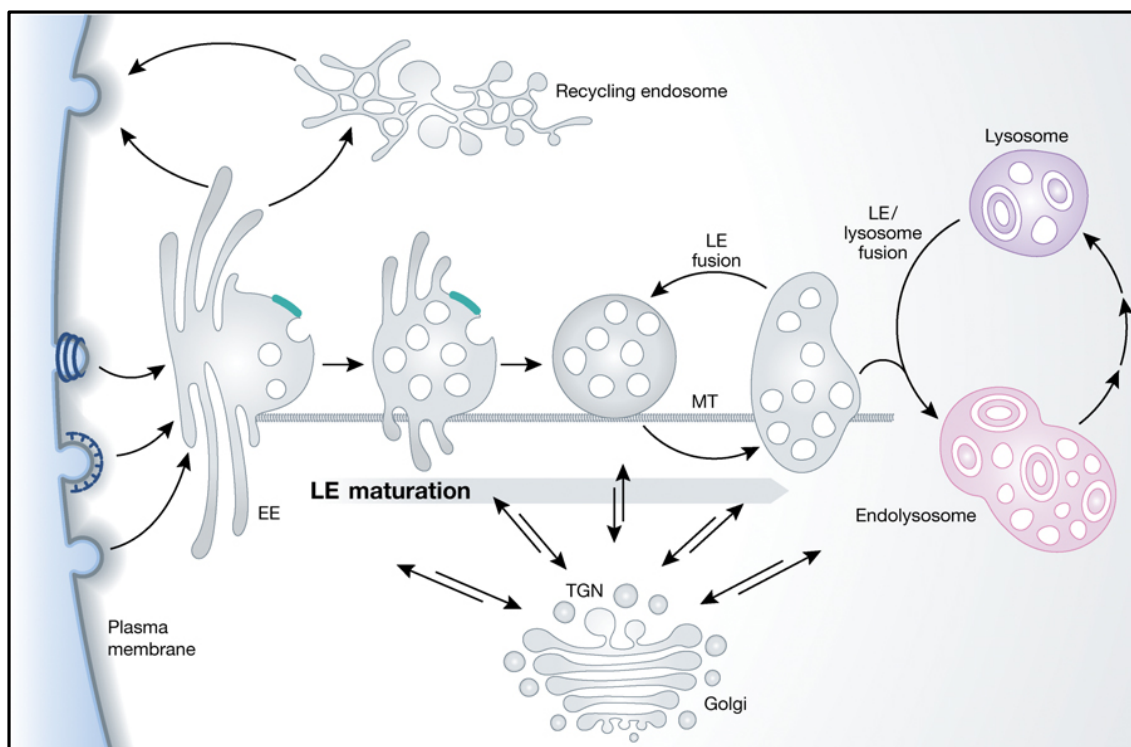


**Figure 10. Endosomal maturation (derived from (Huotari and Helenius 2011))**- After internalization, vesicles deliver their contents and their membrane to early endosomes (EEs) in the peripheral cytoplasm. After a period of recycling to the plasma membrane (directly or via recycling endosomes in the perinuclear region), conversion of the early endosomes to the late endosomes (LEs) occurs. As the endosomes move towards the perinuclear space along microtubules (MT), the nascent LE are formed by the vacuolar domains of the EE network. They carry a selected subset of endocytosed cargo from the EE and also receive input with lysosomal hydrolases and components from the secretory pathway. They undergo homotypic fusion reactions, grow in size, and acquire more intraluminal vesicles (ILVs). LEs undergo a maturation process preparing them progressively for fusion with lysosomes to generate a transient hybrid compartment, the endolysosome, in which active degradation takes place. The endolysosome is finally converted to pure lysosome (resolution phase), which constitutes a storage organelle for lysosomal hydrolases and membrane components.

### Early endosome formation and regulation

How early endosomes exactly arise remains still elusive. One of the key events however, is the recruitment and activation of the small GTPase Rab5 to the cytosolic membrane of the early endosome, which depend on the GEF Rabex-5 (Ohya, Miaczynska et al. 2009). By homodimeric fusion, the active GTP-bound Rab-5 form promotes further Rab5 binding and the recruitment of effector proteins including the PI3K complex. The PI3K Vps34 subunit will generate the phosphatidylinositol triphosphate (PtdIns3P) that is highly enriched at the early endosome membranes and can bind other proteins through their PI-binding motifs (Hurley and Stenmark 2011). Early endosomes are heterogeneous structures regarding their

size, their distribution among the cells, their morphology and their composition. They include domains enriched in the recycling process such as Rab4 and Rab11 small GTPases that mediate the recycling back to the plasma membrane, or in the retrograde traffic to the TGN, such as the retromer and caveolae (Galvez, Gilleron et al. 2012). The intraluminal vesicles (n: 1-10) that will give rise to the multivesicular bodies are already visualized in the lumen of early endosomes and the cytosolic membranes of early endosomes harbor the machinery responsible for the sorting of ubiquitinated proteins into ILVs. Finally, the biochemical examination of the early endosomes has revealed that early endosomes are weakly acidic (pH ranges: 6.8-5.9) and contain a relatively low  $\text{Ca}^{2+}$  concentration. The bi-directional transport between the TGN and the maturing endosome is responsible for the delivery of lysosomal component such hydrolases as well as the removal of endosomal components (Huotari and Helenius 2011, Scott, Vacca et al. 2014). The retrograde traffic to the TGN requires specific factors including the small GTPases Rab7, Rab9 and the retromer complex. The retromer complex is composed by a sorting nexin dimer that associates some sorting nexin proteins (SNX) and a cargo-recognition trimer that associates Vps26, Vps29 and Vps35. The SNX proteins exhibit two specific domains (PX and BAR) that bind to PtdIns3P rich-membranes (Huotari and Helenius 2011, Scott, Vacca et al. 2014).

### **Biogenesis of intraluminal vesicles and multivesicular bodies**

The formation of ILVs is a critical process to sort membrane-associated cargo that are addressed to the degradative lysosomes as well as for the termination of some signaling receptors. These structures are not capable of homotypic fusion. The formation of ILVs and multivesicular bodies is controlled by the activity of specific complexes referred to as endosomal sorting complexes required for transport (ESCRT) complexes that will help with the sorting of ubiquitinated complexes (Huotari and Helenius 2011, Scott, Vacca et al. 2014). The newly formed ILVs-multivesicular bodies complexes will rapidly acidify to pH 6.0-5.5 and mediate microtubule-dependent transport toward late endosomes, with which they fuse, resulting in the delivery of their lipid and protein cargo (Huotari and Helenius 2011, Scott, Vacca et al. 2014). As mentioned earlier, the Rab5/Rab7 exchange is a crucial step in the transition from early-to-late endosomes and this process is regulated on the membrane of ILVs-multivesicular bodies by the Sand1/Mon1-Ccz1 complex (Poteryaev, Datta et al. 2010).

### **Late endosomes.**



Mature late endosomes are fueled with a broad variety of proteins that are delivered from the endocytic membrane transport, from TGN-derived vesicles and from autophagosomes. For instance, late endosome membranes harbor lysosomal membrane proteins such as lysosomal-associated membrane protein 1 (LAMP1) and their lumen contains a series of acid lysosomal hydrolases as well as numerous ILVs ( $n > 30$ ). From the early endosome to the late endosome, a drop of 1.0 in pH is generally noticed, with ranges 6.0-4.9 (Huotari and Helenius 2011, Scott, Vacca et al. 2014). Late endosomes are motile organelles, since after their formation in the peripheral cytoplasm they rapidly move to the perinuclear region where they form larger bodies by homotypic fusion and transiently fusion with lysosomes to form a hybrid organelle, the endolysosomes, by a series of “kiss-and-run” processes (Huotari and Helenius 2011, Scott, Vacca et al. 2014). The transition toward the late endosome might involve at least two mechanisms: the dissociation of Rab5 together with its effectors, or a fission phenomenon in which the late endosome will be separated from the hybrid compartment. In the current opinion, Rab5 is thought to recruit and activate Rab7, and Rab7 displays auto-activation and suppresses Rab5 activity to favor its removal from the early endosome cytosolic membrane (Peplowska, Markgraf et al. 2007). Additional proteins recently identified are two cytosolic factors, SAND-1/Mon1 and Ccz1: these proteins are thought to bind to the active GTP-bound Rab5 form to recruit Rab7 and disassemble the complex formed between Rab5 and its effectors (Poteryaev, Datta et al. 2010). SAND-1/Mon1 recognizes PtdIns3P to mediate Rab5 inactivation. In addition to the Rab5/Rab7 switch, other Rabs including Rab4 and Rab11 are replaced by Rab9; further modifications include a change in size and morphology with the acquisition of a round shape and increase in size, a conversion in the phosphoinositide species with a replacement of PtdIns3P in phosphatidylinositol 3,5 bisphosphate (PtdIns3,5P2) by the recruitment of the Phosphoinositide Kinase, FYVE-Type Zinc Finger Containing (PIKfyve) enzyme through its PtdIns3P-binding FYVE domain (Huotari and Helenius 2011, Scott, Vacca et al. 2014). The PIKfyve enzyme also regulates the acidification and ion flux (for instance the  $\text{Ca}^{2+}$  flux). As mentioned above, another striking modification concerns the endosome motility. The endosome motility is indispensable to achieve the maturation process. Indeed, the disruption of microtubules impairs the endosomal maturation and subsequent degradation, presumably by delaying the access to the acidic compartment. The motility is strictly dependent on kinesin and dynein motor proteins, providing opposing forces that move endosomes in opposite directions. Kinesin and dynein proteins are required for the fission of early endosomes, the sorting of lipid and protein cargos into both the degradative and recycling compartments (Huotari and Helenius 2011, Scott, Vacca et al. 2014). As an

example, the Kinesin Family Member 16b KIF16b is a kinesin 3 motor protein responsible for plus-end-directed movements of early endosomes. KIF16b attaches early endosomes through its PtdIns-binding PX domain when Rab5 is under its active GTP-bound form. Manipulating the level of KIF16b expression influences the balance between cargo recycling or degradation: while depleting KIF16b triggers a block in cargo recycling and an increased routing to lysosome degradation, overexpression of the kinesin leads to the opposite observation (Hoepfner, Severin et al. 2005). Finally, the endosome acidification gradually observed during endosome maturation is essential for the endosome functions: a low pH is beneficial for the activation of lysosomal hydrolases, for the inactivation of trapped pathogens and for membrane traffic. One source for the endosome acidification is the V-Adenosine TriPhosphatase (V-ATPase) complex proton pumps, composed by a V0 complex that acts like a transmembrane pore unit for protons and by a V1 cytosolic complex that binds and hydrolyzes the ATP. The acidification of endosome lumen is influenced by the density of V-ATPase complexes, the selective distribution of their isoforms and the proportion of V0 and V1 complexes (Lafourcade, Sobo et al. 2008). Additional molecules regulating the endoluminal pH are ion channels or the Na/K ATPase. Of interest, endosome acidification is accompanied by drastic ion modifications that contribute to the endosome homeostasis: for instance, calcium efflux might be a regulator for fusion with lysosomes and for lysosome reformation from the endolysosomes (Huotari and Helenius 2011, Scott, Vacca et al. 2014).

### **Resolution of the endolysosomes**

The lysosomes are heterogeneous regarding their size, morphology, location and density, presumably influenced by their cargo and the multiple pathways that feed them, or fusion events. The endolysosomes possess a high number of lysosome-derived hydrolases, used to degrade most of the endosome-derived components, yet some of the molecules that resist to the degradation contribute to the lysosome homeostasis. The formation of endolysosomes and the lysosome biogenesis are both orchestrated by the Transcription Factor EB (TFEB) (Luzio, Pryor et al. 2007).

## **2) Phagosome formation, maturation and resolution**

### **Phagosome system overview**

Phagocytosis is defined as the regulated uptake of large particles (usually  $> 0.5 \mu\text{m}$  in diameter) into cytosolic, membrane-bound vacuoles called phagosomes. Phagocytosis is a common characteristic shared by the mononuclear phagocyte system and the neutrophils. The

neutrophils use phagocytosis to eliminate pathogen by injecting a broad variety of microbial compounds into the phagosomes. Macrophages can also clear pathogens at sites of infection, but serve the additional function of cleaning up the collateral damage caused by the exuberant microbicidal response of neutrophils. Dendritic cells, and some types of macrophages, have the specific capacity to selectively sort antigens from material digested in phagosomes for further processing and presentation to T lymphocytes, thereby eliciting immunological effector and memory responses. Phagocytosis is a dynamic process that can be divided in three different consecutive steps: 1) the recognition and adhesion/attachment of the particle to the phagocyte, 2) the engulfment/internalization of the particle into a specific vesicle, the phagosome, and 3) the digestion of the particle.

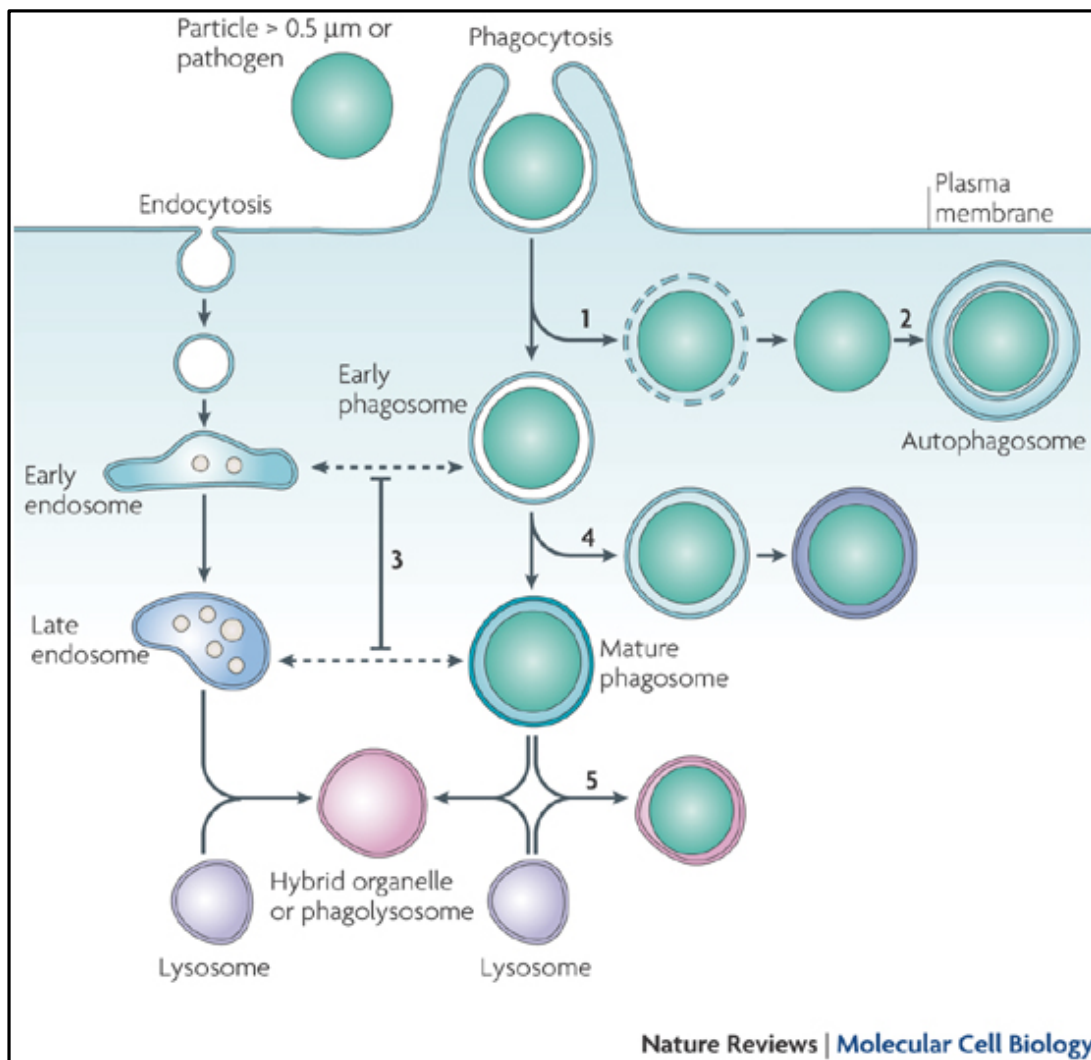


**Figure 11. Phagosome maturation (derived from (Luzio, Pryor et al. 2007)).** Phagosome maturation includes multiple interactions with endocytic compartments to generate a mature phagosome. The phagosome fuses with lysosomes to form a transient hybrid organelle, the phagolysosome, where digestion of the phagocytic particle occurs.

## Phagosome formation

The phagosome formation is generally an active and actin-dependent process. However, an alternative passive phagocytosis has been identified in splenic macrophages involved in the clearance of end-of-life erythrocytes; in this scenario, passive contacts with the target particles are favored by the particular architecture of the splenic marginal sinus, where the blood flows progressively slows down (Levin, Grinstein et al. 2016). During “active phagocytosis”, the sensing of particles by phagocytes is allowed by their unique properties including migration and membrane protrusions. Migration to the sites of scavenging depends on signals that are sometimes referred to as “find-me” signals released by the pathogens, the cell debris or by the inflammatory cells. Additionally, dendritic cells and macrophages continuously and actively extend membrane protrusions in a process called membrane “ruffling” resulting in an enhanced sensing of particles. Membrane extensions are driven by active cytoskeleton remodeling through an actin-dependent manner. This remodeling generally involves actin-related protein 2 and 3 (Arp2/3) complex that is conditionally activated by nucleation-promoting factors that remain to be identified for the majority (Levin, Grinstein et al. 2016). Wondering how is regulated membrane ruffling the group of S. Grinstein has identified the calcium-sensing receptor as a crucial activator of nucleation-promoting factors. In their publication, the authors demonstrated that the activation of calcium-sensing receptor promotes the generation of phosphatidylinositol 3,4,5 trisphosphate (PtdIns3,4,5P3) and phosphatidic acid at the plasma membrane, resulting in the activation of two complexes required for nucleation and subsequent membrane extension (Canton, Schlam et al. 2016). Sensing and attachment of the particles to the phagocytes are dependent on surface pattern-recognition receptors expressed by dendritic cells and macrophages that will be specifically described in more details. Binding of the particles to their specific receptors triggers intracellular signal transduction that mediates either the formation of phagosome for internalization via “eat-me” signals or the rejection of the particle via “don't-eat-me” signals (Levin, Grinstein et al. 2016). The first steps of cascade signaling generally involve specific signaling motifs that can mediate either activating or inhibitory signals. For instance, the Fc-gamma receptors (FcγRs) exhibit immunoreceptor-tyrosine based activation motifs (ITAM) in their cytosolic tail that are phosphorylated by specific kinases including the spleen tyrosine kinases (Syks), found in macrophages and some Src-family tyrosine kinases (SFKs). In homeostatic conditions, the activation of ITAM is prevented by the constitutive inhibitory action of tyrosine phosphatases that mediate the phosphorylation of inhibitory tyrosine

residues (Levin, Grinstein et al. 2016). Productive signals triggering the phagosome formation only occur when the basal inhibition is overcome. This involves at least two mechanisms that depend on membrane ruffling: the local accumulation and clustering of positive kinases and the exclusion of negative phosphatases. Importantly, activating Fc $\gamma$ Rs can also aggregate with inhibitory Fc $\gamma$ Rs that express in their cytosolic tail an immunoreceptor-tyrosine based inhibition motifs (ITIM) that might regulate or terminate the cascade signaling (Levin, Grinstein et al. 2016). When productive signals occur, the activating kinases will phosphorylate nearby ITAM motifs to amplify the signal and also recruit adaptor proteins that will in turn recruit cytosolic effectors to support the cytoskeletal and lipid remodeling. Such adaptor proteins include for example the growth factor receptor-bound protein (Grb2) or the Grb-2-associated-binding protein 2 (Gab2) (Levin, Grinstein et al. 2016). Among membrane lipid modifications of the plasma membrane, an increase in phosphatidylinositol 4,5-bisphosphate (PtdIns4,5P2) is one of the first modification observed, triggered by the phosphatidylinositol 4-phosphate 5-kinases (PIP5K) that is recruited by locally activated Phospholipase D. Shortly after its accumulation, PtdIns4,5P2 is rapidly converted by the PI3K into PtdIns3,4,5P3, then into diacylglycerol and inositol (1,4,5)-trisphosphate by phospholipase C $\gamma$ . While the generation of PtdIns3,4,5P3 is mandatory for the phagosome formation in the context of large particles, it is dispensable for the internalization of small size particles. Hydrolysis of PtdIns3,4,5P3 into diacylglycerol and inositol (1,4,5)-trisphosphate is also important for initiating cytoskeleton remodeling. Indeed, inositol (1,4,5)-trisphosphate binding to its receptor will mediate calcium release from the ER whereas diacylglycerol will regulate and recruit a large number of effector proteins involved in the cytoskeleton remodeling (Levin, Grinstein et al. 2016). The cytoskeleton remodeling requires nucleation-promoting factors to activate the Arp2/3 complex and nucleate the branched actin networks and the actin polymerization around the phagocytic particles. Phagosome sealing is the last step of the phagosome formation. This “zipper-like” phenomenon leads to the coalescence of membrane protrusions at their distal margins, but it remains poorly understood. After phagosome sealing, tyrosine phosphatases are recruited to the phagosome cups to dephosphorylate and inactivate ITAMs and SFKs, Syks and PI3K. The termination of sealing is tightly regulated in both space and time and starts as soon as actin polymerization has started (Levin, Grinstein et al. 2016).

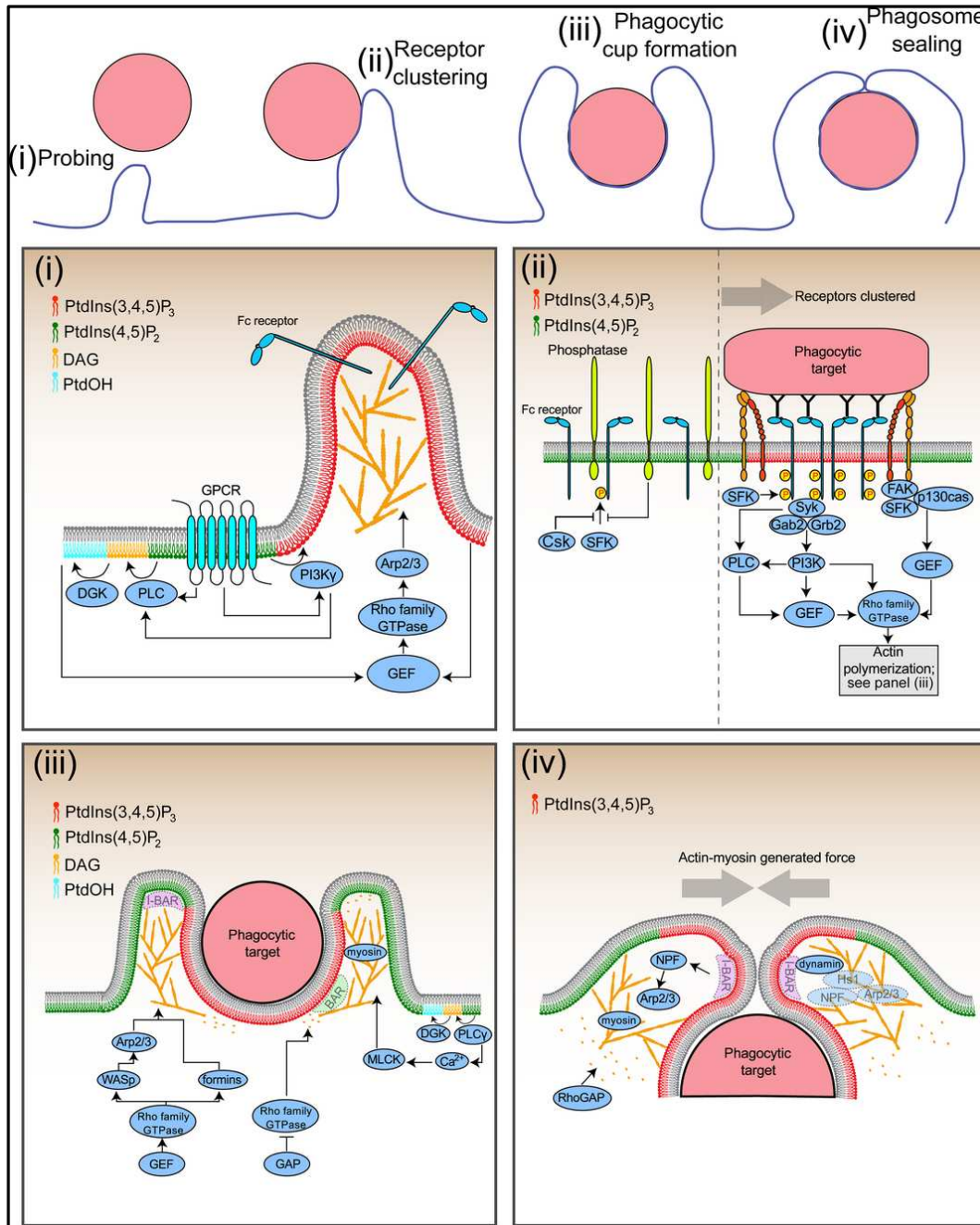


**Figure 12. Phagosome formation. (derived from (Levin, Grinstein et al. 2016))**

### Pattern Recognition Receptors

Pathogen recognition and internalization by the innate immune system is mediated by a series of PRRs that are either soluble or membrane-bound. The PRRs can recognize conserved pathogen structures, mainly lipid or sugar motifs that are PAMPs. Membrane-bound PRRs directly recognize conserved motifs on microbes and consequently mediate their internalization (Drickamer and Taylor 2015). Here is a non-exhaustive description of some PRRs.

Opsinin receptors. FcγRs bind to IgG-opsonized particles, triggering an actin-rich pseudopodia extension circumferentially around the targeted particle with a “zippered phagosome” as the final result (Griffin, Bianco et al. 1975). Signaling resulting from the FcγR engagement is mediated through ITAM motifs, PI3K, and the small GTPases Rac and cell division control protein 42 homolog (Cdc42). All the effector molecules are involved in actin and membrane reorganization and phagosome sealing (Caron and Hall 1998). Although this general process was initially deciphered in macrophages, it also takes place in other phagocytes such as neutrophils, monocytes and dendritic cells and involves various receptors, with specific substrates and affinities. Another example is the complement receptor 3, already extensively reviewed (Kerrigan and Brown 2009).

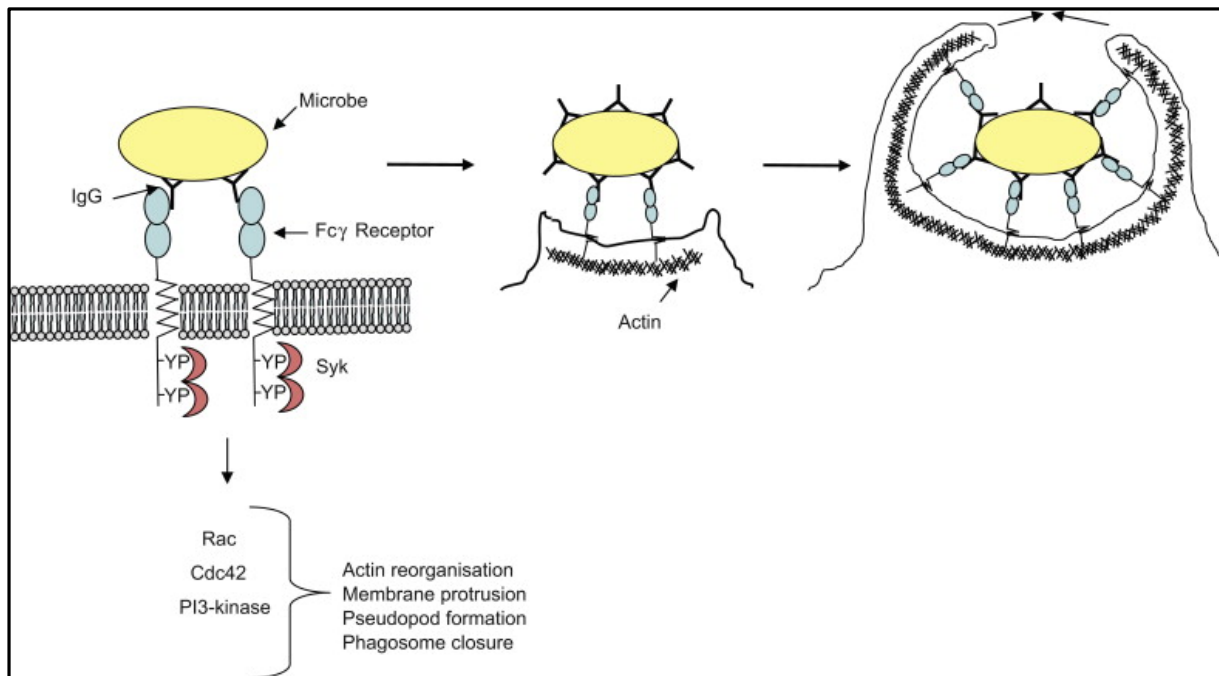


**Figure 13. FcγR signaling leads to the phagocytosis of the microbe (derived from (Kerrigan and Brown 2009))**

C-type lectins superfamily. C-type lectin superfamily is a large group of protein receptors characterized by the presence of at least one C-type lectin-like domain. These proteins have been involved not only in microbial recognition and phagocytosis but also in a large set of biological processes such as endocytosis, cell adhesion, platelet activation, tissue remodeling, complement recruitment. Here are some examples of C-type lectin receptors. **SIGN-R1.** SIGN-R1 is the murine homologue of human DC-SIGN and is type II transmembrane protein (Drickamer and Taylor 2015). Initially, its expression was thought to be restricted to dendritic cell populations but is now considered as mainly expressed by selected macrophage

populations (Kang, Yamazaki et al. 2003). DC-SIGN recognizes internal mannose branched motifs as well as terminal di-mannoses. SIGN-R1 has been additionally shown to be a receptor for the complement protein C1q and to regulate the C3 deposition on blood-borne *Streptococcus pneumoniae* (Kang, Kim et al. 2004). Furthermore, SIGN-R1 by interacting with 2,6 sialylated motifs present on Fc fragments of immunoglobulins contributes to the anti-inflammatory activity of intravenous immunoglobulin infusions, widely used in autoimmune settings to treat patients (Yu, Vasiljevic et al. 2013). In the mouse spleen, SIGN-R1 is selectively expressed on a marginal sinus macrophage subset, the outer marginal zone macrophage subset and is strictly required *in vivo* for the uptake/phagocytosis of circulating apoptotic cells and their clearance. Finally, the recognition of apoptotic cells by SIGN-R1 is dependent on C1q since phagocytosis is enhanced in the presence of increasing amounts of purified C1q protein (Kang, Do et al. 2006, Prabagar, Do et al. 2013). To date, no report has elucidated the molecular effectors responsible for the phagocytosis of apoptotic cells by the marginal zone macrophages. **CLEC9A**. CLEC9A is a disulphide-bonded homo-dimeric type II transmembrane protein of the C-type lectin superfamily, with a selective high expression in the cDC1 subset. CLEC9A is the major pathway for initiating immunity against tumors and some viruses (Huysamen, Willment et al. 2008). The protein recognizes specifically some motifs exposed by dead cells, the filamentous form of actin (F-actin), one of the most abundant intracellular components of eukaryotic cells (Zhang, Czabotar et al. 2012). Altogether, these observations have revealed a new mechanism unsuspected for informing about cell damage: cytoskeleton exposure. Recent reports from the group of C. Reis e Sousa have contributed for the elucidation of the receptor structure and of the motifs involved in F-actin recognition (Hanc, Fujii et al. 2015). Supporting the role for CLEC9A in adaptive immune responses, lack of functional CLEC9A impairs cross presentation of dead-cell associated antigens by cDC1 subset *in vitro* and *in vivo* in mouse (Schulz and Reis e Sousa 2002, Schreiber, Klinkenberg et al. 2012). Importantly, while the absence of CELC9A is not associated with the impairment of dead-cell phagocytosis by dendritic cells, its expression is mandatory for initiating adaptive immune responses. Whether or not the receptor can mediate phagocytosis of dead cells remains unknown to date.

Scavenger receptors. Scavenger receptors constitute a large family of proteins, initially characterized by Brown and Goldstein as receptors for scavenging oxidized but not native low-density lipoprotein. In addition to recognize modified self-molecules, scavenger receptors also recognize pathogen-derived molecules to mediate microbe phagocytosis. Scavenger



receptors are divided into 10 classes (from A to J). As an example, MARCO is a member of the class A scavenger receptor family that shares a similar structure to SR-A, but totally lacks the  $\alpha$ -helical coiled coil domain (Elomaa, Kangas et al. 1995). Expression of MARCO is exclusively restricted to macrophage subsets (van der Laan, Kangas et al. 1997). Again, the *in vivo* relevance of MARCO as crucial for host protection against bacteria has been supported by challenging MARCO<sup>-/-</sup> mice with *Streptococcus pneumoniae* (Arredouani, Yang et al. 2004).

### **Phagosome maturation**

During its maturation, the phagosome undergoes a drastic and gradual transformation to incorporate components that *in fine* create a degradative and hostile local environment for the ingested particle, favoring its clearance. Phagosome maturation parallels the endosome maturation process and several intermediate states have been described such as early phagosome, late phagosome and phagolysosome (Levin, Grinstein et al. 2016). The early phagosome is formed after scission with the plasma membrane. After particle internalization, the phagosome undergoes a series of fusion events to incorporate new material required for its maturation. One of the crucial events is the recruitment and the activation of the small GTPase Rab5 that mediates early fusion events (Roberts, Barbieri et al. 2000). This activation is dependent on its GEFs such as the small GTPase Rab22a that activates Rab5 through the recruitment of the Rab5 GEF Rabex-5. GTP-bound active Rab5 form directly recruits the Vps34 to generate PtdIns3P that is highly enriched at the early phagosome membrane. PtdIns3P and Vps34 activity are strictly required for phagosome maturation, early endosomal antigen-1 (EEA-1) recruitment to the phagosome membrane, a protein important for promoting fusion by docking target membranes and interacting with the fusion-mediating SNAREs Syntaxin 6 and Syntaxin 13 (Vieira, Botelho et al. 2001). At the early phagosome step, some of the phagosome components are not targeted to degradation and are recycled to the plasma membrane or the TGN through the retrograde protein transport. Proteins associated to recycling compartments have been detected such the vesicle-associated membrane protein 3 (VAMP-3) or the transferrin receptor. Rab11 and Rab4 mediate the recycling events in the case of slow recycling and fast recycling, respectively. Both these small GTPases have been detected in early phagosome preparations, paralleling the endosome formation and maturation. The retrograde traffic of phagosome material to the TGN occurs through tubule-vesicular structures that are dependent for their formation on SNXs. SNXs are recruited in a PtdIns-3P dependent fashion through their PX domain whereas their BAR

domains are involved in the tubulation and vesiculation processes (Levin, Grinstein et al. 2016). The transition from early-to-late phagosome requires the fusion of the early phagosome with late endosomes, that is an acidic low-pH compartment due to the presence of the proton-pumping V-ATPase complexes. This transition is strictly dependent on an exchange of Rab5 with Rab7 that is thought to be mediated by the Mon1-Mcz1 GEF (Levin, Grinstein et al. 2016). Moreover, this exchange is associated with the CORVET/HOPS complex switch. At the late phagosome stage, retrograde protein transport from the phagosome to the TGN can also occur and involves the retromer complex, initially recruited by PtdIns3P to the early phagosome and a trimer of Vps26-Vps29-Vps35 that associates with active Rab7 (Levin, Grinstein et al. 2016). During the transition early-to-late phagosome, hydrolysis of PtdIns3P triggers the recruitment of PtdIns4P, a lipid marker of the late phagosome by the Phosphatidylinositol 4-Kinase Type 2 Alpha (PI4K2A) kinase. Phagolysosome biogenesis is dependent on Rab7 and some SNARE proteins including VAMP7, Syntaxins 7 and 8. The phagolysosome is a highly degradative microenvironment due to the low pH, the oxidative components and the presence of lytic enzymes (Levin, Grinstein et al. 2016). Regarding the phagocyte cell type as well as the nature of the particle, striking variations have been observed for the pH of phagolysosomes. Production of phagolysosomal reactive oxygen species is highly dependent on the NOX2 oxidase protein, a member of the NADPH oxidase family. NOX2 transfers electrons from the cytosolic NADPH to the intraluminal O<sub>2</sub> molecule to generate superoxide, a microbicidal compound. NOX2 oxidase is a multimeric protein that is formed under inflammatory conditions and is progressively incorporated at the phagosome membranes, yet it is only active in the phagolysosomes, in macrophages and neutrophils (Nunes, Demaurex et al. 2013).

### **Phagosome termination or resolution**

Phagosome resolution is the ultimate but facultative step of the phagocytosis. Generally, phagosome cargo is fully degraded but the products of this breakdown have to be proceeded in order to allow the phagocyte to return to the homeostatic state. During the phagosome resolution, nucleic acids are digested by the DNase-II enzyme, proteins are degraded by proteases such as the cathepsins, and aminoacids are presumably translocated to the cytosol through a mTORC1 dependent manner. Lipids and cholesterol are also degraded by various hydrolases or lipase proteins (Levin, Grinstein et al. 2016).

### **Chapter 3. Antigenic material internalized is processed into peptides that will be presented to T lymphocytes after loading onto MHC molecules**

Antigen presentation is a complex and dynamic process that can be divided into three main successive steps: antigen uptake, antigen degradation into antigenic peptides and peptide loading onto MHC-I or MHC-II molecules. As mentioned before in this introduction, antigen presentation is a *sine qua non* condition to activate CD4<sup>+</sup> and CD8<sup>+</sup> T cell responses since T cells activate when their TcR antigen receptor binds to the specific complex MHC-II-peptide or MHC-I-peptide, respectively. Initially, two antigen presentation pathways have been identified and characterized, depending on the origin of antigen and consequently the T cell subtype that is stimulated. Intracellular-residing antigens are degraded into peptides that are loaded on MHC-I molecules and are recognized only by CD8<sup>+</sup> T lymphocytes whereas extracellular antigens are degraded after internalization in peptides suitable for MHC-II molecules that are required for CD4<sup>+</sup> T cell activation. However, restricting antigen presentation pathways to a strict dichotomy does not solve a major issue: how a fraction of antigen presenting cells are capable of stimulating naïve CD8<sup>+</sup> T lymphocytes that are specific from exogenous antigen? This question has only been recently solved with the demonstration of the occurrence of this process, referred to as antigen cross-presentation, and the characterization of various related intracellular pathways. The outcomes of cross-presentation are tolerance (cross-tolerance) or productive activation (cross-priming) and depend on antigen presenting cell types, maturation state of antigen presenting cells and on the local environment. Almost all the current literature points out the role of dendritic cells in cross-tolerance and cross-priming. I will describe in details and successively the current state of the art about the structure of MHC molecules and how the MHC-I and MHC-II ligands are generated through the MHC-I direct antigen presentation, the MHC-II antigen presentation and the MHC-I antigen cross-presentation.

### 1) classic direct MHC-I antigen presentation

#### Origin of antigenic peptides for MHC-I

*Physiological protein turnover.* Protein degradation physiologically occurs in two different organelles that are the cytosol and the lysosomes. However, the vast majority of MHC-I ligands are produced by the cytosolic proteolysis that allows for the degradation of both cytosolic and nuclear proteins as well as membrane and secreted proteins addressed to the ER-associated degradation (ERAD) pathway from the ER (Ciechanover 2005). Importantly, not only cellular aging proteins but also viral proteins synthesized by cellular ribosomes employ cytosolic proteolysis. If the source of antigenic peptides depends only on the physiological protein turn-over, the rate of ligand production should be related to protein

abundance and half-life (van Endert 2016). This model is supported by several reports (Farfan-Arribas, Stern et al. 2012, Rock, Farfan-Arribas et al. 2014).

Ribosomal translation. Next to the physiological protein turnover, recent studies have documented the presence of a second source for MHC-I ligands production, which would provide ligands for MHC-I faster than proteolysis (Yewdell 2011). Reducing the ribosomal translation or blocking the proteasome cytosolic degradation result in an unexpected fast arrest of production of new peptide-MHC-I complexes (Reits, Vos et al. 2000). The nature of Defective Ribosomal products (DRiPs) is thought to be diverse compiling protein misfolding, failed assembly of protein complexes, premature protein termination or nonstandard translation. In this model, the rate of MHC-I ligands is predicted by the rate of messenger ribonucleic acid (RNA (mRNA)) translation and not the protein abundance and half-life (van Endert 2016). The postulate of the DRiPs model is that non-functional products of RNA translation are a major source for MC-I ligands. In recent studies using dynamic mass spectrometric quantification of ligand production, vaccinia virus-encoded MHC-I ligands occurred in the same time as protein neo-synthesis and was not correlated with protein abundance, supporting the role of DRiPs as MHC-I ligands. However, mature proteins were also detected (Croft, Smith et al. 2013).

### **Antigen processing for MHC-I ligands**

Production of ligands for MHC-I ligands mainly involves a pathway that starts with the protein cleavage by the cytosolic proteasome complexes followed by additional processing by various exopeptidases. The proteasome is the principal cytosolic protease in eukaryote cells and responsible for a large part of the cellular protein turnover.

Proteasomes. The proteasome complexes are assemblies of a core catalytic particle associated with regulatory cap particles, each component being named by its sedimentation coefficient. The 20S core particle is made of four stacked heptameric rings, with two outer rings of  $\alpha$  and two inner rings of  $\beta$  subunits enclosing a sequestered axial channel where proteolytic cleavage occurs (Goldberg 2007). Unfolded protein substrates enter activated 20S particles through gates at the end of the cylinder for processive degradation by three distinct catalytic subunits. Together with the regulatory 19S particles, the 20S particles form the 26S complex, which is the major form of proteasome. The 19S particle includes several ATPases that recognize the unfolded substrates and open the 20S gate, allowing substrates to enter into the cylinder. The 19S particle can be replaced by another regulatory particle, the 11S particle,

which is induced by the cell exposure to IFN- $\gamma$ . This alternative complex enhances the proteolytic generation of antigenic peptides suitable for loading onto MHC-I molecules. To favor their degradation by the 26S complex, the protein substrates have to be tagged with multiple ubiquitins that mainly and covalently attach the target substrates by binding to the C-terminus glycine and lysine residues. The three catalytic beta-subunits,  $\beta 1$ ,  $\beta 2$ ,  $\beta 5$  have caspase-like (cleavage after Asp and Glu), trypsin-like (Arg, Lys) and chymotrypsin-like (Leu, Ile, Tyr, Phe) specificities, respectively (van Endert 2016). Two alternative proteasomes have been identified. The thymoproteasome is selectively expressed in thymic epithelial cells and drives the positive selection of CD8<sup>+</sup> T lymphocytes (Takahama, Takada et al. 2012). This proteasome variant exhibits a single catalytic unit with chymotrypsin-like activity. The immunoproteasome variant is expressed in professional antigen presenting cells (dendritic cells, macrophages, B cells) and is recruited under inflammatory environment; exposure to TNF- $\alpha$  or IFN- $\gamma$  promotes the expression of immunoproteasome specifically in the professional antigen presenting cell (Kruger and Kloetzel 2012). The catalytic subunits  $\beta 1i$ ,  $\beta 2i$ ,  $\beta 5i$  display no caspase-like activity. The relevance of these variants has been demonstrated by different studies: the group of B. Van den Eynde has noticed that some epitopes are exclusively produced by one variant specifically whereas some epitopes are preferentially (but not selectively), resulting in differences in T cell responses (Vigneron and Van den Eynde 2012). Examination of the proteasome function in the generation of antigenic peptides suitable for MHC-I molecules has been mainly achieved by the use of efficient inhibitors. Supporting a critical role for the proteasome activity in generating MHC-I ligands, incubating cell lines with epoxomicin or MG132 leads to a massive decrease of MHC-I expression at the cell surface and to the inhibition of peptide presentation by MHC-I (Rock, Gramm et al. 1994, van Endert 2016). Interestingly not all the MHC-I allomorphs and MHC-I epitopes are affected by the inhibition of proteasome activity, suggesting the presence of alternative cytosolic proteases to process MHC-I ligands (Saveanu, Fruci et al. 2002). Among the candidates, tripeptidyl-peptidase II and the insulin-degrading enzyme (IDE) have been proposed (Seifert, Maranon et al. 2003, Parmentier, Stroobant et al. 2010). Altogether, examination of the proteasome function has revealed its predominant role in the generation of antigenic peptides for the loading into MHC-I molecules, with an eventual non-redundant role for alternative cytosolic proteases. In any case, products generated by the proteasome are peptides with a length ranging 2-25 residues and are mainly not suitable for a direct loading on MHC-I molecules, since the target length is expected to be 8-10 residues (Kisselev,

Akopian et al. 1999). Consequently, proteasome products have to be additionally trimmed from their N-terminal residues. This work is achieved by cytosolic exopeptidases and ER aminopeptidases.

*Cytosolic exopeptidases.* In the cytosol, exopeptidases involved in the digestion of proteasome products complement their action one to each other, as they usually display specific affinities depending on the substrate length. Consequently, tripeptidyl-peptidase II preferentially degrades peptides longer than 15 residues (Reits, Neijssen et al. 2004), whereas cytosolic aminopeptidases such as leucine aminopeptidase, bleomycin hydrolase or puromycin-sensitive aminopeptidase remove any N-terminal residue from the peptides (Saveanu, Fruci et al. 2002). All these peptidases have been identified as potential but marginal actors in the generation of MHC-I ligands. However, cytosolic peptidases usually generate single amino acid residues and only in rare cases precursors of MHC-I ligands (van Endert 2016).

### **TAP transport and ER aminopeptidases**

The precursors of MHC-I epitopes generated in the cytosol enter into the ER through active transporters, the transporters associated with antigen processing (TAP). TAP is a dimeric transporter protein mainly found in the ER membrane and is composed of two subunits, TAP1 and TAP2 that are highly homologous. Each subunit displays six helices in the C-terminal part required for transporter activity, and four helices in the N-terminus required to interact with the peptide loaded complex (Abele and Tampe 2011). The TAP dimers have been demonstrated to prefer substrates with a length ranging from 8-16 residues and the selection among the candidates is decided by the affinity for the three N-terminal residues and the first C-terminal residue, with a preference for hydrophobic C-terminal residues (Gubler, Daniel et al. 1998). In the ER, additional trimming can be performed by ER resident aminopeptidases (ERAP), including ERAP1 (Saric, Chang et al. 2002, Serwold, Gonzalez et al. 2002), present in both human and mouse (also referred to as ERAAP in mouse) and ERAP2 (Saveanu, Carroll et al. 2005), selectively expressed in human. ERAP1 displays a preference for substrates with a length of 9-16 residues (Chang, Momburg et al. 2005). The important role of ERAP is demonstrated by the decreased MHC-I levels at the surface of cells lacking ERAP1 expression (Hammer, Gonzalez et al. 2007). In humans, both ERAP1 and ERAP2 are up-regulated in the presence of IFN- $\gamma$ , they display preferences for hydrophobic and positively charged residues and can form dimers, with an enhanced trimming activity (Evnouchidou, Weimershaus et al. 2014). Supporting a defective trimming activity required for generating

peptides with the target length for loading onto MHC-I molecules, the quantities of longer peptides have been found to be increased by a 3-fold factor when examining ERAAP deficient splenocytes (Blanchard, Kanaseki et al. 2010). The relevance of the role of ERAPs *in vivo* has been verified in the context of *Toxoplasma gondii* infection. Indeed, a single MHC-I epitope has been shown to promote the protection against this pathogen and in addition to require aminoterminal trimming by ERAPs. Supporting these findings, infection of ERAAP<sup>-/-</sup> mice resulted in a lack of protection and in animal death because of the impaired activation of adaptive cellular immunity (Blanchard, Gonzalez et al. 2008). The presence of alternative processing mechanisms is supported by the fact that patients suffering from TAP-deficiency do not fail in controlling viral infections. Prompted by this original observation, several groups have investigated the existence of TAP-independent pathways and a TAP-independent repertoire has been identified (Abele and Tampe 2011, Del Val, Lazaro et al. 2013, Oliveira, Sluijter et al. 2014). Among candidates, several compartments and pathways, including golgi and autophagic or endocytic pathways have been suggested. However, the mechanisms involved remain poorly elucidated.

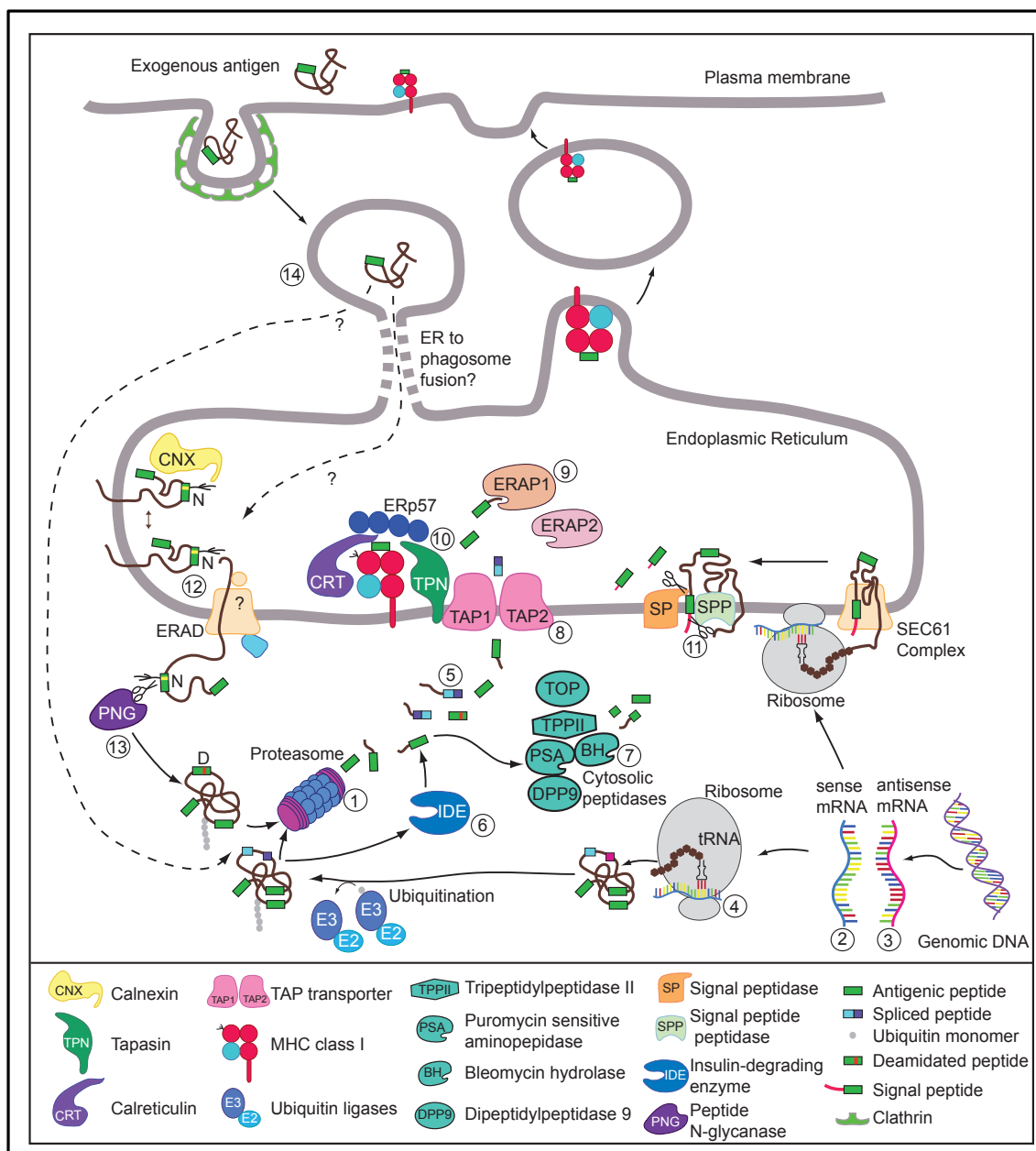


**Figure 14. MHC-I endogenous (classical) antigen presentation (derived from (van Endert 2016))**

### Peptide loading onto MHC-I molecules in the endoplasmic reticulum

Newly synthesized MHC-I molecules in the ER are stabilized into the ER by a specific complex that also drives the loading of peptides onto the MHC-I molecules, the peptide loading complex (Hulpke and Tampe 2013). After *de novo* synthesis, heavy chains are translocated to the ER and first encounter the chaperones Binding Immunoglobulin Protein and calnexin. On  $\beta$ 2-microglobulin association, calnexin is replaced by calreticulin, a chaperone which connects TAP with the remaining peptide loading complex elements to form a complex that catalyzes MHC-I recognition, translocation and loading with high-affinity



ligands (Chapman and Williams 2010). This preassembled sub-complex docks to the TAP/tapasin/ERp57 complex to form the loading-competent active peptide loading complex. By this spatial organization, TAP supplies for the MHC-I ligands and provides the proximity of MHC-I ligands by the recruitment of tapasin (Momburg and Tan 2002). Additionally, tapasin proof-reads the peptide-MHC-I complexes and thereby catalyzes the peptide exchange in favor of peptides with high affinities (Chen and Bouvier 2007, Sieker, Straatsma et al. 2008, Wearsch, Peaper et al. 2011). When stable complexes are formed, they are released from the peptide loading complex before their export to the plasma membrane through the secretory pathway. If a suboptimal peptide was loaded, a re-glycosylation and peptide exchange takes place (Zhang, Wearsch et al. 2011). The contribution of the different components of the peptide loaded complex is supported by the examination of the consequences on MHC-I molecules in deficient-cells. Tapasin-deficient cells exhibit a significant reduction in MHC-I surface levels because of their reduced stability (Grande, Golovina et al. 2000). Consequently, tapasin has been suggested to regulate the quality control of MHC-I molecules that traffic from the ER to the Golgi (Momburg and Tan 2002). ERp57 protein is covalently bound to tapasin through disulfide bonds between the two proteins (Dick and Cresswell 2002). ERp57-deficient cells exhibit a reduction in the formation of the peptide loading complex and a decrease in surface MHC-I expression (Garbi, Hammerling et al. 2007). The calreticulin deficient-fibroblasts exhibit reduced peptide loading and cell surface expression of MHC-I molecules, in part due to an impairment in quality control (Gao, Adhikari et al. 2002).

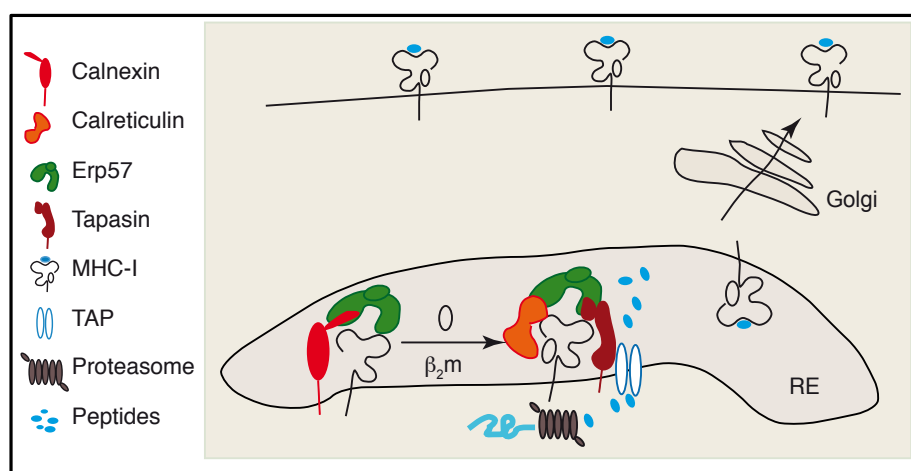


**Figure 15. The peptide loading complex dynamic (derived from (Adiko, Babdor et al. 2015))**

## 2) MHC-II antigen presentation

The distribution of MHC-II molecules strikingly differs from MHC-I and is selectively restricted to professional antigen presenting cells, including B lymphocytes, dendritic cells and macrophages (Watts 1997) under homeostatic conditions; MHC-II is also expressed in cortical and medullary thymic epithelial cells and contributes to the positive and negative CD4<sup>+</sup> T cells selections (Fukui, Ishimoto et al. 1997). In particular circumstances, upon inflammation for instance, MHC-II expression can be induced in other cell types, such as epithelium or endothelium. MHC-II antigen presentation engages peptides in endosomes and lysosomes and provides a read-out of protein antigens that enter that pathway, whatever they derive from exogenous pathogens internalized by phagocytosis or endocytosis or from self-antigens that have gained access to the pathway. I will review the processing of MHC-II ligands in the endocytic pathway and their loading onto MHC-II molecules.

### Processing of MHC-II ligands

Processing of MHC-II ligands requires the digestion of protein antigens by the action of endosomal and lysosomal proteases. Among the candidates, the cathepsin family plays a crucial role. The cysteine protease cathepsins B, C, F, H, K, L, V, W and X as well as the aspartic endoprotease cathepsin D (Lautwein, Kraus et al. 2004), are active after the removal of the amino-terminal pro-domain, which occurs by auto-catalytic mechanism with the pH acidification during endosome maturation or by the action of additional proteases (Zavasnik-Bergant and Turk 2007, van Kasteren and Overkleeft 2014). Importantly, the cathepsin family displays a complementary activity, with carboxy-exopeptidases (cathepsins B and X), amino-exopeptidases (cathepsins C and H) and endopeptidases (other cathepsins among the above mentioned) (Zavasnik-Bergant and Turk 2007, van Kasteren and Overkleeft 2014). These cathepsins are expressed in professional antigen presenting cells, with gradual distribution and activities during the course of endosome maturation. Starting from the beginning of the endocytic pathway, cathepsins B and X are mainly found in the early endosomes, a weak acidic compartment that favors their activities (Lautwein, Burster et al. 2002, Lennon-Dumenil, Bakker et al. 2002, Lennon-Dumenil, Bakker et al. 2002). Cathepsin S is enriched in endolysosomes whereas cathepsin D is predominantly found in lysosomes, consistent with their *in vitro*-determined pH ranges of activities (Lautwein, Burster et al. 2002, Lennon-Dumenil, Bakker et al. 2002, Lennon-Dumenil, Bakker et al. 2002). Unexpectedly, while cathepsins B, C, H and X exhibit amino-peptidase or carboxy-peptidase activity that promotes the breakdown of precursor MHC-II ligands *in vitro*, testing the relevance of these proteases

*in vivo* reveals a dispensable role for most of these cathepsins in generating MHC-II ligands, presumably because of a redundant activity (Riese and Chapman 2000). Two exceptions have been however identified with the cathepsins L and S. Cathepsin L is mainly involved in the thymic T cell selection, by processing the invariant chain (Ii) and epitopes for T cell selection. Cathepsin S displays similar roles in the periphery (Riese and Chapman 2000, Pluger, Boes et al. 2002). However, it is difficult to directly assess the role of both cathepsins in the direct processing of MHC-II ligands since they also contribute to the processing of Ii, an important chaperone for peptide loading onto MHC-II molecules (Nakagawa, Roth et al. 1998, Shi, Villadangos et al. 1999). Finally, the role of cathepsin D *in vivo* is controversial and might affect the generation of a specific range of MHC-II epitopes (Koike, Nakanishi et al. 2000, Moss, Villadangos et al. 2005). Another protease has also been involved in the generation of MHC-II ligands, the asparagine endopeptidase, a caspase-related enzyme that has a specific trimming activity after asparagine residues. Asparagine endopeptidase contributes to the generation of MHC-II ligands both *in vitro* and *in vivo*. Indeed, the tetanus toxin C fragment, a model antigen, depends exclusively on asparagine endopeptidase for its processing *in vitro* (Manoury, Hewitt et al. 1998). However, the reduction in MHC-II presentation of this model antigen was only partially reduced *in vivo*, suggesting the use of alternative proteases (Matthews, Werber et al. 2010). Interestingly, asparagine endopeptidase displays a dual role in the generation of MHC-II ligands, since the enzyme drives the destruction of the myelin basic protein, another model antigen (Beck, Schwarz et al. 2001, Burster, Beck et al. 2004). Finally, in the context of disulphide bonded antigens, an additional enzyme promotes the generation of MHC-II ligands derived from soluble, tumor or auto-antigens, the gamma-interferon inducible lysosomal thiol reductase enzyme (GILT) (Maric, Arunachalam et al. 2001, Bergman, Marta et al. 2012). As previously mentioned, the activity of endosomal and lysosomal proteases is mainly influenced by the pH of a given compartment. In the recent years, several molecular factors have been involved in the regulation of pH in the endocytic pathway, yet the precise relative contribution of these candidates remains to be elucidated since they may be inter-related one to each other. For example, the NADPH oxidase complex, by regulating the ROS production and the pH, is involved in the generation of MHC-II ligands as assessed by the examination of antigen presentation by cells derived from patients with mutation in the subunits of the NADPH complex (Crotzer, Matute et al. 2012). The activation of TFEB, a crucial regulator of lysosome biogenesis and function (Sardiello, Palmieri et al. 2009), has been very recently identified by the group of P. Cresswell to activate the MHC-II antigen presentation, by promoting lysosome fusion with the plasma membrane

and increasing MHC-II expression levels as well as by increasing the acidification of endolysosomes (Samie and Cresswell 2015).

### **MHC-II origin and loading with ligands**

The class II  $\alpha$  and  $\beta$  chains are synthesized in the endoplasmic reticulum where they associate under the form of three  $\alpha\beta$  dimers together with a trimer of a chaperone protein, Ii. This association results in a complex that prevents premature binding of peptides (Landsverk, Bakke et al. 2009). Importantly, the Ii chaperone drives the correct folding of MHC  $\alpha\beta$  dimers to prevent their early degradation. This complex exits from the ER to the golgi apparatus before its final sorting to the endolysosome compartment (Watts 2004, Landsverk, Bakke et al. 2009). Resident aspartic and cysteine proteases, including the cathepsins S and L, digest the Ii molecules with the exception of a small protein of 24 residues that remains bind to the MHC-II  $\alpha\beta$  chain complex, the class-II-associated invariant chain peptide (CLIP). In parallel time within the same structures, antigens are digested by the same sets of resident proteases. In lysosomes,  $\alpha\beta$ -CLIP complex interacts with another class-II related  $\alpha\beta$  dimer, the H2-M in mouse or HLA-DM in human, resulting in the detachment of the CLIP fragment (Denzin and Cresswell 1995, Kropshofer, Vogt et al. 1996). Peptides present in this compartment can bind the MHC-II-binding pocket, before the export of the complex to the cell surface. The specialized compartment where the CLIP fragment detaches and is replaced by peptides is the MHC-II complex loading compartment, often referred to as MIIC (Peters, Neefjes et al. 1991). An alternative source of MHC-II molecules for MHC-II presentation is the MHC-II  $\alpha\beta$  dimers that recycle back from the plasma membrane to the early endosomes, and that can bind new peptides in a Ii and DM-independent manner (Rock and Goldberg 1999). The export of peptides-loaded MHC-II molecules involved a specific microtubule-dependent lysosomal tubular network (Jordens, Fernandez-Borja et al. 2001, Kleijmeer, Ramm et al. 2001). A recent report has identified a new mechanism that enhances MHC-II presentation for phagocytosed antigens: a late-onset phagosomal microtubule-dependent tubular structure is formed during phagocytosis. This intriguing structure is not involved in the delivery of phagosomal material to the plasma membrane such as the MHC-II/peptide complexes but rather in the material exchange from various phagosomal structures, in a TLR-dependent and MyD88-dependent manner. This results in an increased antigen presentation and CD4+ T cell activation (Mantegazza, Zajac et al. 2014).

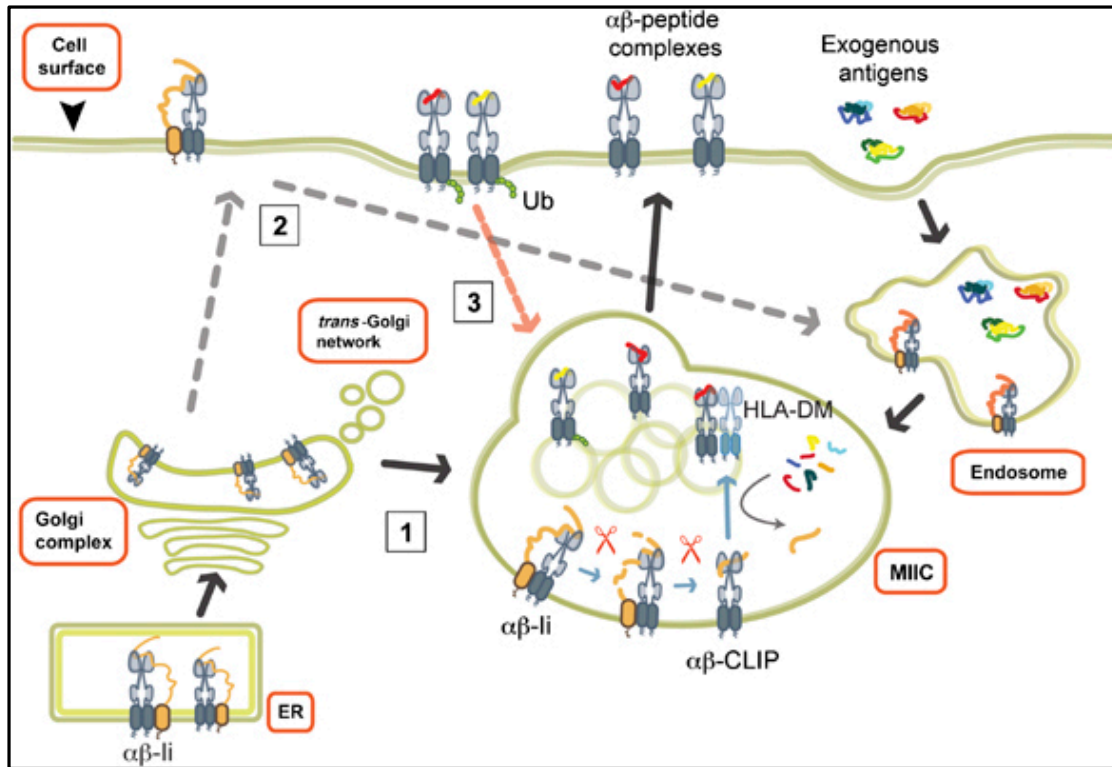


**Figure 16. MHC-II antigen presentation (derived from (Rocha and Neefjes 2008))**

### 3) MHC-I antigen cross-presentation

#### Cytosolic pathway

Cytosolic pathway for antigen cross-presentation has been the most studied pathway in dendritic cells and is defined as a proteasome-dependent or sensitive pathway (Joffre, Segura et al. 2012). As previously mentioned in this introduction, proteasome complex is mainly found in the cytosol. Therefore, and contrasting with classical MHC-II antigen presentation pathway the intact or pre-processed antigen has to shuttle from the endosomal or phagosomal compartment to the cytosol to be degraded by the proteasome (Kovacs-Bankowski and Rock 1995). *What is the evidence level for phagosome to cytosol export during cross-presentation?* Experimental evidence for antigen export to the cytosol has been collected from various independent studies that mostly used reporter assays. The first evidence was provided by the observation that after the phagocytosis of a latex bead coated with a ribosome inactivating toxin (Kovacs-Bankowski and Rock 1995), the protein synthesis was abolished in the phagocytes, indirectly suggesting a phagosome-to-cytosol export. Using horseradish peroxidase (HRP)-dextran or fluorescein isothiocyanate (FITC)-dextran Norbury et al. demonstrated that macropinocytosed antigens gain access to the cytosol in macrophages and dendritic cells differentiated from murine bone marrow progenitors

(Norbury, Hewlett et al. 1995, Norbury, Chambers et al. 1997). The observations by the group of S. Amigorena of a size-dependent transport pathway for internalized model antigens to the cytosol that is only present in dendritic cells but not macrophages allowed him to propose the existence of an active and dendritic cell specific transporter that remained to be identified (Rodriguez, Regnault et al. 1999). The group of J. Villadangos compared the capacity of cDC1 and cDC2 mouse subsets in transporting phagocytosed antigens from the phagosome to the cytosol: by incubating *in vitro* conventional dendritic cell subsets purified from the mouse spleen with equine cytochrome c, a known inducer of apoptotic peptidase activating factor 1-mediated cell death when it is present in the cytosol, a significant higher mortality in cDC1 subset compared to pDCs or cDC2 subset was observed (Lin, Zhan et al. 2008). Systemic infusion of mice with equine cytochrome c selectively depleted cDC1 subset. However, using a  $\beta$ -lactamase assay the group of S. Amigorena demonstrated that human conventional dendritic cell subsets equally transfer antigen from the phagosome to the cytosol, but not pDCs and macrophages (Segura, Durand et al. 2013). *What are the proposed mechanisms for phagosome-to-cytosol export during cross-presentation?* The group of P. Creswell was the first to suggest a role for the machinery usually involved in the ERAD pathway, including the ERAD proteins Derlin-1, Sec61 and p97 (Ackerman, Giodini et al. 2006). The role of such proteins is also supported by the groups of S. Amigorena and C. Kurts that respectively showed that Sec22b is involved in the recruitment of proteins from the ER to the phagosomes (Cebrian, Visentin et al. 2011) and that the Mannose Receptor might play a role in this process (Burgdorf, Lukacs-Kornek et al. 2006, Burgdorf, Schuette et al. 2010). A very recent work from the group of S. Burgdorf recently demonstrated that Sec61 is an antigen transport channel required for cross-presentation *in vitro* and *in vivo* in cDC1 mouse subset; in this publication, the authors suggest that the recruitment of Sec61 is dependent on the secretory pathway (Zehner, Marschall et al. 2015). However, in a commentary on F1000 (<http://f1000.com/prime/725499865>), Karin Romisch challenged the conclusions made by the authors arguing that the fusion protein system used by the authors is not suitable for tracking the recruitment of Sec61 channels to the phagosomes by the secretory pathway. In addition, she underlines that due to the presence of cholesterol-rich membranes in endosomes, the Sec61 translocon should not be active in these compartments (Nilsson, Ohvo-Rekila et al. 2001). She also discusses an alternative mechanism to explain the recruitment of Sec61 to the phagosomes, by the transient connections formed between ER and phagosomes through the “kiss-and-run” mechanism (Ackerman, Giodini et al. 2006). Further experimental work is consequently required to further conclude how Sec61 is recruited to the phagosome to

mediate the phagosome-to-cytosol export. Altogether, the literature about the cytosolic pathway converges towards the concept that active export of antigenic materials to the cytosol is one of the key feature that contributes to the excellence of dendritic cells in cross-presenting exogenous antigens. Alternative “passive” mechanisms have been documented in the context of bacterial infection: toxins secreted by the bacteria might trigger pore formation and allow for phagosome material escape to the cytosol, before pathogen is destroyed by lysosomal pH and proteases. *What are the routes of antigenic peptides after proteasome digestion during cross-presentation?* Because proteasome generates longer peptides than 8-10 residues that is the suitable size for loading onto MHC-I molecules, additional processing is further required by accessory peptidases that are mainly located in the cytosol, in the ER or in the endosome or phagosome. While the first above described steps are common in the different cytosolic pathways, diverging routes for completing the digestion of proteasome products have led to the description of the different models currently published in the literature. The first cytosolic pathway historically characterized parallels the classical endogenous direct MHC-I presentation: proteasome products gain access to the ER lumen through an active TAP-dependent transport during cross presentation, where the final processing by ERAP enzymes and the loading of antigenic peptides on MHC-I molecules occur, before the export at the cell surface of complexes through the secretory pathway (Firat, Saveanu et al. 2007). In other models, proteasome products re-enter into phagosomes (Guermontprez, Saveanu et al. 2003) or endosomes (Burgdorf, Scholz et al. 2008, Saveanu, Carroll et al. 2009) by a retro-transporter, for final trimming and peptide-loading on empty MHC-I molecules. One of the main proposed retro-transport model postulates that after proteasome digestion, peptides can re-enter into the phagosomes (Guermontprez, Saveanu et al. 2003). In this model, a prerequisite is that ER and phagosome membranes fusion to fuel the phagosomes with the ER peptide loading machinery. Existence of connections between ER and phagosomes is supported by the presence of ER-resident proteins in dendritic cell phagosomes, especially the peptide loading complex proteins. Fusion events during phagosomal maturation have been reported first by the group of M. Desjardins mostly using proteomic studies in macrophage (Gagnon, Duclos et al. 2002) but this work was challenged by an independent study (Touret, Paroutis et al. 2005) from the group of S. Grinstein few years later. However, the latter experimental work cannot totally exclude the existence of selective transition of ER membrane proteins to the endophagosomal membrane. Since these two reports additional works from other groups have given numerous evidence to support the model of fusion between ER and phagosome membranes. For instance, the group of P.

Cresswell observed that a ER-restricted phenomenon, the N-glycosylation of a peptide attached to a synthetic bead can occur without the export of the bead from the phagosome, indirectly suggesting that ER-phagosome membrane fusion have occurred (Ackerman, Giodini et al. 2006). Furthermore, the group of S. Amigorena recently proposed the SNARE Sec22b as a critical actor in recruiting a specific cargo of ER proteins to phagosomes in dendritic cells. Depleting dendritic cells from Sec22b inhibited cross-presentation of phagocytosed antigen but not endogenous MHC-I or MHC-II antigen presentation. They showed by elegant and biochemical analysis that phagosome maturation was impaired and accelerated, promoting the premature degradation of antigenic peptides; phagosome preparations were deprived from ER proteins; antigen exit to the cytosol was inhibited (Cebrian, Visentin et al. 2011). A rapid transfer between parasite vacuole and host ER has been reported in *Toxoplasma gondii*-infected cells, where the parasitophorous vacuole fuses not with endosomes, lysosomes, or phagosomes but with adjacent ER so that there is an open connection between the two. Thus, antigens can diffuse into the ER and access Sec61 channels embedded in the ER membrane (Goldszmid, Coppens et al. 2009). In phagosomes, no stable connections to the ER were observed, but the group of P. Cresswell reported transient connections and suggested a “kiss-and-run” mechanism (Ackerman, Giodini et al. 2006). *What is the contribution of endosomes during MHC-I cross-presentation?* The endocytic pathway is thought to contribute to cross-presentation by several complementary processes: 1) the endosomes are a compartment where cross-presentation directly occurs; 2) the endosomes regulate cross-presentation by delivering critical tools to degrade or prevent the premature degradation of MHC-I ligands; 3) a specific class of endosomes may regulate the maturation of phagosomal and endosomal compartments where cross-presentation occurs. Most of the antigens are internalized through micropinocytosis and phagocytosis, yet internalization can occur through endocytosis as this is the case for artificial settings that use soluble proteins or experimental systems, in which antigens are fused with specific antibodies targeted to receptors preferentially expressed by the desired antigen presenting cell type. The use of antigen-antibody systems that allow for antigen targeting to a specific receptor is mostly an artificial way to promote the access of antigens to the endocytic pathway, through receptor-mediated endocytosis. Several groups, including our group, have developed distinct strategies to couple the model antigen to specific antibodies and to develop vaccine strategies (Kratzer, Mauvais et al. 2010). All these studies demonstrated that antigen targeting to receptors is a very efficient way to activate naïve CD8<sup>+</sup> T cells by cross-priming (Bonifaz, Bonnyay et al. 2002, Bonifaz, Bonnyay et al. 2004, Bozzacco, Trumpfheller et al. 2007,



Kratzer, Mauvais et al. 2010). However, an efficient cross-presentation has been mainly observed when the antigen is targeted to a receptor mostly expressed by the cross-presenting cDC1 subset. Consistent with this, the groups of R.M. Steinman and M. Nussenzweig have reported that antigen targeting to the dendritic and epithelial cells, 205 kDa (DEC-205) C-type lectin receptor resulted in an efficient activation of CD8+ T cells *in vivo*, compared to the dendritic cell inhibitor receptor 2 (DCIR2) receptor, mostly found in the cDC2 subset (Dudziak, Kamphorst et al. 2007). One possible explanation would be that this effect is mediated by the cell type; however, an alternative hypothesis would be that the antigen gain access to different endocytic compartments depending on the receptor targeted. To discriminate between the two, the group of M.C. Nussenzweig has forced the expression of the human DEC-205 receptor on both the cDC1 and cDC2 subsets and analyzed the cross-presentation capacity of these two subsets upon antigen targeting to human DEC-205. Interestingly, the authors unexpectedly observed an efficient cross-presentation by the two subsets of dendritic cells, and within the cDC2 subset they demonstrated that DEC-205 targeting was more efficient than DCIR2 targeting (Kamphorst, Guermonprez et al. 2010). Such results were confirmed in a more physiological setting, using immune complexes infused *in vivo*, a setting that mediates the antigen endocytosis through FcγRs (den Haan and Bevan 2002). Consequently, it is admitted that the receptor and the subsequent internalization of antigen dictates the cross-presentation capacity. An elegant study from the group of C. Kurts has identified an unsuspected contribution of endosomes in the cross-presentation of the model antigen OVA. Focusing on the endocytosed OVA form, the authors observed that the model antigen was found in a mannose receptor-expressing early endosomal compartment and that the expression of mannose receptor was required for the OVA uptake. In addition, they made the original and elegant observation that the mannose receptor-expressing endosomes were also a MHC-I loading compartment in a TAP-dependent manner. Supporting the original mechanism, this compartment fused less with lysosomes, and cross-presentation was proteasome-sensitive (Burgdorf, Scholz et al. 2008).

In the current opinion, essentially based on observations made from the examination of cross-presenting dendritic cells, one of the hallmarks of cross-presentation is the relatively poor endolysosomal proteolytic activities compared with other phagocytes. An indirect evidence is the relatively low amount of lysosomal proteases in *ex vivo* purified dendritic cells that correlates with the antigen-cross presentation capacity of mouse and human conventional dendritic cell subsets (Dudziak, Kamphorst et al. 2007, Cohn, Chatterjee et al. 2013). Beside

the amount of proteases, the pH within the endocytic pathway independently influences the cross-presentation capacity of conventional dendritic cells, since the use of pharmacological inhibitors of pH acidification or of proteases enhances the cross-presentation by the cDC2 subset (Trombetta, Ebersold et al. 2003, Accapezzato, Visco et al. 2005, Chatterjee, Smed-Sorensen et al. 2012, Garulli, Di Mario et al. 2013). How these two parameters are regulated in cross-presenting dendritic cells have started to be recently addressed: the low levels of activity of the V-ATPase and high levels of NOX2 have been identified in both endosomes and phagosomes to be a feature of cross-presenting dendritic cells, resulting in a strikingly decreased level of activation of pH-sensitive proteases (Joffre, Segura et al. 2012). Furthermore, the group of S. Amigorena has identified how the NOX2 gains access to the maturing phagosomes: under homeostatic conditions, NOX2 is mainly found in a particular secretory lysosome compartment, and the fusion during phagocytosis with the maturing phagosomes is under the control of the small GTPase Rab27a (Jancic, Savina et al. 2007).

A complementary role for endosomes has been identified by two studies from my host laboratory. In the first study, my laboratory has investigated the role of the insulin-regulated aminopeptidase (IRAP), which presents close homology with ERAPs, in the MHC-I endogenous and cross-presentation. While no role in direct antigen presentation was observed, the absence of IRAP strikingly impaired the cross-presentation of a model antigen in a proteasome-sensitive, TAP-independent and ERAP-independent manners. Importantly, examination of the distribution of IRAP within the dendritic cells supported the role of endosomes as a compartment for peptide final trimming and loading onto MHC-I molecules, as IRAP was selectively expressed in a specific subclass of endosomes, defined by the co-expression of Rab14 and Syntaxin 6 (Saveanu, Carroll et al. 2009). The physiological relevance of these findings is reinforced by additional observations that IRAP-deficient animals have reduced cross-presentation *in vivo* after immunization with endocytic or phagocytic antigens and that the Rab14+Syntaxin6+IRAP+ compartment is restricted to the cDC1 subset in the spleen (Weimershaus, Maschalidi et al. 2012). Finally, a surprising finding was the observation of an accelerated phagosome maturation resulting in an enhanced phagosomal antigen digestion, that might by an unknown mechanism also affect antigen cross-presentation in addition to the defect in the IRAP trimming activity (Weimershaus, Maschalidi et al. 2012).

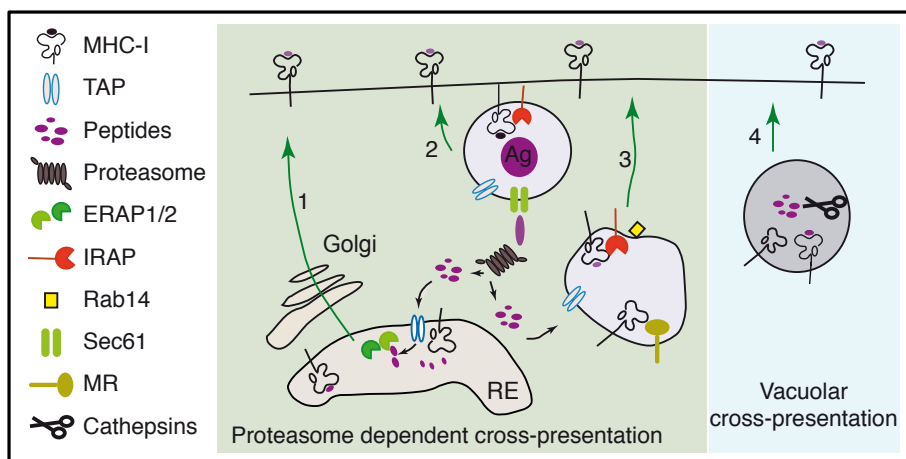


**Figure 17. Antigen cross-presentation pathways in dendritic cells (derived from (Adiko, Babdor et al. 2015)).** (Left): three distinct cytosolic (proteasome-sensitive) pathways have been identified, depending on the location of the peptide loading onto MHC-I molecules, in the endoplasmic reticulum (1), in the phagosome (2) or in endosomes (3) by an active retro-transport from the cytosol. In the vacuolar (proteasome-insensitive) pathway, the processing and the peptide loading occur in the endocytic pathway only (4).

### Proteasome-independent vacuolar pathway

A second alternative cross-presentation pathway that is strikingly different from the cytosolic pathway has been initially identified and is reminiscent from the classical MHC-II pathway. In this alternative pathway, the antigen does not gain access to the cytosol and to the ER and antigen processing and peptide loading is exclusively performed in the endocytic pathway. Vacuolar pathway has been first identified by the group of C.V. Harding as a TAP transport-independent pathway that does not require antigen transfer from the vacuole to the cytosol (Pfeifer, Wick et al. 1993). While proteasome inhibition does not affect cross-presentation, broad inhibition of endolysosomal proteases activity reduces cross-presentation. Protein antigens engaged in the proteasome-independent pathway are retained in the endosomal compartment where the antigen processing and the peptide loading onto MHC-I molecules exclusively occur. Examination of this pathway has allowed for the identification of cathepsin S as the major enzyme responsible for proteolysis in this pathway (Shen, Sigal et al. 2004, Kurotaki, Tamura et al. 2007). Indeed, *in vitro* cross-presentation and *in vivo* cross-priming were found to be totally abolished in TAP and cathepsin S double deficient mice compared to TAP-deficient mice or wild-type mice (Kurotaki, Tamura et al. 2007). Because of its relatively poor efficiency and the small numbers of antigens identified to be processed in it (Bertholet, Goldszmid et al. 2006), the proteasome-independent pathway has been barely studied and characterized.

## **What are the contributions of and the factors regulating the cytosolic and vacuolar pathways during immune responses?**

*Cytosolic versus vacuolar pathways.* All the reports that have compared the efficiency of the two main cross-presentation pathways point out the superiority of the cytosolic pathways. A quantitative examination has estimated that the cytosolic pathway is at least 10-fold more efficient than vacuolar pathway (Mant, Chinnery et al. 2012). Indirect supporting evidence gained by the comparison of conventional dendritic cell subsets for various antigens are also available. Indeed, cross-presentation by cDC1 subset is very sensitive to proteasome inhibition (Schulz and Reis e Sousa 2002) but not to a broad endosomal protease inhibitor (Thacker and Janssen 2012) whereas cDC2 is as sensitive to proteasome inhibition as to broad protease inhibition (Schulz and Reis e Sousa 2002). However, for some antigens vacuolar pathway might be better suited than the proteasome-dependent pathways. To date, the precise determinants that dictate the route of antigens toward a preferential pathway remain elusive, even if some of them are (at least) indirectly suspected: the size of the particles in the case of a phagocytosed antigen; the nature (endocytic or phagocytic) of the antigen considered (Mant, Chinnery et al. 2012). In this context, our laboratory has started to address this question and observed that antigen expressed at the surface of yeast cells are processed by a proteasome-dependent but TAP-independent pathway that does not occur in the context of an endocytic antigen (Merzougui, Kratzer et al. 2011). However, the relevance of this pathway as well as the transporter that allows for retro-transport of peptides into the phagosomes for the final trimming and loading onto MHC-I remain totally elusive.

*The “peptide loading onto MHC-I” compartments.* Whatever the cross-presentation pathway considered, the current view proposes that endosomes and phagosomes are the compartments where the peptides are loaded onto MHC-I molecules. However, the source of MHC-I, that is newly synthesized or recycling MHC-I, responsible for cross-presentation is thought to differ between the cytosolic and the vacuolar pathways. In the cytosolic pathway, an important set of experiments support the fact that newly synthesized MHC-I in the ER is the major source of MHC-I. Indeed, incubating cells with specific inhibitors of the anterograde protein transport from the ER through the secretory pathway, such as brefeldin A and/or monensin, impairs cross-presentation and triggers a drastic reduction in the MHC-I levels at the cell surface. Additionally, TAP deficient dendritic cells and macrophages exhibit impaired cross-presentation and reduced MHC-I levels (Van Kaer, Ashton-Rickardt et al. 1992, Day, Esquivel et al. 1995, Chefalo, Grandea et al. 2003). Supporting this idea, examination of

phagosome composition has revealed the presence of several components from an ER origin, such as TAP2 or proteins from the peptide loading complex are recruited in a Sec22b-dependent manner (Guermonprez, Saveanu et al. 2003, Ackerman, Giodini et al. 2006, Cebrian, Visentin et al. 2011). Importantly, MHC-I levels in the phagosomes seem to be unchanged in the cells lacking of Sec22b (Cebrian, Visentin et al. 2011). Recent reports from my laboratory have revisited the role of TAP in the cross-presentation of antigens by mouse dendritic cells (Merzougui, Kratzer et al. 2011). Prompted by the observation that low-temperature restores physiological MHC-I levels at the surface of TAP deficient splenocytes, my group has confirmed that this is also the case for dendritic cells and surprisingly, this is accompanied by the restoration of cross-presentation of phagocytosed antigens. In this proteasome-sensitive cytosolic pathway, the restoration of the cross-presentation due to normal levels of surface MHC-I and additional experiments suggest that recycling MHC-I molecules play an important role in providing MHC-I for newly synthesized peptides during cross-presentation. Importantly, this effect was specifically observed for phagocytosed antigens and not endocytosed antigens, suggesting that either the source of MHC-I for cross-presentation is different for endosomes and phagosomes or an alternative mechanism supports peptide import into the phagosomes only, that remains to be identified (Merzougui, Kratzer et al. 2011). Reinforcing these results, my group has recently revisited the role of the TAP protein in the peptide transport into phagosomes during the cross-presentation of phagocytosed antigens. This study confirmed a TAP-dependent ATP-dependent peptide transport into the phagosome when the peptides have a high-affinity for this transporter whereas a TAP-independent ATP-dependent transport of the OVA peptide SIINFEKL was observed (Lawand, Abramova et al. 2016).

In the vacuolar pathway, the source of MHC-I for cross-presentation is the recycling MHC-I molecules, as assessed by several reports (Reid and Watts 1990, Pfeifer, Wick et al. 1993, Chiu, Davis et al. 1999). A conserved tyrosine motif in the intracytoplasmic tail of MHC-I molecules has been identified as crucial for MHC-I endocytosis and targeting to a lysosomal-like compartment, but the adaptor molecules remain still elusive (Lizee, Basha et al. 2003). Furthermore, examining how the HIV Nef protein down-regulates surface MHC-I molecules has allowed for the identification of a binding site on MHC-I for its binding on the AP-1 clathrin adaptor protein and the targeting to the endocytic pathway (Roeth, Williams et al. 2004). Furthermore, the cross-presentation of soluble OVA has been recently shown to be dependent on both the tyrosine residue in the cytoplasmic tail and on the AP-1 protein (Kulpa,

Del Cid et al. 2013), suggesting an alternative endogenous protein for routing of MHC-I to the endocytic pathway, in the absence of the Nef protein. Such protein might be the invariant chain Ii, which can bind to AP-1 and is required for routing MHC-I to the endosomes or lysosomes (Basha, Omilusik et al. 2012). Additional information on the precise nature of the compartment involved in the recycling of MHC-I molecules that are also a source for cross-presentation has been given by the examination of a proteasome-independent antigen cross-presentation by human pDCs (Di Pucchio, Chatterjee et al. 2008). Surprisingly, the authors found that ready-to-use MHC-I are stored into a recycling endocytic compartment that also contains the transferrin receptor and that can be mobilized rapidly to fuel the endolysosomes and the cross-presentation of exogenous antigens.

As previously mentioned, MHC-I recruitment to endosomes has been shown to be influenced by TLR signaling by the group of C. Kurts, after stimulation with a synthetic TLR4 ligand, LPS (Burgdorf, Scholz et al. 2008). In the context of phagocytosed antigens, the group of J.M. Blander has recently reported that LPS stimulation of dendritic cells triggers a cascade signaling that activates the phosphorylation of the SNAP23 protein on the phagosomes and together with syntaxin 4 the target SNARE VAMP3 and its endosomal compartment defined by the high expression of Rab11 are recruited to the phagosome resulting in the provision of MHC-I for cross-presentation (Nair-Gupta, Baccharini et al. 2014). However, how MHC-I are routed to be stored in this recycling compartment as well as where do the MHC-I come from and what is the role of tyrosine residues in MHC-I routing in this compartment remain open questions.

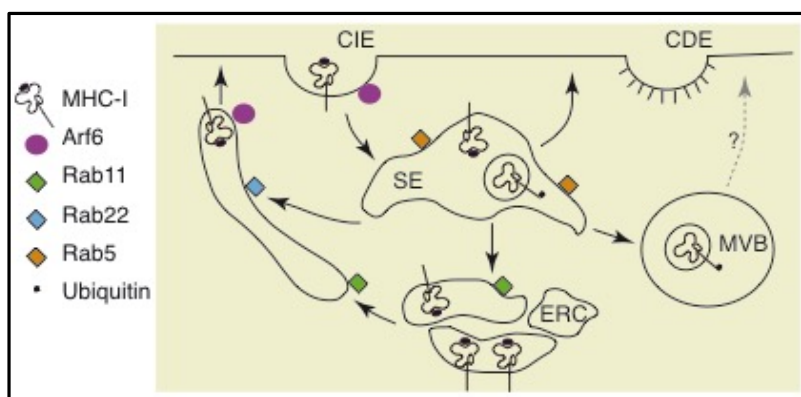


**Figure 18. MHC-I recycling within the endocytic pathway (derived from (Adiko, Babdor et al. 2015))**

### **What are the barriers in determining the relevance of the cross-presentation pathways under physiologic and pathologic conditions?**

Most of the groups that have identified and characterize antigen cross-presentation pathways have used dendritic cells and macrophages cell lines. The main source for these myeloid cells are the differentiation of bone marrow progenitors with a growth factor cocktail. Cultures of bone marrow derived dendritic cells and macrophages allow for the generation of large number of cells, thus limiting the numbers of animals to be included in the experimental work. Also, these cells are easy to manipulate *in vitro* and gene silencing or mutant protein transfection tools might be applied to these cells allowing for robust biological studies. However, variations about dose or culture time might alter results. Importantly very recently the precise nature of the pre-supposed bone marrow derived dendritic cells using the widely used protocol (Weimershaus and van Endert 2013) has been revisited. Surprisingly the group of C. Reis e Sousa observed by gene and protein expression analysis that bone marrow derived dendritic cells generated in the presence of granulocyte-macrophage colony-stimulating factor is a mixture of heterogeneous myeloid cells that are close to either dendritic cells or macrophages (Guilliams and Malissen 2015, Helft, Bottcher et al. 2015). These findings remain still controversial and an intense subject of debate and will probably require further independent work to be fully admitted by the dendritic cell community (Helft, Bottcher et al. 2016, Lutz, Inaba et al. 2016). These recent discussed limitations prompt to design or use novel technologies for studying the cell biology of natural phagocyte subsets from rodents and from human *ex vivo*. Pertinent technologies will be discussed later in the manuscript.

#### **Chapter 4. Concluding remarks**

Exogenous antigenic material is actively internalized by phagocytosis, micropinocytosis and micropinocytosis and routed to the phagocytic or endocytic pathway to be processed by endolysosomal proteases for loading onto MHC-II molecules and subsequent presentation to CD4<sup>+</sup> T cells or for loading onto MHC-I molecules and presentation to CD8<sup>+</sup> T cells in the context of antigen vacuolar cross-presentation pathway. However, the contribution of the vacuolar pathway in generating MHC-I ligands is thought to be marginal and less efficient than the cytosolic pathway. In the cytosolic pathway, antigenic material exits from the phagosome to the cytosol and is degraded by the proteasome before further processing by proteases, mainly aminopeptidases located in the ER (following the endogenous MHC-I antigen presentation); or in the phagosome or in endosomes, in this case requiring an active

retro-transport through specific channels. The precise contribution of the pools of neosynthesized and recycling MHC-I molecules to fuel antigen cross-presentation remains still elusive. Dendritic cells are professional antigen presenting cells that excel in antigen cross-presentation by MHC-I and the examination of the mechanisms involved has led to the identification of hallmarks for an efficient cross-presentation, relative to other phagocytes: the (exclusive) use of cytosolic pathway, an efficient phagosome-to-cytosol export, a slow phagosomal maturation, a weak acid endolysosomal pH and a lower endosomal protease activity, the presence of specific endosomal and lysosomal compartments that protect antigenic material from degradation and that act as platforms for MHC-I routing to the compartments where peptide loading occurs.



## PART IV - CD169+ MACROPHAGES ARE TISSUE RESIDENT MACROPHAGES WITH UNIQUE FUNCTIONS AND BEHAVIORS

### Chapter 1. What are the structure and the functions of the CD169 molecule?

CD169 antigen (also called sialoadhesin or siglec-1) was originally published as a marker of a tissue macrophage sub-population that was isolated from primary (bone marrow), secondary (lymph nodes and spleen) and tertiary (liver) lymphoid organs and had the capacity of binding erythrocytes (Crocker and Gordon 1985). More recently, CD169 antigen was found to be expressed by alveolar macrophages (Ducreux, Crocker et al. 2009) and an intestinal and a colonic macrophage sub-population (Hiemstra, Beijer et al. 2014, Asano, Takahashi et al. 2015). This marker was shown to be absent from serosal pleural and peritoneal cavities. Sialoadhesin molecule was historically described in 1985 as a non-phagocytic sheep erythrocyte receptor on resident bone marrow macrophages (Crocker and Gordon 1985).

CD169 protein is 185 kDa under non-denaturing conditions and 170 kDa under reducing conditions and a member of the lectin-like receptor family. Its structure includes 17 Ig-like domains, classifying CD169 as a member of the immunoglobulin superfamily (Crocker, Mucklow et al. 1994). Murine protein was predicted to be a type I transmembrane glycoprotein composed of 1,694 residues with a short intracellular region of 35 residues, a 21-residues transmembrane segment and a long extracellular part of 1,619 residues composed of 15 N-linked glycans (Crocker, Mucklow et al. 1994, Mucklow, Gordon et al. 1997). In the short cytosolic tail 5 putative phosphorylation sites were suspected. However, the short cytoplasmic tail totally lacks signaling motifs (Crocker, Mucklow et al. 1994). The first domain of the extracellular tail was shown to be a V-set domain containing an unusual arrangement of predicted disulphide bond between beta-strands B and E and an inter-domain disulphide linking the V-set domain to the adjacent immunoglobulin domain (Crocker, Mucklow et al. 1994). The 16 other extracellular domains were reported to be C2-like, with strong similarities between domains regarding their length and sequence. Importantly, the first two Ig domains share both strong sequence and structure similarities with two members of Ig superfamily proteins CD22 and CD33 (Freeman, Kelm et al. 1995) and all the three proteins due to their ability to bind sialic acid were included by consensus in a sialic acid binding Ig-like lectins family, previously described; due to the identification of the binding sialic acid activity first on sialoadhesin, it has been considered as the founder member of this family (Siglec-1). The location of the sialic acid region is located in the N-terminus V-set domain,

more specifically arginine-97 is crucial for the recognition and binding of carbohydrates, as also assessed by its conservation in all species tested (Crocker, Vinson et al. 1999). Arginine-97 forms a bidentate salt bridge with the carboxylate group of N-acetylneuraminic acid and with conserved tryptophans at positions 2 and 106 to make hydrophobic interaction with the N-acetyl and glycerol moieties, respectively. Arginine-97 is crucial for binding (Crocker, Vinson et al. 1999). Sialoadhesin specifically binds to  $\alpha$ Neu5Ac but not Neu5Gc or Neu5Ac9Ac (Kelm, Schauer et al. 1994, Crocker, Vinson et al. 1999), with a very low binding affinity (approximately  $10^{-3}$  M range) for natural sialylated glycoconjugated ligands (Crocker, Vinson et al. 1999).

CD169 distribution in rodents, pig and human is exclusively restricted to the mononuclear phagocyte system, with the highest expression observed in tissue macrophages residing in the secondary lymphoid organs (Klaas and Crocker 2012). Similar to observations in rodents, CD169 was found to be expressed in human spleen, liver, lymph nodes, bone marrow, colon, kidney and lungs but not on blood monocytes derived from healthy donors (Hartnell, Steel et al. 2001). Contrasting with the literature on rodent, CD169 is expressed by perifollicular resident spleen macrophages and not marginal zone macrophages, an anatomical location that is quite similar to the red pulp zone and that is enriched with high numbers of erythrocytes (Pack, Trumpfheller et al. 2008). Unexpected CD169 expression has been observed in human immunopathology, in patients suffering from inflammatory and/or type I IFN associated disorders. Inflammatory macrophages purified from synovial membranes of rheumatoid arthritis patients (Hartnell, Steel et al. 2001, Xiong, Cheng et al. 2014), blood monocytes from Human Immunodeficiency Virus-1 (HIV-1)-exposed patients (van der Kuyl, van den Burg et al. 2007), systemic lupus (Rose, Grutzkau et al. 2013), early-stage type 1 diabetes (Ferreira, Guo et al. 2014) or systemic sclerosis (York, Nagai et al. 2007) were unexpectedly found to express high levels of CD169. Interestingly, all these conditions have been associated to high levels of type I IFN responses. Incubating monocytes with natural or synthetic stimuli known to trigger type I IFN responses was also shown to trigger or up-regulate CD169 surface expression (Puryear, Akiyama et al. 2013). A recent report has suggested that human monocytes-derived dendritic cells might express CD169 after exposure to rhinovirus *in vitro* through a mechanism that probably involves type I IFN production (Seyerl, Kirchberger et al. 2010). However, to date no clear expression has been reported on tissue or migratory dendritic cells at the protein level questioning the relevance and the role of CD169 in dendritic cells.

### **Pathogen recognition, capture and trapping**

The main documented roles of the CD169 molecule are the binding and internalization of various pathogens (PRRSV, HIV-1, *Trypanosoma cruzi*, *Neisseria meningitidis*, *Campylobacter jejuni*) *in vitro*, with a strong contribution of sialic-acid binding activity (Klaas and Crocker 2012). As previously mentioned, CD169 molecular and protein expressions in blood monocytes from HIV-1 exposed patients were found to be significantly increased (van der Kuyl, van den Burg et al. 2007); reinforcing a putative role for virus handling, protein level expression correlated with viral load. *In vitro* examination of the role of CD169 demonstrated that glycoprotein 120 kDa (gp120) envelope glycoprotein exhibits sialic acid residues that are recognized by the sialic acid binding domain of CD169 (Rempel, Calosing et al. 2008, Izquierdo-Useros, Lorizate et al. 2012, Izquierdo-Useros, Lorizate et al. 2014, Pino, Erkizia et al. 2015). However, a recent report challenges the role of Siglec-1 as a receptor required for HIV-1 infectivity: by analyzing siglec-1 activity from null patients *ex vivo* the authors found that HIV-1 capture was not impacted in this context, as well as AIDS outcomes *in vivo*, suggesting that previously classical routes for HIV-1 infection might compensate for the lack of sialic acid binding activity (Martinez-Picado, McLaren et al. 2016). *Campylobacter jejuni* causes invasive gastro-enteritis and is also implicated in the pathophysiology of Guillain-Barré syndrome. Some *Campylobacter jejuni* strains carry sialylated lipooligosaccharides, this feature being associated with higher infectivity of target epithelial cells. These observations led to investigate the role of siglec receptors in the recognition of sialylated bacteria (Heikema, Bergman et al. 2010, Klaas, Oetke et al. 2012, Heikema, Koning et al. 2013). *Trypanosoma cruzi* is a sialylated parasite responsible for Chagas diseases that naturally infects macrophages in a sialic acid-dependent manner. Loss of sialic acid motifs was shown to decrease association with macrophages. Moreover, trypomastigotes distribution after infection was found to be restricted to CD169+ macrophages (Monteiro, Lobato et al. 2005). A recent report extends the role of siglec-1 in the recognition of parasites with *Leishmania donovani* (Roy and Mandal 2016).

### **Chapter 2. How are CD169 macrophage development and maintenance regulated?**

In the secondary lymphoid organs, the ontogeny and the maintenance of CD169+ macrophages remain still elusive and poorly investigated, with some exceptions. Indeed, the groups of J.G. Cyster and U.H von Andrian have identified lymphotoxin- $\alpha$ 1 $\beta$ 2 as required for the maintenance of subcapsular sinus macrophages in the lymph nodes: in the first study, a specific and drastic reduction of the numbers of subcapsular sinus but not medullary

macrophages was observed in lymphotoxin- $\alpha$ 1 $\beta$ 2-deficient mice (Phan, Green et al. 2009), whereas the second report directly showed that B cells specifically produced lymphotoxin- $\alpha$ 1 $\beta$ 2, underlying the role of B cells in the maintenance of subcapsular sinus macrophages (Moseman, Iannacone et al. 2012). Interestingly, similar observations have been made in the spleen for outer marginal zone and metallophilic macrophages, with a direct implication of B cells (Matsumoto, Fu et al. 1997, Nolte, Arens et al. 2004). The requirement of B cells for maintenance of spleen marginal zone macrophages is also supported by the study of B cell-activating factor receptor-deficient mice (Xu, Huang et al. 2015). A recent study has identified another factor that controls the differentiation of macrophages in the marginal zone of the spleen, the nuclear receptor  $LXR\alpha^{-/-}$ : examination of the spleen of  $LXR\alpha^{-/-}$  mice showed a disappearance of the outer marginal zone and the metallophilic macrophages and intact macrophage populations in other tissues, including the lymph nodes; highlighting the interdependency of marginal zone macrophages and marginal zone B cells,  $LXR\alpha^{-/-}$  mice also exhibited a significant reduction of marginal zone B cells. Confirming the total lack of marginal zone macrophages,  $LXR\alpha^{-/-}$  exhibited abnormal responses to blood-born antigens (N, Guillen et al. 2013). Importantly, CD169 expression by itself is not required for the development of spleen and lymph node macrophages (Oetke, Vinson et al. 2006). To date, with the exception of the use of clodronate liposomes, there is no available technique to properly and selectively deplete CD169<sup>+</sup> macrophages or outer marginal zone macrophages. Additionally, conditional depletion of CD169<sup>+</sup> cells by CD169-dtr mice has been shown to also eliminate SIGN-R1<sup>+</sup> macrophages suggesting either a not detectable expression of CD169 by the outer marginal zone macrophages with the techniques currently used or because of an interdependency of these two populations for their maintenance (Miyake, Asano et al. 2007).

### **Chapter 3. CD169<sup>+</sup> macrophages display a crucial role of immune-surveillance**

#### **1) Apoptotic clearance**

The clearance of apoptotic cells by macrophages is an important process in the regulation and maintenance of peripheral tolerance, as assessed by the emergence of autoimmune disorders in animal and human settings with a defective clearance (Miyake, Asano et al. 2007, McGaha, Chen et al. 2011). In the rodent spleen, both dendritic cells and marginal sinus macrophages strongly express surface receptors that bind and internalize signals from dead cells. In physiological settings, systemic intravenous apoptotic cells are mainly visualized in the

marginal sinus in both outer marginal zone macrophages and metallophilic marginal zone macrophages (Miyake, Asano et al. 2007, McGaha, Chen et al. 2011). However, depletion of marginal sinus macrophages by clodronate liposomes apoptotic cell clearance is not significantly impaired due to the phagocytosis by other phagocytes such as the red pulp macrophages or the cDC1 dendritic cell subset (McGaha, Chen et al. 2011). This modification in the distribution of cell debris was associated with an up-regulation of efferocytosis, the latter being also associated with an inflammatory phenotype (Miyake, Asano et al. 2007). Additionally, cDC1 dendritic cell subtype classically described as responsible for the induction of tolerance by cross-presentation exhibited reduced efferocytosis (Miyake, Asano et al. 2007). By contrast, when the marginal sinus macrophages were depleted tolerance was not achieved because of the presentation of dead cell-associated antigens by cDC2 dendritic cells (Miyake, Asano et al. 2007). Following this work, the group of T.L. McGaha proposed a mechanism responsible for the regulation of tolerance against apoptotic cells governed by spleen marginal sinus macrophages: marginal zone macrophages phagocytose cell debris and in turn produce type I IFNs responsible for the autocrine induction of indoleamine 2,3-dioxygenase resulting in the inhibition of IL-12 translation but not IL-10 during efferocytosis in cDC1s that allow for the maintenance of tolerance (Ravishankar, Liu et al. 2012). They also demonstrated that indoleamine 2,3-dioxygenase drives the expression of the protein general control nonderepressible 2, the molecule responsible for IL-12 repression and IL-10 promotion (Ravishankar, Liu et al. 2012, Ravishankar, Liu et al. 2015). Additionally, metallophilic macrophages exposed to cell debris secrete CCL22, a chemokine ligand for CCR4 that is expressed on Treg and on CD103+ cDC1 tolerogenic dendritic cells promoting their migration and accumulation, thereby dendritic cell-Treg interaction in the white pulp (Ravishankar, Shinde et al. 2014).

## **2) Clearing of infections *in vivo***

Due to their anatomic distribution within the secondary lymphoid organs and the expression of a broad variety of pathogen-recognition receptors, CD169+ macrophages act like scavenger cells, trapping the pathogens and developing molecular responses after integration of the pathogen or particles recognized. Outer marginal zone macrophages express SIGN-R1 and have been shown to interact and phagocytose various pathogens such as yeast cells, *Mycobacterium tuberculosis*, *Streptococcus pneumoniae*, *Escherichia coli* and *Salmonella typhimurium* (Borges da Silva, Fonseca et al. 2015). Next to phagocytosis, SIGN-R1 also contributes in the clearing of *Streptococcus pneumoniae* by binding and activating

complement cascade. MARCO receptor is mainly found in outer marginal zone macrophages as well as medullary lymph node macrophages and is thought to play a role in the uptake of Gram-negative bacteria. In addition, MARCO in outer marginal zone macrophages phagocytose directly *Escherichia coli* and *Staphylococcus aureus* (Borges da Silva, Fonseca et al. 2015). Outer marginal zone and metallophilic macrophages are fundamental in controlling early infection as assessed by the rapid death observed by fulminant massive bacteremia after macrophage depletion (Borges da Silva, Fonseca et al. 2015). Importantly, in these experimental settings, T-cell responses were still present in the absence of macrophages, limiting, even if not excluding, the contribution of macrophages as antigen presenting cells. Similar findings were reported for *Neisseria meningitidis* (Borges da Silva, Fonseca et al. 2015). Adenovirus (Alba, Bradshaw et al. 2010) as well as vesicular stomatitis virus and lymphocytic choriomeningitis virus co-localize as soon as few minutes with marginal zone macrophages (Oehen, Odermatt et al. 2002), suggesting a role for pathogen trapping *in vivo*. In the lymph nodes, several studies have revealed a similar role for subcapsular sinus macrophages in limiting the spreading of various pathogens and in some cases in preventing animal death: gammaherpesvirus (Frederico, Chao et al. 2015), west nile virus (Winkelmann, Widman et al. 2014), cytomegalovirus (Farrell, Davis-Poynter et al. 2015), vaccinia virus, vesicular stomatitis virus (Junt, Moseman et al. 2007, Iannacone, Moseman et al. 2010, Moseman, Iannacone et al. 2012). Two mechanisms have been proposed to support this antiviral function independently of adaptive immunity, the production of type I IFNs (Junt, Moseman et al. 2007, Iannacone, Moseman et al. 2010, Moseman, Iannacone et al. 2012) and the recruitment and accumulation of NK cells (Garcia, Lemaitre et al. 2012). The group of K.S. Lang has provided a significant insight on the mechanisms responsible for control of acute and chronic viral infections by splenic metallophilic macrophages. In a first study, his group identified type I IFN responses and especially usp18 small IFN responsive protein to be required to allow viral replication of trapped viral particle in the metallophilic macrophages, this being crucial for the generation of robust antiviral adaptive immunity and control of chronic infection (Honke, Shaabani et al. 2012). Interestingly, in the context of a chronic viral infection, the enforced viral replication was totally absent due to a sustained type-I IFN response, thereby impairing the generation of protective adaptive immunity (Honke, Shaabani et al. 2016). An additional proof of the role of CD169<sup>+</sup> macrophages in the control of acute viral infections has been recently published: mice lacking B cell-activating factor receptor showed drastically reduced number of CD169<sup>+</sup> macrophages resulting in: reduced viral amplification, reduced antigen presentation following viral infection, and impaired antiviral T

cell responses (Xu, Huang et al. 2015), resulting in animal death. Reinforcing the particularity of marginal metallophilic macrophages, specific antibodies to virus produced in primary responses were shown to enforce the viral replication in metallophilic macrophages, thereby boosting adaptive immunity, whereas in the peripheral organs the same antibodies limited viral replication (Duhan, Khairnar et al. 2016).

### **3) Induction of inflammation**

The role of spleen and lymph node CD169<sup>+</sup> macrophages in inducing inflammation has been described in different parts of the manuscript and mainly involves an early production of type I IFNs and pro-inflammatory cytokines through the recruitment of the inflammasome complex. These inflammatory responses are crucial in controlling viral infections (Junt, Moseman et al. 2007, Iannacone, Moseman et al. 2010, Honke, Shaabani et al. 2012, Xu, Huang et al. 2015, Duhan, Khairnar et al. 2016, Honke, Shaabani et al. 2016, Pucci, Garris et al. 2016, Sagoo, Garcia et al. 2016, Shaabani, Khairnar et al. 2016).

## **Chapter 4. CD169<sup>+</sup> cells can activate adaptive immune responses by antigen transfer or by antigen presentation to cognate cells**

Due to their anatomical location in spleen and lymph nodes, CD169 macrophages act as filters for blood-borne and lymph-borne antigens, respectively. CD169<sup>+</sup> macrophages are distributed in a transitional marginal (or subcapsular) area where the fluid flows slow down and antigens derived from cell debris or pathogens are in direct contact with these macrophages. In addition to macrophages, other immune cells such as marginal zone B cells, migratory dendritic cells, resident dendritic cells or circulating T and B lymphocytes also pass throughout or in close proximity to this transitional area in the spleen. Altogether these simple observations suggest potential interactions between T lymphocytes and marginal sinus macrophages, at least a potential role for marginal sinus macrophages in T and B cell adaptive immunity.

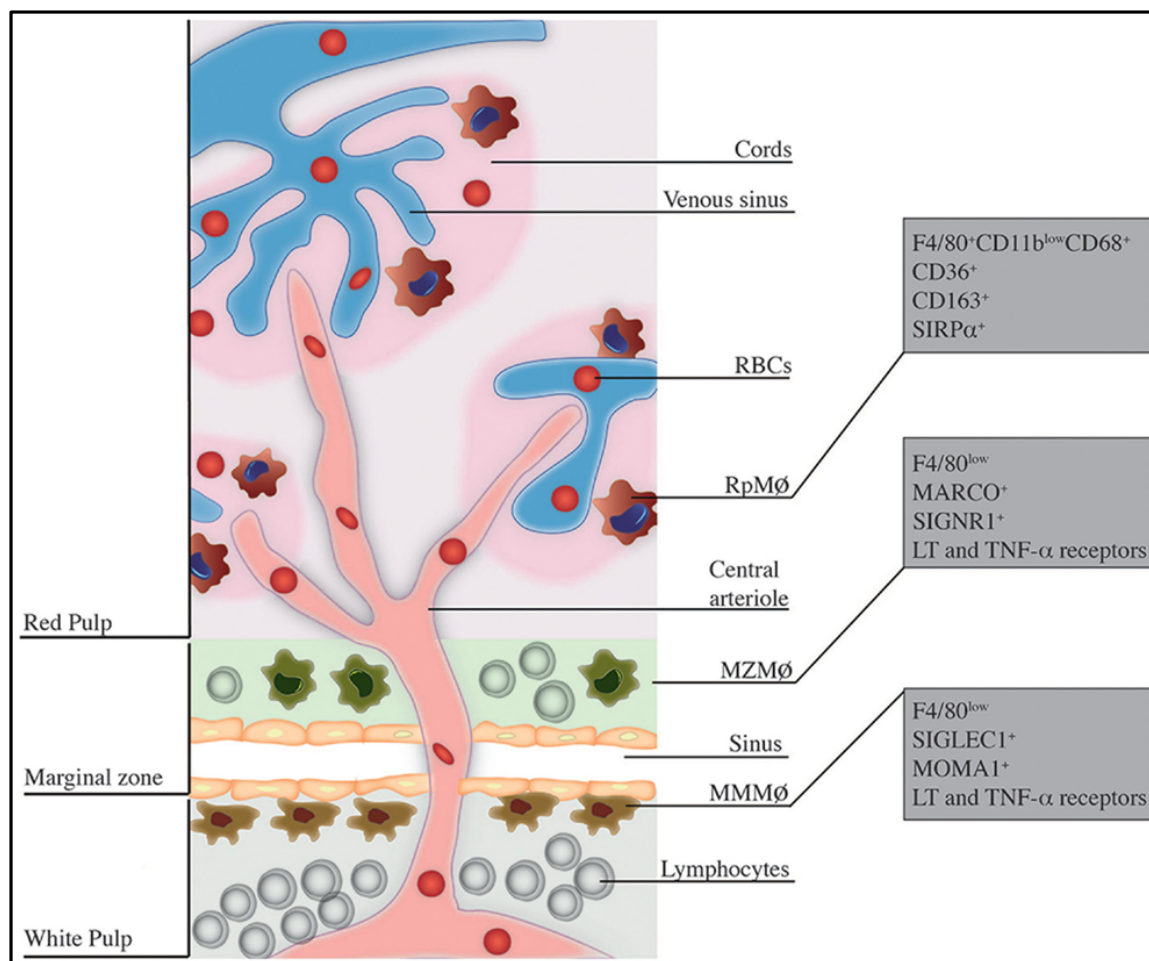


**Figure 19. Distribution and markers of macrophage subsets in the mouse spleen (derived from (Borges da Silva, Fonseca et al. 2015))**

### 1) Antigen presentation to B cells

The regulation of antigen presentation to marginal zone B cells and follicular B cells by spleen and lymph node CD169<sup>+</sup> macrophages, respectively, has been already exposed earlier in the manuscript. Briefly, several reports have demonstrated that lymph node subcapsular sinus macrophages control antigen presentation to follicular B cells: for antigens with low molecular weight, they limit their passive and massive spreading in the organ, allowing for a regulated antigen presentation by dendritic cells; for larger antigens, subcapsular sinus macrophages trap the antigen and transfer them to cognate B cells that in turn migrate to the follicles for relaying antigens to follicular dendritic cells (Junt, Moseman et al. 2007, Phan, Grigorova et al. 2007, Phan, Green et al. 2009, Suzuki, Grigorova et al. 2009). A similar role in the spleen has been recently reported (You, Myers et al. 2011) and they induce strong high-affinity humoral responses by promoting T<sub>fh</sub> responses (Veninga, Borg et al. 2015).



## 2) Antigen presentation to invariant NK-T cells

Initiation of adaptive immune responses by CD169<sup>+</sup> macrophages is not only limited to a sole role of directed antigen capture and transfer to *bona fide* antigen presenting cells as this is the case for B lymphocytes. Indeed, in addition to internalize a glycolipidic lymph-borne antigen, the group of F.D. Batista has demonstrated that the subcapsular sinus macrophages are directly responsible for the antigen processing and presentation to cognate invariant NK-T cells, thereby resulting in their early activation, expansion and cytokine production; the depletion of CD169<sup>+</sup> cells resulted in the total lack of antigen capture and presentation of glycolipid antigen. Reinforcing these results, a direct visualization by live microscopy of invariant NK-T cells and CD169<sup>+</sup> cells was also achieved (Barral, Polzella et al. 2010). Unexpectedly these findings were recently extended to marginal zone macrophages (Kawasaki, Vela et al. 2013). Another surprising finding was that in both cases, CD169<sup>+</sup> macrophages were able to generate antigenic peptides suggesting a relatively poor degradative endocytic pathway, more efficiently than dendritic cells.

## 3) Regulation of antigen presentation to T cells

Recent published reports have unraveled unsuspected functions for secondary lymphoid organs resident CD169<sup>+</sup> macrophages, especially in antigen recognition and presentation to cognate cells. In the context of dead cell-associated model antigen injected subcutaneously, the group of M. Tanaka has provided evidence for a direct role in the priming of transgenic naïve CD8<sup>+</sup> T cell into cytotoxic T cells targeted against the model antigen OVA by a unique subset of subcapsular sinus macrophages co-expressing CD169<sup>+</sup> and CD11c<sup>+</sup> in the draining lymph nodes (Asano, Nabeyama et al. 2011). In addition to phagocytose the model antigen, the CD169<sup>+</sup>CD11c<sup>+</sup> cells directly cross-presented the antigen to specific CD8<sup>+</sup> T cells *in vitro* and *in vivo*, resulting in the rejection of tumor cells *in vivo* (Asano, Nabeyama et al. 2011). Importantly and reinforcing the role of CD11c<sup>+</sup>CD169<sup>+</sup> lymph node macrophages in this protection, a conditional depletion of CD169<sup>+</sup> cells from the mice resulted in a reduction in T cell cytotoxicity and the failure of tumor rejection *in vivo*. Moreover, depletion of migratory or resident DCs did not affect CD8<sup>+</sup> T cell priming in these settings (Asano, Nabeyama et al. 2011). Taken together the results collected by the group of M. Tanaka strongly suggest that a specific subset of CD169<sup>+</sup> subcapsular sinus macrophages is strictly required to control tumor immunity, by cross-presenting tumor derived antigens to specific CD8<sup>+</sup> T cells. However, whether these myeloid cells are dendritic cells or macrophages is controversial (Meredith, Liu et al. 2012, Satpathy, Kc et al. 2012). Furthermore, how the

antigens are processed into antigenic peptides by these cells in comparison to dendritic cells remains elusive, yet it could bring some insight in the design of anti-tumor vaccine strategies. We also observed that antigen targeting to CD169 injected subcutaneously resulted in efficient cross priming of OT-I T cells *in vivo*, comparable to the targeting to dendritic cell subsets, yet the quality of the priming and the direct visualization of antigen-bearing CD169+ macrophages and cognate T cells were not assessed (Kratzer, Mauvais et al. 2010). Consequently, a scenario in which antigen is transferred to dendritic cells for presentation to T cells is not excluded, paralleling the model of antigen presentation to B cells. Interestingly such a scenario might occur in the spleen as proposed by the group of J.M. den Haan. They observed that antigen targeting to metallophilic macrophages in the spleen *in vivo* resulted in a CD8+ T cell cross-priming as efficient as when antigen was targeted to conventional dendritic cells. However, when dendritic cells were depleted from the spleen before the antigen was targeted to either dendritic cells or metallophilic macrophages, a total absence of cytotoxic CD8+ T cells responses was observed, indirectly suggesting that CD169+ macrophages in the spleen may act as a platform for antigen transfer to cross-presenting dendritic cells (Backer, Schwandt et al. 2010). However, no further direct evidence was provided to support this hypothesis: no cross-presentation assays to CD8+ T cells by sorted dendritic cells and macrophages were performed *ex vivo* or *in vitro*, and no visualization of CD8+ T cell/antigen presenting cell contacts or antigen transfer from macrophages to dendritic cells was achieved. This is probably due to technical limitations. Importantly, the depletion model used to eliminate dendritic cells also eliminates marginal zone macrophages, due to either a direct toxicity of toxin on these cells (Probst, Tschannen et al. 2005) or a significant expression of CD11c by the macrophages. Consequently, the capacity of CD169+ macrophages in the spleen in antigen cross-presentation and cross-priming both *in vitro* and *in vivo* remains an open question. Supporting a potential role in direct cross-presentation to T lymphocytes, CD169+ macrophages are capable of presenting exogenous antigens to invariant NK-T cells (Barral, Polzella et al. 2010) and present some of the hallmarks of cross-presenting dendritic cell subsets: they are poorly degradative for pathogens and for model antigens (Veninga, Borg et al. 2015); they are equipped with low endosomal protease contents (Phan, Green et al. 2009). However, these features are not exclusive with a role of antigen transfer platform. Finally, supporting a direct role for CD169+ macrophages in activating adaptive immune responses, two recent reports have demonstrated their crucial role in promoting the diversity of antiviral T cell repertoire compared to dendritic cells, through a robust endogenous MHC-I antigen presentation (Bernhard, Ried et al. 2015) at variance with

another study (Hickman, Takeda et al. 2008) and in directly presenting antigen to memory but not naïve Tfh CD4<sup>+</sup> T cells thereby promoting their early activation and effector functions (Suan, Nguyen et al. 2015).

In conclusion, CD169<sup>+</sup> macrophages are strategically distributed within the lymphoid organs where they are in direct and prolonged contacts with the pathogens. They display not only classical functions devoted to macrophages, such as the clearance of cell debris and pathogens, the initiation of inflammatory responses and to tissue homeostasis by orchestrating indirectly adaptive immune responses through their capacity to transfer antigens to follicular dendritic cells and to cross-presenting dendritic cells. More surprisingly, they can also display unconventional dendritic cell-like functions and may directly present exogenous protein and glycolipid antigens to cognate lymphocytes, promoting adaptive responses more robust than when performed by dendritic cells.

## PART V - High-dimensional technologies and analytic tools to unravel the complexity and the variability of immune responses

As described above, the immune system is particularly complex regarding the nature of the cellular actors, how they form interconnections to communicate, and their ability to analyze and react to exogenous signals. Additionally, there is a high heterogeneity regarding these parameters depending on the tissue and the nature of the ongoing immune responses. Finally, due to the inter-individual variability as well as the non-naïve repertoire of human in comparison to the mice model, a higher degree in heterogeneity is expected. In this context, strategies capable to simultaneously collect and analyze a large number of parameters at different scales including the whole tissues, the cellular level, and the protein and gene levels are required. In the recent years, a high number of live or static imaging techniques, of single-cell measurement techniques, as well as methods for high-throughput data acquisition and computational integration of the resulting data sets has emerged with promising and encouraging impact on our understanding on how the immune system operates. I will review and discuss briefly such technologies, from the tissue to the gene levels.

### **Chapter 1. How to study immune responses in the lymphoid organs by multiplex technologies?**

The question of new imaging developments for the immune system has been largely developed and reviewed (Tang, van Panhuys et al. 2013). Therefore, I will discuss two emerging technologies that allow for a multiplex whole-organ imaging in the context of the examination of immune responses. The group of R. Germain has recently developed a multiplex imaging technology (Gerner, Kastenmuller et al. 2012, Gerner, Torabi-Parizi et al. 2015) that combines multi-parametric 3D confocal imaging, spillover and deconvolution correction, image processing and display. The aim of the “histo-cytometry” is to allow for the visualization, quantification, and positional analysis directly in tissue sections of diverse immune cell populations. The sole (published) application of the histo-cytometry by the same group has led to the identification of a rare dendritic cell population distributed with the lymphatic sinus endothelium and responsible for the priming of T cells after capture of lymph-borne particulate pathogens (Gerner, Torabi-Parizi et al. 2015). Another technology, the light sheet fluorescence microscopy and one of its implementations, selective plane illumination microscopy, is based on the generation of a thin laser sheet oriented orthogonally to the detection axis, illuminating a single plane at the focal distance of the detection

objective. By moving the sample through the light sheet, a 3D image stack is quickly obtained for quantitative analysis within the intact lymphoid tissues (Brede, Friedrich et al. 2012, Mayer, Swoger et al. 2012, Coelho, Natale et al. 2013, Abe, Ozga et al. 2016), even allowing for the detection of rare events (Abe, Ozga et al. 2016) or events at the nanometer scale (Hu, Cang et al. 2016).

## **Chapter 2. How to study immune responses at the cellular level by multiplex technologies?**

At the cellular level, the major technological achievement has been the development of imaging flow cytometry that allows for the study of cell biological processes. Imaging flow cytometry combines high-throughput cytometry with high-resolution bright-field and fluorescent microscopy. The most common imaging cytometry platform, ImageStream system (Amnis, Seattle, WA), captures image data for each of the cells (events) that pass through the detector system using 20x, 40x or 60x microscope objectives. Once the LED light and the excitation lasers strike each cell, pictures of each cell are taken by a high-speed camera apparatus as the cell passes through the sensors. With imaging flow cytometry, each event has an associated set of pictures, in contrast to traditional flow cytometry in which no cell images are captured. The most popular applications non-exhaustively include experiments elucidating cell–cell interactions, cell signaling localization, co-localization of multiple intracellular targets, apoptosis, transfection efficiency, cell–pathogen interactions. However, this technique is slower than traditional flow cytometry. Because this technology uses fluorescent dyes, it continues to be subject to signal spillover, which limits the number of simultaneous targets that can be read on a single cell, yet the new fluorochromes available can overcome/reduce signal spillover. Although the resolution and the number of stacks in the z-dimension per cell are far inferior than confocal imaging, imaging flow cytometry displays a major interest for studying rare cell populations, non-adherent cells, for performing comparisons between cell populations present in the same sample, for collecting a high number of events to ensure a reliable biostatistics analysis. In the immune system analysis, the imaging flow cytometry has been used to study the cell biology of phagocytes: pathogen tracking among the endocytic pathway (van de Laar, Saelens et al. 2016), the phagosome maturation (Johansson, Karlsson et al. 2015), the MHC trafficking (Hennies, Lehn et al. 2015), the interaction between T cell and dendritic cell (Markey, Gartlan et al. 2015), the activation/recruitment of molecules involved in signaling pathways (Vakkila, DeMarco et al. 2004, Schmidt, Pietkiewicz et al. 2015). Imaging flow cytometry has also been extensively used to study T cell biology

including the measurement of calcium flux (Cerveira, Begum et al. 2015), T cell contacts, detection and quantification of miRNAs and mRNAs (Porichis, Hart et al. 2014) and translocation of factors within the cells (Ellis, Carthy et al. 2014). Variations from the ImageStream technologies have been recently proposed to study biological processes without the requirement of fluorescent probes (Feng, Zhang et al. 2014, Blasi, Hennig et al. 2016), yet this approach is limited to one cell population per sample. These two techniques have several significant limitations that reside in the time required for image processing and analysis in the case of histo-cytometry or for sample processing in the context of light sheet microscopy. Indeed, tissue clearing is a prerequisite before image acquisition with a light sheet microscope and depending on the protocol it can last for several weeks. Moreover, some of the reagents used may alter fluorophores or target antigens for fluorochrome-conjugated antibodies (Susaki, Tainaka et al. 2015).

### **Chapter 3. How to study immune responses at the molecular level by multiplex technologies?**

Various complementary technologies, including multiplex flow cytometry, mass cytometry, cytokine secretome and single-cell transcription profiling, have been developed and applied for the study of complex and heterogeneous biological processes at the protein- and gene-expression levels. Importantly, such technologies have been applied to human immunopathology, supporting their potential for translational medicine.

#### **1) Multiplex flow cytometry.**

Flow cytometry is one of the commonly used technologies to measure the heterogeneity and the diversity of immune cell populations. In addition to the phenotypic examination of cell suspensions from cultured cells or organ-derived cell suspensions, flow cytometry allows for the purification of cell populations for further phenotypic or functional analysis. This versatile technology is still improving and with the development of new fluorophores that display less spectral overlap or of machines capable of deciphering the spectral of single cells, the most recent configurations can detect up to 20 parameters (Chattopadhyay and Roederer 2012, Futamura, Sekino et al. 2015). In addition to the increasing number of parameters analyzed simultaneously, flow cytometry has also improved by the analysis of signaling pathways through the detection of phosphorylated proteins (Krutzik, Crane et al. 2008) or of mRNA (Porichis, Hart et al. 2014). With the advent of multiplex flow cytometry, analytic strategies using bioinformatics tools have been developed allowing for high-dimensional analysis (Qiu,

Simonds et al. 2011, Aghaeepour, Finak et al. 2013). Although still useful, the main limitation of the multiplex flow cytometry is the number of parameters, due to the emission spectral overlap and the availability of fluorophores (Newell and Davis 2014).

## **2) Mass cytometry**

Mass cytometry is a fusion of two technologies: flow cytometry and elemental mass spectrometry, allowing for increasing the number of cellular parameters that can be quantified simultaneously. The use of probes coupled to unique stable, heavy metal isotopes is a clear advantage because elemental mass spectrometry is able to discriminate isotopes of different atomic weights with high accuracy. This is in direct contrast with the use of fluorophores that are often the main limitation of multiplex flow cytometry, due to the emission spectra overlap. Static mass cytometry allows for the simultaneous detection of up to 40 parameters, but is imagined to reach the level of a hundred parameters in the next years (Spitzer and Nolan 2016). Mass cytometry has been applied on mouse and human phagocyte populations to unravel the heterogeneity among dendritic cell and macrophage subsets (Becher, Schlitzer et al. 2014) as well as the patterns specifically associated to their activation (Fernandez and Maecker 2015, Fernandez and Maecker 2015, Guilliams, Dutertre et al. 2016). Applications of mass cytometry for T and B cell biology include TcR signalization (Mingueneau, Krishnaswamy et al. 2014), cytokine production (Newell, Sigal et al. 2012, Wong, Ong et al. 2016), activation of signaling pathways or transcription factors at both the mRNA and protein levels (Frei, Bava et al. 2016), lymphocyte differentiation (Bendall, Davis et al. 2014) or the analysis of antigen specific responses (Leong and Newell 2015). Supporting its potential for translation to human immunopathology, mass cytometry is efficient to detect and analyze rare immune cell populations (Yao, Liu et al. 2014), and to identify new biomarkers or signatures associated to disease outcomes (Gaudilliere, Fragiadakis et al. 2014, Mingueneau, Boudaoud et al. 2016). With the advent of mass cytometry, a significant attention has been given to the development of bioinformatics tools as well as for the rationalization of experimental design (Chester and Maecker 2015, Chen, Lau et al. 2016, Spitzer and Nolan 2016). Excitingly, such technologies have been implemented with imaging technologies to propose new multiplex imaging methods with promising impact (Angelo, Bendall et al. 2014, Giesen, Wang et al. 2014).

### **3) Cytokine secretome**

Recent technologies also include assays to monitor the cytokine signatures from various cell types at both the bulk and the single cell levels such as the Simoa technology (Rissin, Kan et al. 2013, Rivnak, Rissin et al. 2015) and the single-cell secretome (Ma, Fan et al. 2011). The single-cell secretome has revealed a massive degree of heterogeneity among the antigen specific single T cells within each donor (Ma, Fan et al. 2011). The Simoa technology has improved the sensitivity of the multiplex detection of cytokines at the femtogram level, thereby proposing a valuable assay for testing the functional capacities of rare cell populations.

### **4) Single-cell gene transcription profiling**

Among the major limitations of multiplex flow cytometry and mass cytometry, even with the most recent advances, the number of parameters analyzed simultaneously ranges between 20-40 and, even if possible, only a limited view of the transcription profile displayed by immune cells can be achieved. Recently, technologies to study the single-cell gene transcription profiling of immune cells have been available. The detection of mRNAs at the single-cell level has been rendering possible by the use of microfluidics technologies, mainly by the technologies developed by the Fluidigm corporation. Current experimental settings include the possibility of analyzing up to 96 single cells and up to 96 genes at the same time, on bulk or prior cell sorted populations. The emergence of single-cell RNA sequencing methods that allow genome wide mRNA transcript quantification (Tang, Barbacioru et al. 2009, Shalek, Satija et al. 2013). These technologies have already been applied to successfully solve some complex questions or provide crucial tools to unravel the heterogeneity of immune responses: the differentiation of myeloid progenitors (Paul, Arkin et al. 2015) and tissue-resident macrophages (Lavin, Winter et al. 2014), the sequencing of the T and B cell repertoires, in combination with barcoding technologies (DeKosky, Ippolito et al. 2013, Han, Newell et al. 2013, Shapiro, Biezuner et al. 2013), the heterogeneity of single dendritic cells and macrophages under homeostasis or after activation upon an inflammatory stimulus (Jaitin, Kenigsberg et al. 2014, Shalek, Satija et al. 2014), the differentiation of CD8<sup>+</sup> T cells (Arsenio, Kakaradov et al. 2014). These technologies have also a promising translational potential, as assessed by the following recent publications: the identification of vaccine correlates (Flatz, Roychoudhuri et al. 2011, Finak, McDavid et al. 2014), the cancer cell biology (Irish and Doxie 2014). Although powerful tools, it will always be important to



evaluate cellular protein levels instead of relying strictly on mRNA levels, since the protein level is probably more biologically relevant.

In conclusion, with the development of a large set of multiplex dynamic and/or static technologies, an impressive number of tools are currently available for dissecting the diversity and the heterogeneity of the immune responses at the tissue, the cellular and the molecular levels. Of particular interest, this technologic boom has open avenues for study of complex biological processes on rare tissue-resident immune cell populations such as phagocytes or lymphocytes, including an examination of: the antigenic material uptake and trafficking among phagocytes, the formation of T cell/antigen presenting cells, the activation of signaling pathways in lymphocytes and antigen presenting cells, the activation, the differentiation and the effector functions of antigen specific T cells. However, these techniques are limited by their cost and/or the time required for processing the samples and computing the high-dimensional data collected. Finally, most of the single-cell protein and transcription profiling techniques have proved their capacity to identify signatures associated to disease outcomes or useful for monitoring patients under immune-modifying therapies. With the exception of some rare reports (McKinney, Lyons et al. 2010, Lee, Lyons et al. 2011, Banchereau, Hong et al. 2016), such technologies have not been tested in autoimmune settings for studying autoreactive T cells. Indeed, antigen-specific techniques for the detection of the autoreactive T cell repertoire such as the fluorescent tetramers or ELISPOT techniques are of limited interest because of the rare frequency of autoreactive cells and of the lack of further phenotypic and functional characterization, respectively.

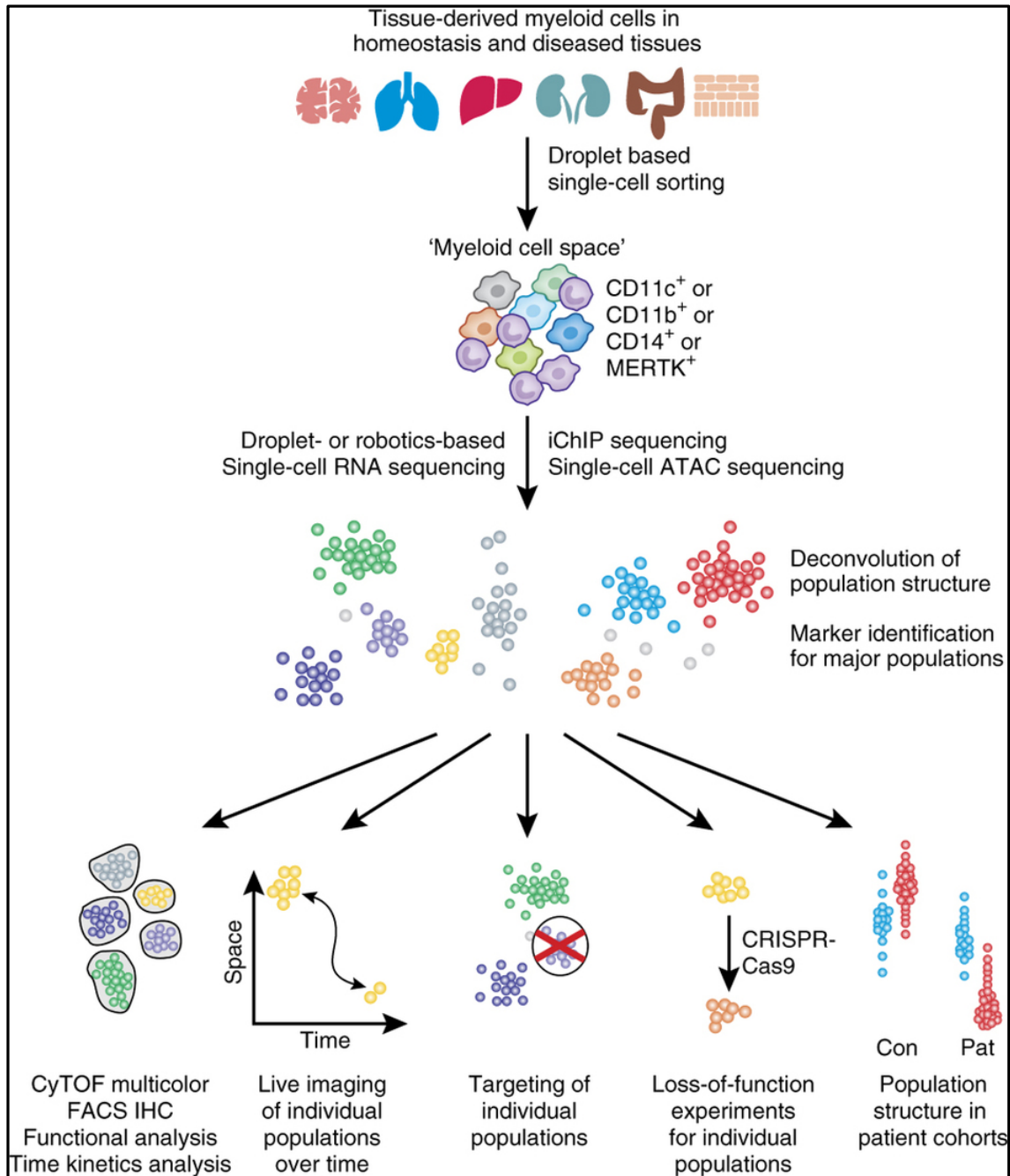


**Figure 20. An example of workflow for a high-resolution analysis of macrophage activation (as proposed by and derived from (Ginhoux, Schultze et al. 2016)).**

## OBJECTIVES

---

The literature discussed in the introduction converges towards the general concept that mononuclear phagocytes, especially dendritic cells and macrophages, occupy a central role in maintaining tissue homeostasis and in inducing and regulating inflammatory and innate and adaptive immune responses. In general, macrophages are resident cells that coordinate innate immune and inflammatory responses whereas dendritic cells are also specialized in the generation of productive adaptive immune responses. Consistent with this, conventional dendritic cells are notably far superior in the generation and the loading of exogenous antigens-derived peptides onto MHC-I molecules to induce cytotoxic CD8<sup>+</sup> T cell responses, by a process called antigen cross-presentation. Despite the crucial role of antigen cross-presentation in the control of infections and tumor, the underlying mechanisms remain partly elusive (Joffre, Segura et al. 2012). Notably, the spectrum of proteases involved in the trimming and processing of exogenous protein antigens is not fully understood (van Endert 2016). Also, the nature of and the mechanisms regulating the cell compartments where antigen is degraded and/or antigenic peptides are loaded into empty MHC-I as well as the precise contribution of newly synthesized or recycling MHC-I molecules in cross-presentation remain poorly studied (Adiko, Babdor et al. 2015), at variance with classical MHC-I and MHC-II presentation. Finally, the relevance of the mechanisms, with respect to the different types of antigen presenting cells, that have been already or that remain to be identified *in vivo* has been barely studied and the translation of results obtained with the bone marrow-derived dendritic cell model has been limited by the presence of contaminant macrophage-like populations (Helft, Bottcher et al. 2015). Addressing all these questions is of particular interest since manipulating dendritic cell functions may open avenues for the design of vaccines or of antiviral and antitumor cell therapies.

Importantly, the functional dichotomy between dendritic cells and macrophages has been recently challenged by the characterization of secondary lymphoid tissue CD169-expressing macrophages: the subcapsular sinus and the medullary macrophages in lymph nodes and the metallophilic marginal sinus macrophages in the spleen (den Haan and Kraal 2012, Gray and Cyster 2012). Consistent with a role in tissue homeostasis, these cells act as filters for pathogens or cell debris and trap circulating antigens from lymph and blood. This unique capacity is not only due to particular molecular features (Honke, Shaabani et al. 2012) but also to their unique anatomic distribution that places them in direct contact with body fluids.

Regarding tissue-resident cells, CD169<sup>+</sup> macrophages may contribute to adaptive immunity either by directly or indirectly present antigens to cognate cells. While their direct and crucial role in presenting exogenous lipid antigens to invariant NK-T lymphocytes is well documented (Barral, Polzella et al. 2010, Kawasaki, Vela et al. 2013), their precise contribution in inducing CD8<sup>+</sup> T cell responses is still a subject of intense debate. In a recent report, in the lymph nodes a particular subset of subcapsular sinus macrophages that also express CD11c is essential for the induction of CD8<sup>+</sup> cytotoxic T cell responses (Asano, Nabeyama et al. 2011), thus controlling tumor growth: they phagocytose and cross-present dead-tumor cells derived antigens. On the contrary, at least in this model, CD207<sup>+</sup> migratory dendritic cells or resident CD8 $\alpha$ <sup>+</sup> conventional dendritic cells occupy a marginal role in conferring protection against tumor. In the rodent spleen, a model has been proposed in which CD169 metallophilic marginal sinus macrophages cooperate with cDC1s to generate cytotoxic CD8<sup>+</sup> T cell responses *in vivo*: after capture, CD169<sup>+</sup> macrophages might transfer antigen to cDC1s, the latter being responsible for CD8<sup>+</sup> T cell activation (Backer, Schwandt et al. 2010). This cooperative role by antigen transfer would parallel what has been already published in the context of the role of CD169<sup>+</sup> macrophages in generating humoral responses. However, these studies have several limitations so that the role of CD169<sup>+</sup> macrophages that reside in the spleen and the lymph nodes in adaptive immune responses remain an open question. Indeed, the precise lineage (macrophages or dendritic cells) of the CD11c<sup>+</sup>CD169<sup>+</sup> cell subset in lymph nodes is still under debate since it has been observed that this population strongly expresses *zbtb46* that is more likely expected to be a dendritic cell lineage marker (Meredith, Liu et al. 2012, Satpathy, Kc et al. 2012). Moreover, the group of J.M. den Haan (Backer, Schwandt et al. 2010) used the CD11c-dtr mouse model aiming to deplete dendritic cells to test the antigen cross-priming by CD169<sup>+</sup> macrophages *in vivo*; however, in a previous report independently confirmed by other groups, CD169<sup>+</sup> cells in the spleen are also depleted by this strategy either because they express significant levels of CD11c or because of a toxic effect due to the diphtheria toxin injection (Probst, Tschannen et al. 2005). Importantly, it is commonly admitted that classical tools have failed to allow for the clear identification and isolation of CD169<sup>+</sup> subsets in the spleen and to a lesser extent in the lymph nodes. This has been explained by the scarcity of the splenic CD169<sup>+</sup> macrophages or by their disappearance after enzymatic digestion of the organ or by the presence of contaminant cells that might limit the conclusions raised in the published reports (den Haan and Kraal 2012, Gray and Cyster 2012, Gray, Friend et al. 2012).

To sum up, regarding spleen and lymph node CD169-expressing cell populations, there are controversies regarding the precise lineage of the cells that have been characterized; regarding their precise role in inducing or regulating adaptive immune responses and the mechanisms that are employed. This absence of knowledge can essentially be explained by two complementary reasons: i) there are no tools to selectively deplete CD169<sup>+</sup> macrophage subsets in the secondary lymphoid organs without affecting other phagocytes; ii) there is no published strategy to identify and purify CD169<sup>+</sup> cell population from the spleen and the lymph nodes deprived from contaminant cells, which is a prerequisite for studying their gene and protein expression profile, their functions and their morphology. Technical tools have recently emerged that allow for the study of the cell biology of *ex vivo* purified populations from lymphoid organs by imaging flow cytometry; or to unravel the complexity and the heterogeneity of both T cell and dendritic cell/macrophage populations at the gene and protein levels, by bulk or single-cell RNA sequencing, single-cell quantitative polymerase chain reaction (qPCR), multiplex flow cytometry and mass cytometry. Recent studies using these tools have started to elucidate some crucial questions regarding: the identification of macrophage and dendritic cell specific signatures resulting in the design of a simple reference classification and of specific tools to manipulate these populations; the origin and development of phagocytes; how memory and effector T cell subsets are related and distinct one from each other; the identification of signatures associated with good or poor outcome in immunopathology. However, these tools have not been applied to characterize CD169<sup>+</sup> macrophages in secondary lymphoid organs or to identify specific and robust signatures in human autoimmunity, a pathological setting in which characterization of autoantigen-specific T cells remains challenging.

At the outset of my thesis work, my starting hypothesis was that due to their specific location and to their particularly low-degradative equipment (Phan, Green et al. 2009), splenic CD169<sup>+</sup> macrophages may cross-present antigenic peptides to efficiently generate effector and memory responses. If CD169<sup>+</sup> macrophages were competent professional cross-presenting cells, it was conceivable that they use cell compartments, proteases or identified presentation pathways/models implicated in the generation of antigenic peptides by the cross-presenting cDC1 subset. However, as CD169<sup>+</sup> macrophages are not *bona fide* dendritic cells, it was also possible that they use alternative pathways to generate antigenic peptides. Consequently, I was also interested in identifying and characterizing the proteases and subcellular compartments implicated in generating antigenic peptides for MHC-I, an issue

also corresponding to the main interest of my laboratory and supervisor. Finally, I was able to participate in a project aiming to demonstrate how single-cell technologies can answer complex biological questions such as the phenotype and the functions of CD8<sup>+</sup> T lymphocytes during an ongoing autoreactive T cell response.

**The main objective of my experimental work was to evaluate the precise contribution of splenic CD169<sup>+</sup> macrophages in adaptive immune responses by CD8<sup>+</sup> T lymphocytes, as well as the underlying cell biological mechanisms.** Next to this, I could also participate in research aiming: 1) to test whether IDE has a broader role in generating antigenic peptides for MHC-I presentation, beyond the MAGE-A3 antigenic epitope identified by the group of B.J. Van den Eynde; 2) to help in the identification of molecules that would help in modulating immune responses by inhibiting aminopeptidase trimming activity; 3) to characterize the mechanisms supporting the role of the Rab14<sup>+</sup>IRAP<sup>+</sup>Syntaxin 6<sup>+</sup> endosome compartment as a platform for cross-presentation in dendritic cells and to determine the role of Rab14 in regulating this compartment; 4) to evaluate the performance of high-throughput single-cell technologies in analyzing cell biological process in phagocytes and in identifying T cell signature specific to outcomes in human autoimmune settings, in which classical antigen specific tools have failed. Importantly, addressing the questions related to these secondary objectives provided me with technical and biological information instrumental for succeeding in the main task.

## EXPERIMENTAL WORK

---

### **No major role for insulin-degrading enzyme in antigen presentation by MHC molecules.**

**Mauvais FX**, Culina S, Hsu HT, Burgevin A, Guénette S, Moser A, van Endert P. PLoS One. 2014 Feb 7;9(2):e88365. doi: 10.1371/journal.pone.0088365. eCollection 2014.

As mentioned in the introduction, although the proteasome is the major cytosolic peptidase that digests proteins for generating MHC-ligands, some reports have suggested the presence of a back-up cytosolic protease that may act in the absence of proteasome activity. This was supported by some reports that used proteasome inhibitors but that are now thought to actually reflect an incomplete proteasome inhibition (van Endert 2016). More recently, the group of B. Van den Eynde in collaboration with our group has shown that IDE can produce an antigenic peptide derived from the tumor antigen MAGE-A3 in a proteasome-independent manner (Parmentier, Stroobant et al. 2010). Interestingly, IDE prefers misfolded proteins, such as amyloid-beta (McCord, Liang et al. 2013), as substrates, suggesting that it might digest such proteins and play a larger role in MHC-I presentation beyond the production of this tumor-derived peptide. We examined the effect of IDE knockdown or knockout on global MHC-I expression as well as presentation of a variety of antigens. Our results did not provide any evidence of such a role for IDE and confirmed that the role of IDE in generating antigenic peptides concerns a limited and marginal number of situations. Together with a former PhD student in the van Endert laboratory, I did a significant set of experiments in this work. Notably, I performed the following experiments: direct antigen presentation assays using the EG7 cell line or the 25.D1 antibody on the IDE<sup>+/+</sup> and IDE<sup>-/-</sup> bone marrow-derived dendritic cells and mouse embryonic fibroblasts; *in vivo* and *in vitro* antigen presentation assays using a self-antigen in the IDE<sup>+/+</sup> and IDE<sup>-/-</sup> mice on the Non Obese Diabetic background; acid-stripping experiments on splenocytes from IDE<sup>+/+</sup> and IDE<sup>-/-</sup> mice on C57BL/6 and Non Obese Diabetic backgrounds.

**3,4-diaminobenzoic acid derivatives as inhibitors of the oxytocinase subfamily of M1 aminopeptidases with immune-regulating properties.** Papakyriakou A, Zervoudi E, Tsoukalidou S, **Mauvais FX**, Sfyroera G, Mastellos DC, van Endert P, Theodorakis EA, Vourloumis D, Stratikos E. *J Med Chem.* 2015 Feb 12;58(3):1524-43. doi: 10.1021/jm501867s. Epub 2015 Jan 30.

**Screening Identifies Thimerosal as a Selective Inhibitor of Endoplasmic Reticulum Aminopeptidase 1.** Stamogiannos A, Papakyriakou A, **Mauvais FX**, van Endert P, Stratikos E. *ACS Med Chem Lett.* 2016 May 31;7(7):681-5. doi: 10.1021/acsmchemlett.6b00084. eCollection 2016 Jul 14.

**Optimization and Structure-Activity Relationships of Phosphinic Pseudotriptide Inhibitors of Aminopeptidases that Generate Antigenic Peptides.** Kokkala P, Mpakali A, **Mauvais FX**, Papakyriakou A, Daskalaki I, Petropoulou I, Kavvalou S, Papanthanasopoulou M, Agrotis S, Fonsou TM, van Endert P, Stratikos E, Georgiadis D. *J Med Chem.* 2016 Sep 20. [Epub ahead of print]

In the work reported in these manuscripts, I have, under the supervision of my director, collaborated with the group of E. Stratikos, a well-known expert in the biochemical characterization of aminoterminal peptidases, especially ERAPs. Very recently, prompted by the accumulating evidence suggesting that manipulating both aminopeptidase expression and activities of these enzymes may influence the outcome of antigen presentation, he started to identify pharmacological inhibitors potentially selective for ERAPs and/or IRAP, through the screening of impressive libraries. Indeed, both the levels of activity and of expression of ERAPs have been associated with predisposition to infections, autoimmunity and tumor escape to the immunosurveillance (Fruci, Romania et al. 2014, Stratikos 2014, Stratikos 2014, Stratikos, Stamogiannos et al. 2014, Aldhamen, Pepelyayeva et al. 2015). Furthermore, a pioneer study of a pharmacological inhibitor, a phosphinic pseudotriptide, the DG013A compound, has demonstrated the interest of inhibiting aminopeptidase activities (Zervoudi, Saridakis et al. 2013). However, identification of selective aminopeptidase activity inhibitors is a critical barrier for preclinical development of such strategies since the lack of selectivity might be associated with potential adverse effects. In this context, the group of E. Stratikos has investigated the specificity and affinity of various candidates for ERAP1, ERAP2 and IRAP enzymes and wanted to confirm their results in an *in vitro* more relevant cell based model. My contribution in these three publications was to examine presentation of



endocytosed and/or phagocytosed antigens in the presence of the candidate compounds as well as in ERAAP and/or IRAP deficient cells to verify effects on antigen cross-presentation by dendritic cells and to confirm inhibitor selectivity for the targeted aminopeptidase. While in the two first studies I used bone marrow-derived dendritic cells, I performed the assays on *ex vivo* purified splenic dendritic cells in the last study. Altogether, these three studies provide various selective inhibitors that should merit consideration for preclinical use in human immunopathology.

**Rab14-kinesin interaction mediates TLR-activated peripheral retention of early endosomes favouring MHC class I cross-presentation.** Saveanu L, Weimershaus M, Babdor J, Lawand M, Evnouchidou I, Vargas P, Zwick M, Brocker T, **Mauvais FX**, van Ender P. (submitted to Science)

Dendritic cells are central actors in mounting adaptive immune responses and they particularly excel in the presentation of antigenic peptides derived from exogenous materials onto the MHC-I molecules, a particular antigen presentation pathway referred to as antigen cross-presentation (Joffre, Segura et al. 2012). Among the specificities that might explain the superiority of dendritic cells in antigen cross-presentation compared to other phagocytes, accumulating evidence converges to the particular composition and regulation of the phagocytic pathway. Indeed, cross-presenting dendritic cells exhibit lower activity of lysosomal proteases and a slightly less acidic environment in their phagosomes during maturation (Joffre, Segura et al. 2012). The group of S. Amigorena has recently provided some insight on the mechanisms regulating the composition of maturing phagosomes and the phagosome maturation process. In a first study his group has identified the ER-Golgi intermediate compartment SNARE Sec22b to be responsible for the recruitment of material from the ER into the maturing phagosomes as well as for the delayed phagosome maturation observed in dendritic cells, thereby controlling antigen cross-presentation (Cebrian, Visentin et al. 2011). In a more recent study, his group has identified an independent mechanism present in maturing dendritic cells to limit the phagosome maturation in an inflammatory environment: exposure of dendritic cells to a synthetic TLR-4 ligand drives a Rab34-dependent re-organization of lysosomal structures into perinuclear clusters, preventing the fusion between the phagosome and the lysosomes and subsequently boosting the cross-presentation during the early phase of dendritic cells maturation (Alloatti, Kotsias et al. 2015). In this context, my host laboratory has previously identified the aminopeptidase IRAP as a new player involved in the antigen cross-presentation by dendritic cells. While a first study demonstrated the role of its trimming activity in the generation of exogenous-derived antigenic peptides suitable for MHC-I loading in model dendritic cells (Saveanu, Carroll et al. 2009), an additional and complementary study has revealed its crucial role as a regulator of cross-presentation by the cDC1 dendritic cell subset *in vitro* and *in vivo*, by delaying the phagosome maturation in addition to its trimming activity (Weimershaus, Maschalidi et al. 2012). Analysis of the IRAP distribution has indicated its selective expression within an endosomal storage compartment characterized by the high co-expression of EEA-1, the small

GTPase Rab14 and the SNARE Syntaxin 6. A more careful examination of this compartment has revealed its peripheral distribution in dendritic cells and intriguingly, dendritic cells deficient for IRAP harbor substantially reduced amounts of this peripheral compartment (Weimershaus, Maschalidi et al. 2012). Altogether, these observations suggest that a tightly-regulated and delayed phagosome maturation occurs in dendritic cells and contributes to prevent the premature degradation of antigenic peptides. Furthermore, in dendritic cells lysosomes exhibit a particular organization and central perinuclear distribution during antigen cross-presentation; the IRAP<sup>+</sup> storage endosomes are peripheral structures also used by dendritic cells to prevent phagosome maturation, yet the molecular mechanism remains elusive. Prompted by this context and the well-documented role of Rab14 in modulating the phagosome maturation, our group suspected that Rab14 might regulate the formation of the storage (or regulatory) endosomes, thereby controlling antigen cross-presentation. In the initial version of the work, submitted to Cell Reports, our group reported that IRAP-deficient cells exhibit a specific defect in the regulatory Syntaxin 6<sup>+</sup>Rab14<sup>+</sup> regulatory compartment but not in mannose receptor-expressing endosomes. This resulted in accelerated phagosome maturation, enhanced pathogen killing and antigen degradation and reduction in cross-presentation. Our group also observed a similar phenotype for Rab14-silenced dendritic cells and an impairment in antigen cross-presentation when Rab14 was absent or mis-localized by forcing the expression of its GDP-bound or GTP-bound forms. In this version of the manuscript, my contribution was to design and perform the antigen cross-presentation assays, the cell sorting of dendritic cells sorted by flow cytometry, flow cytometric examination of the consequences of Rab14 silencing or manipulation on the phenotype of dendritic cells. I also significantly contributed in the scientific discussions.

As this version of the manuscript was not accepted for publication, we decided to significantly extend mechanistic exploration of phagosome maturation and the role of Rab14<sup>+</sup> endosomes in it, and to focus the message of the project on the Rab14 GTPase and its effector proteins.

The new set of experimental work has allowed us to identify the role of the Kinesin KIF16b and of dynein proteins in the regulation of the Rab14<sup>+</sup> compartment formation, stability and peripheral distribution and in the subsequent consequences on phagosome maturation and antigen cross-presentation. During the revision, I was implicated in designing and performing experiments to test whether the imaging flow cytometry might be used for the examination of phagosome maturation by dendritic cells. This successful contribution has been incorporated in the new version of the manuscript and provided key aspects that support our findings such

as the evaluation of phagocytosis and a quantitative and qualitative comparison on how phagosome maturation is affected when the Rab14+ compartment is manipulated. I have also performed all the cell sorting and cross-presentation experiments and made a significant contribution during the scientific discussions.

**IRAP endosomes restrict TLR9 activation and signaling.** Babdor J, Descamps D, Adiko Assi AC, Tohmé M, Maschalidi S, Vasconcellos L, De Luca M, **Mauvais FX**, Garfa-Traore M, M. Brinkmann M, Chignard M, Manoury B, Saveanu L. (**submitted, under revision in Nature Immunology**)

In a parallel work supervised by a former scientist in the van Endert laboratory, L. Saveanu, I contributed to identify a role of the IRAP+Rab14+ compartment in controlling the TLR9 activation and signaling in dendritic cells. Prompted by the fact that, on the one hand intracellular TLRs require their transfer to and traffic through the endocytic pathway to be activated and signal and that, on the other hand the IRAP+Rab14+ storage endosomes plays a role in the regulation of phagosome maturation, a process during which TLRs can be recruited, we wondered whether the Rab14+ regulatory endosomes could control endosomal trafficking and/or signaling in dendritic cells. Exposure of IRAP-deficient bone marrow-derived or splenic dendritic cells to TLR3, TLR4 and TLR9 ligands, led to a hyper-secretion of pro-inflammatory cytokines including type I IFNs, only when the cells were treated with the synthetic TLR9 ligand CpG. This increase in cytokine production was due to an enhanced TLR9 MyD88-dependent and IRF-7-dependent signaling. Importantly, IRAP-deficient mice were highly susceptible to *Pseudomonas aeruginosa* infection, resulting in animal death in a presumable TLR9-dependent manner. When examining TLR9 distribution and trafficking in bone marrow-derived dendritic cells, we observed an aberrant trafficking of TLR9 to the Lamp-1+ compartment under basal conditions in IRAP-deficient cells and that TLR9 traffics to IRAP+ endosomes upon stimulation in IRAP-sufficient cells. Altogether, these results suggest that IRAP endosomes control TLR9 trafficking and activation by slowing its routing to lysosomes where it signals to promote cytokine production. Finally, looking for the molecular actors that drive the traffic of IRAP+ endosomes to lysosomes, we identified a crucial role for a protein member of the formin homology domain-containing proteins (FHOD), FHOD4. My contribution to this work was to perform the cell sorting of splenic cDC1, cDC2 and plasmacytoid dendritic cell subsets so that the consequences of IRAP deficiency on the TLR9 activation could be tested *ex vivo*, by detecting pro-inflammatory cytokines at the gene and protein levels.

**Beta cell antigens in type 1 diabetes: triggers in pathogenesis and therapeutic targets.**

**Mauvais FX**, Diana J, van Endert P. *F1000Res.* 2016 Apr 22;5. pii: F1000 Faculty Rev-728. doi: 10.12688/f1000research.7411.1. eCollection 2016. Review.

**A unique CD8(+) T lymphocyte signature in pediatric type 1 diabetes. Mauvais FX,**

Hamel Y, Pham HP, Kratzer R, Marchi C, Barilleau É, Waeckel-Enée E, Arnoux JB, Hartemann A, Cordier C, Mégret J, Rocha B, de Lonlay P, Beltrand J, Six A, Robert JJ, van Endert P. *J Autoimmun.* 2016 Sep;73:54-63. doi: 10.1016/j.jaut.2016.06.003. Epub 2016 Jun 16.

The outcome of cross-presentation is the activation of CD8+T cells that can be either productive (cross-priming) or inefficient, resulting in tolerance (cross-tolerance) (Joffre, Segura et al. 2012). The gold standard to study specific adaptive cellular immune responses is antigen-based techniques, including fluorescent tetramers. However, in autoimmune settings, which involve pathogenic and/or regulatory CD4+ and/or CD8+ T lymphocytes, the study of autoreactive T cell responses by autoantigen-based techniques are of limited interest as described for type 1 diabetes in more details in the following review: the low frequency of autoreactive T cells questions the reliability of fluorescent tetramers; the ELISPOT techniques do not allow for further phenotypic or functional characterization. Detailed information about the phenotype and functions of CD8+ T lymphocytes in type 1 diabetes is of particular interest due to their well-documented pathogenic role; the identification of biomarkers suitable for prediction of disease risk or progress, as well as for monitoring patients under immunotherapies are a major research axis. In this context, recent high-dimensional multiplex single-cell technologies have provided crucial tools to unravel the heterogeneity of antigen-specific CD4+ and CD8+ T cells in infectious or vaccine settings. We aimed to test single-cell technologies in recent-onset human type 1 diabetes patients to identify a specific CD8+ T cell signature. By multiplex single-cell PCR and flow cytometry we identified global perturbations at both the gene and protein expression levels in pediatric but not adult patients relative to age-matched controls. Furthermore, by using bioinformatics we identified a unique population in pediatric patients characterized by the co-expression of effector (Perforin, Granzyme B) and regulatory (TGF- $\beta$ , IL-10R) molecules that persists after metabolic equilibrium and that correlate with disease severity at the diagnosis. My contribution to this work was to design the flow cytometry panel, to perform the flow cytometry experiments, to help with the statistical analyses and to contribute to scientific discussions.

Highly efficient cross-priming of CD8<sup>+</sup> T cells by splenic CD169<sup>+</sup> macrophages employing a unique endosomal processing pathway. **Mauvais FX**, Hamel Y, Garfa-Traore M, Diana J, van Ender P. **(manuscript in preparation, not submitted)**

# No Major Role for Insulin-Degrading Enzyme in Antigen Presentation by MHC Molecules

Slobodan Culina<sup>1,2,3</sup>, François-Xavier Mauvais<sup>1,2,3</sup>, Hsiang-Ting Hsu<sup>1,2</sup>, Anne Burgevin<sup>1,2</sup>, Suzanne Guénette<sup>3</sup>, Anna Moser<sup>1,2</sup>, Peter van Endert<sup>1,2\*</sup>

**1** Institut National de la Santé et de la Recherche Médicale, Unité 1013, Paris, France, **2** Université Paris Descartes, Sorbonne Paris Cité, Faculté de Médecine Paris Descartes, Paris, France, **3** Genetics and Aging Research Unit, MassGeneral Institute for Neurodegenerative Disease, Charlestown, Massachusetts, United States of America

## Abstract

Antigen presentation by MHC class I molecules requires degradation of epitope source proteins in the cytosol. Although the preeminent role of the proteasome is clearly established, evidence suggesting a significant role for proteasome-independent generation of class I ligands has been reported repeatedly. However, an enzyme responsible for such a role has not been identified. Recently insulin-degrading enzyme (IDE) was shown to produce an antigenic peptide derived from the tumor antigen MAGE-A3 in an entirely proteasome-independent manner, raising the question of the global impact of IDE in MHC class I antigen processing. Here we report that IDE knockdown in human cell lines, or knockout in two different mouse strains, has no effect on cell surface expression of various MHC class I molecules, including allomorphs such as HLA-A3 and HLA-B27 suggested to be loaded in an at least a partly proteasome-independent manner. Moreover, reduced or absent IDE expression does not affect presentation of five epitopes including epitopes derived from beta amyloid and proinsulin, two preferred IDE substrates. Thus, IDE does not play a major role in MHC class I antigen processing, confirming the dominant and almost exclusive role of the proteasome in cytosolic production of MHC class I ligands.

**Citation:** Culina S, Mauvais F-X, Hsu H-T, Burgevin A, Guénette S, et al. (2014) No Major Role for Insulin-Degrading Enzyme in Antigen Presentation by MHC Molecules. PLoS ONE 9(2): e88365. doi:10.1371/journal.pone.0088365

**Editor:** Jacques Zimmer, Centre de Recherche Public de la Santé (CRP-Santé), Luxembourg

**Received:** September 25, 2013; **Accepted:** January 6, 2014; **Published:** February 7, 2014

**Copyright:** © 2014 Culina et al. This is an open-access article distributed under the terms of the Creative Commons Attribution License, which permits unrestricted use, distribution, and reproduction in any medium, provided the original author and source are credited.

**Funding:** This work was supported by grant 05-Blanc-0162 of the Agence Nationale de Recherche (Paris, France). The funders had no role in study design, data collection and analysis, decision to publish, or preparation of the manuscript.

**Competing Interests:** The authors have declared that no competing interests exist.

\* E-mail: peter.van-endert@inserm.fr

These authors contributed equally to this work.

## Introduction

The principal task of MHC class I (MHC-I) molecules is to present breakdown products of proteins synthesized by the presenting cell. The proteases involved in production of MHC-I ligands have been characterized in detail [1]. In the vast majority of cases, cytosolic proteasome complexes initiate degradation of the source proteins, producing peptides with a length of about 5 to 20 amino acids. These can be shortened by various aminopeptidases in the cytosol which in some cases have been shown to be involved in production of antigenic peptides, although the net effect tends to be a loss in class I ligands [2]. Endoplasmic reticulum aminopeptidases play a more important role in epitope production [3], while carboxypeptidases residing in the cytosol and the endoplasmic reticulum have only recently been described to trim some MHC-I ligands [4,5].

Although the dominant role of the proteasome is well documented and widely recognized, observations suggestive of alternative proteases responsible for the initial attack of source proteins yielding class I ligands have been known for a long time [6]. Among these, the long-term survival of cell lines in the presence of proteasome inhibitors was initially interpreted as evidence for a back-up protease but then turned out to reflect incomplete proteasome inhibition [7]. The fact that cell surface expression of some MHC-I allomorphs is not affected, or even increased, in the presence of proteasome inhibitors, might also be

due to partial inhibition, although some studies observed the phenomenon when the relevant proteasome subunits were inhibited at 70 to 80 percent [8,9]. MHC-I allomorphs preferring ligands with a carboxyterminal lysine such as HLA-A3 appeared to be especially “proteasome independent” although peptides with hydrophobic residues in this position could also be eluted from proteasome-inhibited HLA-A3-expressing cells [8,10]. Another interesting case is HLA-B27; according to a recent report, about 20 to 30 percent of its ligands appear proteasome-independent and are derived from small basic proteins [11]. Thus, a significant contribution of proteases other than the proteasome to initial antigen degradation in the cytosolic MHC-I processing pathway cannot be ruled out.

The first protease suggested to produce proteasome-independent ligands was tripeptidyl peptidase II (TPPII), a large cytosolic aminopeptidase [12]. Due to its (weak) trypsin-like endoprotease activity, TPPII was a candidate for production of peptides with basic carboxyterminal residues [13]. However, although the enzyme could be shown to contribute to production of some peptides [14,15], analysis of TPPII-deficient mice produced by several groups did not support a more general role in antigen processing [16,17]. Moreover, degradation of a complete antigenic protein by TPPII *in vitro* has never been demonstrated.

More recently, the group of B. van den Eynde in collaboration with us has shown that IDE can produce an antigenic peptide derived from the tumor antigen MAGE-A3 in a proteasome-



independent manner [18]. IDE is a ubiquitous enzyme with a predominant cytosolic location that degrades preferentially small substrates such as insulin or glucagon although oxidized hemoglobin can also be broken down by it [19]. IDE is unusual in that it seems to select structural features of substrates rather than specific sequences. Thus it has been proposed that IDE prefers substrates with a tendency to form amyloids, consistent with its capacity to degrade amyloid beta, shared by few proteases [20]. Given that amyloid formation generally is a type of misfolding, and that current evidence suggests that many source proteins for class I ligands correspond to defective and therefore possibly misfolded proteins [21], it was conceivable that IDE plays a larger role in MHC-I antigen processing. In this study we examined the effect of IDE knockdown or knockout on global MHC-I expression as well as presentation of a variety of antigens. Our results demonstrate that IDE does not play a more general role in peptide supply to MHC molecules.

## Materials and Methods

### Cell Lines

Human cervix carcinoma (HeLa) and colon carcinoma (HCT116) cell lines were purchased from ATCC. A human embryonic kidney (HEK293) cell line was kindly provided by G. de Saint Basile, Paris; H-2D<sup>d</sup> transfected HeLa cells by M. delVal, Madrid [22]; H-2K<sup>b</sup> transfected HeLa cells by I. York, Worcester, MA [17]; HLA-A2 and B27-transfected HeLa cells by J. Lopez de Castro, Madrid (unpublished); H-2K<sup>d</sup>-transfected HEK293 cells expressing a fusion between islet-specific glucose-6-phosphate catalytic subunit related protein (IGRP) and GFP by P. Santamaria, Calgary [23]; the mouse thymoma EL4 cell line (H-2<sup>b</sup>) and an EL4 clone transfected with ovalbumin (EG7) were kindly provided by E. Tartour, Paris. All cell lines were cultured in DMEM media supplemented by heat-inactivated FBS, 100 U/ml penicillin, 100 µg/ml streptomycin and 1% non-essential amino acids.

### siRNA Transfection

Cell lines were transfected with an siRNA set of 4 *Smart pool* heteroduplexes (Thermo Scientific) specific for human IDE (siIDE, duplex 1:5' UCA AAG GGC UGG GUU AAU AUU 3', 5' UAU UAA CCC AGC CCU UUG AUU 3'; duplex 2:5' ACA CUG AGG UUG CAU AUU UUU 3', 5' AAA UAU GCA ACC UCA GUG UUU 3'; duplex 3:5' GAA CAA AGA AAU ACC CUA AUU 3', 5' UUA GGG UAU UUC UUU GUU CUU 3'; duplex 4:5' GAA GUU ACG UGC AGA AGG AUU 3', 5' UCC UUC UGC ACG UAA CUU CUU 3'). 5×10<sup>6</sup> cells were resuspended in 250 µl of transfection buffer (PBS, 10 mM HEPES pH 8.2) and transfected with a final concentration of 100 nM or 400 nM of each duplex by electroporation (250 V, 960 µF). A non-targeting siRNA duplex pool (siNTG) was used as control. Twenty-four hours, 36 h, 48 h and 72 h after transfection, knockdown efficiency was verified by immunoblotting, reverse transcriptase-PCR (RT-PCR) and fluorescence microscopy.

### RNA Isolation, cDNA Synthesis and Real-time Quantitative RT-PCR

Total RNA was extracted from 2×10<sup>6</sup> siRNA-transfected cells with the QuickPrep<sup>TM</sup> extraction kit (GE Healthcare). Total RNA was reverse transcribed into cDNA using the ImProm-II<sup>TM</sup> Reverse Transcription System (Promega). Quantitative real-time PCR was performed and quantified with a Prism 7700 System (ABI/Life Technologies) using the SYBR Green master mix. The conditions for PCR were as follows: 1 cycle 50°C for 2 min, 1

cycle 95°C for 5 min, and 40 cycles 95°C for 30 s, 55°C for 30 s and 68°C for 1 min. The Ct values obtained were normalized to GAPDH and Actin B expression. The following primer sequences were used: IDE forward 5'-AAA AAG AGG CGA CAC CAT ACC -3', IDE reverse 5'- AGG TAC AAA TAG GCC ATG TT -3', GAPDH forward 5'-TGC ACC ACC AAC TGC TTA GC-3', GAPDH reverse 5'- GGC ATG GAC TGT GGT CAT GAG-3', Actin B forward 5'- CTG GAA CGG TGA AGG TGA CA-3' and Actin B reverse 5'- AAG GGA CTT CCT GTA ACA ATG-3'.

### Western Blotting

siRNA transfected cells were lysed in Laemmli buffer, denatured by boiling for 15 min, separated on a 10% SDS-PAGE gel and transferred onto polyvinylidene fluoride membranes (GE Healthcare). Membranes were blocked using non-fat dry milk in Tris-buffered saline with 0.1% Tween 20 overnight at 4°C and probed with an IDE-specific monoclonal antibody (mAb; clone 9B12, 0.5 µg/mL; Covance) and an actin B-specific (1:5000, Sigma) mAb as loading control. Staining was visualized using HRP-conjugated secondary Abs (1:25,000; Jackson ImmunoResearch), an ECL substrate (Immobilon<sup>TM</sup>, Millipore) and a Fuji LAS-1000 CCD camera.

### Immunofluorescence

Three days after siRNA transfection, 1×10<sup>5</sup> HeLa cells were cultured on 0.033% poly-L-lysine-treated 12 mm glass coverslips. Cells were fixed with 4% paraformaldehyde in PBS and quenched with 100 mM glycine, washed in PBS, treated with 0.2% BSA, 0.05% saponin (Sigma) and incubated for 45 min with 5 µg/ml of anti-IDE mAb. After washing, cells were incubated for 45 min with 10 µg/ml FITC-labeled goat anti-mouse antibodies (Abs; Jackson), washed again, fixed with 2% paraformaldehyde followed by glycine quenching and mounted with Fluoprep (BioMérieux). Images were taken with a DMI 6000B fluorescence microscope (Leica, Rueil-Malmaison, France) equipped with a 63x PlanApo objective and analyzed by 3D deconvolution using MetaMorph<sup>®</sup>6.2 software (Universal Imaging Corp., Downingtown, PA).

### Flow Cytometry

Twenty-four hours after siRNA transfection, cells were plated in complete DMEM in 6 well plates with or without 400 U/ml IFN-γ (R&D Systems) at 9×10<sup>5</sup> or 6×10<sup>5</sup> cells per well, respectively. Two days later, cells were washed with FACS buffer (PBS, 1.5% BSA, 0.05% NaN<sub>3</sub>), incubated with mAb W6/32 for 1 h at 4°C, washed and stained with FITC-labeled goat anti-mouse Abs (Jackson). Samples were acquired on a FACSCalibur<sup>TM</sup> (BD Bioscience) and analyzed using FlowJo<sup>TM</sup> software. Dead cells were excluded by propidium iodide staining.

Expression of MHC molecules was also evaluated on splenocytes of previously described IDE-deficient mice on both C57BL/6 and non-obese diabetic (NOD) backgrounds; the latter mice were produced by back-crossing the published strain [19] ten times to NOD mice (AM and PVE, manuscript in preparation). Cells were stained with anti-CD19/PE (clone 6D5; Biologend), anti-CD11c/eFluor450 (clone N418; eBioscience), anti-CD11b/PE-Cy (clone M1/70; BD Biosciences), anti-TCR-β/APC (clone H57-597; eBioscience), anti-F4-80/APC-Cy7 (clone RM8; Biologend), anti-H2-K<sup>b</sup>/biotin (clone AF6-88.5; Biologend), anti-H2-K<sup>d</sup>/biotin (clone SF1-1.1; Biologend) or anti-I-A<sup>k</sup>/biotin (cross-reacting with I-A<sup>g7</sup>; clone 10-3.6; Biologend) or rat anti-mouse IgG2a (Biologend) Abs followed by streptavidin/PE-CF594 (BD Biosciences). Prior to analysis on a FACSFortessa or a FACSCanto II flow cytometer, cells were stained with 7-AAD (BD Biosciences).

At least 3 independent experiments with 2–3 mice per group were performed.

### Flow Cytometry on Acid-stripped Cells

Sixty-five hours after transfection of HEK293 or HeLa B27 cells with siRNA, 1  $\mu$ M epoxomicin or 10  $\mu$ g/ml brefeldin A (both from Sigma) was added to the cells for 2 h or 30 min, respectively. Drug treatment was followed by acid removal of surface class I molecules, using a 90 s incubation in cold citrate buffer (pH = 3) for HEK293 cells, and a 120 s incubation in cold glycine buffer (pH = 2.8) for HeLa B27 cells, followed by neutralization with five volumes of DMEM without FBS. The stripped cells were split in two parts, one of which was stained immediately for HLA class I expression, while the other was suspended in DMEM with 10% FBS and incubated for 6 h in the presence of the drugs used before stripping, or without drugs. Finally the cells were stained for expression of HLA-A,B,C (mAb W6/32), HLA A3 (mAb GAP.A3) or HLA-B27 (mAb ME-1), as described above. Alternatively, splenocytes from C57BL/6 mice or NOD IDE wild type (wt) or knockout (ko) mice were treated with cold glycine buffer (pH = 2.8) for 90 s before neutralization by successive washes with five volumes of IMDM without FBS. The acid-stripped cells were either immediately stained for MHC-I expression, or suspended in IMDM with 10% FBS and incubated at 37°C for several periods. Finally the cells were stained for expression of H-2K<sup>b</sup> (mAb AF6.88-5) or H-2K<sup>d</sup> (mAb SF1-1.1) in combination with anti-CD19 and anti-CD11c as described above.

### Antigen Presentation Assays

**Vaccinia-ovalbumin.**  $3 \times 10^6$  HeLa-K<sup>b</sup> cells were transfected with siRNA. Three days later, the cells were infected with vaccinia viruses expressing ovalbumin (OVA) or peptide SIINFEKL (S8L) for 2 h at a multiplicity of infection (MOI) of 30 and 10, respectively. Then the cells were fixed with 1% formaldehyde, washed successively with 0.2 M glycine pH7.4, pH 7.0 and PBS, and added to T cell receptor (TCR)-transgenic OT-I T cells [24] seeded at  $2 \times 10^5$ /well in 96 well plates so that an effector:target (E:T) ratio of 2:1 and 4:1 resulted. HeLa cells not expressing H-2K<sup>b</sup> and HeLa-K<sup>b</sup> cells pulsed for 2 h with  $10^{-10}$ M S8L peptide were negative and positive controls, respectively. IFN- $\gamma$  secretion by OT-I cells was analyzed after a 12 h incubation by standard ELISA. Capture anti-IFN- $\gamma$  mAb was clone R4-6A<sub>2</sub> and detection mAb was clone XMG1.2 (both BD Pharmingen), both used at 0.2  $\mu$ g/50  $\mu$ l/well. Incubation times were 5 h for supernatant, 45 min for detection mAb, and 30 min for streptavidin-HRP (Sigma). Tetramethylbenzidine was used as substrate. Alternatively 400,000 C57BL/6 IDE wt or ko Mouse Embryonic Fibroblasts (MEFs) or Bone Marrow-derived Dendritic Cells (BM-DCs), prepared as described elsewhere [25] were infected with a vaccinia virus expressing OVA or the control strain WR1354 (obtained from ATCC) at an MOI of 30 and 10 for 2 h or 6 h. H-2K<sup>b</sup>-S8L complexes were detected by sequential incubation with mAb 25D1.16 (10  $\mu$ g/mL), FITC-labeled goat anti-mouse Abs (1:50; Biolegend), and Alexa488-labeled goat anti-FITC Abs (1:100; Invitrogen) and the fluorescence analyzed on a BD FACSCANTO-II analyzer.

**Vaccinia-gp160.**  $2 \times 10^6$  HeLa-D<sup>d</sup> cells were transfected with siRNA and infected with vaccinia viruses expressing the HIV envelope glycoprotein protein (gp160) or wt vaccinia virus at an MOI of 30, as described for vaccinia-OVA. Six hours after infection, the cells were added to a previously described CD8+ T cell clone recognizing the epitope RGPGRAVTI at an E:T ratio of 2:1 ( $1 \times 10^5$  CTLs/well in a 96-well plate). HeLa-D<sup>d</sup> cells pulsed with  $10^{-7}$ M peptide G9I for 2 h, and cells transfected 24 h before

addition of CTL with plasmid pMACS4-IRES.II encoding G9I, were used as controls. Cell lysis was assessed using the CytoTox-One™ assay (Promega), which measures release of lactate dehydrogenase by permeable dying cells. The percentage of specific lysis was calculated as: (experimental result – medium background) divided by (maximum lysis – medium background) multiplied with 100.

**IGRP-GFP.**  $3 \times 10^6$  HEK293-K<sup>d</sup> cells stably expressing an IGRP-GFP fusion protein were transfected with siRNA. Two days later, the cells were acid-stripped for 120 s with citrate buffer (pH = 2.8) followed by an overnight incubation in DMEM 10% FBS in the presence or absence of 0.1  $\mu$ M epoxomicin. P815 cells pulsed for 2 h with  $10^{-6}$ M superagonist peptide NRP-V7 were used as positive controls. HEK293 and P815 cells were added to TCR-transgenic 8.3 cells recognizing epitope IGRP<sub>206-14</sub> for 12 h at an E:T ratio of 2:1 before quantification of IFN- $\gamma$  secretion by ELISA as described above. 8.3 effector cells were prepared by stimulation of splenocytes from 8.3 mice with irradiated splenocytes from NOD mice and  $10^{-6}$ M peptide IGRP<sub>206-14</sub>, and used 5 or 6 days after stimulation.

**Amyloid-beta and proinsulin-S8L.** Amyloid beta and proinsulin expression plasmids were constructed in the vector pTRE-Tight (Clontech) containing the Tet Response Element. Initially the pTRE-Tight cloning site was modified by insertion between the SalI and XbaI sites of complementary oligonucleotides encoding the OVA epitope S8L. Then a cDNA encoding proinsulin was amplified from a previously described cloned human preproinsulin sequence [26], using primers containing BamHI (5') and SalI (3') sites, and subcloned into the modified vector. Sequences encoding human beta amyloid 1–42 preceded by the signal peptide from the rat Ig kappa-chain or not were synthesized by GeneArt (Munich, Germany) and subcloned as NcoI/SalI fragments into modified pTRE-Tight. HeLa Tet-on cells (Clontech) stably transfected with H-2K<sup>b</sup> (Hsu et al., submitted) were nucleofected with  $4 \times 100$  nM siRNA. One day later, the cells were electroporated with 20  $\mu$ g of the described pTRE-Tight plasmids. Expression was induced immediately by addition of 1  $\mu$ g/mL of doxycycline. Forty-two hours later, half of the cells were pulsed for 90 min with  $10^{-8}$ M S8L peptide. Finally H-2K<sup>b</sup>-S8L complexes were detected by sequential incubation with mAb 25D1.16 (10  $\mu$ g/mL), FITC-labeled goat anti-mouse Abs (1:50; Biolegend), and Alexa488-labeled goat anti-FITC Abs (1:100; Invitrogen). Fluorescence was read on a FACSCalibur cytometer.

**Cell line transfected with OVA.** After a 36 Gy gamma-irradiation of cell lines, EG7 cells were diluted with EL4 cells while keeping a final number of 100,000 cells/well constant. One hundred thousand OT-I T cells labeled with 5  $\mu$ M Carboxy-Fluorescein Succinimidyl Ester (CFSE; Invitrogen) for 12 min at 37°C were added to culture. After 20 h, supernatants were collected for quantification of IL-2 by ELISA whereas CFSE staining was measured after 48 h and 72 h using a BD FACSCanto II cytometer (BD Biosciences) and FlowJo v10 software, and proliferation calculated as previously described [27]. For IL-2 ELISA, the capture anti-IL-2 mAb was clone JES6-1A12 and the detection mAb was clone JES6-5H4 (both BD Pharmingen), both used at 0.2  $\mu$ g/50  $\mu$ l/well. Incubation times were 2 h for supernatant, 45 min for detection mAb, and 30 min for streptavidin-HRP (Sigma). Tetramethylbenzidine was used as substrate.

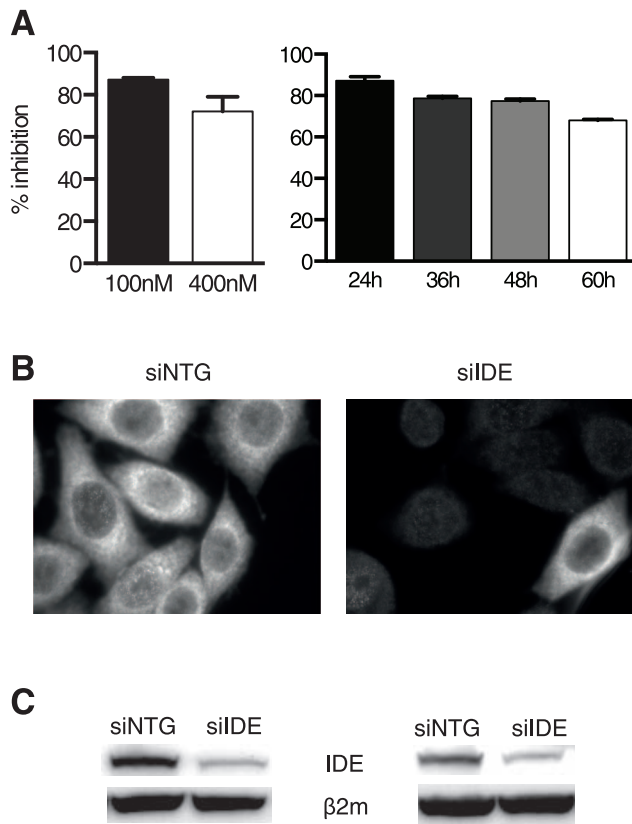


**Figure 1. Efficiency of IDE down-regulation by siRNA.** **A**, percentage of IDE mRNA inhibition, measured by qRT-PCR, in HeLa HHD cells transfected with different concentrations ( $4 \times 100$  or  $4 \times 400$  nM) of specific siRNA (left panel), and at different time points after transfection by  $4 \times 100$  nM siRNA (right panel). **B**, fluorescence microscopy analysis of HeLa HHD cells transfected with 400 nM of siIDE and siNTG 72 h after transfection. IDE expression was detected by staining with anti-IDE mAb 9B12. **C**, IDE expression by HeLa cells (left panel) and HEK293 cells (right panel) transfected with  $4 \times 100$  nM of siIDE or siNTG and probed 48 h later by immunoblot.  $\beta_2m$  served as a loading control. siNTG, small interfering RNA, non-targeted; siIDE, small interfering RNA, IDE-specific;  $\beta_2m$ , beta 2-microglobulin. One out of 5 (**A**, **C**) and 2 (**B**) experiments is shown. doi:10.1371/journal.pone.0088365.g001

### Ethics Statement

Animal experimentation performed in this study was approved by the Comité Régional d'Éthique pour l'Expérimentation Animale Ile de France – René Descartes (n° P2.LS.012.06).

### CD4+ T Lymphocyte Priming *in vitro* and *in vivo*

***In vivo* experiments.** TCR-transgenic CD4+ T cells purified from skin-draining lymph nodes of BDC2.5/NOD mice were labeled with  $10 \mu\text{M}$  CFSE for 12 min at  $37^\circ\text{C}$  and injected i.v. at  $2 \times 10^6$ /mouse into sex-matched non-diabetic NOD IDE wt or ko recipient mice. Twenty-four hours later, the mice were anesthetized using Xylazine plus Ketamine and injected in the four footpads with 500 ng of an OVA fusion protein modified to carry the p31 mimotope (P3UOp31) that is specifically recognized by the BDC2.5 TCR, or with unmodified OVA fusion protein (P3UO). Prior to injection, the fusion proteins were non-covalently coupled to a mAb recognizing CD11c (clone N418; ATCC), as described previously [27]. Four days later, skin draining lymph nodes and pancreatic lymph nodes were purified and stained with rat anti-mouse CD4/Pacific Blue (clone RM4-5; BD Biosciences)

and anti-mouse V $\beta$ 4/PE (clone KT4; BD Biosciences) Abs to identify the BDC2.5 cells. CFSE staining of BDC2.5 cells was measured using a FACSCFortessa™ flow cytometer (BD Biosciences) and FlowJo v10 software, and proliferation calculated as previously described [27].

***In vitro* experiments.** Splens from non-diabetic NOD IDE wt or ko were digested with collagenase D (Roche) for 40 min at  $37^\circ\text{C}$  and cell suspensions were enriched in DCs by performing a very low density gradient with OptiPrep (Axis-Shield); cells were stained for 30 min with anti-CD19/PE (clone 6D5; Biolegend), anti-CD11c/eFluor450 (clone N418; eBioscience) and 7-AAD was added prior cell sorting on a BD FACS ARIA-II cell sorter. Conventional DCs were sorted as 7-AAD-CD19-CD11c<sup>hi</sup> cells. Fifty thousand cells were then incubated with serial dilutions of P3UOp31 or P3UO complexed with anti-CD11c as described above for 1 h before the addition of 50,000 TCR-transgenic CD4+ T cells purified from skin-draining lymph nodes of BDC2.5/NOD mice and labeled with  $5 \mu\text{M}$  CFSE. On day 2, supernatants were collected to measure IL-2 concentration by ELISA, as described above. On day 4, proliferation of CD4+ T cells was evaluated by flow cytometry, as described above.

## Results

### Down-regulation of IDE Expression by siRNA Transfection of Human Cell Lines

Because the previous observation of a role of IDE in class I antigen processing was made in a human cell line [18], we first set up protocols to reduce IDE expression in a selection of human cell lines. We electroporated cells with pools of 4 siRNA sequences and analyzed the effect on IDE expression using quantitative PCR (qPCR), fluorescence microscopy, and immunoblotting (Fig. 1). Expression of IDE mRNA was reduced by >80 percent at 24 h after transfection and then recovered slightly to ~30 percent of controls at 60 h; optimal siRNA efficacy was observed at 100 nM duplex concentration, which was therefore used in further experimentation (Fig. 1A). Incomplete reduction of IDE expression as seen by qPCR likely was due to unaltered IDE expression in a small percentage of cells combined with complete extinction in the majority rather than uniform reduction in all cells, as suggested by microscopy analysis of HeLa cells (Fig. 1B). Efficient down-regulation of IDE expression was confirmed by immunoblots on HeLa and HEK293 cells analyzed 2 days after transfection (Fig. 1C). Knockdown protocols reducing IDE protein expression by at least 70 percent were established for all human cell lines used in this study, using the methods shown in Fig. 1.

### Effect of IDE Expression on Global Cell Surface HLA Class I Expression

We next examined the effect of reduced IDE expression on the level of HLA-A, B, C molecules or of specific human or murine MHC-I allomorphs on the surface of human cell lines. IDE knockdown had no effect on steady state levels of total HLA class I molecules by HEK293, HCT116 and HeLa cells (Fig. 2A, B, F, left hand panels), including clones transfected by H-2K<sup>d</sup> or HLA-A2 (Fig. 2D, E, left). Abs detecting the transfected class I molecules H-2D<sup>d</sup>, H-2K<sup>d</sup> and HLA-A2 (Fig. 2C left and 2D, E right) also did not reveal an effect of the IDE expression levels on cell surface class I levels. Treatment with IFN- $\gamma$  increases synthesis of MHC-I molecules but also may increase the number of oxidized proteins [28]. Reasoning that an effect of IDE knockdown might only be revealed in the presence of a high demand for class I ligands by newly synthesized class I molecules and/or damaged proteins, we treated cells with IFN- $\gamma$  for 24 h, however again without noting

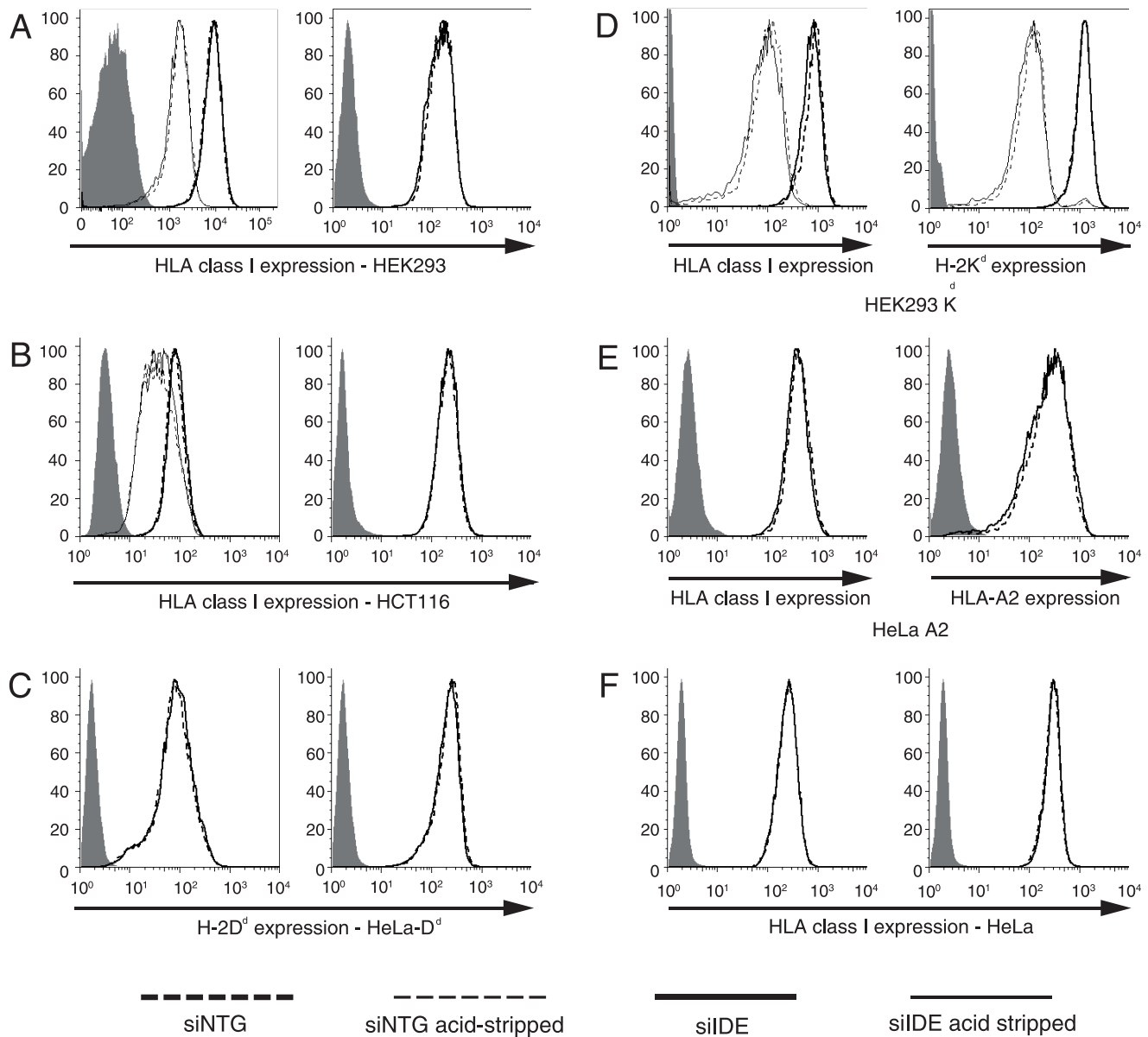


**Figure 2. Effect of IDE knockdown on HLA class I expression.** The indicated cell types were transfected with  $4 \times 100$  nM siIDE and expression of MHC-I molecules was detected 48 h later by flow cytometry. In **A**, **B** and **D** (left panels) cells were acid-stripped 24 h prior to analysis. In **A**, **B**, **C**, **F** (right panels), cells were incubated with 400 U/ml of IFN- $\gamma$  24 h after transfection. Cell surface expression of "HLA class I" was assessed using mAb W6/32, while expression of H-2D<sup>d</sup> was measured using mAb34-5-8, H-2K<sup>d</sup> using mAb20-8-4 and HLA-A2 using mAb BB7.2. Filled histograms: secondary Ab only. One of 3 experiments is shown.  
doi:10.1371/journal.pone.0088365.g002

any impact of IDE knockdown on HLA A, B, C expression by HEK293, HCT116 and HeLa cells (Fig. 2A, B, F right). Recovery of HLA class I expression, measured 24 h after acid stripping of cell surface molecules, also was not affected by IDE expression levels. Thus, IDE did not have any measurable impact on global HLA class I expression at all conditions tested.

#### Effect of IDE on Antigen Presentation by MHC-I Molecules

Although IDE did not affect global cell surface MHC-I expression, it was possible that the enzyme affected presentation of individual epitopes produced in the endogenous MHC-I processing pathway. Because up to 30 percent of transfected

cells retained IDE expression after siRNA transfection (Fig. 1), we first examined the sensitivity of our T cell assays. For this, we mixed transfected EG7 cells stably expressing OVA with non-transfected parent EL4 cells, keeping the total cell number constant, and incubated the mixture with OT-I CD8<sup>+</sup> T cells that recognize the H-2K<sup>b</sup>-restricted epitope OVA<sub>257-64</sub> (S8L). Using both IL-2 secretion and proliferation as readout, absence of OVA presentation by 60 percent or more of the cells was clearly detectable, ruling out a plateau effect for the highly sensitive OT-I T cells (Fig. 3A). Next we tested the effect of IDE knockdown on presentation of S8L and of two additional epitopes derived from the envelope protein of HIV and the type 1 diabetes autoantigen IGRP. The two former were expressed through recombinant vaccinia viruses and the latter in a stable

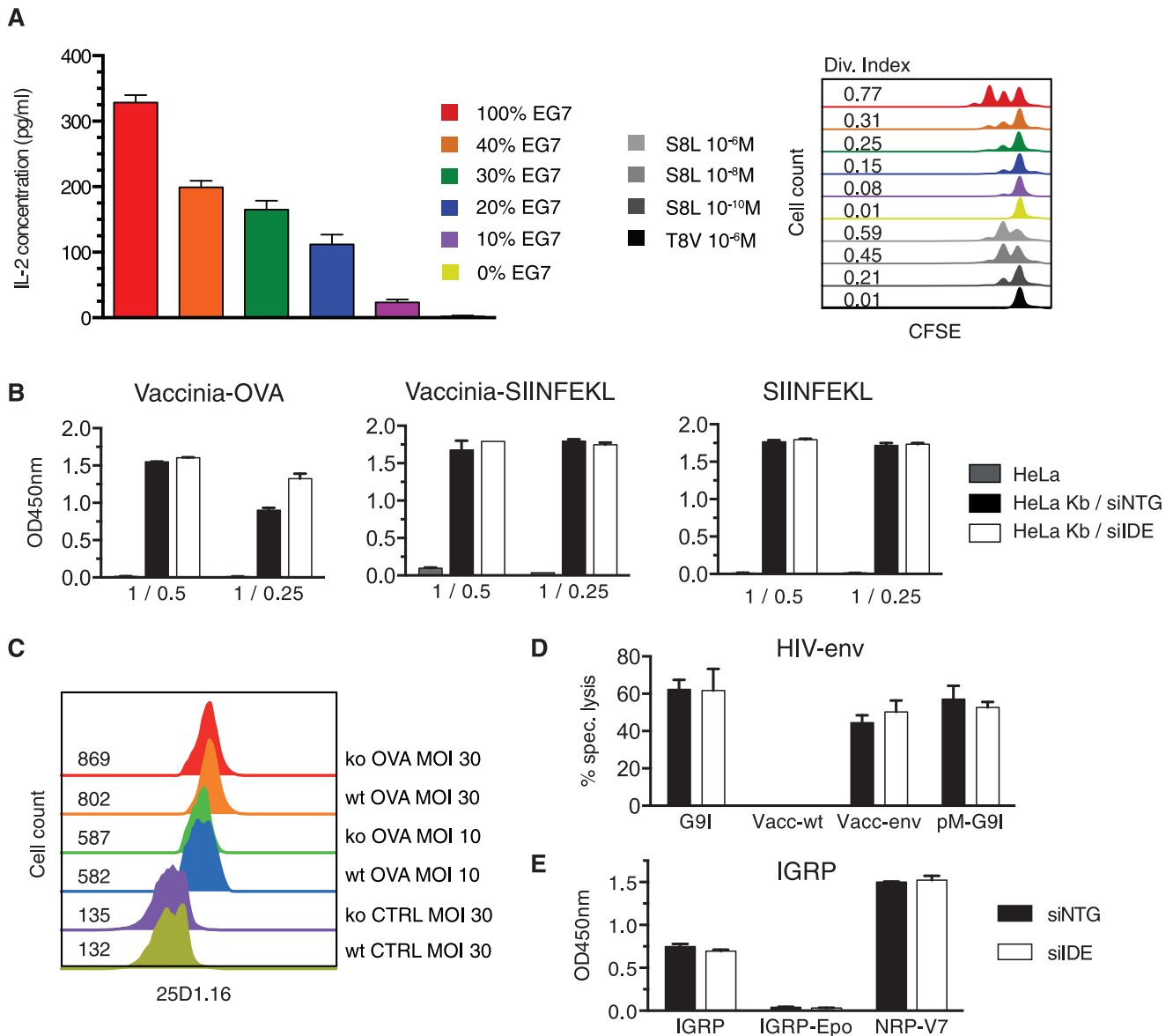


**Figure 3. IDE is not involved in endogenous MHC-I presentation of viral antigens and a self antigen.** A, 150,000 CFSE-labeled OT-I T cells were incubated with EG7 cells complemented to 100,000 cells with EL4 cells, with the percentage of EG7 cells in the mixture indicated in the legend. As control, 100,000 EL4 cells were incubated with S8L or irrelevant peptide TSYFESEV (T8V). After 16 h (left) and 48 h (right), T cell activation was assessed by measuring the IL-2 concentration in the supernatants and T cell proliferation by the dilution of CFSE, respectively. B, HeLa-K<sup>b</sup> cells were transfected with siRNA. Seventy-two hours later, the cells were infected with a recombinant vaccinia virus encoding ovalbumin or the H-2K<sup>b</sup> restricted epitope SIINFEKL, or pulsed with 10<sup>-10</sup>M SIINFEKL peptide and incubated with SIINFEKL-specific OT-I T cells, using different effector to target ratios. Secretion of IFN- $\gamma$  by OT-I cells was measured by ELISA. In panel C, formation of S8L/H2-K<sup>b</sup> complexes at the cell surface of IDE wt and ko C57BL/6 MEFs was evaluated 6 h after infection with vaccinia viruses expressing OVA or not (CTRL), by staining cells with mAb 25D1.16; numbers indicate the MFI for 25D1.16. Panel D shows an equivalent experiment with siRNA transfected HeLa-D<sup>d</sup> cells and CTL recognizing a peptide from HIV gp160. Here the antigens were (from left to right) 10<sup>-7</sup>M cognate peptide G9I, wt vaccinia virus, vaccinia virus encoding HIV-env, and a plasmid encoding peptide G9I (pM-G9I). Presentation was assessed using a standard kill assay with an effector to target ratio of 2:1. E, HEK293-K<sup>d</sup> cells stably expressing an IGRP-GFP fusion protein were transfected with siRNA and acid stripped 56 h after transfection (IGRP). Prior to addition of CTLs at an E:T ratio of 1:1, 72 h after transfection, part of the target cells was incubated with epoxomicin (Epo). Secretion of IFN- $\gamma$  by CTLs was measured by standard ELISA. Cells treated as described and pulsed with 10<sup>-6</sup>M super-agonist peptide NRP-V7 were positive controls. One out of 3 (A, B, D), 2 (C) or 5 (E) experiments is shown. doi:10.1371/journal.pone.0088365.g003

transfectant. All epitopes were presented by murine class I molecules transfected in HeLa or HEK293 cells. Presentation of S8L pulsed on HeLa-K<sup>b</sup> cells, expressed as mini-gene or as full-length protein, was not affected by IDE knockdown (Fig. 3B). Thus, cell surface expression of H-2K<sup>b</sup>, intracellular loading of K<sup>b</sup> molecules, and proteolytic generation of the OVA epitope

did not require IDE. To further corroborate the absence of an IDE effect on S8L presentation, we took advantage of the TCR-like mAb 25D1.16 [29] that provides quantitative information on the number of H-2K<sup>b</sup> complexes. MEFs produced from published IDE-deficient C57BL/6 mice and infected with vaccinia viruses encoding OVA or not expressed

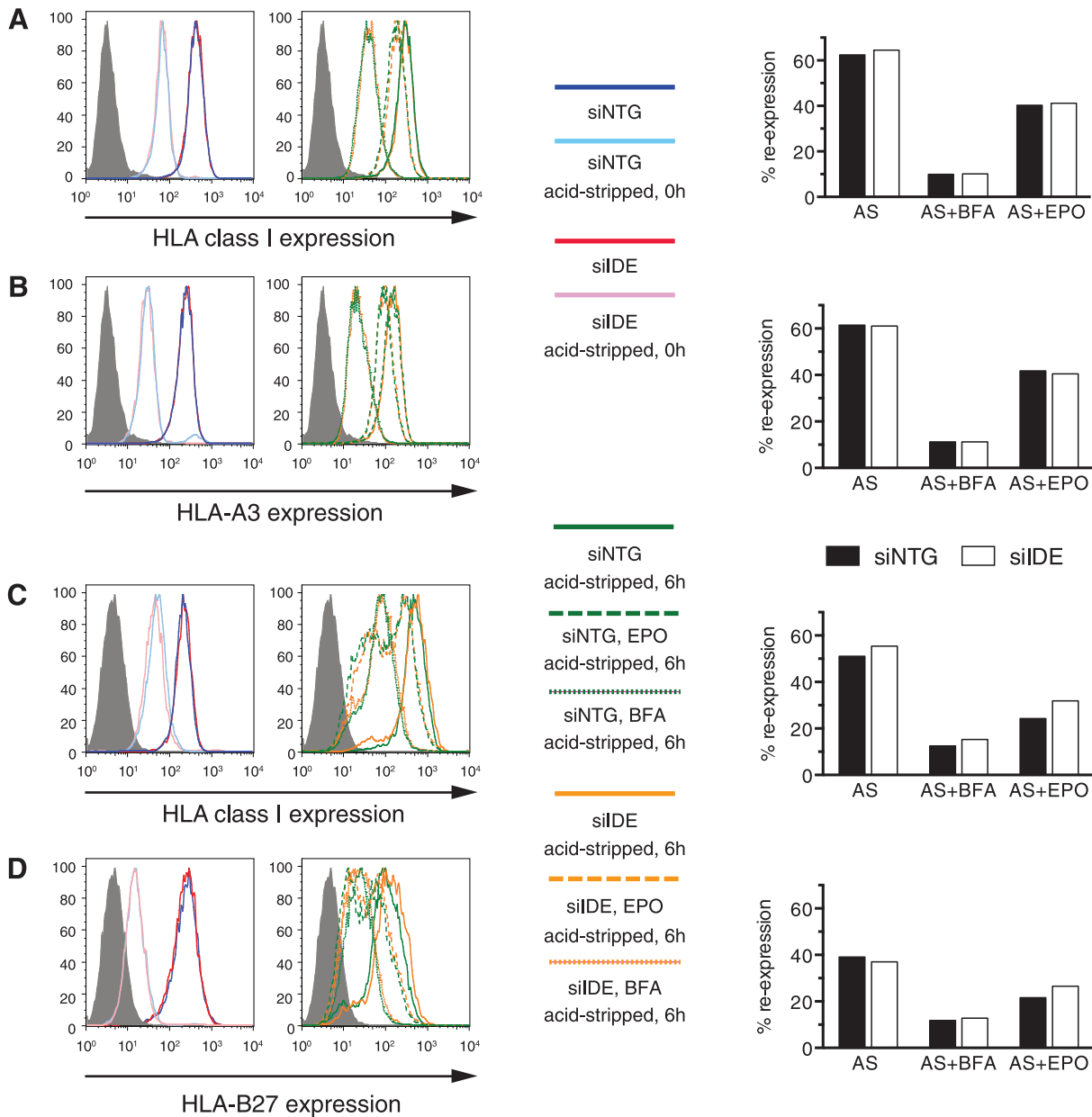


**Figure 4. Role of IDE in expression of "proteasome-independent" HLA class I alleles.** HLA-A3-expressing HEK293 cells and HLA-B27-transfected HeLa cells were transfected with  $4 \times 100$  nM siRNA. Sixty-five hours later,  $1 \mu\text{M}$  epoxomicin or  $10 \mu\text{g/ml}$  brefeldin A were added to the cultures for 2 h or 30 min, respectively, before removal of most cell surface class I molecules by acid stripping and another 6 h incubation with the same drugs. HLA class I expression was detected using mAb W6/32 immediately after acid stripping (**A, C** left panel) and after the 6 h incubation (**A, C** center panel). The panels on the right show HLA class I re-expression relative to untreated cells as histograms. The panels in **B** and **D** show an evaluation of HEK293 cells using mAb GAP.A3 with specificity for HLA-A3 (**B**) and of HeLa-B27 cells using mAb ME-1 recognizing HLA-B27 (**D**). AS, acid stripping; BFA, brefeldin A; EPO, epoxomicin; filled histogram, secondary Ab only. One out of 3 experiments is shown.  
doi:10.1371/journal.pone.0088365.g004

the same number of H-2K<sup>b</sup>/S8L complexes as wild type MEFs (Fig. 3C), confirming that IDE was not involved in endogenous OVA processing for MHC-I presentation. Equivalent results were obtained when infecting BM-DCs (not shown). Similarly, presentation of the H-2D<sup>d</sup>-restricted HIV-envelope epitope encoded in a vaccinia virus or introduced by transfection with a plasmid encoding HIV-env was not affected by IDE knockdown (Fig. 3D). Finally, reduced IDE expression affected neither the presentation of a synthetic variant (NRP-V7) of the IGRP epitope nor the presentation of the epitope by a stable IGRP transfectant tested 16 hrs after removal of H-2K<sup>d</sup>-

IGRP<sub>206-14</sub> complexes by acid stripping, while treatment with the proteasome inhibitor epoxomicin abolished presentation (Fig. 3E). Thus, proteolytic generation of three viral and self-epitopes did not involve IDE.

#### Effect of IDE knockdown on Cell Surface Expression of HLA-A3 and HLA-B27

The effect of proteasome inhibition on global MHC-I loading has been described to vary greatly according to the allomorph considered. The relative insensitivity of HLA-A3 to proteasome

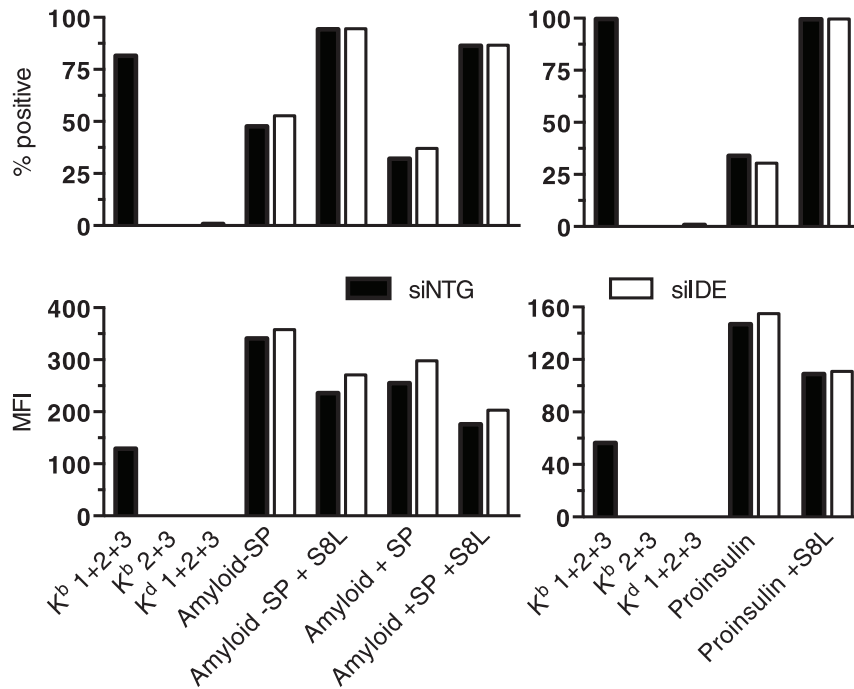


**Figure 5. HeLa Tet-on cells expressing H-2K<sup>b</sup> were nucleofected with 4×100 nM siRNA.** Twenty-four hours later, the cells were electroporated with inducible plasmids encoding amyloid beta preceded by a signal peptide (+SP) or not (−SP), or encoding proinsulin, all tagged with the S8L peptide at the C-terminus. Protein expression was induced immediately by addition of 1 μg/ml doxycyclin. Forty-eight hours later, K<sup>b</sup>/S8L complexes on the cell surface were detected using mAb 25D1.16 (Ab1) followed by FITC-labeled goat anti-mouse Abs (Ab2) and Alexa488-labeled goat anti-FITC Ab (Ab3). Control samples were HeLa-K<sup>b</sup> cells pulsed for 2 h with 10<sup>−8</sup> M S8L and stained with Abs 1, 2 and 3 or with Abs 2 and 3 only, as well as peptide-pulsed HeLa cells expressing H-2K<sup>d</sup> stained with Abs 1, 2 and 3. One of two experiments is shown. doi:10.1371/journal.pone.0088365.g005

inhibitors is ascribed to its preference for Lys at the C-terminus [10], while the reason for the reported proteasome resistance of a 30 percent proportion of HLA-B27 ligands, most of which are derived from small basic proteins, remains unclear [11]. Although we had found that expression of the HLA and H-2 class I molecules expressed by HeLa, HEK and HCT cells did not correlate with IDE expression levels, it was conceivable that IDE was involved in ligand production for the mentioned particularly “proteasome-independent” allomorphs. To study this, we subjected HEK293 cells naturally expressing HLA-A3, and HLA-B27-transfected HeLa cells to acid stripping of cell surface class I molecules, and examined re-expression of total HLA-A, B, C molecules versus re-expression of the presumed proteasome-independent or partly independent molecules. Six hours after stripping, global class I and A3 re-expression reached 50 to 60 percent of levels prior to acid treatment (Fig. 4A–C), while B27 re-expression was 40 percent (Fig. 4D). Incubation with Brefeldin A after acid-stripping reduced re-expression to 10 percent, as expected. Addition of epoxomicin after stripping reduced re-expression by no more than one third to one half, consistent with the reported proteasome-independence of the allomorphs studied [8,10,11]. Note that the epoxomicin sensitivity of HLA-A3 did not differ from that of the HLA-A,B,C molecules expressed by HEK293, while HLA-B27 appeared more “proteasome independent” than the endogenous HLA-A,B,C molecules expressed by HeLa cells. Knockdown of IDE had no effect on the recovery of HLA-A3 and HLA-B27 (Fig. 4). Thus, IDE is not responsible for the reported “proteasome independence” of HLA-A3 and HLA-B27.

### Effect of IDE Knockdown on Presentation of Amyloid Beta and Proinsulin

Although IDE played no role in class I presentation of 3 standard epitopes (Fig. 3), we reasoned that a role was more likely in presentation of substrates known to be degraded by IDE and to be relatively resistant to other proteases. Only a small number of proteases can degrade beta amyloid [30] and proinsulin, though having lower affinity for IDE than insulin, is known to be an IDE substrate [31]. Lacking suitable CD8+ T cells recognizing beta amyloid and proinsulin, we tagged the two autoantigens with the epitope S8L, expressed them in H-2K<sup>b</sup>-transfected HeLa cells, and measured presentation using mAb 25D1.16. Expression of both beta amyloid (preceded or not by a signal peptide) and proinsulin resulted in presentation of S8L by 30 to 50 percent of transfected cells, suggesting that both proteins were efficiently processed (Fig. 5). However, IDE knockdown did not reduce presentation.

### Analysis of IDE Deficient Mice for Expression of MHC Molecules and MHC Class II Antigen Presentation

Although IDE has a dominant cytosolic location, a small percentage of the enzyme is thought to localize to endosomes and may participate in the degradation of internalized insulin according to some older papers [31]. To further address a possible role of IDE in production of MHC-I ligands, and to examine its role in production of MHC-II ligands, we used the published IDE knockout mice generated on the C57BL/6 background, which we also back-crossed to the NOD strain (AM and PVE, manuscript in preparation). IDE-deficient mice on both genetic backgrounds harbor normal numbers of splenic B, T and dendritic cells which express normal amounts of MHC-I molecules, confirming results

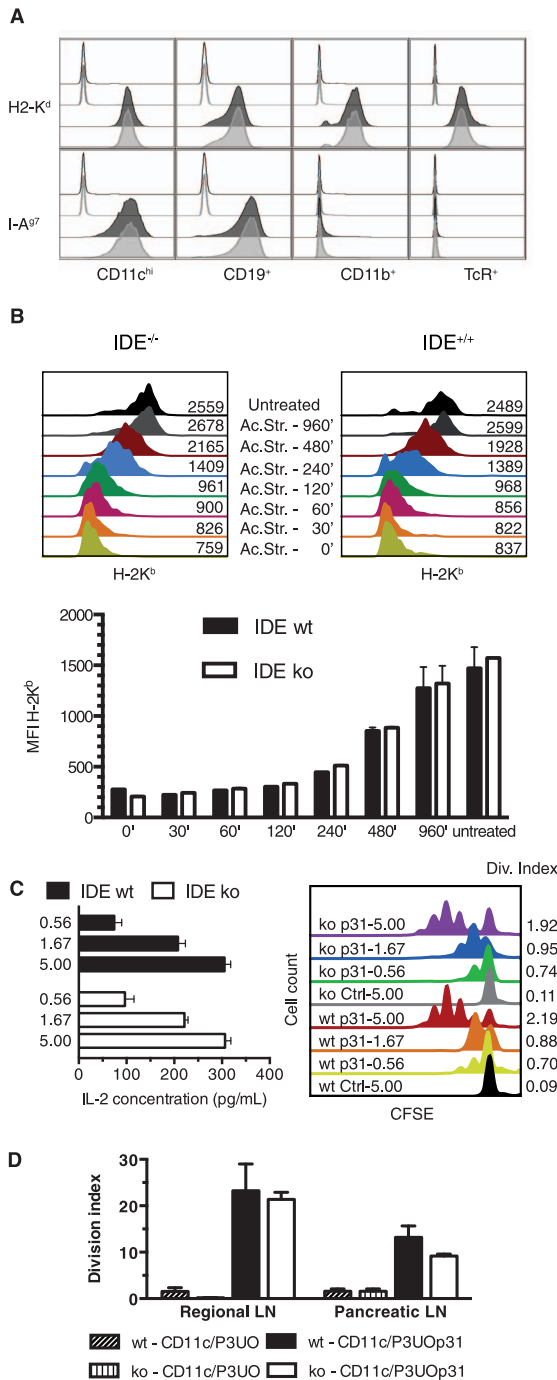


**Figure 6. Characterization of IDE ko mice.** **A**, expression of MHC molecules on wt (black lines) and IDE ko (grey lines) NOD splenocytes. Live cells were gated on TcR-β<sup>+</sup> cells, CD19<sup>+</sup> cells, CD11c<sup>hi</sup> cells or CD11b<sup>+</sup>CD11c<sup>-</sup> cells, and analyzed for expression of H-2K<sup>d</sup> and I-A<sup>97</sup>. Isotype controls are shown in open, and specific stainings in filled histograms. **B**, Splenocytes from IDE wt and ko C57BL/6 mice were subjected to a 90 s treatment with acid, incubated with 10% FCS complete medium for the indicated periods to allow for re-expression of MHC-I molecules, and then stained for H-2K<sup>b</sup> with mAb AF6-88.5, using gates on CD11c<sup>+</sup> DCs (top panels, experiment represented as FACS plots) and CD19<sup>+</sup> B cells (bottom panel, means ± SDEV of 2 experiments represented as histogram). Numbers on histograms in the top panels indicate MFI for AF6-88.5. **C**, 25,000 TCR-transgenic CFSE-labeled BDC2.5 CD4<sup>+</sup> T cells were put in contact with 20,000 sorted splenic CD11c<sup>hi</sup> DCs incubated with graded amounts of the fusion proteins P3UOp31 or P3UO (Ctrl) in complexes with an anti-CD11c mAb.

After 2 days (left panel) or 4 days (right panel), T cell activation was assessed by measuring the IL-2 concentration in the culture supernatant and proliferation was measured by flow cytometry as dilution of CFSE, respectively. The numbers next to the FACS plots indicate the division index of progenitor cells, calculated as previously described [27]. One out of 2 experiments. **D**, priming of CD4<sup>+</sup> T cells in IDE-deficient mice. CFSE-labeled BDC2.5 T cells were injected into wt and IDE-deficient mice. Twenty-four hours later, 500 ng of the P3UOp31 or P3UO fusion proteins in complexes with a CD11c-specific mAb were injected s.c. Four days after antigen injection, CD4<sup>+</sup>Vβ4<sup>+</sup> T cells recovered from draining and pancreatic lymph nodes were assessed for CFSE dilution by flow cytometry and the division index of injected precursors was calculated. Two independent experiments were performed, with a total of 5 or 6 mice per condition. Means and SDEV are shown.

doi:10.1371/journal.pone.0088365.g006

obtained with human cell lines using RNA interference (Fig. 6A, Table 1). We reasoned that, although the steady state levels of MHC-I molecules on IDE ko cells are normal, a potential limited role of IDE in endogenous antigen processing might cause a delay in production and export of new class I molecules. To address this, we subjected IDE wt and ko C57BL/6 splenic DCs and B lymphocytes to a short acid treatment that removed 85% of cell surface H-2K<sup>b</sup> molecules and monitored re-expression of H-2K<sup>b</sup> over up to 16 h (Fig. 6B). IDE ko cells recovered class I expression with the same kinetics as wt cells. Similar results were obtained with NOD splenocytes (not shown).

DCs, B and T cells and macrophages of IDE ko NOD mice also expressed normal levels of cell surface MHC-II molecules (Fig. 6A). Importantly, the murine cell types tested by us for MHC-I and II expression all physiologically express IDE (between 3,000 and 7,000 IDE mRNA copies per cell; J. Kim and PvE, unpublished observations), consistent with the known ubiquitous nature of its expression. To study MHC-II-restricted antigen presentation, we used complexes of a fusion protein consisting of OVA preceded by streptococcal Ig-binding domains and ubiquitin, and a mAb with specificity for the dendritic cell receptor CD11c [27]. Two versions of the fusion protein were used: protein P3UOp31 containing the p31 mimotope [32] inserted into OVA and recognized by TCR-transgenic CD4<sup>+</sup> BDC2.5 T cells (specific for the pancreatic autoantigen chromogranin A [33]), and protein P3UO containing unmodified OVA. Upon incubation with graded amounts of fusion protein *in vitro*, IDE-sufficient and deficient NOD DCs induced IL-2 secretion by, and proliferation of BDC2.5 CD4<sup>+</sup> T cells with undistinguishable efficiency (Fig. 6C). We also injected mice with CFSE-labeled BDC2.5 cells followed 1 day later by the antigenic complexes, and another 4 days later by analysis of T cell proliferation (Fig. 6B). While the control protein P3UO did not stimulate BDC2.5 proliferation, injection of CD11c-targeted P3UOp31 triggered vigorous proliferation of BDC2.5 cells

**Table 1. MHC-I expression by splenocyte sub-populations of IDE ko mice.**

Strain	MFI* control	% B cells	MFI	% T cells	MFI	% DCs	MFI
C57/BL6 wt	3.0	64	93	31	93	5.9	90
C57/BL6 ko	—	64	114	31	113	5.0	120
NOD wt	3.7	46	146	17	132	4.2	166
NOD ko	—	48	150	17	124	4.0	138

\*MFI, mean fluorescence intensity.

doi:10.1371/journal.pone.0088365.t001



recovered both from regional and from pancreatic lymph nodes. However, IDE deficiency did not have a significant impact on the extent of BDC2.5 proliferation.

## Discussion

Prompted by the published finding that IDE can process a tumor antigen [18], in this study we examined the hypothesis that proteolysis by IDE may account for the phenomenon of proteasome-independent MHC-I loading with peptides, suggested by various reports in the literature. Studying human and murine cells, and using both RNA interference and gene invalidation, we conclude that IDE neither has a detectable effect on cell surface expression of various MHC-I molecules including allomorphs described to be especially proteasome-independent, nor on presentation of five different antigens including two proteins known to be preferred IDE substrates. Thus, implication of IDE in MHC-I processing as described for MAGE-A3 is unlikely to be a common phenomenon.

Given the number of MHC-I allomorphs studied and the different approaches used in this study, we conclude that a general major role of IDE in MHC-I loading can be ruled out. Our findings therefore parallel earlier studies of TPPII, the second protease initially described to produce an antigenic epitope in a proteasome-independent manner and subsequently shown to be dispensable for efficient MHC-I loading. Thus, despite substantial efforts undertaken in this and previous studies, it remains impossible to identify a protease capable of making a significant proteasome-independent contribution to cytosolic MHC-I antigen processing. One way, and possibly the most plausible one, of interpreting this fact is that such a protease does not exist, and that previous reports of substantial proteasome-independent MHC-I loading simply reflect the conundrum that complete proteasome inhibition (and more so knockout) of the proteasome is not feasible, and that some class I allomorphs are more readily loaded in the presence of low proteasome activity than others. It also cannot be ruled out that some allomorphs rely more on non-cytosolic sources of ligands than others.

Our examination of the presentation of defined epitopes by cells lacking IDE demonstrated that the enzyme is not implicated in presentation of three standard epitopes as well as two epitopes linked to proteins known to be preferred IDE substrates. Although these results are consistent with the lack of a global role of IDE in antigen processing, they do not rule out a role of the enzyme in processing and presentation of peptides derived from preferred substrates. Lacking CD8+ T cells recognizing beta amyloid, we attached an OVA epitope to the protein and examined its

presentation to OT-I T cells. It is conceivable that other proteases, e.g. the proteasome, can remove the C-terminal tag from our beta amyloid protein without degrading the amyloid 42-mer. However, our results obtained in an independent project suggest that IDE is not required for processing and presentation of an immunodominant epitope in the insulin B chain by beta cells (AM and PVE, manuscript in preparation), confirming the results obtained with the tagged insulin molecule examined in this study. Nevertheless, it needs to be emphasized that our results do not rule out an effect of IDE in processing of other antigens, or minor effects on presentation of the epitopes studied here. On the other hand, the absence of other “accessory” proteases involved in MHC-I antigen processing, such as ERAPI or immunoproteasome subunits, consistently results in decreased cell surface expression of class I molecules [34,35], suggesting that the extensive screening of different class I allomorphs undertaken in this study should have allowed for detecting a global role of IDE in antigen processing.

Although the negative results reported here might seem little surprising as they are in line with earlier studies of other proteases, we contend that the complete lack of a role of IDE in substrates such as amyloid beta and insulin is a non-trivial observation. Few proteases including IDE but not the proteasome are able to degrade beta amyloid efficiently [30]. Moreover, although the proteasome is known to cleave the insulin B chain efficiently, insulin and proinsulin are highly preferred IDE substrates [31]. IDE also has been demonstrated to degrade proinsulin processed by the endoplasmic reticulum-associated degradation pathway [36]. Thus a role for IDE in the processing of at least these substrates was expected. We speculate that these proteins may not be readily accessible to IDE when they are processed to antigenic epitopes, consistent with the so far entirely hypothetical model of an “immunoribosome” [37] including a co-translational mechanism for peptide degradation in which the proteasome would occupy a privileged and exclusive place.

## Acknowledgments

We are grateful to G. de Saint-Basile and E. Tartour (Paris), M. del Val and J. Lopez de Castro (Madrid), P. Santamaria (Calgary), and I. York (Worcester) for the gift of cell lines and transfectants.

## Author Contributions

Conceived and designed the experiments: SC FXM PVE. Performed the experiments: SC HTH FXM AB AM. Analyzed the data: SC FXM PVE. Contributed reagents/materials/analysis tools: HTH SG. Wrote the paper: PVE.

## References

1. Rock KL, Farfan-Arribas DJ, Shen L (2010) Proteases in MHC class I presentation and cross-presentation. *J Immunol* 184: 9–15.
2. van Endert P (2011) Post-proteasomal and proteasome-independent generation of MHC class I ligands. *Cellular and molecular life sciences: Cell Mol Life Sci* 68: 1553–1567.
3. Weimershaus M, Evnouchidou I, Saveanu L, van Endert P (2013) Peptidases trimming MHC class I ligands. *Curr Opin Immunol* 25: 90–96.
4. Shen XZ, Billet S, Lin C, Okwan-Duodu D, Chen X, et al. (2011) The carboxypeptidase ACE shapes the MHC class I peptide repertoire. *Nat Immunol* 12: 1078–1085.
5. Kessler JH, Khan S, Seifert U, Le Gall S, Chow KM, et al. (2011) Antigen processing by nardilysin and thimet oligopeptidase generates cytotoxic T cell epitopes. *Nat Immunol* 12: 45–53.
6. Saveanu L, Fruci D, van Endert P (2002) Beyond the proteasome: trimming, degradation and generation of MHC class I ligands by auxiliary proteases. *Mol Immunol* 39: 203–215.
7. Princiotto MF, Schubert U, Chen W, Benmink JR, Myung J, et al. (2001) Cells adapted to the proteasome inhibitor 4-hydroxy-5-iodo-3-nitrophenylacetyl-Leu-Leu-leucinal-vinyl sulfone require enzymatically active proteasomes for continued survival. *Proc Natl Acad Sci U S A* 98: 513–518.
8. Benham AM, Gromme M, Neeffjes J (1998) Allelic differences in the relationship between proteasome activity and MHC class I peptide loading. *J Immunol* 161: 83–89.
9. Vinitzky A, Anton LC, Snyder HL, Orlowski M, Benmink JR, et al. (1997) The generation of MHC class I-associated peptides is only partially inhibited by proteasome inhibitors: involvement of nonproteasomal cytosolic proteases in antigen processing? *J Immunol* 159: 554–564.
10. Luckey CJ, Marto JA, Partridge M, Hall E, White FM, et al. (2001) Differences in the expression of human class I MHC alleles and their associated peptides in the presence of proteasome inhibitors. *J Immunol* 167: 1212–1221.
11. Marcilla M, Cragolini JJ, Lopez de Castro JA (2007) Proteasome-independent HLA-B27 ligands arise mainly from small basic proteins. *Mol Cell Proteomics* 6: 923–938.
12. van Endert P (2008) Role of tripeptidyl peptidase II in MHC class I antigen processing - the end of controversies? *Eur J Immunol* 38: 609–613.

13. Geier E, Pfeifer G, Wilm M, Lucchiari-Hartz M, Baumeister W, et al. (1999) A giant protease with potential to substitute for some functions of the proteasome. *Science* 283: 978–981.
14. Seifert U, Maranon C, Shmueli A, Desoutter JF, Wesoloski L, et al. (2003) An essential role for tripeptidyl peptidase in the generation of an MHC class I epitope. *Nat Immunol* 4: 375–379.
15. Guil S, Rodriguez-Castro M, Aguilar F, Villasevil EM, Anton LC, et al. (2006) Need for tripeptidyl-peptidase II in major histocompatibility complex class I viral antigen processing when proteasomes are detrimental. *J Biol Chem* 281: 39925–39934.
16. Firat E, Huai J, Saveanu L, Gaedicke S, Aichele P, et al. (2007) Analysis of Direct and Cross-Presentation of Antigens in TPPH Knockout Mice. *J Immunol* 179: 8137–8145.
17. York IA, Bhutani N, Zendzian S, Goldberg AL, Rock KL (2006) Tripeptidyl peptidase II is the major peptidase needed to trim long antigenic precursors, but is not required for most MHC class I antigen presentation. *J Immunol* 177: 1434–1443.
18. Parmentier N, Stroobant V, Colau D, de Diesbach P, Morel S, et al. (2010) Production of an antigenic peptide by insulin-degrading enzyme. *Nat Immunol* 11: 449–454.
19. Farris W, Mansourian S, Chang Y, Lindsley L, Eckman EA, et al. (2003) Insulin-degrading enzyme regulates the levels of insulin, amyloid beta-protein, and the beta-amyloid precursor protein intracellular domain in vivo. *Proc Natl Acad Sci U S A* 100: 4162–4167.
20. Kurochkin IV (2001) Insulin-degrading enzyme: embarking on amyloid destruction. *Trends Biochem Sci* 26: 421–425.
21. Dolan BP, Bennink J, Yewdell J (2011) Translating DRiPs: progress in understanding the viral and cellular sources of MHC class I peptide ligands. *Cell Mol Life Sci* 68: 1481–1489.
22. Saveanu L, Carroll O, Lindo V, Del Val M, Lopez D, et al. (2005) Concerted peptide trimming by human ERAP1 and ERAP2 aminopeptidase complexes in the endoplasmic reticulum. *Nat Immunol* 6: 689–697.
23. Tsai S, Shameli A, Yamanouchi J, Clemente-Casares X, Wang J, et al. (2010) Reversal of autoimmunity by boosting memory-like autoregulatory T cells. *Immunity* 32: 568–580.
24. Hogquist KA, Jameson SC, Heath WR, Howard JL, Bevan MJ, et al. (1994) T cell receptor antagonist peptides induce positive selection. *Cell* 76: 17–27.
25. Weimershaus M, van Endert P (2013) Preparation of dendritic cells by in vitro cultures. *Methods Mol Biol* 960: 351–357.
26. Hassainya Y, Garcia-Pons F, Kratzer R, Lindo V, Greer F, et al. (2005) Identification of naturally processed HLA-A2-restricted proinsulin epitopes by reverse immunology. *Diabetes* 54: 2053–2059.
27. Kratzer R, Mauvais FX, Burgevin A, Barilleau E, van Endert P (2010) Fusion proteins for versatile antigen targeting to cell surface receptors reveal differential capacity to prime immune responses. *J Immunol* 184: 6855–6864.
28. Ebstein F, Voigt A, Lange N, Warnatsch A, Schroter F, et al. (2013) Immunoproteasomes are important for proteostasis in immune responses. *Cell* 152: 935–937.
29. Porgador A, Yewdell JW, Deng Y, Bennink JR, Germain RN (1997) Localization, quantitation, and in situ detection of specific peptide-MHC class I complexes using a monoclonal antibody. *Immunity* 6: 715–726.
30. Miners JS, Barua N, Kehoe PG, Gill S, Love S (2011) Abeta-degrading enzymes: potential for treatment of Alzheimer disease. *J Neuropathol Exp Neurol* 70: 944–959.
31. Fernandez-Gamba A, Leal MC, Morelli L, Castano EM (2009) Insulin-degrading enzyme: structure-function relationship and its possible roles in health and disease. *Curr Pharm Des* 15: 3644–3655.
32. Judkowski V, Pinilla C, Schroder K, Tucker L, Sarvetnick N, et al. (2001) Identification of MHC class II-restricted peptide ligands, including a glutamic acid decarboxylase 65 sequence, that stimulate diabetogenic T cells from transgenic BDC2.5 nonobese diabetic mice. *J Immunol* 166: 908–917.
33. Stadinski BD, Delong T, Reisdorph N, Reisdorph R, Powell RL, et al. (2010) Chromogranin A is an autoantigen in type 1 diabetes. *Nat Immunol* 11: 225–231.
34. Fehling HJ, Swat W, Laplace C, Kuhn R, Rajewski K, et al. (1994) MHC class I expression in mice lacking the proteasome subunit LMP-7. *Science* 265: 1234–1237.
35. Firat E, Saveanu L, Aichele P, Staeheli P, Huai J, et al. (2007) The role of endoplasmic reticulum-associated aminopeptidase 1 in immunity to infection and in cross-presentation. *J Immunol* 178: 2241–2248.
36. Schmitz A, Schneider A, Kummer MP, Herzog V (2004) Endoplasmic reticulum-localized amyloid beta-peptide is degraded in the cytosol by two distinct degradation pathways. *Traffic* 5: 89–101.
37. Yewdell JW (2007) Plumbing the sources of endogenous MHC class I peptide ligands. *Curr Opin Immunol* 19: 79–86.

# 3,4-Diaminobenzoic Acid Derivatives as Inhibitors of the Oxytocinase Subfamily of M1 Aminopeptidases with Immune-Regulating Properties

Athanasios Papakyriakou,<sup>†,‡</sup> Efthalia Zervoudi,<sup>†</sup> Sofia Tsoukalidou,<sup>†</sup> Francois-Xavier Mauvais,<sup>§</sup> Georgia Sfyroera,<sup>†</sup> Dimitrios C. Mastellos,<sup>†</sup> Peter van Endert,<sup>§</sup> Emmanuel A. Theodorakis,<sup>‡</sup> Dionisios Vourloumis,<sup>\*,†</sup> and Efstratios Stratikos<sup>\*,†</sup>

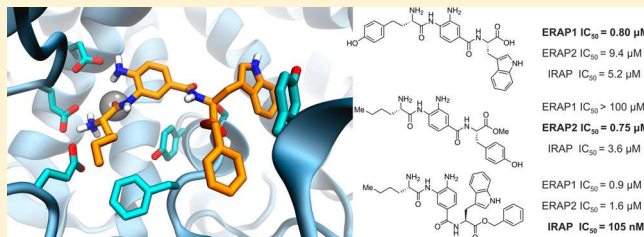
<sup>†</sup>National Center for Scientific Research “Demokritos”, Aghia Paraskevi, 15310 Athens, Greece

<sup>‡</sup>Department of Chemistry and Biochemistry, University of California—San Diego, 9500 Gilman Drive, San Diego, California 92093-0358, United States

<sup>§</sup>Institut National de la Santé et de la Recherche Médicale, Unité 1151; Université Paris Descartes, Sorbonne Paris Cité; Centre National de la Recherche Scientifique, Unité 8253, 75015 Paris, France

## Supporting Information

**ABSTRACT:** Members of the oxytocinase subfamily of M1 aminopeptidases (ERAP1, ERAP2, and IRAP) play important roles in both the adaptive and innate human immune responses. Their enzymatic activity can contribute to the pathogenesis of several major human diseases ranging from viral and parasitic infections to autoimmunity and cancer. We have previously demonstrated that diaminobenzoic acid derivatives show promise as selective inhibitors for this group of aminopeptidases. In this study, we have thoroughly explored a series of 3,4-diaminobenzoic acid derivatives as inhibitors of this class of enzymes, achieving submicromolar inhibitors for ERAP2 ( $IC_{50} = 237$  nM) and IRAP ( $IC_{50} = 105$  nM). Cell-based analysis indicated that the lead compounds can be effective in downregulating macrophage activation induced by lipopolysaccharide and interferon- $\gamma$  as well as cross-presentation by bone marrow-derived dendritic cells. Our results indicate that this class of inhibitors may be useful for the targeted downregulation of immune responses.



## INTRODUCTION

The three members of the oxytocinase subfamily of M1 aminopeptidases,<sup>1</sup> namely, endoplasmic reticulum aminopeptidases 1 and 2 (ERAP1 and ERAP2) and insulin regulated aminopeptidase (IRAP), henceforth referred to as antigen processing aminopeptidases (APAs), have been, during recent years, shown to have important biological functions, primarily in the regulation of human adaptive and innate immune responses. ERAP1 and ERAP2 act in intracellular antigen processing and are responsible not only for the correct generation of many antigenic epitopes but also for the destruction of others.<sup>2–4</sup> By this function, these enzymes can regulate cellular immune responses to infected or diseased cells and contribute to immune evasion by pathogens and cancer cells as well as to autoimmunity.<sup>5</sup> IRAP combines the specificity of ERAP1 and ERAP2 and functions in a specialized pathway of antigen processing and presentation called cross-presentation, present in dendritic cells (DCs), possibly regulating early stages of inflammatory immune responses.<sup>6,7</sup> ERAP1 and ERAP2 are polymorphic, and several coding single nucleotide polymorphisms in these genes have been associated with predisposition to major human diseases, ranging from viral

and parasitic infections to cancer and inflammatory diseases with autoimmune etiology (reviewed in refs 8 and 9). Recently, a secreted form of ERAP1 has also been implicated in innate immunity responses: macrophages activated by interferon- $\gamma$  and liposaccharides secrete ERAP1 in a TLR-dependent pathway,<sup>10,11</sup> resulting in the enhancement of their phagocytic activity and inflammatory potential. Similarly, ERAP1 knockout mice show increased activation of NK and NKT cells,<sup>12</sup> consistent with a role of ERAP1 in regulating both adaptive and innate immune responses. ERAP1 polymorphic variation was recently shown to quantitatively affect innate immune responses.<sup>13</sup> Since natural polymorphic variation of ERAP1 and ERAP2 can generate a range of enzymatic activities in the population, it has been hypothesized that the activity of these enzymes is an important regulator of immune responses in humans.<sup>14</sup>

Inhibition of APAs is a promising approach for selectively regulating immune responses. ERAP1 knockout mice present a distinct repertoire of antigenic peptides on their cell sur-

Received: December 3, 2014

Published: January 18, 2015

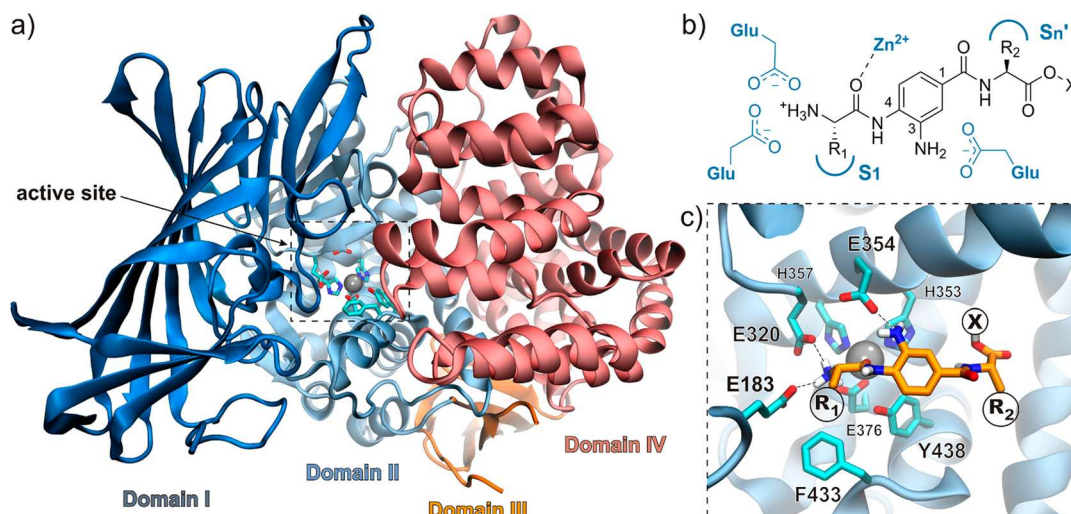


**Figure 1.** (a) Crystallographic structure of ERAP1 in the closed conformation (PDB ID: 2YD0), illustrating the domain organization and the active site of the enzyme. The catalytic zinc is shown as a gray sphere, and protein residues are shown as sticks with carbon in cyan, nitrogen in blue, oxygen in red, and sulfur in yellow. (b) Schematic representation of the 1,4-disubstituted DABA inhibitors, where  $R_1$  and  $R_2$  are  $L$ - $\alpha$ -amino acid side chains targeting the S1 and  $S_n'$  subsites of the aminopeptidases, respectively, and  $X = H, Me, \text{ or } Bn$ . (c) Molecular model of the 1,4-disubstituted DABA scaffold (carbon atoms shown in orange) docked at the active site of ERAP1. The  $\alpha$ -amino terminal docking residues are E183 and E320; the zinc-binding residues are H353, H357, and E376, whereas the catalytic E354 is expected to interact with the free aniline of the inhibitors. Catalytically important Y438 and conserved F433 that forms the bottom of S1 are also shown.

face.<sup>15–17</sup> Genetic downregulation of ERAP1 can lead to novel cellular immune responses, including nonclassical cellular responses, through the activation of cytotoxic-T lymphocytes and natural killer cells.<sup>18–20</sup> A pseudophosphinic peptide APA inhibitor has been demonstrated recently to enhance antigen presentation and elicit potent anti-cancer CTL responses toward a cryptic antigenic epitope that is normally destroyed by ERAP1.<sup>21</sup> On the other hand, downregulation of ERAP1 has been recently shown to reduce CTL responses against a viral epitope associated with the pathogenesis of autoimmunity.<sup>22</sup> As a result, the pharmacological regulation of APA activity has attracted significant scientific interest over the past few years as a promising area with therapeutic potential. Unfortunately, most characterized APA inhibitors suffer either from low potency or low selectivity, necessitating the exploration of other approaches. Selectively targeting only one of the members of this family of aminopeptidases may be highly desirable in order to fine-tune immune responses while minimizing potential side effects.

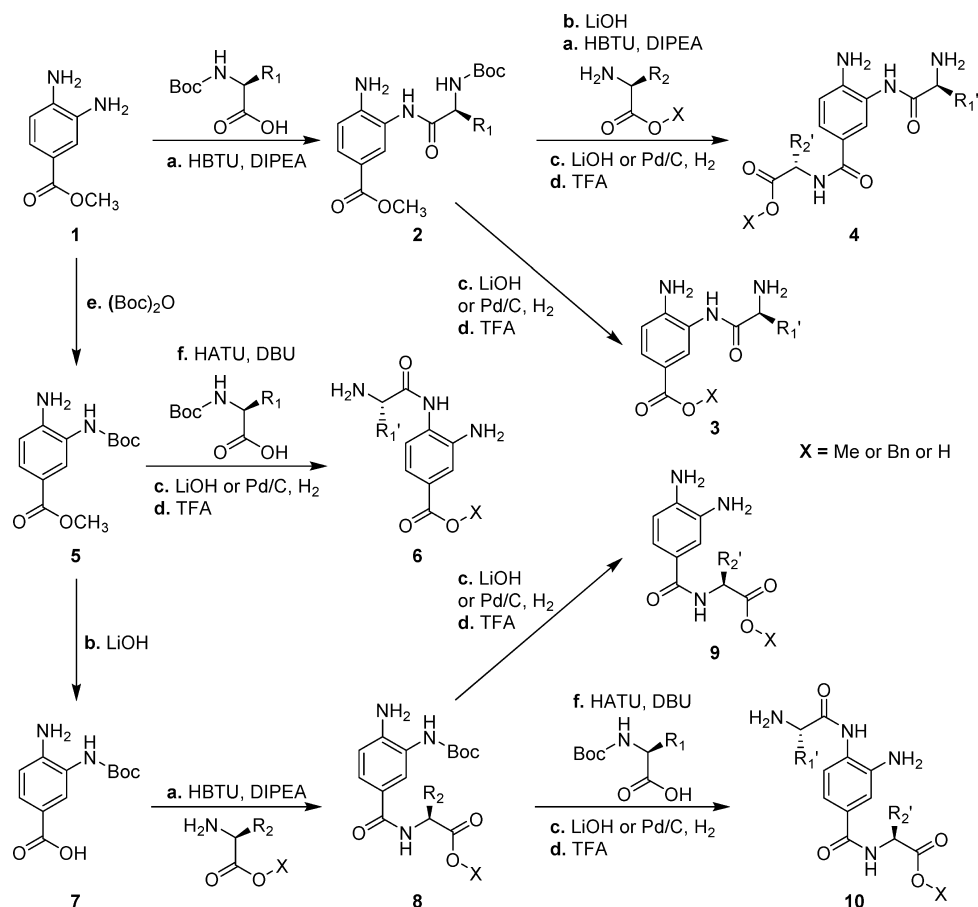
We recently demonstrated that using 3,4-diaminobenzoic acid (DABA) as a scaffold is a valid approach for generating inhibitors for this class of aminopeptidases with promising selectivity profiles.<sup>23</sup> In this study, we explored the DABA derivatives more extensively, with the aim of improving their potency and selectivity toward ERAP1, ERAP2, and IRAP. By employing a rational, structure-based optimization procedure, we identified potent inhibitors for ERAP2 (237 nM) and IRAP (105 nM) as well as a highly selective ERAP2 inhibitor (755 nM) in comparison to ERAP1 (>100  $\mu$ M).

To evaluate the biological potential of the discovered inhibitors, we utilized two specialized cellular assays relevant to innate and adaptive inflammatory immune responses. The low-micromolar ERAP1 inhibitor, **4a** (2  $\mu$ M), was able to inhibit macrophage activation by inflammatory mediators with submicromolar potency. The most potent IRAP inhibitor, **4u**, was able to block the IRAP-dependent cross-presentation pathway in dendritic cells with low-nanomolar potency. These

results suggest that these compounds may hold promise upon further development as targeted modulators of inflammatory immune responses.

## RESULTS AND DISCUSSION

**Inhibitor Design.** Selection of the amino acid side chains used for inhibitor design was based on a previous study on the selectivity profile of the S1 subsite of ERAP1, ERAP2, and IRAP using a library of 82 fluorogenic substrates.<sup>24</sup> Specifically, it was suggested that ERAP1 displays a general preference for substrates comprising long, aromatic or hydrophobic,  $R_1$  side chains (Figure 1). In contrast, the S1 subsite of ERAP2 exhibits higher selectivity for positively charged groups, especially Arg and homo-Arg, whereas IRAP combines the specificity of ERAP1 and ERAP2. All  $D$ -amino acid-based substrates were poorly processed by the three enzymes, suggesting that the  $L$  configuration is a prerequisite for binding. In our initial efforts,<sup>23</sup> we utilized homo-Phe (hPhe), which is predicted to be ideally accommodated within the S1 specificity pocket of ERAP1 due to  $\pi$ -stacking interactions with a conserved aromatic residue (F433/450/544 for ERAP1/ERAP2/IRAP, respectively). In combination with the positively charged side chain of Lys for  $R_2$ , 1,3-substituted derivative **4a** displayed low-micromolar affinity for ERAP1 ( $IC_{50} = 2.0 \pm 0.6 \mu$ M) and >10-fold selectivity for ERAP2. In this study, we explored the contribution of hydrophobic (Leu and nor-Leu), aromatic (Phe, Tyr, homo-Tyr(OBn), Ser-OBn), and positively charged Arg side chains at position  $R_1$ , while keeping lysine in the  $R_2$  position (Figure 1). Subsequently, a series of 1,3-substituted DABA derivatives was synthesized by combining the above-mentioned  $R_1$  amino acids with hydrophobic (Val), polar (Thr), aromatic (Tyr and Trp), and positively charged Arg side chains at position  $R_2$ . Our collection of 1,3-disubstituted DABA analogues was enriched with a selection of 1,4-disubstituted DABA to evaluate the different binding orientations of the inhibitors. A subset of monosubstituted DABA derivatives was also evaluated for direct comparison.

Scheme 1. Synthesis of the 1,3- and 1,4-Substituted 3,4-Diaminobenzoic Acid Derivatives<sup>a</sup>

<sup>a</sup>Reagents and conditions: (a) protected amino acid (1.1–1.5 equiv), HBTU (2.0–3.0 equiv), DIEA (3.0–4.0 equiv), DMF, 4–12 h, rt, 65–92%; (b) LiOH 1 M (20 equiv), dioxane/H<sub>2</sub>O (1:1), 3–6 h, rt, 87–95%. (c) LiOH 1 M (20 equiv), dioxane/H<sub>2</sub>O (1:1), 3–6 h, rt, or cat. Pd/C (10 wt %), H<sub>2</sub>, MeOH, 1–2 h, rt, 90–95%. (d) TFA/CH<sub>2</sub>Cl<sub>2</sub> (1:2), 20–40 min, rt, 95–98%. (e) (Boc)<sub>2</sub>O (1.0 equiv), Gu·HCl (15 mol %), EtOH, 40 min, 45 °C, 78%. (f) Protected amino acid (2.0 equiv), HATU (3.0 equiv), DBU (4.0 equiv), DMF, 24–36 h, rt, 45–72%. R<sub>1</sub>: side chain of L-α-amino acid selected from Leu, nor-Leu, Ser(OBn), Phe, homo-Phe, Tyr(OBn), homo-Tyr(OBn), or Arg(Z)<sub>2</sub>. R<sub>2</sub>: side chain of L-α-amino acid selected from Val, Thr, Tyr(O-tBu), Trp, Lys(Boc), ornithine(Boc), or Arg(Z)<sub>2</sub>. R<sub>1</sub>' , R<sub>2</sub>': the corresponding deprotected L-amino acid side chains. X: H, OMe, or OBn.

**Chemistry.** General synthetic routes for all new analogues are presented in Scheme 1. As described previously,<sup>23</sup> 1,3-disubstituted DABA derivatives **4** were obtained through the coupling of *N*-Boc-protected amino acids, furnishing intermediates **2**, followed by saponification of the corresponding methyl ester, formation of the second amide bond using *O*-methyl or *O*-benzyl protected amino acids, and global removal of the protecting groups. Following an analogous route, our approach was extended to furnish 1,4-disubstituted DABA derivatives **10** starting from 3-*N*-Boc protected DABA intermediate **7**. In this case, the second amide bond formation at the less reactive 4-NH<sub>2</sub> was achieved in higher yields by utilizing a combination of HATU as the coupling reagent and DBU as the base. As mentioned before, monosubstituted DABA derivatives **3**, **6**, and **9** were also prepared, as presented in Scheme 1, for direct comparison.

**In Vitro Evaluation.** The inhibitory potency of the synthesized compounds for the three enzymes was determined using an established fluorogenic assay.<sup>23</sup> Regarding monosubstituted DABA derivatives **3a–3g'** (Table 1), **6a–6f**, and **9a–9d** (Table 2), the in vitro evaluation did not reveal any low-micromolar (<10 μM) ERAP1 inhibition. In contrast, 4-amino substituted DABA derivatives **6e** (R<sub>1</sub>=Nle) and **6f** (R<sub>1</sub>=Arg)

displayed IC<sub>50</sub> values of 1.1 and 2.5 μM for ERAP2, respectively, whereas **6b** (R<sub>1</sub>=Tyr(OBn)) exhibits IC<sub>50</sub> = 1.7 μM for IRAP.

In the effort to optimize our previous hit **4a**, we initially substituted R<sub>2</sub>=Lys for the shorter side chain of L-ornithine (Orn). Surprisingly, both the methyl ester and the carboxylic acid of 1,3-hPhe-DABA-Orn derivatives (**4d** and **4d'**, respectively) were found to be inactive (IC<sub>50</sub> > 100 μM) for all three aminopeptidases (Table 1), indicating a very important interaction associated with the longer Lys side chain. Substitution of hPhe by the shorter Phe side chain yielded compound **4e**, which is inactive for ERAP1, although it is more potent than **4a** for ERAP2 and IRAP, demonstrating the importance of the longer hPhe side chain, as proposed previously.<sup>23</sup> From the remaining 1,3-disubstituted DABA-Lys derivatives, **4e–4l**, the in vitro evaluation revealed several moderate inhibitors (IC<sub>50</sub> = 2–8 μM) for ERAP2 and IRAP only, with most compounds being inactive toward ERAP1 (Table 1).

The next generation of 1,3-disubstituted DABA derivatives, **4m–4y**, was designed by combining Tyr, hTyr, Nle, and Arg for R<sub>1</sub> with Val, Tyr, and Trp for R<sub>2</sub> (Table 1). Although Tyr in the R<sub>1</sub> position yielded low-affinity inhibitors (**4m–4p'**) for all

Table 1. In Vitro Evaluation of the Designed 1,3-Substituted DABA Derivatives for ERAP1, ERAP2, and IRAP\*

ID	Chemical Structure		IC <sub>50</sub> (μM)		
	R <sub>1</sub>	R <sub>2</sub>	ERAP1	ERAP2	IRAP
3a	NH <sub>2</sub> -L-Tyr(OBn)	OMe	NI	NI	10.0±1.0
3a'	NH <sub>2</sub> -L-Tyr(OBn)	OH	NI	NI	10.7±1.5
3b	NH <sub>2</sub> -L-Tyr	OMe	NI	>100	57±9.5
3b'	NH <sub>2</sub> -L-Tyr	OH	>100	3.2±0.8	10.9±1.9
3c	NH <sub>2</sub> -L-hTyr(OBn)	OMe	NI	NI	2.1±0.4
3d	NH <sub>2</sub> -L-hTyr-OMe	OMe	>100	NI	12±2.0
3e	NH <sub>2</sub> -L-Leu	OMe	NI	NI	NI
3e'	NH <sub>2</sub> -L-Leu	OH	NI	NI	NI
3f	NH <sub>2</sub> -L-Nle	OMe	>100	9.8±1.0	7.2±1.0
3g	NH <sub>2</sub> -L-Arg	OMe	NI	3.7±0.5	14.6±2.0
3g'	NH <sub>2</sub> -L-Arg	OH	NI	>100	34±7.5
4a <sup>a</sup>	NH <sub>2</sub> -L-hPhe	L-Lys-OMe	2.0±0.6	24.9±1.2	10.3±0.6
4b <sup>a</sup>	NH <sub>2</sub> -L-hPhe	L-Trp-OBn	NI	23.9 ± 0.8	1.3±0.1
4c <sup>a</sup>	NH <sub>2</sub> -L-hPhe	L-Tyr-OMe	7.7±0.4	>100	3.6±0.4
4d	NH <sub>2</sub> -L-hPhe	L-Orn-OMe	NI	NI	NI
4d'	NH <sub>2</sub> -L-hPhe	L-Orn-OH	NI	NI	>100
4e	NH <sub>2</sub> -L-Phe	L-Lys-OH	NI	2.6±0.3	3.8±0.6
4f	NH <sub>2</sub> -L-Tyr	L-Lys-OH	NI	4.5±0.4	4.8±0.4
4g	NH <sub>2</sub> -L-hTyr	L-Lys-OMe	>100	4.8±0.8	10.7±2.8
4h	NH <sub>2</sub> -L-hTyr(OBn)	L-Lys-OMe	>100	13±2.5	5.7±0.5
4i	NH <sub>2</sub> -L-Ser(OBn)	L-Lys-OMe	NI	NI	NI
4j	NH <sub>2</sub> -L-Leu	L-Lys-OMe	NI	52±13	NI
4j'	NH <sub>2</sub> -L-Leu	L-Lys-OH	6.8±1.1	2.1±0.2	4.1±0.8
4k	NH <sub>2</sub> -L-Nle	L-Lys-OMe	18.3±0.3	8.3±1.5	>100
4l	NH <sub>2</sub> -L-Arg	L-Lys-OMe	42±8	17±3	NI
4m	NH <sub>2</sub> -L-Tyr	L-Val-OBn	NI	50±14	12±1.0
4m'	NH <sub>2</sub> -L-Tyr	L-Val-OH	NI	>100	>100
4n	NH <sub>2</sub> -L-Tyr	L-Tyr-OMe	110±50	33±6.5	22±4.5
4o	NH <sub>2</sub> -L-Tyr	L-Thr-OMe	>100	39±9.5	>100
4p	NH <sub>2</sub> -L-Tyr	L-Trp-OBn	9.8±0.8	40±14.5	7.1±1.2
4p'	NH <sub>2</sub> -L-Tyr	L-Trp-OH	>100	>100	>100
4q	NH <sub>2</sub> -L-hTyr(OBn)	L-Trp-OBn	>100	>100	0.933±0.14
4r	NH <sub>2</sub> -L-hTyr	L-Trp-OH	38.4±9.5	>100	4.4±0.7
4s	NH <sub>2</sub> -L-Nle	L-Val-OBn	>100	>100	1.3±0.4
4s'	NH <sub>2</sub> -L-Nle	L-Val-OH	NI	>100	>100
4t	NH <sub>2</sub> -L-Nle	L-Tyr-OMe	>100	6.4±0.4	1.2±0.4
4u	NH <sub>2</sub> -L-Nle	L-Trp-OBn	0.92±0.20	1.6±0.3	0.105±0.063
4u'	NH <sub>2</sub> -L-Nle	L-Trp-OH	3.6±0.6	3.8±0.3	0.296±0.090
4v	NH <sub>2</sub> -L-Nle	L-Arg-OMe	10.7±2.1	2.5±0.3	31±7.5
4w	NH <sub>2</sub> -L-Arg	L-Val-OH	NI	5.0±1.0	3.3±0.6
4x	NH <sub>2</sub> -L-Arg	L-Tyr-OMe	9.6±0.2	0.518±0.043	0.966±0.050
4y	NH <sub>2</sub> -L-Arg	L-Trp-OH	1.2±0.2	0.589±0.109	0.655±0.040

\*NI, no inhibition observed up to 100 μM; >100 indicates that a limited inhibition is observed in the 50–100 μM range. <sup>a</sup>Data taken from ref 23.

three enzymes, hTyr in combination with Trp displayed low-micromolar inhibition for IRAP (4q and 4r). In particular, 4q proved to be the most selective IRAP inhibitor against both ERAP1 and ERAP2 (IC<sub>50</sub> > 100 μM). The combination of R<sub>1</sub>=Nle (4s–4v) or Arg (4w–4y) with R<sub>2</sub>=Tyr or Trp provided the most potent inhibitors. Compound 4u is the most potent inhibitor of ERAP1 (IC<sub>50</sub> = 0.92 μM) and IRAP (IC<sub>50</sub> = 105 nM), followed by its corresponding carboxylic acid 4u' (IC<sub>50</sub> = 296 nM for IRAP). It is interesting to note that 4s and 4t are both significantly selective inhibitors of IRAP (IC<sub>50</sub> = 1.2–1.3 μM) with respect to ERAP1 (IC<sub>50</sub> > 100 μM). As predicted, Arg in the R<sub>1</sub> position provided two more submicromolar inhibitors, 4x and 4y, for both ERAP2 and IRAP, with 4x (IC<sub>50</sub> = 518 nM) displaying a ~20-fold selectivity with respect to ERAP1 (IC<sub>50</sub> = 9.6 μM).

Concerning the in vitro evaluation of the 1,4-disubstituted DABA derivatives (Table 2), our results indicate a significant structural effect from the orientation of the two amino acid substituents on their inhibitory effect, especially regarding ERAP1. A striking example is inactive compound 10a, which is the regioisomer of the initial ERAP1 hit, 4a (IC<sub>50</sub> = 2.0 μM). In

Table 2. In Vitro Evaluation of the Designed 1,4-Substituted DABA Derivatives for ERAP1, ERAP2, and IRAP\*

ID	Chemical Structure		IC <sub>50</sub> (μM)		
	R <sub>1</sub>	R <sub>2</sub>	ERAP1	ERAP2	IRAP
6a	NH <sub>2</sub> -L-hPhe	OMe	>100	58±18	31±4.0
6b	NH <sub>2</sub> -L-Tyr(OBn)	OMe	NI	NI	1.7±0.2
6c	NH <sub>2</sub> -L-Tyr	OMe	NI	58±12	8.3±1.0
6d	NH <sub>2</sub> -L-Leu	OMe	NI	>100	NI
6e	NH <sub>2</sub> -L-Nle	OMe	NI	1.1±0.2	3.3±0.5
6f	NH <sub>2</sub> -L-Arg	OMe	NI	2.5±0.7	39.6±2.1
9a	H	L-Lys-OMe	>100	NI	>100
9b	H	L-Tyr-OMe	NI	NI	9.9±2.7
9c	H	L-Trp-OBn	NI	>100	22.5±2.5
9c'	H	L-Trp-OH	>100	1.9±0.3	>100
9d	H	L-Arg-OMe	35±10	NI	2.5±0.9
10a	NH <sub>2</sub> -L-hPhe	L-Lys-OMe	NI	NI	20.6±4.0
10b	NH <sub>2</sub> -L-hPhe	L-Val-OBn	NI	>100	14.4±3.0
10b'	NH <sub>2</sub> -L-hPhe	L-Val-OH	NI	>100	20.2±2.5
10c	NH <sub>2</sub> -L-hPhe	L-Tyr-OMe	9.4±0.7	5.5±0.6	1.3±0.2
10d	NH <sub>2</sub> -L-hPhe	L-Trp-OBn	13.4±3.0	11±2.5	2.4±0.6
10e	NH <sub>2</sub> -L-hPhe	L-Arg-OMe	12±1.3	11.8±1.5	4.7±0.6
10f	NH <sub>2</sub> -L-Tyr(OBn)	L-Tyr-OMe	NI	16±4.5	2.9±0.4
10g	NH <sub>2</sub> -L-Tyr	L-Tyr-OMe	16.7±1.5	15.1±2.5	3.7±0.5
10h	NH <sub>2</sub> -L-Tyr(OBn)	L-Trp-OBn	1.1±0.3	20.5±2.0	3.8±0.7
10h'	NH <sub>2</sub> -L-Tyr	L-Trp-OH	19.5±4.0	4.8±0.8	1.3±0.2
10i	NH <sub>2</sub> -L-Tyr	L-Lys-OMe	>100	>100	70±19
10j	NH <sub>2</sub> -L-hTyr(OBn)	L-Trp-OBn	NI	70±10	3.4±0.5
10j'	NH <sub>2</sub> -L-hTyr	L-Trp-OH	0.80±0.16	9.4±1.6	5.2±0.6
10k	NH <sub>2</sub> -L-Leu	L-Trp-OBn	8.9±1.5	21±4.5	3.7±0.9
10l	NH <sub>2</sub> -L-Leu	L-Lys-OMe	NI	NI	>100
10m	NH <sub>2</sub> -L-Nle	L-Val-OBn	>100	6.2±1.9	3.9±1.0
10m'	NH <sub>2</sub> -L-Nle	L-Val-OH	NI	38±12	>100
10n	NH <sub>2</sub> -L-Nle	L-Tyr-OMe	>100	0.755±0.100	3.6±0.7
10o	NH <sub>2</sub> -L-Nle	L-Trp-OBn	2.5±0.5	0.709±0.050	0.438±0.010
10o'	NH <sub>2</sub> -L-Nle	L-Trp-OH	2.8±0.5	0.237±0.030	1.7±0.4
10p	NH <sub>2</sub> -L-Nle	L-Lys-OMe	NI	30.6±12	35.7±12.5
10q	NH <sub>2</sub> -L-Arg	L-Tyr-OMe	2.6±0.3	1.4±0.4	2.2±0.2
10r	NH <sub>2</sub> -L-Arg	L-Trp-OH	38.2±9.5	1.1±0.1	7.6±0.6
10s	NH <sub>2</sub> -L-Arg	L-Lys-OMe	NI	11.8±1.0	4.9±0.6

\*NI, no inhibition observed up to 100 μM; >100 indicates that a limited inhibition is observed in the 50–100 μM range.

contrast, the inhibitory effect of low-micromolar IRAP inhibitors 4b (IC<sub>50</sub> = 1.3 μM) and 4c (IC<sub>50</sub> = 2.8 μM) is marginally affected at their corresponding para-isomers 10d (IC<sub>50</sub> = 2.4 μM) and 10c (IC<sub>50</sub> = 1.3 μM), respectively.

By employing Tyr in the R<sub>1</sub> position, we obtained two more potent inhibitors, 10h, with IC<sub>50</sub> = 1.1 μM for ERAP1, and 10h', with IC<sub>50</sub> = 1.3 μM for IRAP. In particular, 10h displayed a 2-fold increase in selectivity for ERAP1 compared to ERAP2, with respect to that of the initial hit, 4a. Interestingly, compound 10j' (R<sub>1</sub>=hTyr and R<sub>2</sub>=Trp), the topoisomer of ERAP1-inactive 4r, exhibits an IC<sub>50</sub> = 0.8 μM for ERAP1 with a ~12-fold selectivity with respect to ERAP2. Similar to the 1,3-analogues, the use of Nle at R<sub>1</sub> (10m–10o') in combination with Tyr or Trp at R<sub>2</sub> provided the most potent ERAP2 and IRAP inhibitors. Among them, 10n, with IC<sub>50</sub> = 755 nM for ERAP2, is the most selective inhibitor against ERAP1 (>130-fold), and 10o' is the most potent inhibitor of ERAP2 (IC<sub>50</sub> = 237 nM). The corresponding benzyl ester of the latter, 10o, displayed a higher potency for IRAP (IC<sub>50</sub> = 438 nM) with respect to ERAP2 (IC<sub>50</sub> = 709 nM). Finally, 10q with R<sub>1</sub>=Arg, the para-isomer of potent ERAP2/IRAP inhibitor 4x, provided an equipotent inhibitor of the three enzymes (IC<sub>50</sub> = 1.4–2.6 μM).

Overall, the in vitro evaluation of the designed DABA derivatives revealed several potent inhibitors for the three M1 aminopeptidases. ERAP1 appears to be the most challenging target in terms of inhibitor potency and selectivity, with 4u

( $IC_{50} = 0.92 \mu\text{M}$ ) and **10j'** ( $IC_{50} = 0.80 \mu\text{M}$ ) being the most effective inhibitors and **10h** being the most selective with respect to ERAP2 ( $\sim 20$ -fold). On the other hand, our optimization efforts resulted in significantly more potent inhibitors of ERAP2 (**10o'**,  $IC_{50} = 237 \text{ nM}$ ) and IRAP (**4u**,  $IC_{50} = 105 \text{ nM}$ ). In addition, we identified two remarkably selective inhibitors, **10n**, displaying  $IC_{50} = 755 \text{ nM}$  for ERAP2 and  $IC_{50} > 100 \mu\text{M}$  for ERAP1, and **4s**, with  $IC_{50} = 1.3 \mu\text{M}$  for IRAP and  $IC_{50} > 100 \mu\text{M}$  for both ERAP1 and ERAP2. Conclusively, the inhibitory potency of the synthesized compounds revealed that Nle as the  $R_1$  and Trp as the  $R_2$  substituents provided the most potent inhibitors for the three aminopeptidases. It is possible that the linear side chain of Nle is easily accommodated within the S1 pocket and facilitates the proper orientation of the inhibitors in both topologies of the DABA derivatives. The indole ring of Trp is most probably mediating key aromatic interactions at the S-primed subsites in addition to potential hydrogen-bonding interactions. Similar observations were drawn from the crystallographic structure of ERAP1 in complex with a phosphinic transition state analogue tripeptide comprising a Trp residue, which was found to be stacked with catalytic Y438.<sup>21</sup>

**Structure–Activity Relationships.** Recent crystallographic studies revealed that ERAP1 can adopt at least two distinct conformational states that involve large interdomain motions, a closed, active-form (Figure 1a) and an open, inactive conformation that exposes a large internal peptide-binding cavity to the solvent.<sup>25</sup> Although ERAP2 has been crystallized in the closed conformation only, the absence of substrate access into the active site in the published structure suggests that ERAP2 should be able to adopt open conformations as well.<sup>26</sup> These two states differ in the organization of key active site residues and the adjacent S1 specificity pocket, which is disordered in the open state, making inhibitor design a challenging task.<sup>14</sup> Specifically, the conserved ERAP1 residue F433 that comprises the bottom of the S1 pocket as well as the catalytic Y438 are both disordered or dislocated in the open-state crystal structure.<sup>27</sup>

It is therefore plausible that inhibitors that target these aminopeptidases may form initial interactions inside the active site at different configurations than those expected by analyzing the closed crystallographic structures. This may be exemplified by a lack of a strong zinc binding group serving as anchor point. As a result, molecular docking calculations of the synthesized compounds reveal multiple putative binding poses inside the active sites of all three aminopeptidases. Still, the most potent inhibitors display a common binding motif among the top-ranked predicted conformations, where the carbonyl group of  $R_1$  is bound to zinc so that the  $R_1$  side chain can be accommodated within the S1 pocket (Figure 1c). In such conformation, the  $\alpha$ -amino acid terminal amine displays salt bridge interactions with two conserved glutamates, E183/200/295 and E320/337/431 (residue numbering of ERAP1/ERAP2/IRAP, respectively), and the free aniline could provide an additional hydrogen bond with the catalytic E354/371/465 residue. It is therefore possible that only the best inhibitors bind in the expected conformation through an induced-fit mechanism that promotes correct folding of the APA active site.

The docked conformation of the most potent ERAP1 inhibitor, **10j'**, displays the side chain of its hTyr stacked above F433 inside the S1 pocket and, at the same time, forms a hydrogen bond with the backbone NH of S869 (Figure 2a), a

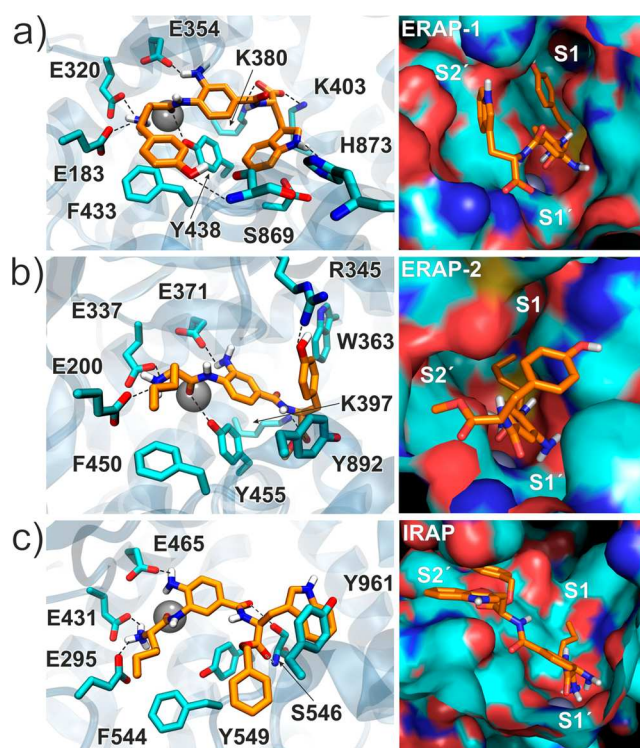


**Figure 2.** Close-up view of the active site from molecular models of (a) ERAP1–**10j'**, (b) ERAP2–**10n**, and (c) IRAP–**4u** complexes. The inhibitors are shown with carbon atoms in orange, and the key interacting residues, with cyan carbons. Potential hydrogen bonds are indicated with dashed lines, and the surface representations illustrate the three potential subsites of the enzymes.

residue that belongs to the C-terminal domain IV. The indole ring of **10j'** could interact with the H873 residue of domain IV, whereas its terminal carboxylic acid might form salt bridges with K308 and K403. Considering the bound conformation of the most selective inhibitor of ERAP2 ( $>100$ -fold with respect to ERAP1), **10n** is predicted to bind in a similar orientation as that for **10j'**. However, the phenolic ring in **10n** could be accommodated between the aromatic side chains of Y892 and W363 so that a hydrogen bond is formed between its hydroxylate group and R345 of ERAP2 (Figure 2b). The nonconserved W363 residue of ERAP2 corresponds to G346 of ERAP1 and therefore such an interaction might not be possible between ERAP1 and **10n**. The most potent IRAP inhibitor, **4u**, is predicted to interact mostly with conserved residues and thus displays low-micromolar affinity for ERAP1 and ERAP2 as well. The high binding affinity of **4u** for IRAP (105 nM) can be attributed to a potential stacking interaction of the indole moiety with Y961 and the two hydrogen bonds with S546 (Figure 2c). The terminal benzyl group of **4u** is predicted to provide minor contacts; therefore, the corresponding deprotected analogue, **4u'**, displayed a marginally lower binding affinity for IRAP (296 nM).

**Biological Evaluation of Inhibitors.** To assess the biological efficacy of this group of inhibitors we utilized two specialized cellular assays that relate to the function of the human innate and adaptive immune responses. It has been recently demonstrated that macrophages respond to the inflammatory modulator interferon- $\gamma$  in combination with lipopolysaccharide (LPS), which is a component of the outer membrane of Gram-negative bacteria, by secreting ERAP1 in a

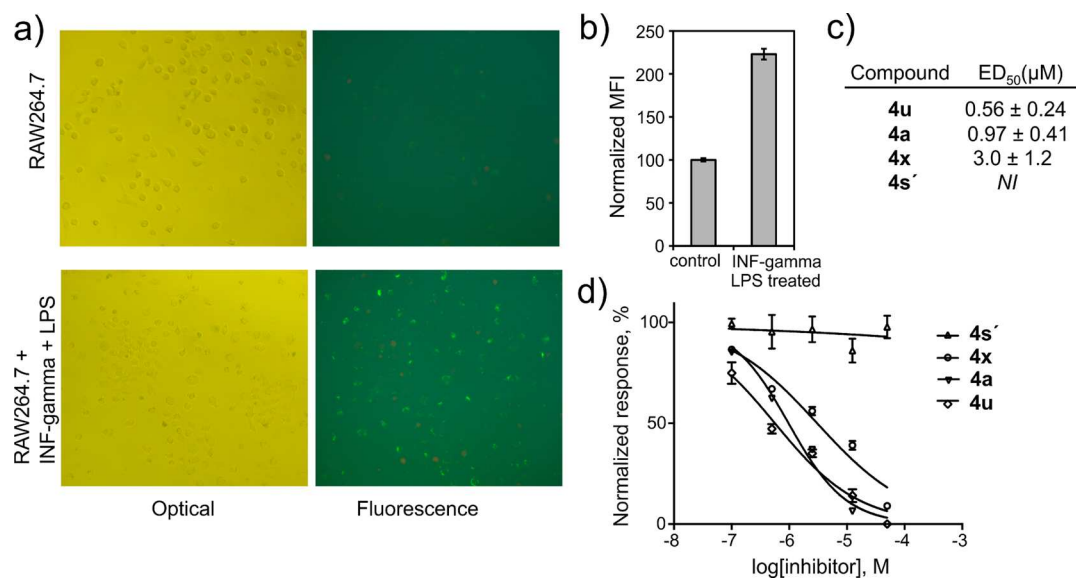


**Figure 3.** (a) Effect of interferon- $\gamma$  and LPS on the phagocytic activity of RAW264.7 macrophages as followed by the internalization of fluorescent latex beads. (b) Fluorescence enhancement due to macrophage activation. (c, d) Reduction of fluorescence enhancement due to inhibition of phagocytosis by the ERAP1 inhibitors and the calculated ED<sub>50</sub> values.

TLR-dependent manner.<sup>10,11</sup> The aminopeptidase activity of the secreted ERAP1 induces the enhancement of phagocytosis by macrophages, which can be followed by the internalization of fluorescently labeled latex beads (Figure 3a). To evaluate the effect of the inhibitors on this process, we measured the total cell fluorescence in stimulated and unstimulated cells. Total fluorescence enhancement upon macrophage stimulation was in the range of 100–150%, which is a sufficient signal change to detect inhibitory effects (Figure 3b). Adding compounds 24 h premeasurement revealed a dose dependent reduction in phagocytosis with calculated ED<sub>50</sub> values (Figure 3c,d) that correspond well to the *in vitro* IC<sub>50</sub> values calculated for ERAP1 using recombinant protein, suggesting that the biological effect was indeed mediated through the inhibition of ERAP1.

Furthermore, we evaluated the effectiveness of the most potent IRAP inhibitor, **4u**, on blocking cross-presentation by bone marrow-derived DCs (BMDCs). To assess the specificity of the inhibitor, we utilized BMDCs from both wild-type and IRAP knockout mice. We first confirmed that **4u** is able to inhibit mouse IRAP using mouse recombinant enzyme and discovered that this compound is 2-fold more effective for mouse IRAP (IC<sub>50,mouse</sub> = 52 nM, Supporting Information Figure S1) compared to that for human IRAP (IC<sub>50,human</sub> = 105 nM). Mouse BMDCs were first exposed to yeast cells expressing surface ovalbumin and then added to CD8<sup>+</sup> T cells from the lymph nodes of transgenic mice expressing a T cell receptor specific for the peptide ovalbumin247–254. T cell activation by the cross-presented epitope was read out as IL-2 secretion (Figure 4a). The same experiment was performed in the presence of increasing doses of **4u** (Figure 4b). In the presence of the inhibitor, cross-presentation was reduced in a dose-dependent manner with an ED<sub>50</sub> of 6.5 nM. No effect was seen when we used BMDCs from IRAP knockout mice, indicating that the effect is specific for the IRAP-dependent cross-presentation pathway. The surprisingly high effectiveness of the inhibitor in this setting may be related to the compartmentalization of the cross-presentation process in which high local concentrations may be obtained due to

continued inhibitor internalization into phagosomes and endosomes.

To date, only a series of phosphinic pseudopeptide transition state analogues has been reported as potent inhibitors of all three APAs,<sup>21</sup> albeit with low selectivity among the three enzymes. Specifically, the most potent inhibitor displayed IC<sub>50</sub> values of 33, 11, and 30 nM for ERAP1, ERAP2, and IRAP, respectively. On the basis of the observation that peptide inhibitors of IRAP can enhance cognitive functions, peptidomimetic analogues of angiotensin IV have been designed using a wide range of synthetic approaches.<sup>28–30</sup> Among the most potent angiotensin IV mimetics reported, a series of macrocyclic compounds attained inhibition constants as low as 1.8 nM for IRAP.<sup>30</sup> With regard to small molecule inhibitors of IRAP, a series of benzopyran compounds that had been identified through a virtual screening approach using a homology model of IRAP<sup>31</sup> led to the development of the first lead compound with K<sub>i</sub> = 30 nM through a medicinal chemistry campaign.<sup>32</sup> Recently, a series of arylsulfonamides was identified as being moderate inhibitors of IRAP, with the most potent exhibiting IC<sub>50</sub> = 1.1 μM.<sup>33</sup> These IRAP inhibitors, however, have either not been tested for their ability to inhibit ERAP1 and ERAP2 or have been tested and found not to be active.<sup>31</sup> As a result, the 3,4-diaminobenzoic acid derivatives described here appear to constitute not only an alternative potent chemical tool for controlling APA activity but also one with very good selectivity properties.

## CONCLUSIONS

In summary, we have investigated the ability of 3,4-diaminobenzoic acid derivatives to act as inhibitors of three critical aminopeptidases involved in the human innate and adaptive immune response, ERAP1, ERAP2, and IRAP. Our analysis revealed potent inhibitors for ERAP2 and IRAP as well as excellent selectivity profiles for all three enzymes. Furthermore, our analysis confirmed previously hypothesized difficulties in the rational design of inhibitors for this class of enzymes based on existing crystal structures, especially for ERAP1, possibly due to the conformational heterogeneity of



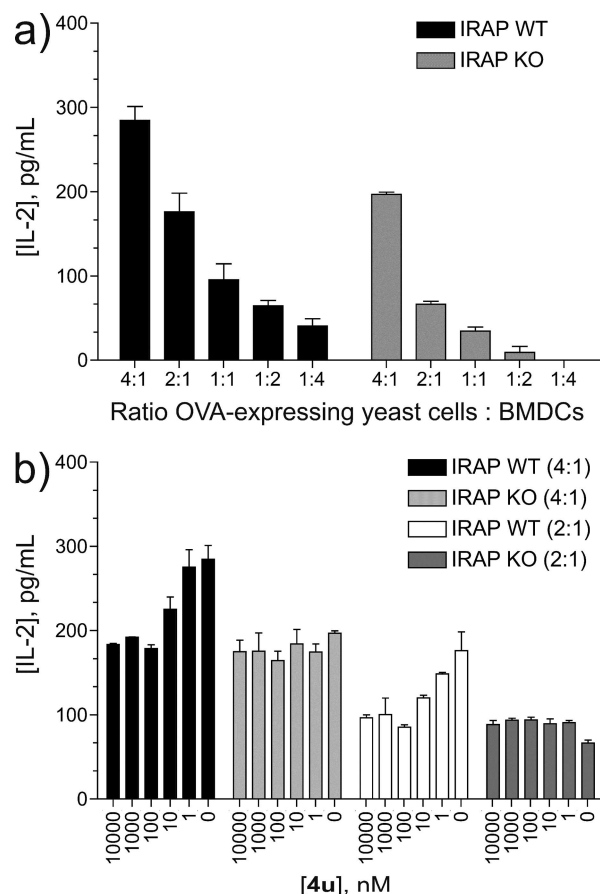


**Figure 4.** (a) Murine BMDCs from either wild-type or IRAP knockout mice were exposed to several ratios of ovalbumin-expressing yeast cells and subsequently to CD8<sup>+</sup> T cells purified from lymph nodes of OT-I mice. T cell activation was evaluated by measuring the IL-2 concentration in the culture supernatant. (b) The same experiment was repeated in the presence of increasing concentrations of **4u**. Note that titration of the inhibitor affected only wild-type, not IRAP knockout, cells and reduced the response of the wild-type cells to the levels of the IRAP knockout cells, indicating complete inhibition of the IRAP-dependent cross-presentation pathway.

this enzyme that greatly affects the folding of the S1 specificity pocket. Our best compounds were found to be active in specialized cellular assays related to their biological functions of the targeted enzymes in regulation of the adaptive and innate immune responses. We conclude that this class of compounds may find important applications in the regulation of inflammatory human immune responses for the treatment of a variety of major human diseases, varying from viral infections to cancer and autoimmunity. More specifically, ERAP1 inhibitors such as **4a** may be useful for reducing inflammation by controlling macrophage activation<sup>11</sup> and selective ERAP2 inhibitors like **10n** may be useful for controlling autoimmune responses brought about by high ERAP2 expression, such as that seen in birdshot chorioretinopathy,<sup>34</sup> or for enhancing immune responses toward immune-evading cancer cells.<sup>35</sup> Finally, potent IRAP inhibitors such as **4u** or **4u'** may find uses in controlling inflammatory autoimmune diseases or as cognitive enhancers.<sup>36,32</sup>

## EXPERIMENTAL SECTION

**Materials and General Procedures.** Unless otherwise noted, all solvents and reagents for organic synthesis were obtained from

commercial suppliers and used without further purification. Reactions requiring anhydrous conditions were carried out in flame-dried (vacuum <0.5 Torr) glassware, using anhydrous, freshly distilled solvents and under an Ar atmosphere. All reactions were stirred with Teflon-coated magnetic stir bars, and temperatures were measured externally. Yields refer to chromatographically and spectroscopically (<sup>1</sup>H NMR) homogeneous materials. Reactions were monitored by thin-layer chromatography (TLC) carried out on 0.25 mm silica gel plates (60 F254, E. Merck). Silica gel (60, particle size: 0.040–0.063 mm, E. Merck) was used for flash column chromatography. NMR spectra were recorded on a Bruker Avance DRX-500 instrument at 298 K using residual undeuterated solvent for <sup>1</sup>H NMR [ $\delta_{\text{H}}$  = 7.26 (CHCl<sub>3</sub>), 2.50 (DMSO-*d*<sub>5</sub>), and 3.31 (MeOH-*d*<sub>3</sub>) ppm] and <sup>13</sup>C deuterated solvent for <sup>13</sup>C NMR [ $\delta_{\text{C}}$  = 77.16 (CDCl<sub>3</sub>), 39.52 (DMSO-*d*<sub>5</sub>), and 49.00 (MeOH-*d*<sub>4</sub>) ppm] as an internal reference. The following abbreviations were used to designate the multiplicities: s, singlet; d, doublet; t, triplet; q, quartet; m, multiplet; and br, broad. Quantitation of the final compounds was achieved using an internal standard of 2,5-dimethylfuran (DMFu, 0.1 mM in MeOD).<sup>37</sup> High-resolution mass spectra (HRMS) were measured on Agilent 6224 Accurate Mass TOF LC/MS at the Faculty of Chemistry and Chemical Technology, University of Ljubljana. Compounds were purified by reversed-phase HPLC on a C18 chromolith column (Merck) using a 0–50% (v/v) acetonitrile gradient in water containing 0.05% TFA while following the absorbance at 257 nm. The purity of all final compounds employed in the biological assays was greater than 95%, and the structures of the synthesized compounds were determined by <sup>1</sup>H NMR, <sup>13</sup>C NMR, and high-resolution mass spectroscopy (HRMS).

**General Methods for the Synthesis of the Inhibitors. Amino Acid Coupling (Method A).** A mixture of **1** (1.0 equiv), the desired *N*-Boc protected amino acid (1.1 equiv), HBTU (2.0 equiv), and DIEA (3.0 equiv) in anhydrous DMF (0.25 mM) was stirred under an Ar atmosphere at ambient temperature for 4 h. Similarly, a mixture of the carboxylic acid derivative of **2** or **7** (1.0 equiv), the desired *O*-Me or *O*-Bn protected amino acid (1.5 equiv), HBTU (3.0 equiv), and DIEA (4.0 equiv) in anhydrous DMF (0.25 mM) was stirred under an Ar atmosphere at ambient temperature for 8–12 h. For the preparation of the 1,4-substituted compounds, a mixture of **5** or **8** (1.0 equiv), the *N*-Boc protected amino acid (2.0 equiv), HATU (3.0 equiv), and DBU (4.0 equiv) in anhydrous DMF (0.25 mM) was stirred under an Ar atmosphere at ambient temperature for 24–36 h. The reaction mixture was then diluted with EtOAc and washed sequentially with aqueous HCl 1.0 N, sat. NaHCO<sub>3</sub>, and sat. NaCl. Consequently, the solvent was evaporated under reduced pressure to provide the crude product, which was purified using a gradient of EtOAc in hexanes to yield the desired products in yields of 45–92%.

**Saponification of Methyl Esters (Method B).** The desired compound was dissolved in a mixture of 1:1 dioxane/aqueous LiOH 1.0 M (20 equiv) under rigorous stirring. After 3–6 h (monitored by TLC) at ambient temperature, the mixture was diluted with aqueous sat. NaCl and the organic solvent was evaporated. The remaining aqueous solution (pH 12) was washed with EtOAc and then acidified with HCl 1.0 N until no further precipitation could be observed (pH 2). The aqueous phase was then extracted three times with EtOAc, and the combined organic extracts were dried with MgSO<sub>4</sub>, filtered, and washed with EtOAc. After evaporating the solvents and drying under high vacuum, the product was obtained at yields of 87–95% and purity > 95% (NMR).

**General Procedure for the Deprotection of *O*-Bn and *N*-Cbz Groups (Method C).** The desired compound (0.1 mmol) was dissolved in MeOH (4 mL, 0.025 mM), and the solution was degassed under an Ar atmosphere. A catalytic amount of activated Pd/C 10% was added and degassed under Ar, followed by the introduction of H<sub>2</sub> gas. The mixture was stirred under H<sub>2</sub> at ambient temperature for 1–2 h (monitored by TLC) and then filtered through Celite and washed with MeOH. The resulting product was acquired in yields of 90–95%.

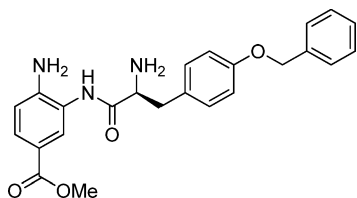
**General Procedure for the Deprotection of *N*-Boc and *O*-tBu Groups (Method D).** The desired compound (0.1 mmol) was dissolved in a mixture of CH<sub>2</sub>Cl<sub>2</sub>/TFA (2:1 mL, 0.033 mM) and

stirred at ambient temperature for 20–40 min (monitored by TLC). Consequently, the solvents were evaporated, and the product was treated with HCl 1.0 N (0.5 mL). The solvents were evaporated using toluene (2 × 2 mL) to azeotrop the remaining aqueous solution and dried under high vacuum overnight to yield the hydrochloric salt of the amine in yields of 95–99%.

**Methyl 4-Amino-3-((tert-butoxycarbonyl)amino)benzoate (5).** To a stirred solution of **1** (500 mg, 3.0 mmol) and Gu-HCl (45 mg, 0.45 mmol) in 5 mL of EtOH was added (Boc)<sub>2</sub>O (650 mg, 3.0 mmol), and the mixture was heated at 45 °C for 40 min. Subsequently, ethanol was evaporated under reduced pressure, and the reaction mixture was redissolved in EtOAc and washed sequentially with aqueous HCl 1.0 N, sat. NaHCO<sub>3</sub>, and sat. NaCl. The organic layer was evaporated under reduced pressure to provide the crude product, which was purified using a gradient of 35–65% EtOAc in hexanes to yield the *N*-Boc protected amine **5** (665 mg, 2.5 mmol, 83%). <sup>1</sup>H NMR (500.13 MHz, CDCl<sub>3</sub>): δ 7.83 (s, 1H), 7.56 (dd, *J* = 8.4, 1.7 Hz, 1H), 6.76 (s, 1H), 6.58 (d, *J* = 8.4 Hz, 1H), 4.39 (s, 2H), 3.74 (s, 3H), 1.41 (s, 9H). <sup>13</sup>C NMR (125.76 MHz, CDCl<sub>3</sub>): δ 167.0, 154.2, 145.8, 128.3, 127.6, 122.7, 119.4, 115.5, 80.5, 51.5, 28.1, 28.1, 28.1.

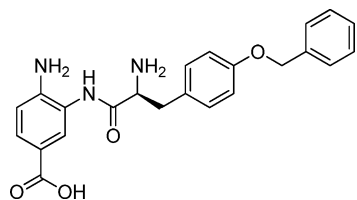
Saponification of methyl ester of **5** using method B yielded **7**, as reported in the literature.<sup>38</sup>

**(S)-Methyl 4-Amino-3-(2-amino-3-(4-(benzyloxy)phenyl)propanamido)benzoate (3a).**



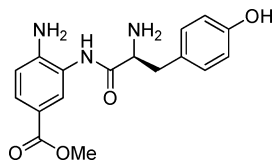
<sup>1</sup>H NMR (500.13 MHz, MeOH-*d*<sub>4</sub>): δ 7.82 (d, *J* = 8.4 Hz, 1H), 7.65 (s, 1H), 7.47–7.42 (m, 2H), 7.38–7.32 (m, 2H), 7.31–7.25 (m, 3H), 7.10–7.06 (m, 1H), 7.04 (d, *J* = 8.5 Hz, 2H), 5.16–5.08 (m, 2H), 4.32–4.25 (m, 1H), 3.85 (s, 3H), 3.25–3.17 (m, 2H). <sup>13</sup>C NMR (125.76 MHz, MeOH-*d*<sub>4</sub>): δ 171.9, 169.4, 160.1, 147.1, 138.6, 131.8, 131.8, 130.5, 130.5, 129.6, 129.5, 129.5, 128.9, 128.6, 127.5, 127.5, 119.3, 116.7, 116.7, 71.1, 56.4, 52.6, 38.0. HRMS (ESI): *m/z* calcd for C<sub>24</sub>H<sub>25</sub>N<sub>3</sub>O<sub>4</sub> + H<sup>+</sup> [M + H<sup>+</sup>], 420.1918; found, 420.1922.

**(S)-4-Amino-3-(2-amino-3-(4-(benzyloxy)phenyl)propanamido)benzoic Acid (3a').**



<sup>1</sup>H NMR (500.13 MHz, MeOH-*d*<sub>4</sub>): δ 7.90 (d, *J* = 8.3 Hz, 1H), 7.71 (s, 1H), 7.46–7.41 (m, 2H), 7.38–7.32 (m, 2H), 7.31–7.25 (m, 3H), 7.23 (dd, *J* = 8.3, 2.5 Hz, 1H), 7.03 (d, *J* = 8.2 Hz, 2H), 5.18–5.03 (m, 2H), 4.34–4.28 (m, 1H), 3.28–3.23 (m, 1H), 3.22–3.16 (m, 1H). <sup>13</sup>C NMR (125.76 MHz, MeOH-*d*<sub>4</sub>): δ 169.5, 168.5, 160.0, 139.6, 138.6, 131.8, 131.8, 131.8, 130.6, 129.6, 129.5, 129.5, 128.9, 128.6, 128.6, 127.5, 127.0, 121.2, 116.7, 116.7, 71.0, 56.3, 37.8. HRMS (ESI): *m/z* calcd for C<sub>23</sub>H<sub>23</sub>N<sub>3</sub>O<sub>4</sub> + H<sup>+</sup> [M + H<sup>+</sup>], 406.1761; found, 406.1767.

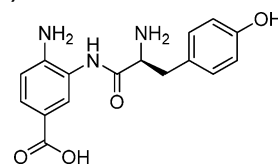
**(S)-Methyl 4-Amino-3-(2-amino-3-(4-hydroxyphenyl)propanamido)benzoate (3b).**



<sup>1</sup>H NMR (500.13 MHz, MeOH-*d*<sub>4</sub>): δ 7.90 (br.d, 1H), 7.71 (s, 1H), 7.28–7.23 (m, 1H), 7.18 (d, *J* = 8.3 Hz, 2H), 6.83 (d, *J* = 8.3 Hz, 2H), 4.33–4.27 (m, 1H), 3.91 (s, 3H), 3.26–3.11 (m, 2H). <sup>13</sup>C NMR (125.76 MHz, MeOH-*d*<sub>4</sub>): δ 174.0, 169.7, 167.3, 158.5, 131.7, 131.7,

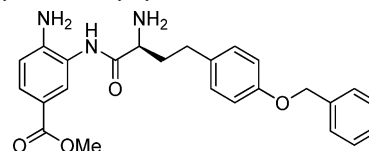
130.2, 129.3, 128.5, 126.9, 125.9, 121.6, 117.0, 117.0, 56.5, 52.8, 37.8. HRMS (ESI): *m/z* calcd for C<sub>17</sub>H<sub>19</sub>N<sub>3</sub>O<sub>4</sub> + H<sup>+</sup> [M + H<sup>+</sup>], 330.1448; found, 330.1444.

**(S)-4-Amino-3-(2-amino-3-(4-hydroxyphenyl)propanamido)benzoic Acid (3b').**



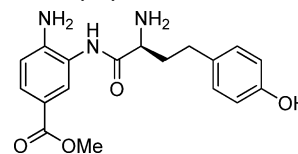
<sup>1</sup>H NMR (500.13 MHz, MeOH-*d*<sub>4</sub>): δ 7.90 (br.d, 1H), 7.81 (s, 1H), 7.25–7.21 (m, 1H), 7.19 (d, *J* = 8.4 Hz, 2H), 6.83 (d, *J* = 8.4 Hz, 2H), 4.33–4.25 (m, 1H), 3.30–3.24 (m, 1H), 3.16–3.08 (m, 1H). <sup>13</sup>C NMR (125.76 MHz, MeOH-*d*<sub>4</sub>): δ 179.0, 169.6, 158.5, 140.5, 131.7, 131.7, 130.6, 129.5, 126.9, 125.8, 121.4, 121.4, 117.0, 117.0, 56.5, 37.9. HRMS (ESI): *m/z* calcd for C<sub>16</sub>H<sub>17</sub>N<sub>3</sub>O<sub>4</sub> + H<sup>+</sup> [M + H<sup>+</sup>], 316.1292; found, 316.1298.

**(S)-Methyl 4-Amino-3-(2-amino-4-(4-(benzyloxy)phenyl)butanamido)benzoate (3c).**



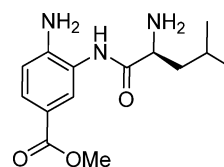
<sup>1</sup>H NMR (500.13 MHz, MeOH-*d*<sub>4</sub>): δ 7.95 (s, 1H), 7.90 (dd, *J* = 8.4, 1.8 Hz, 1H), 7.42–7.37 (m, 2H), 7.37–7.32 (m, 2H), 7.32–7.25 (m, 2H), 7.20 (d, *J* = 8.6 Hz, 2H), 6.92 (d, *J* = 8.6 Hz, 2H), 5.02 (s, 2H), 4.33–4.26 (m, 1H), 3.87 (s, 3H), 2.84–2.74 (m, 2H), 2.42–2.33 (m, 1H), 2.32–2.24 (m, 1H). <sup>13</sup>C NMR (125.76 MHz, MeOH-*d*<sub>4</sub>): δ 169.9, 167.3, 158.9, 138.8, 133.5, 130.4, 130.4, 130.1, 130.1, 129.4, 129.4, 128.9, 128.8, 128.5, 128.5, 127.9, 127.3, 122.1, 116.2, 116.2, 71.1, 55.0, 52.8, 34.5, 31.3. HRMS (ESI): *m/z* calcd for C<sub>25</sub>H<sub>27</sub>N<sub>3</sub>O<sub>4</sub> + H<sup>+</sup> [M + H<sup>+</sup>], 434.2074; found, 434.2079.

**(S)-Methyl 4-Amino-3-(2-amino-4-(4-hydroxyphenyl)butanamido)benzoate (3d).**

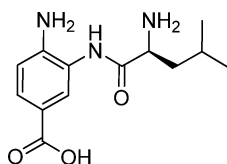


<sup>1</sup>H NMR (500.13 MHz, MeOH-*d*<sub>4</sub>): δ 7.93 (s, 1H), 7.86 (d, *J* = 8.4 Hz, 1H), 7.21 (d, *J* = 8.4 Hz, 1H), 7.10 (d, *J* = 8.3 Hz, 2H), 6.73 (d, *J* = 8.3 Hz, 2H), 4.30–4.22 (m, 1H), 3.88 (s, 3H), 2.80–2.68 (m, 2H), 2.41–2.28 (m, 1H), 2.28–2.20 (m, 1H). <sup>13</sup>C NMR (125.76 MHz, MeOH-*d*<sub>4</sub>): δ 169.9, 167.6, 157.1, 140.4, 131.9, 130.3, 130.3, 130.2, 129.1, 126.7, 125.8, 121.0, 116.5, 116.5, 54.9, 52.7, 34.8, 31.3. HRMS (ESI): *m/z* calcd for C<sub>18</sub>H<sub>21</sub>N<sub>3</sub>O<sub>4</sub> + H<sup>+</sup> [M + H<sup>+</sup>], 344.1605; found, 344.1607.

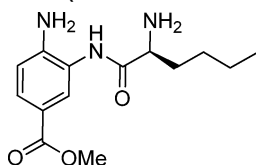
**(S)-Methyl 4-Amino-3-(2-amino-4-methylpentanamido)benzoate (3e).**



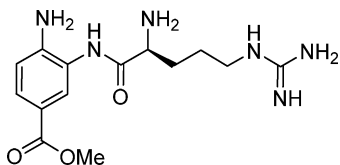
<sup>1</sup>H NMR (500.13 MHz, MeOH-*d*<sub>4</sub>): δ 7.94 (s, 1H), 7.88 (d, *J* = 8.0, 1H), 7.21 (d, *J* = 8.0 Hz, 1H), 4.25–4.15 (m, 1H), 3.88 (s, 3H), 1.97–1.76 (m, 3H), 1.11–1.05 (m, 6H). <sup>13</sup>C NMR (125.76 MHz, MeOH-*d*<sub>4</sub>): δ 170.6, 167.6, 140.6, 130.4, 129.2, 126.7, 125.7, 121.0, 53.5, 52.7, 41.5, 25.6, 23.3, 21.9. HRMS (ESI): *m/z* calcd for C<sub>14</sub>H<sub>21</sub>N<sub>3</sub>O<sub>3</sub> + H<sup>+</sup> [M + H<sup>+</sup>], 280.1656; found, 280.1659.

**(S)-4-Amino-3-(2-amino-4-methylpentanamido)benzoic Acid (3e').**

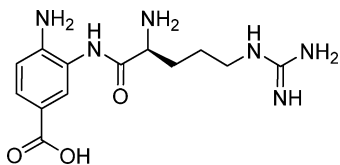
$^1\text{H}$  NMR (500.13 MHz, MeOH- $d_4$ ):  $\delta$  8.08–7.88 (m, 2H), 7.42–7.35 (m, 1H), 4.27–4.19 (m, 1H), 2.01–1.75 (m, 3H), 1.11–1.05 (m, 6H).  $^{13}\text{C}$  NMR (125.76 MHz, MeOH- $d_4$ ):  $\delta$  170.7, 168.2, 136.5, 130.4, 129.4, 129.1, 123.0, 115.4, 53.5, 41.4, 25.6, 23.3, 21.9. HRMS (ESI):  $m/z$  calcd for  $\text{C}_{13}\text{H}_{19}\text{N}_3\text{O}_3 + \text{H}^+$  [ $\text{M} + \text{H}^+$ ], 266.1499; found, 266.1500.

**(S)-Methyl 4-Amino-3-(2-aminohexanamido)benzoate (3f).**

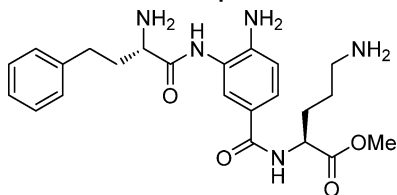
$^1\text{H}$  NMR (500.13 MHz, MeOH- $d_4$ ):  $\delta$  7.99 (d,  $J = 1.9$  Hz, 1H), 7.90 (dd,  $J = 8.4, 1.9$  Hz, 1H), 7.35 (d,  $J = 8.4$  Hz, 1H), 4.34–4.16 (m, 1H), 3.89 (s, 3H), 2.15–1.94 (m, 2H), 1.61–1.36 (m, 4H), 1.09–0.87 (m, 3H).  $^{13}\text{C}$  NMR (125.76 MHz, MeOH- $d_4$ ):  $\delta$  170.4, 167.1, 136.2, 130.0, 129.1, 128.8, 123.3, 115.3, 55.1, 52.9, 32.2, 28.1, 23.4, 14.0. HRMS (ESI):  $m/z$  calcd for  $\text{C}_{14}\text{H}_{21}\text{N}_3\text{O}_3 + \text{H}^+$  [ $\text{M} + \text{H}^+$ ], 280.1656; found, 280.1655.

**(S)-Methyl 4-Amino-3-(2-amino-5-guanidinopentanamido)benzoate (3g).**

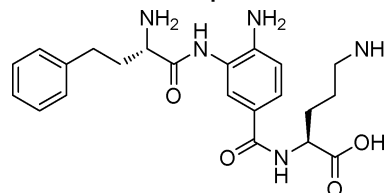
$^1\text{H}$  NMR (500.13 MHz, MeOH- $d_4$ ):  $\delta$  8.11 (s, 1H), 7.97 (d,  $J = 8.3$  Hz, 1H), 7.53–7.46 (m, 1H), 4.40–4.28 (m, 1H), 3.92 (s, 3H), 3.37–3.32 (m, 2H), 2.27–2.20 (m, 1H), 2.16–2.07 (m, 1H), 1.91–1.80 (m, 2H).  $^{13}\text{C}$  NMR (125.76 MHz, MeOH- $d_4$ ):  $\delta$  170.0, 166.9, 158.6, 144.8, 130.2, 129.9, 128.7, 124.3, 124.2, 54.6, 53.0, 41.8, 29.6, 25.7. HRMS (ESI):  $m/z$  calcd for  $\text{C}_{14}\text{H}_{22}\text{N}_6\text{O}_3 + \text{H}^+$  [ $\text{M} + \text{H}^+$ ], 323.1826; found, 323.1818.

**(S)-4-Amino-3-(2-amino-5-guanidinopentanamido)benzoic Acid (3g').**

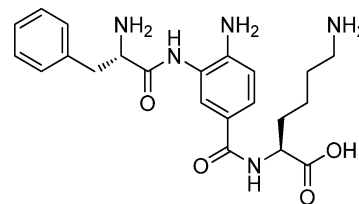
$^1\text{H}$  NMR (500.13 MHz, MeOH- $d_4$ ):  $\delta$  8.12 (br.s, 1H), 8.04–7.97 (m, 1H), 7.60–7.47 (m, 1H), 4.40–4.28 (m, 1H), 3.38–3.32 (m, 2H), 2.29–2.20 (m, 1H), 2.15–2.06 (m, 1H), 1.90–1.80 (m, 2H).  $^{13}\text{C}$  NMR (125.76 MHz, MeOH- $d_4$ ):  $\delta$  170.0, 167.8, 158.6, 131.7, 130.6, 130.1, 128.8, 124.7, 124.4, 54.6, 41.8, 29.6, 25.7. HRMS (ESI):  $m/z$  calcd for  $\text{C}_{13}\text{H}_{20}\text{N}_6\text{O}_3 + \text{H}^+$  [ $\text{M} + \text{H}^+$ ], 309.1670; found, 309.1677.

**(S)-Methyl 5-Amino-2-(4-amino-3-((S)-2-amino-4-phenylbutanamido)benzamido)pentanoate (4d).**

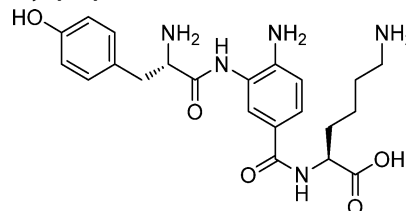
$^1\text{H}$  NMR (500.13 MHz, MeOH- $d_4$ ):  $\delta$  7.73 (s, 1H), 7.60 (dd,  $J = 8.4, 1.9$  Hz, 1H), 7.30–7.14 (m, 5H), 6.84 (d,  $J = 8.4$  Hz, 1H), 4.64–4.56 (m, 1H), 3.91–3.83 (m, 1H), 3.72 (s, 3H), 3.02–2.89 (m, 2H), 2.86–2.72 (m, 2H), 2.28–2.19 (m, 1H), 2.14–1.97 (m, 2H), 1.94–1.68 (m, 3H).  $^{13}\text{C}$  NMR (125.76 MHz, MeOH- $d_4$ ):  $\delta$  173.9, 173.5, 169.9, 148.1, 142.1, 129.6, 129.5, 129.4, 128.3, 127.7, 127.3, 123.2, 122.9, 122.4, 116.6, 55.6, 53.6, 52.8, 40.3, 36.6, 32.7, 29.3, 25.3. HRMS (ESI):  $m/z$  calcd for  $\text{C}_{23}\text{H}_{31}\text{N}_5\text{O}_4 + \text{H}^+$  [ $\text{M} + \text{H}^+$ ], 442.2449; found, 442.2450.

**(S)-5-Amino-2-(4-amino-3-((S)-2-amino-4-phenylbutanamido)benzamido)pentanoic Acid (4d').**

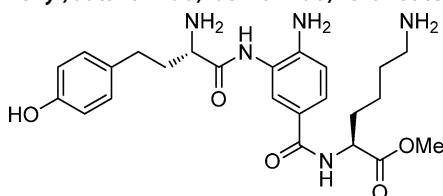
$^1\text{H}$  NMR (500.13 MHz, MeOH- $d_4$ ):  $\delta$  7.68 (s, 1H), 7.56 (dd,  $J = 8.4, 1.9$  Hz, 1H), 7.32–7.09 (m, 5H), 6.81 (d,  $J = 8.4$  Hz, 1H), 4.49–4.40 (m, 1H), 3.90–3.75 (m, 1H), 2.88–2.72 (m, 2H), 2.32 (s, 1H), 2.26–2.20 (m, 1H), 2.17–2.13 (m, 1H), 2.12–2.03 (m, 1H), 2.00–1.84 (m, 4H).  $^{13}\text{C}$  NMR (125.76 MHz, MeOH- $d_4$ ):  $\delta$  173.4, 173.3, 169.4, 147.8, 142.1, 129.6, 129.5, 129.4, 128.1, 127.5, 127.3, 123.7, 123.1, 122.5, 116.7, 55.6, 51.4, 42.8, 36.7, 32.7, 28.9, 22.5. HRMS (ESI):  $m/z$  calcd for  $\text{C}_{22}\text{H}_{29}\text{N}_5\text{O}_4 + \text{H}^+$  [ $\text{M} + \text{H}^+$ ], 428.2292; found, 428.2299.

**(S)-6-Amino-2-(4-amino-3-((S)-2-amino-3-phenylpropanamido)benzamido)hexanoic Acid (4e).**

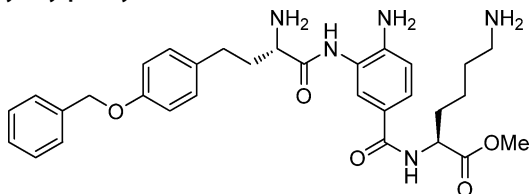
$^1\text{H}$  NMR (500.13 MHz, MeOH- $d_4$ ):  $\delta$  7.92 (d,  $J = 8.3$  Hz, 1H), 7.69 (s, 1H), 7.55 (d,  $J = 8.3$  Hz, 1H), 7.47–7.34 (m, 5H), 4.64–4.55 (m, 1H), 4.53–4.46 (m, 1H), 3.51–3.43 (m, 1H), 3.29–3.21 (m, 1H), 3.00–2.93 (m, 2H), 2.12–1.88 (m, 2H), 1.83–1.70 (m, 2H), 1.68–1.50 (m, 2H).  $^{13}\text{C}$  NMR (125.76 MHz, MeOH- $d_4$ ):  $\delta$  175.0, 173.0, 169.8, 168.3, 135.4, 130.8, 130.7, 130.7, 130.3, 130.3, 129.1, 128.1, 127.1, 127.0, 125.0, 56.4, 54.2, 40.5, 38.4, 31.8, 28.1, 24.2. HRMS (ESI):  $m/z$  calcd for  $\text{C}_{22}\text{H}_{29}\text{N}_5\text{O}_4 + \text{H}^+$  [ $\text{M} + \text{H}^+$ ], 428.2292; found, 428.2289.

**(S)-6-Amino-2-(4-amino-3-((S)-2-amino-3-(4-hydroxyphenyl)propanamido)benzamido)hexanoic Acid (4f).**

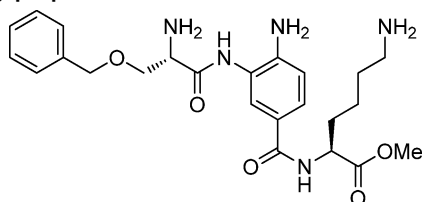
$^1\text{H}$  NMR (500.13 MHz, MeOH- $d_4$ ):  $\delta$  7.92 (d,  $J = 8.3$  Hz, 1H), 7.82 (s, 1H), 7.59 (d,  $J = 8.3$  Hz, 1H), 7.25 (d,  $J = 8.1$  Hz, 2H), 6.83 (d,  $J = 8.1$  Hz, 2H), 4.62–4.55 (m, 1H), 4.49–4.38 (m, 1H), 3.45–3.37 (m, 1H), 3.19–3.10 (m, 1H), 3.02–2.91 (m, 2H), 2.09–1.90 (m, 2H), 1.85–1.70 (m, 2H), 1.67–1.48 (m, 2H).  $^{13}\text{C}$  NMR (125.76 MHz, MeOH- $d_4$ ):  $\delta$  175.1, 170.0, 168.3, 158.3, 141.3, 131.8, 131.8, 129.6, 129.5, 128.1, 127.0, 125.9, 125.3, 117.0, 117.0, 56.6, 54.3, 40.5, 37.6, 31.7, 28.1, 24.2. HRMS (ESI):  $m/z$  calcd for  $\text{C}_{22}\text{H}_{29}\text{N}_5\text{O}_4 + \text{H}^+$  [ $\text{M} + \text{H}^+$ ], 444.2241; found, 444.2251.

**(S)-Methyl 6-Amino-2-(4-amino-3-((S)-2-amino-4-(4-hydroxyphenyl)butanamido)benzamido)hexanoate (4g).**

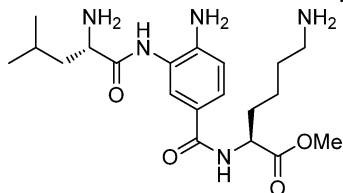
$^1\text{H}$  NMR (500.13 MHz, MeOH- $d_4$ ):  $\delta$  7.99–7.85 (m, 2H), 7.54–7.46 (m, 1H), 7.13 (d,  $J$  = 8.2 Hz, 2H), 6.74 (d,  $J$  = 8.2 Hz, 2H), 4.64–4.54 (m, 1H), 4.38–4.32 (m, 1H), 3.74 (s, 3H), 3.00–2.90 (m, 2H), 2.83–2.69 (m, 2H), 2.44–2.33 (m, 1H), 2.32–2.22 (m, 1H), 2.06–1.87 (m, 2H), 1.80–1.68 (m, 2H), 1.64–1.46 (m, 2H).  $^{13}\text{C}$  NMR (125.76 MHz, MeOH- $d_4$ ):  $\delta$  173.9, 170.2, 168.5, 157.0, 134.1, 133.1, 132.0, 130.4, 130.4, 130.1, 128.2, 127.0, 124.2, 116.4, 116.4, 55.1, 54.3, 52.9, 40.5, 34.8, 31.6, 31.4, 28.0, 24.1. HRMS (ESI):  $m/z$  calcd for  $\text{C}_{24}\text{H}_{33}\text{N}_5\text{O}_5 + \text{H}^+$  [M + H $^+$ ], 472.2554; found, 472.2554.

**(S)-Methyl 6-Amino-2-(4-amino-3-((S)-2-amino-4-(benzyloxy)phenyl)butanamido)benzamido)hexanoate (4h).**

$^1\text{H}$  NMR (500.13 MHz, MeOH- $d_4$ ):  $\delta$  8.05–7.93 (m, 2H), 7.67–7.57 (m, 1H), 7.50–7.19 (m, 7H), 7.00–6.88 (m, 2H), 5.04 (s, 2H), 4.66–4.56 (m, 1H), 4.46–4.31 (m, 1H), 3.82–3.68 (m, 3H), 3.02–2.90 (m, 2H), 2.88–2.77 (m, 2H), 2.52–2.24 (m, 2H), 2.10–1.88 (m, 2H), 1.82–1.68 (m, 2H), 1.67–1.46 (m, 2H).  $^{13}\text{C}$  NMR (125.76 MHz, MeOH- $d_4$ ):  $\delta$  173.8, 170.3, 168.2, 158.9, 138.8, 135.9, 133.5, 131.6, 130.5, 130.5, 129.5, 129.5, 128.8, 128.8, 128.5, 128.5, 128.1, 126.9, 125.6, 116.2, 116.2, 71.0, 55.0, 54.4, 52.9, 40.5, 34.6, 31.6, 31.4, 28.0, 24.2. HRMS (ESI):  $m/z$  calcd for  $\text{C}_{31}\text{H}_{39}\text{N}_5\text{O}_5 + \text{H}^+$  [M + H $^+$ ], 562.3024; found, 562.3026.

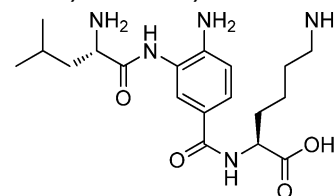
**(S)-Methyl 6-Amino-2-(4-amino-3-((S)-2-amino-3-(benzyloxy)propanamido)benzamido)hexanoate (4i).**

$^1\text{H}$  NMR (500.13 MHz, MeOH- $d_4$ ):  $\delta$  7.95–7.83 (m, 2H), 7.48 (m, 1H), 7.45–7.23 (m, 5H), 4.74–4.64 (m, 2H), 4.64–4.56 (m, 1H), 4.55–4.50 (m, 1H), 4.11–4.02 (m, 2H), 3.79–3.68 (m, 3H), 2.99–2.90 (m, 2H), 2.07–1.86 (m, 2H), 1.82–1.68 (m, 2H), 1.64–1.48 (m, 2H).  $^{13}\text{C}$  NMR (125.76 MHz, MeOH- $d_4$ ):  $\delta$  173.9, 168.5, 167.9, 138.4, 133.7, 129.6, 129.6, 129.2, 129.2, 129.2, 128.2, 127.2, 123.9, 123.8, 115.8, 74.6, 68.8, 55.2, 54.3, 52.9, 40.5, 31.7, 28.0, 24.2. HRMS (ESI):  $m/z$  calcd for  $\text{C}_{24}\text{H}_{33}\text{N}_5\text{O}_5 + \text{H}^+$  [M + H $^+$ ], 472.2554; found, 472.2550.

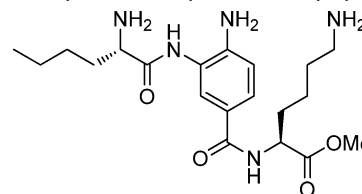
**(S)-Methyl 6-Amino-2-(4-amino-3-((S)-2-amino-4-methylpentanamido)benzamido)hexanoate (4j).**

$^1\text{H}$  NMR (500.13 MHz, MeOH- $d_4$ ):  $\delta$  7.94–7.80 (m, 2H), 7.42–7.35 (m, 1H), 4.63–4.57 (m, 1H), 4.28–4.22 (m, 1H), 3.78–3.70 (m, 3H), 2.98–2.90 (m, 2H), 2.09–1.79 (m, 5H), 1.78–1.69 (m, 2H), 1.64–

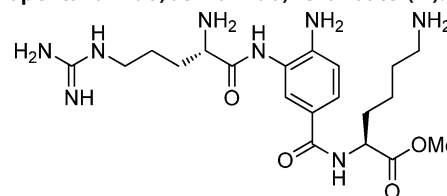
1.45 (m, 2H), 1.11–1.06 (m, 6H).  $^{13}\text{C}$  NMR (125.76 MHz, MeOH- $d_4$ ):  $\delta$  174.0, 170.8, 168.7, 151.2, 132.0, 128.6, 128.3, 127.3, 122.7, 54.2, 53.5, 52.8, 41.5, 40.5, 31.7, 28.0, 25.6, 24.2, 23.4, 21.9. HRMS (ESI):  $m/z$  calcd for  $\text{C}_{20}\text{H}_{33}\text{N}_5\text{O}_4 + \text{H}^+$  [M + H $^+$ ], 408.2605; found, 408.2606.

**(S)-6-Amino-2-(4-amino-3-((S)-2-amino-4-methylpentanamido)benzamido)hexanoic Acid (4j').**

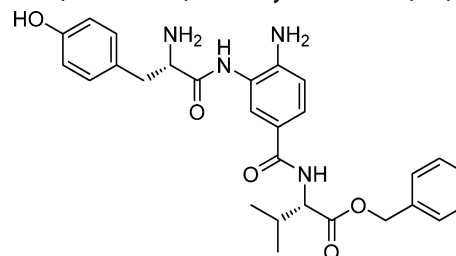
$^1\text{H}$  NMR (500.13 MHz, MeOH- $d_4$ ):  $\delta$  7.96–7.85 (m, 2H), 7.46 (d,  $J$  = 8.2 Hz, 1H), 4.65–4.53 (m, 1H), 4.34–4.21 (m, 1H), 2.12–1.68 (m, 9H), 1.64–1.48 (m, 2H), 1.14–1.01 (m, 6H).  $^{13}\text{C}$  NMR (125.76 MHz, MeOH- $d_4$ ):  $\delta$  175.1, 170.8, 168.5, 151.2, 129.5, 128.2, 127.2, 123.7, 123.5, 54.1, 53.6, 41.4, 40.6, 31.9, 28.1, 25.6, 24.2, 23.4, 21.9. HRMS (ESI):  $m/z$  calcd for  $\text{C}_{19}\text{H}_{31}\text{N}_5\text{O}_4 + \text{H}^+$  [M + H $^+$ ], 394.2449; found, 394.2455.

**(S)-Methyl 6-Amino-2-(4-amino-3-((S)-2-amino-3-aminohexanamido)benzamido)hexanoate (4k).**

$^1\text{H}$  NMR (500.13 MHz, MeOH- $d_4$ ):  $\delta$  7.92 (s, 1H), 7.88 (d,  $J$  = 8.4 Hz, 1H), 7.45 (d,  $J$  = 8.4 Hz, 1H), 4.63–4.57 (m, 1H), 4.28–4.22 (m, 1H), 3.76 (s, 3H), 2.99–2.92 (m, 2H), 2.15–2.06 (m, 1H), 2.05–1.96 (m, 2H), 1.95–1.88 (m, 1H), 1.78–1.68 (m, 2H), 1.62–1.43 (m, 6H), 1.03–0.97 (m, 3H).  $^{13}\text{C}$  NMR (125.76 MHz, MeOH- $d_4$ ):  $\delta$  173.9, 170.5, 168.6, 134.3, 133.2, 129.5, 128.2, 127.1, 123.6, 55.1, 54.3, 52.9, 40.5, 32.3, 31.6, 28.2, 28.0, 24.2, 23.4, 14.1. HRMS (ESI):  $m/z$  calcd for  $\text{C}_{20}\text{H}_{33}\text{N}_5\text{O}_4 + \text{H}^+$  [M + H $^+$ ], 408.2605; found, 408.2603.

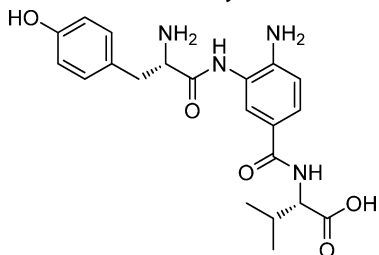
**(S)-Methyl 6-Amino-2-(4-amino-3-((S)-2-amino-5-guanidinopentanamido)benzamido)hexanoate (4l).**

$^1\text{H}$  NMR (500.13 MHz, MeOH- $d_4$ ):  $\delta$  8.00 (s, 1H), 7.88 (d,  $J$  = 8.2 Hz, 1H), 7.47–7.38 (m, 1H), 4.63–4.56 (m, 1H), 4.35–4.29 (m, 1H), 3.75 (s, 3H), 3.37–3.32 (m, 2H), 2.99–2.91 (m, 2H), 2.17–2.07 (m, 2H), 2.05–1.90 (m, 2H), 1.90–1.81 (m, 2H), 1.79–1.68 (m, 2H), 1.64–1.49 (m, 2H).  $^{13}\text{C}$  NMR (125.76 MHz, MeOH- $d_4$ ):  $\delta$  174.0, 171.5, 169.9, 168.6, 158.6, 129.1, 128.3, 127.2, 123.4, 123.3, 54.7, 54.4, 52.9, 41.9, 40.7, 31.8, 29.8, 28.2, 25.8, 24.3. HRMS (ESI):  $m/z$  calcd for  $\text{C}_{20}\text{H}_{34}\text{N}_8\text{O}_4 + \text{H}^+$  [M + H $^+$ ], 451.2776; found, 451.2777.

**(S)-Benzyl 2-(4-Amino-3-((S)-2-amino-3-(4-hydroxyphenyl)propanamido)benzamido)-3-methylbutanoate (4m).**

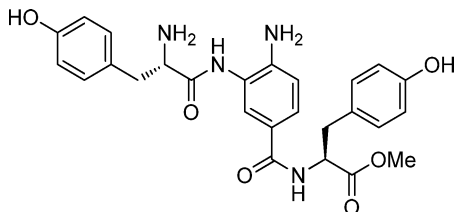
$^1\text{H}$  NMR (500.13 MHz, MeOH- $d_4$ ):  $\delta$  7.78 (d,  $J$  = 8.2 Hz, 1H), 7.69 (s, 1H), 7.41–7.29 (m, 6H), 7.21 (d,  $J$  = 8.3 Hz, 2H), 6.83 (d,  $J$  = 8.3 Hz, 2H), 5.26–5.21 (m, 1H), 5.19–5.14 (m, 1H), 4.51–4.46 (m, 1H), 4.39–4.33 (m, 1H), 3.36–3.32 (m, 1H), 3.16–3.08 (m, 1H), 2.32–2.22 (m, 1H), 1.06–0.94 (m, 6H).  $^{13}\text{C}$  NMR (125.76 MHz, MeOH- $d_4$ ):  $\delta$  173.0, 169.9, 169.1, 167.3, 158.5, 137.2, 131.8, 131.8, 131.8, 129.6, 129.5, 129.5, 129.4, 129.4, 128.2, 127.3, 125.8, 122.9, 117.0, 117.0, 117.0, 67.9, 60.5, 56.5, 37.8, 31.7, 19.6, 19.2. HRMS (ESI):  $m/z$  calcd for  $\text{C}_{28}\text{H}_{32}\text{N}_4\text{O}_5 + \text{H}^+$  [ $\text{M} + \text{H}^+$ ], 505.2445; found, 505.2447.

**(S)-2-(4-Amino-3-((S)-2-amino-3-(4-hydroxyphenyl)propanamido)benzamido)-3-methylbutanoic Acid (4m')**



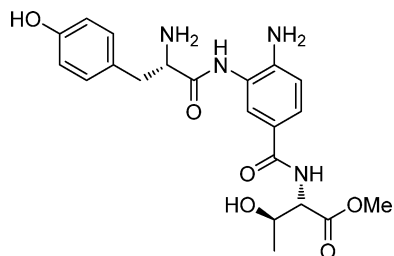
$^1\text{H}$  NMR (500.13 MHz, MeOH- $d_4$ ):  $\delta$  7.86 (d,  $J$  = 8.3 Hz, 1H), 7.74 (s, 1H), 7.51 (d,  $J$  = 8.3 Hz, 1H), 7.22 (d,  $J$  = 8.3 Hz, 2H), 6.83 (d,  $J$  = 8.3 Hz, 2H), 4.52–4.46 (m, 1H), 4.43–4.37 (m, 1H), 3.40–3.33 (m, 1H), 3.18–3.07 (m, 1H), 2.35–2.24 (m, 1H), 1.09–1.01 (m, 6H).  $^{13}\text{C}$  NMR (125.76 MHz, MeOH- $d_4$ ):  $\delta$  174.8, 169.9, 168.7, 167.1, 158.4, 135.4, 131.8, 131.8, 130.4, 128.1, 127.1, 125.8, 124.6, 117.0, 117.0, 60.1, 56.6, 37.7, 31.7, 19.7, 18.9. HRMS (ESI):  $m/z$  calcd for  $\text{C}_{21}\text{H}_{26}\text{N}_4\text{O}_5 + \text{H}^+$  [ $\text{M} + \text{H}^+$ ], 415.1976; found, 415.1982.

**(S)-Methyl 2-(4-Amino-3-((S)-2-amino-3-(4-hydroxyphenyl)propanamido)benzamido)-3-(4-hydroxyphenyl)propanoate (4n).**



$^1\text{H}$  NMR (500.13 MHz, MeOH- $d_4$ ):  $\delta$  7.70 (d,  $J$  = 8.3 Hz, 1H), 7.63 (s, 1H), 7.34 (dd,  $J$  = 8.4, 3.1 Hz, 1H), 7.21 (d,  $J$  = 8.4 Hz, 2H), 7.07 (d,  $J$  = 8.4 Hz, 2H), 6.83 (d,  $J$  = 8.4 Hz, 2H), 6.70 (d,  $J$  = 8.4 Hz, 2H), 4.80–4.74 (m, 1H), 4.38–4.32 (m, 1H), 3.72 (s, 3H), 3.23–3.15 (m, 2H), 3.14–3.07 (m, 1H), 3.06–2.99 (m, 1H).  $^{13}\text{C}$  NMR (125.76 MHz, MeOH- $d_4$ ):  $\delta$  173.7, 169.9, 168.4, 158.5, 157.4, 132.9, 131.8, 131.8, 131.2, 129.0, 128.9, 128.0, 127.2, 125.9, 123.1, 117.1, 117.1, 116.9, 116.3, 116.3, 56.6, 56.2, 52.8, 37.8, 37.4. HRMS (ESI):  $m/z$  calcd for  $\text{C}_{26}\text{H}_{28}\text{N}_4\text{O}_6 + \text{H}^+$  [ $\text{M} + \text{H}^+$ ], 493.2082; found, 493.2081.

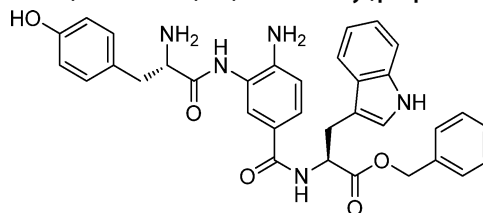
**(2S,3R)-Methyl 2-(4-Amino-3-((S)-2-amino-3-(4-hydroxyphenyl)propanamido)benzamido)-3-hydroxybutanoate (4o).**



$^1\text{H}$  NMR (500.13 MHz, MeOH- $d_4$ ):  $\delta$  7.80 (d,  $J$  = 8.4 Hz, 1H), 7.69 (s, 1H), 7.26 (d,  $J$  = 8.4 Hz, 1H), 7.20 (d,  $J$  = 8.3 Hz, 2H), 6.84 (d,  $J$  = 8.3 Hz, 2H), 4.69–4.65 (m, 1H), 4.43–4.37 (m, 1H), 4.33–4.27 (m, 1H), 3.78 (s, 3H), 3.29–3.25 (m, 1H), 3.15–3.09 (m, 1H), 1.27–1.23 (m, 3H).  $^{13}\text{C}$  NMR (125.76 MHz, MeOH- $d_4$ ):  $\delta$  169.6, 169.2, 165.1, 158.5, 158.2, 131.7, 131.7, 128.3, 127.5, 125.9, 120.6, 120.5, 120.4,

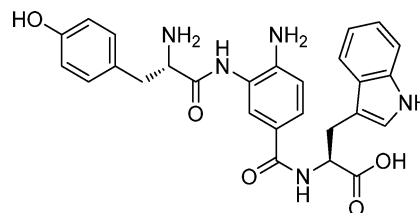
117.1, 117.1, 68.6, 60.3, 56.7, 52.8, 37.4, 20.1. HRMS (ESI):  $m/z$  calcd for  $\text{C}_{21}\text{H}_{26}\text{N}_4\text{O}_6 + \text{H}^+$  [ $\text{M} + \text{H}^+$ ], 431.1925; found, 431.1931.

**(S)-Benzyl 2-(4-Amino-3-((S)-2-amino-3-(4-hydroxyphenyl)propanamido)benzamido)-3-(1H-indol-3-yl)propanoate (4p).**



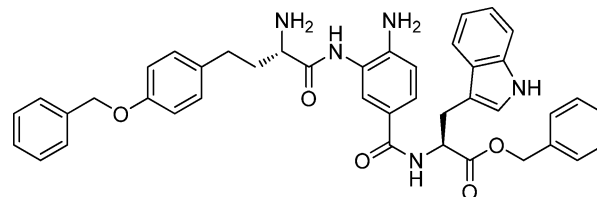
$^1\text{H}$  NMR (500.13 MHz, MeOH- $d_4$ ):  $\delta$  7.55 (d,  $J$  = 7.9 Hz, 1H), 7.49 (s, 1H), 7.46–7.41 (m, 1H), 7.34 (d,  $J$  = 7.9 Hz, 1H), 7.30–7.25 (m, 3H), 7.19–7.14 (m, 2H), 7.14–7.05 (m, 3H), 7.03–6.97 (m, 2H), 6.78–6.71 (m, 3H), 5.07 (s, 2H), 4.93–4.87 (m, 1H), 3.82–3.76 (m, 1H), 3.43–3.37 (m, 1H), 3.35–3.33 (m, 1H), 3.05–2.97 (m, 1H), 2.95–2.86 (m, 1H).  $^{13}\text{C}$  NMR (125.76 MHz, MeOH- $d_4$ ):  $\delta$  175.3, 173.8, 169.8, 157.5, 148.0, 138.1, 137.1, 131.6, 131.6, 129.5, 129.2, 129.2, 128.9, 128.8, 128.3, 127.7, 124.5, 123.1, 122.5, 122.2, 120.0, 119.2, 117.2, 116.7, 116.6, 116.6, 116.2, 112.5, 110.8, 68.2, 57.8, 55.6, 41.5, 28.6. HRMS (ESI):  $m/z$  calcd for  $\text{C}_{34}\text{H}_{33}\text{N}_5\text{O}_5 + \text{H}^+$  [ $\text{M} + \text{H}^+$ ], 592.2554; found, 592.2564.

**(S)-2-(4-Amino-3-((S)-2-amino-3-(4-hydroxyphenyl)propanamido)benzamido)-3-(1H-indol-3-yl)propanoic Acid (4p').**

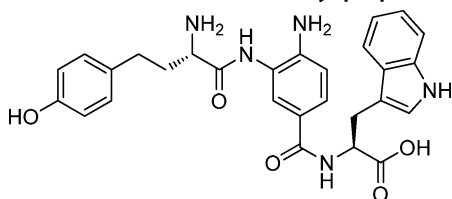


$^1\text{H}$  NMR (500.13 MHz, MeOH- $d_4$ ):  $\delta$  7.71–7.50 (m, 3H), 7.39–7.29 (m, 2H), 7.20 (d,  $J$  = 8.4 Hz, 2H), 7.15 (s, 1H), 7.11–7.02 (m, 1H), 7.02–6.63 (m, 1H), 6.82 (d,  $J$  = 8.4 Hz, 2H), 4.95–4.90 (m, 1H), 4.42–4.30 (m, 1H), 3.55–3.40 (m, 1H), 3.40–3.32 (m, 1H), 3.25–3.15 (m, 1H), 3.14–3.04 (m, 1H).  $^{13}\text{C}$  NMR (125.76 MHz, MeOH- $d_4$ ):  $\delta$  175.1, 169.9, 168.2, 158.4, 138.1, 133.9, 131.7, 131.7, 129.5, 128.8, 127.9, 127.0, 125.8, 124.5, 123.6, 122.4, 122.1, 119.9, 119.3, 117.1, 117.1, 112.4, 111.1, 56.5, 55.5, 37.8, 28.3. HRMS (ESI):  $m/z$  calcd for  $\text{C}_{27}\text{H}_{27}\text{N}_5\text{O}_5 + \text{H}^+$  [ $\text{M} + \text{H}^+$ ], 502.2085; found, 502.2080.

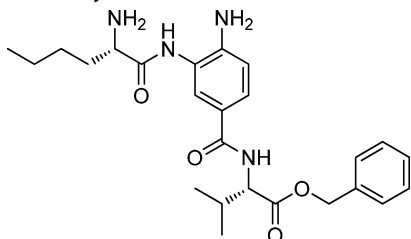
**(S)-Benzyl 2-(4-Amino-3-((S)-2-amino-4-(4-(benzyloxy)phenyl)butanamido)benzamido)-3-(1H-indol-3-yl)propanoate (4q).**



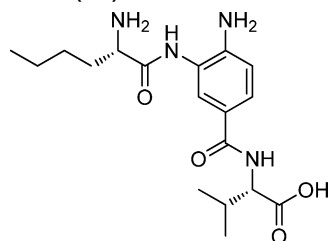
$^1\text{H}$  NMR (500.13 MHz, MeOH- $d_4$ ):  $\delta$  7.75–7.63 (m, 2H), 7.55–7.48 (m, 1H), 7.41–7.11 (m, 14H), 7.07–6.86 (m, 5H), 5.06 (br.d, 2H), 4.99 (br.d, 2H), 4.95–4.89 (m, 1H), 4.38–4.22 (m, 1H), 3.49–3.35 (m, 1H), 3.36–3.30 (m, 1H), 2.87–2.67 (m, 2H), 2.41–2.31 (m, 1H), 2.29–2.19 (m, 1H).  $^{13}\text{C}$  NMR (125.76 MHz, MeOH- $d_4$ ):  $\delta$  173.4, 170.1, 168.4, 158.9, 138.7, 138.0, 137.0, 134.9, 133.5, 132.8, 130.4, 130.4, 129.4, 129.4, 129.2, 129.2, 129.1, 129.1, 128.9, 128.8, 128.8, 128.7, 128.5, 128.5, 128.1, 127.0, 124.6, 123.2, 122.5, 119.9, 119.1, 116.2, 116.2, 112.4, 110.7, 71.0, 68.0, 55.9, 54.9, 34.6, 31.4, 28.3. HRMS (ESI):  $m/z$  calcd for  $\text{C}_{42}\text{H}_{41}\text{N}_5\text{O}_5 + \text{H}^+$  [ $\text{M} + \text{H}^+$ ], 696.3180; found, 696.3174.

**(S)-2-(4-Amino-3-((S)-2-amino-4-(4-hydroxyphenyl)butanamido)benzamido)-3-(1H-indol-3-yl)propanoic Acid (4r).**

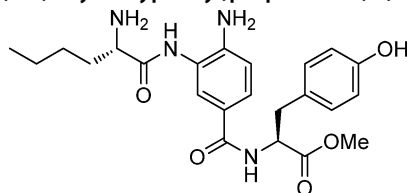
$^1\text{H}$  NMR (500.13 MHz, MeOH- $d_4$ ):  $\delta$  7.65 (s, 1H), 7.59–7.39 (m, 3H), 7.29 (br.d, 1H), 7.14–6.91 (m, 5H), 6.74 (br.d, 2H), 4.71–4.49 (m, 1H), 4.30–4.04 (m, 1H), 3.46–3.38 (m, 1H), 3.30–3.28 (m, 1H), 2.76–2.64 (m, 2H), 2.32–2.22 (m, 1H), 2.23–2.13 (m, 1H).  $^{13}\text{C}$  NMR (125.76 MHz, MeOH- $d_4$ ):  $\delta$  175.3, 169.8, 168.9, 157.1, 141.2, 138.0, 132.0, 130.3, 130.3, 128.4, 128.2, 127.6, 127.3, 125.5, 124.4, 122.4, 120.0, 119.8, 119.2, 116.5, 116.5, 112.3, 111.1, 55.3, 54.9, 35.0, 31.4, 28.3. HRMS (ESI):  $m/z$  calcd for  $\text{C}_{28}\text{H}_{29}\text{N}_5\text{O}_5 + \text{H}^+$  [ $\text{M} + \text{H}^+$ ], 516.2241; found, 516.2248.

**(S)-Benzyl 2-(4-Amino-3-((S)-2-aminohexanamido)benzamido)-3-methylbutanoate (4s).**

$^1\text{H}$  NMR (500.13 MHz, MeOH- $d_4$ ):  $\delta$  7.85–7.77 (m, 2H), 7.40–7.29 (m, 6H), 5.27–5.13 (m, 2H), 4.50–4.46 (m, 1H), 4.24–4.18 (m, 1H), 2.31–2.22 (m, 1H), 2.15–2.04 (m, 1H), 2.03–1.93 (m, 1H), 1.57–1.42 (m, 4H), 1.04–0.95 (m, 9H).  $^{13}\text{C}$  NMR (125.76 MHz, MeOH- $d_4$ ):  $\delta$  173.0, 170.4, 168.9, 151.1, 137.2, 129.6, 129.6, 129.5, 129.4, 128.6, 128.2, 128.2, 127.2, 127.2, 122.8, 67.9, 60.5, 55.1, 32.3, 31.6, 28.1, 23.4, 19.6, 19.2, 14.1. HRMS (ESI):  $m/z$  calcd for  $\text{C}_{25}\text{H}_{34}\text{N}_4\text{O}_4 + \text{H}^+$  [ $\text{M} + \text{H}^+$ ], 455.2653; found, 455.2653.

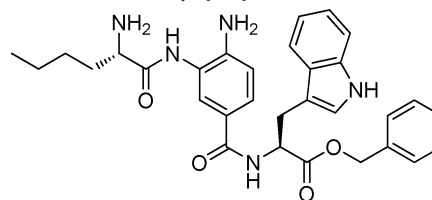
**(S)-2-(4-Amino-3-((S)-2-aminohexanamido)benzamido)-3-methylbutanoic Acid (4s').**

$^1\text{H}$  NMR (500.13 MHz, MeOH- $d_4$ ):  $\delta$  7.91–7.86 (m, 2H), 7.56 (br.d, 1H), 4.50–4.46 (m, 1H), 4.28–4.22 (m, 1H), 2.34–2.25 (m, 1H), 2.16–2.06 (m, 1H), 2.03–1.96 (m, 1H), 1.58–1.42 (m, 4H), 1.08–1.02 (m, 6H), 1.02–0.96 (m, 3H).  $^{13}\text{C}$  NMR (125.76 MHz, MeOH- $d_4$ ):  $\delta$  178.5, 171.0, 169.0, 147.6, 127.9, 127.3, 124.2, 122.3, 116.8, 61.7, 55.2, 33.1, 33.0, 28.3, 23.5, 20.2, 18.7, 14.1. HRMS (ESI):  $m/z$  calcd for  $\text{C}_{18}\text{H}_{28}\text{N}_4\text{O}_4 + \text{H}^+$  [ $\text{M} + \text{H}^+$ ], 365.2183; found, 365.2177.

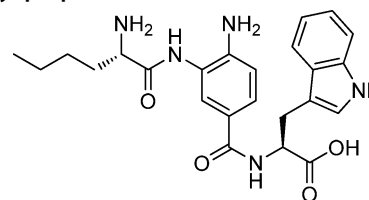
**(S)-Methyl 2-(4-Amino-3-((S)-2-aminohexanamido)benzamido)-3-(4-hydroxyphenyl)propanoate (4t).**

$^1\text{H}$  NMR (500.13 MHz, MeOH- $d_4$ ):  $\delta$  7.83–7.72 (m, 2H), 7.51 (d,  $J = 8.3$  Hz, 1H), 7.13–7.02 (m, 2H), 6.74–6.65 (m, 2H), 4.81–4.74 (m, 1H), 4.26–4.19 (m, 1H), 3.72 (s, 3H), 3.26–3.16 (m, 1H), 3.08–2.96 (m, 1H), 2.15–2.05 (m, 1H), 2.05–1.95 (m, 1H), 1.57–1.41 (m, 4H),

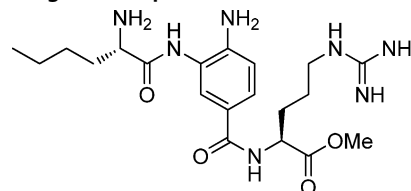
1.04–0.93 (m, 3H).  $^{13}\text{C}$  NMR (125.76 MHz, MeOH- $d_4$ ):  $\delta$  174.7, 173.5, 170.7, 168.0, 157.4, 135.4, 131.2, 131.2, 131.0, 129.0, 127.9, 126.8, 125.0, 116.3, 116.3, 56.3, 55.1, 52.8, 37.3, 32.2, 28.1, 23.4, 14.1. HRMS (ESI):  $m/z$  calcd for  $\text{C}_{23}\text{H}_{30}\text{N}_4\text{O}_5 + \text{H}^+$  [ $\text{M} + \text{H}^+$ ], 443.2289; found, 443.2291.

**(S)-Benzyl 2-(4-Amino-3-((S)-2-aminohexanamido)benzamido)-3-(1H-indol-3-yl)propanoate (4u).**

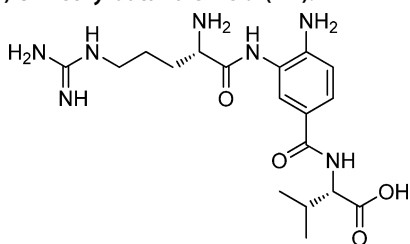
$^1\text{H}$  NMR (500.13 MHz, MeOH- $d_4$ ):  $\delta$  7.78 (s, 1H), 7.70 (d,  $J = 7.8$  Hz, 1H), 7.54 (d,  $J = 7.8$  Hz, 1H), 7.40–7.30 (m, 2H), 7.30–7.25 (m, 3H), 7.22–7.16 (m, 2H), 7.11–7.06 (m, 1H), 7.04 (s, 1H), 7.01–6.95 (m, 1H), 5.09 (s, 2H), 4.24–4.16 (m, 1H), 3.48–3.38 (m, 1H), 3.38–3.32 (m, 2H), 2.12–2.04 (m, 1H), 2.03–1.93 (m, 1H), 1.56–1.39 (m, 4H), 1.02–0.94 (m, 3H).  $^{13}\text{C}$  NMR (125.76 MHz, MeOH- $d_4$ ):  $\delta$  173.4, 170.4, 168.3, 138.1, 137.0, 133.3, 129.5, 129.5, 129.2, 129.2, 129.1, 129.1, 128.7, 128.0, 127.0, 124.5, 123.5, 123.4, 122.5, 119.9, 119.1, 112.4, 110.8, 68.0, 55.9, 55.1, 32.3, 28.3, 28.1, 23.4, 14.0. HRMS (ESI):  $m/z$  calcd for  $\text{C}_{31}\text{H}_{35}\text{N}_5\text{O}_4 + \text{H}^+$  [ $\text{M} + \text{H}^+$ ], 542.2762; found, 542.2759.

**(S)-2-(4-Amino-3-((S)-2-aminohexanamido)benzamido)-3-(1H-indol-3-yl)propanoic Acid (4u').**

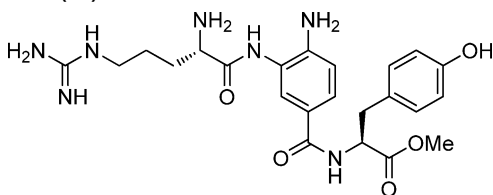
$^1\text{H}$  NMR (500.13 MHz, MeOH- $d_4$ ):  $\delta$  7.76 (s, 1H), 7.70–7.64 (m, 1H), 7.58 (d,  $J = 7.8$  Hz, 1H), 7.41–7.36 (m, 1H), 7.32 (d,  $J = 7.8$  Hz, 1H), 7.15 (s, 1H), 7.09–7.03 (m, 1H), 7.00–6.93 (m, 1H), 4.93–4.90 (m, 1H), 4.26–4.18 (m, 1H), 3.53–3.44 (m, 1H), 3.37–3.32 (m, 1H), 2.14–2.04 (m, 1H), 2.02–1.94 (m, 1H), 1.55–1.40 (m, 4H), 1.02–0.92 (m, 3H).  $^{13}\text{C}$  NMR (125.76 MHz, MeOH- $d_4$ ):  $\delta$  175.1, 170.5, 168.2, 138.0, 134.3, 133.2, 129.9, 128.8, 127.9, 126.9, 124.5, 124.0, 122.4, 119.8, 119.2, 112.3, 111.2, 55.5, 55.1, 32.2, 28.2, 28.1, 23.4, 14.1. HRMS (ESI):  $m/z$  calcd for  $\text{C}_{24}\text{H}_{29}\text{N}_5\text{O}_4 + \text{H}^+$  [ $\text{M} + \text{H}^+$ ], 452.2292; found, 452.2302.

**(S)-Methyl 2-(4-Amino-3-((S)-2-aminohexanamido)benzamido)-5-guanidinopentanoate (4v).**

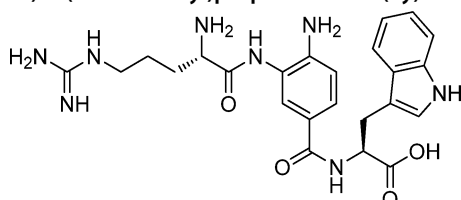
$^1\text{H}$  NMR (500.13 MHz, MeOH- $d_4$ ):  $\delta$  8.00 (s, 1H), 7.98–7.94 (d,  $J = 7.8$  Hz, 1H), 7.63 (d,  $J = 7.8$  Hz, 1H), 4.65–4.58 (m, 1H), 4.33–4.27 (m, 1H), 3.75 (s, 3H), 2.17–1.92 (m, 4H), 1.85–1.62 (m, 3H), 1.60–1.40 (m, 5H), 1.04–0.92 (m, 3H).  $^{13}\text{C}$  NMR (125.76 MHz, MeOH- $d_4$ ):  $\delta$  173.6, 170.6, 168.2, 158.6, 135.8, 131.5, 130.6, 128.1, 126.9, 125.6, 55.1, 54.2, 53.0, 42.0, 32.1, 29.2, 28.1, 26.6, 23.4, 14.1. HRMS (ESI):  $m/z$  calcd for  $\text{C}_{20}\text{H}_{33}\text{N}_7\text{O}_4 + \text{H}^+$  [ $\text{M} + \text{H}^+$ ], 436.2667; found, 436.2670.

**(S)-2-(4-Amino-3-((S)-2-amino-5-guanidinopentanamido)benzamido)-3-methylbutanoic Acid (4w).**

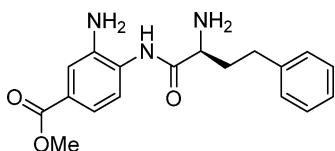
$^1\text{H}$  NMR (500.13 MHz, MeOH- $d_4$ ):  $\delta$  7.91 (s, 1H), 7.83 (d,  $J$  = 8.3 Hz, 1H), 7.44–7.37 (m, 1H), 4.50–4.45 (m, 1H), 4.33–4.27 (m, 1H), 3.36–3.32 (m, 2H), 2.35–2.05 (m, 3H), 1.89–1.80 (m, 2H), 1.08–1.01 (m, 6H).  $^{13}\text{C}$  NMR (125.76 MHz, MeOH- $d_4$ ):  $\delta$  174.9, 169.9, 169.1, 169.0, 158.7, 128.3, 128.1, 127.2, 122.5, 122.3, 60.0, 54.6, 41.8, 31.7, 29.7, 25.6, 19.7, 19.6. HRMS (ESI):  $m/z$  calcd for  $\text{C}_{18}\text{H}_{29}\text{N}_7\text{O}_4 + \text{H}^+$  [ $\text{M} + \text{H}^+$ ], 408.2354; found, 408.2354.

**(S)-Methyl 2-(4-Amino-3-((S)-2-amino-5-guanidinopentanamido)benzamido)-3-(4-hydroxyphenyl)propanoate (4x).**

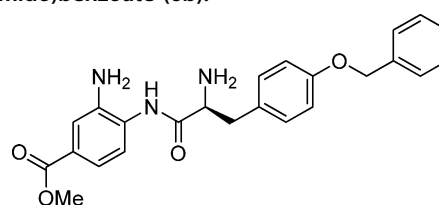
$^1\text{H}$  NMR (500.13 MHz, MeOH- $d_4$ ):  $\delta$  7.90 (s, 1H), 7.76 (br.d, 1H), 7.60–7.47 (m, 1H), 7.08 (br.d, 2H), 6.70 (br.d, 2H), 4.82–4.74 (m, 1H), 4.39–4.29 (m, 1H), 3.72 (s, 3H), 3.40–3.27 (m, 2H), 3.26–3.14 (m, 1H), 3.13–2.97 (m, 1H), 2.25–2.06 (m, 2H), 1.92–1.76 (m, 2H).  $^{13}\text{C}$  NMR (125.76 MHz, MeOH- $d_4$ ):  $\delta$  173.6, 170.0, 167.9, 158.6, 157.3, 151.2, 135.8, 131.2, 131.2, 129.0, 127.9, 126.8, 126.6, 125.3, 116.3, 116.3, 56.3, 54.6, 52.8, 41.8, 37.3, 29.6, 25.6. HRMS (ESI):  $m/z$  calcd for  $\text{C}_{23}\text{H}_{31}\text{N}_7\text{O}_5 + \text{H}^+$  [ $\text{M} + \text{H}^+$ ], 486.2459; found, 486.2466.

**(S)-2-(4-Amino-3-((S)-2-amino-5-guanidinopentanamido)benzamido)-3-(1H-indol-3-yl)propanoic Acid (4y).**

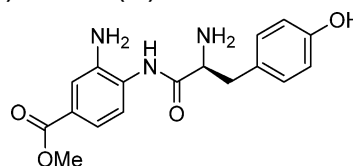
$^1\text{H}$  NMR (500.13 MHz, MeOH- $d_4$ ):  $\delta$  7.83–7.55 (m, 2H), 7.39–7.21 (m, 2H), 7.20–6.88 (m, 4H), 4.32–4.24 (m, 1H), 3.93–3.81 (m, 1H), 3.69–3.49 (m, 2H), 3.34–3.40 (m, 2H), 2.17–2.00 (m, 2H), 1.88–1.76 (m, 2H).  $^{13}\text{C}$  NMR (125.76 MHz, MeOH- $d_4$ ):  $\delta$  174.1, 170.5, 169.7, 168.6, 158.6, 138.0, 128.0, 127.2, 125.9, 124.5, 122.5, 121.6, 120.1, 119.8, 119.6, 119.1, 112.4, 110.9, 55.6, 54.5, 41.8, 29.7, 28.3, 25.6. HRMS (ESI):  $m/z$  calcd for  $\text{C}_{24}\text{H}_{30}\text{N}_8\text{O}_4 + \text{H}^+$  [ $\text{M} + \text{H}^+$ ], 495.2463; found, 495.2470.

**(S)-Methyl 3-Amino-4-(2-amino-4-phenylbutanamido)benzoate (6a).**

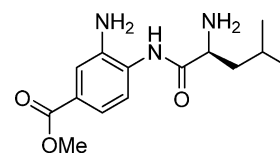
$^1\text{H}$  NMR (500.13 MHz, MeOH- $d_4$ ):  $\delta$  8.17–8.06 (m, 2H), 7.67–7.58 (m, 1H), 7.35–7.27 (m, 4H), 7.25–7.18 (m, 1H), 4.45–4.36 (m, 1H), 3.94 (s, 3H), 2.90–2.80 (m, 2H), 2.48–2.37 (m, 1H), 2.36–2.26 (m, 1H).  $^{13}\text{C}$  NMR (125.76 MHz, MeOH- $d_4$ ):  $\delta$  170.1, 166.4, 141.2, 135.6, 131.2, 131.1, 130.7, 129.7, 129.6, 129.4, 127.6, 127.1, 126.6, 126.5, 55.2, 53.1, 34.5, 32.3. HRMS (ESI):  $m/z$  calcd for  $\text{C}_{18}\text{H}_{21}\text{N}_3\text{O}_3 + \text{H}^+$  [ $\text{M} + \text{H}^+$ ], 328.1656; found, 328.1661.

**(S)-Methyl 3-Amino-4-(2-amino-3-(4-(benzyloxy)phenyl)propanamido)benzoate (6b).**

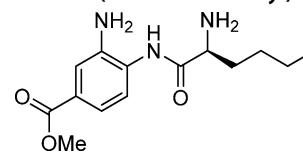
$^1\text{H}$  NMR (500.13 MHz, MeOH- $d_4$ ):  $\delta$  7.90–7.85 (m, 1H), 7.79 (dd,  $J$  = 8.3, 1.7 Hz, 1H), 7.45–7.40 (m, 2H), 7.38–7.32 (m, 2H), 7.31–7.24 (m, 4H), 7.02 (d,  $J$  = 8.5 Hz, 3H), 5.18–4.99 (m, 2H), 4.45–4.27 (m, 1H), 3.95–3.85 (m, 3H), 3.37–3.32 (m, 1H), 3.20–3.10 (m, 1H).  $^{13}\text{C}$  NMR (125.76 MHz, MeOH- $d_4$ ):  $\delta$  169.5, 167.0, 159.9, 143.4, 138.6, 133.1, 131.8, 131.8, 130.5, 129.5, 129.5, 128.9, 128.5, 128.4, 127.8, 127.5, 126.9, 124.3, 116.6, 116.6, 70.9, 56.4, 52.9, 37.7. HRMS (ESI):  $m/z$  calcd for  $\text{C}_{24}\text{H}_{25}\text{N}_3\text{O}_4 + \text{H}^+$  [ $\text{M} + \text{H}^+$ ], 420.1845; found, 420.1843.

**(S)-Methyl 3-Amino-4-(2-amino-3-(4-hydroxyphenyl)propanamido)benzoate (6c).**

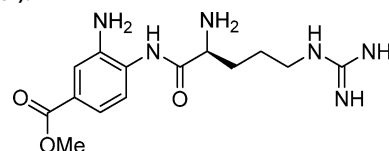
$^1\text{H}$  NMR (500.13 MHz, MeOH- $d_4$ ):  $\delta$  7.63 (s, 1H), 7.50 (d,  $J$  = 8.2 Hz, 1H), 7.30–7.16 (m, 3H), 6.81 (d,  $J$  = 8.1 Hz, 2H), 4.40–4.30 (m, 1H), 3.95–3.85 (m, 3H), 3.30–3.07 (m, 2H).  $^{13}\text{C}$  NMR (125.76 MHz, MeOH- $d_4$ ):  $\delta$  169.2, 167.8, 158.4, 143.4, 131.8, 131.8, 130.3, 126.8, 125.9, 123.7, 121.5, 121.3, 116.9, 116.9, 56.4, 52.7, 37.9. HRMS (ESI):  $m/z$  calcd for  $\text{C}_{17}\text{H}_{19}\text{N}_3\text{O}_4 + \text{H}^+$  [ $\text{M} + \text{H}^+$ ], 330.1448; found, 330.1457.

**(S)-Methyl 3-Amino-4-(2-amino-4-methylpentanamido)benzoate (6d).**

$^1\text{H}$  NMR (500.13 MHz, MeOH- $d_4$ ):  $\delta$  8.15–8.04 (m, 2H), 7.62 (dd,  $J$  = 8.5, 3.2 Hz, 1H), 4.33–4.25 (m, 1H), 3.94 (s, 3H), 2.00–1.76 (m, 3H), 1.12–1.04 (m, 6H).  $^{13}\text{C}$  NMR (125.76 MHz, MeOH- $d_4$ ):  $\delta$  170.8, 166.5, 135.4, 130.8, 130.8, 127.2, 126.4, 115.9, 53.7, 53.1, 41.3, 25.5, 23.4, 21.8. HRMS (ESI):  $m/z$  calcd for  $\text{C}_{14}\text{H}_{21}\text{N}_3\text{O}_3 + \text{H}^+$  [ $\text{M} + \text{H}^+$ ], 280.1656; found, 280.1650.

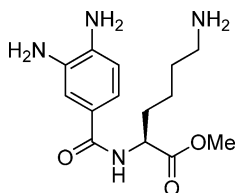
**(S)-Methyl 3-Amino-4-(2-amino-4-phenylbutanamido)benzoate (6e).**

$^1\text{H}$  NMR (500.13 MHz, MeOH- $d_4$ ):  $\delta$  8.10 (s, 1H), 8.04 (d,  $J$  = 8.4 Hz, 1H), 7.64 (d,  $J$  = 8.4 Hz, 1H), 4.31–4.25 (m, 1H), 3.94 (s, 3H), 2.16–1.96 (m, 2H), 1.58–1.39 (m, 4H), 1.02–0.94 (m, 3H).  $^{13}\text{C}$  NMR (125.76 MHz, MeOH- $d_4$ ):  $\delta$  170.4, 166.5, 143.4, 135.3, 130.6, 128.0, 127.0, 126.2, 55.2, 53.1, 32.2, 28.1, 23.4, 14.1. HRMS (ESI):  $m/z$  calcd for  $\text{C}_{14}\text{H}_{21}\text{N}_3\text{O}_3 + \text{H}^+$  [ $\text{M} + \text{H}^+$ ], 280.1656; found, 280.1663.

**(S)-Methyl 3-Amino-4-(2-amino-5-guanidinopentanamido)benzoate (6f).**

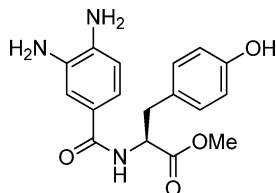
$^1\text{H}$  NMR (500.13 MHz, MeOH- $d_4$ ):  $\delta$  8.13 (s, 1H), 8.08 (dd,  $J$  = 8.4, 1.8 Hz, 1H), 7.71 (d,  $J$  = 8.4 Hz, 1H), 4.40–4.33 (m, 1H), 3.94 (s, 3H), 3.29–3.24 (m, 2H), 2.25–2.16 (m, 1H), 2.13–2.04 (m, 1H), 1.87–1.78 (m, 2H).  $^{13}\text{C}$  NMR (125.76 MHz, MeOH- $d_4$ ):  $\delta$  167.9, 166.7, 158.3, 145.0, 131.6, 130.3, 126.8, 121.1, 118.6, 53.5, 52.8, 41.8, 29.3, 25.4. HRMS (ESI):  $m/z$  calcd for  $\text{C}_{14}\text{H}_{22}\text{N}_6\text{O}_3 + \text{H}^+$  [ $\text{M} + \text{H}^+$ ], 323.1826; found, 323.1822.

**(S)-Methyl 6-Amino-2-(3,4-diaminobenzamido)hexanoate (9a).**



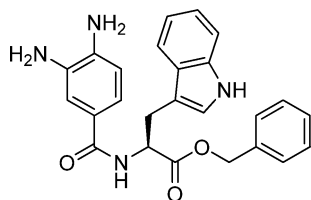
$^1\text{H}$  NMR (500.13 MHz, MeOH- $d_4$ ):  $\delta$  7.80 (s, 1H), 7.75–7.70 (m, 1H), 7.04 (d,  $J$  = 8.5 Hz, 1H), 4.60–4.52 (m, 1H), 3.74 (s, 3H), 2.99–2.91 (m, 2H), 2.06–1.87 (m, 2H), 1.73 (m, 2H), 1.63–1.45 (m, 2H).  $^{13}\text{C}$  NMR (125.76 MHz, MeOH- $d_4$ ):  $\delta$  174.1, 169.0, 142.9, 128.9, 125.8, 124.7, 120.1, 118.8, 54.2, 52.8, 40.5, 31.6, 28.0, 24.2. HRMS (ESI):  $m/z$  calcd for  $\text{C}_{14}\text{H}_{22}\text{N}_4\text{O}_3 + \text{H}^+$  [ $\text{M} + \text{H}^+$ ], 295.1765; found, 295.1765.

**(S)-Methyl 2-(3,4-Diaminobenzamido)-3-(4-hydroxyphenyl)propanoate (9b).**



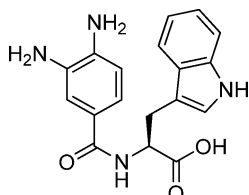
$^1\text{H}$  NMR (500.13 MHz, MeOH- $d_4$ ):  $\delta$  7.68 (s, 1H), 7.60 (d,  $J$  = 8.3 Hz, 1H), 7.06 (d,  $J$  = 8.4 Hz, 2H), 7.02 (d,  $J$  = 8.3 Hz, 1H), 6.70 (d,  $J$  = 8.4 Hz, 2H), 4.76–4.68 (m, 1H), 3.70 (s, 3H), 3.21–3.12 (m, 1H), 3.07–2.97 (m, 1H).  $^{13}\text{C}$  NMR (125.76 MHz, MeOH- $d_4$ ):  $\delta$  173.8, 168.7, 157.3, 142.5, 131.2, 131.2, 129.0, 128.7, 126.1, 124.6, 120.3, 119.0, 116.3, 116.3, 56.2, 52.7, 37.3. HRMS (ESI):  $m/z$  calcd for  $\text{C}_{17}\text{H}_{19}\text{N}_3\text{O}_4 + \text{H}^+$  [ $\text{M} + \text{H}^+$ ], 330.1448; found, 330.1447.

**(S)-Benzyl 2-(3,4-Diaminobenzamido)-3-(1H-indol-3-yl)propanoate (9c).**



$^1\text{H}$  NMR (500.13 MHz, MeOH- $d_4$ ):  $\delta$  7.63 (s, 1H), 7.58–7.46 (m, 2H), 7.38–7.23 (m, 4H), 7.20–7.11 (m, 2H), 7.11–6.88 (m, 4H), 5.09 (s, 2H), 4.92–4.85 (m, 1H), 3.47–3.34 (m, 2H).  $^{13}\text{C}$  NMR (125.76 MHz, MeOH- $d_4$ ):  $\delta$  173.6, 168.8, 152.0, 143.4, 138.1, 137.1, 132.1, 129.5, 129.2, 129.2, 128.6, 126.9, 125.4, 125.4, 124.5, 122.5, 119.9, 119.2, 118.3, 117.6, 112.4, 110.8, 68.0, 55.8, 28.3. HRMS (ESI):  $m/z$  calcd for  $\text{C}_{25}\text{H}_{24}\text{N}_4\text{O}_3 + \text{H}^+$  [ $\text{M} + \text{H}^+$ ], 429.1921; found, 429.1930.

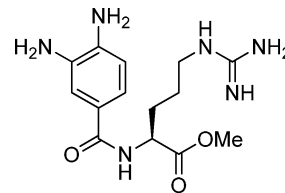
**(S)-2-(3,4-Diaminobenzamido)-3-(1H-indol-3-yl)propanoic Acid (9c').**



$^1\text{H}$  NMR (500.13 MHz, MeOH- $d_4$ ):  $\delta$  7.63–7.53 (m, 2H), 7.49 (dd,  $J$  = 8.5, 2.0 Hz, 1H), 7.32 (d,  $J$  = 8.1 Hz, 1H), 7.12 (s, 1H), 7.09–7.04

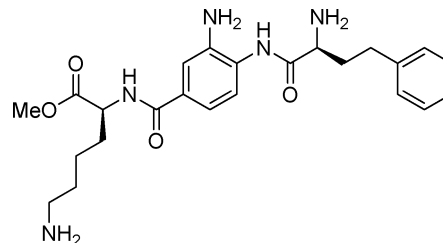
(m, 1H), 6.99–6.94 (m, 1H), 6.92–6.87 (m, 1H), 4.92–4.85 (m, 1H), 3.53–3.40 (m, 2H).  $^{13}\text{C}$  NMR (125.76 MHz, MeOH- $d_4$ ):  $\delta$  175.4, 168.7, 138.1, 131.9, 128.9, 128.1, 126.6, 124.4, 124.1, 122.4, 119.8, 119.3, 118.1, 117.5, 112.3, 111.2, 55.3, 28.3. HRMS (ESI):  $m/z$  calcd for  $\text{C}_{18}\text{H}_{18}\text{N}_4\text{O}_3 + \text{H}^+$  [ $\text{M} + \text{H}^+$ ], 339.1452; found, 339.1447.

**(S)-Methyl 2-(3,4-Diaminobenzamido)-5-guanidinopentanoate (9d).**



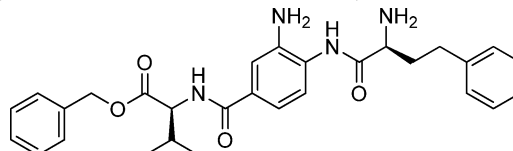
$^1\text{H}$  NMR (500.13 MHz, MeOH- $d_4$ ):  $\delta$  7.77 (d,  $J$  = 1.9 Hz, 1H), 7.72 (dd,  $J$  = 8.5, 1.9 Hz, 1H), 7.00 (d,  $J$  = 8.5 Hz, 1H), 4.62–4.53 (m, 1H), 3.73 (s, 3H), 3.28–3.18 (m, 2H), 2.10–1.85 (m, 2H), 1.84–1.63 (m, 2H).  $^{13}\text{C}$  NMR (125.76 MHz, MeOH- $d_4$ ):  $\delta$  174.0, 169.1, 158.6, 143.6, 128.8, 125.2, 124.6, 119.7, 118.4, 53.9, 52.8, 42.0, 29.4, 26.6. HRMS (ESI):  $m/z$  calcd for  $\text{C}_{14}\text{H}_{22}\text{N}_6\text{O}_3 + \text{H}^+$  [ $\text{M} + \text{H}^+$ ], 323.1826; found, 323.1821.

**(S)-Methyl 6-Amino-2-(3-amino-4-((S)-2-amino-4-phenylbutanamido)benzamido)hexanoate (10a).**



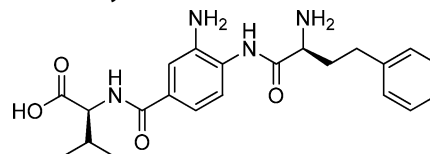
$^1\text{H}$  NMR (500.13 MHz, MeOH- $d_4$ ):  $\delta$  8.05 (s, 1H), 8.00 (br.d, 1H), 7.62 (br.d, 1H), 7.33–7.16 (m, 5H), 4.64–4.56 (m, 1H), 4.46–4.40 (m, 1H), 3.75 (s, 3H), 3.03–2.91 (m, 2H), 2.92–2.84 (m, 2H), 2.52–2.40 (m, 1H), 2.38–2.28 (m, 1H), 2.08–1.80 (m, 2H), 1.82–1.70 (m, 2H), 1.66–1.46 (m, 2H).  $^{13}\text{C}$  NMR (125.76 MHz, MeOH- $d_4$ ):  $\delta$  173.8, 170.1, 168.0, 141.3, 134.4, 129.7, 129.6, 129.6, 129.4, 129.4, 129.2, 127.6, 127.5, 127.1, 125.1, 55.2, 54.4, 52.9, 40.5, 34.4, 32.3, 31.6, 28.0, 24.2. HRMS (ESI):  $m/z$  calcd for  $\text{C}_{24}\text{H}_{33}\text{N}_5\text{O}_4 + \text{H}^+$  [ $\text{M} + \text{H}^+$ ], 456.2605; found, 456.2596.

**(S)-Benzyl 2-(3-Amino-4-((S)-2-amino-4-phenylbutanamido)benzamido)-3-methylbutanoate (10b).**



$^1\text{H}$  NMR (500.13 MHz, MeOH- $d_4$ ):  $\delta$  7.90 (s, 1H), 7.85 (d,  $J$  = 8.3 Hz, 1H), 7.56 (d,  $J$  = 8.3 Hz, 1H), 7.40–7.25 (m, 9H), 7.23–7.15 (m, 1H), 5.25–5.20 (m, 1H), 5.18–5.13 (m, 1H), 4.52–4.47 (m, 1H), 4.44–4.38 (m, 1H), 2.90–2.83 (m, 2H), 2.48–2.38 (m, 1H), 2.37–2.23 (m, 2H), 1.04–0.96 (m, 6H).  $^{13}\text{C}$  NMR (125.76 MHz, MeOH- $d_4$ ):  $\delta$  172.9, 170.0, 168.6, 141.3, 137.1, 134.6, 133.6, 130.2, 130.1, 129.8, 129.6, 129.5, 129.3, 128.8, 128.6, 128.1, 127.6, 127.4, 127.0, 126.9, 124.5, 67.9, 60.3, 55.1, 32.3, 31.8, 31.3, 19.6, 19.3. HRMS (ESI):  $m/z$  calcd for  $\text{C}_{29}\text{H}_{34}\text{N}_4\text{O}_4 + \text{H}^+$  [ $\text{M} + \text{H}^+$ ], 503.2653; found, 503.2649.

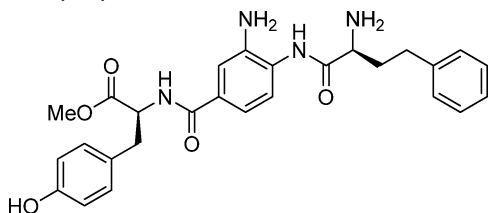
**(S)-2-(3-Amino-4-((S)-2-amino-4-phenylbutanamido)benzamido)-3-methylbutanoic Acid (10b').**





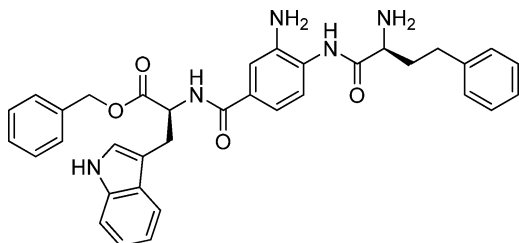
$^1\text{H}$  NMR (500.13 MHz, MeOH- $d_4$ ):  $\delta$  7.61 (s, 1H), 7.54 (d,  $J$  = 8.2 Hz, 1H), 7.45 (d,  $J$  = 8.2 Hz, 1H), 7.36–7.13 (m, 5H), 4.51–4.44 (m, 1H), 4.36–4.30 (m, 1H), 2.87–2.78 (m, 2H), 2.44–2.20 (m, 3H), 1.05 (d,  $J$  = 6.4 Hz, 6H).  $^{13}\text{C}$  NMR (125.76 MHz, MeOH- $d_4$ ):  $\delta$  174.8, 169.5, 169.4, 141.3, 135.7, 134.7, 130.2, 129.7, 129.7, 129.4, 129.4, 127.5, 126.8, 123.1, 121.0, 59.9, 55.0, 34.7, 32.2, 31.7, 19.7, 18.9. HRMS (ESI):  $m/z$  calcd for  $\text{C}_{22}\text{H}_{28}\text{N}_4\text{O}_4 + \text{H}^+$  [ $\text{M} + \text{H}^+$ ], 413.2183; found, 413.2185.

**(S)-Methyl 2-(3-Amino-4-((S)-2-amino-4-phenylbutanamido)benzamido)-3-(4-hydroxyphenyl)propanoate (10c).**



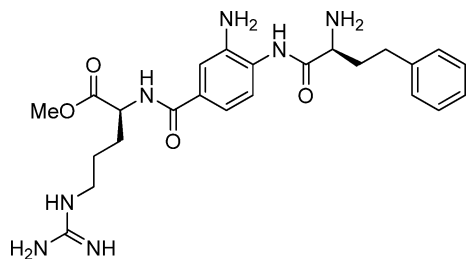
$^1\text{H}$  NMR (500.13 MHz, MeOH- $d_4$ ):  $\delta$  7.89 (s, 1H), 7.84 (d,  $J$  = 8.3 Hz, 1H), 7.56 (d,  $J$  = 8.3 Hz, 1H), 7.31–7.28 (m, 4H), 7.24–7.15 (m, 1H), 7.08 (d,  $J$  = 8.4 Hz, 2H), 6.70 (d,  $J$  = 8.4 Hz, 2H), 4.82–4.76 (m, 1H), 4.43–4.32 (m, 1H), 3.72 (s, 3H), 3.24–3.15 (m, 1H), 3.08–3.00 (m, 1H), 2.91–2.81 (m, 2H), 2.49–2.37 (m, 1H), 2.36–2.24 (m, 1H).  $^{13}\text{C}$  NMR (125.76 MHz, MeOH- $d_4$ ):  $\delta$  173.6, 170.1, 167.6, 157.4, 141.2, 134.6, 134.5, 131.2, 131.2, 129.7, 129.7, 129.4, 129.4, 129.1, 128.9, 127.5, 127.1, 126.8, 125.2, 116.3, 116.3, 56.3, 55.1, 52.8, 37.3, 34.4, 32.3. HRMS (ESI):  $m/z$  calcd for  $\text{C}_{27}\text{H}_{30}\text{N}_4\text{O}_5 + \text{H}^+$  [ $\text{M} + \text{H}^+$ ], 491.2289; found, 491.2298.

**(S)-Benzyl 2-(3-Amino-4-((S)-2-amino-4-phenylbutanamido)benzamido)-3-(1H-indol-3-yl)propanoate (10d).**



$^1\text{H}$  NMR (500.13 MHz, MeOH- $d_4$ ):  $\delta$  7.75 (s, 1H), 7.66 (dd,  $J$  = 8.4, 1.7 Hz, 1H), 7.55 (d,  $J$  = 7.9 Hz, 1H), 7.46 (d,  $J$  = 8.4 Hz, 1H), 7.36–7.15 (m, 11H), 7.12–6.96 (m, 3H), 5.10 (s, 2H), 4.98–4.92 (m, 1H), 4.40–4.32 (m, 1H), 3.50–3.40 (m, 1H), 3.38–3.32 (m, 1H), 2.90–2.77 (m, 2H), 2.45–2.35 (m, 1H), 2.34–2.21 (m, 1H).  $^{13}\text{C}$  NMR (125.76 MHz, MeOH- $d_4$ ):  $\delta$  173.4, 169.9, 168.2, 141.2, 138.1, 137.0, 134.5, 132.8, 130.3, 129.7, 129.7, 129.5, 129.5, 129.4, 129.4, 129.2, 129.2, 128.7, 127.6, 126.9, 126.7, 126.7, 124.5, 123.6, 122.5, 119.9, 119.1, 112.4, 110.7, 68.1, 55.9, 55.1, 34.5, 32.2, 28.3. HRMS (ESI):  $m/z$  calcd for  $\text{C}_{35}\text{H}_{35}\text{N}_5\text{O}_4 + \text{H}^+$  [ $\text{M} + \text{H}^+$ ], 590.2762; found, 590.2759.

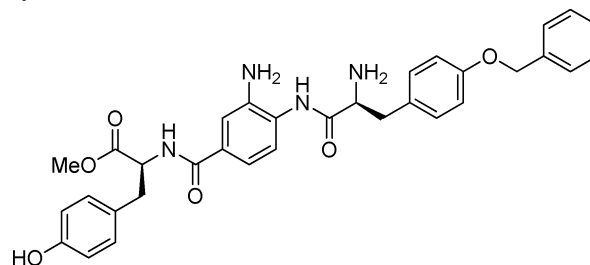
**(S)-Methyl 2-(3-Amino-4-((S)-2-amino-4-phenylbutanamido)benzamido)-5-guanidinopentanoate (10e).**



$^1\text{H}$  NMR (500.13 MHz, MeOH- $d_4$ ):  $\delta$  8.07–7.91 (m, 2H), 7.58 (br.d, 1H), 7.34–7.16 (m, 5H), 4.67–4.58 (m, 1H), 4.43–4.35 (m, 1H), 3.75 (s, 3H), 3.29–3.20 (m, 2H), 2.91–2.81 (m, 2H), 2.47–2.24 (m, 2H), 2.13–1.89 (m, 2H), 1.89–1.66 (m, 2H).  $^{13}\text{C}$  NMR (125.76 MHz, MeOH- $d_4$ ):  $\delta$  173.7, 171.9, 170.1, 168.1, 158.6, 154.2, 141.3,

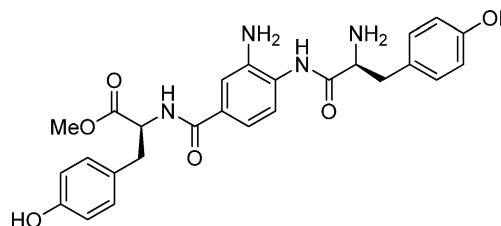
134.3, 129.7, 129.6, 129.4, 127.6, 127.5, 127.1, 125.1, 124.8, 55.1, 54.2, 53.0, 41.9, 34.5, 32.3, 29.3, 26.6. HRMS (ESI):  $m/z$  calcd for  $\text{C}_{24}\text{H}_{33}\text{N}_7\text{O}_4 + \text{H}^+$  [ $\text{M} + \text{H}^+$ ], 484.2667; found, 484.2660.

**(S)-Methyl 2-(3-Amino-4-((S)-2-amino-3-(4-benzyloxyphenyl)propanamido)benzamido)-3-(4-hydroxyphenyl)propanoate (10f).**



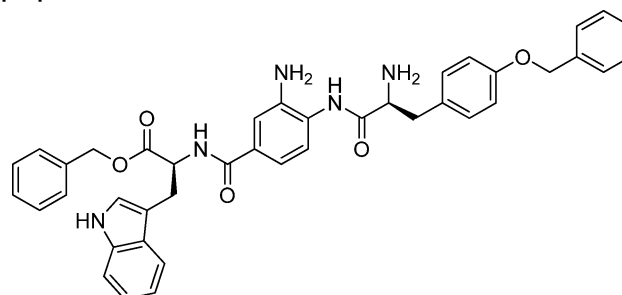
$^1\text{H}$  NMR (500.13 MHz, MeOH- $d_4$ ):  $\delta$  7.74 (s, 1H), 7.69–7.65 (m, 1H), 7.47–7.41 (m, 2H), 7.39–7.34 (m, 2H), 7.31–7.26 (m, 3H), 7.24–7.20 (m, 1H), 7.09–7.00 (m, 4H), 6.73–6.68 (m, 2H), 5.13–5.10 (m, 2H), 4.82–4.77 (m, 1H), 4.42–4.36 (m, 1H), 3.74–3.71 (m, 3H), 3.37–3.32 (m, 1H), 3.24–3.14 (m, 2H), 3.08–2.97 (m, 1H).  $^{13}\text{C}$  NMR (125.76 MHz, MeOH- $d_4$ ):  $\delta$  173.6, 169.6, 168.0, 165.8, 159.9, 157.4, 138.6, 135.8, 134.8, 131.8, 131.8, 131.2, 131.2, 129.9, 129.6, 128.9, 128.9, 128.5, 127.4, 127.0, 127.0, 123.7, 121.7, 116.8, 116.8, 116.3, 116.3, 71.0, 56.5, 56.2, 52.8, 37.7, 37.4. HRMS (ESI):  $m/z$  calcd for  $\text{C}_{33}\text{H}_{34}\text{N}_4\text{O}_6 + \text{H}^+$  [ $\text{M} + \text{H}^+$ ], 583.2511; found, 583.2504.

**(S)-Methyl 2-(3-Amino-4-((S)-2-amino-3-(4-hydroxyphenyl)propanamido)benzamido)-3-(4-hydroxyphenyl)propanoate (10g).**



$^1\text{H}$  NMR (500.13 MHz, MeOH- $d_4$ ):  $\delta$  7.79 (br.s, 1H), 7.74 (br.d, 1H), 7.27 (br.d, 1H), 7.19 (d,  $J$  = 8.3 Hz, 2H), 7.07 (br.d, 2H), 6.82 (d,  $J$  = 8.3 Hz, 2H), 6.69 (br.d, 2H), 4.82–4.76 (m, 1H), 4.41–4.35 (m, 1H), 3.73 (s, 3H), 3.28–3.09 (m, 3H), 3.06–2.99 (m, 1H).  $^{13}\text{C}$  NMR (125.76 MHz, MeOH- $d_4$ ):  $\delta$  173.6, 169.8, 167.8, 158.4, 157.4, 134.8, 133.4, 131.8, 131.8, 131.2, 131.2, 128.9, 127.8, 127.7, 127.1, 125.8, 124.2, 117.0, 117.0, 116.3, 116.3, 56.6, 56.3, 52.8, 37.7, 37.4. HRMS (ESI):  $m/z$  calcd for  $\text{C}_{26}\text{H}_{28}\text{N}_4\text{O}_6 + \text{H}^+$  [ $\text{M} + \text{H}^+$ ], 493.2082; found, 493.2082.

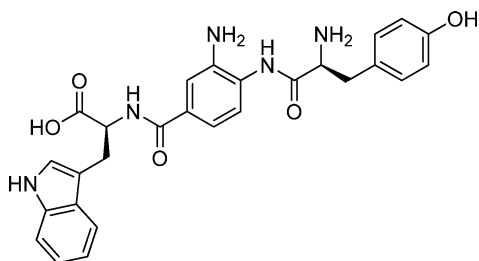
**(S)-Benzyl 2-(3-Amino-4-((S)-2-amino-3-(4-benzyloxyphenyl)propanamido)benzamido)-3-(1H-indol-3-yl)propanoate (10h).**



$^1\text{H}$  NMR (500.13 MHz, MeOH- $d_4$ ):  $\delta$  7.72 (s, 1H), 7.61 (br.d, 1H), 7.55 (d,  $J$  = 7.9 Hz, 1H), 7.46–7.39 (m, 2H), 7.38–7.32 (m, 3H), 7.31–7.23 (m, 6H), 7.22–7.16 (m, 3H), 7.11–6.95 (m, 5H), 5.14–5.06 (m, 4H), 4.98–4.92 (m, 1H), 4.38–4.33 (m, 1H), 3.49–3.40 (m, 1H), 3.38–3.32 (m, 2H), 3.20–3.10 (m, 1H).  $^{13}\text{C}$  NMR (125.76 MHz, MeOH- $d_4$ ):  $\delta$  173.3, 169.7, 167.8, 159.9, 138.6, 138.0, 137.0, 134.6, 131.8, 131.8, 131.6, 129.5, 129.5, 129.4, 129.4, 129.2, 129.2, 128.9, 128.7, 128.5, 128.5, 128.3, 128.1, 127.4, 127.0, 124.6, 124.6,

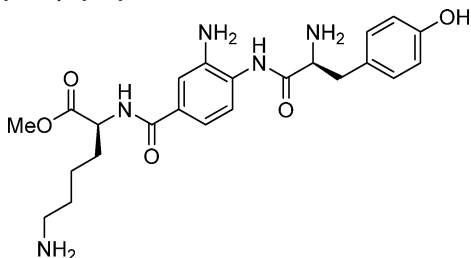
122.5, 119.9, 119.1, 116.6, 116.6, 116.5, 112.5, 110.7, 70.9, 68.1, 56.5, 55.9, 37.6, 28.3. HRMS (ESI):  $m/z$  calcd for  $C_{41}H_{39}N_5O_5 + H^+$  [ $M + H^+$ ], 682.3024; found, 682.3020.

**(S)-2-(3-Amino-4-((S)-2-amino-3-(4-hydroxyphenyl)propanamido)benzamido)-3-(1H-indol-3-yl)propanoic Acid (10h').**



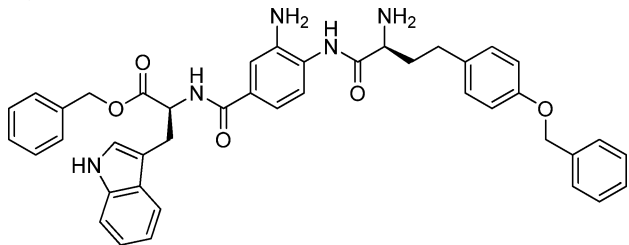
$^1H$  NMR (500.13 MHz, MeOH- $d_4$ ):  $\delta$  7.58 (br.d, 1H), 7.46–6.90 (m, 9H), 6.84–6.76 (m, 2H), 4.92–4.88 (m, 1H), 4.31–4.21 (m, 1H), 3.50–3.42 (m, 1H), 3.25–3.07 (m, 3H).  $^{13}C$  NMR (125.76 MHz, MeOH- $d_4$ ):  $\delta$  175.3, 169.8, 168.7, 158.4, 143.1, 138.1, 134.4, 131.8, 129.5, 128.9, 128.5, 126.7, 126.0, 124.4, 122.4, 119.9, 119.3, 117.5, 116.9, 116.9, 116.7, 112.3, 111.1, 56.3, 55.2, 38.1, 28.3. HRMS (ESI):  $m/z$  calcd for  $C_{27}H_{27}N_5O_5 + H^+$  [ $M + H^+$ ], 502.2085; found, 502.2088.

**(S)-Methyl 6-Amino-2-(3-amino-4-((S)-2-amino-3-(4-hydroxyphenyl)propanamido)benzamido)hexanoate (10i).**



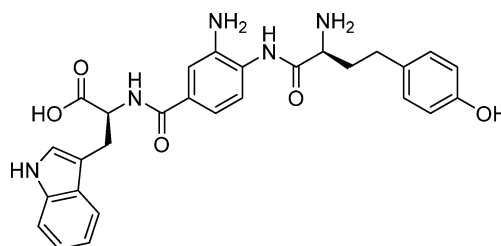
$^1H$  NMR (500.13 MHz, MeOH- $d_4$ ):  $\delta$  7.86 (s, 1H), 7.79 (br.d, 1H), 7.30 (br.d, 1H), 7.20 (br.d, 2H), 6.81 (br.d, 2H), 4.63–4.55 (m, 1H), 4.43–4.36 (m, 1H), 3.75 (s, 3H), 3.38–3.32 (m, 1H), 3.23–3.10 (m, 1H), 3.00–2.90 (m, 2H), 2.11–1.86 (m, 2H), 1.81–1.67 (m, 2H), 1.59–1.50 (m, 2H).  $^{13}C$  NMR (125.76 MHz, MeOH- $d_4$ ):  $\delta$  173.9, 169.6, 168.5, 158.3, 134.4, 132.6, 131.8, 131.8, 130.8, 127.1, 126.7, 125.8, 123.4, 116.9, 116.9, 56.5, 54.4, 52.9, 40.6, 37.7, 31.6, 28.0, 24.2. HRMS (ESI):  $m/z$  calcd for  $C_{23}H_{31}N_5O_5 + H^+$  [ $M + H^+$ ], 458.2398; found, 458.2407.

**(S)-Benzyl 2-(3-Amino-4-((S)-2-amino-4-(4-(benzyloxy)phenyl)butanamido)benzamido)-3-(1H-indol-3-yl)propanoate (10j).**



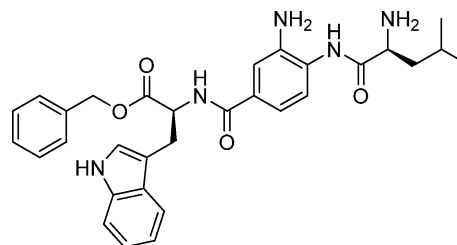
$^1H$  NMR (500.13 MHz, MeOH- $d_4$ ):  $\delta$  7.62 (br.s, 1H), 7.58–7.49 (m, 2H), 7.44–7.23 (m, 10H), 7.23–6.89 (m, 9H), 5.12–5.01 (m, 4H), 4.98–4.90 (m, 1H), 4.31–4.23 (m, 1H), 3.48–3.39 (m, 1H), 3.27–3.20 (m, 1H), 2.82–2.71 (m, 2H), 2.38–2.29 (m, 1H), 2.28–2.19 (m, 1H).  $^{13}C$  NMR (125.76 MHz, MeOH- $d_4$ ):  $\delta$  173.4, 169.7, 168.6, 159.0, 138.8, 138.1, 137.1, 134.6, 133.5, 132.3, 131.3, 130.4, 130.4, 130.4, 129.5, 129.5, 129.3, 129.2, 128.8, 128.8, 128.5, 126.8, 124.5, 124.5, 122.5, 122.4, 122.0, 119.9, 119.2, 119.2, 116.3, 116.3, 112.4, 110.8, 109.7, 71.1, 68.1, 55.9, 55.0, 34.7, 31.3, 28.3. HRMS (ESI):  $m/z$  calcd for  $C_{42}H_{41}N_5O_5 + H^+$  [ $M + H^+$ ], 696.3175; found, 696.3180.

**(S)-2-(3-Amino-4-((S)-2-amino-4-(4-hydroxyphenyl)butanamido)benzamido)-3-(1H-indol-3-yl)propanoic Acid (10j').**



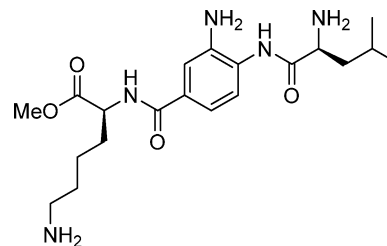
$^1H$  NMR (500.13 MHz, MeOH- $d_4$ ):  $\delta$  7.90 (s, 1H), 7.84 (br.d, 1H), 7.58–7.50 (m, 2H), 7.33 (d,  $J = 8.3$  Hz, 1H), 7.14–6.96 (m, 4H), 6.76–6.69 (m, 3H), 4.93–4.91 (m, 1H), 4.40–4.31 (m, 1H), 3.38–3.32 (m, 2H), 2.81–2.70 (m, 2H), 2.43–2.32 (m, 1H), 2.31–2.20 (m, 1H).  $^{13}C$  NMR (125.76 MHz, MeOH- $d_4$ ):  $\delta$  175.0, 170.3, 167.6, 157.1, 138.1, 134.7, 131.9, 130.4, 130.4, 129.5, 127.1, 125.5, 125.4, 124.5, 122.5, 122.4, 119.9, 119.2, 119.1, 116.4, 116.4, 112.4, 112.4, 55.7, 55.1, 34.7, 31.4, 28.2. HRMS (ESI):  $m/z$  calcd for  $C_{28}H_{29}N_5O_5 + H^+$  [ $M + H^+$ ], 516.2241; found, 516.2249.

**(S)-Benzyl 2-(3-Amino-4-((S)-2-amino-4-methylpentanamido)benzamido)-3-(1H-indol-3-yl)propanoate (10k).**

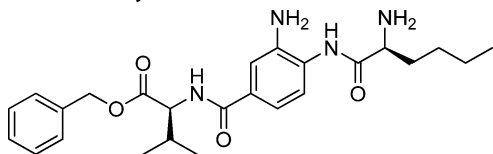


$^1H$  NMR (500.13 MHz, MeOH- $d_4$ ):  $\delta$  7.78 (s, 1H), 7.72 (br.d, 1H), 7.54 (d,  $J = 7.7$  Hz, 1H), 7.50 (d,  $J = 8.3$  Hz, 1H), 7.36–7.25 (m, 4H), 7.22–7.16 (m, 2H), 7.11–6.96 (m, 3H), 5.13–5.06 (s, 2H), 4.98–4.92 (m, 1H), 4.30–4.21 (m, 1H), 3.48–3.40 (m, 1H), 3.39–3.33 (m, 1H), 1.96–1.76 (m, 3H), 1.11–1.04 (br.s, 6H).  $^{13}C$  NMR (125.76 MHz, MeOH- $d_4$ ):  $\delta$  173.3, 170.7, 168.1, 138.1, 137.1, 134.8, 133.2, 129.8, 129.5, 129.4, 129.3, 129.2, 128.8, 128.2, 127.3, 127.0, 124.5, 124.0, 122.5, 119.9, 119.2, 112.4, 110.8, 68.1, 55.9, 53.7, 41.4, 28.3, 25.5, 23.4, 21.9. HRMS (ESI):  $m/z$  calcd for  $C_{31}H_{35}N_5O_4 + H^+$  [ $M + H^+$ ], 542.2762; found, 542.2761.

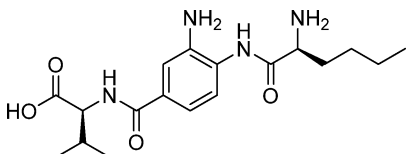
**(S)-Methyl 6-Amino-2-(3-amino-4-((S)-2-amino-4-methylpentanamido)benzamido)hexanoate (10l).**



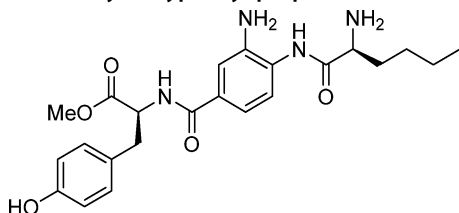
$^1H$  NMR (500.13 MHz, MeOH- $d_4$ ):  $\delta$  7.99–7.93 (m, 2H), 7.60 (d,  $J = 8.4$  Hz, 1H), 4.65–4.57 (m, 1H), 4.32–4.23 (m, 1H), 3.76 (s, 3H), 3.00–2.90 (m, 2H), 2.11–1.81 (m, 5H), 1.79–1.68 (m, 2H), 1.67–1.46 (m, 2H), 1.13–1.04 (m, 6H).  $^{13}C$  NMR (125.76 MHz, MeOH- $d_4$ ):  $\delta$  173.9, 170.8, 168.2, 134.6, 133.9, 128.4, 128.3, 127.1, 124.6, 54.4, 53.6, 52.9, 41.4, 40.5, 31.7, 28.1, 25.5, 24.2, 23.4, 21.8. HRMS (ESI):  $m/z$  calcd for  $C_{20}H_{33}N_5O_4 + H^+$  [ $M + H^+$ ], 408.2605; found, 408.2604.

**(S)-Benzyl 2-(3-Amino-4-((S)-2-aminohexanamido)benzamido)-3-methylbutanoate (10m).**

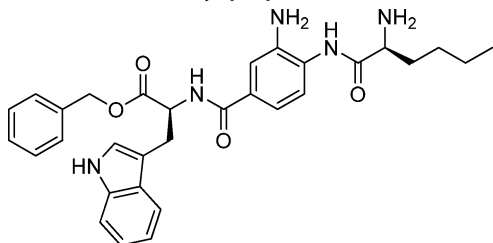
$^1\text{H}$  NMR (500.13 MHz, MeOH- $d_4$ ):  $\delta$  7.92–7.68 (m, 2H), 7.58 (d,  $J$  = 8.4 Hz, 1H), 7.42–7.28 (m, 5H), 5.26–5.14 (m, 2H), 4.52–4.47 (m, 1H), 4.27–4.22 (m, 1H), 2.35–2.20 (m, 1H), 2.14–2.06 (m, 1H), 2.05–1.96 (m, 1H), 1.56–1.41 (m, 4H), 1.05–0.94 (m, 9H).  $^{13}\text{C}$  NMR (125.76 MHz, MeOH- $d_4$ ):  $\delta$  172.9, 170.4, 168.5, 137.2, 134.8, 133.9, 129.6, 129.5, 129.5, 129.4, 129.4, 128.4, 126.9, 124.7, 67.9, 60.5, 55.2, 32.3, 31.6, 28.1, 23.4, 19.6, 19.2, 14.1. HRMS (ESI):  $m/z$  calcd for  $\text{C}_{25}\text{H}_{34}\text{N}_4\text{O}_4 + \text{H}^+$  [ $\text{M} + \text{H}^+$ ], 455.2653; found, 455.2653.

**(S)-2-(3-Amino-4-((S)-2-aminohexanamido)benzamido)-3-methylbutanoic Acid (10m').**

$^1\text{H}$  NMR (500.13 MHz, MeOH- $d_4$ ):  $\delta$  7.99–7.92 (m, 2H), 7.60 (d,  $J$  = 7.9 Hz, 1H), 4.51–4.46 (m, 1H), 4.29–4.22 (m, 1H), 2.34–2.24 (m, 1H), 2.15–2.06 (m, 1H), 2.05–1.95 (m, 1H), 1.58–1.35 (m, 4H), 1.08–1.03 (m, 6H), 1.02–0.96 (m, 3H).  $^{13}\text{C}$  NMR (125.76 MHz, MeOH- $d_4$ ):  $\delta$  174.7, 170.5, 168.2, 135.0, 134.3, 129.0, 127.3, 127.0, 125.1, 60.1, 55.2, 32.2, 31.6, 28.1, 23.4, 19.7, 18.9, 14.1. HRMS (ESI):  $m/z$  calcd for  $\text{C}_{18}\text{H}_{28}\text{N}_4\text{O}_4 + \text{H}^+$  [ $\text{M} + \text{H}^+$ ], 365.2183; found, 365.2177.

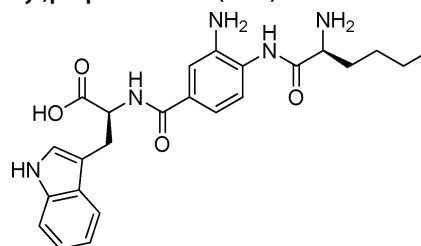
**(S)-Methyl 2-(3-Amino-4-((S)-2-aminohexanamido)benzamido)-3-(4-hydroxyphenyl)propanoate (10n).**

$^1\text{H}$  NMR (500.13 MHz, MeOH- $d_4$ ):  $\delta$  7.86–7.76 (m, 2H), 7.56 (br.d, 1H), 7.11–7.04 (m, 2H), 6.72–6.67 (m, 2H), 4.82–4.75 (m, 1H), 4.27–4.18 (m, 1H), 3.73 (s, 3H), 3.24–3.16 (m, 1H), 3.07–2.97 (m, 1H), 2.15–2.04 (m, 1H), 2.02–1.93 (m, 1H), 1.58–1.42 (m, 4H), 1.03–0.94 (m, 3H).  $^{13}\text{C}$  NMR (125.76 MHz, MeOH- $d_4$ ):  $\delta$  173.6, 170.4, 167.8, 157.4, 134.7, 134.0, 131.2, 131.2, 128.9, 128.4, 126.9, 124.7, 116.3, 116.2, 56.3, 55.2, 52.8, 37.4, 32.2, 28.1, 23.4, 14.1. HRMS (ESI):  $m/z$  calcd for  $\text{C}_{23}\text{H}_{30}\text{N}_4\text{O}_5 + \text{H}^+$  [ $\text{M} + \text{H}^+$ ], 443.2289; found, 443.2288.

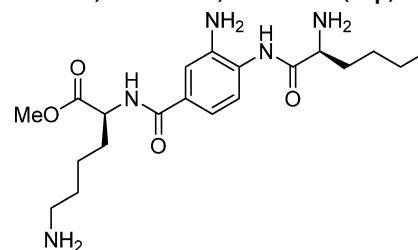
**(S)-Benzyl 2-(3-Amino-4-((S)-2-aminohexanamido)benzamido)-3-(1H-indol-3-yl)propanoate (10o).**

$^1\text{H}$  NMR (500.13 MHz, MeOH- $d_4$ ):  $\delta$  7.77 (s, 1H), 7.70 (br.d, 1H), 7.55 (d,  $J$  = 7.8 Hz, 1H), 7.50 (d,  $J$  = 8.3 Hz, 1H), 7.36–7.26 (m, 4H), 7.23–7.16 (m, 2H), 7.12–6.96 (m, 3H), 5.11 (s, 2H), 4.98–4.92 (m, 1H), 4.25–4.18 (m, 1H), 3.48–3.40 (m, 1H), 3.37–3.32 (m, 1H), 1.55–1.37 (m, 6H), 1.02–0.94 (m, 3H).  $^{13}\text{C}$  NMR (125.76 MHz, MeOH- $d_4$ ):  $\delta$  173.4, 170.3, 168.1, 138.1, 137.1, 134.6, 134.5, 133.1,

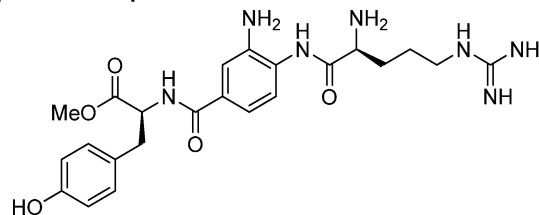
129.5, 129.5, 129.3, 129.2, 128.8, 127.1, 126.8, 124.5, 123.9, 122.5, 119.9, 119.2, 112.4, 110.8, 110.7, 68.1, 55.9, 55.2, 32.3, 28.3, 28.1, 23.4, 14.1. HRMS (ESI):  $m/z$  calcd for  $\text{C}_{31}\text{H}_{35}\text{N}_5\text{O}_4 + \text{H}^+$  [ $\text{M} + \text{H}^+$ ], 542.2762; found, 542.2760.

**(S)-2-(3-Amino-4-((S)-2-aminohexanamido)benzamido)-3-(1H-indol-3-yl)propanoic Acid (10o').**

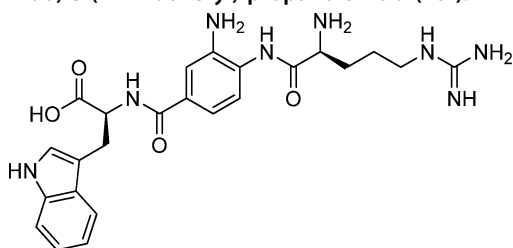
$^1\text{H}$  NMR (500.13 MHz, MeOH- $d_4$ ):  $\delta$  7.81 (s, 1H), 7.75 (br.d, 1H), 7.58 (d,  $J$  = 7.9 Hz, 1H), 7.51 (d,  $J$  = 8.3 Hz, 1H), 7.32 (d,  $J$  = 8.0 Hz, 1H), 7.14 (s, 1H), 7.10–7.04 (m, 1H), 7.02–6.94 (m, 1H), 4.95–4.91 (m, 1H), 4.26–4.18 (m, 1H), 3.56–3.39 (m, 2H), 2.10–1.90 (m, 2H), 1.56–1.36 (m, 4H), 1.03–0.92 (m, 3H).  $^{13}\text{C}$  NMR (125.76 MHz, MeOH- $d_4$ ):  $\delta$  170.4, 167.8, 159.6, 138.1, 133.8, 128.3, 128.1, 126.9, 124.5, 124.4, 122.5, 122.4, 119.9, 119.8, 119.2, 119.1, 112.3, 61.3, 55.2, 32.3, 28.2, 28.1, 23.4, 14.1. HRMS (ESI):  $m/z$  calcd for  $\text{C}_{24}\text{H}_{29}\text{N}_5\text{O}_4 + \text{H}^+$  [ $\text{M} + \text{H}^+$ ], 452.2292; found, 452.2297.

**(S)-Methyl 6-Amino-2-(3-amino-4-((S)-2-aminohexanamido)benzamido)hexanoate (10p).**

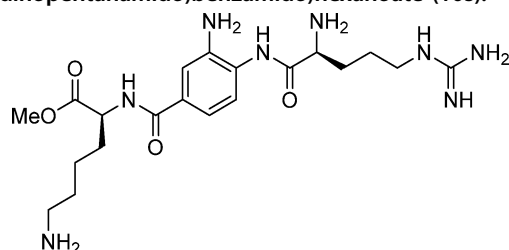
$^1\text{H}$  NMR (500.13 MHz, MeOH- $d_4$ ):  $\delta$  8.07–7.94 (m, 2H), 7.62 (d,  $J$  = 8.3 Hz, 1H), 4.63–4.57 (m, 1H), 4.32–4.22 (m, 1H), 3.75 (s, 3H), 3.00–2.90 (m, 2H), 2.17–1.90 (m, 4H), 1.91–1.66 (m, 2H), 1.65–1.32 (m, 6H), 1.06–0.83 (m, 3H).  $^{13}\text{C}$  NMR (125.76 MHz, MeOH- $d_4$ ):  $\delta$  173.9, 170.4, 168.1, 134.4, 134.3, 128.9, 127.5, 127.0, 125.0, 55.2, 54.4, 52.9, 40.5, 32.2, 31.6, 28.1, 28.0, 24.2, 23.4, 14.1. HRMS (ESI):  $m/z$  calcd for  $\text{C}_{20}\text{H}_{33}\text{N}_5\text{O}_4 + \text{H}^+$  [ $\text{M} + \text{H}^+$ ], 408.2605; found, 408.2608.

**(S)-Methyl 2-(3-Amino-4-((S)-2-amino-5-guanidinopentanamido)benzamido)-3-(4-hydroxyphenyl)propanoate (10q).**

$^1\text{H}$  NMR (500.13 MHz, MeOH- $d_4$ ):  $\delta$  7.95–7.82 (m, 2H), 7.67 (d,  $J$  = 8.4 Hz, 1H), 7.09 (d,  $J$  = 8.0 Hz, 2H), 6.71 (d,  $J$  = 8.0 Hz, 2H), 4.82–4.74 (m, 1H), 4.40–4.28 (m, 1H), 3.73 (s, 3H), 3.38–3.32 (m, 2H), 3.23–3.15 (m, 1H), 3.09–2.99 (m, 1H), 2.30–2.17 (m, 1H), 2.16–2.05 (m, 1H), 1.95–1.76 (m, 2H).  $^{13}\text{C}$  NMR (125.76 MHz, MeOH- $d_4$ ):  $\delta$  173.6, 169.9, 167.6, 158.6, 157.4, 134.7, 134.6, 131.2, 131.2, 129.4, 128.9, 127.1, 126.4, 125.4, 116.3, 116.3, 56.3, 54.7, 52.8, 41.8, 37.3, 29.6, 25.7. HRMS (ESI):  $m/z$  calcd for  $\text{C}_{23}\text{H}_{31}\text{N}_7\text{O}_5 + \text{H}^+$  [ $\text{M} + \text{H}^+$ ], 486.2459; found, 484.2458.

**(S)-2-(3-Amino-4-((S)-2-amino-5-guanidinopentanamido)-benzamido)-3-(1H-indol-3-yl) propanoic Acid (10r).**

<sup>1</sup>H NMR (500.13 MHz, MeOH-*d*<sub>4</sub>): δ 7.80 (s, 1H), 7.74 (d, *J* = 8.1 Hz, 1H), 7.63–7.56 (m, 2H), 7.32 (d, *J* = 8.1 Hz, 1H), 7.14 (s, 1H), 7.10–7.05 (m, 1H), 7.01–6.94 (m, 1H), 4.97–4.89 (m, 1H), 4.37–4.26 (m, 1H), 3.37–3.32 (m, 2H), 3.25–3.20 (m, 2H), 2.28–2.03 (m, 2H), 1.91–1.79 (m, 2H). <sup>13</sup>C NMR (125.76 MHz, MeOH-*d*<sub>4</sub>): δ 175.0, 169.9, 167.8, 158.7, 138.1, 133.8, 128.06, 126.9, 124.6, 124.4, 122.5, 122.4, 119.9, 119.2, 119.1, 112.4, 112.3, 111.2, 64.9, 54.7, 41.8, 29.7, 28.3, 25.7. HRMS (ESI): *m/z* calcd for C<sub>24</sub>H<sub>30</sub>N<sub>8</sub>O<sub>4</sub> + H<sup>+</sup> [*M* + H<sup>+</sup>], 495.2463; found, 495.2468.

**(S)-Methyl 6-Amino-2-(3-amino-4-((S)-2-amino-5-guanidinopentanamido)benzamido)hexanoate (10s).**

<sup>1</sup>H NMR (500.13 MHz, MeOH-*d*<sub>4</sub>): δ 8.02–7.94 (m, 2H), 7.70 (br.d, 1H), 4.65–4.58 (m, 1H), 4.37–4.30 (m, 1H), 3.76 (s, 3H), 3.37–3.32 (m, 2H), 2.99–2.91 (m, 2H), 2.14–1.90 (m, 4H), 1.89–1.69 (m, 4H), 1.65–1.48 (m, 2H). <sup>13</sup>C NMR (125.76 MHz, MeOH-*d*<sub>4</sub>): δ 173.9, 169.9, 168.1, 158.8, 134.5, 134.1, 128.6, 127.1, 126.9, 124.9, 54.7, 54.4, 52.9, 41.9, 40.6, 31.7, 29.7, 28.1, 25.7, 24.1. HRMS (ESI): *m/z* calcd for C<sub>20</sub>H<sub>34</sub>N<sub>8</sub>O<sub>4</sub> + H<sup>+</sup> [*M* + H<sup>+</sup>], 451.2776; found, 451.2778.

**Protein Expression and Purification.** The expression and purification of recombinant human endoplasmic reticulum aminopeptidase 1 (ERAP1), endoplasmic reticulum aminopeptidase 2 (ERAP2), and insulin-regulated aminopeptidase (IRAP) have been described before.<sup>23,24</sup> Recombinant baculovirus containing each ERAP1 variant was produced in sf9 cells according to the manufacturer's instructions (Bac-to-Bac baculovirus expression system, Invitrogen). Recombinant proteins were expressed in Hi5 cells after infection with the appropriate recombinant baculovirus and purified as previously described.<sup>24</sup> Proteins were aliquoted in and stored in a buffer containing 10 mM HEPES, pH 7, 100 mM NaCl, and 10% glycerol at –80 °C, until needed.

**Enzymatic Assays.** The enzymatic activity of the enzymes was calculated by following the time-dependent increase in fluorescence at 460 nm (excitation was at 380 nm) of the fluorogenic substrates L-leucine-7-amido-4-methyl coumarin (L-AMC; Sigma) for ERAP1 and IRAP and L-arginyl-7-amido-4-methyl coumarin (R-AMC; Sigma) for ERAP2. All measurements were performed on a TECAN infinite M200 microplate fluorescence reader. For evaluation of the effect of the compound on activity, 30 nM ERAP1, 6 nM ERAP2, or 6 nM IRAP was added to each well along with 50 μM substrate and varied concentrations of compound. In all cases, the enzyme concentration used was significantly less than the calculated IC<sub>50</sub> values for the inhibitors in order to avoid ligand depletion artifacts. The reaction was followed for 5–10 min, and activity was calculated by measuring the slope of the time course. For calculation of the in vitro IC<sub>50</sub> values, experimental data were fit to the following equation using the GraphPad Prism software package

$$Y = \text{bottom} + (\text{top} - \text{bottom}) / (1 + 10^{((\text{Log IC}_{50} - X) \times \text{Hill Slope})})$$

where *Y* is the enzymatic activity and *X* is the inhibitor concentration.

**Phagocytosis Assay.** Murine macrophage cell line RAW264.7 cells were cultured in RPMI 1640 containing 10% heat-inactivated fetal bovine serum. For assays, cells were transferred to and cultured in a 96-well black culture plate (2 × 10<sup>4</sup> cells/well) for 24 h at 37 °C, 5% CO<sub>2</sub>. The next day, they were washed twice with cold phosphate-buffered saline (PBS) and activated with IFN-γ (100 IU/mL) and LPS (1 μg/mL) in the presence or absence of various inhibitor concentrations. Phagocytosis was assessed by measuring the amount of uptake of latex beads coated with FITC-labeled rabbit IgG into cells using a phagocytosis assay kit (FITC) (Cayman Chemical, Ann Arbor, MI) according to the instruction manual. In brief, cells with or without various stimulants were treated with the beads and cultured in RPMI 1640 without FBS (1% FBS) for 24 h at 37 °C, 5% CO<sub>2</sub>. Twenty-four hours after stimulation, cells were washed twice with cold phosphate-buffered saline (PBS). The uptake of the beads into cells was calculated by measuring fluorescence intensity in a TECAN infinite M200 microplate fluorescence reader using an excitation of 485 nm and an emission of 535 nm. The cell supernatant from treated cells was used for measuring aminopeptidase activity. The enzymatic activity of ERAP1 was determined with L-leucine-7-amido-4-methyl coumarin (L-AMC; Sigma). The reaction mixture containing 100 μM Leu-AMC and 50 μL of culture medium in 50 mM HEPES pH 7.0, 100 mM NaCl. The amount of 7-amino-4-methylcoumarin released was measured by a TECAN infinite M200 microplate fluorescence reader at an excitation wavelength of 380 nm and an emission wavelength of 460 nm. For calculation of the ED<sub>50</sub> values, experimental data were fit to the equation described in the Enzymatic Assay section using the GraphPad Prism software.

**Mice.** Previously described IRAP knockout mice on an Sv129 background obtained from S. Keller were backcrossed up to 10 times to C57BL/6 mice obtained from Janvier (St. Quentin-Fallavier, France). Control mice were mixed-background mice bred in our facility. RAG1-deficient OT-1 T cell receptor transgenic mice were obtained from Taconic (Germantown, NY) and bred in our animal facility. Animal experimentation was approved by the Comité d'éthique pour l'expérimentation animale Paris Descartes (no. P2.LS.156.10).

**In Vitro Cross-Presentation Assays.** Murine BMDCs were generated in vitro by culturing progenitor cells extruded from large bones for 7 days in complete medium (IMDM medium completed with 10% FCS, 2 mM glutamine, 100 IU/mL penicillin, 100 μg/mL streptomycin, 50 mM β-mercaptoethanol) supplemented with J558 supernatant containing 20 μg/mL GM-CSF. On day 6, BMDCs were seeded at 50 000 cells/well into a 96-well flat bottom culture plate with increasing concentrations of inhibitor **4u**. On day 7, cells were washed twice with PBS and incubated with serial dilutions of yeast cells expressing ovalbumin on their cell surface in complete medium (prepared as described in ref 39), in the presence of the same concentration of **4u** as that used before. After 6 h, the cells were washed twice with PBS, and CD8<sup>+</sup> T cells purified from lymph nodes of OT-I mice were added to the culture for 20 h at a ratio T/BMDCs of 1.5:1, again in the presence of inhibitor **4u**. To assess T cell activation, the IL-2 concentration in supernatants was measured by sandwich ELISA using Nunc Maxisorp plates, streptavidin/horse radish peroxidase (Thermo Scientific), and OptEIA TMB substrate (BD Biosciences). As negative controls, an aliquot of BMDCs were fixed with 0.04% glutaraldehyde (as described in ref 39) prior to the addition of antigen, and the signal obtained was set as the background and subtracted from all OD values. Results represent the means of duplicate wells.

**Computational Methods.** The crystallographic structures of ERAP1 (PDB ID: 2YD0),<sup>40</sup> ERAP2 (PDB ID: 3SE6),<sup>24</sup> and IRAP (PDB ID: 4PJ6)<sup>41</sup> were used without any further refinement. Polar hydrogen atoms were added and Gasteiger charges were applied using AutoDock Tools 1.5.6.<sup>42</sup> The initial conformations of the inhibitors were generated from SMILES representations using the program Omega 2.4,<sup>43</sup> and then Gasteiger charges were applied. The search space was defined by a grid box centered next to the catalytic zinc and comprised 81 × 81 × 81 grid points of 0.375 Å spacing. For each

complex, 100 docking rounds were calculated with AutoDock 4.2 using the Lamarckian genetic algorithm with the default parameters of AutoDock 3.<sup>44</sup> The maximum number of energy evaluations was set to  $10 \times 10^6$ , and the docked conformations were clustered using a tolerance of 2.0 Å. Visual examination of the complexes and rendering of the figures were performed with VMD 1.9.<sup>45</sup> Calculations were carried out using Intel Xeon workstations running Linux 2.6.32 kernels.

## ■ ASSOCIATED CONTENT

### 📄 Supporting Information

<sup>1</sup>H and <sup>13</sup>C NMR spectra of biologically active compounds **4a**, **4u**, **4x**, and **10n**; titration curve of **4u** with recombinant mouse IRAP. This material is available free of charge via the Internet at <http://pubs.acs.org>.

## ■ AUTHOR INFORMATION

### Corresponding Authors

\*(D.V.) E-mail: [vourloumis@chem.demokritos.gr](mailto:vourloumis@chem.demokritos.gr). Phone: (+30)2106503624. Fax: (+30)2106511766.

\*(E.S.) E-mail: [stratos@rrp.demokritos.gr](mailto:stratos@rrp.demokritos.gr). Phone: (+30)2106503918. Fax: (+30)2106503918.

### Author Contributions

A.P. performed the computational design, synthesis, and characterization of the compounds; E.Z. prepared the recombinant enzymes and performed the in vitro and phagocytosis assays measurements and HPLC analysis; S.T. assisted in the synthesis of the compounds; F.-X.M. and P.v.E. designed and performed the cross-presentation assay; G.S. and D.C.M. helped to establish the macrophage activation assay; E.A.T. co-supervised the project along with D.V. and E.S., who conceived the experiments and analyzed the results. All authors contributed to the preparation of the manuscript and have approved its final version.

### Notes

The authors declare no competing financial interest.

## ■ ACKNOWLEDGMENTS

This research was financed by the European Union (European Social Fund) and Greek national funds through the Operational Program "Education and Lifelong Learning" of the National Strategic Reference Framework: Research Funding Program of the General Secretariat for Research & Technology (grant nos. LS7-2199 and ERC-14). F.-X.M. was supported by a grant from INSERM (poste d'accueil). Work in the laboratory of P.v.E. was supported by the Fondation pour la Recherche Médicale (grant no. DEQ20130326539).

## ■ ABBREVIATIONS USED

DABA, 3,4-diaminobenzoic acid; hPhe, L-homophenylalanine; hTyr, L-homotyrosine; Nle, L-norleucine; TFA, trifluoroacetic acid; HBTU, *N,N,N',N'*-tetramethyl-*O*-(1*H*-benzotriazol-1-yl)-uronium hexafluorophosphate; HATU, 1-[bis(dimethylamino)-methylene]-1*H*-1,2,3-triazolo[4,5-*b*]pyridinium 3-oxid hexafluorophosphate; DIEA, *N,N*-diisopropylethylamine; DBU, 1,8-diazabicyclo[5.4.0]undec-7-ene; DMF, *N,N*-dimethylformamide

## ■ REFERENCES

(1) Tsujimoto, M.; Hattori, A. The oxytocinase subfamily of M1 aminopeptidases. *Biochim. Biophys. Acta* **2005**, *1751*, 9–18.

(2) Evnouchidou, I.; Papakyriakou, A.; Stratikos, E. A new role for Zn(II) aminopeptidases: antigenic peptide generation and destruction. *Curr. Pharm. Des.* **2009**, *15*, 3656–3670.

(3) Serwold, T.; Gonzalez, F.; Kim, J.; Jacob, R.; Shastri, N. ERAAP customizes peptides for MHC class I molecules in the endoplasmic reticulum. *Nature* **2002**, *419*, 480–3.

(4) Saveanu, L.; Carroll, O.; Lindo, V.; Del Val, M.; Lopez, D.; Lepelletier, Y.; Greer, F.; Schomburg, L.; Fruci, D.; Niedermann, G.; van Endert, P. M. Concerted peptide trimming by human ERAAP1 and ERAAP2 aminopeptidase complexes in the endoplasmic reticulum. *Nat. Immunol.* **2005**, *6*, 689–97.

(5) Weimershaus, M.; Evnouchidou, I.; Saveanu, L.; van Endert, P. Peptidases trimming MHC class I ligands. *Curr. Opin Immunol.* **2013**, *25*, 90–6.

(6) Saveanu, L.; Carroll, O.; Weimershaus, M.; Guernonprez, P.; Firat, E.; Lindo, V.; Greer, F.; Davoust, J.; Kratzer, R.; Keller, S. R.; Niedermann, G.; van Endert, P. IRAP identifies an endosomal compartment required for MHC class I cross-presentation. *Science* **2009**, *325*, 213–7.

(7) Segura, E.; Albiston, A. L.; Wicks, I. P.; Chai, S. Y.; Villadangos, J. A. Different cross-presentation pathways in steady-state and inflammatory dendritic cells. *Proc. Natl. Acad. Sci. U.S.A.* **2009**, *106*, 20377–81.

(8) Cifaldi, L.; Romania, P.; Lorenzi, S.; Locatelli, F.; Fruci, D. Role of endoplasmic reticulum aminopeptidases in health and disease: from infection to cancer. *Int. J. Mol. Sci.* **2012**, *13*, 8338–52.

(9) Alvarez-Navarro, C.; Lopez de Castro, J. A. ERAAP1 structure, function and pathogenetic role in ankylosing spondylitis and other MHC-associated diseases. *Mol. Immunol.* **2014**, *57*, 12–21.

(10) Goto, Y.; Ogawa, K.; Nakamura, T. J.; Hattori, A.; Tsujimoto, M. TLR-mediated secretion of endoplasmic reticulum aminopeptidase 1 from macrophages. *J. Immunol.* **2014**, *192*, 4443–52.

(11) Goto, Y.; Ogawa, K.; Hattori, A.; Tsujimoto, M. Secretion of endoplasmic reticulum aminopeptidase 1 is involved in the activation of macrophages induced by lipopolysaccharide and interferon-gamma. *J. Biol. Chem.* **2011**, *286*, 21906–14.

(12) Aldhamen, Y. A.; Seregin, S. S.; Rastall, D. P.; Aylsworth, C. F.; Pepelyayeva, Y.; Busuito, C. J.; Godbehere-Roosa, S.; Kim, S.; Amalfitano, A. Endoplasmic reticulum aminopeptidase-1 functions regulate key aspects of the innate immune response. *PLoS One* **2013**, *8*, e69539.

(13) Aldhamen, Y. A.; Pepelyayeva, Y.; Rastall, D. P. W.; Seregin, S. S.; Zervoudi, E.; Koumantou, D.; Aylsworth, C. F.; Quiroga, D.; Godbehere, S.; Georgiadis, D.; Stratikos, E.; Amalfitano, A. Auto-immune disease-associated variants of extracellular endoplasmic reticulum aminopeptidase 1 induce altered innate immune responses by human immune cells. *J. Innate Immun.* **2015**, Jan 14. DOI:10.1159/000368899.

(14) Stratikos, E. Regulating adaptive immune responses using small molecule modulators of aminopeptidases that process antigenic peptides. *Curr. Opin. Chem. Biol.* **2014**, *23C*, 1–7.

(15) York, I. A.; Brehm, M. A.; Zendzian, S.; Towne, C. F.; Rock, K. L. Endoplasmic reticulum aminopeptidase 1 (ERAAP1) trims MHC class I-presented peptides in vivo and plays an important role in immunodominance. *Proc. Natl. Acad. Sci. U.S.A.* **2006**, *103*, 9202–7.

(16) Hammer, G. E.; Gonzalez, F.; James, E.; Nolla, H.; Shastri, N. In the absence of aminopeptidase ERAAP, MHC class I molecules present many unstable and highly immunogenic peptides. *Nat. Immunol.* **2007**, *8*, 101–8.

(17) Rastall, D. P.; Aldhamen, Y. A.; Seregin, S. S.; Godbehere, S.; Amalfitano, A. ERAAP1 functions override the intrinsic selection of specific antigens as immunodominant peptides, thereby altering the potency of antigen-specific cytolytic and effector memory T-cell responses. *Int. Immunol.* **2014**, *26*, 685–95.

(18) Cifaldi, L.; Lo Monaco, E.; Forloni, M.; Giorda, E.; Lorenzi, S.; Petrini, S.; Tremante, E.; Pende, D.; Locatelli, F.; Giacomini, P.; Fruci, D. Natural killer cells efficiently reject lymphoma silenced for the endoplasmic reticulum aminopeptidase associated with antigen processing. *Cancer Res.* **2011**, *71*, 1597–606.

- (19) James, E.; Bailey, I.; Sugiyarto, G.; Elliott, T. Induction of protective antitumor immunity through attenuation of ERAAP function. *J. Immunol.* **2013**, *190*, 5839–46.
- (20) Nagarajan, N. A.; Gonzalez, F.; Shastri, N. Nonclassical MHC class Ib-restricted cytotoxic T cells monitor antigen processing in the endoplasmic reticulum. *Nat. Immunol.* **2012**, *13*, 579–86.
- (21) Zervoudi, E.; Saridakis, E.; Birtley, J. R.; Seregin, S. S.; Reeves, E.; Kokkala, P.; Aldhamen, Y. A.; Amalfitano, A.; Mavridis, I. M.; James, E.; Georgiadis, D.; Stratikos, E. Rationally designed inhibitor targeting antigen-trimming aminopeptidases enhances antigen presentation and cytotoxic T-cell responses. *Proc. Natl. Acad. Sci. U.S.A.* **2013**, *110*, 19890–5.
- (22) Chen, L.; Fischer, R.; Peng, Y.; Reeves, E.; McHugh, K.; Ternette, N.; Hanke, T.; Dong, T.; Elliott, T.; Shastri, N.; Kollnberger, S.; James, E.; Kessler, B.; Bowness, P. Critical role of endoplasmic reticulum aminopeptidase 1 in determining the length and sequence of peptides bound and presented by HLA-B27. *Arthritis Rheumatol.* **2014**, *66*, 284–94.
- (23) Papakyriakou, A.; Zervoudi, E.; Theodorakis, E. A.; Saveanu, L.; Stratikos, E.; Vourloumis, D. Novel selective inhibitors of aminopeptidases that generate antigenic peptides. *Bioorg. Med. Chem. Lett.* **2013**, *23*, 4832–6.
- (24) Zervoudi, E.; Papakyriakou, A.; Georgiadou, D.; Evnouchidou, I.; Gajda, A.; Poreba, M.; Salvesen, G. S.; Drag, M.; Hattori, A.; Swevers, L.; Vourloumis, D.; Stratikos, E. Probing the S1 specificity pocket of the aminopeptidases that generate antigenic peptides. *Biochem. J.* **2011**, *435*, 411–20.
- (25) Stratikos, E.; Stern, L. J. Antigenic peptide trimming by ER aminopeptidases—insights from structural studies. *Mol. Immunol.* **2013**, *55*, 212–9.
- (26) Birtley, J. R.; Saridakis, E.; Stratikos, E.; Mavridis, I. M. The crystal structure of human endoplasmic reticulum aminopeptidase 2 reveals the atomic basis for distinct roles in antigen processing. *Biochemistry* **2012**, *51*, 286–295.
- (27) Nguyen, T. T.; Chang, S. C.; Evnouchidou, I.; York, I. A.; Zikos, C.; Rock, K. L.; Goldberg, A. L.; Stratikos, E.; Stern, L. J. Structural basis for antigenic peptide precursor processing by the endoplasmic reticulum aminopeptidase ERAP1. *Nat. Struct. Mol. Biol.* **2011**, *18*, 604–13.
- (28) Lukaszuk, A.; Demaegdt, H.; Szemenyei, E.; Toth, G.; Tymecka, D.; Misicka, A.; Karoyan, P.; Vanderheyden, P.; Vauquelin, G.; Tourwe, D. Beta-homo-amino acid scan of angiotensin IV. *J. Med. Chem.* **2008**, *51*, 2291–6.
- (29) Andersson, H.; Demaegdt, H.; Vauquelin, G.; Lindeberg, G.; Karlen, A.; Hallberg, M.; Erdelyi, M.; Hallberg, A. Disulfide cyclized tripeptide analogues of angiotensin IV as potent and selective inhibitors of insulin-regulated aminopeptidase (IRAP). *J. Med. Chem.* **2010**, *53*, 8059–71.
- (30) Andersson, H.; Demaegdt, H.; Johnsson, A.; Vauquelin, G.; Lindeberg, G.; Hallberg, M.; Erdelyi, M.; Karlen, A.; Hallberg, A. Potent macrocyclic inhibitors of insulin-regulated aminopeptidase (IRAP) by olefin ring-closing metathesis. *J. Med. Chem.* **2011**, *54*, 3779–92.
- (31) Albiston, A. L.; Morton, C. J.; Ng, H. L.; Pham, V.; Yeatman, H. R.; Ye, S.; Fernando, R. N.; De Bundel, D.; Ascher, D. B.; Mendelsohn, F. A.; Parker, M. W.; Chai, S. Y. Identification and characterization of a new cognitive enhancer based on inhibition of insulin-regulated aminopeptidase. *FASEB J.* **2008**, *22*, 4209–17.
- (32) Mountford, S. J.; Albiston, A. L.; Charman, W. N.; Ng, L.; Holien, J. K.; Parker, M. W.; Nicolazzo, J. A.; Thompson, P. E.; Chai, S. Y. Synthesis, structure-activity relationships and brain uptake of a novel series of benzopyran inhibitors of insulin-regulated aminopeptidase. *J. Med. Chem.* **2014**, *57*, 1368–77.
- (33) Borhade, S. R.; Rosenström, U.; Sävmarker, J.; Lundbäck, T.; Jenmalm-Jensen, A.; Sigmundsson, K.; Axelsson, H.; Svensson, F.; Konda, V.; Sköld, C.; Larhed, M.; Hallberg, M. Inhibition of insulin-regulated aminopeptidase (IRAP) by arylsulfonamides. *ChemistryOpen* **2014**, *3*, 256–263.
- (34) Kuiper, J. J.; Van Setten, J.; Ripke, S.; Van 't Slot, R.; Mulder, F.; Missotten, T.; Baarsma, G. S.; Francioli, L. C.; Pulit, S. L.; De Kovel, C. G.; Ten Dam-Van Loon, N.; Den Hollander, A. I.; Veld, P. H.; Hoyng, C. B.; Cordero-Coma, M.; Martin, J.; Llorens, V.; Arya, B.; Thomas, D.; Bakker, S. C.; Ophoff, R. A.; Rothova, A.; De Bakker, P. I.; Mutis, T.; Koelman, B. P. A genome-wide association study identifies a functional ERAP2 haplotype associated with birdshot chorioretinopathy. *Hum. Mol. Genet.* **2014**, *23*, 6081–7.
- (35) Fruci, D.; Ferracuti, S.; Limongi, M. Z.; Cunsolo, V.; Giorda, E.; Fraioli, R.; Sibilio, L.; Carroll, O.; Hattori, A.; van Endert, P. M.; Giacomini, P. Expression of endoplasmic reticulum aminopeptidases in EBV-B cell lines from healthy donors and in leukemia/lymphoma, carcinoma, and melanoma cell lines. *J. Immunol.* **2006**, *176*, 4869–79.
- (36) Albiston, A. L.; Diwakarla, S.; Fernando, R. N.; Mountford, S. J.; Yeatman, H. R.; Morgan, B.; Pham, V.; Holien, J. K.; Parker, M. W.; Thompson, P. E.; Chai, S. Y. Identification and development of specific inhibitors for insulin-regulated aminopeptidase as a new class of cognitive enhancers. *Br. J. Pharmacol.* **2011**, *164*, 37–47.
- (37) Gerritz, S. W.; Seffler, A. M. 2,5-Dimethylfuran (DMFu): an internal standard for the “traceless” quantitation of unknown samples via <sup>1</sup>H NMR. *J. Comb. Chem.* **2000**, *2*, 39–41.
- (38) Jahani, F.; Tajbakhsh, M.; Golchoubian, H.; Khaksar, S. Guanidine hydrochloride as an organocatalyst for N-Boc protection of amino groups. *Tetrahedron Lett.* **2011**, *52*, 1260–1264.
- (39) Saveanu, L.; van Endert, P. Preparing antigens suitable for cross-presentation assays in vitro and in vivo. *Methods Mol. Biol.* **2013**, *960*, 389–400.
- (40) Kochan, G.; Krojer, T.; Harvey, D.; Fischer, R.; Chen, L.; Vollmar, M.; von Delft, F.; Kavanagh, K. L.; Brown, M. A.; Bowness, P.; Wordsworth, P.; Kessler, B. M.; Oppermann, U. Crystal structures of the endoplasmic reticulum aminopeptidase-1 (ERAP1) reveal the molecular basis for N-terminal peptide trimming. *Proc. Natl. Acad. Sci. U.S.A.* **2011**, *108*, 7745–50.
- (41) Hermans, S. J.; Ascher, D. B.; Hancock, N. C.; Holien, J. K.; Mitchell, B. J.; Yeen Chai, S.; Morton, C. J.; Parker, M. W. Crystal structure of human insulin-regulated aminopeptidase with specificity for cyclic peptides. *Protein Sci.* **2014**, *24*, 190–9.
- (42) Morris, G. M.; Huey, R.; Lindstrom, W.; Sanner, M. F.; Belew, R. K.; Goodsell, D. S.; Olson, A. J. AutoDock4 and AutoDockTools4: automated docking with selective receptor flexibility. *J. Comput. Chem.* **2009**, *30*, 2785–91.
- (43) Hawkins, P. C.; Skillman, A. G.; Warren, G. L.; Ellingson, B. A.; Stahl, M. T. Conformer generation with OMEGA: algorithm and validation using high quality structures from the Protein Databank and Cambridge Structural Database. *J. Chem. Inf. Model.* **2010**, *50*, 572–84.
- (44) Huey, R.; Morris, G. M.; Olson, A. J.; Goodsell, D. S. A semiempirical free energy force field with charge-based desolvation. *J. Comput. Chem.* **2007**, *28*, 1145–1152.
- (45) Humphrey, W.; Dalke, A.; Schulten, K. VMD: visual molecular dynamics. *J. Mol. Graphics* **1996**, *14*, 33–8.

3,4-diaminobenzoic acid derivatives as  
inhibitors of the oxytocinase subfamily of M1  
aminopeptidases with immune regulating  
properties

*Athanasios Papakyriakou,<sup>†,‡</sup> Efthalia Zervoudi,<sup>†</sup> Sofia Tsoukalidou,<sup>†</sup> Francois-Xavier  
Mauvais,<sup>§</sup> Georgia Sfyroera,<sup>†</sup> Dimitrios C. Mastellos,<sup>†</sup> Peter van Endert,<sup>§</sup> Emmanuel A.  
Theodorakis,<sup>‡</sup> Dionisios Vourloumis<sup>\*,†</sup> and Efstratios Stratikos<sup>\*,†</sup>*

<sup>†</sup>National Center for Scientific Research "Demokritos", Aghia Paraskevi, 15310 Athens,  
Greece

<sup>‡</sup>Department of Chemistry and Biochemistry, University of California San Diego, 9500  
Gilman Drive, San Diego, CA, 92093-0358, United States

<sup>§</sup>Institut National de la Santé et de la Recherche Médicale, Unité 1151, 75015 Paris;  
Université Paris Descartes, Sorbonne Paris Cité, 75015 Paris; Centre National de la  
Recherche Scientifique, Unité 8253, 75015 Paris, France

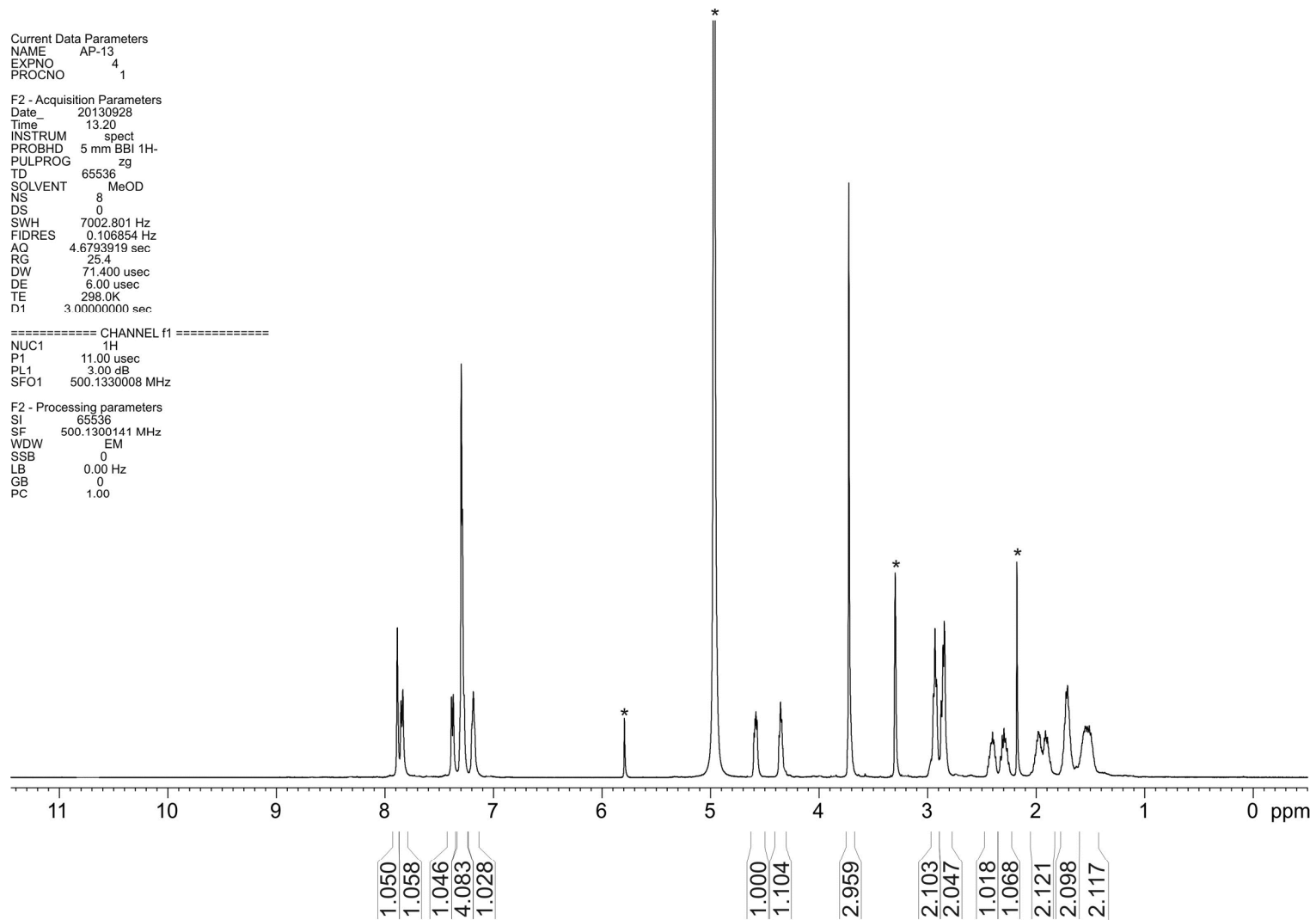
## SUPPORTING INFORMATION

### Table of contents

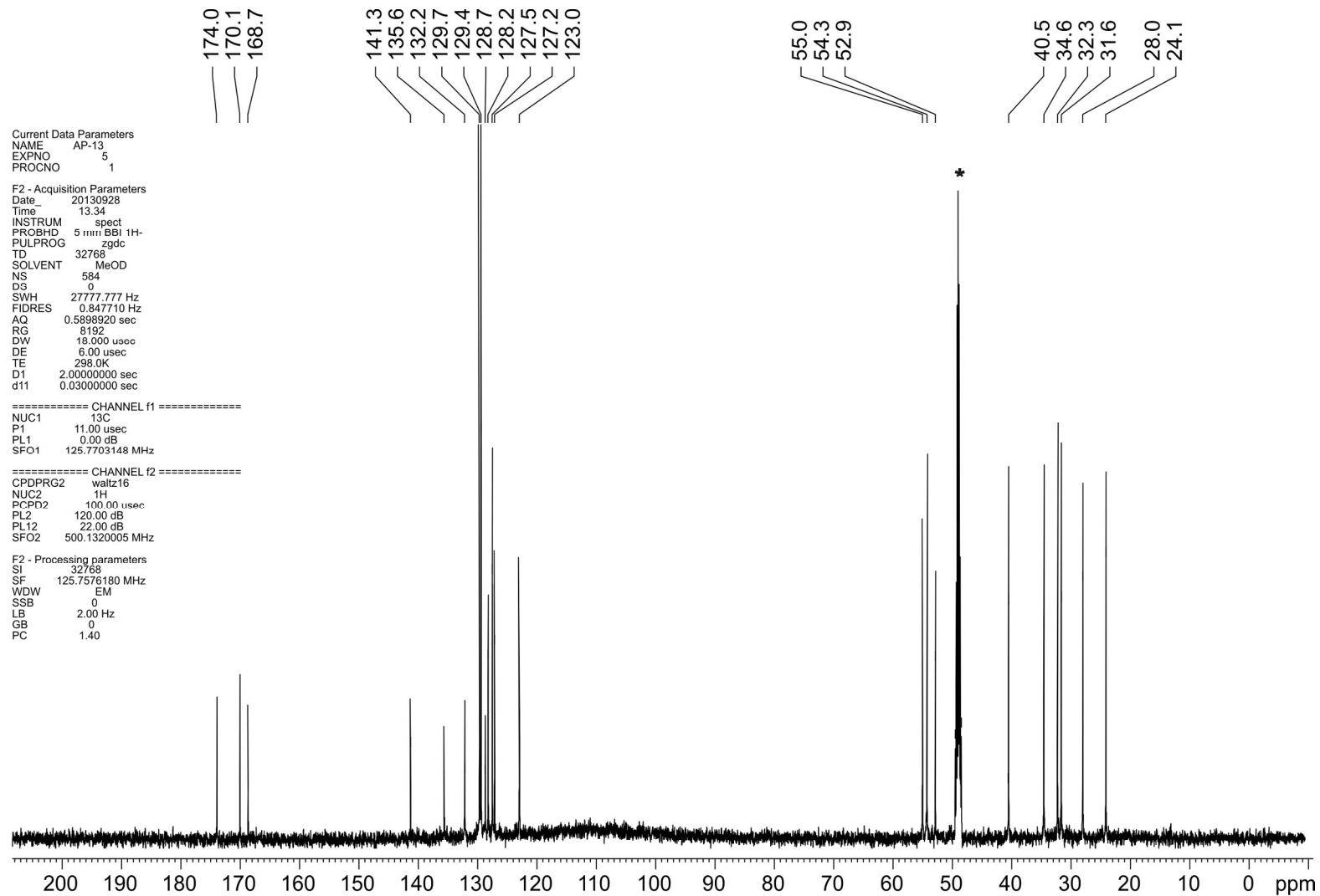
$^1\text{H}$  and  $^{13}\text{C}$  NMR spectra of the biologically active compounds **4a**, **4u**, **4x** and **10n**.

Titration curve of **4u** with mouse recombinant IRAP.





$^1\text{H}$  NMR spectrum of **4a** in MeOD in the presence of DMFu internal standard. Asterisks indicate solvent and internal standard peaks.



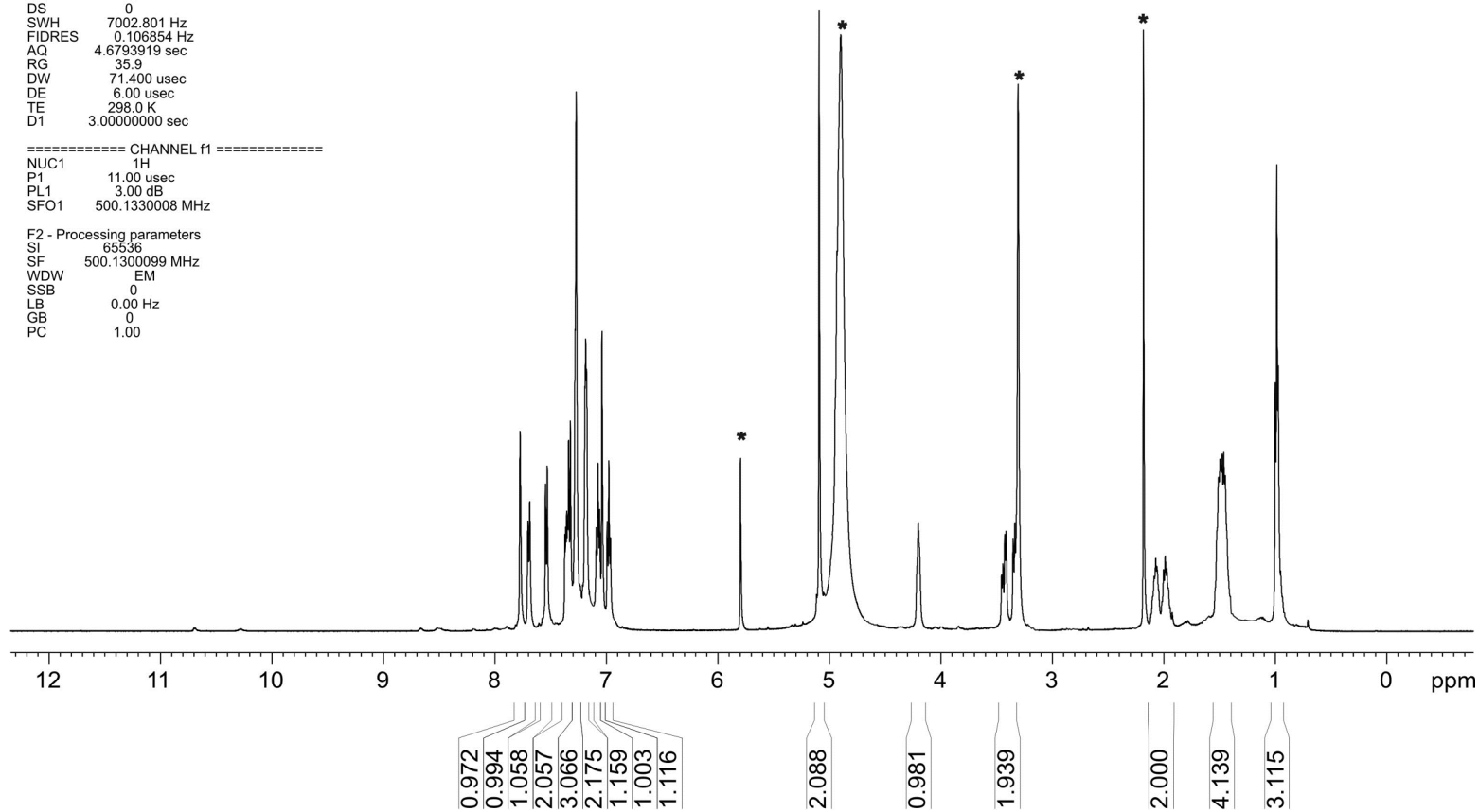
$^{13}\text{C}$  NMR spectrum of **4a** in MeOD in the presence of DMFu internal standard. Asterisks indicate solvent and internal standard peaks.

Current Data Parameters  
NAME AP-64  
EXPNO 1  
PROCNO 1

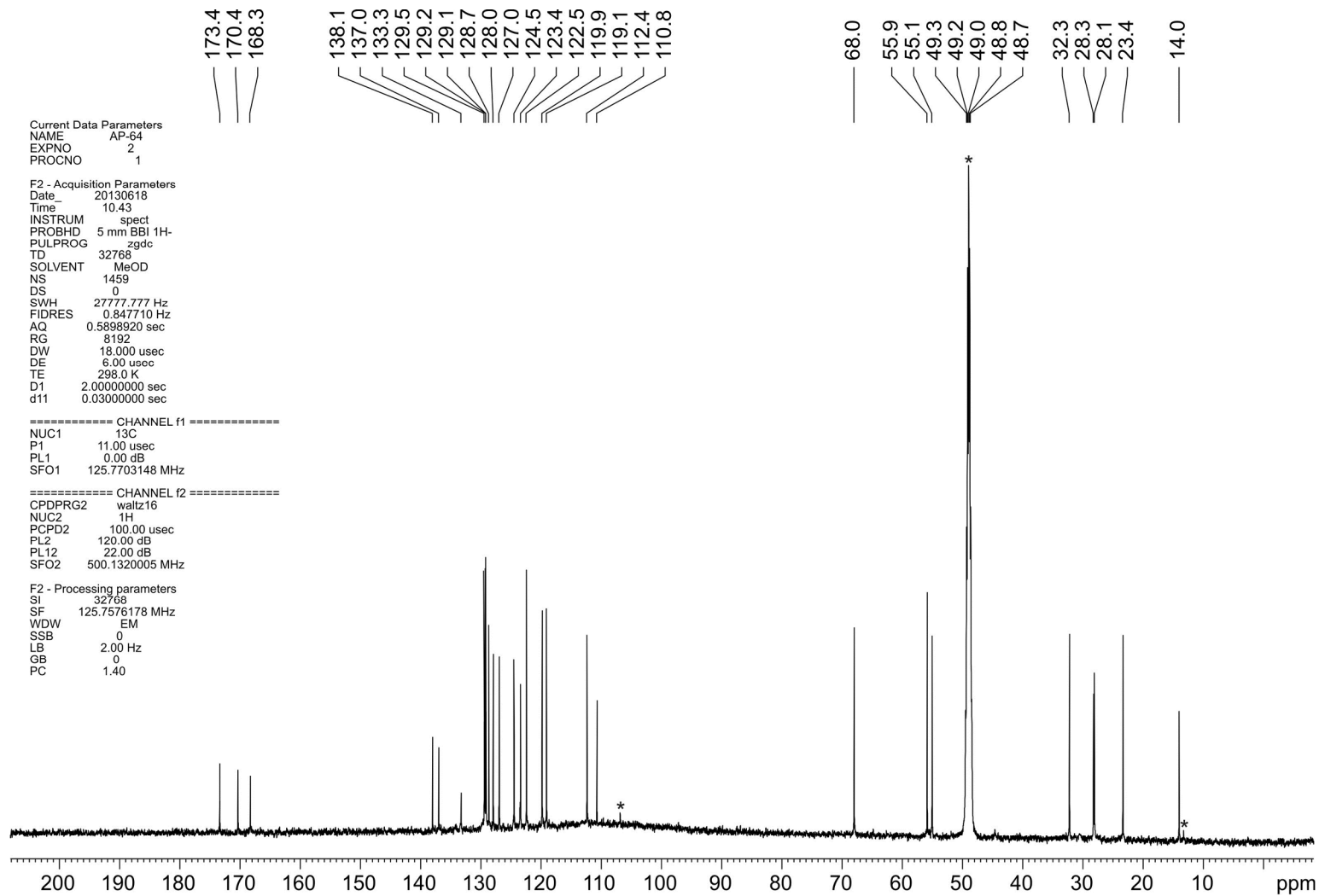
F2 - Acquisition Parameters  
Date\_ 20130618  
Time 10.39  
INSTRUM spect  
PROBHD 5 mm BBI 1H-  
PULPROG zg  
TD 65536  
SOLVENT MeOD  
NS 16  
DS 0  
SWH 7002.801 Hz  
FIDRES 0.106854 Hz  
AQ 4.6793919 sec  
RG 35.9  
DW 71.400 usec  
DE 6.00 usec  
TE 298.0 K  
D1 3.0000000 sec

===== CHANNEL f1 =====  
NUC1 1H  
P1 11.00 usec  
PL1 3.00 dB  
SFO1 500.1330008 MHz

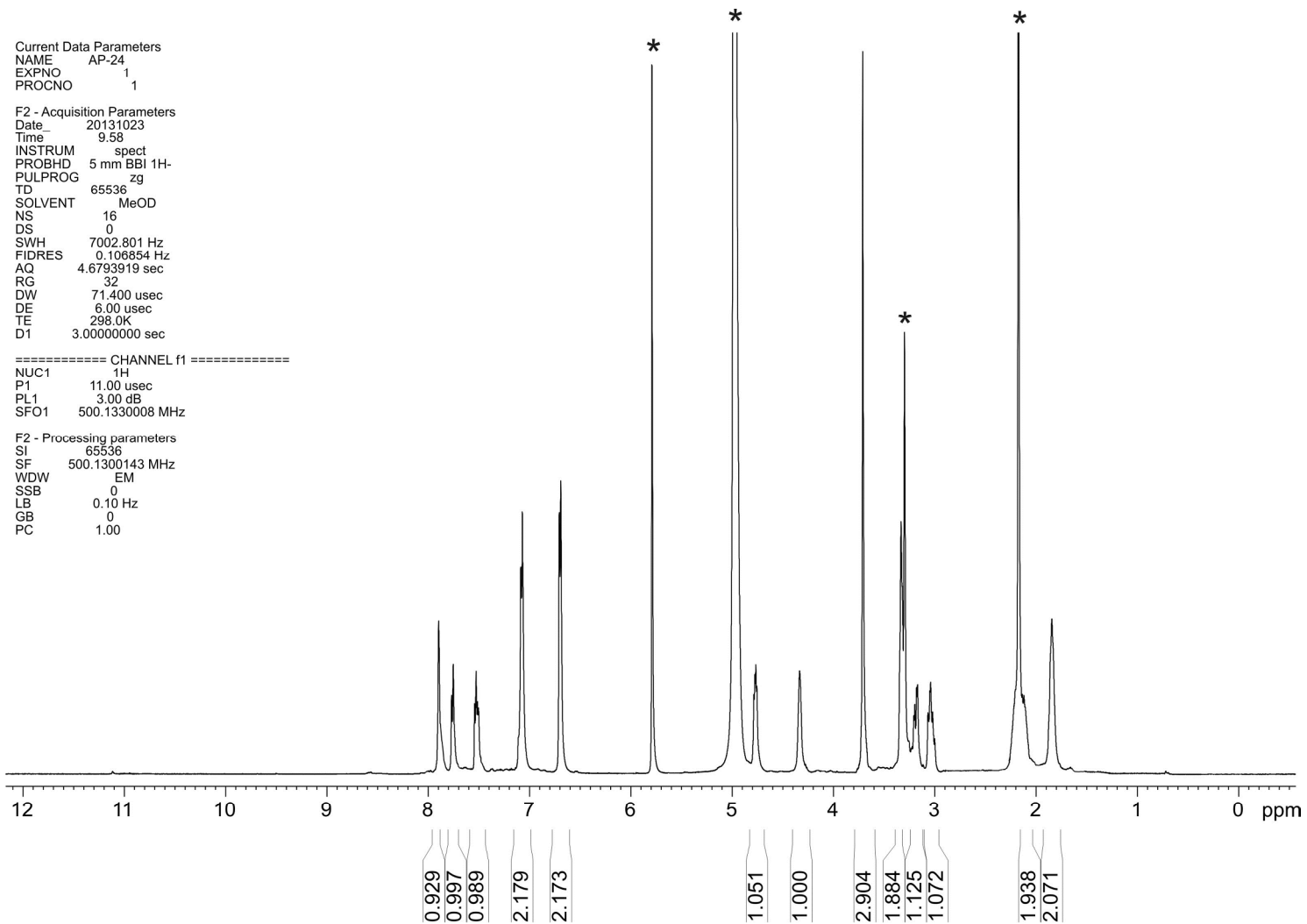
F2 - Processing parameters  
SI 65536  
SF 500.1300099 MHz  
WDW EM  
SSB 0  
LB 0.00 Hz  
GB 0  
PC 1.00



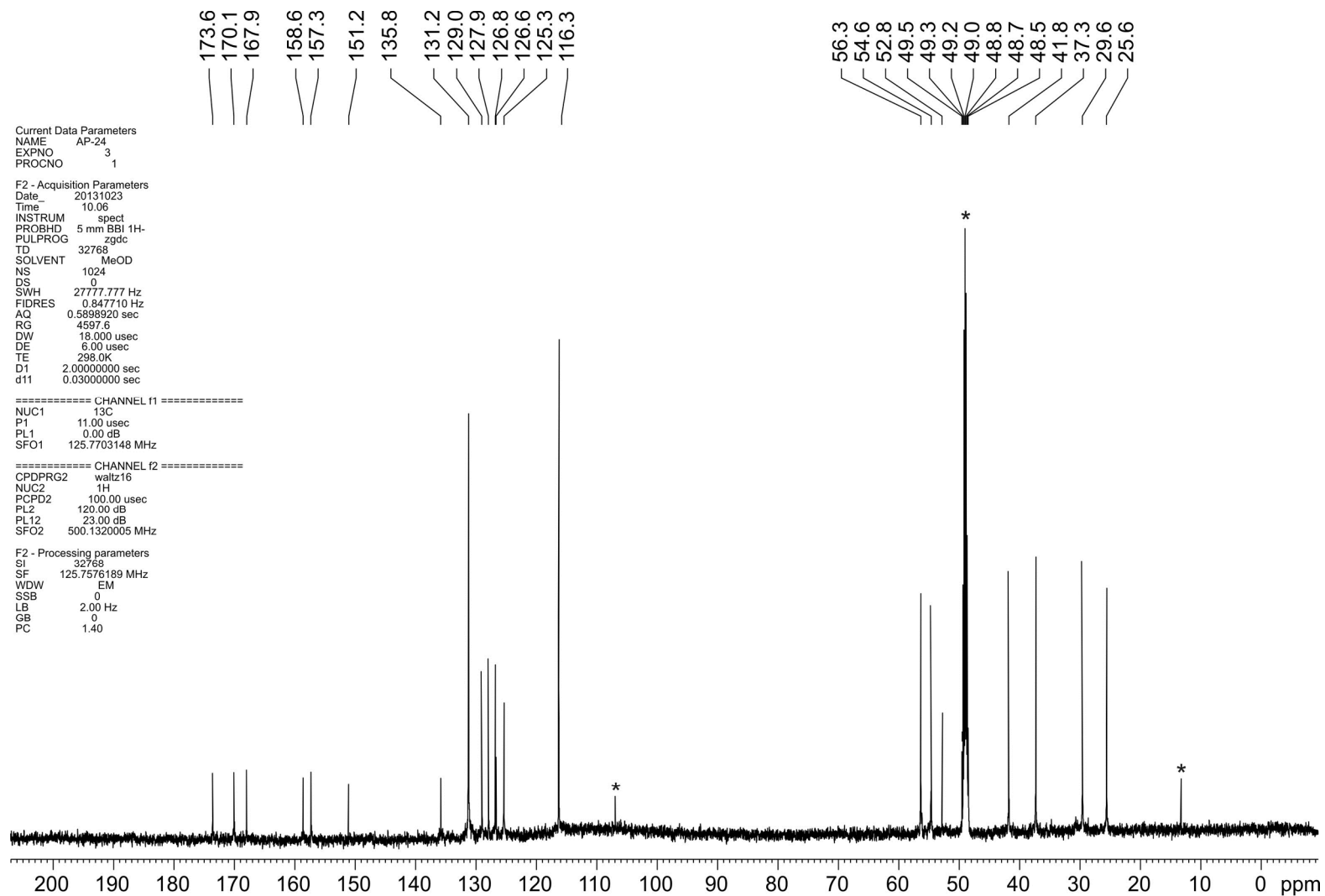
<sup>1</sup>H NMR spectrum of **4u** in MeOD in the presence of DMFu internal standard. Asterisks indicate solvent and internal standard peaks.



<sup>13</sup>C NMR spectrum of **4u** in MeOD in the presence of DMFu internal standard. Asterisks indicate solvent and internal standard peaks.



$^1\text{H}$  NMR spectrum of **4x** in MeOD in the presence of DMFu internal standard. Asterisks indicate solvent and internal standard peaks.



$^{13}\text{C}$  NMR spectrum of **4x** in MeOD in the presence of DMFu internal standard. Asterisks indicate solvent and internal standard peaks.

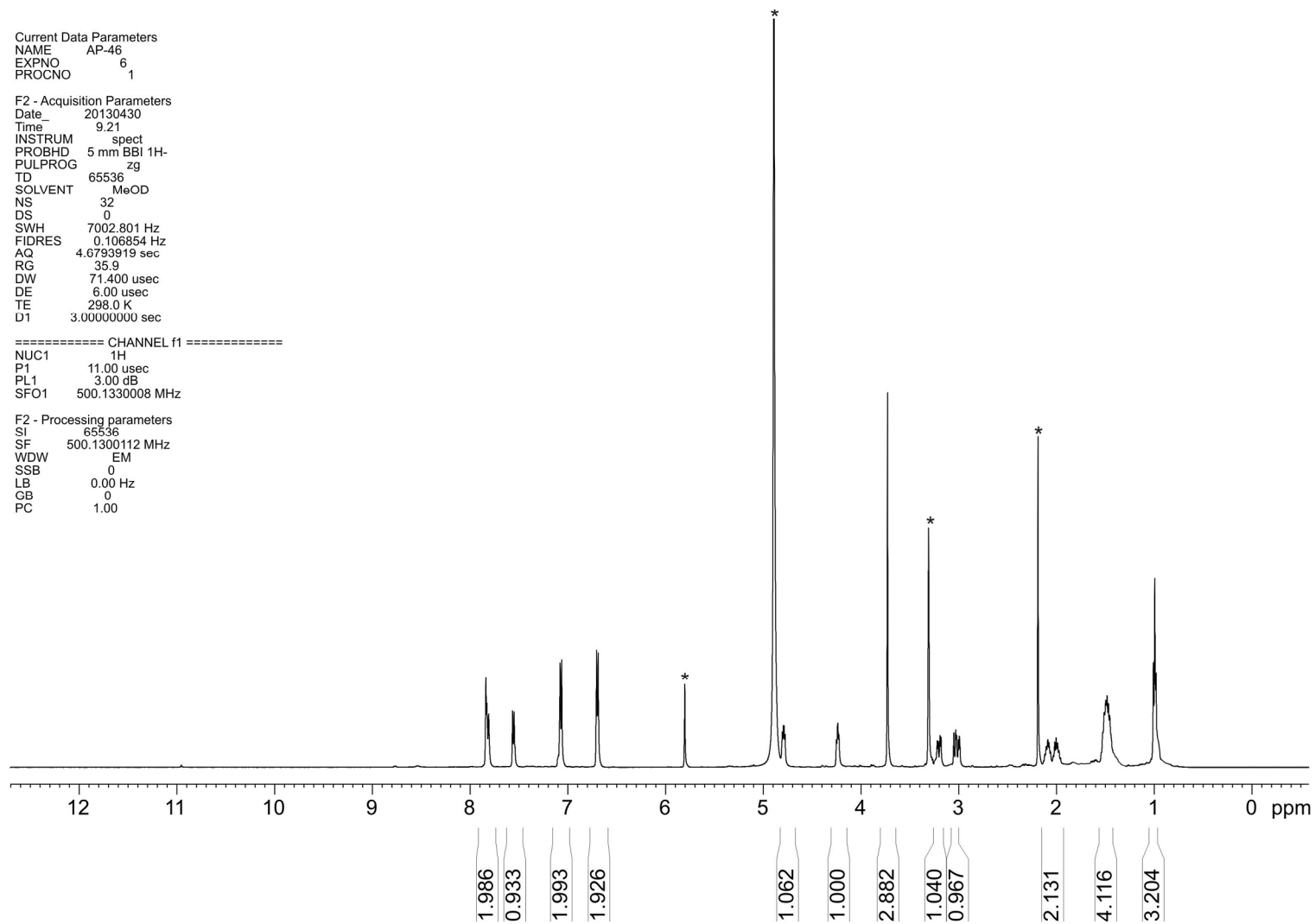
Current Data Parameters  
NAME AP-46  
EXPNO 6  
PROCNO 1

F2 - Acquisition Parameters  
Date\_ 20130430  
Time 9.21  
INSTRUM spect  
PROBHD 5 mm BBI 1H-  
PULPROG zg  
TD 65536  
SOLVENT MeOD  
NS 32  
DS 0  
SWH 7002.801 Hz  
FIDRES 0.106854 Hz  
AQ 4.6793919 sec  
RG 35.9  
DW 71.400 usec  
DE 6.00 usec  
TE 298.0 K  
D1 3.00000000 sec

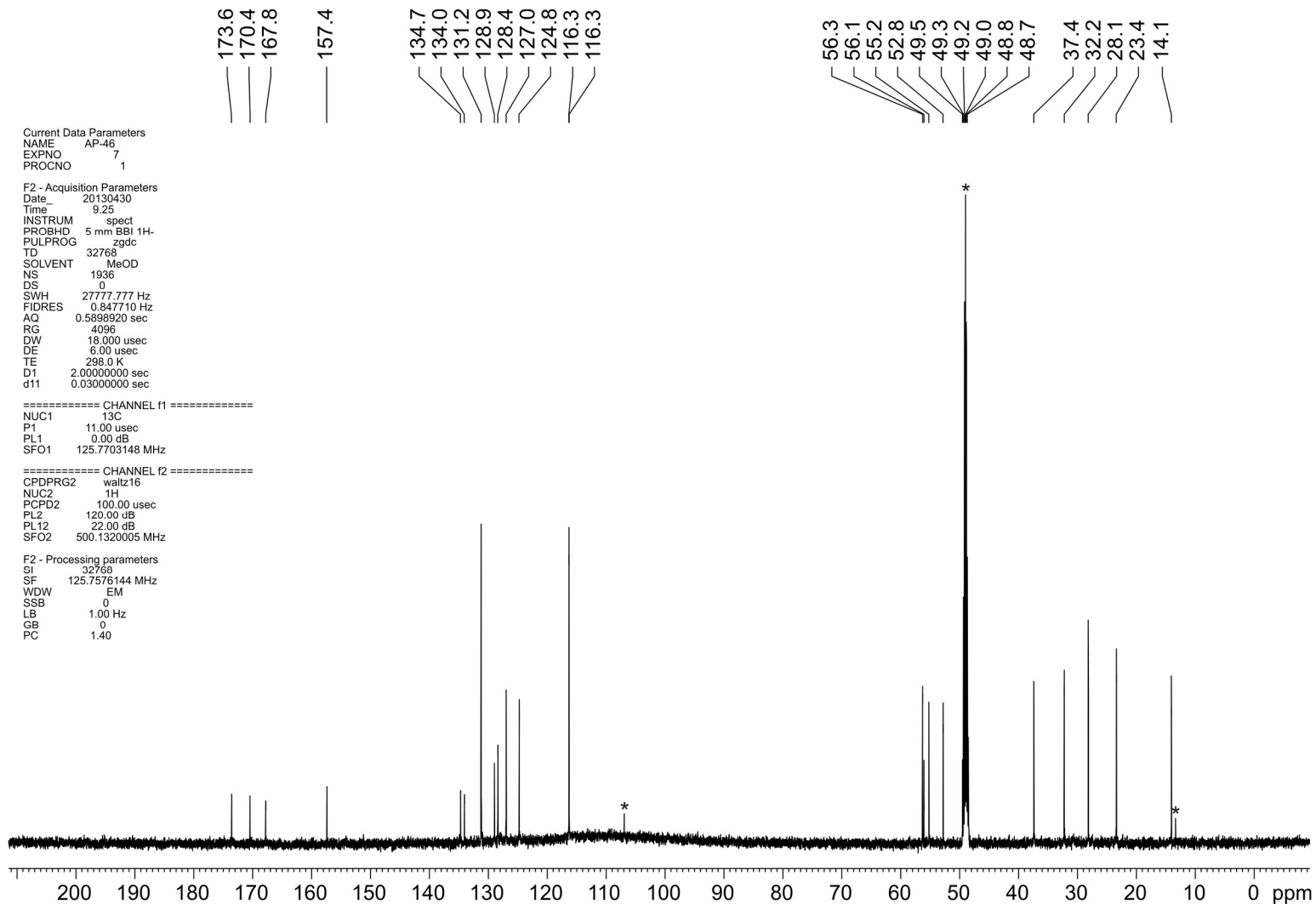
===== CHANNEL f1 =====

NUC1 1H  
P1 11.00 usec  
PL1 3.00 dB  
SFO1 500.1330008 MHz

F2 - Processing parameters  
SI 65536  
SF 500.1300112 MHz  
WDW EM  
SSB 0  
LB 0.00 Hz  
GB 0  
PC 1.00



<sup>1</sup>H NMR spectrum of **10n** in MeOD in the presence of DMFu internal standard. Asterisks indicate solvent and internal standard peaks.



$^{13}\text{C}$  NMR spectrum of **10n** in MeOD in the presence of DMFu internal standard. Asterisks indicate solvent and DMFu peaks.



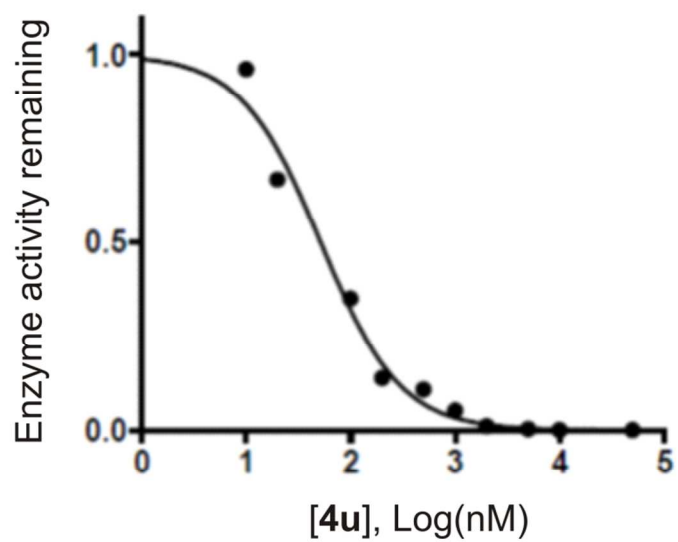


**Figure S1.** Titration of **4u** with mouse recombinant IRAP while following L-AMC hydrolysis by the enzyme.

# Screening Identifies Thimerosal as a Selective Inhibitor of Endoplasmic Reticulum Aminopeptidase 1

Athanasios Stamogiannos,<sup>†,‡</sup> Athanasios Papakyriakou,<sup>†,‡</sup> Francois-Xavier Mauvais,<sup>§</sup> Peter van Endert,<sup>§</sup> and Efstratios Stratikos<sup>\*,†</sup>

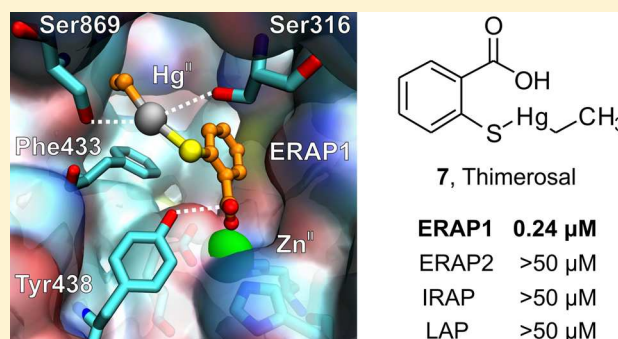
<sup>†</sup>National Center for Scientific Research Demokritos, Agia Paraskevi GR-15310, Athens, Greece

<sup>§</sup>Institut National de la Santé et de la Recherche Médicale, Unité1151; Université Paris Descartes, Sorbonne Paris Cité; Centre National de la Recherche Scientifique, Unité 8253, 75015 Paris, France

## S Supporting Information

**ABSTRACT:** We employed virtual screening followed by *in vitro* evaluation to discover novel inhibitors of ER aminopeptidase 1, an important enzyme for the human adaptive immune response that has emerged as an attractive target for cancer immunotherapy and the control of autoimmunity. Screening hits included three structurally related compounds carrying the (*E*)-*N'*-((1*H*-indol-3-yl)methylene)-1*H*-pyrazole-5-carbohydrazide scaffold and (2-carboxylatophenyl)sulfanyl-ethylmercury as novel ERAP1 inhibitors. The latter, also known as thimerosal, a common component in vaccines, was found to inhibit ERAP1 in the submicromolar range and to present strong selectivity versus the homologous aminopeptidases ERAP2 and IRAP. Cell-based analysis indicated that thimerosal can effectively reduce ERAP1-dependent cross-presentation by dendritic cells in a dose-dependent manner.

**KEYWORDS:** ERAP1, ERAP2, IRAP, aminopeptidase, inhibitor, immune system, antigenic peptide, docking



Endoplasmic reticulum (ER) aminopeptidases generate antigenic peptides for loading onto Major Histocompatibility Class I molecules (MHCI), which then interact with receptors on cytotoxic T-lymphocytes to initiate adaptive immune responses against infected or cancerous cells.<sup>1,2</sup> ER aminopeptidase 1 (ERAP1) is particularly effective in this function, and many *in vitro* and *in vivo* studies have established its role in regulating adaptive immune responses. For these reasons, ERAP1 is an attractive target for both cancer immunotherapy and the control of autoimmune reactions.<sup>3,4</sup> Indeed, ERAP1 down-regulation by available inhibitors has been reported to enhance cytotoxic responses versus cancer and suppress cellular autoimmune responses in Ankylosing Spondylitis.<sup>4–6</sup> Despite its biological importance, however, no clinical application of ERAP1 inhibitors have been reported, in part due to the lack of pharmacologically appropriate potent and selective inhibitors. Bestatin (ubenimex), a typical aminopeptidase inhibitor, has been evaluated in clinical settings but is a poor inhibitor of ERAP1.<sup>7</sup> Recent rational design efforts have yielded promising leads including a phosphinic pseudopeptide nanomolar inhibitor (DG013A, Chart 1) that displayed however low selectivity toward homologous enzymes, and 3,4-diaminobenzoic acid derivatives (such as 3, Chart 1) that displayed a better selectivity profile albeit with modest potency.<sup>8,9</sup> In an effort to discover novel, nonpeptidic scaffolds that inhibit ERAP1 as leads for preclinical development we applied a combination of structure-based, ligand-based, and

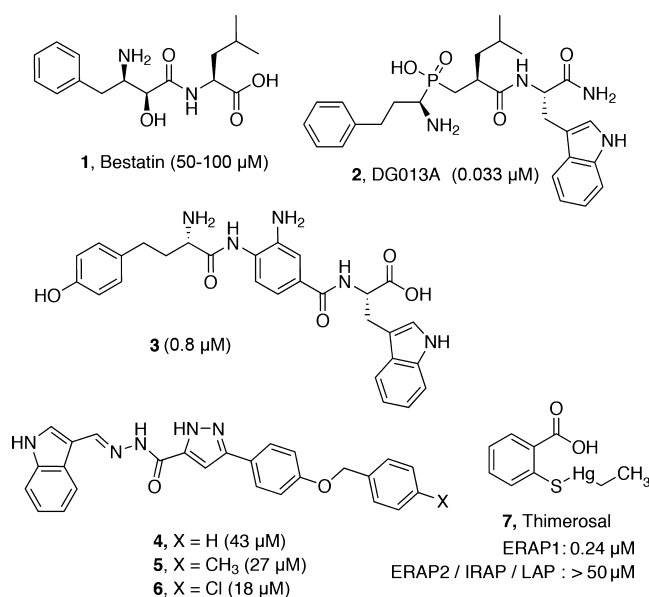
knowledge-based virtual screening approaches, taking advantage of key structural characteristics revealed in the recent crystal structures of ERAP1 and ERAP2 and their complexes with 1 and 2, respectively.<sup>8,10,11</sup>

Toward this goal, we compiled a library of more than 265,000 compounds from selected collections of chemical vendors that are focused on drug-likeness and structural diversity (Table S1). The library was enriched with the National Cancer Institute's diversity set II (1364 compounds) and the DrugBank database comprising 6590 FDA-approved and experimental small-molecule drugs.<sup>12</sup> We also performed a 3D pharmacophore search against the purchasable subset of the ZINC database (more than 20 million compounds)<sup>13</sup> using the online interface of ZINCPharmer.<sup>14</sup> The pharmacophore features of the query were extracted from the X-ray crystal structures of ERAP1 complex with bestatin and ERAP2 complex with DG013A,<sup>8,10,11</sup> which were further refined to a consensus pharmacophore (see the Computational Methods section, Table S2, and Figure S1 in the Supporting Information for more details). The filtered query results (3959 compounds) supplemented our small-molecule library for docking to ERAP1.

**Received:** February 26, 2016

**Accepted:** May 31, 2016

**Published:** May 31, 2016

**Chart 1. Chemical Structures of Known ERAP1 Inhibitors and Inhibitors Identified in This Study<sup>a</sup>**

<sup>a</sup>Values in parentheses indicate the IC<sub>50</sub> for ERAP1.

Molecular docking was performed with AutoDock Vina,<sup>15</sup> using ERAP1 in the closed state as the target structure (PDB ID: 2YD0).<sup>10</sup> Approximately 2500 top-ranked complexes were examined on the basis of three knowledge-based criteria: (i) their zinc-binding potential, (ii) accommodation of an aromatic ring system inside the S1 pocket, and (iii) additional hydrogen bonding and hydrophobic interactions at the S1'-S2' subsites. Accordingly, 24 compounds that satisfied all three criteria (Supporting Information, Table S3) were obtained and screened against ERAP1 using a previously established fluorogenic assay.<sup>16</sup>

The *in vitro* evaluation of the selected compounds revealed 4 as a low micromolar inhibitor of ERAP1 (Chart 1). The top-ranked predicted pose of 4 displayed coordination to the active site Zn(II) via the carbonyl group and a stacking interaction between the indole ring of 4 and Phe433 (Figure 1). The accommodation of the indole ring inside the S1 pocket of ERAP1 can be stabilized further via a hydrogen bond with the backbone carbonyl group of Glu183. The pyrazole carbohy-

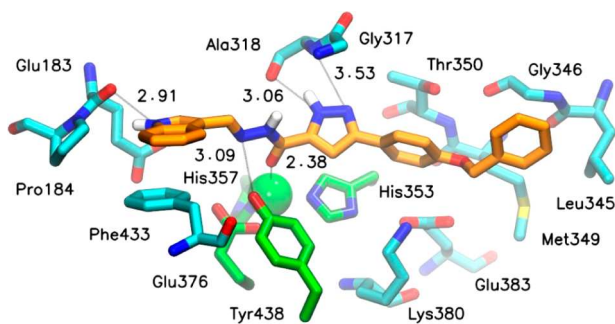


**Figure 1.** Predicted conformation of 4 bound to the active site of ERAP1. The inhibitor is shown with orange C, the interacting residues with cyan C, and the zinc-bound residues including the catalytic Tyr438 with green C; all N are blue, O are red, S are yellow, and Zn(II) is shown as a green sphere. Intermolecular hydrogen bonding distances between heavy atoms are given in Å.

drazide moiety of 4 is predicted to interact with the active site Tyr438 and the backbone of Ala318, whereas the benzyloxybenzene moiety is mainly engaged in aromatic-hydrophobic interactions.

To examine the potential of 4 for further optimization as ERAP1 inhibitor we performed a similarity search at 70% cutoff of the (*E*)-*N'*-((1*H*-indol-3-yl)methylene)-3-phenyl-1*H*-pyrazole-5-carbohydrazide scaffold against the purchasable ZINC database. The query results (1320 compounds) were docked against ERAP1, and visual inspection of the predicted bound conformations assisted the selection of a subset of 20 compounds for experimental evaluation (Table S4). The second round of *in vitro* screening revealed two inhibitors of ERAP1, 5 and 6 (Chart 1), with an approximately 2-fold increase in potency (representative titrations are shown in Figure 2). The activity gain of 5 and 6 can be attributed to a

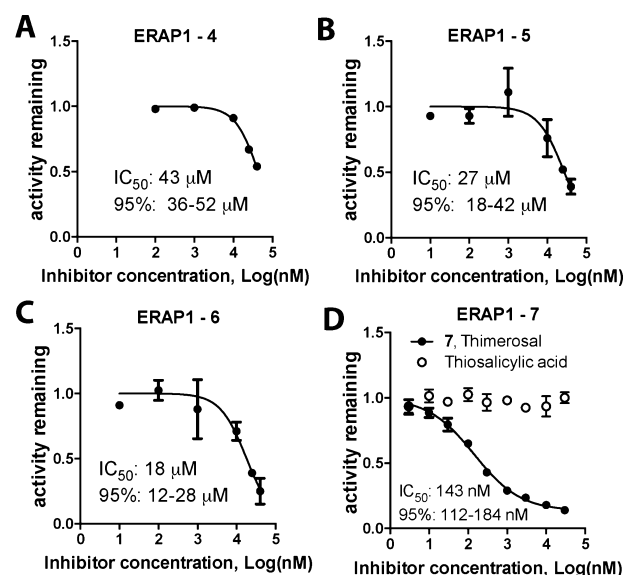


**Figure 2.** Representative titrations showing the ability of selected compounds to inhibit the ability of ERAP1 to hydrolyze the model fluorogenic substrate L-leucine-7-amino-4-methylcoumarin. Calculated IC<sub>50</sub> values and 95% confidence interval are indicated.

potential CH...O hydrogen or halogen bond with the hydroxyl group of Ser342, respectively (Figure S2). Although the identified inhibitors 4–6 are quite large and lipophilic (MW  $\approx$  450,  $x \log P > 5$ ) to be considered for further lead optimization, our data indicate that (*E*)-*N'*-((1*H*-indol-3-yl)methylene)-1*H*-pyrazole-5-carbohydrazide is a promising scaffold for the design of nonpeptidic inhibitors for ER aminopeptidases.

Motivated by successful structure-based design strategies that were based on the use of a zinc-binding group,<sup>17</sup> we selected an additional subset of nine small-molecule drugs from the DrugBank database (Table S5). Their selection was assisted by visual inspection of the docked conformations but was based on their zinc-chelating potential, regardless of their estimated binding affinity for ERAP1 (see the Compound Selection section in the Supporting Information).

Of the small-molecule drugs that were evaluated (Table S5) only one was found to inhibit ERAP1. Compound 7 (Chart 1) displayed submicromolar inhibition of ERAP1 with an IC<sub>50</sub> of  $0.24 \pm 0.11 \mu\text{M}$  (average of three separate experiments, representative titration shown in Figure 2D). Compound 7 was

initially selected for its potential bidentate coordination to the thiophilic Zn(II) through the thiosalicylic acid moiety. However, *in vitro* evaluation of thiosalicylic acid revealed no measurable inhibition of ERAP1 up to 30  $\mu\text{M}$  (Figure 2D), suggesting that 7 inhibits ERAP1 through a different mechanism.

To examine the selectivity of the discovered ERAP1 inhibitors, we evaluated the two most potent compounds (6 and 7) against ERAP2 and IRAP, two enzymes that are homologous to ERAP1 and are also important for the generation of antigenic epitopes and the function of the adaptive immune system. Compound 6 inhibited ERAP2 and IRAP with similar potency (34 and 28  $\mu\text{M}$ , respectively), but 7 was essentially inactive toward the two enzymes (Figure S3). The remarkable selectivity of 7 for ERAP1 with respect to the highly homologous ERAP2 and IRAP (51% and 46% sequence identity, respectively) suggests that inhibition is mediated by structural features that are unique to ERAP1. This idea is further supported by the inactivity of 7 against another zinc aminopeptidase of the M17 peptidase family, leucyl-amino-peptidase (LAP, Figure S4).

The inhibition profile of thimerosal (Figure 2D) displayed some atypical parameters and specifically a less than complete inhibition (10–20% residual enzymatic activity) and a hill constant of 0.73, which could indicate either negative cooperativity or multiple binding sites. To rule out any potential artifacts due to the nature of the fluorogenic enzymatic assay we also tested the ability of thimerosal to inhibit ERAP1 in a more physiologically relevant HPLC-based peptide trimming assay.<sup>18</sup> The rate of trimming of the N-terminus of the natural antigenic epitope precursor YTAFTIPSI was followed by reversed-phase HPLC in the presence or absence of 7 at 1  $\mu\text{M}$  concentration (Figure 3). Thimerosal was able to

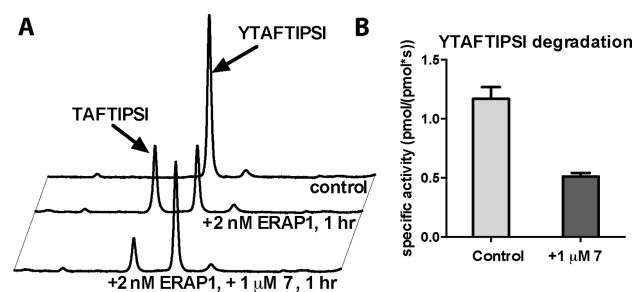


**Figure 3.** (A) Characteristic chromatograms showing the trimming of peptide YTAFTIPSI by ERAP1 in the presence or absence of 7. (B) Calculated specific activity based on the surface of the peptide peaks in the chromatograms (average of three separate experiments).

reduce the rate of trimming by 2.3-fold, which is overall consistent with the previous *in vitro* measurements of inhibitor activity versus ERAP1. Still, the residual ERAP1 activity seen in this assay suggests that thimerosal may be less potent in inhibiting the trimming of large peptides by ERAP1.

To further investigate the mechanism by which 7 inhibits ERAP1 we employed Michaelis–Menten analysis using the chromogenic substrate L-pNA (Leucine-*para*-Nitroanilide).<sup>8</sup> The  $V_{\text{max}}$  of the reaction was unaffected by the presence of the inhibitor, whereas  $K_{\text{M}}$  was increased according to the expected inhibition, indicating that thimerosal acts as a competitive inhibitor of ERAP1 (Figure 4A,B).

Since thimerosal has been reported to be able to release ethylmercury that can bind covalently to cysteine residues, we

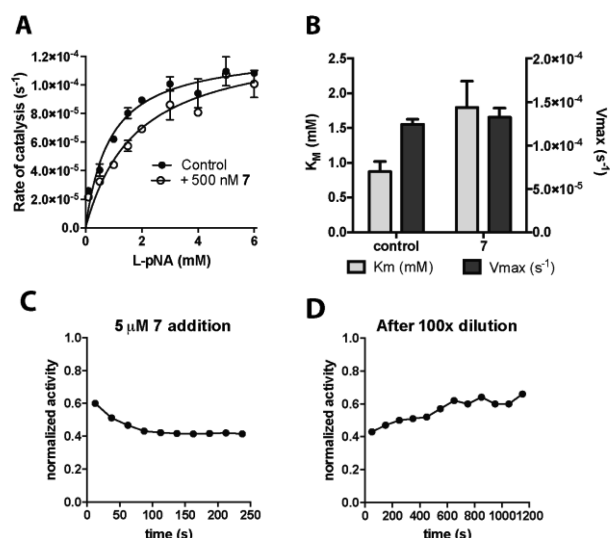


**Figure 4.** Kinetic analysis of inhibition of ERAP1 by 7 (thimerosal). (A) Michaelis–Menten analysis in the absence or presence of 500 nM 7. (B) Calculated enzymatic parameters by fitting the experimental data of panel A to the classical Michaelis–Menten equation. (C) Normalized ERAP1 activity following the addition of 7 (15 s of dead mixing time). (D) Recovery of ERAP1 activity after 100-fold dilution of the sample used in (C).

investigated the reversibility of ERAP1 inhibition by 7.<sup>19</sup> Rapid mixing of 5  $\mu\text{M}$  thimerosal with ERAP1 in the presence of L-AMC resulted in loss of the majority of the enzymatic activity, although a slow-rate component was also evident. Dilution of this mixture by 100-fold resulted in a time-dependent recovery of enzymatic activity indicating that the interaction of ERAP1 with thimerosal is characterized by relatively slow  $k_{\text{on}}$  and  $k_{\text{off}}$  rates and is mostly reversible (Figure 4C,D). Overall, the selectivity of thimerosal for ERAP1 over other highly homologous enzymes, the competitive type of inhibition, in addition to evidence for reversibility, indicate that thimerosal inhibits ERAP1 through noncovalent interactions with non-conserved residues of the active site.

To provide a structural rationale for the ability of thimerosal to inhibit ERAP1 we evaluated its docked conformations at the active sites of ERAP1, ERAP2, and IRAP.<sup>10,20,21</sup> Several top-ranked poses among the docked conformations of 7 displayed monodentate binding of the carboxylate group (Figure 5A), in accordance with crystallographic structures of Zn(II) model

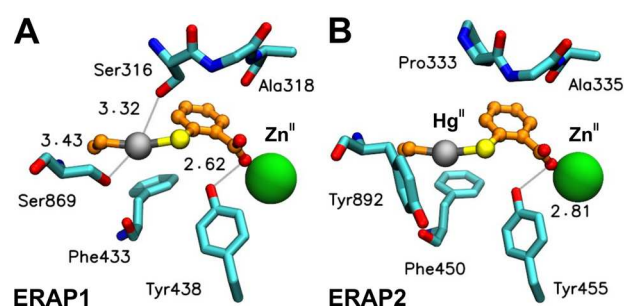


**Figure 5.** Putative binding mode of thimerosal at the catalytic zinc of ERAP1 (A) and ERAP2 (B). Hg(II) is shown as gray sphere, and all other atom colors are the same as those in Figure 1. Interactions between the ethylmercury moiety and the two nonconserved serine residues 316 and 869 are unique for ERAP1 and may be underlying the observed selectivity.

complexes with salicylate ligands, including thiosalicylic acid.<sup>22</sup> The complex of ERAP1 with **7** suggested two potential contacts between the mercury atom and the hydroxyl groups of Ser316 and Ser869 (Figure 5A). This type of interaction has been also observed in the X-ray structure of methylmercury complex with L-serine, where Hg(II) exhibits short intermolecular contacts with the carboxylate and the hydroxyl groups of the coordinated amino acid.<sup>23</sup> In contrast, such a configuration does not exhibit any contact with the corresponding residues Pro333 and Tyr892 of ERAP2 (Figure 5B). These two residues are also not conserved in IRAP or LAP, an observation that could explain the high selectivity of thimerosal for ERAP1.

ERAP1 has been described as a key enzyme for the generation of antigenic peptides in both direct and cross-presentation.<sup>1,24</sup> Cross-presentation by dendritic cells can proceed by at least two separate biochemical pathways, only one of which is dependent on ERAP1 enzymatic activity.<sup>25</sup>

To test whether thimerosal can affect ERAP1-dependent antigen presentation in live cells we incubated ERAP<sup>+/+</sup> and ERAP<sup>-/-</sup> BMDCs (bone marrow derived dendritic cells) with a fixed dose of ovalbumin (OVA) and increasing dosages of the inhibitor and then exposed them to transgenic OT-I CD8<sup>+</sup> T cells as described in the methods section. Antigen cross-presentation to CD8<sup>+</sup> T cells was quantified by measuring the IL-2 secretion by OT-I T cells, reflecting their activation.<sup>26,27</sup> Increasing concentrations of thimerosal reduced OVA presentation by ERAP<sup>+/+</sup> but not ERAP<sup>-/-</sup> BMDCs, consistent with an ERAP1-specific effect (Figure 6A). The calculated ED<sub>50</sub>

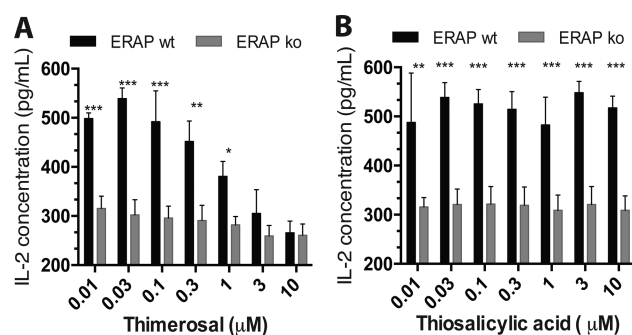


**Figure 6.** *In vitro* inhibitory effect of **7** (thimerosal) and inactive analogue thiosalicylic acid on cross-presentation by BMDCs. The IL-2 secretion of transgenic OT-I CD8<sup>+</sup> T cells incubated with OVA loaded-ERAP<sup>+/+</sup> and ERAP<sup>-/-</sup> BMDCs in the presence of **7** (thimerosal) (A) or thiosalicylic acid (B) was assessed by ELISA. \*,  $P < 0.05$ ; \*\*,  $P < 0.01$ ; \*\*\*,  $P < 0.001$ , as calculated by a two-way ANOVA test, with correction for multiple comparisons by the Bonferroni method. Histograms represent the mean of triplicates obtained in four independent experiments.

for this effect was found to be 930 nM, consistent with the *in vitro* affinity of thimerosal for ERAP1. No significant toxicity was observed with the concentrations of thimerosal tested in the cross-presentation assays (Figure S5). The inactive homologue thiosalicylic acid had no dose-dependent effect on OVA cross-presentation for either ERAP<sup>+/+</sup> or ERAP<sup>-/-</sup> BMDCs (Figure 6B). We conclude that thimerosal can affect ERAP1-dependent antigen presentation in cells.

Thimerosal is commonly used as a preservative in vaccines because it is a potent antiseptic and antifungal agent. Although several concerns have been raised over the years regarding its safety due to its potential to release ethylmercury, a toxic substance, thimerosal is generally considered safe at the

amounts used in vaccines (25–50 μg per dosage).<sup>28,29</sup> Still, other biological effects have been described including effects on mitochondrial respiration and the function of dendritic cells.<sup>30,31</sup> Our experiments indicate that thimerosal is a potent ERAP1 inhibitor and can affect cross-presentation by dendritic cells, a cell type important for vaccination responses. Although the low dosages of thimerosal in vaccines probably rule out any systemic effects, local, short-term effects on dendritic cells at the site of vaccination cannot be readily ruled out and should be further investigated.

In summary, we evaluated a collection of compounds as putative inhibitors of ERAP1, an enzyme important for adaptive immune responses and target for immunotherapy approaches.<sup>3,4</sup> We discovered two novel scaffolds as possible inhibitors of ERAP1, including thimerosal, a known pharmaceutical agent. Thimerosal was found to be a selective inhibitor of ERAP1 and to be able to affect antigen cross presentation by DCs. Although toxicity concerns may discourage the pharmacological use of thimerosal as an ERAP1 inhibitor, its strong selectivity profile and the effective utilization of unique structural elements in the active site of ERAP1 may constitute a valuable starting point for the development of potent and selective ERAP1 inhibitors that are currently lacking from the literature.

## ■ ASSOCIATED CONTENT

### 📄 Supporting Information

The Supporting Information is available free of charge on the ACS Publications website at DOI: 10.1021/acsmchemlett.6b00084.

Detailed description of computational and biochemical methods; collection of libraries screened; description of the 3D pharmacophore query; compounds used in this study and *in vitro* screening results; illustration of the predicted ERAP1–**6** complex; selectivity versus ERAP2 and IRAP; the effect of **7** on the activity of LAP; the toxicity of **7** on BMDCs; and supporting references (PDF)

## ■ AUTHOR INFORMATION

### Corresponding Author

\*E-mail: stratos@rrp.demokritos.gr or stratikos@gmail.com.

### Author Contributions

‡A.S. and A.P. contributed equally to this work. A.S. performed all enzymatic experiments and analyzed data. A.P. designed and performed the virtual library screen, compound selection, and structural analysis. F.X.M. and P.v.E. designed and implemented the cross-presentation assay. E.S. supervised the project, analyzed data, and interpreted results. The manuscript was written through contributions of all authors, and all authors have given approval to the final version of the manuscript.

### Funding

This research was funded by the European Union (EU Social Fund) and Greek National funds through the Operational Program “Education and Lifelong Learning” of the National Strategic Reference Framework: Research Funding Program of the General Secretariat for Research and Technology (Grant ERC-14 to E.S.). Funding was also provided by grants DEQ20130326539 from the Fondation pour la Recherche Médicale and ANR-14-CE11-0014 from the Agence Nationale de Recherche to P.v.E.

## Notes

The authors declare no competing financial interest.

## ■ ABBREVIATIONS

ER, endoplasmic reticulum; MHC, major histocompatibility molecules; ERAP1&2, endoplasmic reticulum aminopeptidase 1 and 2; IRAP, insulin regulated aminopeptidase; LAP, leucyl aminopeptidase; BMDCs, bone marrow derived dendritic cells; OVA, ovalbumin; IL-2, interleukin-2

## ■ REFERENCES

- (1) Weimershaus, M.; Evnouchidou, I.; Saveanu, L.; van Endert, P. Peptidases trimming MHC class I ligands. *Curr. Opin. Immunol.* **2013**, *25*, 90–96.
- (2) Evnouchidou, I.; Papakyriakou, A.; Stratikos, E. A New Role for Zn(II) Aminopeptidases: Antigenic Peptide Generation and Destruction. *Curr. Pharm. Des.* **2009**, *15*, 3656–3670.
- (3) Stratikos, E. Regulating adaptive immune responses using small molecule modulators of aminopeptidases that process antigenic peptides. *Curr. Opin. Chem. Biol.* **2014**, *23C*, 1–7.
- (4) Stratikos, E. Modulating antigen processing for cancer immunotherapy. *Oncimmunology* **2014**, *3*, e27568.
- (5) Cifaldi, L.; Romania, P.; Falco, M.; Lorenzi, S.; Meazza, R.; Petrini, S.; Andreani, M.; Pende, D.; Locatelli, F.; Fruci, D. ERAP1 regulates natural killer cell function by controlling the engagement of inhibitory receptors. *Cancer Res.* **2015**, *75*, 824–834.
- (6) Chen, L.; Ridley, A.; Hammitzsch, A.; Al-Mossawi, M. H.; Bunting, H.; Georgiadis, D.; Chan, A.; Kollnberger, S.; Bowness, P. Silencing or inhibition of endoplasmic reticulum aminopeptidase 1 (ERAP1) suppresses free heavy chain expression and Th17 responses in ankylosing spondylitis. *Ann. Rheum. Dis.* **2016**, *75*, 916.
- (7) Hattori, A.; Matsumoto, H.; Mizutani, S.; Tsujimoto, M. Molecular cloning of adipocyte-derived leucine aminopeptidase highly related to placental leucine aminopeptidase/oxytocinase. *J. Biochem.* **1999**, *125*, 931–938.
- (8) Zervoudi, E.; Saridakis, E.; Birtley, J. R.; Seregin, S. S.; Reeves, E.; Kokkala, P.; Aldhamen, Y. A.; Amalfitano, A.; Mavridis, I. M.; James, E.; Georgiadis, D.; Stratikos, E. Rationally designed inhibitor targeting antigen-trimming aminopeptidases enhances antigen presentation and cytotoxic T-cell responses. *Proc. Natl. Acad. Sci. U. S. A.* **2013**, *110*, 19890–19895.
- (9) Papakyriakou, A.; Zervoudi, E.; Tsoukalidou, S.; Mauvais, F. X.; Sfyroera, G.; Mastellos, D. C.; van Endert, P.; Theodorakis, E. A.; Vourloumis, D.; Stratikos, E. 3,4-Diaminobenzoic Acid Derivatives as Inhibitors of the Oxytocinase Subfamily of M1 Aminopeptidases with Immune-Regulating Properties. *J. Med. Chem.* **2015**, *58*, 1524.
- (10) Kochan, G.; Krojer, T.; Harvey, D.; Fischer, R.; Chen, L.; Vollmar, M.; von Delft, F.; Kavanagh, K. L.; Brown, M. A.; Bowness, P.; Wordsworth, P.; Kessler, B. M.; Oppermann, U. Crystal structures of the endoplasmic reticulum aminopeptidase-1 (ERAP1) reveal the molecular basis for N-terminal peptide trimming. *Proc. Natl. Acad. Sci. U. S. A.* **2011**, *108*, 7745–7750.
- (11) Nguyen, T. T.; Chang, S. C.; Evnouchidou, I.; York, I. A.; Zikos, C.; Rock, K. L.; Goldberg, A. L.; Stratikos, E.; Stern, L. J. Structural basis for antigenic peptide precursor processing by the endoplasmic reticulum aminopeptidase ERAP1. *Nat. Struct. Mol. Biol.* **2011**, *18*, 604–613.
- (12) Knox, C.; Law, V.; Jewison, T.; Liu, P.; Ly, S.; Frolkis, A.; Pon, A.; Banco, K.; Mak, C.; Neveu, V.; Djoumbou, Y.; Eisner, R.; Guo, A. C.; Wishart, D. S. DrugBank 3.0: a comprehensive resource for 'omics' research on drugs. *Nucleic Acids Res.* **2011**, *39*, D1035–1041.
- (13) Irwin, J. J.; Sterling, T.; Mysinger, M. M.; Bolstad, E. S.; Coleman, R. G. ZINC: a free tool to discover chemistry for biology. *J. Chem. Inf. Model.* **2012**, *52*, 1757–1768.
- (14) Koes, D. R.; Camacho, C. J. ZINCPharmer: pharmacophore search of the ZINC database. *Nucleic Acids Res.* **2012**, *40*, W409–414.
- (15) Trott, O.; Olson, A. J. AutoDock Vina: improving the speed and accuracy of docking with a new scoring function, efficient optimization, and multithreading. *J. Comput. Chem.* **2010**, *31*, 455–461.
- (16) Zervoudi, E.; Papakyriakou, A.; Georgiadou, D.; Evnouchidou, I.; Gajda, A.; Poreba, M.; Salvesen, G. S.; Drag, M.; Hattori, A.; Swevers, L.; Vourloumis, D.; Stratikos, E. Probing the S1 specificity pocket of the aminopeptidases that generate antigenic peptides. *Biochem. J.* **2011**, *435*, 411–420.
- (17) Jacobsen, J. A.; Major Jourden, J. L.; Miller, M. T.; Cohen, S. M. To bind zinc or not to bind zinc: an examination of innovative approaches to improved metalloproteinase inhibition. *Biochim. Biophys. Acta, Mol. Cell Res.* **2010**, *1803*, 72–94.
- (18) Georgiadou, D.; Hearn, A.; Evnouchidou, I.; Chroni, A.; Leondiadis, L.; York, I. A.; Rock, K. L.; Stratikos, E. Placental leucine aminopeptidase efficiently generates mature antigenic peptides in vitro but in patterns distinct from endoplasmic reticulum aminopeptidase 1. *J. Immunol.* **2010**, *185*, 1584–1592.
- (19) Trumpler, S.; Lohmann, W.; Meermann, B.; Buscher, W.; Sperling, M.; Karst, U. Interaction of thimerosal with protein-ethylmercury adduct formation of human serum albumin and beta-lactoglobulin A. *Metallomics* **2009**, *1*, 87–91.
- (20) Birtley, J. R.; Saridakis, E.; Stratikos, E.; Mavridis, I. M. The Crystal Structure of Human Endoplasmic Reticulum Aminopeptidase 2 Reveals the Atomic Basis for Distinct Roles in Antigen Processing. *Biochemistry* **2012**, *51*, 286–295.
- (21) Mpakali, A.; Saridakis, E.; Harlos, K.; Zhao, Y.; Papakyriakou, A.; Kokkala, P.; Georgiadis, D.; Stratikos, E. Crystal Structure of Insulin-Regulated Aminopeptidase with Bound Substrate Analogue Provides Insight on Antigenic Epitope Precursor Recognition and Processing. *J. Immunol.* **2015**, *195*, 2842–2851.
- (22) Jacobsen, F. E.; Cohen, S. M. Using model complexes to augment and advance metalloproteinase inhibitor design. *Inorg. Chem.* **2004**, *43*, 3038–3047.
- (23) Corbeil, M. C.; Beauchamp, A. L. Conformational-Changes in Serine on Methylmercury Complexation. *Can. J. Chem.* **1988**, *66*, 1379–1385.
- (24) Firat, E.; Saveanu, L.; Aichele, P.; Staeheli, P.; Huai, J.; Gaedicke, S.; Nil, A.; Besin, G.; Kanzler, B.; van Endert, P.; Niedermann, G. The role of endoplasmic reticulum-associated aminopeptidase 1 in immunity to infection and in cross-presentation. *J. Immunol.* **2007**, *178*, 2241–2248.
- (25) Saveanu, L.; Carroll, O.; Weimershaus, M.; Guermontprez, P.; Firat, E.; Lindo, V.; Greer, F.; Davoust, J.; Kratzer, R.; Keller, S. R.; Niedermann, G.; van Endert, P. IRAP Identifies an Endosomal Compartment Required for MHC Class I Cross-Presentation. *Science* **2009**, *325*, 213–217.
- (26) Weimershaus, M.; van Endert, P. Preparation of dendritic cells by in vitro cultures. *Methods Mol. Biol.* **2013**, *960*, 351–357.
- (27) Merzougui, N.; Kratzer, R.; Saveanu, L.; van Endert, P. A proteasome-dependent, TAP-independent pathway for cross-presentation of phagocytosed antigen. *EMBO Rep.* **2011**, *12*, 1257–1264.
- (28) Baker, J. P. Mercury, vaccines, and autism: one controversy, three histories. *Am. J. Public Health* **2008**, *98*, 244–253.
- (29) Dorea, J. G.; Farina, M.; Rocha, J. B. Toxicity of ethylmercury (and Thimerosal): a comparison with methylmercury. *J. Appl. Toxicol.* **2013**, *33*, 700–711.
- (30) Goth, S. R.; Chu, R. A.; Gregg, J. P.; Cherednichenko, G.; Pessah, I. N. Uncoupling of ATP-mediated calcium signaling and dysregulated interleukin-6 secretion in dendritic cells by nanomolar thimerosal. *Environ. Health Perspect.* **2006**, *114*, 1083–1091.
- (31) Sharpe, M. A.; Livingston, A. D.; Baskin, D. S. Thimerosal-Derived Ethylmercury Is a Mitochondrial Toxin in Human Astrocytes: Possible Role of Fenton Chemistry in the Oxidation and Breakage of mtDNA. *J. Toxicol.* **2012**, *2012*, 373678.

# Screening identifies Thimerosal as a Selective Inhibitor of Endoplasmic Reticulum Aminopeptidase 1

Athanasios Stamogiannos<sup>†,‡</sup>, Athanasios Papakyriakou<sup>†,‡</sup>, Francois-Xavier Mauvais<sup>§</sup>, Peter van Endert<sup>§</sup> and Efstratios Stratikos<sup>†,\*</sup>

<sup>†</sup>National Center for Scientific Research Demokritos, GR-15310, Agia Paraskevi, Athens, Greece

<sup>§</sup>Institut National de la Santé et de la Recherche Médicale, Unité 1151; Université Paris Descartes, Sorbonne Paris Cité; Centre National de la Recherche Scientifique, Unité 8253, 75015 Paris, France

\*Corresponding author: stratos@rrp.demokritos.gr or stratikos@gmail.com

## Supporting Information

### Table of contents

<b>Computational Methods</b> .....	2
Table S1 .....	2
Table S2 .....	3
Figure S1.....	4
Table S3 .....	6
Table S4 .....	10
Table S5 .....	13
Figure S2.....	15
<b>Biochemical Methods</b> .....	16
Figure S3.....	19
Figure S4.....	20
Figure S5.....	20
<b>Supporting References</b> .....	21

## Computational Methods

**Database collection and preparation.** A collection of commercially available compounds was compiled from the in-house synthesized compounds of Asinex,<sup>S1</sup> ChemBridge,<sup>S2</sup> KeyOrganics,<sup>S3</sup> TimTec and Sigma-Aldrich.<sup>S4</sup> In particular, we selected the diversity-focused screening libraries shown in Table S1, which comprise, but are not limited to, drug-like compounds according to Lipinski's rule of five,<sup>S5</sup> and have been filtered from undesirable chemical groups, such as Michael acceptors, epoxides, crown-ethers, triflates, perchlorates. This collection was supplemented with the NCI Diversity Set II<sup>S6</sup> and all the approved and experimental drugs available at the DrugBank v.3 (www.drugbank.ca).<sup>S7</sup> The libraries were downloaded as SDF files and 3D coordinates in MOL2 format were generated using OMEGA v2.4.<sup>S8</sup> Molecules that failed conversion were examined individually and were manually converted to a 3D model, if possible, using VIDA v4.2 (OpenEye Scientific, <http://eyesopen.com>). The final input files for docking were prepared using the Python scripts available from MGLTools v1.5.4.<sup>S9</sup> In the case of drugs that contained metal ions not supported by AutoDock Vina (arsenic, mercury, platinum),<sup>S10</sup> the metals were replaced by phosphorus atoms.

**Table S1.** Collection of small-molecule libraries employed in the structure-based virtual screen against ERAP1

<b>Chemical Library</b>	<b>No. Compounds</b>
Asinex Platinum Collection (2013)	113,962
ChemBridge DIVERSet Library (EXP+CL)	100,000
KeyOrganics Screening Library (2013)	41,612
MyriaScreen Diversity Collection II	10,000
National Cancer Institute Diversity Set	1,364
DrugBank ver.3.0 (2013)	6,590
3D pharmacophore search of ZINC database	3,959
<b>Total number of compounds</b>	<b>277,487</b>



**Pharmacophore search.** Taking advantage of the crystallographic structures of bestatin bound to ERAP1 in the closed state,<sup>S11</sup> and the phosphinic pseudopeptide transition state analog DG013A bound to ERAP2,<sup>S12</sup> we employed a pharmacophore-based screening of the ZINC database.<sup>S13</sup> The corresponding X-ray structures (PDB IDs: 2YDO and 4JBS) were superimposed with respect to the backbone atoms of the domains I and II (46–529 in ERAP1) and the superimposed ligand structures were extracted (Figure S1). The four critical pharmacophoric features that were identified visually are:

- i) An aromatic group inside the S1 specificity pocket that is stacked with Phe433 of ERAP1.
- ii) A positive ion docked at the substrate N-terminus site by Glu183 and Glu320 residues.
- iii) A negative ion that will bind to the catalytic Zn(II).
- iv) A hydrophobic element at the S1' subsite.

The aromatic element was defined mainly on the basis of the benzyl ring of DG013A that is in exact perpendicular orientation with respect to Phe433 of ERAP1, whereas the negative ion pharmacophore was selected so as to include both oxygen ligands of bestatin and DG013A that are coordinated to zinc. The positive ion indicates the common position of the primary amine of the two inhibitors, and the hydrophobic pharmacophore was expanded in order to include the major moiety of the leucine side chain that is part of both inhibitors. These pharmacophore elements (Figure S1 and Table S2) were employed manually for a search of the purchasable subset of the ZINC database using ZINCpharmer web server.<sup>S14</sup> Results were limited to a single conformation per molecule and were filtered using a MW range of 250–600 and less than 10 rotatable bonds. The resulting 3,959 compounds were retrieved in MOL2 format and were included in the small-molecule collection employed for docking to ERAP1.

**Table S2.** Pharmacophore elements employed in the ZINCPharmer query. Their centers in x, y, z coordinates are given with respect to PDB ID: 2YD0, and their radii are in Å.

Description	Coordinates	Radius
Aromatic	7.8, 77.5, 26.2	1.8
Positive ion	6.2, 75.5, 21.2	1.2
Negative ion	7.7, 72.4, 21.5	1.4
Hydrophobic	10.9, 68.8, 23.1	2.0

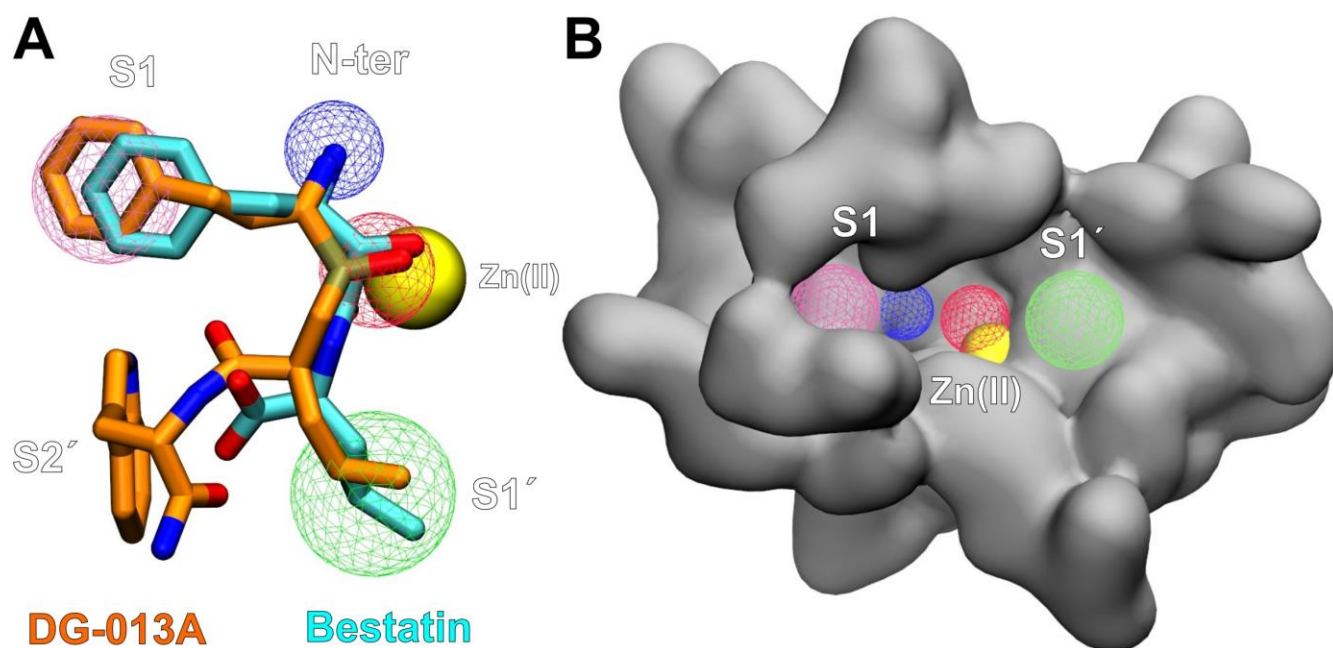


**Figure S1.** (A) Superposition of the X-ray structure of bestatin (cyan C atoms) and DG-013A (orange C atoms) from their complexes with ERAP1 and ERAP2, respectively. The pharmacophoric elements identified are color-coded as follows: aromatic (purple), positive ion (blue), negative ion (red) and hydrophobic (green). The yellow sphere is the catalytic Zn(II). (B) Surface representation of ERAP1 active site residues indicating the position of the subsites and pharmacophores as defined in (A).

**Target structure preparation.** The crystal structure of ERAP1 complex with bestatin in the closed state (PDB ID: 2YD0)<sup>S11</sup> was employed as the target structure. The protein atoms of residues 46–940 and the zinc ion were extracted from the PDB file. The alternative location–A residues D284, C736, C743 and H873 were retained, and the missing residues 111–114 and 553–557 were added using MODELLER (v9.10).<sup>S15</sup> The missing loop residues 486–513 were not modeled considering their distance from the active site. The protonation state of histidine residues was set after estimation of their pK<sub>a</sub> values using H++ (v3.1)<sup>S16</sup> and visual inspection of their neighboring residues for putative hydrogen bonding interactions. In particular, the two zinc-bound histidines (H353 and H357), and H468, H501, H511, H738 were set to be protonated at H<sup>δ1</sup>, whereas all the remaining histidine residues were protonated at H<sup>ε2</sup>. Two disulfide bonds were added between C404–C443 and C736–C743, polar hydrogen atoms were added, and then Gasteiger charges were applied to the protein atoms using AutoDockTools 1.4.5.<sup>S17</sup> The atomic charge of Zn(II) was manually set to +1.0 e<sup>-</sup> and the remaining

+1.0 e<sup>-</sup> was equally distributed among the zinc-bound atoms of His353, His357 and the two carboxylate oxygen atoms of Glu386.

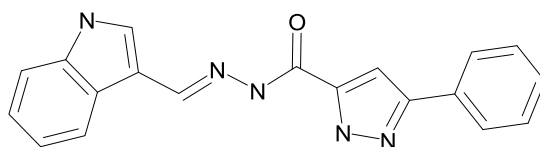
**Molecular docking.** The collection of compounds was docked at the active site of ERAP1 in the closed state using AutoDock Vina.<sup>S10</sup> The search space was defined so as to include all critical residues of the S1 and S1'–S2' specificity pockets of ERAP1 that interact with known inhibitors. Specifically, the search space comprised a cube of 25 Å edge that was centered at 8.6, 73.6, 22.6 (x, y, z with respect to PDB ID 2YD0).<sup>S11</sup> The exhaustiveness level and the number of modes were both set to 10, and calculations were performed at Intel Xeon clusters running Linux x86 v2.6.32 kernels.

**Compound selection.** Selection of the compounds for *in vitro* examination was assisted by examination of their complexes using VMD (v1.9)<sup>S18</sup> and on the basis of the following three criteria:

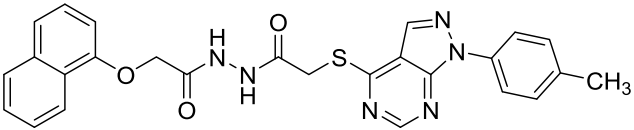
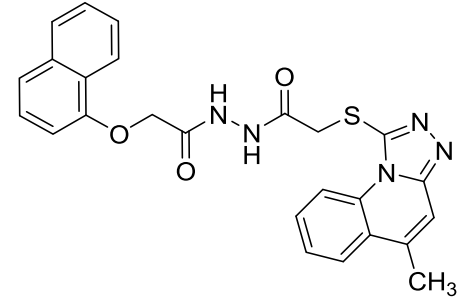
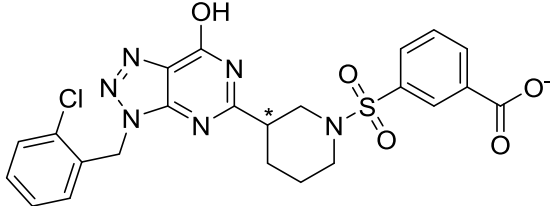
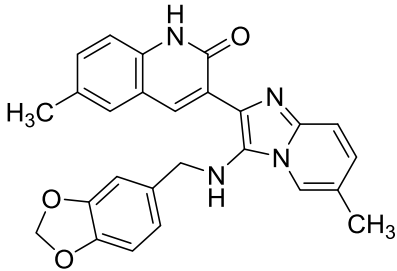
- i) The appropriate coordination to the catalytic zinc via a carbonyl, hydroxyl or sulfonyl group
- ii) Accommodation of an aromatic ring system inside the S1 pocket
- iii) Additional hydrogen bonding and hydrophobic interactions at the S1'–S2' subsites

Approximately 2,500 of complexes from the top-ranked results were visually examined and those that satisfied all the above-mentioned criteria were re-evaluated using physiochemical- and diversity-based criteria, and in particular, using the Ligand Efficiency metric ( $\Delta G$  per number of non-hydrogen atoms), the calculated octanol-water partition coefficient (xLogP) and the number of rotatable bonds (NRB). The 24 selected compounds shown in Table S3 were purchased from commercial vendors and used for experimental validation.

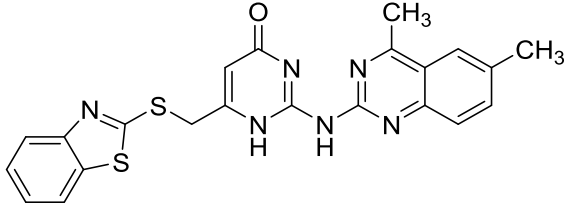
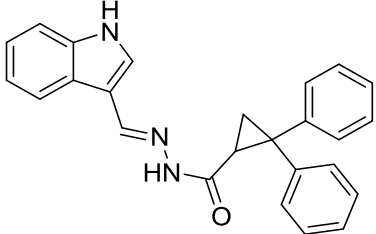
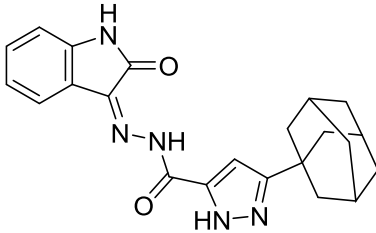
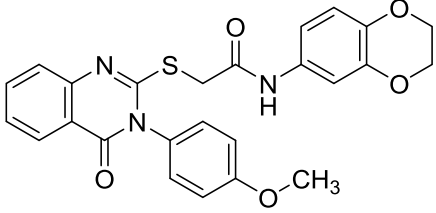
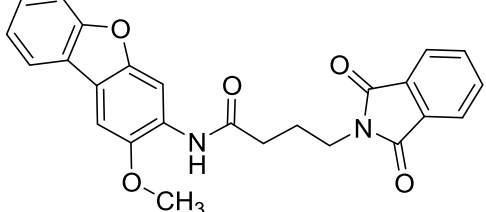
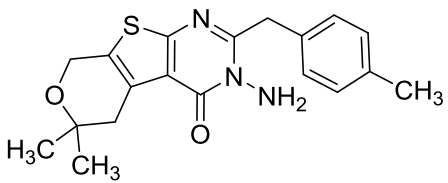
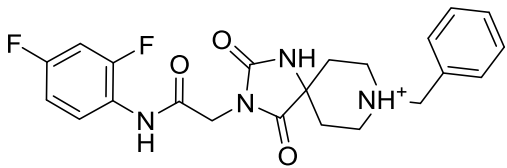
After identifying **4** as an ERAP1 inhibitor, we performed a similarity search at 70% level of the (E)-N'-((1H-indol-3-yl)methylene)-3-phenyl-1H-pyrazole-5-carbohydrazide scaffold (shown below) against the purchasable subset of the ZINC database. The resulting unique compounds were downloaded in MOL2 format and were evaluated by molecular docking to ERAP1 as described above. The bound poses of several highly-ranked compounds were visually inspected for additional interactions at the S1'–S2' subsites of ERAP1, and with the aim to explore the structure-activity relationships of the indole, the carbohydrazide and the substituted benzene moieties of the scaffold. The subset of 20 compounds that was selected for further evaluation is given in Table S4.



**Table S3.** Initial selection of compounds based on the virtual screening for ERAP1 inhibitors. Multiple ZINC ID codes correspond to chiral compounds indicated with an asterisk. Molecular weight (MW/g·mol<sup>-1</sup>), topological polar surface area (tPSA/Å<sup>2</sup>), computed octanol/water partition coefficient (xlogP), and number of rotatable bonds (RB) at reference pH=7 were taken from the ZINC database.<sup>S13</sup> The half maximal inhibitory concentration for ERAP1 (IC<sub>50</sub>) and 95% confidence intervals are given in μM. For the cases that no significant inhibition was observed up to the highest possible concentration tested due to solubility restraints, the IC<sub>50</sub> is only indicated as an estimate.

ZINC ID	Structure	MW	tPSA	xlogP	RB	IC <sub>50</sub>
12643186		498.6	111	3.6	8	>40
06195120		471.5	98	4.4	7	>100
38145715 38145716		527.0	157	3.2	6	>100
35312113		438.5	81	4.2	4	>40

ZINC ID	Structure	MW	tPSA	xlogP	RB	IC <sub>50</sub>
12637537 12637541		524.6	114	2.5	7	>40
12496502 12496507		507.6	89	5.7	7	>40
00901013 00901019		498.6	97	4.1	6	>100
06161768		532.5	113	3.5	6	>40
01354670		519.6	97	4.6	5	>40
13083792 13083794		430.4	116	3.4	5	>100
<b>00867876</b> <b>(4)</b>		<b>435.5</b>	<b>95</b>	<b>5.2</b>	<b>7</b>	<b>43</b> <b>95%:</b> <b>36-52</b>

ZINC ID	Structure	MW	tPSA	xlogP	RB	IC <sub>50</sub>
08682430		446.6	96	5.6	5	>40
00704204		379.5	57	5.4	5	>40
05093080		389.5	103	4.1	3	>40
01088858		475.5	91	3.6	6	>40
02849847		428.4	90	4.5	6	>40
01076692		355.5	70	3.7	2	>100
08769214		429.4	82	2.5	5	>100

ZINC ID	Structure	MW	tPSA	xlogP	RB	IC <sub>50</sub>
08781733		516.6	64	6.8	7	>40
12949796		558.8	97	4.6	6	>40
52537818		500.5	151	4.8	11	>100
03134263		568.4	82	7.6	8	>40
12958828		465.3	53	6.8	8	>40
n.a.		572.7	105 <sup>a</sup>	5.1 <sup>a</sup>	6	>40

n.a. not registered at ZINC (vendor catalog ID: ASN05342805)

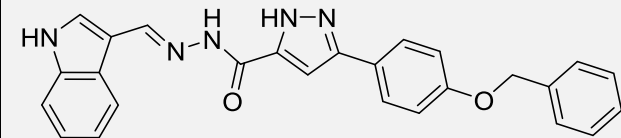
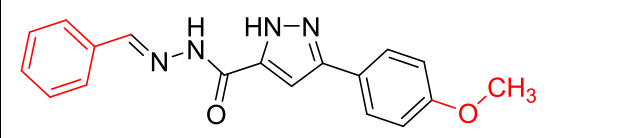
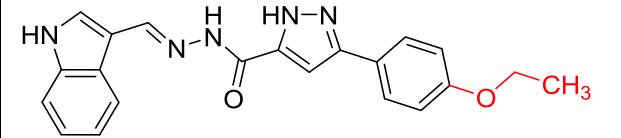
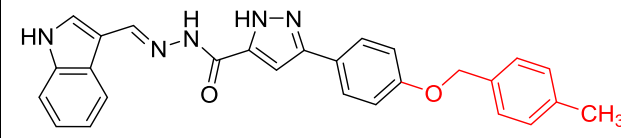
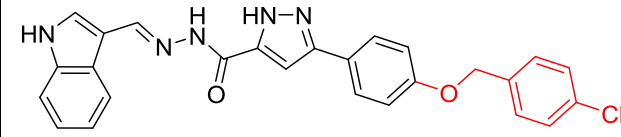
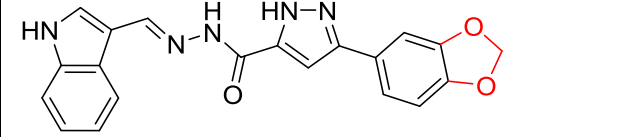
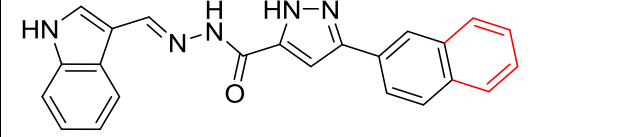
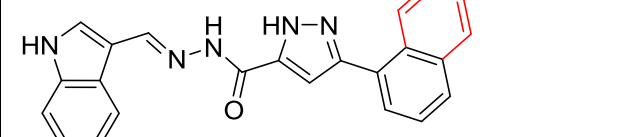
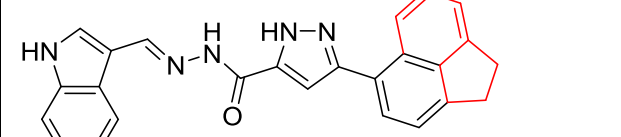
<sup>a</sup> estimated using the Plugin Calculator of Marvin<sup>S19</sup>

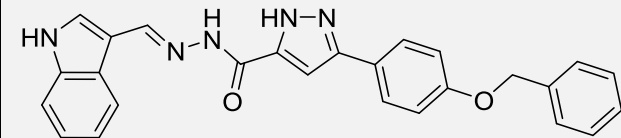
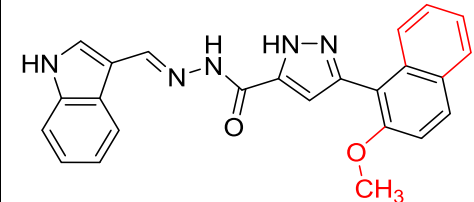
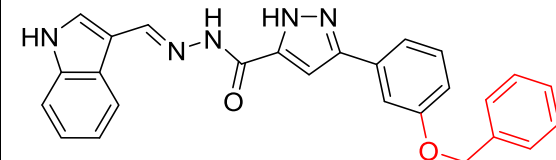
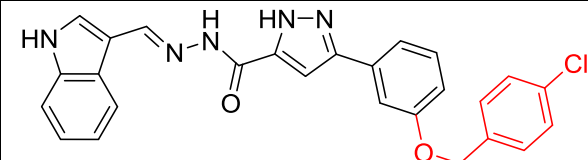
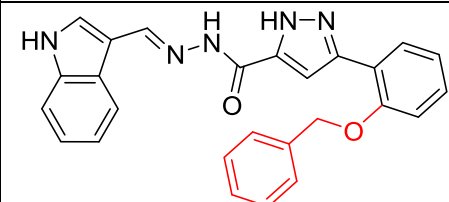
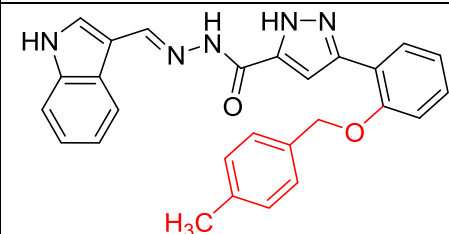
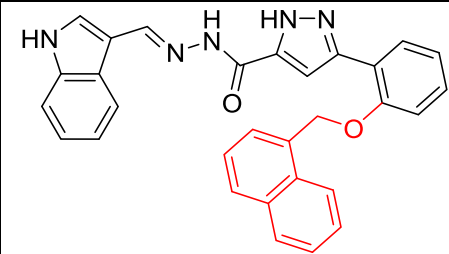
\* indicates a chiral center

**Table S4.** Selected analogues of hit compound **4** employed in the second round of screening for ERAP1 inhibitors. Modified moieties of the (E)-N'-((1H-indol-3-yl)methylene)-3-phenyl-1H-pyrazole-5-carbohydrazide scaffold are indicated with red color. Molecular weight (MW/g·mol<sup>-1</sup>), topological polar surface area (tPSA/Å<sup>2</sup>), computed octanol/water partition coefficient (xlogP), and number of rotatable bonds (RB) at reference pH=7 were taken from the ZINC database.<sup>S13</sup> The half maximal inhibitory concentration for ERAP1 (IC<sub>50</sub>) and 95% confidence intervals are given in μM. For the cases that no significant inhibition was observed up to the highest possible concentration tested due to solubility restraints, the IC<sub>50</sub> is only indicated as an estimate.

ZINC ID	Structure	MW	tPSA	xlogP	RB	IC <sub>50</sub>
00867876 (4)		435.5	95	5.2	7	43 95%: 36–52
00229172		267.3	85	2.1	3	>40
08683438		329.4	86	3.5	4	>40
01050817		363.8	86	4.2	4	>40
09301959		359.4	95	3.6	5	>25
01190000		373.4	95	3.8	5	>40
13548665		360.4	83	3.4	6	>40

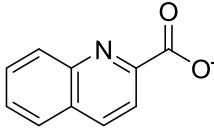
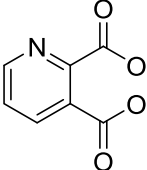
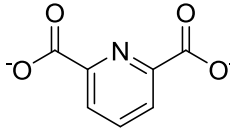


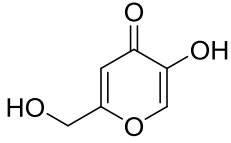
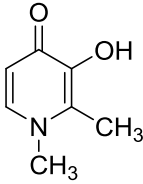
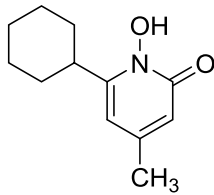
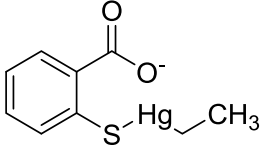
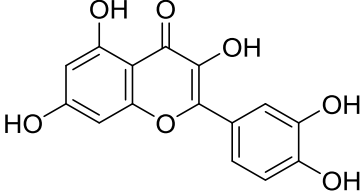
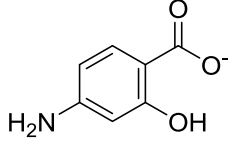
ZINC ID	Structure	MW	tPSA	xlogP	RB	IC <sub>50</sub>
00867876 (4)		435.5	95	5.2	7	43 95%: 36–52
09043273		320.4	79	3.4	5	>40
09011889		373.4	95	4.0	6	>25
09374837 (5)		449.5	95	5.6	7	27 95%: 18–42
09088951 (6)		469.9	95	5.9	7	18 95%: 12–28
01469005		373.4	104	3.4	4	>40
08690033		379.4	86	4.7	4	>40
08683431		379.4	86	4.7	4	>25
05297058		405.5	86	4.8	4	>25

ZINC ID	Structure	MW	tPSA	xlogP	RB	IC <sub>50</sub>
00867876 (4)		435.5	95	5.2	7	43 95%: 36–52
08973566		409.4	95	4.7	5	>25
09088076		435.5	95	5.2	7	>25
09363640		469.9	95	5.8	7	>25
18148616		435.5	95	5.2	7	>25
09008747		449.5	95	5.6	7	>25
04527990		485.5	95	6.3	7	>25

A number of approved and experimental drugs were selected irrespective of their estimated binding affinity from docking to ERAP1. The compounds given in Table S5 were acquired as potential zinc chelating agents after visual inspection of the predicted bound conformations of selected compounds from DrugBank. More specifically, the first 3 compounds in Table S5 were obtained to investigate the putative inhibition of ERAP1 via chelation of pyridine carboxylate or dicarboxylate moieties. Kojic acid, deferiprone (an iron-chelating agent) and ciclopirox were selected to examine the potential of zinc chelation by the hydroxypyranone, hydroxypyridinone and *N*-hydroxypyridinone moieties, respectively. Thimerosal was acquired based on the assumption that the thiosalicylic acid moiety could bind strongly to the active site Zn(II). Quercetin was chosen as a representative member of the flavonol family that displayed diverse but promising zinc-bound conformations in the active site of ERAP1, and finally, aminosalicylic acid for the possibility to chelate the catalytic zinc via its 2-hydroxybenzoate moiety.

**Table S5.** Compounds from DrugBank<sup>S7</sup> selected based on their potential as zinc-binding chelators. The half maximal inhibitory concentration for ERAP1 (IC<sub>50</sub>) and 95% confidence intervals are given in μM. For the cases that no significant inhibition was observed up to the highest possible concentration tested due to solubility restraints, the IC<sub>50</sub> is only indicated as an estimate.

ZINC ID	DrugBank ID	Name (Status)	Structure	MW	IC <sub>50</sub>
00084153	DB02428	Quinaldic acid (Experimental)		172.2	>100
00331671	DB01796	Quinolinic acid (Experimental)		165.1	>100
00105246	DB04267	Dipicolinic acid (Experimental)		165.1	>100

ZINC ID	DrugBank ID	Name (Status)	Structure	MW	IC <sub>50</sub>
13831818	DB01759	Kojic acid (Experimental)		142.1	>100
00006226	DB08826	Deferiprone (Approved)		139.2	>100
00001145	DB01188	Ciclopirox (Approved)		206.3	>100
<i>n.a.</i> (7)	DB02731	<b>Thimerosal</b> (Experimental)		382.8	0.24±0.11
03869685	DB04216	Quercetin (Experimental)		302.2	>10
00000922	DB00233	Aminosalicylic acid (Approved)		152.1	>100

*n.a.*: not registered at ZINC (PubChem CID: 16684434)

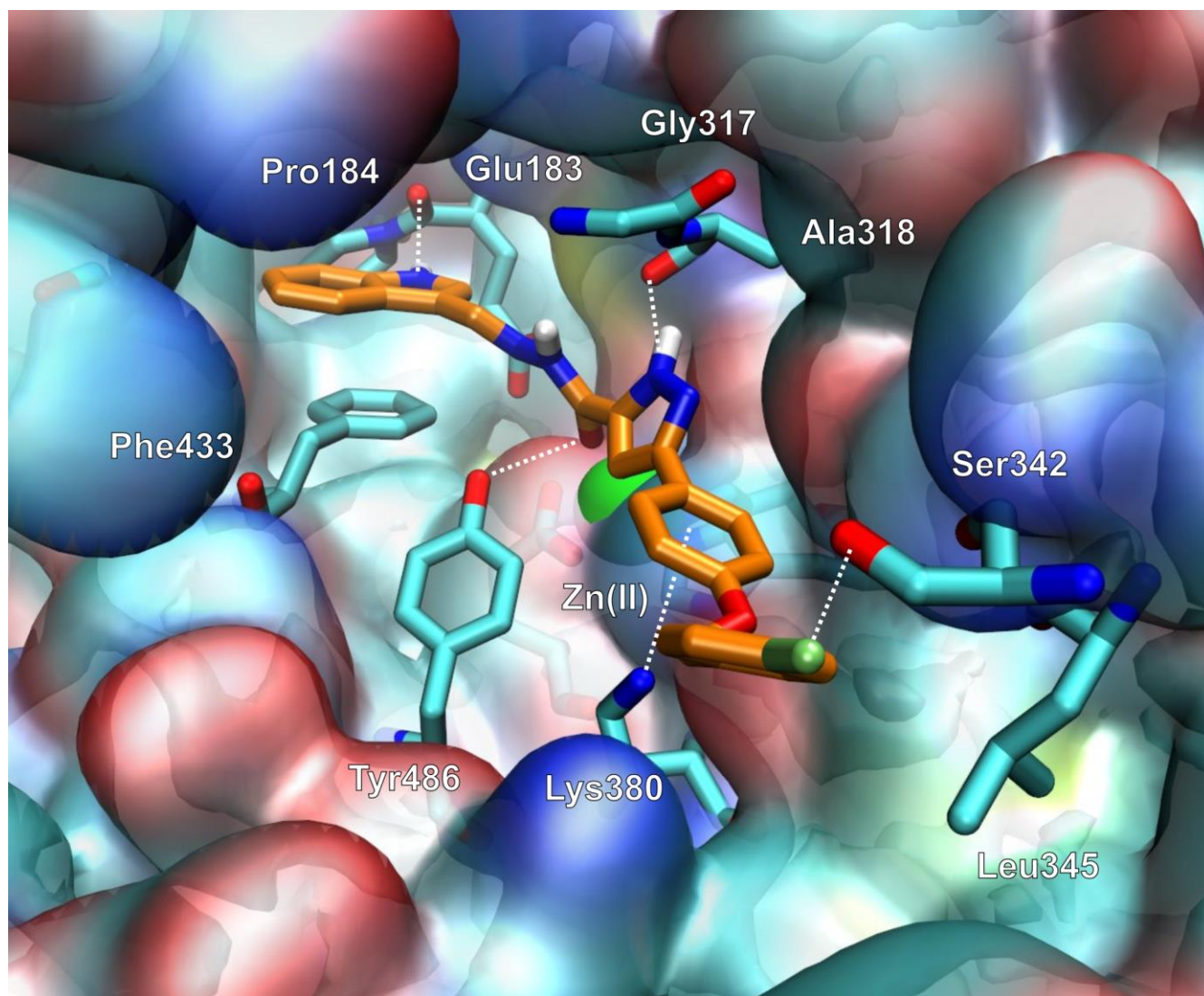


**Figure S2.** Predicted conformation of **6** (orange C atoms) within the substrate binding site of ERAP1, illustrating the interacting residues (cyan C atoms) and the specificity subsites of the enzyme.

The model of ERAP1 complex with thimerosal (**7**) shown in Figure 5 of the manuscript was obtained by docking of the optimized structure of **7** at the B3LYP/6-31G(d) level using Gaussian03.<sup>S20</sup> The Stuttgart/Dresden (SDD) ECP basis set was used for Hg(II).<sup>S21</sup>

## Biochemical Methods

**Materials.** The compounds for the initial screen (Table S3) were purchased from Asinex, ChemBridge and KeyOrganics, the compounds used for the second round of screening were acquired from Ambinter (Table S4), and the compounds selected from the DrugBank (Table S5) and thiosalicylic acid were purchased from Sigma-Aldrich. Thimerosal was also purchased from Applichem (A1278) for verification of the observed activity. L-leucine-7-amido-4-methyl coumarin (L-AMC), L-arginine-7-amido-4-methyl coumarin (R-AMC) and Leucine aminopeptidase (LAP, L5006) were purchased from Sigma-Aldrich. All compounds were of the highest purity available (at least >90% for the screening compounds) and were used without any further purification.

**Recombinant enzyme production and purification.** ERAP1, ERAP2 and IRAP were produced by insect cells in suspension culture (Hi5 cells) after infection with recombinant baculovirus carrying the respective gene with an additional poly-histidine tag fused at the C-terminus for purification purposes. The expression of recombinant ERAP1, ERAP2 and IRAP has been described before.<sup>S22,S23</sup> Briefly, Hi5 insect cells grown in sf900II serum-free medium (Invitrogen), were infected with baculoviruses carrying ERAP1, ERAP2 or IRAP genes and 3–4 days later the cell medium was harvested by centrifugation. The cell supernatant was extensively dialyzed against a 10 mM phosphate buffer pH 8.0 containing 100 mM NaCl. After the dialysis, the supernatant composition was adjusted to 50 mM sodium phosphate pH 8.0, 300 mM sodium chloride and 10 mM imidazole and then mixed with Ni-NTA resin and allowed to bind with mild stirring for 2 h. The slurry was packed to a gravity column and washed. The protein was eluted using a 20–150 mM imidazole step-gradient. The fractions collected were tested for aminopeptidase enzymatic activity, using as substrates L-leucine 7-amido-4-methyl coumarin (L-AMC, Sigma) for ERAP1, IRAP and L-Arginine 7-amido-4-methyl coumarin (R-AMC) for ERAP2 and the enzyme purity was validated with SDS-PAGE. The enzyme-containing fractions were dialyzed against a 10 mM Hepes pH 7.0, 100 mM NaCl buffer and stored as single use aliquots with 10% glycerol at –80°C. The proteins were quantified by SDS-PAGE densitometry, using ImageJ software and known concentration standards.

**Enzymatic assays.** The enzymatic activity of the enzymes was calculated by following the time-dependent increase in fluorescence at 460 nm (excitation was at 380 nm) of the fluorogenic substrates L-leucine-7-amido-4-methyl coumarin (L-AMC) for ERAP1 and IRAP and L-arginine-7-amido-4-methyl coumarin (R-AMC) for ERAP2. All measurements were performed on a TECAN infinite M200

microplate fluorescence reader. For evaluation of the effect of the compound on activity, 20 nM ERAP1, 4 nM ERAP2, or 1 nM IRAP was added to each well along with 50  $\mu$ M substrate and varied concentrations of compound. The reaction was followed for 5–10 min, and activity was calculated by measuring the slope of the time course. For calculation of the in vitro IC<sub>50</sub> values, experimental data were fit to the following equation using the GraphPad Prism software package:

$$Y = \text{bottom} + (\text{top} - \text{bottom}) / (1 + 10^{((\text{LogIC}_{50} - X) \times \text{Hill Slope})})$$

where Y is the enzymatic activity and X is the inhibitor concentration. For the calculation of the IC<sub>50</sub> values of **4,5** and **6**, the parameters “top” and “bottom” were constrained to 1 and 0 respectively. This was necessary due to the lack of experimental data at high concentrations due to limited solubility of the compounds. For the calculation of the IC<sub>50</sub> values of **7** the parameter “bottom” was not constrained since the experimental data suggested that a plateau was achieved at a value above zero.

For analysis of the digestion of the YTAFTIPSI peptide, 10  $\mu$ M of peptide was incubated with 2 nM of ERAP1, in the presence or absence of 1  $\mu$ M of Thimerosal, at 37 °C for 1 h, in a 50 mM Hepes pH 7.0, 100 mM NaCl buffer. The reactions were analyzed in a reverse phase-HPLC (chromolith C-18 column, Merck) by following the absorbance at 220 nm. A linear gradient elution system was used (5%–50% acetonitrile). The percentage of the substrate cleaved was calculated by integration of the area under each peptide peak, using appropriate standards. Specific activity was calculated using the GraphPad software, by fitting the results in a one phase decay equation:  $Y = Y_0 \times e^{(-k \times X)}$ , where X is the reaction time, Y<sub>0</sub> the substrate fraction left intact after t = 0 s (constrained as Y = 1), Y the substrate fraction left intact after the end of the reaction and k the reaction rate constant.

Michaelis-Menten kinetics were performed by measuring the rate of hydrolysis of the chromogenic substrate L-Leucine-p-nitroanilide (L-pNA) for a series of substrate concentration in the presence or absence of thimerosal. The measurements were performed on a TECAN infinite M200 microplate fluorescence reader. The data were fit to a standard Michaelis-Menten model using Graphpad Prism to allow for the calculation of the enzymatic parameter V<sub>max</sub> and K<sub>M</sub> in the presence or absence of thimerosal.

The reversibility experiment was performed on a QuantaMaster 400 (Photon Technology International, Birmingham, NJ). Briefly, 300  $\mu$ M of the fluorogenic substrate L-leucine-7-amido-4-methyl coumarin (L-AMC) were mixed with 150 nM of ERAP1 in the presence or absence of 5  $\mu$ M thimerosal, in a 50

mM Hepes pH 7.0, 100 mM NaCl buffer. The time-dependent increase in fluorescence at 460 nm (excitation was at 380 nm) was followed for 5 min. To measure the recovery of ERAP1 activity the mixture was diluted 100-fold in buffer containing 300  $\mu$ M of L-AMC and the fluorescence was followed for 20 min. Activity was calculated by measuring the slope every 25 s before dilution, 100 s after dilution, and was normalized with the corresponding controls.

### ***In vitro* cross-presentation assay**

BMDCs from 8-10 weeks-old C57Bl/6 JRj ERAP<sup>+/+</sup> and ERAP<sup>-/-</sup> JRj mice that were bred in the animal facility of INSERM U1151 were differentiated from bone marrow progenitors as described before,<sup>S24</sup> and used at day 7. After a pre-incubation of 90 min with DMSO or serial dilutions of thimerosal or thiosalicylic acid, 15,000 BMDCs were incubated with DMSO or an inhibitor for another 3hrs or 18hrs in the presence of a model antigen OVA (500  $\mu$ g/mL) or the control antigen BSA (500  $\mu$ g/mL). Then cells were fixed with a solution of PBS-Glutaraldehyde 0.008% for 30sec, followed by neutralization using PBS-glycine 0.2 M. After 3 washes with PBS, 75,000 CD8+ T cells purified from lymph nodes of a sex-matched OT-I Rag1<sup>-/-</sup> mouse were added per well. After an 18-hour incubation, supernatants were collected and the IL-2 concentration, reflecting CD8+ T cell activation, was measured using a sandwich ELISA.<sup>S25</sup> The optical density measured for wells containing BMDCs incubated with BSA was used to define the background and subtracted from all values. Toxicity of inhibitors on BMDCs was evaluated by determining the percentage of dead cells using a 7-Actinomycin D (7-AAD, BD Biosciences) assay and the BD LSR Fortessa FACS analyzer.



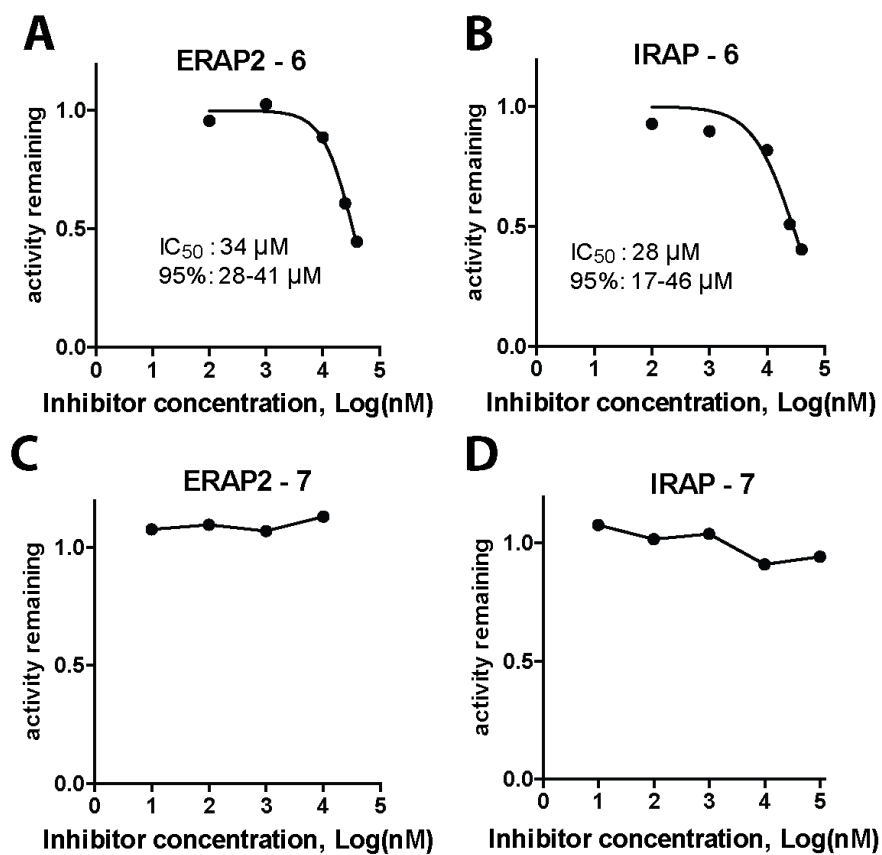


**Figure S3.** Representative titrations showing the ability of selected compounds to inhibit the ability of ERAP2 and IRAP to hydrolyze the fluorogenic substrate L-arginine-7-amino-4-methylcoumarin (for ERAP2) or L-leucine-7-amino-4-methylcoumarin (for IRAP). Calculated IC<sub>50</sub> values and 95% confidence intervals are indicated.

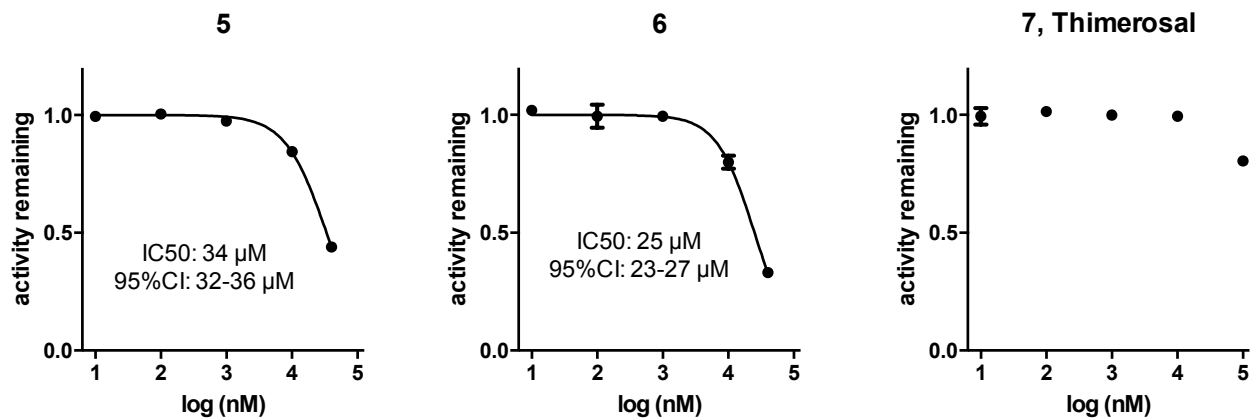


**Figure S4.** Effect of compounds **5**, **6** and **7** on the activity of Leucine-aminopeptidase (LAP).

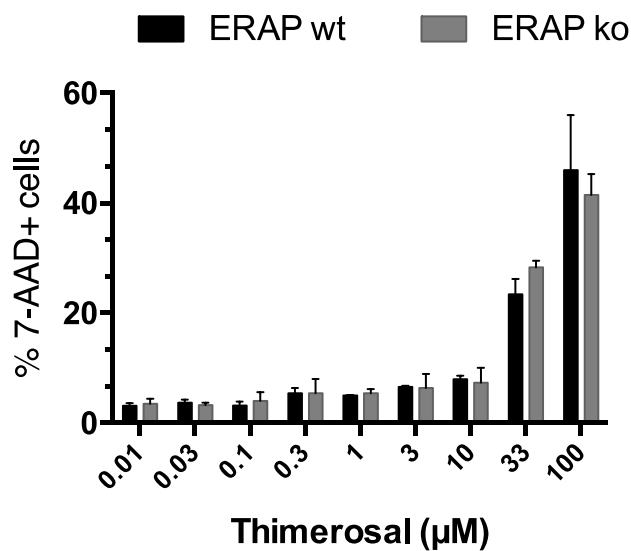


**Figure S5:** Toxicity assay of thimerosal on murine BMDCs. ERAP<sup>+/+</sup> and ERAP<sup>-/-</sup> BMDCs were incubated with increasing concentrations of thimerosal for 3 h before the addition of 7-AAD; cell death was evaluated by FACS, by determining the percentage of 7-AAD<sup>+</sup> cells. Histograms show the mean of duplicates collected in one representative out of two independent experiments.

## Supporting References

- (S1) [http://www.asinex.com/libraries\\_gold\\_platinum.html](http://www.asinex.com/libraries_gold_platinum.html)
- (S2) [http://www.chembridge.com/screening\\_libraries/diversity\\_libraries/diverset/](http://www.chembridge.com/screening_libraries/diversity_libraries/diverset/)
- (S3) <http://www.keyorganics.net/services/bionet-products/screening-compounds/>
- (S4) <http://www.myriascreeen.com/>
- (S5) Lipinski, C.A.; Lombardo, F.; Dominy, B.W.; Feeney, P.J. Experimental and computational approaches to estimate solubility and permeability in drug discovery and development settings". *Adv Drug Deliv Rev* **2001**, *46*, 3–26
- (S6) <https://wiki.nci.nih.gov/display/NCIDTPdata/Compound+Sets>
- (S7) Knox, C.; Law, V.; Jewison, T. et al. DrugBank 3.0: a comprehensive resource for “Omics” research on drugs. *Nucleic Acids Res* **2011**, *39*, D1035–D1041.
- (S8) Hawkins, P.C.D.; Skillman, A.G.; Warren, G.L.; Ellingson, B.A.; Stahl, M.T. Conformer Generation with OMEGA: Algorithm and Validation Using High Quality Structures from the Protein Databank and the Cambridge Structural Database. *J. Chem. Inf. Model* **2010**, *50*, 572–584.
- (S9) Sanner, M. F. Python: a programming language for software integration and development. *J Mol Graph Model* **1999**, *17*, 57–61.
- (S10) Trott, O.; Olson, A. J. AutoDock Vina: improving the speed and accuracy of docking with a new scoring function, efficient optimization, and multithreading. *J Comput Chem* **2010**, *31*, 455–461.
- (S11) Kochan, G.; Krojer, T.; Harvey, D.; Fischer, R.; Chen, L.; Vollmar, M.; von Delft, F.; Kavanagh, K. L.; Brown, M. A.; Bowness, P.; Wordsworth, P.; Kessler, B. M.; Oppermann, U. Crystal structures of the endoplasmic reticulum aminopeptidase-1 (ERAP1) reveal the molecular basis for N-terminal peptide trimming. *Proc Natl Acad Sci USA* **2011**, *108*, 7745–7750.
- (S12) Zervoudi, E.; Saridakis, E.; Birtley, J. R.; Seregin, S. S.; Reeves, E.; Kokkala, P.; Aldhamen, Y. A.; Amalfitano, A.; Mavridis, I. M.; James, E.; Georgiadis, D.; Stratikos, E. Rationally designed inhibitor targeting antigen-trimming aminopeptidases enhances antigen presentation and cytotoxic T-cell responses. *Proc Natl Acad Sci U S A* **2013**, *110*, 19890–19895.
- (S13) Irwin, J. J.; Sterling, T.; Mysinger, M. M.; Bolstad, E. S.; Coleman, R. G. ZINC: a free tool to discover chemistry for biology. *J Chem Inf Model* **2012**, *52*, 1757–1768.
- (S14) Koes, D. R.; Camacho, C. J. ZINCPharmer: pharmacophore search of the ZINC database. *Nucleic Acids Res* **2012**, *40*, W409–414.

- (S15) Fiser, A.; Sali, A. MODELLER: Generation and refinement of homology-based protein structure models, *Macromolecular Crystallography. Methods Enzymol* **2003**, *374*, 461–491.
- (S16) Anandakrishnan, R.; Aguilar, B.; Onufriev, A.V. H++ 3.0: automating pK prediction and the preparation of biomolecular structures for atomistic molecular modeling and simulations, *Nucleic Acids Res* **2012**, *40*, W537–541.
- (S17) Morris, G. M.; Huey, R.; Lindstrom, W.; Sanner, M. F.; Belew, R. K.; Goodsell, D. S.; Olson, A. J. Autodock4 and AutoDockTools4: automated docking with selective receptor flexibility. *J Comput Chem* **2009**, *16*, 2785–2791.
- (S18) Humphrey, W.; Dalke, A.; Schulten, K. VMD: visual molecular dynamics. *J Mol Graph* **1996**, *14*, 33–38.
- (S19) Marvin 5.7, 2012, ChemAxon, <http://www.chemaxon.com>
- (S20) Gaussian 03, Revision D.01, M. J. Frisch, G. W. Trucks, H. B. Schlegel, G. E. Scuseria, M. A. Robb, J. R. Cheeseman, J. A. Montgomery, Jr., T. Vreven, K. N. Kudin, J. C. Burant, J. M. Millam, S. S. Iyengar, J. Tomasi, V. Barone, B. Mennucci, M. Cossi, G. Scalmani, N. Rega, G. A. Petersson, H. Nakatsuji, M. Hada, M. Ehara, K. Toyota, R. Fukuda, J. Hasegawa, M. Ishida, T. Nakajima, Y. Honda, O. Kitao, H. Nakai, M. Klene, X. Li, J. E. Knox, H. P. Hratchian, J. B. Cross, V. Bakken, C. Adamo, J. Jaramillo, R. Gomperts, R. E. Stratmann, O. Yazyev, A. J. Austin, R. Cammi, C. Pomelli, J. W. Ochterski, P. Y. Ayala, K. Morokuma, G. A. Voth, P. Salvador, J. J. Dannenberg, V. G. Zakrzewski, S. Dapprich, A. D. Daniels, M. C. Strain, O. Farkas, D. K. Malick, A. D. Rabuck, K. Raghavachari, J. B. Foresman, J. V. Ortiz, Q. Cui, A. G. Baboul, S. Clifford, J. Cioslowski, B. B. Stefanov, G. Liu, A. Liashenko, P. Piskorz, I. Komaromi, R. L. Martin, D. J. Fox, T. Keith, M. A. Al-Laham, C. Y. Peng, A. Nanayakkara, M. Challacombe, P. M. W. Gill, B. Johnson, W. Chen, M. W. Wong, C. Gonzalez, and J. A. Pople, Gaussian, Inc., Wallingford CT, 2004.
- (S21) Häussermann, U.; Dolg, M.; Stoll, H.; Preuss, H.; Schwerdtfeger, P., Pitzer R. M. Accuracy of energy-adjusted quasirelativistic ab initio pseudopotentials. *Mol Phys* **1993**, *78*, 1211–1224.
- (S22) Zervoudi, E.; Papakyriakou, A.; Georgiadou, D.; Evnouchidou, I.; Gajda, A.; Poreba, M.; Salvesen, G. S.; Drag, M.; Hattori, A.; Swevers, L.; Vourloumis, D.; Stratikos, E. Probing the S1 specificity pocket of the aminopeptidases that generate antigenic peptides. *Biochem J* **2011**, *435*, 411–420.
- (S23) Mpakali, A.; Saridakis, E.; Harlos, K.; Zhao, Y.; Papakyriakou, A.; Kokkala, P.; Georgiadis, D.; Stratikos, E. Crystal Structure of Insulin-Regulated Aminopeptidase with Bound Substrate Analogue

Provides Insight on Antigenic Epitope Precursor Recognition and Processing. *J Immunol* **2015**, *195*, 2842-2851.

(S24) Weimershaus M, van Endert P. Preparation of dendritic cells by in vitro cultures. *Methods Mol Biol*, **2013**;960:351-7.

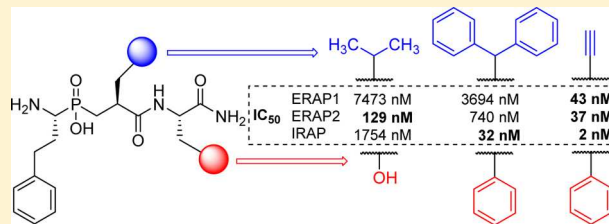
(S25) Merzougui N, Kratzer R, Saveanu L, van Endert P. A proteasome-dependent, TAP-independent pathway for cross-presentation of phagocytosed antigen. *EMBO reports*, **2011**;12:1257-64.

## Optimization and Structure–Activity Relationships of Phosphinic Pseudotriptide Inhibitors of Aminopeptidases That Generate Antigenic Peptides

Paraskevi Kokkala,<sup>†</sup> Anastasia Mpakali,<sup>‡</sup> Francois-Xavier Mauvais,<sup>§</sup> Athanasios Papakyriakou,<sup>‡</sup> Ira Daskalaki,<sup>†</sup> Ioanna Petropoulou,<sup>†</sup> Sofia Kavvalou,<sup>†</sup> Mirto Papatanasopoulou,<sup>†</sup> Stefanos Agrotis,<sup>†</sup> Theodora-Markisia Fonsou,<sup>†</sup> Peter van Endert,<sup>§</sup> Efstratios Stratikos,<sup>\*,‡</sup> and Dimitris Georgiadis<sup>\*,†</sup><sup>†</sup>Laboratory of Organic Chemistry, Department of Chemistry, National and Kapodistrian University of Athens, Panepistimiopolis, Zografou, 15771, Athens, Greece<sup>‡</sup>National Center for Scientific Research “Demokritos”, GR 15310 Agia Paraskevi, Attikis, Greece<sup>§</sup>Institut National de la Santé et de la Recherche Médicale, Unité 1151, Université Paris Descartes, Sorbonne Paris Cité, Centre National de la Recherche Scientifique, Unité 8253, 75015 Paris, France

## Supporting Information

**ABSTRACT:** The oxytocinase subfamily of M1 aminopeptidases, consisting of ER aminopeptidase 1 (ERAP1), ER aminopeptidase 2 (ERAP2), and insulin-regulated aminopeptidase (IRAP), plays critical roles in the generation of antigenic peptides and indirectly regulates human adaptive immune responses. We have previously demonstrated that phosphinic pseudotriptides can constitute potent inhibitors of this group of enzymes. In this study, we used synthetic methodologies able to furnish a series of stereochemically defined phosphinic pseudotriptides and demonstrate that side chains at P<sub>1</sub>' and P<sub>2</sub>' positions are critical determinants in driving potency and selectivity. We identified low nanomolar inhibitors of ERAP2 and IRAP that display selectivity of more than 2 and 3 orders of magnitude, respectively. Cellular analysis demonstrated that one of the compounds that is a selective IRAP inhibitor can reduce IRAP-dependent but not ERAP1-dependent cross-presentation by dendritic cells with nanomolar efficacy. Our results encourage further preclinical development of phosphinic pseudotriptides as regulators of adaptive immune responses.



## INTRODUCTION

Antigen processing aminopeptidases (APAs) trim antigenic peptide precursors and generate peptides for binding onto major histocompatibility complex class I (MHCI) molecules.<sup>1</sup> The peptide–MHCI complex is then transported to the cell surface of somatic cells and presented to circulating T lymphocytes. Interactions between specialized T-cell receptors and peptide–MHCI complexes are used to determine if the cell is infected or otherwise aberrant, initiating biochemical cascades that lead to apoptosis.<sup>2</sup> Three major APAs have been identified to date: ER aminopeptidase 1 (ERAP1), ER aminopeptidase 2 (ERAP2), and insulin-regulated aminopeptidase (IRAP).<sup>3</sup> The first two are localized in the ER and trim antigenic peptide precursors translocated into the ER but generated in the cytosol.<sup>2</sup> IRAP trims antigenic peptide precursor generated by endocytosed proteins in dendritic cells for cross-presentation.<sup>4</sup> These three enzymes are highly homologous (50% sequence identity on average) and have conserved active sites, although key amino acid differences defining the specificity pockets can account for different substrate preferences.<sup>5</sup> Structural differences between the three enzymes also include a unique orientation of the GAMEN motif in IRAP<sup>5b</sup> and an overall

conformational change that reorganizes the structure from an open to a closed form, affecting the folding of the active site and nearby specificity pockets.<sup>6</sup>

The enzymatic activity and expression level of APAs, frequently affected by polymorphic variation, has been repeatedly associated with predisposition to autoimmunity, infections, and cancer immune evasion.<sup>7</sup> Functional studies have established that alterations in the enzymatic activity of APAs can result in changes in the presented antigenic peptides and concomitant cytotoxic responses by T-cells.<sup>8</sup> Furthermore, the activity of ERAP1 has been also linked to the function of innate immune responses.<sup>9</sup> Accumulating evidence has therefore established the tractability of these enzymes as pharmaceutical targets for the regulation of immune responses.<sup>10</sup>

We have previously demonstrated that a phosphinic pseudotriptide, **6e** (DG013A), can act as a highly potent inhibitor of all three APAs and is able to regulate antigen presentation in cellular systems (Figure 1).<sup>11</sup> This nanomolar

Received: July 12, 2016

Published: September 8, 2016

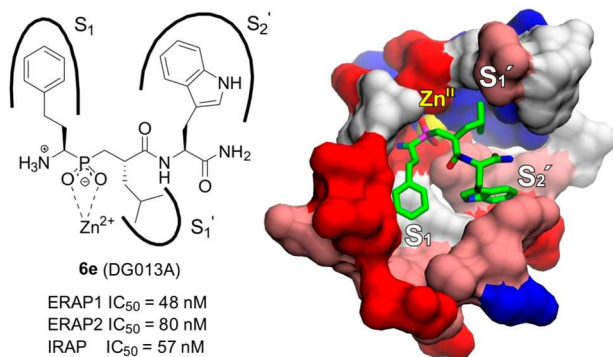


**Figure 1.** Structure, in vitro inhibition data, and schematic representation of **6e** in the active site of ERAP2 (PDB code 4JBS), illustrating the three interacting subsites that are color-coded per residue type (white, nonpolar; pink, polar; red, acidic; blue, basic). The inhibitor is shown as sticks with green C, blue N, red O, magenta P, and the catalytic Zn(II) as a yellow sphere.

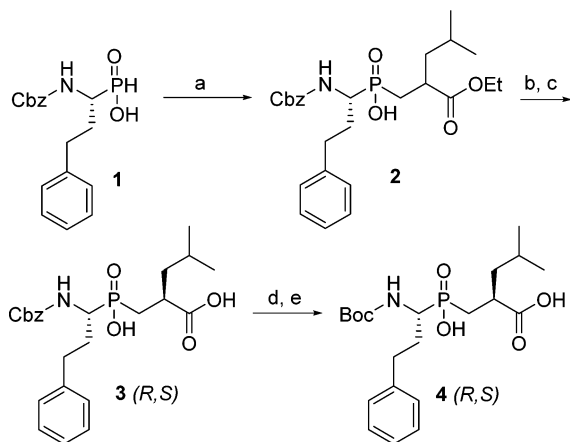
potency inhibitor was shown to be able to enhance anticancer cytotoxic responses and to down-regulate T-cell mediated and innate inflammatory responses, indicating that this class of compounds holds promise for pharmaceutical applications.<sup>11,12</sup> Low selectivity between the three APAs, however, limits options for preclinical development. However, since this inhibitor utilizes the three first specificity pockets of these aminopeptidases, as it was revealed by X-ray crystallographic analysis of **6e**/ERAP2 complex (Figure 1),<sup>11</sup> varying the side chains that occupy these pockets can be a valid approach for optimizing both selectivity and potency. The ability of phosphinic pseudopeptides to successfully discriminate active sites with high structural homology and functional similarity has been well-demonstrated in several demanding cases in the past, such as the development of domain-selective inhibitors of angiotensin-converting enzyme<sup>13</sup> and a selective subnanomolar inhibitor of MMP-12.<sup>14</sup> This property of phosphinic peptides, as compared to other classes of protease inhibitors, is attributed to the weak zinc-binding ability of phosphinic group which allows for inhibitor affinity to be determined by proper optimization of weaker but more specific enzyme–ligand interactions and not by the dominance of tight chelating interactions with the zinc ion.<sup>15</sup>

In this study, we focused on the structure–activity relationships (SAR) of P<sub>1</sub>' and P<sub>2</sub>' side chains in driving potency and selectivity for APAs, by synthesizing a series of stereochemically defined phosphinic pseudotriptide derivatives. In vitro evaluation and molecular modeling revealed that while aromatic residues at P<sub>2</sub>' position are critical for achieving potency for ERAP1, hydrophilic residues at the same site can enhance selectivity for ERAP2. Conversely, although small P<sub>1</sub>' side chains are important for achieving potency, bulkier groups can be well tolerated only by IRAP resulting in selective inhibitors. We identified several new nanomolar-affinity selective inhibitors for ERAP2 and IRAP that displayed selectivity for each enzyme of over 2 and 3 orders of magnitude, respectively. Proof-of-concept cellular analysis using a cross-presentation model system indicated that one of the selective IRAP inhibitors can reduce IRAP-dependent but not ERAP1-dependent cross-presentation by dendritic cells with nanomolar efficacy. Our results encourage further preclinical development of phosphinic pseudotriptides for therapeutic applications.

## RESULTS AND DISCUSSION

**Inhibitor Design.** In previous studies, it has been demonstrated that **6e** influences with high efficacy antigen presentation in several cell-based systems. For this reason, we were based on the core structure of **6e** and used it as a template for screening various modifications at P<sub>1</sub>' and P<sub>2</sub>' positions, aiming to enhance potency and selectivity. The factor of stereochemical purity was set as a priority, even though available synthetic possibilities to achieve this goal are extremely limited.<sup>16</sup> This requirement can be critical for the accurate evaluation of structure–activity relationships and the discovery of improved inhibitors, especially in terms of selectivity. Interestingly, inversion of the selectivity exhibited by different diastereoisomers has been recently highlighted in the case of phosphinic tripeptide inhibitors of neprilysin (NEP) and endothelin-converting enzyme (ECE-1).<sup>17</sup> In a noteworthy example from this report, the 20-fold selectivity for NEP achieved by using a mixture of P<sub>1</sub>'-epimers of a phosphinic tripeptide dropped down to a 5-fold selectivity for NEP when the “natural” P<sub>1</sub>'-epimer was employed, and this was inverted to a 500-fold selectivity for ECE-1 when the “unnatural” P<sub>1</sub>'-epimer was examined. Notably, most of the studies related to phosphinic peptide inhibitors of Zn aminopeptidases involve evaluation of diastereoisomeric mixtures,<sup>18</sup> with only a few exceptions.<sup>19</sup> To our knowledge, in the only relevant systematic study a large selection of stereochemically pure phosphinic tripeptides was evaluated but all of them were isolated after separation by RP-HPLC of the final diastereoisomeric mixtures of inhibitors.<sup>19a</sup> In our case, considering the 2–3 orders of magnitude difference in affinity between two different diastereoisomers of **6e** (epimers at P<sub>1</sub>' position, **6e** and **6e'**)<sup>11</sup> and with the aim to eliminate possible inaccuracies during SAR analysis, we devised appropriately adjusted synthetic plans to control the stereochemical purity and identity of final compounds. Most of the inhibitors presented herein were obtained as single diastereoisomers directly from the synthesis, using late-stage diversification approaches on stereochemically pure building blocks. In order to explore the S<sub>1</sub>' cavity of target aminopeptidases, we based our synthesis on a well-studied postmodification protocol of phosphinic peptides, which has been developed several years ago in our laboratory.<sup>20</sup> This strategy affords diverse, linear isoxazole-substituted P<sub>1</sub>' side chains and has been successfully applied in the past to the discovery of inhibitors for other families of Zn metalloproteases<sup>14,17a,21</sup> but not for aminopeptidases. Finally, nonlinear P<sub>1</sub>' substitutions were pursued in order to estimate the effect of expanding the bulk of side chains toward more than one direction. This differentiation in the spatial installation of bulky groups at P<sub>1</sub>' position revealed significant variations between inhibitors with linear “extended” and nonlinear “expanded” P<sub>1</sub>' side chains, as it will be discussed below.

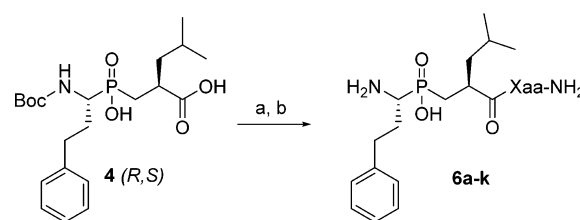
**Chemistry.** For the synthesis of compounds **6a–k**, our efforts were focused on the preparation of parent phosphinic building block **4** in a stereochemically pure form (Scheme 1). Stereochemical purity was considered essential during our design in order to extract accurate structure–activity relationships that would eventually reveal the structural determinants responsible for high potency and selectivity. Given the lack of general synthetic methods able to provide stereochemical control during the formation of P<sub>1</sub>' stereogenic center of phosphinic peptides,<sup>15</sup> we explored the possibility of resolving diastereoisomeric mixtures by selective crystallization, a

Scheme 1. Synthesis of Phosphinic Building Block 4<sup>a</sup>

<sup>a</sup>Reagents and conditions: (a) HMDS,  $\text{H}_2\text{C}=\text{C}[\text{CH}_2\text{CH}(\text{CH}_3)_2]\text{COOEt}$ , 110 °C, 1 h, then 90 °C, 3 h, then EtOH, 70 °C, 30 min; (b) NaOH, EtOH,  $\text{H}_2\text{O}$ , rt, 24 h, then  $\text{H}_3\text{O}^+$ ; (c) 2× recrystallizations by AcOEt, 46%, three steps; (d) HBr/AcOH 33%, rt, 1 h; (e)  $\text{Boc}_2\text{O}$ ,  $\text{Et}_3\text{N}$ , DMF, rt, 24 h, 92%, two steps.

technique that has previously succeeded in several cases of phosphinic dipeptide and tripeptide isomers.<sup>17a,20,22</sup> In this regard, the preparation of enantiomerically pure amino-phosphinic acid **1** by a scalable method was an absolute requirement for accomplishing our goal. It has been previously described in the literature that optically pure **1** can be obtained by HPLC enantiomeric separation of the corresponding racemic mixture;<sup>23</sup> however this approach is limited to milligram quantities.<sup>19b</sup> In contrast with earlier reports,<sup>19b</sup> we were pleased to find that resolution of diastereoisomeric salts of racemic **1** with (*S*)-(-)- $\alpha$ -methylbenzylamine by crystallization, following the protocol of Baylis et al., was highly efficient.<sup>24</sup> By this procedure, the levorotatory (*R*)-isomer (**1**)<sup>23</sup> [salt with (*S*)-(-)-amine,  $[\alpha]_{\text{D}}^{20} -22.3$  (*c* 1, EtOH); free acid,  $[\alpha]_{\text{D}}^{20} -35.7$  (*c* 1, EtOH)] was successfully isolated in a multigram quantities. P-Michael addition of **1** to ethyl 4-methyl-2-methylenepentanoate<sup>25</sup> using silylating conditions afforded **2** as a mixture of two diastereoisomers in nearly equimolar ratio (Scheme 1). All attempts of diastereoisomeric separation by crystallization at this stage failed; therefore compound **2** was subjected to saponification and crystallization efforts were repeated at racemic diacid **3**. Two recrystallizations by ethyl acetate proved sufficient for the gram-scale isolation of the less soluble **3** (*R,S*) isomer with *dr* > 95%, as determined by <sup>31</sup>P NMR. Finally, the Cbz group was exchanged by Boc following a two-step procedure. This exchange was considered necessary due to the advantageous behavior of Boc group during the final deprotection of target tripeptides, as compared to the Cbz group.

With the stereochemically pure building block **4** in hand, the synthesis of inhibitors **6a–k** required a coupling protocol that does not involve prior protection of the hydroxyphosphinyl moiety. In this regard, we employed a previously described, epimerization-free protocol based on the EDC/HOBt coupling system (Scheme 2).<sup>20,22a</sup> During optimization, high concentrations (0.5 mmol of substrate/1 mL of solvent) were found to be essential for efficient coupling reactions. Aiming to reach the final tripeptides **6a–k** in a single deprotection step, amino acid carboxamides **5a–k** with acid-labile protecting groups (if necessary) were employed (see Supporting Information for

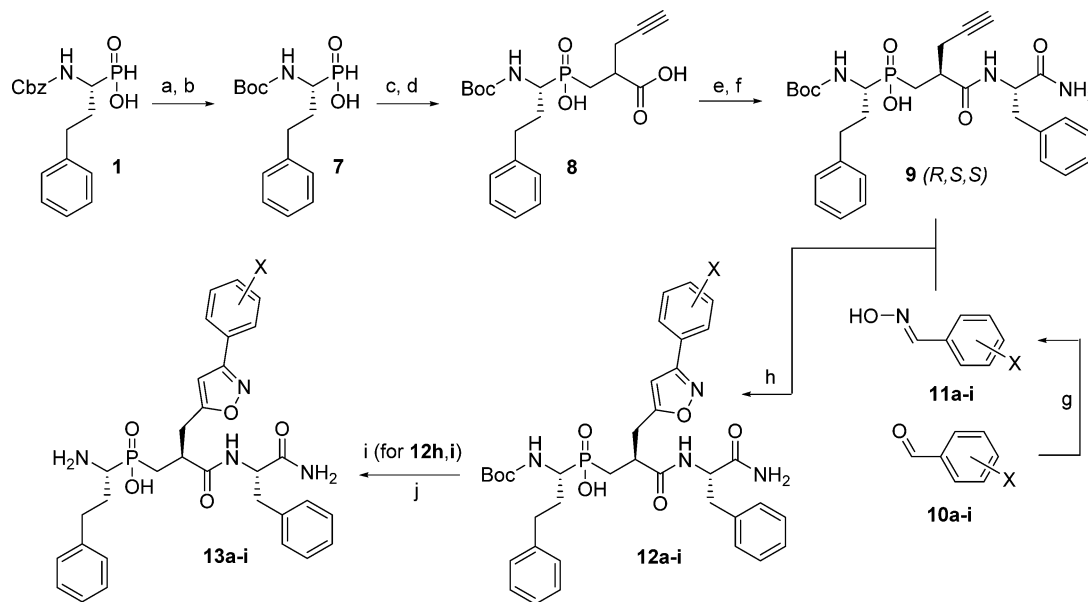
Scheme 2. Synthesis of P<sub>2</sub>' Diversified Phosphinic Pseudotriptide Inhibitors **6a–k**<sup>a</sup>

<sup>a</sup>Reagents and conditions: (a) H-Xaa-NH<sub>2</sub> (**5a–k**), [Xaa for **5a**: L-Ala. **5b**: L-Leu. **5c**: L-Phe. **5d**: L-Pro. **5e**: L-Trp. **5f**: L-Tyr(*t*-Bu). **5g**: L-Ser(TBS). **5h**: L-Lys(Boc). **5i**: L-His(Boc). **5j**: L-Glu(*t*-Bu). **5k**: D-Phe], EDC·HCl, HOBt, DIPEA,  $\text{CH}_2\text{Cl}_2$ , rt, 2–4 h; (b) TFA/ $\text{CH}_2\text{Cl}_2$ /TIS/ $\text{H}_2\text{O}$  48:49:2:1, rt, 2 h, [yields for two steps, for **6a** (L-Ala): 65%. **6b** (L-Leu): 59%. **6c** (L-Phe): 32%. **6d** (L-Pro): 41%. **6e** (L-Trp): 32%. **6f** (L-Tyr): 55%. **6g** (L-Ser): 43%. **6h** (L-Lys): 56%. **6i** (L-His): 10%. **6j** (L-Glu): 52%. **6k** (D-Phe): 31%].

experimental details). Compound **6e** obtained by this procedure was found to be spectroscopically and chromatographically identical to previously described inhibitor **6e** (whose stereochemistry was confirmed by X-ray crystallographic analysis),<sup>11</sup> which confirms both the stereochemical purity and identity of building block **4** used for the synthesis of inhibitors of type **6**.

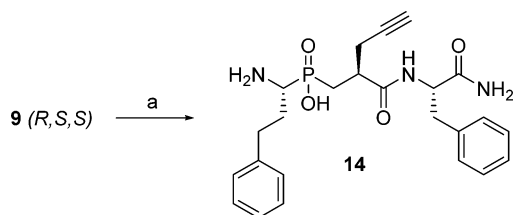
For the structural diversification of P<sub>1</sub>' position of phosphinic tripeptides, we employed a postmodification protocol<sup>20</sup> that has been successfully used in the past to the development of important inhibitors of various Zn metalloproteases.<sup>14,17a,21</sup> This protocol involves the application of a 1,3-dipolar cycloaddition reaction (1,3-DCR) between readily accessible nitrile oxides and an appropriate dipolarophilic precursor, such as tripeptide **9**, bearing a propargyl chain in P<sub>1</sub>' position (Scheme 3). The synthesis of stereochemically pure precursors of similar type has been described by our group in the past;<sup>20</sup> therefore we decided to apply this chemistry to the preparation of compound **9**. Phosphinic acid **7** [ $[\alpha]_{\text{D}}^{20} -41.3$  (*c* 1, EtOH)] was prepared based on literature protocols<sup>26</sup> and subjected to a P-Michael addition with ethyl 2-methylenepent-4-ynoate as the electrophile. In accordance to previous observations,<sup>17a,20</sup> the reaction proceeded with a significant degree of diastereoselectivity (*dr* ≈ 2:1, based on <sup>31</sup>P NMR). Saponification and coupling of the resulting diacid **8** with phenylalanine carboxamide **5c** afforded **9** which allowed the efficient isolation of the major isomer **9** (*R,S,S*) after two recrystallizations by ethyl acetate in satisfactory overall yield. This stereochemically pure building block afforded inhibitors **13a–i** after application of the one-pot Huisgen protocol,<sup>20</sup> which involves the use of *N*-chlorosuccinimide (NCS) as an oxidant for the in situ generation of necessary nitrile oxides from the corresponding oximes,<sup>27</sup> and final acidic deprotection. Compound **13a** was resynthesized as a mixture of two epimers at P<sub>1</sub>', **13a** (*R,S,S*) and **13a'** (*R,R,S*), by using the corresponding diastereoisomeric mixture of **9**. Inhibitor **13a** obtained from the stereocontrolled synthesis corresponds to the first RP-HPLC eluted isomer of the diastereoisomeric mixture obtained from the nonstereocontrolled synthesis. On the basis of previous studies which correlate the stereochemical configuration of P<sub>1</sub>' position of phosphinic peptides with their elution order in RP-HPLC,<sup>17a,19a,20</sup> this is a strong indication of the *R,S,S* stereochemical assignment for propargylic precursor **9**. This was further supported after isolation of the two isomers by



Scheme 3. Synthesis of P<sub>1</sub>' Isoxazole-Diversified Phosphinic Pseudotriptide Inhibitors 13a–i<sup>a</sup>

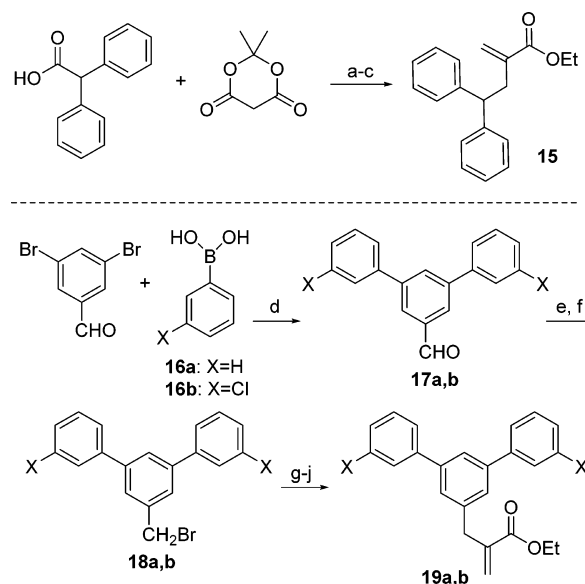
<sup>a</sup>Reagents and conditions: (a) 33% HBr/AcOH, rt, 1 h; (b) Boc<sub>2</sub>O, Et<sub>3</sub>N, DMF, rt, 24 h, 89%, two steps; (c) HMDS, H<sub>2</sub>C=C(CH<sub>2</sub>C≡CH)COOEt, 110 °C, 1 h, then 90 °C, 3 h, then EtOH, 70 °C, 30 min; (d) NaOH, MeOH, H<sub>2</sub>O, rt, 24 h, then H<sub>3</sub>O<sup>+</sup>, 99%, two steps; (e) HBr·H-Phe-NH<sub>2</sub> (5c), EDC·HCl, HOBT, DIPEA, CH<sub>2</sub>Cl<sub>2</sub>, rt, 2 h; (f) recrystallization by AcOEt, 41%, two steps. (g) 10a–i (X for 10a: H. 10b: *o*-OMe. 10c: *m*-OMe. 10d: *p*-OMe. 10e: *o*-Cl. 10f: *m*-Cl. 10g: *p*-Cl. 10h: *o*-OTBS. 10i: *p*-OTBS). HCl·H<sub>2</sub>NOH, CH<sub>3</sub>COONa, MeOH, H<sub>2</sub>O, rt, 24 h, 85–95%; (h) 11, NCS, pyridine (cat.), CHCl<sub>3</sub>, 45 °C, 3–4 h, then 9, Et<sub>3</sub>N, 45 °C, 3 d, 1–6 repetitions; (i) Cs<sub>2</sub>CO<sub>3</sub>, DMF/H<sub>2</sub>O, rt, 2–3 d; (j) TFA/CH<sub>2</sub>Cl<sub>2</sub>/TIS/H<sub>2</sub>O 48:49:2:1, rt, 2 h, two steps. For 13a: 80%. 13b: 85%. 13c: 75%. 13d: 76%. 13e: 73%. 13f: 67%. 13g: 66%. 13h (X = *o*-OH, three steps): 51%. 13i (X = *p*-OH, three steps): 61%.

semipreparative RP-HPLC and evaluation of the inhibitory potency of individual isomers. Inhibition values showed that the first-eluted RP-HPLC-eluted isomer (13a) was 1–2 orders of magnitude more potent than its *R,R,S*-epimer (13a') toward all aminopeptidases, a profile that is consistent with the higher potency observed for 6e (possessing the stereochemical configuration of a natural substrate) as compared to its *R,R,S*-epimer 6e'. Finally, inhibitor 14 was obtained by cleavage of the Boc group from 9, using standard acidic deprotection conditions (Scheme 4).

Scheme 4. Synthesis of Phosphinic Inhibitor 14<sup>a</sup>

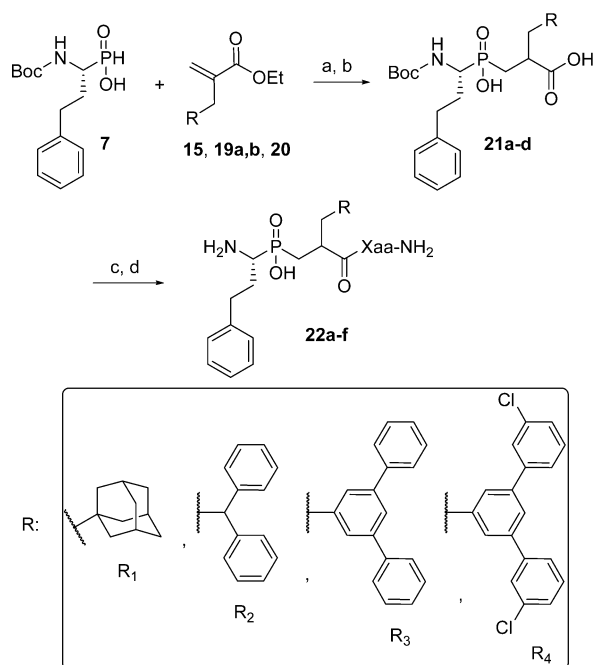
<sup>a</sup>Reagents and conditions: (a) TFA/CH<sub>2</sub>Cl<sub>2</sub>/TIS/H<sub>2</sub>O 48:49:2:1, rt, 2 h, 87%.

Next, we proceeded to the synthesis of compounds 22a–f, according to the general synthetic strategy outlined in Scheme 6. In particular, the synthesis of acrylic derivatives 15 and 19a,b was initially performed as it is described in Scheme 5 (adamantyl-substituted acrylic ester 20 was prepared according to literature procedures<sup>28</sup>). Benzhydryl derivative 15 was prepared in good yield according to the protocol of Hin et al. which involves DCC-mediated coupling of 2,2-diphenylacetic acid with Meldrum's acid, reduction of the resulting enol,

Scheme 5. Synthesis of Acrylic Esters 15 and 19a,b<sup>a</sup>

<sup>a</sup>Reagents and conditions: (a) DCC, DMAP, CH<sub>2</sub>Cl<sub>2</sub>, rt, 3 h; (b) NaBH<sub>4</sub>, AcOH, CH<sub>2</sub>Cl<sub>2</sub>, rt, 24 h, 49%, two steps; (c) [(CH<sub>3</sub>)<sub>2</sub>N=CH<sub>2</sub>]<sub>2</sub>I, THF, EtOH, 65 °C, 24 h, 93%; (d) 16a/16b Pd(PPh<sub>3</sub>)<sub>4</sub>, Na<sub>2</sub>CO<sub>3</sub>, DME, H<sub>2</sub>O, 24 h. For 17a: 98%. 17b: 82%. (e) NaBH<sub>4</sub>, EtOH, rt, 1.5 h; (f) PBr<sub>3</sub>, CH<sub>2</sub>Cl<sub>2</sub>, rt, 1 h, two steps. For 18a: 91%. 18b: 81%. (g) HC(CO<sub>2</sub>Et)<sub>3</sub>, K<sub>2</sub>CO<sub>3</sub>, DMF/toluene, reflux, 1.5 h; (h) KOH, EtOH, rt, 24 h; (i) (HCHO)<sub>n</sub>, Et<sub>2</sub>NH, AcOEt, reflux, 4 h; (j) EtOH, EDC·HCl, DMAP, DIPEA, CH<sub>2</sub>Cl<sub>2</sub>, rt, 24 h, four steps. For 19a: 56%. 19b: 25%.

and final Mannich reaction using Eschenmosher's salt and EtOH as a scavenger of the ketene intermediate.<sup>29</sup> For the

Scheme 6. Synthesis of P<sub>1</sub>' Diversified Phosphinic Pseudotriptide Inhibitors 22a–f<sup>a</sup>

<sup>a</sup>Reagents and conditions: (a) HMDS, acrylic ester **15** or **19a,b** or **20** (R = 1-Ad), 110 °C, 1 h, then 90 °C, 3 h, then EtOH, 70 °C, 30 min; (b) NaOH, EtOH, H<sub>2</sub>O, rt, 24 h, then H<sub>3</sub>O<sup>+</sup>, two steps. For **21a** (R = R<sub>1</sub>): 79%. **21b** (R = R<sub>2</sub>): 61%. **21c** (R = R<sub>3</sub>): 88%. **21d** (R = R<sub>4</sub>): 87%. (c) HBr-H-(L)Leu-NH<sub>2</sub> (**5b**) or HBr-H-(L)Phe-NH<sub>2</sub> (**5c**), EDC-HCl, HOBT, DIPEA, CH<sub>2</sub>Cl<sub>2</sub>, rt, 2–4 h; (b) TFA/CH<sub>2</sub>Cl<sub>2</sub>/TIS/H<sub>2</sub>O 48:49:2:1, rt, 2 h, two steps. For **22a** (R = R<sub>1</sub>, Xaa = L-Phe): 79%. **22b** (R = R<sub>2</sub>, Xaa = L-Phe): 80%. **22c** (R = R<sub>2</sub>, Xaa = L-Leu): 75%. **22d** (R = R<sub>3</sub>, Xaa = L-Phe): 78%. **22e** (R = R<sub>3</sub>, Xaa = L-Leu): 65%. **22f** (R = R<sub>4</sub>, Xaa = L-Leu): 40%.

synthesis of terphenyl derivatives **19a** and **19b**, aldehydes of type **17** were readily synthesized via Suzuki coupling of 3,5-dibromobenzaldehyde with the appropriate boronic acids.<sup>30</sup> The resulting aldehydes were converted to the corresponding bromides of type **18** after reduction with NaBH<sub>4</sub> and subsequent treatment with PBr<sub>3</sub>. Substitution of the latter intermediates by the anion of triethyl methanetricarboxylate, followed by saponification/decarboxylation, Knoevenagel condensation of the crude substituted malonic acids with paraformaldehyde, and esterification of the resulting acrylic acids with EtOH successfully afforded the target acrylates **19**.<sup>25,31</sup> P-Michael addition of phosphinic acid **7** to acrylates **15**, **19a,b**, and **20** afforded dipeptides of type **21** as mixtures of two diastereoisomers with dr values ranging from 1:1 (**21a**) to 4:1 (**21d**). Coupling of **5b** or **5c** to diacids of type **21** followed by TFA-mediated deprotection afforded target compounds **22a–f**. For **22a,b** and **22d**, two isomers were obtained which were separated by semipreparative HPLC and evaluated separately (annotated as **22a'**, **22b'**, and **22d'** in Tables 1 and 2), whereas for **22c,e** and **22f** single isomers were obtained due to efficient separation during column purification of coupling products.

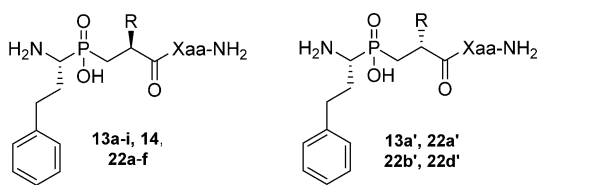
**Structure–Activity Relationships: P<sub>2</sub>' Position.** Our first goal was to evaluate the effect of various proteinogenic amino acid side chains at P<sub>2</sub>' position (with the only exception of **6k**) on the overall inhibition profile of APAs (Table 1). This side chain has been found to occupy the S<sub>2</sub>' specificity pocket of ERAP2 in a previously determined crystal structure of

Table 1. In Vitro Evaluation of Phosphinic Pseudotriptides 6a–k Varying at Position P<sub>2</sub>'

compd	Xaa	IC <sub>50</sub> (nM)		
		ERAP1	ERAP2	IRAP
<b>6a</b>	L-Ala	2518 ± 390	96 ± 6	102 ± 9
<b>6b</b>	L-Leu	682 ± 40	118 ± 40	32 ± 2
<b>6c</b>	L-Phe	155 ± 38	109 ± 8	41 ± 6
<b>6d</b>	L-Pro	949 ± 236	144 ± 57	14 ± 1
<b>6e</b>	L-Trp	48 ± 16	80 ± 10	57 ± 35
<b>6f</b>	L-Tyr	340 ± 56	55 ± 7	29 ± 9
<b>6g</b>	L-Ser	7473 ± 1566	129 ± 11	1754 ± 631
<b>6h</b>	L-Lys	3093 ± 968	271 ± 55	1800 ± 411
<b>6i</b>	L-His	1969 ± 548	128 ± 23	381 ± 43
<b>6j</b>	L-Glu	2660 ± 174	243 ± 17	4024 ± 273
<b>6k</b>	D-Phe	2650 ± 212	211 ± 21	185 ± 5

ERAP2 with the inhibitor **6e**.<sup>11</sup> In vitro evaluation demonstrated that having aromatic residues at that position (**6c**, **6e,f**) is a prerequisite for retaining sufficient potency for ERAP1, although a small hydrophobic residue (**6b**) can also be well accommodated. Charged or hydrophilic residues (**6g–j**) greatly reduced the affinity for ERAP1 and so did the unnatural stereochemistry of P<sub>2</sub>' in **6k**. In contrast, virtually all tested side chains could be well tolerated by ERAP2, leading to nanomolar inhibition for all compounds of type **6**, even for **6k** that possesses (*R*)-stereochemistry at P<sub>2</sub>'. Hydrophobic side chains were also preferred by IRAP, in contrast to polar and charged residues that resulted in significantly reduced affinities. Overall, our analysis suggests that the P<sub>2</sub>' position is more important for controlling inhibitor potency for ERAP1, less so for IRAP, and highly permissive for ERAP2. This comes largely as a surprise, since the crystal structure of ERAP2 with **6e** showed that the indole moiety of Trp at P<sub>2</sub>' position is sandwiched between two Tyr residues that form the opposing sides of the S<sub>2</sub>' pocket. One of these Tyr residues (Y438) is conserved in both ERAP1 and IRAP and is actually important for catalysis.<sup>32</sup> This apparent paradox can be rationalized by taking into account the conformational changes that ERAP1 (and probably ERAP2 and IRAP) undergoes during the catalytic cycle.<sup>6b</sup> ERAP1 has been crystallized in two distinct conformational states, a “closed” and an “open” state, as defined by the interactions between domains II and IV. The “open” state is considered to be less active and is characterized by disorder at the S<sub>1</sub> specificity pocket and a distinct conformation for the catalytic Y438. The “closed” state is correspondingly characterized by the lack of access of the catalytic site to the external solvent. Since any encounter complex between the inhibitor and ERAP1 would have to be with the “open” state, interactions that may facilitate the transition to the “closed” state which promotes the formation of the S<sub>1</sub> pocket would favor inhibitor affinity. It is conceivable therefore that aromatic side chains at P<sub>2</sub>' may affect inhibitor affinity differently depending on the conformation of the catalytic Tyr residue. Indeed, the orientation of the catalytic Tyr is different among the three enzymes (Figure 2). The

**Table 2.** In Vitro Evaluation of Phosphinic Pseudotripeptides 13a–i, 14, and 22a–f Varying at Position P<sub>1</sub>'



ID	R	Xaa	IC <sub>50</sub> (nM)		
			ERAP1	ERAP2	IRAP
13a		L-Phe	126±31	190±24	18±3
13a'		L-Phe	2087±347	878±334	434±50
13b		L-Phe	178±67	130±15	13±2
13c		L-Phe	98±11	217±76	20±4
13d		L-Phe	48±9	84±21	10±2
13e		L-Phe	102±11	123±14	13±4
13f		L-Phe	143±14	225±67	41±5
13g		L-Phe	71±8	345±138	34±9
13h		L-Phe	65±38	83±11	9±2
13i		L-Phe	33±5	56±9	4±1
14		L-Phe	43±4	37±4	2±1
22a		L-Phe	726±157	412±89	46±17
22a'		L-Phe	27008±7715	2271±486	561±66
22b		L-Phe	3694±908	740±129	32±9
22b'		L-Phe	>100000	1922±199	221±24
22c		L-Leu	31212±6939	246±7	16±2
22d		L-Phe	>35000	105±15	21±3
22d'		L-Phe	>100000	4622±2517	281±100
22e		L-Leu	21229±907	2565±47	317±20
22f		L-Leu	25111±6363	13814±566	577±21

importance for aromatic residues at P<sub>2</sub>' appears to correlate well with the known orientation of this Tyr (most important for ERAP1, less so for IRAP, and not important for ERAP2). These observations suggest that SAR for inhibitors that occupy the S<sub>2</sub>' pocket of APAs these enzymes may be complicated by the conformational states available to each enzyme.

**Structure–Activity Relationships: P<sub>1</sub>' Position.** Evaluation of the P<sub>1</sub>' position was performed along two separate routes involving (a) isoxazole-based, linearly extended side chains (13a–i) to explore the depth of S<sub>1</sub>' pocket and (b) “expanded” bulky side chains (22a–f) to explore the base of the same pocket. Our results showed that the bulky side chains of inhibitors 22a–f were poorly tolerated by ERAP1 whereas

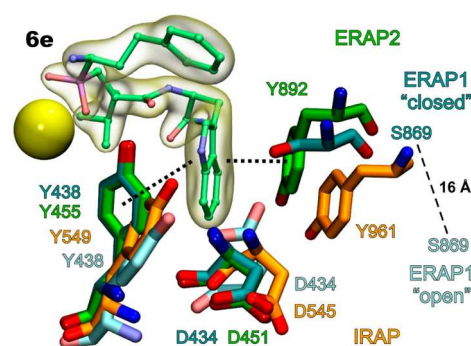


**Figure 2.** Three key residues that comprise the S<sub>2</sub>' subsite of APAs. The X-ray crystal structure of ERAP2 complex with 6e (green C, PDB code 4JBS) is superimposed with ERAP1 complexes with bestatin (PDB codes 2YD0, 3MDJ) in the closed and open states (dark and light cyan C, respectively), and IRAP in its ligand-free form (orange C, PDB code 5C97). Note the different orientations of the catalytic Y438, the conserved D434, and the nonconserved S869, especially in the open and closed states of ERAP1.

the extended isoxazole side chains of 13h,i were well tolerated (Table 2). A similar but less striking phenomenon was evident for ERAP2, albeit with some notable exceptions, such as 22d. In contrast, IRAP was able to easily accommodate the P<sub>1</sub>' side chains of both groups of compounds (13h,i and 22a–f), resulting in most cases in low nanomolar inhibition. This was more evident in the case of linear isoxazole side chains, considering that all inhibitors of type 13 were able to potentially inhibit IRAP with IC<sub>50</sub> values ranging between 4 and 41 nM. The ability of IRAP to accommodate bulky side chains at P<sub>1</sub>' position may be explained by the different orientation that the conserved GAMEN motif adopts in this enzyme, an orientation that allows for a more open catalytic site and has been hypothesized to allow processing of cyclic peptides that may also require additional space around the base of S<sub>1</sub>' pocket.<sup>3c</sup> Interestingly, inversion of the stereochemical configuration at P<sub>1</sub>' position caused a dramatic drop in the potency of all examples presented in Table 2 (13a', 22a', 22b', and 22d'), which is consistent with previously reported observations for the pair of P<sub>1</sub>'-epimers 6e and 6e'<sup>11</sup> and emphasizes the importance of stereochemical control in the development of optimized inhibitors of APAs, in terms of both potency and selectivity.

**Critical Parameters for Maximizing Potency.** As it is demonstrated in Tables 1 and 2, the potency of phosphinic tripeptide inhibitors against ERAP1 can be greatly affected by both P<sub>1</sub>' and P<sub>2</sub>' side chain composition. Aromatic residues are preferred at P<sub>2</sub>' position presumably due to the importance of interaction with Y438 that facilitates the conformational change to the closed form of the enzyme. Long side chains at P<sub>1</sub>' position, such as the aryl-substituted isoxazole derivatives 13a–i, are well accommodated but do not confer any additional affinity compared to a small hydrophobic residue (such as Leu, 6b) at the same position. In contrast, bulky substituents are highly disfavored at P<sub>1</sub>' position.

The effectiveness of phosphinic tripeptides against ERAP2 was found to be highly permissive with respect to position P<sub>2</sub>', since all compounds exhibited activity in the nanomolar range (with the exception of 22e, 22f, and all primed diastereoisomers listed in Table 2). Similar to ERAP1, bulky residues at P<sub>1</sub>' position may not be optimal but are well tolerated and in some cases can result in highly potent inhibitors (such as 22d).

$P_2'$  position is also important for potency against IRAP: polar and charged residues lead to reduction of the affinity, presumably reporting a hydrophobic environment for subsite  $S_2'$ . Inhibitor potency was also affected by the nature of the  $P_1'$  side chain, especially for bulky substituents, but in general IRAP was able to accommodate bulky side chains while retaining nanomolar potency.

The affinity displayed by inhibitor **14** that bears a propargyl group at  $P_1'$  position is also highly notable, since it appears to outperform leucine (**6c**) for all enzymes and especially IRAP, resulting in an  $IC_{50}$  value of 2 nM. This affinity is in the same range as for several macrocyclic angiotensin IV analogues developed by Hallberg and co-workers which are among the most potent known IRAP inhibitors.<sup>33</sup> Moreover, to the best of our knowledge, **14** is the most potent inhibitor of ERAP2 described to date ( $IC_{50} = 37$  nM) and parallels **6e** for potency against ERAP1 ( $IC_{50} = 43$  nM for **14** and  $IC_{50} = 48$  nM for **6e**). Although the origin of this outstanding behavior is not clear, putative interactions between the electron-rich triple bond of the propargyl group and the catalytic Zn(II) atom at certain orientations may provide a reasonable explanation.<sup>34</sup> Given the absence of any literature precedent concerning propargyl substituted phosphinic inhibitors of Zn metallopeptidases, further investigations including crystallographic analysis will be necessary to clarify this effect.

**Critical Parameters for Maximizing Selectivity.** Our screening results revealed several compounds to be selective inhibitors of ERAP2 and IRAP with respect to ERAP1 but afforded only few compounds displaying selectivity for ERAP1, consistent with previous reports (Figure 3).<sup>10b,11,35</sup> This is likely a result of the conformational dynamics of ERAP1, which samples more open states than ERAP2 and IRAP with partially disordered  $S_1$  and  $S_2'$  subsites, rendering inhibitor targeting quite challenging.<sup>6c,10b</sup> Still, some selectivity was evident for some of the isoxazole derivatives, indicating that the  $P_1'$  position can be valuable in enhancing ERAP1 selectivity over ERAP2. For example, compound **13g** is about 5-fold more selective for ERAP1 versus ERAP2. In an attempt to rationalize this observation, we examined the predicted conformations of **13g** from docking calculations, which showed that the  $P_1'$  side chain extends in a linear fashion down the elongated shallow  $S_1'$  pocket of ERAP1 (Figure 4A). This pocket is much shallower in ERAP2 (Figure 4B), making this conformation inaccessible to extended  $P_1'$  side chains and possibly explaining the observed selectivity. Another informative observation that supports the aforementioned shape description of  $S_1'$  subsite for ERAP1 and ERAP2 is the fact that among the isoxazole series, ortho-substituted aryl substituents (**13b**, **13e**, and **13h**) result in the least ERAP1-selective compounds (in fact, **13b** bearing the bulkier -OMe group displays higher potency for ERAP2 than ERAP1). Evidently, in contrast to **13g**, inhibitors **13b**, **13e**, and **13h** require a wider, more spacious  $S_1'$  channel for favorable accommodation of their  $P_1'$  side chains, which results in reduction of their affinity for ERAP1.

Both  $P_1'$  and  $P_2'$  side chains of phosphinic tripeptides offer opportunities for the optimization of ERAP2 selective inhibitors. Screening of  $P_2'$  position resulted in several compounds that were selective for ERAP2 over ERAP1 (Figure 3A). In particular, polar and charged side chains were well tolerated by ERAP2 but not ERAP1, thus providing selective inhibitors, such as **6g** that exhibits 50-fold selectivity for ERAP2. In regard to the  $P_1'$  position, some of the bulky side chains that were tolerated by ERAP2 resulted in highly selective

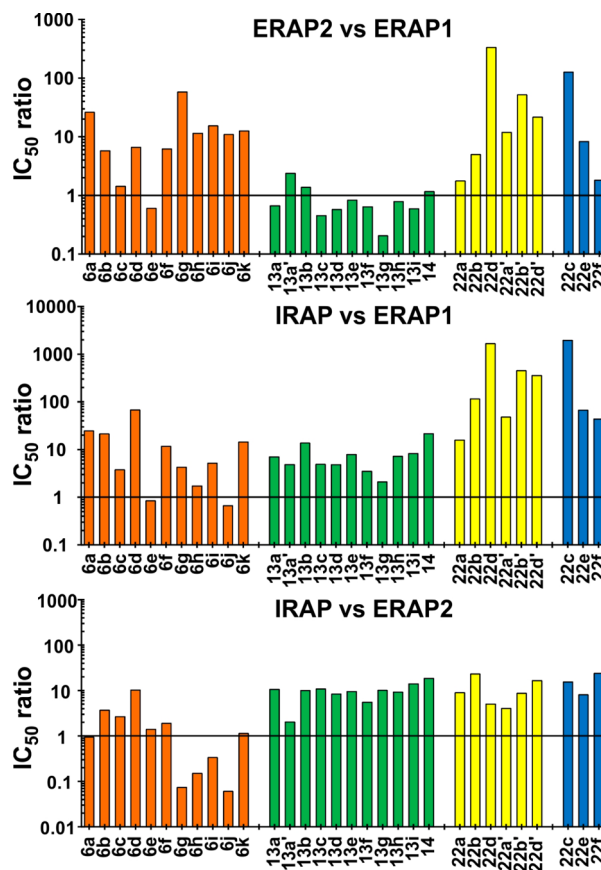


**Figure 3.** Ratio of  $IC_{50}$  values showing the selectivity of phosphinic tripeptide inhibitors (A, top) for ERAP2 over ERAP1, (B, middle) IRAP over ERAP1, and (C, bottom) IRAP over ERAP2.

inhibitors. For example, **22d** was found to be over 350-fold selective for ERAP2 over ERAP1. Docking calculations suggest that **22d** binds to ERAP2 with the  $P_1'$  side chain abutting to the extension of the GAMEN loop (Figure 5). At this site, the presence of two nonconserved residues in ERAP1 (Q315 and S316) that could interfere with this configuration of **22d** possibly accounts for the observed selectivity.

The highest selectivity during our screening analysis was observed for IRAP, with several derivatives reaching selectivity of over 3 orders of magnitude (Figure 2). This was true for screening of both the  $P_1'$  and  $P_2'$  positions with respect to ERAP1 but only for the  $P_1'$  position with respect to ERAP2. Taken together, the  $P_1'$  position proved to be an exceptional modification site for generating IRAP-selective inhibitors. This ability of IRAP to accommodate in its  $S_1'$  subsite very bulky groups justifies the nanomolar affinity for IRAP observed by all listed compounds of Table 2. In fact, this feature is more striking in IRAP than in ERAP2, considering that in the most extreme case of bulky  $P_1'$  side chain (**22f**) examined in this work, nanomolar affinity for IRAP was still attainable ( $IC_{50} = 577$  nM) whereas  $IC_{50}$  value for ERAP2 was dramatically increased to 13  $\mu$ M. This may be due to the alternative configuration of the GAMEN loop in IRAP that generates additional space around that site, making it more permissive, especially for bulky side chains. In an effort to put these observations under a structural perspective we docked IRAP-selective inhibitor **22b** in the active site of IRAP. Two major low-energy configurations were identified and shown in Figure 6. Interestingly, in both configurations the  $P_1'$  side chain does

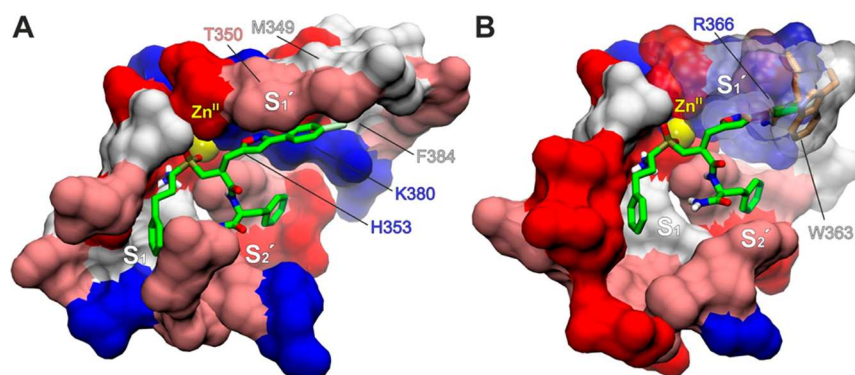


**Figure 4.** (A) Docked conformation of **13g** in the active site of ERAP1 (PDB code 2YD0), where the P1' side chain extends inside the deep, elongated S<sub>1</sub>' pocket. (B) Active site of ERAP2 (PDB code 4JBS) shown from an identical view, where the shallower S<sub>1</sub>' subsite renders such an extended configuration of **13g** inaccessible due to steric clashes with R366 and W363. Colors are as in Figure 1.

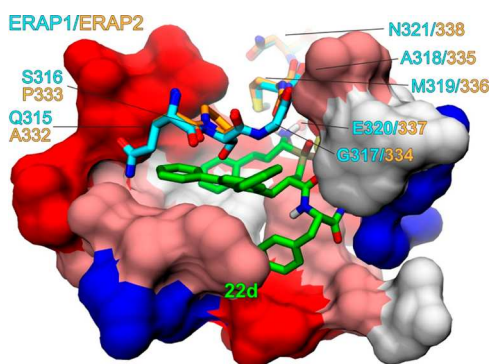


**Figure 5.** Lowest energy conformation of **22d** (green C) docked inside the active site of ERAP2 (orange C), superimposed with ERAP1 (cyan C) to illustrate the conserved GAMEN motif and the two nonconserved preceding residues that probably restrict the accommodation of similar conformations of **22d** in ERAP1 (PDB codes 2YD0 for ERAP1, 4JBS for ERAP2).

not interact with the GAMEN-motif residues but rather forces either the P<sub>1</sub> or P<sub>2</sub>' side chain to occupy the free space adjacent to the GAMEN loop. This space is not readily available in ERAP1, making these configurations inaccessible (Figure 6).

**Biological Evaluation.** To access the efficacy and selectivity of this group of inhibitors in regulating antigenic peptide processing in live cells, we evaluated the ability of one of the IRAP-selective inhibitors, **22b** (DG026A), to regulate cross-presentation by dendritic cells (DCs) as described in the Experimental Section. DCs can perform cross-presentation by at least two distinct pathways, one of which is dependent on

ERAP1 activity and the other is dependent on IRAP activity.<sup>4a</sup> To confirm the selectivity of any effect, we compared BMDCs from both wild-type and IRAP<sup>-/-</sup> knockout mice. Mouse CD8 $\alpha^+$  and CD11b<sup>+</sup> DCs were exposed to soluble ovalbumin (OVA) in the presence of increasing concentrations of the inhibitor. After 6 h the cells were fixed to stop antigen processing and mixed with CD8<sup>+</sup> T-cells isolated from the lymph nodes of Rag-1<sup>-/-</sup> C57Bl/6 OT-I mice. T-cell activation was evaluated by measuring the levels of secreted IL-2 by the activated CD8<sup>+</sup> T-cells. The OT-I T cell response to increasing levels of soluble OVA (Figure S1) was first evaluated to determine the optimal concentration of OVA for all subsequent experiments (set to 500  $\mu$ g/mL) (Figure S1). For both CD8 $\alpha^+$  and CD11b<sup>+</sup> DCs, titration of the inhibitor **22b** resulted in a dose-dependent reduction of cross-presentation down to a plateau that corresponds to IRAP-independent cross-presentation (Figure 7A). No effect was evident when using DCs isolated from IRAP<sup>-/-</sup> knockout mice, indicating that the effect was IRAP-specific (Figure 7B). A limited additional effect was seen at the highest inhibitor concentration (3.3  $\mu$ M) which may be attributable to toxicity. In conclusion, we demonstrate a dose-dependent and target-specific effect of the IRAP selective inhibitor **22b** on the cross-presentation by both subsets of conventional DCs, which indicates that this compound may be useful in regulating DC-triggered adaptive immune responses.

## CONCLUSIONS

In this study, we expanded on our previous observation that phosphinic pseudotriptides are potent inhibitors of aminopeptidases that are involved in the generation of antigenic

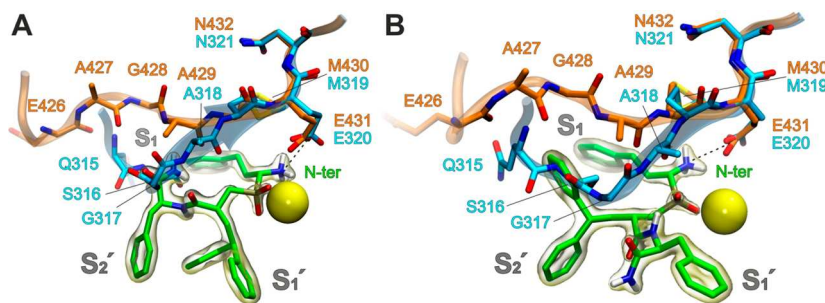


**Figure 6.** Two docked conformations of **22b** (green C) inside the active site of IRAP (orange C), superimposed with the structure of closed ERAP1 (cyan C). The more “closed” configuration of the GAMEN motif and of the two preceding residues in ERAP1 with respect to IRAP probably renders such bound poses of **22b** inaccessible (PDB codes 2YD0 for ERAP1, 5C97 for IRAP).

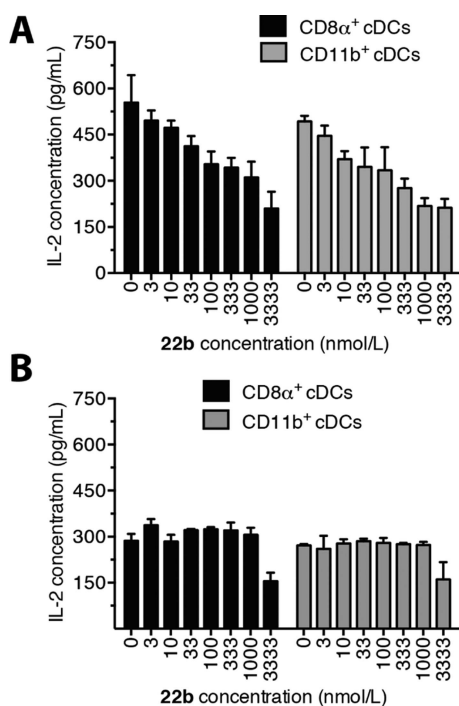


**Figure 7.** Response of CD8 $^+$  T-cells isolated from the lymph nodes of Rag-1 $^{-/-}$  C57Bl/6 OT-I mice to FACS-sorted splenic CD8 $\alpha^+$  and CD11b $^+$  conventional DCs exposed to soluble OVA in the presence of the inhibitor **22b**. DCs were isolated either from wild-type (A) or from IRAP $^{-/-}$  knockout mice (B). A dose-dependent inhibition of the response by DCs from wild-type mice is evident (A) down to the level of activation seen for DCs isolated from knockout mice (B).

peptides, by thoroughly investigating the P $_1'$  and P $_2'$  positions for their effect on inhibitor potency and selectivity. Special attention was given to the control of chirality during the preparation of target compounds, considering the difference in affinity of 2–3 orders of magnitude previously observed for the P $_1'$ -epimers **6e** and **6e'** and verified in this study for several more cases of phosphinic tripeptides. This requirement is of paramount importance for the accurate evaluation of reported structure–activity relationships and the discovery of improved inhibitors, especially in terms of selectivity. In this regard, appropriately adjusted synthetic plans able to confer stereochemical control were devised and employed. Our strategy succeeded in providing several low nanomolar inhibitors for all APAs, such as **14** which is among the most potent inhibitors ever reported for all three enzymes. Important inhibitors in terms of selectivity have also been identified, such as the ERAP2 selective inhibitor **6g** and the IRAP selective inhibitor **22b**. Our analysis suggests that the P $_2'$  position is more important for controlling inhibitor potency for ERAP1 than for ERAP2 and IRAP. Moreover, selectivity for ERAP2 can be controlled by polar residues at P $_2'$  position while selectivity for IRAP is mainly determined by the presence of bulky groups at P $_1'$  position. A notable observation concerning the effect of shape of P $_1'$  side chains in ERAP1/ERAP2 selectivity is that ERAP1 accommodates better than ERAP2 long, linear ligands whereas this preference is inverted in the case of more “expanded” bulky groups (e.g., **22d**). Biological evaluation demonstrated that one of the selective IRAP inhibitors (**22b**) was able to regulate cross-presentation by dendritic cells *ex vivo* in a dose-dependent and target-specific fashion. Our results suggest that this class of compounds can be useful for the

targeted regulation of adaptive immune responses and encourage their preclinical evaluation for applications in cancer immunotherapy or the control of autoimmunity. Possible bioavailability concerns associated with the high polarity of the described structures can be overcome either by prodrug-based strategies, as it has been successfully demonstrated in the past with fosinopril,<sup>36</sup> a known marketed phosphinic inhibitor of angiotensin-converting enzyme, and with a series of structurally relevant phosphinic inhibitors of NEP and APN (aminopeptidase N) that exhibit analgesic properties,<sup>22a</sup> or with intravenous (iv) or intraperitoneal (ip) administration to animals.

## EXPERIMENTAL SECTION

**Materials and General Procedures.** Solvents for reactions were purchased as anhydrous grade and stored over 4 Å activated molecular sieves before use. Reagents were purchased from commercial sources and were used without further purification. Column chromatography was performed on silica gel (E. Merck, 70–230 mesh). TLC analyses were performed on silica gel plates (E. Merck, silica gel 60 F254), and components were visualized by the following methods: UV light absorbance, ninhydrin spraying and/or charring after spraying with a solution of NH $_4$ HSO $_4$ . Coupling reactions were monitored by LC/MS analysis. Melting points (measured on an Electrothermal apparatus) are uncorrected. Optical rotation data were acquired on a PerkinElmer 343 polarimeter at 25 °C. NMR spectra were recorded on a Varian 200 MHz Mercury or a Bruker Avance DRX-500 instrument at 25 °C.  $^1$ H and  $^{13}$ C spectra are referenced according to the residual peak of the solvent based on literature data.<sup>37</sup>  $^{31}$ P NMR chemical shifts are reported in ppm downfield from 85% H $_3$ PO $_4$  (external standard), and the corresponding spectra are fully proton decoupled. The following abbreviations are used to designate the multiplicities: s, singlet; d, doublet; t, triplet; q, quartet; m, multiplet; br, broad. ESI mass spectral analysis was performed on a MSQ Surveyor, Finnigan mass spectrometer, using direct sample injection. Negative or positive ion ESI spectra were acquired by adjusting the needle and cone voltages accordingly. HRMS spectra were recorded on a Bruker Maxis Impact QTOF spectrometer or a 4800 MALDI-TOF mass spectrometer (Applied Biosystems, Foster City, CA, USA) in positive reflectron mode in the  $m/z$  range of 100–700. Each spectrum was the result of 1000–2000 shots (20 different positions into each spot and 50 shots per subspectrum), and internal calibration was applied by using 4-HCCA matrix  $m/z$ . Stereochemical purity of intermediates and final inhibitors was determined using  $^{31}$ P NMR and/or RP-HPLC analysis. RP-HPLC analyses were performed on a Hewlett-Packard 1100 model (C18-Cromasil-RP, 5  $\mu$ m, UV/vis detector, flow of 0.5 mL/min, 254 and/or 280 nm detection). Conditions and gradients used for each compound are reported in Supporting Information. Purity of compounds after preparative reverse-phase HPLC was assessed by analytical HPLC (Merck Chromolith C-18 column) using a 0.05% TFA–acetonitrile gradient (5–40%). On the basis of these criteria, all compounds possess purity of >95%.

**General Procedure A: P-Michael Addition of P–H Phosphinic Acids to Acrylic Derivatives.** A mixture of the appropriate N-protected aminophosphinic acid (1.0 mmol), the appropriate acrylic derivative (1.1–1.5 mmol), and HMDS (1.05 mL, 5.0 mmol) was heated at 110 °C for 1 h and then at 90 °C for 3 h under Ar. Then, the mixture was slowly cooled to 70 °C, dry EtOH (1.5 mL) was slowly added, and the resulting mixture was stirred at 70 °C for 20 min. After removal of the volatiles in vacuo, the residue was taken up by AcOEt (20 mL) and the organic solution was washed with 2 M HCl (2  $\times$  10 mL) and brine (10 mL). The organic layer was dried over Na $_2$ SO $_4$  and evaporated in vacuo to afford the crude product. Purification details are described for each case separately.

**General Procedure B: Saponification of P-Michael Adducts.** The appropriate P-Michael addition product (1.0 mmol) was dissolved in EtOH (10 mL), and the solution was cooled to 0 °C. 1 M NaOH (5 mL) was added portionwise, and the mixture was stirred at rt for 24 h.

After removal of the volatiles in vacuo, the residue was suspended in H<sub>2</sub>O (10 mL) and AcOEt (20 mL) and acidified with 2 M HCl to pH 1. The aqueous phase was extracted twice more with AcOEt (2 × 10 mL), and the combined organic layers were dried over Na<sub>2</sub>SO<sub>4</sub> and evaporated in vacuo.

**General Procedure C: TFA-Mediated Deprotection of Final Inhibitors.** A solution of the appropriate protected pseudopeptide (0.2 mmol) in TFA/CH<sub>2</sub>Cl<sub>2</sub>/TIS/H<sub>2</sub>O 48:49:2:1 (2 mL) was stirred at rt for 2 h. After removal of the volatiles in vacuo, the residue was dried azeotropically using toluene, and then it was treated with dry Et<sub>2</sub>O at 0 °C. The precipitate was collected by centrifugation, washed twice with dry Et<sub>2</sub>O, and dried over P<sub>2</sub>O<sub>5</sub> to afford the final product.

**General Procedure D: Coupling of Amino acid Carboxamides to Phosphinic Building Blocks.** The appropriate phosphinic pseudodipeptide building block (0.5 mmol) was suspended/dissolved in CH<sub>2</sub>Cl<sub>2</sub> (1.0 mL) and DIPEA (174 μL, 1.0 mmol), and the appropriate amino acid carboxamide (0.65 mmol), HOBt (68 mg, 0.5 mmol), and EDC·HCl (480 mg, 2.5 mmol) were added. The mixture was stirred at rt and the reaction was monitored by TLC until complete consumption of the starting phosphinic acid (2–4 h). Then, the solvent was evaporated, AcOEt (10 mL) and 1 M HCl (10 mL) were added, and the organic layer was separated and washed with 1 M HCl (3 × 10 mL), H<sub>2</sub>O (5 mL), and brine (5 mL). The organic phase was dried over Na<sub>2</sub>SO<sub>4</sub>, evaporated in vacuo and the residue was purified by column chromatography (CHCl<sub>3</sub>/MeOH/AcOH 7:0.1:0.1 → 7:0.5:0.5) to afford the target protected pseudotripeptide.

**General Procedure E: 1,3-Dipolar Cycloaddition toward the Synthesis of Isoxazole Inhibitors.** The appropriate oxime (3.0 mmol) was dissolved in CHCl<sub>3</sub> (10 mL), and 2 drops of pyridine were added. Then, NCS (401 mg, 3.0 mmol) was added at rt, and after 10 min the resulting mixture was stirred at 40–50 °C for 3 h. In this solution, phosphinic tripeptide **13** (167 mg, 0.3 mmol) was added, followed by slow addition of Et<sub>3</sub>N (0.49 mL, 3.5 mmol) at the same temperature. The reaction mixture was stirred for 3 days at 40–50 °C. Then, the solvent was evaporated, AcOEt (10 mL) and 1 M HCl (10 mL) were added, and the organic layer was separated and washed with 1 M HCl (3 × 10 mL), H<sub>2</sub>O (5 mL), and brine (5 mL). The organic phase was dried over Na<sub>2</sub>SO<sub>4</sub> and evaporated in vacuo. In case of incomplete reaction, the procedure was repeated as many times as necessary using the product of each reaction as starting material for the next reaction. When the starting material was fully consumed, the crude product was purified by column chromatography (CHCl<sub>3</sub>/MeOH/AcOH 7:0.1:0.1 → 7:0.5:0.5) to afford the target isoxazole pseudotripeptide.

**((1R)-1-[(Benzyloxy)carbonyl]amino)-3-phenylpropyl[2'-(ethoxycarbonyl)-4'-methylpentyl]phosphinic Acid (2).** Phosphinic acid **1** (7.0 g, 21 mmol) was converted to compound **2** according to general procedure A. The crude product was used at the next step without further purification. For analytical reasons, a small sample was purified by column chromatography (CHCl<sub>3</sub>/MeOH/AcOH 7:0.1:0.1 → 7:0.5:0.5) to afford compound **2** as a white solid. <sup>1</sup>H NMR (200 MHz, DMSO-*d*<sub>6</sub>/2% TFA) δ 0.79 (t, *J* = 6.5 Hz, 6H), 1.11 (t, *J* = 7.0 Hz, 3H), 1.18–1.51 (m, 3H), 1.52–2.09 (m, 4H), 2.31–2.88 (m, 3H), 3.48–3.78 (m, 1H), 4.00 (q, *J* = 6.8 Hz, 2H), 5.06 (s, 2H), 7.04–7.42 (m, 10H), 7.62 (d, *J* = 9.6 Hz, 1H); <sup>13</sup>C NMR (50 MHz, CDCl<sub>3</sub>) δ 14.2, 22.0, 22.8, 25.9, 28.8 (d, <sup>1</sup>*J*<sub>PC</sub> = 85.4 Hz), 29.3 (d, <sup>1</sup>*J*<sub>PC</sub> = 90.7 Hz), 29.9, 32.0, 32.1, 32.2, 32.3, 37.2, 37.3, 43.2, 43.3, 43.4, 43.6, 49.2 (d, <sup>1</sup>*J*<sub>PC</sub> = 104 Hz), 50.1 (d, <sup>1</sup>*J*<sub>PC</sub> = 104 Hz), 60.9, 67.3, 125.4, 126.2, 128.1, 128.2, 128.5, 128.6, 129.1, 136.4, 136.5, 140.9, 140.9, 156.3, 156.4, 175.2, 175.3, 175.4; <sup>31</sup>P NMR (81 MHz, DMSO-*d*<sub>6</sub>) δ 45.7, 46.0. ES-MS *m/z*: calcd for [C<sub>26</sub>H<sub>36</sub>NO<sub>6</sub>P – H]<sup>–</sup> 488.2; found, 488.2. HRMS (*m/z*): [M + Na]<sup>+</sup> calcd for C<sub>26</sub>H<sub>36</sub>NNaO<sub>6</sub>P<sup>+</sup>, 512.2172; found, 512.2178.

**(2'S)-2'-{[(1R)-1-[(Benzyloxy)carbonyl]amino)-3-phenylpropyl](hydroxy)phosphoryl}methyl-4'-methylpentanoic Acid (3).** The crude product **2** from the above preparation was subjected to saponification according to general procedure B. The resulting crude product was recrystallized twice by AcOEt to afford compound **3** as a white solid (4.45 g, 46% starting from **1**). Mp 160–

162 °C; <sup>1</sup>H NMR (200 MHz, DMSO-*d*<sub>6</sub>/2% TFA) δ 0.82 (t, *J* = 5.9 Hz, 6H), 1.20–2.09 (m, 7H), 2.36–2.83 (m, 3H), 3.50–3.72 (m, 1H), 5.07 (s, 2H), 7.04–7.42 (m, 10H), 7.63 (d, *J* = 9.4 Hz, 1H); <sup>13</sup>C NMR (50 MHz, DMSO-*d*<sub>6</sub>) δ 21.8, 23.0, 25.6, 28.9 (d, <sup>1</sup>*J*<sub>PC</sub> = 88.2 Hz), 29.2, 29.3, 31.5, 31.8, 36.7, 36.8, 42.6, 42.7, 50.4 (d, <sup>1</sup>*J*<sub>PC</sub> = 105.9 Hz), 65.6, 126.0, 127.7, 127.9, 128.4, 128.5, 128.5, 137.3, 141.3, 156.4, 156.4, 176.4, 176.5; <sup>31</sup>P NMR (81 MHz, DMSO-*d*<sub>6</sub>/3% TFA) δ 47.3. ES-MS *m/z*: calcd for [C<sub>24</sub>H<sub>32</sub>NO<sub>6</sub>P – H]<sup>–</sup> 460.2; found, 460.2. HRMS (*m/z*): [M + H]<sup>+</sup> calcd for C<sub>24</sub>H<sub>33</sub>NO<sub>6</sub>P<sup>+</sup>, 462.2040; found, 462.2046.

**(2'S)-2'-{[(1R)-1-[(tert-Butoxy)carbonyl]amino)-3-phenylpropyl](hydroxy)phosphoryl}methyl-4'-methylpentanoic acid (4).** A solution of compound **3** (4 g, 8.7 mmol) in 33% HBr/AcOH (7 mL) was stirred at rt for 1 h. After removal of the volatiles in vacuo, the residue was dried azeotropically using toluene and then it was dissolved in DMF (20 mL). To this solution, Et<sub>3</sub>N (6.0 mL, 43 mmol) and (Boc)<sub>2</sub>O (2.3 g, 10.4 mmol) were added at 0 °C, and the final mixture was stirred at rt for 24 h. Then, the mixture was diluted with AcOEt (100 mL) and 1 M HCl (100 mL) and the organic phase was washed with 1 M HCl (2 × 20 mL), H<sub>2</sub>O (2 × 20 mL), and brine (10 mL). The organic phase was dried over Na<sub>2</sub>SO<sub>4</sub> and evaporated in vacuo. The residue was dissolved in 5% NaHCO<sub>3</sub> (70 mL), washed with Et<sub>2</sub>O (3 × 10 mL), and acidified with 1 M HCl to pH 1. The aqueous suspension was extracted with AcOEt (2 × 30 mL) and the organic layers were dried over Na<sub>2</sub>SO<sub>4</sub> and evaporated under vacuum to afford compound **4** as a white solid (3.4 g, 92%). Mp 128–132 °C; <sup>1</sup>H NMR (200 MHz, DMSO-*d*<sub>6</sub>/2% TFA) δ 0.83 (t, *J* = 5.9 Hz, 6H), 1.38 (s, 9H), 1.05–1.58 (m, 3H), 1.60–2.13 (m, 4H), 2.35–2.79 (m, 3H), 3.35–3.64 (m, 1H), 7.02–7.33 (m, 5H); <sup>13</sup>C NMR (50 MHz, DMSO-*d*<sub>6</sub>) δ 22.0, 23.2, 25.8, 28.4, 29.0 (d, <sup>1</sup>*J*<sub>PC</sub> = 89.7 Hz), 29.3, 31.8, 32.0, 36.9, 37.0, 42.6, 42.8, 49.8 (d, <sup>1</sup>*J*<sub>PC</sub> = 105.2 Hz), 78.6, 126.1, 128.5, 128.7, 141.5, 155.9, 156.0, 176.6, 176.8; <sup>31</sup>P NMR (81 MHz, DMSO-*d*<sub>6</sub>) δ 46.8. ES-MS *m/z*: calcd for [C<sub>21</sub>H<sub>34</sub>NO<sub>6</sub>P – H]<sup>–</sup> 427.2; found, 426.2. HRMS (*m/z*): [MNa]<sup>+</sup> calcd for C<sub>21</sub>H<sub>34</sub>NNaO<sub>6</sub>P 450.2016; found, 450.2022.

**((1R)-1-Amino-3-phenylpropyl){(2'S)-2'-{[(2'S)-1'-amino-1'-oxopropan-2'-yl]carbamoyl}-4'-methylpentyl}phosphinic Acid (6a).** Coupling of **4** with H-(L)Ala-NH<sub>2</sub> (**5a**) according to general procedure D and subsequent deprotection according to general procedure C afforded compound **6a** as a white solid (yield for two steps: 65%). <sup>1</sup>H NMR (200 MHz, DMSO-*d*<sub>6</sub>/2% TFA) δ 0.84 (dd, *J* = 5.7, 11.4 Hz, 6H), 1.19 (d, *J* = 7.1 Hz, 3H), 1.14–1.50 (m, 3H), 1.70–2.23 (m, 4H), 2.56–2.90 (m, 3H), 3.11–3.37 (m, 1H), 4.15 (quint, *J* = 7.1 Hz, 1H), 6.81–7.58 (m, 7H), 8.09 (d, *J* = 7.4 Hz, 1H), 8.25 (br s, 3H); <sup>13</sup>C NMR (50 MHz, DMSO-*d*<sub>6</sub>/2% TFA) δ 18.1, 22.4, 22.9, 25.2, 29.7 (d, <sup>1</sup>*J*<sub>PC</sub> = 91.8 Hz), 29.7, 31.6, 31.8, 37.7, 37.7, 43.2, 43.4, 48.5, 48.7 (d, <sup>1</sup>*J*<sub>PC</sub> = 93.8 Hz), 126.4, 128.5, 128.7, 141.0, 173.9, 174.0, 174.6; <sup>31</sup>P NMR (81 MHz, DMSO-*d*<sub>6</sub>) δ 41.7. HRMS (*m/z*): [M – H]<sup>–</sup> calcd for C<sub>19</sub>H<sub>31</sub>N<sub>3</sub>O<sub>4</sub>P<sup>–</sup>, 396.2058; found, 396.2059.

**((1R)-1-Amino-3-phenylpropyl){(2'S)-2'-{[(2'S)-1'-amino-4'-methyl-1'-oxopentan-2'-yl]carbamoyl}-4'-methylpentyl}phosphinic Acid (6b).** Coupling of **4** with HBr-H-(L)Leu-NH<sub>2</sub> (**5b**) according to general procedure D and subsequent deprotection according to general procedure C afforded compound **6b** as a white solid (yield for two steps: 59%). <sup>1</sup>H NMR (200 MHz, DMSO-*d*<sub>6</sub>/2% TFA) δ 0.67–0.98 (m, 12H), 1.19–1.68 (m, 6H), 1.71–2.30 (m, 4H), 2.56–2.96 (m, 3H), 3.15–3.40 (m, 1H), 4.16 (dd, *J* = 7.8, 14.2 Hz, 1H), 6.70–7.76 (m, 7H), 8.02 (d, *J* = 7.9 Hz, 1H), 8.25 (br s, 3H); <sup>13</sup>C NMR (50 MHz, DMSO-*d*<sub>6</sub>/2% TFA) δ 21.6, 22.3, 23.0, 23.2, 24.4, 25.3, 29.7 (d, <sup>1</sup>*J*<sub>PC</sub> = 92.8 Hz), 29.9, 31.8, 31.9, 38.1, 43.4, 43.6, 48.9 (d, <sup>1</sup>*J*<sub>PC</sub> = 94.0 Hz), 51.4, 126.4, 128.5, 128.7, 141.0, 174.2, 174.3, 174.7; <sup>31</sup>P NMR (81 MHz, DMSO-*d*<sub>6</sub>/2% TFA) δ 42.0. HRMS (*m/z*): [M – H]<sup>–</sup> calcd for C<sub>22</sub>H<sub>37</sub>N<sub>3</sub>O<sub>4</sub>P<sup>–</sup>, 438.2527; found, 438.2524.

**((1R)-1-Amino-3-phenylpropyl){(2'S)-2'-{[(2'S)-1'-amino-1'-oxo-3'-phenylpropan-2'-yl]carbamoyl}-4'-methylpentyl}phosphinic Acid (10c).** Coupling of **4** with HBr-H-(L)Phe-NH<sub>2</sub> (**5c**) according to general procedure D and subsequent deprotection according to general procedure C afforded compound **6c** as a white solid (yield for two steps: 32%). <sup>1</sup>H NMR (200 MHz, DMSO-*d*<sub>6</sub>/2% TFA) δ 0.59–0.85 (m, 6H), 1.10–1.41 (m, 3H), 1.57–2.20 (m, 4H),

2.55–2.94 (m, 4H), 2.97–3.36 (m, 2H), 4.29–4.51 (m, 1H), 6.97–7.76 (m, 12H), 8.10 (d,  $J = 7.4$  Hz, 1H), 8.25 (br s, 3H);  $^{13}\text{C}$  NMR (50 MHz, DMSO- $d_6$ /2% TFA)  $\delta$  22.1, 23.0, 25.0, 29.6, 29.6 (d,  $^1\text{J}_{\text{PC}} = 95.2$  Hz), 31.5, 31.6, 32.6, 37.1, 42.8, 43.0, 48.5 (d,  $^1\text{J}_{\text{PC}} = 95.0$  Hz), 54.1, 126.2, 128.1, 128.3, 128.6, 129.2, 138.4, 140.8, 173.1, 173.8, 173.9;  $^{31}\text{P}$  NMR (81 MHz, DMSO- $d_6$ )  $\delta$  41.7. HRMS ( $m/z$ ):  $[\text{M} - \text{H}]^-$  calcd for  $\text{C}_{25}\text{H}_{35}\text{N}_3\text{O}_4\text{P}^-$ , 472.2371; found, 472.2366.

**((1R)-1-Amino-3-phenylpropyl)((2'S)-2'-((2''S)-2''-carbamoylpyrrolidine-1''-carbonyl)-4'-methylpentyl]phosphinic Acid (6d).** Coupling of **4** with H-(L)Pro-NH<sub>2</sub> (**5d**) according to general procedure D and subsequent deprotection according to general procedure C afforded compound **6d** as a white solid (yield for two steps: 41%).  $^1\text{H}$  NMR (200 MHz, DMSO- $d_6$ /2% TFA)  $\delta$  0.84 (t,  $J = 6.3$  Hz, 6H), 1.01–2.27 (m, 11H), 2.53–2.99 (m, 3H), 3.02–3.27 (m, 1H), 3.31–3.79 (m, 2H), 4.05–4.26 (m, 0.75H, major rotamer), 4.26–4.37 (m, 0.25H, minor rotamer), 6.73–7.86 (m, 7H), 8.22 (br s, 4H);  $^{13}\text{C}$  NMR (50 MHz, DMSO- $d_6$ /2% TFA), signals for major rotamer  $\delta$  22.4, 23.0, 24.5, 24.8, 29.3 (d,  $^1\text{J}_{\text{PC}} = 93.4$  Hz), 29.4, 29.6, 31.5, 31.7, 34.8, 42.7, 42.9, 47.1, 48.7 (d,  $^1\text{J}_{\text{PC}} = 93.3$  Hz), 59.5, 126.2, 128.3, 128.6, 140.9, 173.2, 173.3, 173.6;  $^{31}\text{P}$  NMR (81 MHz, DMSO- $d_6$ /2% TFA)  $\delta$  40.9 (minor), 41.2 (major), 42.0 (minor). HRMS ( $m/z$ ):  $[\text{M} - \text{H}]^-$  calcd for  $\text{C}_{21}\text{H}_{33}\text{N}_3\text{O}_4\text{P}^-$ , 422.2214; found, 422.2209.

**((1R)-1-Amino-3-phenylpropyl)((2'S)-2'-((2''S)-1''-amino-3''-(1H-indol-3-yl)-1''-oxopropan-2''-yl)carbamoyl)-4'-methylpentyl]phosphinic Acid (6e).** Coupling of **4** with H-(L)Trp-NH<sub>2</sub> (**5e**) according to general procedure D and subsequent deprotection according to general procedure C afforded compound **6e** as a white solid (yield for two steps: 32%).  $^1\text{H}$  NMR (200 MHz, DMSO- $d_6$ /2% TFA)  $\delta$  0.74 (dd,  $J = 4.3, 15.1$  Hz, 6H), 1.14–1.50 (m, 3H), 1.68–2.26 (m, 4H), 2.53–2.91 (m, 3H), 2.92–3.39 (m, 3H), 4.44 (dd,  $J = 6.5, 12.9$  Hz, 1H), 6.83–7.63 (m, 13H), 8.08 (d,  $J = 7.7$  Hz, 1H), 8.24 (br s, 3H);  $^{13}\text{C}$  NMR (50 MHz, DMSO- $d_6$ /2% TFA)  $\delta$  22.2, 22.8, 25.1, 27.4, 29.7 (d,  $^1\text{J}_{\text{PC}} = 92.4$  Hz), 29.7, 31.5, 31.7, 38.0, 38.0, 43.1, 43.2, 48.5, 48.7 (d,  $^1\text{J}_{\text{PC}} = 93.1$  Hz), 53.8, 110.6, 111.4, 118.3, 118.6, 120.9, 123.6, 126.3, 127.5, 128.4, 128.6, 136.2, 140.9, 173.6, 174.0, 174.1;  $^{31}\text{P}$  NMR (81 MHz, DMSO- $d_6$ /2% TFA)  $\delta$  41.9. HRMS ( $m/z$ ):  $[\text{M} - \text{H}]^-$  calcd for  $\text{C}_{27}\text{H}_{36}\text{N}_4\text{O}_4\text{P}^-$ , 511.2480; found, 511.2462.

**((1R)-1-Amino-3-phenylpropyl)((2'S)-2'-((2''S)-1''-amino-3''-(4-hydroxyphenyl)-1''-oxopropan-2''-yl)carbamoyl)-4'-methylpentyl]phosphinic Acid (6f).** Coupling of **4** with H-(L)Tyr(*t*-Bu)-NH<sub>2</sub> (**5f**) according to general procedure D and subsequent deprotection according to general procedure C afforded compound **6f** as a white solid (yield for two steps: 55%).  $^1\text{H}$  NMR (200 MHz, DMSO- $d_6$ /2% TFA)  $\delta$  0.76 (dd,  $J = 4.8, 12.4$  Hz, 6H), 1.14–1.48 (m, 3H), 1.67–2.24 (m, 4H), 2.55–3.03 (m, 5H), 3.08–3.32 (m, 1H), 4.31 (dd,  $J = 8.2, 13.6$  Hz, 1H), 6.62 (d,  $J = 8.2$  Hz, 2H), 6.90 (d,  $J = 8.2$  Hz, 2H), 7.09–7.62 (m, 7H), 8.02 (d,  $J = 7.9$  Hz, 1H), 8.23 (br s, 3H);  $^{13}\text{C}$  NMR (50 MHz, DMSO- $d_6$ /2% TFA)  $\delta$  22.2, 23.1, 25.2, 29.8 (d,  $^1\text{J}_{\text{PC}} = 91.7$  Hz), 29.9, 31.7, 31.8, 36.5, 43.2, 43.4, 48.8 (d,  $^1\text{J}_{\text{PC}} = 94.2$  Hz), 54.7, 115.1, 126.4, 128.5, 128.7, 130.2, 141.0, 156.0, 173.6, 174.0, 174.2;  $^{31}\text{P}$  NMR (81 MHz, DMSO- $d_6$ /2% TFA)  $\delta$  41.3. HRMS ( $m/z$ ):  $[\text{M} - \text{H}]^-$  calcd for  $\text{C}_{25}\text{H}_{35}\text{N}_3\text{O}_5\text{P}^-$ , 488.2320; found, 488.2322.

**((1R)-1-Amino-3-phenylpropyl)((2'S)-2'-((2''S)-1''-amino-3''-hydroxy-1''-oxopropan-2''-yl)carbamoyl)-4'-methylpentyl]phosphinic Acid (6g).** Coupling of **4** with H-(L)Ser(TBS)-NH<sub>2</sub> (**5g**) according to general procedure D and subsequent deprotection according to general procedure C afforded compound **6g** as a white solid (yield for two steps: 43%).  $^1\text{H}$  NMR (200 MHz, DMSO- $d_6$ /2% TFA)  $\delta$  0.83 (dd,  $J = 5.4, 11.9$  Hz, 6H), 1.06–1.32 (m, 1H), 1.33–1.59 (m, 2H), 1.67–2.26 (m, 4H), 2.56–2.94 (m, 3H), 3.19–3.43 (m, 1H), 3.44–3.78 (m, 2H), 4.05–4.39 (m, 1H), 6.94–7.59 (m, 7H), 7.96 (d,  $J = 7.7$  Hz, 1H), 8.24 (br s, 3H);  $^{13}\text{C}$  NMR (50 MHz, DMSO- $d_6$ /2% TFA)  $\delta$  22.4, 23.1, 25.4, 29.9, 30.3 (d,  $^1\text{J}_{\text{PC}} = 92.0$  Hz), 31.7, 31.9, 37.7, 37.8, 43.4, 43.7, 48.5 (d,  $^1\text{J}_{\text{PC}} = 95.5$  Hz), 55.6, 62.3, 126.5, 128.6, 128.8, 141.1, 172.3, 174.2, 174.3;  $^{31}\text{P}$  NMR (81 MHz, DMSO- $d_6$ /2% TFA)  $\delta$  41.6. HRMS ( $m/z$ ):  $[\text{M} - \text{H}]^-$  calcd for  $\text{C}_{19}\text{H}_{31}\text{N}_3\text{O}_5\text{P}^-$ , 412.2007; found, 412.2005.

**((1R)-1-Amino-3-phenylpropyl)((2'S)-2'-((2''S)-1''-6''-diamino-1''-oxohexan-2''-yl)carbamoyl)-4'-methylpentyl]phosphinic Acid (6h).** Coupling of **4** with H-(L)Lys(Boc)-NH<sub>2</sub> (**5h**) according to general procedure D and subsequent deprotection according to general procedure C afforded compound **6h** as a white solid (yield for two steps: 56%).  $^1\text{H}$  NMR (200 MHz, DMSO- $d_6$ /2% TFA)  $\delta$  0.84 (dd,  $J = 6.0, 11.4$  Hz, 6H), 1.15–2.30 (m, 13H), 2.58–2.94 (m, 5H), 3.14–3.41 (m, 1H), 3.99–4.24 (m, 1H), 6.86–7.51 (m, 7H), 7.66 (br s, 2H), 8.01 (d,  $J = 7.7$  Hz, 1H), 8.25 (br s, 3H);  $^{13}\text{C}$  NMR (50 MHz, DMSO- $d_6$ /2% TFA)  $\delta$  22.7, 22.8, 23.1, 25.6, 27.0, 29.9 (d,  $^1\text{J}_{\text{PC}} = 93.3$  Hz), 30.1, 31.5, 32.1, 32.3, 44.0, 44.2, 49.3 (d,  $^1\text{J}_{\text{PC}} = 93.3$  Hz), 53.0, 126.8, 128.9, 129.1, 141.3, 174.9, 175.0, 175.1;  $^{31}\text{P}$  NMR (81 MHz, DMSO- $d_6$ /2% TFA)  $\delta$  40.8. HRMS ( $m/z$ ):  $[\text{M} - \text{H}]^-$  calcd for  $\text{C}_{22}\text{H}_{38}\text{N}_4\text{O}_4\text{P}^-$ , 453.2636; found, 453.2634.

**((1R)-1-Amino-3-phenylpropyl)((2'S)-2'-((2''S)-1''-amino-3''-(1H-imidazol-4-yl)-1''-oxopropan-2''-yl)carbamoyl)-4'-methylpentyl]phosphinic Acid (6i).** Coupling of **4** with H-(L)His(Boc)-NH<sub>2</sub> (**5i**) according to general procedure D and subsequent deprotection according to general procedure C afforded compound **6i** as a white solid (yield for two steps: 10%).  $^1\text{H}$  NMR (200 MHz, DMSO- $d_6$ /2% TFA)  $\delta$  0.53–0.94 (m, 6H), 0.99–1.61 (m, 3H), 1.66–2.28 (m, 4H), 2.55–2.92 (m, 4H), 2.94–3.15 (m, 1H), 3.16–3.50 (m, 1H), 4.39–4.61 (m, 1H), 6.98–7.77 (m, 9H), 8.10 (d,  $J = 7.8$  Hz, 1H), 8.27 (br s, 3H), 8.89 (br s, 1H);  $^{31}\text{P}$  NMR (81 MHz, DMSO- $d_6$ /2% TFA)  $\delta$  41.9, (41.7: minor rotamer). HRMS ( $m/z$ ):  $[\text{M} - \text{H}]^-$  calcd for  $\text{C}_{22}\text{H}_{33}\text{N}_5\text{O}_4\text{P}^-$ , 462.2276; found, 462.2274.

**(4''S)-5''-Amino-4''-((2'S)-2'-(((1R)-1-amino-3-phenylpropyl)(hydroxy)phosphoryl)methyl)-4'-methylpentanamido-5''-oxopentanoic Acid (6j).** Coupling of **4** with HCl·H-(L)Glu(*t*-Bu)-NH<sub>2</sub> (**5j**) according to general procedure D and subsequent deprotection according to general procedure C afforded compound **6j** as a white solid (yield for two steps: 52%).  $^1\text{H}$  NMR (200 MHz, DMSO- $d_6$ /2% TFA)  $\delta$  0.84 (dd,  $J = 5.5, 11.2$  Hz, 6H), 1.13–1.38 (m, 1H), 1.38–1.60 (m, 2H), 1.66–2.33 (m, 8H), 2.60–2.94 (m, 3H), 3.12–3.38 (m, 1H), 4.01–4.26 (m, 1H), 6.82–7.53 (m, 7H), 8.09 (d,  $J = 7.6$  Hz, 1H), 8.23 (br s, 3H);  $^{13}\text{C}$  NMR (50 MHz, DMSO- $d_6$ /2% TFA)  $\delta$  22.4, 23.0, 25.2, 27.2, 29.7 (d,  $^1\text{J}_{\text{PC}} = 94.7$  Hz), 29.8, 30.6, 31.6, 31.8, 37.8, 37.9, 43.3, 43.6, 48.7 (d,  $^1\text{J}_{\text{PC}} = 94.5$  Hz), 52.2, 126.3, 128.5, 128.7, 141.0, 173.5, 174.2, 174.4;  $^{31}\text{P}$  NMR (81 MHz, DMSO- $d_6$ /2% TFA)  $\delta$  41.2. HRMS ( $m/z$ ):  $[\text{M} - \text{H}]^-$  calcd for  $\text{C}_{21}\text{H}_{33}\text{N}_3\text{O}_6\text{P}^-$ , 454.2112; found, 454.2110.

**((1R)-1-Amino-3-phenylpropyl)((2'S)-2'-(((2''R)-1''-amino-3''-oxo-3''-phenylpropan-2''-yl)carbamoyl)-4'-methylpentyl]phosphinic Acid (6k).** Coupling of **4** with HBr·H-(D)Phe-NH<sub>2</sub> (**5k**) according to general procedure D and subsequent deprotection according to general procedure C afforded compound **6k** as a white solid (yield for two steps: 31%).  $^1\text{H}$  NMR (200 MHz, DMSO- $d_6$ /2% TFA)  $\delta$  0.61 (dd,  $J = 3.6, 16.4$  Hz, 6H), 0.81–1.36 (m, 3H), 1.56–2.21 (m, 4H), 2.42–2.94 (m, 4H), 3.11–3.39 (m, 2H), 4.25–4.56 (m, 1H), 6.91–7.41 (m, 12H), 8.21 (br s, 3H), 8.35 (d,  $J = 8.0$  Hz, 1H);  $^{13}\text{C}$  NMR (50 MHz, DMSO- $d_6$ /2% TFA)  $\delta$  22.2, 23.3, 24.7, 29.7, 30.0 (d,  $^1\text{J}_{\text{PC}} = 90.1$  Hz), 31.7, 31.9, 37.1, 37.6, 44.0, 44.3, 49.0 (d,  $^1\text{J}_{\text{PC}} = 95.0$  Hz), 54.6, 126.4, 126.5, 128.3, 128.6, 129.4, 138.9, 141.0, 174.2, 174.4, 174.5;  $^{31}\text{P}$  NMR (81 MHz, DMSO- $d_6$ /2% TFA)  $\delta$  41.6. HRMS ( $m/z$ ):  $[\text{M} - \text{H}]^-$  calcd for  $\text{C}_{25}\text{H}_{35}\text{N}_3\text{O}_4\text{P}^-$ , 472.2371; found, 472.2357.

**2'-(((1R)-1-((tert-Butoxy)carbamoyl)amino)-3-phenylpropyl)-(hydroxy)phosphoryl)methyl]pent-4'-ynoic Acid (8).** Addition of phosphinic acid **7** (1.0 g, 3.3 mmol) to ethyl 2-methylenepent-4-ynoate<sup>25</sup> (0.59 g, 4.3 mmol) according to general procedure A and subsequent saponification according to general procedure B afforded compound **8** as a mixture of two diastereoisomers RS/RR = 67:33 (1.34 g, 99% starting from **7**).  $^1\text{H}$  NMR (500 MHz, DMSO- $d_6$ )  $\delta$  [1.36 (s, minor rotamer) + 1.40 (s, 9H)], 1.66–1.88 (m, 2H), 1.88–2.13 (m, 2H), 2.44–2.65 (m, 3H), 2.66–2.90 (m, 3H), 3.42–3.71 (m, 1H), [6.65 (d,  $J = 9.8$  Hz, minor rotamer) + 6.69 (d,  $J = 9.1$  Hz), 1H], 7.05–7.42 (m, 5H);  $^{13}\text{C}$  NMR (50 MHz, DMSO- $d_6$ ), signals for major rotamer  $\delta$  21.5, 21.6, 26.5 ( $^1\text{J}_{\text{PC}} = 89.0$  Hz), 28.3, 29.0, 31.7, 31.9, 37.6, 49.2 ( $^1\text{J}_{\text{PC}} = 107$  Hz), 72.9, 78.4, 81.4, 126.0, 128.4, 128.6, 141.4, 155.7, 155.8, 174.2, 174.5;  $^{31}\text{P}$  NMR (81 MHz, DMSO- $d_6$ )  $\delta$  47.5, 47.1. ES-MS  $m/z$ : calcd for  $[\text{C}_{20}\text{H}_{28}\text{NO}_6\text{P} - \text{H}]^-$  408.2; found, 408.3. HRMS ( $m/z$ ):  $[\text{M} + \text{H}]^+$  calcd for  $\text{C}_{20}\text{H}_{29}\text{NO}_6\text{P}^+$ , 410.1727; found, 410.1733.



**((1R)-1-[[tert-Butoxy]carbonyl]amino]-3-phenylpropyl)-{(2'S)-2'-[[[(2'S)-1'-amino-1'-oxo-3''-phenylpropan-2''-yl]-carbamoyl]pent-4''-yn-1''-yl]phosphinic Acid (9).** Phosphinic tripeptide **9** was isolated as a white solid after coupling of **8** (1.3 g, 3.2 mmol) with HBr-H-(L)Phe-NH<sub>2</sub> (**5c**) according to general procedure D and recrystallization of the crude product by AcOEt (0.73 g, 41% starting from **8**). <sup>1</sup>H NMR (500 MHz, DMSO-*d*<sub>6</sub>) δ [1.35 (s, minor rotamer) + 1.42 (s, 9H), 1.70–1.84 (m, 3H), 1.88–2.00 (m, 1H), 2.21 (dd, *J* = 6.3, 16.5, 1H), 2.33 (dd, *J* = 6.3, 16.7, 1H), 2.43–2.49 (m, 1H), 2.65–2.77 (m, 2H), 2.74 (s, 1H), 2.83 (dd, *J* = 9.4, 13.7, 1H), 3.08 (dd, *J* = 4.7, 13.7, 1H), 3.58 (dd, *J* = 9.2, 20.5, 1H), 4.33 (dt, *J* = 5.2, 8.7, 1H), 7.02 (br s, 1H), 7.07 (d, *J* = 9.4 Hz, 1H), 7.11–7.33 (m, 10H), 7.55 (br s, 1H), 8.07 (d, *J* = 7.5 Hz, 1H); <sup>13</sup>C NMR (125 MHz, DMSO-*d*<sub>6</sub>, signals for major rotamer) δ 22.2, 22.3, 27.2 (<sup>1</sup>*J*<sub>PC</sub> = 87.4 Hz), 28.3, 29.2, 31.7, 31.8, 37.0, 38.8, 49.6 (<sup>1</sup>*J*<sub>PC</sub> = 106.2 Hz), 54.1, 72.5, 78.3, 81.9, 125.9, 126.1, 128.0, 128.3, 128.5, 129.2, 138.3, 141.4, 155.7, 172.1, 172.1, 172.9; <sup>31</sup>P NMR (81 MHz, DMSO-*d*<sub>6</sub>) δ 47.3, (47.0: minor rotamer). ES-MS *m/z*: calcd for [C<sub>29</sub>H<sub>38</sub>N<sub>3</sub>O<sub>6</sub>P – H]<sup>–</sup> 554.3; found, 554.3. HRMS (*m/z*): [M + H]<sup>+</sup> calcd for C<sub>29</sub>H<sub>39</sub>N<sub>3</sub>O<sub>6</sub>P<sup>+</sup>, 556.2571; found, 556.2566.

**((1R)-1-Amino-3-phenylpropyl){(2'S)-3'-[[[(2'S)-1'-amino-1'-oxo-3''-phenylpropan-2''-yl]amino]-2''-[[3-(phenylisoxazol-5-yl)methyl]propyl]phosphinic Acid (13a).** 1,3-DCR between **9** and oxime **11a** according to general procedure E (no repetition was necessary for completion) and subsequent deprotection according to general procedure C afforded compound **13a** as a white solid (yield for two steps: 80%). <sup>1</sup>H NMR (500 MHz, DMSO-*d*<sub>6</sub>/3% TFA) δ 1.81–1.93 (m, 2H), 1.96–2.10 (m, 2H), 2.60–2.70 (m, 1H), 2.76–2.90 (m, 2H), 3.00–3.09 (m, 2H), 3.09–3.15 (m, 1H), 3.19 (d, *J* = 4.7, 14.8 Hz, 1H), 3.22–3.30 (m, 1H), 4.43 (dt, *J* = 5.7, 8.7 Hz, 1H), 6.70 (s, 1H), 7.01–7.85 (m, 17H), 8.28 (br s, 3H), 8.43 (d, *J* = 8.2 Hz, 1H); <sup>13</sup>C NMR (125 MHz, DMSO-*d*<sub>6</sub>/2% TFA) δ 29.3 (d, <sup>1</sup>*J*<sub>PC</sub> = 92.3 Hz), 29.7, 31.6, 31.7, 37.5, 37.9, 48.7 (d, <sup>1</sup>*J*<sub>PC</sub> = 94.9 Hz), 54.2, 100.4, 126.2, 126.3, 126.6, 128.1, 128.3, 128.5, 128.9, 129.1, 129.2, 130.1, 138.1, 140.9, 161.9, 171.4, 172.3, 172.4, 173.0; <sup>31</sup>P NMR (81 MHz, DMSO-*d*<sub>6</sub>/3% TFA) δ 40.5. HRMS (*m/z*): [M – H]<sup>–</sup> calcd for C<sub>31</sub>H<sub>34</sub>N<sub>4</sub>O<sub>5</sub>P<sup>–</sup>, 573.2272; found, 573.2216.

**((1R)-1-Amino-3-phenylpropyl){(2'S)-3'-[[[(2'S)-1'-amino-1'-oxo-3''-phenylpropan-2''-yl]amino]-2''-[[3-(2-methoxyphenyl)isoxazol-5-yl)methyl]-3'-oxopropyl]phosphinic Acid (13b).** 1,3-DCR between **9** and oxime **11b** according to general procedure E (no repetition was necessary for completion) and subsequent deprotection according to general procedure C afforded compound **13b** as a white solid (yield for two steps: 85%). <sup>1</sup>H NMR (200 MHz, DMSO-*d*<sub>6</sub> + CDCl<sub>3</sub>/3% TFA) δ 1.55–2.20 (m, 4H), 2.54–3.34 (m, 8H), 3.83 (s, 3H), 4.26–4.56 (m, 1H), 6.58 (s, 1H), 6.84–7.79 (m, 16H), 8.02–8.53 (m, 4H); <sup>13</sup>C NMR (50 MHz, DMSO-*d*<sub>6</sub> + CDCl<sub>3</sub>/3% TFA) δ 29.1 (d, <sup>1</sup>*J*<sub>PC</sub> = 92.5 Hz), 29.9, 31.7, 31.9, 37.6, 38.0, 48.7 (d, <sup>1</sup>*J*<sub>PC</sub> = 96.1 Hz), 54.3, 55.7, 103.5, 112.1, 117.5, 120.8, 126.3, 128.1, 128.4, 128.6, 128.9, 129.4, 131.5, 138.2, 140.9, 157.0, 159.6, 170.1, 172.3, 172.5, 173.0; <sup>31</sup>P NMR (81 MHz, DMSO-*d*<sub>6</sub>/3% TFA) δ 40.1. HRMS (*m/z*): [M – H]<sup>–</sup> calcd for C<sub>32</sub>H<sub>36</sub>N<sub>4</sub>O<sub>6</sub>P<sup>–</sup>, 603.2378; found, 603.2351.

**((1R)-1-Amino-3-phenylpropyl){(2'S)-3'-[[[(2'S)-1'-amino-1'-oxo-3''-phenylpropan-2''-yl]amino]-2''-[[3-(3-methoxyphenyl)isoxazol-5-yl)methyl]-3'-oxopropyl]phosphinic Acid (13c).** 1,3-DCR between **9** and oxime **11c** according to general procedure E (one repetition was necessary for completion) and subsequent deprotection according to general procedure C afforded compound **13c** as a white solid (yield for two steps: 75%). <sup>1</sup>H NMR (200 MHz, DMSO-*d*<sub>6</sub>/5% TFA) δ 1.66–2.14 (m, 4H), 2.52–2.94 (m, 3H), 2.95–3.38 (m, 5H), 3.80 (s, 3H), 4.33–4.56 (m, 1H), 6.74 (s, 1H), 6.84–7.68 (m, 16H), 8.30 (br s, 3H), 8.48 (d, *J* = 7.4 Hz, 1H); <sup>13</sup>C NMR (50 MHz, DMSO-*d*<sub>6</sub>/5% TFA) δ 29.4 (d, <sup>1</sup>*J*<sub>PC</sub> = 93.9 Hz), 29.9, 31.7, 31.9, 37.0, 37.7, 38.0, 48.9 (d, <sup>1</sup>*J*<sub>PC</sub> = 93.9 Hz), 54.4, 55.5, 100.7, 112.1, 116.2, 119.1, 126.4, 128.3, 128.4, 128.5, 128.7, 129.4, 130.1, 130.5, 131.5, 137.7, 138.3, 141.0, 159.9, 162.0, 171.6, 172.5, 172.7, 173.1, 173.2; <sup>31</sup>P NMR (81 MHz, DMSO-*d*<sub>6</sub>/5% TFA) δ 40.5. HRMS (*m/z*): [M – H]<sup>–</sup> calcd for C<sub>32</sub>H<sub>36</sub>N<sub>4</sub>O<sub>6</sub>P<sup>–</sup>, 603.2378; found, 603.2379.

**((1R)-1-Amino-3-phenylpropyl){(2'S)-3'-[[[(2'S)-1'-amino-1'-oxo-3''-phenylpropan-2''-yl]amino]-2''-[[3-(4-methoxyphenyl)-**

**isoxazol-5-yl]methyl]-3'-oxopropyl]phosphinic Acid (13d).** 1,3-DCR between **9** and oxime **11d** according to general procedure E (2 repetitions were necessary for completion) and subsequent deprotection according to general procedure C afforded compound **13d** as a white solid (yield for two steps: 76%). <sup>1</sup>H NMR (200 MHz, DMSO-*d*<sub>6</sub>/5% TFA) δ 1.70–2.21 (m, 4H), 2.35–2.94 (m, 3H), 2.94–3.40 (m, 5H), 3.79 (s, 3H), 4.33–4.55 (m, 1H), 6.63 (s, 1H), 6.82–7.85 (m, 16H), 8.27 (br s, 3H), 8.47 (d, *J* = 7.7 Hz, 1H); <sup>13</sup>C NMR (50 MHz, DMSO-*d*<sub>6</sub>/5% TFA) δ 29.3 (d, <sup>1</sup>*J*<sub>PC</sub> = 94.6 Hz), 29.9, 31.7, 31.9, 37.7, 38.1, 48.8 (d, <sup>1</sup>*J*<sub>PC</sub> = 95.6 Hz), 54.4, 55.4, 100.4, 114.7, 121.4, 126.4, 128.3, 128.5, 128.8, 129.5, 138.3, 141.0, 160.9, 161.7, 171.1, 172.4, 172.6, 173.2; <sup>31</sup>P NMR (81 MHz, DMSO-*d*<sub>6</sub>/5% TFA) δ 41.2. HRMS (*m/z*): [M – H]<sup>–</sup> calcd for C<sub>32</sub>H<sub>36</sub>N<sub>4</sub>O<sub>6</sub>P<sup>–</sup>, 603.2378; found, 603.2382.

**((1R)-1-Amino-3-phenylpropyl){(2'S)-3'-[[[(2'S)-1'-amino-1'-oxo-3''-phenylpropan-2''-yl]amino]-2''-[[3-(2-chlorophenyl)isoxazol-5-yl]methyl]-3'-oxopropyl]phosphinic Acid (13e).** 1,3-DCR between **9** and oxime **11e** according to general procedure E (no repetition was necessary for completion) and subsequent deprotection according to general procedure C afforded compound **13e** as a white solid (yield for two steps: 73%). <sup>1</sup>H NMR (200 MHz, DMSO-*d*<sub>6</sub>/4% TFA) δ 1.69–2.21 (m, 4H), 2.53–2.93 (m, 3H), 2.93–3.36 (m, 5H), 4.29–4.52 (m, 1H), 6.58 (s, 1H), 6.81–7.71 (m, 16H), 8.28 (br s, 3H), 8.40 (d, *J* = 8.2 Hz, 1H); <sup>13</sup>C NMR (50 MHz, DMSO-*d*<sub>6</sub>/4% TFA) δ 29.8 (d, <sup>1</sup>*J*<sub>PC</sub> = 92.6 Hz), 29.9, 31.6, 31.8, 37.0, 37.7, 38.0, 48.7 (d, <sup>1</sup>*J*<sub>PC</sub> = 94.7 Hz), 54.2, 103.4, 126.4, 127.8, 128.2, 128.3, 128.4, 128.7, 129.4, 130.6, 131.2, 131.6, 132.0, 138.2, 140.9, 160.7, 170.9, 172.2, 172.4, 172.9; <sup>31</sup>P NMR (81 MHz, DMSO-*d*<sub>6</sub>/4% TFA) δ 40.8. HRMS (*m/z*): [M – H]<sup>–</sup> calcd for C<sub>31</sub>H<sub>33</sub>ClN<sub>4</sub>O<sub>5</sub>P<sup>–</sup>, 607.1883; found, 607.1876.

**((1R)-1-Amino-3-phenylpropyl){(2'S)-3'-[[[(2'S)-1'-amino-1'-oxo-3''-phenylpropan-2''-yl]amino]-2''-[[3-(3-chlorophenyl)isoxazol-5-yl]methyl]-3'-oxopropyl]phosphinic Acid (13f).** 1,3-DCR between **9** and oxime **11f** according to general procedure E (5 repetitions were necessary for completion) and subsequent deprotection according to general procedure C afforded compound **13f** as a white solid (yield for two steps: 67%). <sup>1</sup>H NMR (500 MHz, DMSO-*d*<sub>6</sub>/3% TFA) δ 1.75–1.95 (m, 2H), 1.96–2.11 (m, 2H), 2.57–2.72 (m, 1H), 2.75–2.91 (m, 2H), 2.95–3.40 (m, 5H), 4.32–4.49 (m, 1H), 6.76 (s, 1H), 7.00–7.93 (m, 16H), 8.30 (br s, 3H), 8.45 (d, *J* = 7.3 Hz, 1H); <sup>13</sup>C NMR (50 MHz, DMSO-*d*<sub>6</sub>/3% TFA) δ 29.3 (d, <sup>1</sup>*J*<sub>PC</sub> = 93.1 Hz), 29.8, 31.5, 31.7, 37.5, 37.8, 37.9, 48.7 (d, <sup>1</sup>*J*<sub>PC</sub> = 94.2 Hz), 54.2, 100.5, 125.2, 126.2, 128.1, 128.3, 128.5, 129.2, 130.0, 130.8, 131.1, 133.9, 138.1, 140.9, 160.8, 171.8, 172.2, 172.4, 173.0; <sup>31</sup>P NMR (81 MHz, DMSO-*d*<sub>6</sub>/3% TFA) δ 39.8. HRMS (*m/z*): [M – H]<sup>–</sup> calcd for C<sub>31</sub>H<sub>33</sub>ClN<sub>4</sub>O<sub>5</sub>P<sup>–</sup>, 607.1883; found, 607.1880.

**((1R)-1-Amino-3-phenylpropyl){(2'S)-3'-[[[(2'S)-1'-amino-1'-oxo-3''-phenylpropan-2''-yl]amino]-2''-[[3-(4-chlorophenyl)isoxazol-5-yl]methyl]-3'-oxopropyl]phosphinic Acid (13g).** 1,3-DCR between **9** and oxime **11g** according to general procedure E (4 repetitions were necessary for completion) and subsequent deprotection according to general procedure C afforded compound **13g** as a white solid (yield for two steps: 67%). <sup>1</sup>H NMR (200 MHz, DMSO-*d*<sub>6</sub>/5% TFA) δ 1.69–2.18 (m, 4H), 2.57–2.95 (m, 3H), 2.95–3.37 (m, 5H), 4.28–4.52 (m, 1H), 6.71 (s, 1H), 6.88–7.91 (m, 16H), 8.30 (br s, 3H), 8.47 (d, *J* = 7.8 Hz, 1H); <sup>13</sup>C NMR (50 MHz, DMSO-*d*<sub>6</sub>/5% TFA) δ 29.4 (d, <sup>1</sup>*J*<sub>PC</sub> = 93.5 Hz), 30.0, 31.8, 32.0, 37.1, 37.7, 48.9 (d, <sup>1</sup>*J*<sub>PC</sub> = 96.2 Hz), 54.5, 100.7, 126.4, 126.5, 128.0, 128.3, 128.6, 128.8, 129.5, 135.1, 138.4, 141.1, 161.2, 172.0, 172.5, 172.7, 173.4; <sup>31</sup>P NMR (81 MHz, DMSO-*d*<sub>6</sub>/5% TFA) δ 40.8. HRMS (*m/z*): [M – H]<sup>–</sup> calcd for C<sub>31</sub>H<sub>33</sub>ClN<sub>4</sub>O<sub>5</sub>P<sup>–</sup>, 607.1883; found, 607.1863.

**((1R)-1-Amino-3-phenylpropyl){(2'S)-3'-[[[(2'S)-1'-amino-1'-oxo-3''-phenylpropan-2''-yl]amino]-2''-[[3-(2-hydroxyphenyl)isoxazol-5-yl]methyl]-3'-oxopropyl]phosphinic Acid (13h).** 1,3-DCR between **9** and oxime **11h** was performed according to general procedure E (no repetition was necessary for completion). The product was dissolved in DMF/H<sub>2</sub>O 10:1 (2 mL/mmol) and Cs<sub>2</sub>CO<sub>3</sub> (2 equiv) was added. After stirring at rt overnight, the mixture was acidified with 1 M HCl to pH 1, extracted with AcOEt (× 3). After concentration in vacuo of the organic layer, the residue was subjected to deprotection according to general procedure C, affording

compound **13h** as a white solid (yield for three steps: 51%). <sup>1</sup>H NMR (200 MHz, DMSO-*d*<sub>6</sub>/2% TFA) δ 1.64–2.20 (m, 4H), 2.36–2.93 (m, 3H), 2.94–3.42 (m, 5H), 4.28–4.50 (m, 1H), 6.75 (s, 1H), 6.62–7.56 (m, 16H), 7.69 (d, *J* = 7.3 Hz, 1H), 8.29 (br s, 3H); <sup>13</sup>C NMR (50 MHz, DMSO-*d*<sub>6</sub>/2% TFA) δ 29.2 (d, <sup>1</sup>*J*<sub>PC</sub> = 91.2 Hz), 29.9, 31.6, 31.8, 37.5, 48.7 (d, <sup>1</sup>*J*<sub>PC</sub> = 94.3 Hz), 54.3, 102.9, 115.2, 116.8, 119.5, 126.3, 128.2, 128.4, 128.6, 129.3, 131.3, 138.2, 141.0, 155.7, 160.4, 170.1, 172.4, 172.5, 172.9; <sup>31</sup>P NMR (81 MHz, DMSO-*d*<sub>6</sub>/2% TFA) δ 40.1. HRMS (*m/z*): [M – H]<sup>–</sup> calcd for C<sub>31</sub>H<sub>34</sub>N<sub>4</sub>O<sub>6</sub>P<sup>–</sup>, 589.2221; found, 589.2219.

((1*R*)-1-Amino-3-phenylpropyl){(2'*S*)-3'-[(2''*S*)-1''-amino-1''-oxo-3''-phenylpropan-2''-yl]amino}-2'-[[3-(4-hydroxyphenyl)-isoxazol-5-yl]methyl]-3'-oxopropyl]phosphonic acid (**13i**). 1,3-DCR between **9** and oxime **11i** was performed according to general procedure E (2 repetitions were necessary for completion). The product was treated with Cs<sub>2</sub>CO<sub>3</sub> as described above and subjected to deprotection according to general procedure C, affording compound **13i** as a white solid (yield for three steps: 61%). <sup>1</sup>H NMR (500 MHz, DMSO-*d*<sub>6</sub>/3.5% TFA) δ 1.76–1.96 (m, 2H), 1.98–2.17 (m, 2H), 2.59–2.73 (m, 1H), 2.73–2.95 (m, 2H), 2.95–3.68 (m, 5H), 4.35–4.54 (m, 1H), 6.54 (s, 1H), 6.78–7.69 (m, 16H), 8.30 (br s, 3H), 8.44 (d, *J* = 7.8 Hz, 1H); <sup>13</sup>C NMR (50 MHz, DMSO-*d*<sub>6</sub>/3.5% TFA) δ 29.5 (d, <sup>1</sup>*J*<sub>PC</sub> = 92.0 Hz), 30.1, 31.9, 32.1, 37.8, 49.0 (d, <sup>1</sup>*J*<sub>PC</sub> = 95.8 Hz), 54.6, 100.3, 116.2, 119.9, 126.5, 126.6, 128.4, 128.6, 128.8, 129.6, 138.4, 141.2, 159.5, 162.1, 171.1, 172.7, 172.8, 173.4; <sup>31</sup>P NMR (81 MHz, DMSO-*d*<sub>6</sub>/23.5% TFA) δ 40.1. HRMS (*m/z*): [M – H]<sup>–</sup> calcd for C<sub>31</sub>H<sub>34</sub>N<sub>4</sub>O<sub>6</sub>P<sup>–</sup>, 589.2221; found, 589.2233.

((1*R*)-1-Amino-3-phenylpropyl){(2'*S*)-2'-[(2''*S*)-1''-amino-1''-oxo-3''-phenylpropan-2''-yl]carbamoyl]pent-4'-yn-1'-yl]-phosphonic acid (**14**). Phosphonic tripeptide **9** (24 mg, 43 μmol) was subjected to deprotection according to general procedure C, affording compound **14** as a white solid (17 mg, 87%). <sup>1</sup>H NMR (250 MHz, DMSO-*d*<sub>6</sub>/5% TFA) δ 1.76–2.19 (m, 4H), 2.35–2.70 (m, 3H), 2.72–2.91 (m, 4H), 3.03 (dd, *J* = 5.2, 13.7, 1H), 3.11–3.26 (m, 1H), 4.38 (dd, *J* = 8.1, 13.5, 1H), 7.01–7.45 (m, 12H), 8.14–8.33 (m, 4H); <sup>13</sup>C NMR (63 MHz, DMSO-*d*<sub>6</sub>/5% TFA) δ 22.7, 22.9, 28.4 (<sup>1</sup>*J*<sub>PC</sub> = 92.9 Hz), 29.7, 31.6, 31.7, 48.7 (<sup>1</sup>*J*<sub>PC</sub> = 95.6 Hz), 54.4, 73.2, 81.8, 126.3, 128.2, 128.4, 128.7, 129.4, 138.2, 140.9, 155.7, 172.3, 172.4, 172.8; <sup>31</sup>P NMR (81 MHz, DMSO-*d*<sub>6</sub>/5% TFA) δ 41.7. HRMS (*m/z*): [M – H]<sup>–</sup> calcd for C<sub>24</sub>H<sub>29</sub>N<sub>3</sub>O<sub>4</sub>P<sup>–</sup>, 454.1901; found, 454.1893.

**Ethyl 2-Methylene-4,4-diphenylbutanoate (15)**. A solution of DCC (1.18 g, 5.72 mmol) in dry CH<sub>2</sub>Cl<sub>2</sub> (11 mL) was added to a solution of 2,2-diphenylacetic acid (1.0 g, 4.7 mmol), Meldrum's acid (0.75 g, 5.2 mmol), and DMAP (0.92 g, 7.5 mmol) in CH<sub>2</sub>Cl<sub>2</sub> (22 mL) at 0 °C over a period of 1 h. After stirring at rt for 3 h, the reaction mixture was cooled at –10 °C overnight. The solid precipitate was removed by filtration through a Celite pad, and the filtrates were concentrated in vacuo. The residue was dissolved in AcOEt (20 mL) and washed with sat. NaHSO<sub>4</sub> (2 × 10 mL) and brine (10 mL). The organic phase was dried over Na<sub>2</sub>SO<sub>4</sub> and evaporated in vacuo. The residue was dissolved in dry CH<sub>2</sub>Cl<sub>2</sub> (15 mL), and AcOH (3.5 mL) was added at 0 °C. Then, NaBH<sub>4</sub> (0.60 g, 15.8 mmol) was added over a period of 2 h. After stirring at rt overnight, the reaction mixture was washed with H<sub>2</sub>O (2 × 10 mL) and brine (10 mL) and the organic phase was dried over Na<sub>2</sub>SO<sub>4</sub> and concentrated in vacuo. The residue was purified by column chromatography (PE 40–60 °C/AcOEt 3:7) to afford the alkylated Meldrum's derivative as a white solid (0.75 g, 49%): mp 145–147 °C; <sup>1</sup>H NMR (200 MHz, CDCl<sub>3</sub>) δ 1.57 (s, 3H), 1.71 (s, 3H), 2.79 (dd, *J* = 6.0, 8.5 Hz, 2H), 3.28 (t, *J* = 6.0 Hz, 1H), 4.59 (t, *J* = 8.5 Hz, 1H), 7.12–7.41 (m, 10H); <sup>13</sup>C NMR (50 MHz, CDCl<sub>3</sub>) δ 26.3, 28.7, 32.0, 44.4, 48.3, 105.1, 127.0, 128.1, 129.0, 143.0, 165.7. A solution of the above derivative (500 mg, 1.54 mmol) and Eschenmoser's salt (712 mg, 3.85 mmol) in THF/abs EtOH 1:3 (15 mL) was heated at 65 °C overnight, and then the mixture was cooled at rt, diluted with AcOEt (20 mL), and washed with 10% Na<sub>2</sub>CO<sub>3</sub> (10 mL), H<sub>2</sub>O (2 × 10 mL), and 2 M HCl (10 mL). The organic phase was dried over Na<sub>2</sub>SO<sub>4</sub> and concentrated in vacuo. The residue was purified by column chromatography (PE 40–60 °C/AcOEt 9.5:0.5 → 2:1) to afford **15** as a light-yellow viscous oil (402 mg, 93%). <sup>1</sup>H NMR (200 MHz, CDCl<sub>3</sub>) δ 1.33 (t, *J* = 7.1 Hz, 3H), 3.14 (dd, *J* = 0.7, 7.8

Hz, 2H), 4.23 (q, *J* = 7.1 Hz, 2H), 4.33 (t, *J* = 7.8 Hz, 1H), 5.36 (d, *J* = 1.2 Hz, 1H), 6.13 (d, *J* = 1.2 Hz, 1H), 7.11–7.41 (m, 10H); <sup>13</sup>C NMR (50 MHz, CDCl<sub>3</sub>) δ 14.3, 38.1, 50.0, 60.7, 126.3, 127.0, 128.1, 128.5, 138.6, 144.1, 167.1. HRMS (*m/z*): [M + Na]<sup>+</sup> calcd for C<sub>19</sub>H<sub>20</sub>NaO<sub>2</sub><sup>+</sup>, 303.1356; found, 303.1359.

**[1,1':3',1''-Terphenyl]-5'-carbaldehyde (17a)**. A mixture of 3,5-dibromobenzaldehyde (0.60 g, 2.27 mmol), DME (24 mL), H<sub>2</sub>O (5 mL), phenylboronic acid (0.75 g, 6.15 mmol), and Na<sub>2</sub>CO<sub>3</sub> (0.96 g, 9.08 mmol) was degassed by applying three freeze–pump–thaw cycles. Then, Pd(PPh<sub>3</sub>)<sub>4</sub> (262 mg, 0.227 mmol) was added, and the resulting suspension was heated at 90 °C overnight. The mixture was diluted with Et<sub>2</sub>O (20 mL), and the organic phase was washed with H<sub>2</sub>O (2 × 10 mL), dried over Na<sub>2</sub>SO<sub>4</sub>, and concentrated in vacuo. The residue was purified by column chromatography (PE 40–60 °C/AcOEt 9.8:0.2 → 0:1) to afford **17a** as a white solid (0.57 g, 98%). Mp 96–98 °C; <sup>1</sup>H NMR (200 MHz, CDCl<sub>3</sub>) δ 7.39–7.59 (m, 6H), 7.62–7.76 (m, 4H), 8.07 (s, 3H), 10.13 (s, 1H); <sup>13</sup>C NMR (50 MHz, CDCl<sub>3</sub>) δ 127.1, 127.2, 128.1, 129.0, 131.7, 137.4, 139.6, 142.6, 192.2. HRMS (*m/z*): [M + Na]<sup>+</sup> calcd for C<sub>19</sub>H<sub>14</sub>NaO<sup>+</sup>, 281.0937; found, 281.0938.

**3,3''-Dichloro-[1,1':3',1''-terphenyl]-5'-carbaldehyde (17b)**. 3,5-Dibromobenzaldehyde (0.75 g, 2.84 mmol) and boronic acid **16b** (1.60 g, 10.2 mmol) were converted to **17b** by following the same procedure as described for the synthesis of **17a**. Compound **17b** was obtained as a white solid (0.76 g, 82%). Mp 131–134 °C; <sup>1</sup>H NMR (200 MHz, CDCl<sub>3</sub>) δ 7.31–7.69 (m, 8H), 7.92–8.15 (m, 3H), 10.16 (s, 1H); <sup>13</sup>C NMR (50 MHz, CDCl<sub>3</sub>) δ 125.4, 127.3, 127.5, 128.3, 130.4, 131.4, 135.0, 137.6, 141.2, 141.5, 191.8.

**5'-(Bromomethyl)-1,1':3',1''-terphenyl (18a)**. In an ice-cooled solution of aldehyde **17a** (504 mg, 1.95 mmol) in EtOH (20 mL), NaBH<sub>4</sub> (74 mg, 1.95 mmol) was slowly added. The mixture was stirred at rt during 1.5 h and then quenched with dilute HCl. The mixture was partitioned with Et<sub>2</sub>O (30 mL) and H<sub>2</sub>O (10 mL), and the aqueous phase was washed with Et<sub>2</sub>O (3 × 10 mL). The combined organic layers were dried over Na<sub>2</sub>SO<sub>4</sub> and concentrated in vacuo. The resulting white solid was dissolved in dry CH<sub>2</sub>Cl<sub>2</sub> (10 mL), and PBr<sub>3</sub> (0.18 mL, 1.95 mmol) was added dropwise at 0 °C over a period of 5 min. After stirring at rt for 1 h, the organic phase was washed with H<sub>2</sub>O (2 × 10 mL), dried over Na<sub>2</sub>SO<sub>4</sub>, and concentrated in vacuo. Compound **18a** was obtained as an off-white solid (0.57 g, 91%). Mp 92–94 °C; <sup>1</sup>H NMR (200 MHz, CDCl<sub>3</sub>) δ 4.62 (s, 2H), 7.30–7.81 (m, 13H); <sup>13</sup>C NMR (50 MHz, CDCl<sub>3</sub>) δ 33.6, 125.6, 126.4, 126.9, 127.4, 127.8, 129.9, 138.8, 140.6, 142.4, 142.5.

**5'-(Bromomethyl)-3,3''-dichloro-1,1':3',1''-terphenyl (18b)**. Compound **17b** (0.77 g, 2.34 mmol) was converted to **18b** by following the same procedure as described for the synthesis of **18a**. White solid (0.74 g, 81%). Mp 96–100 °C; <sup>1</sup>H NMR (200 MHz, CDCl<sub>3</sub>) δ 4.60 (s, 2H), 7.16–7.66 (m, 11H); <sup>13</sup>C NMR (50 MHz, CDCl<sub>3</sub>) δ 33.1, 125.5, 126.1, 127.3, 127.5, 128.0, 130.3, 134.9, 139.3, 141.3, 142.1. ES-MS *m/z*: calcd for [C<sub>19</sub>H<sub>13</sub>BrCl<sub>2</sub> – H]<sup>–</sup> 391.0; found, 390.8.

**Ethyl 2-([1,1':3',1''-Terphenyl]-5'-ylmethyl)acrylate (19a)**. A suspension of compound **18a** (0.58 g, 1.78 mmol), triethyl methanetricarboxylate (0.42 mL, 1.95 mmol), and K<sub>2</sub>CO<sub>3</sub> (0.27 mg, 1.97 mmol) in DMF/toluene 1:1 (30 mL) was refluxed over a period of 1.5 h. Then, H<sub>2</sub>O (50 mL) was added, the organic phase was separated, and the aqueous phase was extracted with AcOEt (2 × 15 mL). The combined organic layers were dried over Na<sub>2</sub>SO<sub>4</sub>, concentrated in vacuo, and the resulting orange oil was dissolved in EtOH (10 mL). A solution of KOH (1.1 g, 19 mmol) in EtOH (3 mL) was added at 0 °C, and the mixture was stirred at rt overnight. After evaporation of the volatiles, the residue was dissolved in H<sub>2</sub>O (20 mL) and the aqueous solution was washed with Et<sub>2</sub>O (3 × 5 mL), acidified to pH 1, and extracted with AcOEt (4 × 20 mL). The combined organic layers were dried over Na<sub>2</sub>SO<sub>4</sub>, concentrated in vacuo, and the resulting yellowish oil was dissolved in AcOEt (7 mL). After the addition of Et<sub>3</sub>NH (0.24 mL, 2.35 mmol) and paraformaldehyde (86 mg, 2.88 mmol), the mixture was refluxed during 4 h. Then, the volatiles were evaporated, and the residue was dissolved in H<sub>2</sub>O (30 mL), acidified to pH 1, and extracted with AcOEt (2 × 20 mL). The

combined organic layers were dried over  $\text{Na}_2\text{SO}_4$  and concentrated in vacuo. The resulting crude acrylic acid (0.38 g, 1.22 mmol) was dissolved in dry  $\text{CH}_2\text{Cl}_2$  (3 mL), and EtOH (0.14 mL, 2.4 mmol), DIPEA (0.28 mL, 1.6 mmol), EDC-HCl (307 mg, 1.6 mmol), and DMAP (15 mg, 0.12 mmol) were successively added. The mixture was stirred overnight at rt, and then it was concentrated to dryness. The residue was dissolved in AcOEt (20 mL) and washed with  $\text{H}_2\text{O}$  ( $2 \times 5$  mL), 5%  $\text{NaHCO}_3$  ( $2 \times 5$  mL), 1 M HCl ( $2 \times 5$  mL), and brine (5 mL). The organic phase was dried over  $\text{Na}_2\text{SO}_4$  and concentrated in vacuo. The residue was purified by column chromatography (PE 40–60 °C/AcOEt 9:1  $\rightarrow$  2:1) to afford **19a** as a colorless viscous oil (341 mg, 56%).  $^1\text{H}$  NMR (200 MHz,  $\text{CDCl}_3$ )  $\delta$  1.29 (t,  $J = 7.1$  Hz, 3H), 3.78 (s, 2H), 4.22 (q,  $J = 7.1$  Hz, 2H), 5.59 (t,  $J = 1.3$  Hz, 1H), 6.31 (s, 1H), 7.30–7.54 (m, 8H), 7.60–7.7 (m, 5H);  $^{13}\text{C}$  NMR (50 MHz,  $\text{CDCl}_3$ )  $\delta$  14.3, 38.3, 61.0, 124.4, 126.5, 127.1, 127.4, 127.5, 128.9, 139.9, 140.3, 141.2, 142.0, 167.0. ES-MS  $m/z$ : calcd for  $[\text{C}_{24}\text{H}_{22}\text{O}_2 + \text{NH}_4]^+$  360.2; found, 360.2. HRMS ( $m/z$ ):  $[\text{M} + \text{Na}]^+$  calcd for  $\text{C}_{24}\text{H}_{22}\text{NaO}_2^+$ , 365.1512; found, 365.1516.

**Ethyl 2-[(3,3'-Dichloro-1,1':3',1''-terphenyl)-5'-yl)methyl]-acrylate (19b).** Compound **18b** (741 mg, 1.89 mmol) was converted to **19b** by following the same procedure as described for the synthesis of **19a**. Colorless viscous oil (194 mg, 25%).  $^1\text{H}$  NMR (200 MHz,  $\text{CDCl}_3$ )  $\delta$  1.27 (t,  $J = 7.1$  Hz, 3H), 3.76 (s, 2H), 4.21 (q,  $J = 7.1$  Hz, 2H), 5.59 (q,  $J = 1.2$  Hz, 1H), 6.30 (br s, 1H), 7.18–7.67 (m, 11H);  $^{13}\text{C}$  NMR (50 MHz,  $\text{CDCl}_3$ )  $\delta$  14.3, 38.3, 61.1, 124.3, 125.6, 126.7, 127.5, 127.7, 130.2, 134.8, 140.1, 140.4, 140.8, 142.8, 166.9. ES-MS  $m/z$ : calcd for  $[\text{C}_{24}\text{H}_{20}\text{Cl}_2\text{O}_2 + \text{NH}_4]^+$  428.1; found, 428.2. HRMS ( $m/z$ ):  $[\text{M} + \text{Na}]^+$  calcd for  $\text{C}_{24}\text{H}_{20}\text{Cl}_2\text{NaO}_2^+$ , 433.0733; found, 433.0737.

**3'-[(1R)-1-[(tert-butoxy)carbonyl]amino]-3-phenylpropyl]-propanoic Acid (21a).** Addition of phosphinic acid **7** (300 mg, 1.00 mmol) to ethyl 2-[(adamant-1-yl)methyl]acrylate<sup>28</sup> (320 mg, 1.30 mmol) according to general procedure A and subsequent saponification according to general procedure B afforded compound **21a** as a mixture of two diastereoisomers (410 mg, 79% starting from **11**).  $^1\text{H}$  NMR (200 MHz,  $\text{DMSO-}d_6$ )  $\delta$  1.19–2.09 (m, 30H), 2.30–2.54 and 2.55–2.82 (m, 3H), 3.32–3.67 (m, 1H), 6.90–7.35 (m, 5H);  $^{13}\text{C}$  NMR (50 MHz,  $\text{DMSO-}d_6$ )  $\delta$  28.1, 28.3, 29.2, 29.8, 29.9, 32.5 (d,  $^1J_{\text{PC}} = 77$  Hz), 32.5, 32.7 (d,  $^1J_{\text{PC}} = 80$  Hz), 36.6, 41.8, 47.0, 47.6, 49.3 (d,  $^1J_{\text{PC}} = 105$  Hz), 49.7 (d,  $^1J_{\text{PC}} = 105$  Hz), 78.2, 78.6, 125.9, 128.4, 128.5, 141.4, 141.5, 155.7, 155.8, 177.4, 177.5, 177.6, 177.7;  $^{31}\text{P}$  NMR (81 MHz,  $\text{DMSO-}d_6$ )  $\delta$  46.5. ES-MS  $m/z$ : calcd for  $[\text{C}_{28}\text{H}_{42}\text{NO}_6\text{P} - \text{H}]^-$  518.3; found, 518.4. HRMS ( $m/z$ ):  $[\text{M} + \text{Na}]^+$  calcd for  $\text{C}_{28}\text{H}_{42}\text{NNaO}_6\text{P}^+$ , 542.2642; found, 542.2645.

**2'-[[(1R)-1-[(tert-butoxy)carbonyl]amino]-3-phenylpropyl]-[hydroxy]phosphoryl]methyl-4',4'-diphenylbutanoic Acid (21b).** Addition of phosphinic acid **7** (300 mg, 1.00 mmol) to acrylic derivative **15** (308 mg, 1.10 mmol) according to general procedure A and subsequent saponification according to general procedure B afforded compound **21b** as a mixture of two diastereoisomers (336 mg, 61% starting from **11**).  $^1\text{H}$  NMR (200 MHz,  $\text{DMSO-}d_6$ )  $\delta$  1.40 + 1.43 ( $2 \times$  s, 9H), 1.63–2.06 (m, 4H), 2.07–2.28 (m, 1H), 2.35–2.81 (m, 4H), 3.41–3.70 (m, 1H), 3.89–4.08 (m, 1H), 6.66 (d,  $J = 9.3$  Hz, 1H), 6.97–7.42 (m, 15H);  $^{13}\text{C}$  NMR (50 MHz,  $\text{DMSO-}d_6$ )  $\delta$  27.9, 28.0, 28.3, 29.2, 29.3, 29.6, 29.7, 31.8, 32.0, 37.2, 48.6, 49.5 (d,  $^1J_{\text{PC}} = 105$  Hz), 49.8 (d,  $^1J_{\text{PC}} = 106$  Hz), 78.3, 78.4, 125.9, 126.2, 127.5, 128.0, 128.4, 128.6, 141.4, 143.6, 145.3, 155.7, 155.8, 176.0, 176.1, 176.2;  $^{31}\text{P}$  NMR (81 MHz,  $\text{DMSO-}d_6$ )  $\delta$  46.5. ES-MS  $m/z$ : calcd for  $[\text{C}_{31}\text{H}_{38}\text{NO}_6\text{P} - \text{H}]^-$  550.2; found, 550.3. HRMS ( $m/z$ ):  $[\text{M} + \text{H}]^+$  calcd for  $\text{C}_{31}\text{H}_{39}\text{NO}_6\text{P}^+$ , 552.2510; found, 552.2515.

**3'-[(1,1':3',1''-Terphenyl)-5'-yl]-2'-[[(1R)-1-[(tert-butoxy)carbonyl]amino]-3-phenylpropyl]-[hydroxy]phosphoryl]-methyl]propanoic Acid (21c).** Addition of phosphinic acid **7** (200 mg, 0.67 mmol) to acrylic derivative **19a** (277 mg, 0.81 mmol) according to general procedure A and subsequent saponification according to general procedure B afforded compound **8** as a mixture of two diastereoisomers (362 mg, 88% starting from **7**).  $^1\text{H}$  NMR (200 MHz,  $\text{DMSO-}d_6$ )  $\delta$  1.34 + 1.41 ( $2 \times$  s, 9H), 1.58–2.08 (m, 4H), 2.37–2.58 (m, 1H), 2.58–2.80 (m, 1H), 2.92–3.20 (m, 3H), 3.47–3.73 (m, 1H), 7.06–7.83 (m, 19H);  $^{13}\text{C}$  NMR (50 MHz,  $\text{DMSO-}d_6$ )  $\delta$

26.4, 27.9, 28.2, 29.0, 29.2, 31.6, 31.9, 49.1 ( $^1J_{\text{PC}} = 107$  Hz), 49.5 ( $^1J_{\text{PC}} = 107$  Hz), 78.3, 78.4, 123.5, 125.9, 126.9, 127.1, 127.7, 128.4, 128.6, 128.8, 129.0, 140.1, 140.3, 141.0, 141.4, 141.5, 155.7, 155.8, 175.2, 175.4, 175.5, 175.6;  $^{31}\text{P}$  NMR (81 MHz,  $\text{DMSO-}d_6$ )  $\delta$  46.7, 47.0. ES-MS  $m/z$ : calcd for  $[\text{C}_{36}\text{H}_{40}\text{NO}_6\text{P} - \text{H}]^-$  612.3; found, 612.4. HRMS ( $m/z$ ):  $[\text{M} + \text{H}]^+$  calcd for  $\text{C}_{36}\text{H}_{41}\text{NO}_6\text{P}^+$ , 614.2666; found, 614.2666.

**3'-[[(1R)-1-[(tert-butoxy)carbonyl]amino]-3-phenylpropyl]-[hydroxy]phosphoryl]-2'-[(3,3'-dichloro-1,1':3',1''-terphenyl)-5'-yl]methyl]propanoic Acid (21d).** Addition of phosphinic acid **7** (175 mg, 0.58 mmol) to acrylic derivative **19b** (292 mg, 0.71 mmol) according to general procedure A and subsequent saponification according to general procedure B afforded compound **21d** as a mixture of two diastereoisomers (344 mg, 87% starting from **7**).  $^1\text{H}$  NMR (200 MHz,  $\text{DMSO-}d_6$ )  $\delta$  1.33 + 1.41 ( $2 \times$  s, 9H), 1.59–2.08 (m, 4H), 2.31–2.51 (m, 1H), 2.58–2.80 (m, 1H), 2.92–3.16 (m, 3H), 3.44–3.71 (m, 1H), 7.03–7.93 (m, 17H);  $^{13}\text{C}$  NMR (50 MHz,  $\text{DMSO-}d_6$ )  $\delta$  26.5, 27.9, 28.2, 28.9, 29.1, 31.6, 31.8, 49.4 ( $^1J_{\text{PC}} = 106$  Hz), 78.2, 78.3, 123.8, 125.8, 126.8, 127.5, 128.3, 128.5, 130.7, 133.8, 139.4, 140.4, 141.4, 142.2, 155.7, 175.3, 175.5;  $^{31}\text{P}$  NMR (81 MHz,  $\text{DMSO-}d_6$ )  $\delta$  46.9, 47.1. ES-MS  $m/z$ : calcd for  $[\text{C}_{36}\text{H}_{38}\text{Cl}_2\text{NO}_6\text{P} - \text{H}]^-$  680.2; found, 680.3. HRMS ( $m/z$ ):  $[\text{M} + \text{Na}]^+$  calcd for  $\text{C}_{36}\text{H}_{38}\text{Cl}_2\text{NNaO}_6\text{P}^+$ , 704.1706; found, 704.1694.

**[(1R)-1-Amino-3-phenylpropyl]2'-[(adamantan-1-yl)-methyl]-3'-[[(2'S)-1'-amino-1''-oxo-3''-phenylpropan-2''-yl]-amino]-3'-oxopropyl]phosphinic Acid (22a).** Coupling of **21a** with HBr-H-(L)Phe-NH<sub>2</sub> (**5c**) according to general procedure D and subsequent deprotection according to general procedure C afforded compound **22a** as a mixture of two diastereoisomers (yield for two steps: 79%) which separated by semipreparative HPLC and tested separately.  $^1\text{H}$  NMR (200 MHz,  $\text{DMSO-}d_6$ )  $\delta$  1.14–1.70 (m, 16H), 1.71–2.26 (m, 5H), 2.60–2.98 (m, 4H), 3.00–3.36 (m, 2H), 4.34–4.56 (m, 1H), 6.97–8.01 (m, 13H), 7.34–8.01 (m, 3H);  $^{13}\text{C}$  NMR (50 MHz,  $\text{DMSO-}d_6/2\%$  TFA)  $\delta$  28.3, 30.0, 30.1, 31.7, 31.9, 32.6, 32.7, 33.9, 34.9, 36.7, 37.1, 37.6, 41.7, 41.9, 47.5, 47.6, 48.5, 48.8, 48.8 (d,  $^1J_{\text{PC}} = 94$  Hz), 49.0 (d,  $^1J_{\text{PC}} = 95$  Hz), 54.4, 126.4, 128.3, 128.6, 128.8, 129.3, 129.5, 138.5, 138.9, 141.1, 141.2, 143.1, 173.4, 174.3, 175.0, 175.2, 175.5, 175.6;  $^{31}\text{P}$  NMR (81 MHz,  $\text{DMSO-}d_6/2\%$  TFA)  $\delta$  45.8, 45.9. HRMS ( $m/z$ ):  $[\text{M} - \text{H}]^-$  calcd for  $\text{C}_{32}\text{H}_{43}\text{N}_3\text{O}_4\text{P}^-$ , 564.2997; found, 564.2996.

**[(1R)-1-Amino-3-phenylpropyl]2'-[[(2'S)-1'-amino-1''-oxo-3''-phenylpropan-2''-yl]carbamoyl]-4',4'-diphenylbutyl]-phosphinic Acid (22b).** Coupling of **21b** with HBr-H-(L)Phe-NH<sub>2</sub> (**5c**) according to general procedure D and subsequent deprotection according to general procedure C afforded compound **22b** as a mixture of two diastereoisomers (yield for two steps: 80%) which were separated by semipreparative HPLC and tested separately.  $^1\text{H}$  NMR (200 MHz,  $\text{DMSO-}d_6/2\%$  TFA)  $\delta$  1.71–2.20 (m, 4H), 2.26–2.97 (m, 6H), 3.00–3.40 (m, 2H), 3.48–3.66 and 3.75–3.92 (m, 1H), 4.37–4.63 (m, 1H), 6.89–7.45 (m, 20H), 7.54–8.45 (m, 6H);  $^{13}\text{C}$  NMR (50 MHz,  $\text{DMSO-}d_6/2\%$  TFA)  $\delta$  29.7, 31.6, 31.8, 36.9, 37.1, 37.1, 37.8, 47.6, 47.6, 47.7, 47.9, 49.6, 49.8, 54.0, 126.3, 127.6, 127.6, 127.8, 128.1, 128.2, 128.5, 128.5, 128.7, 129.3, 138.4, 138.9, 140.9, 141.0, 144.2, 144.4, 144.6, 145.2, 173.3, 173.4, 173.6, 173.9, 174.1, 174.1;  $^{31}\text{P}$  NMR (81 MHz,  $\text{DMSO-}d_6/2\%$  TFA)  $\delta$  41.0. HRMS ( $m/z$ ):  $[\text{M} + \text{H}]^+$  calcd for  $\text{C}_{35}\text{H}_{41}\text{N}_3\text{O}_4\text{P}^+$ , 598.2829; found, 598.2830.

**[(1R)-1-Amino-3-phenylpropyl]2'-[[(2'S)-1'-amino-4''-methyl-1''-oxopentan-2''-yl]carbamoyl]-4',4'-diphenylbutyl]-phosphinic Acid (22c).** Coupling of **21b** with HBr-H-(L)Leu-NH<sub>2</sub> (**5b**) according to general procedure D and subsequent deprotection according to general procedure C afforded compound **22c** as a white solid (yield for two steps: 75%). Due to the efficient chromatographic separation of diastereoisomers before the deprotection step, the isolation of the desired RSS (first eluted) isomer became feasible.  $^1\text{H}$  NMR (500 MHz,  $\text{DMSO-}d_6/3\%$  TFA)  $\delta$  0.84 (t,  $J = 5.9$  Hz, 6H), 1.41–1.53 (m, 2H), 1.54–1.65 (m, 1H), 1.76–1.88 (m, 1H), 1.91–2.10 (m, 3H), 2.11–2.27 (m, 2H), 2.44–2.67 (m, 2H), 2.79 (dt,  $J = 4.7, 13.0$  Hz, 1H), 3.16–3.27 (m, 1H), 3.95 (dd,  $J = 4.7, 10.0$  Hz, 1H), 4.26 (dd,  $J = 8.0, 15.1$  Hz, 1H), 7.01–7.55 (m, 17H), 7.80 (d,  $J = 7.9$  Hz, 1H), 8.24 (br s, 3H);  $^{13}\text{C}$  NMR (125 MHz,  $\text{DMSO-}d_6/3\%$  TFA)  $\delta$  21.6, 23.1, 24.3, 29.6, 30.3, 31.6, 31.6, 38.5, 38.5, 40.6, 48.0, 48.6 ( $^1J_{\text{PC}} = 94.5$  Hz), 51.2, 126.1, 126.2, 127.4, 128.0, 128.3, 128.5, 128.5,

128.6, 140.8, 145.0, 146.5, 173.4, 173.4, 174.3;  $^{31}\text{P}$  NMR (81 MHz, DMSO- $d_6$ /3% TFA)  $\delta$  41.4. HRMS ( $m/z$ ):  $[\text{M} - \text{H}]^-$  calcd for  $\text{C}_{32}\text{H}_{41}\text{N}_3\text{O}_4\text{P}^-$ , 562.2840; found, 562.2840.

**((1R)-1-Amino-3-phenylpropyl){2'-[[1,1':3',1''-terphenyl]-5'-ylmethyl]-3'-[[2''(S)-1'-amino-1''-oxo-3''-phenylpropan-2''-yl]-amino]-3'-oxopropyl}phosphinic Acid (22d).** Coupling of 21c with HBr·H-(L)Phe-NH<sub>2</sub> (5c) according to general procedure D and subsequent deprotection according to general procedure C afforded compound 22d as a mixture of two diastereoisomers (yield for two steps: 78%), separated by semipreparative HPLC and tested separately.  $^1\text{H}$  NMR (200 MHz, DMSO- $d_6$ /3% TFA)  $\delta$  1.56–2.11 (m, 4H), 2.28–2.89 (m, 4H), 2.93–3.50 (m, 4H), 4.28–4.57 (m, 1H), 6.91–7.89 (m, 25H), 8.22 (br s, 3H), 8.40 (d,  $J = 8.9$  Hz, 1H);  $^{13}\text{C}$  NMR (50 MHz, DMSO- $d_6$ )  $\delta$  27.1 ( $^1J_{\text{PC}} = 92$  Hz), 29.7, 31.6, 31.7, 37.7, 41.2, 48.6 ( $^1J_{\text{PC}} = 95$  Hz), 54.2, 123.6, 126.3, 127.0, 127.2, 127.7, 128.2, 128.3, 128.4, 128.6, 129.0, 129.4, 138.2, 140.3, 140.4, 140.9, 141.1, 172.9, 173.4, 173.5;  $^{31}\text{P}$  NMR (81 MHz, DMSO- $d_6$ /3% TFA)  $\delta$  41.3, 41.9. HRMS ( $m/z$ ):  $[\text{M} - \text{H}]^-$  calcd for  $\text{C}_{40}\text{H}_{41}\text{N}_3\text{O}_4\text{P}^-$ , 658.2840; found, 658.2846.

**((1R)-1-Amino-3-phenylpropyl){2'-[[1,1':3',1''-terphenyl]-5'-ylmethyl]-3'-[[2''(S)-1'-amino-4''-methyl-1''-oxopentan-2''-yl]-amino]-3'-oxopropyl}phosphinic Acid (22e).** Coupling of 21c with HBr·H-(L)Leu-NH<sub>2</sub> (5b) according to general procedure D and subsequent deprotection according to general procedure C afforded compound 22e as a white solid (yield for two steps: 65%). Due to the efficient chromatographic separation of diastereoisomers before the deprotection step, the isolation of the desired RSS (first eluted) isomer became feasible.  $^1\text{H}$  NMR (500 MHz, DMSO- $d_6$ /3% TFA)  $\delta$  0.80 (dd,  $J = 6.4, 21.2$  Hz, 6H), 1.39–1.61 (m, 3H), 1.71–1.87 (m, 2H), 1.93–2.05 (m, 1H), 2.29 (dt,  $J = 9.9, 15.2$  Hz, 1H), 2.53–2.62 (m, 1H), 2.76 (dt,  $J = 4.8, 12.9$  Hz, 1H), 2.91 (dt,  $J = 7.7, 13.0$  Hz, 1H), 3.09–3.29 (m, 3H), 4.22 (dd,  $J = 8.7, 14.4$  Hz, 1H), 6.84–7.91 (m, 20H), 8.25 (br s, 3H), 8.30 (d,  $J = 8.3$  Hz, 1H);  $^{13}\text{C}$  NMR (50 MHz, DMSO- $d_6$ /3% TFA) 21.6, 23.2, 24.2, 28.2 ( $^1J_{\text{PC}} = 94.4$  Hz), 29.6, 31.6, 31.7, 41.0, 48.6 ( $^1J_{\text{PC}} = 90.5$  Hz), 51.2, 124.1, 126.2, 127.0, 127.1, 127.6, 128.2, 128.5, 128.9, 140.1, 140.3, 140.8, 141.0, 173.3, 173.4, 174.2;  $^{31}\text{P}$  NMR (81 MHz, DMSO- $d_6$ /3% TFA)  $\delta$  41.9. HRMS ( $m/z$ ):  $[\text{M} - \text{H}]^-$  calcd for  $\text{C}_{37}\text{H}_{43}\text{N}_3\text{O}_4\text{P}^-$ , 624.2997; found, 624.2999.

**((1R)-1-Amino-3-phenylpropyl){3'-[[2''(S)-1'-amino-4''-methyl-1''-oxopentan-2''-yl]amino]-2'-[[3,3''-dichloro-[1,1':3',1''-terphenyl]-5'-yl)methyl]-3'-oxopropyl}phosphinic Acid (22f).** Coupling of 21d with HBr·H-(L)Leu-NH<sub>2</sub> (5b) according to general procedure D and subsequent deprotection according to general procedure C afforded compound 22f as a white solid (yield for two steps: 40%). Due to the efficient chromatographic separation of diastereoisomers before the deprotection step, the isolation of the desired RSS (first eluted) isomer became feasible.  $^1\text{H}$  NMR (200 MHz, DMSO- $d_6$ /2% TFA)  $\delta$  0.63–0.98 (m, 6H), 1.35–1.64 (m, 3H), 1.65–2.09 (m, 3H), 2.18–2.40 (m, 1H), 2.50–3.37 (m, 6H), 4.06–4.32 (m, 1H), 6.84–7.91 (m, 19H), 8.29 (br s, 3H);  $^{13}\text{C}$  NMR (50 MHz, DMSO- $d_6$ /2% TFA) 21.6, 23.3, 24.4, 28.3 ( $^1J_{\text{PC}} = 91.4$  Hz), 29.8, 31.7, 31.9, 41.1, 41.2, 48.8 ( $^1J_{\text{PC}} = 95.4$  Hz), 51.4, 126.1, 126.4, 127.0, 127.7, 127.8, 128.4, 128.7, 139.7, 140.6, 140.9, 142.4, 173.4, 173.5, 174.5;  $^{31}\text{P}$  NMR (81 MHz, DMSO- $d_6$ /2% TFA)  $\delta$  41.9. HRMS ( $m/z$ ):  $[\text{M} - \text{H}]^-$  calcd for  $\text{C}_{37}\text{H}_{41}\text{Cl}_2\text{N}_3\text{O}_4\text{P}^-$ , 692.2217; found, 692.2228.

**Protein Expression and Purification.** ERAP1 and ERAP2 were expressed by insect cell culture (Hi5) after infection with recombinant baculovirus as described.<sup>5b,6c</sup> IRAP was expressed by HEK 293S GnTI<sup>(-)</sup> as previously described.<sup>5c</sup>

**In Vitro Enzymatic Assays.** Evaluation of the inhibitory potency of the compounds was carried out using an in vitro fluorimetric assay as previously described.<sup>35</sup>

**Cross-Presentation Assay.** Spleens from C57Bl/6 wild-type (Janvier Labs, France) and from IRAP<sup>-/-</sup> mice bred in the animal facility of INSERM U1151 were digested with Liberase 500  $\mu\text{g}/\text{mL}$  and DNase-1 10  $\text{ng}/\text{mL}$  (Roche Laboratories) for 30 min at 37 °C in PBS. Enzymatic digestion was terminated by incubating cells on ice and adding IMDM medium supplemented with 10% FBS. After washing, CD11c+ cells were positively selected using paramagnetic

beads (Miltenyi Biotec), following the manufacturer's protocol. The cells were then incubated with anti-CD11c/Brilliant Violet 421 (clone N418, Sony Biotechnology), anti-CD8 $\alpha$ /Brilliant Violet 605 (clone 53-6.7, BD Biosciences), and anti-CD11b/PE-Cy7 (clone M1/70, BD Biosciences) for 30 min on ice. After washes and addition of 7-actinomycin D (7-AAD), the two main subsets of conventional dendritic cells (cDCs) were sorted using a BD FACS ARIA-II cell sorter as 7-AAD-CD11c+CD11b<sup>low</sup>CD8 $\alpha$ + cells for CD8 $\alpha$ + cDCs, and 7-AAD-CD11c+CD11b<sup>high</sup>CD8 $\alpha$ - cells for CD11b+ cDCs. 15 000 sorted and washed cDCs resuspended in IMDM medium supplemented with penicillin, streptomycin, and 10% FBS were added per well in a 96-well plate with round bottom. Serial dilutions from 3 to 3333 nM of the inhibitor 22b or DMSO was added to the cells for 60 min before the addition of 500  $\text{ng}/\text{mL}$  of soluble ovalbumin in the presence of the same concentration of 22b or DMSO. After 6 h, cells were washed in PBS and fixed with 50  $\mu\text{L}$  of a PBS-glutaraldehyde 0.008% solution for 30 s to stop antigen processing and washed again twice with a solution containing PBS-glycine 0.2 M and once with PBS. As a negative control, some of the cells were fixed before the addition of 22b. Finally, 45 000 TCR-transgenic CD8+ T cells per well, prepared from lymph nodes of Rag-1<sup>-/-</sup> C57Bl/6 OT-I mice, were added to the fixed cells and supernatants were collected after 24 h. OT-I T cell activation was assessed by dosing IL-2 concentration in supernatants using a sandwich ELISA assay: anti-IL2 (clone JES6-1A12, BD Biosciences) was used as a capture antibody, and anti-IL-2-biotin (clone JES6-SH4, BD Biosciences), streptavidin/horseradish peroxidase (HRP, Pierce), and tetramethylbenzidine substrate (BD Biosciences) were used for the detection of captured IL-2. Optical density was measured on a Mithras plate reader. Background (optical density from wells that contained prefixed cells) was subtracted from all specific values. All conditions were tested in triplicate.

**Computational Methods.** Docking calculations were performed as described previously,<sup>35</sup> using the crystallographic structures of ERAP1 (PDB code 2YD0), ERAP2 (PDB code 3SE6), and IRAP (PDB code 4PJ6) without further refinement.

## ■ ASSOCIATED CONTENT

### Supporting Information

The Supporting Information is available free of charge on the ACS Publications website at DOI: 10.1021/acs.jmedchem.6b01031.

Experimental procedures and characterization for compounds 1, 5b, 5c, 5f–j, 11h, and 11i; list of RP-HPLC retention times and MS data for all tested compounds; titration of T-cell responses versus BMDCs exposed to different amounts of soluble ovalbumin (PDF)

Molecular formula strings and some data (CSV)

## ■ AUTHOR INFORMATION

### Corresponding Authors

\*E.S.: e-mail, [stratos@rrp.demokritos.gr](mailto:stratos@rrp.demokritos.gr); phone, (+30) 2106503918; fax, (+30)2106503918.

\*D.G.: e-mail, [dgeorgia@chem.uoa.gr](mailto:dgeorgia@chem.uoa.gr); phone, (+30) 2107274903; fax, (+30)2107274761.

### Author Contributions

P.K. designed the synthetic routes and performed the synthesis and characterization of reported inhibitors with the contributions of I.D., I.P., S.K., M.P., S.A., and T.-M.F.; A.M. prepared the recombinant enzymes and performed the HPLC purification and in vitro assays. F.-X.M. and P.v.E. designed and performed the cross-presentation assay. A.P. contributed to SAR by performing molecular modeling analysis. D.G. and E.S. conceived the experiments, designed the inhibitors, analyzed the results, and supervised the project. All authors contributed

to the preparation of the manuscript and have approved its final version.

## Notes

The authors declare no competing financial interest.

## ACKNOWLEDGMENTS

This research was financed by the Special Account for Research Grants of National and Kapodistrian University of Athens and by the European Union (European Social Fund) and Greek national funds through the Operational Program “Education and Lifelong Learning” of the National Strategic Reference Framework: Research Funding Program of the General Secretariat for Research and Technology (Grant ERC-14 to E.S.). Funding was also provided by an award from the Harry J. Lloyd Charitable trust to E.S. Work in the laboratory of P.v.E. was supported by Grant DEQ20130326539 from the Fondation pour la Recherche Medicale and Grant ANR-14-CE11-0014 from the Agence Nationale de Recherche. D.G. thanks Dr. Vincent Dive and Dr. Laurent Devel for their kind support and valuable discussions and Dr. Maroula Kokotou for HRMS measurements.

## ABBREVIATIONS USED

CCR2, CC chemokine receptor 2; CCL2, CC chemokine ligand 2; CCR5, CC chemokine receptor 5; DCC, *N,N'*-dicyclohexylcarbodiimide; DIPEA, *N,N*-diisopropylethylamine; DMAP, 4-dimethylaminopyridine; DMF, *N,N*-dimethylformamide; EDC-HCl, *N*-(3-dimethylaminopropyl)-*N'*-ethylcarbodiimide hydrochloride; HMDS, 1,1,1,3,3,3-hexamethyldisilazane; HOBt, 1-hydroxybenzotriazole; MMP, matrix metalloproteinase; TBS, *tert*-butyldimethylsilyl; TFA, trifluoroacetic acid; TIS, triisopropylsilane; TLC, thin layer chromatography

## REFERENCES

- (1) Evnouchidou, I.; Papakyriakou, A.; Stratikos, E. A new role for Zn(II) aminopeptidases: antigenic peptide generation and destruction. *Curr. Pharm. Des.* **2009**, *15*, 3656–3670.
- (2) Weimershaus, M.; Evnouchidou, I.; Saveanu, L.; van Endert, P. Peptidases trimming MHC class I ligands. *Curr. Opin. Immunol.* **2013**, *25*, 90–96.
- (3) Tsujimoto, M.; Hattori, A. The oxytocinase subfamily of M1 aminopeptidases. *Biochim. Biophys. Acta, Proteins Proteomics* **2005**, *1751*, 9–18.
- (4) (a) Saveanu, L.; Carroll, O.; Weimershaus, M.; Guermontprez, P.; Firat, E.; Lindo, V.; Greer, F.; Davoust, J.; Kratzer, R.; Keller, S. R.; Niedermann, G.; van Endert, P. IRAP identifies an endosomal compartment required for MHC class I cross-presentation. *Science* **2009**, *325*, 213–217. (b) Segura, E.; Albiston, A. L.; Wicks, I. P.; Chai, S. Y.; Villadangos, J. A. Different cross-presentation pathways in steady-state and inflammatory dendritic cells. *Proc. Natl. Acad. Sci. U. S. A.* **2009**, *106*, 20377–20381.
- (5) (a) Zervoudi, E.; Papakyriakou, A.; Georgiadou, D.; Evnouchidou, I.; Gajda, A.; Poreba, M.; Salvesen, G. S.; Drag, M.; Hattori, A.; Swevers, L.; Vourloumis, D.; Stratikos, E. Probing the S1 specificity pocket of the aminopeptidases that generate antigenic peptides. *Biochem. J.* **2011**, *435*, 411–420. (b) Mpakali, A.; Giastas, P.; Mathioudakis, N.; Mavridis, I. M.; Saridakis, E.; Stratikos, E. Structural basis for antigenic peptide recognition and processing by ER aminopeptidase 2. *J. Biol. Chem.* **2015**, *290*, 26021–26032. (c) Mpakali, A.; Saridakis, E.; Harlos, K.; Zhao, Y.; Papakyriakou, A.; Kokkala, P.; Georgiadis, D.; Stratikos, E. Crystal structure of insulin-regulated aminopeptidase with bound substrate analogue provides insight on antigenic epitope precursor recognition and processing. *J. Immunol.* **2015**, *195*, 2842–2851.

- (6) (a) Birtley, J. R.; Saridakis, E.; Stratikos, E.; Mavridis, I. M. The crystal structure of human endoplasmic reticulum aminopeptidase 2 reveals the atomic basis for distinct roles in antigen processing. *Biochemistry* **2012**, *51*, 286–295. (b) Stratikos, E.; Stern, L. J. Antigenic peptide trimming by ER aminopeptidases—Insights from structural studies. *Mol. Immunol.* **2013**, *55*, 212–219. (c) Stamogiannos, A.; Koumantou, D.; Papakyriakou, A.; Stratikos, E. Effects of polymorphic variation on the mechanism of Endoplasmic Reticulum Aminopeptidase 1. *Mol. Immunol.* **2015**, *67*, 426–435.

- (7) (a) Cagliani, R.; Riva, S.; Biasin, M.; Fumagalli, M.; Pozzoli, U.; Lo Caputo, S.; Mazzotta, F.; Piacentini, L.; Bresolin, N.; Clerici, M.; Sironi, M. Genetic diversity at endoplasmic reticulum aminopeptidases is maintained by balancing selection and is associated with natural resistance to HIV-1 infection. *Hum. Mol. Genet.* **2010**, *19*, 4705–4714. (b) Fierabracci, A.; Milillo, A.; Locatelli, F.; Fruci, D. The putative role of endoplasmic reticulum aminopeptidases in autoimmunity: insights from genomic-wide association studies. *Autoimmun. Rev.* **2012**, *12*, 281–288. (c) Seregin, S. S.; Rastall, D. P. W.; Evnouchidou, I.; Aylsworth, C. F.; Quiroga, D.; Kamal, R. P.; Godbehere-Roosa, S.; Blum, C. F.; York, I. A.; Stratikos, E.; Amalfitano, A. Endoplasmic reticulum aminopeptidase-1 alleles associated with increased risk of ankylosing spondylitis reduce HLA-B27 mediated presentation of multiple antigens. *Autoimmunity* **2013**, *46*, 497–508. (d) Stratikos, E.; Stamogiannos, A.; Zervoudi, E.; Fruci, D. A role for naturally occurring alleles of endoplasmic reticulum aminopeptidases in tumor immunity and cancer pre-disposition. *Front. Oncol.* **2014**, *4*, 363.

- (8) Fruci, D.; Romania, P.; D'Alicandro, V.; Locatelli, F. Endoplasmic reticulum aminopeptidase 1 function and its pathogenic role in regulating innate and adaptive immunity in cancer and major histocompatibility complex class I-associated autoimmune diseases. *Tissue Antigens* **2014**, *84*, 177–186.

- (9) Goto, Y.; Ogawa, K.; Nakamura, T. J.; Hattori, A.; Tsujimoto, M. TLR-mediated secretion of endoplasmic reticulum aminopeptidase 1 from macrophages. *J. Immunol.* **2014**, *192*, 4443–4452.

- (10) (a) Stratikos, E. Modulating antigen processing for cancer immunotherapy. *Oncoimmunology* **2014**, *3*, e27568. (b) Stratikos, E. Regulating adaptive immune responses using small molecule modulators of aminopeptidases that process antigenic peptides. *Curr. Opin. Chem. Biol.* **2014**, *23*, 1–7.

- (11) Zervoudi, E.; Saridakis, E.; Birtley, J. R.; Seregin, S. S.; Reeves, E.; Kokkala, P.; Aldhamen, Y. A.; Amalfitano, A.; Mavridis, I. M.; James, E.; Georgiadis, D.; Stratikos, E. Rationally designed inhibitor targeting antigen-trimming aminopeptidases enhances antigen presentation and cytotoxic T-cell responses. *Proc. Natl. Acad. Sci. U. S. A.* **2013**, *110*, 19890–19895.

- (12) (a) Aldhamen, Y. A.; Pepelyayeva, Y.; Rastall, D. P. W.; Seregin, S. S.; Zervoudi, E.; Koumantou, D.; Aylsworth, C. F.; Quiroga, D.; Godbehere, S.; Georgiadis, D.; Stratikos, E.; Amalfitano, A. Auto-immune disease-associated variants of extracellular endoplasmic reticulum aminopeptidase 1 induce altered innate immune responses by human immune cells. *J. Innate Immun.* **2015**, *7*, 275–289. (b) Chen, L.; Ridley, A.; Hammitzsch, A.; Al-Mossawi, M. H.; Bunting, H.; Georgiadis, D.; Chan, A.; Kollnberger, S.; Bowness, P. Silencing or inhibition of endoplasmic reticulum aminopeptidase 1 (ERAP1) suppresses free heavy chain expression and Th17 responses in ankylosing spondylitis. *Ann. Rheum. Dis.* **2016**, *75*, 916–923.

- (13) (a) Dive, V.; Cotton, J.; Yiotakis, A.; Michaud, A.; Vassiliou, S.; Jiracek, J.; Vazeux, G.; Chauvet, M. T.; Cuniassse, P.; Corvol, P. RXP 407, a phosphinic peptide, is a potent inhibitor of angiotensin I converting enzyme able to differentiate between its two active sites. *Proc. Natl. Acad. Sci. U. S. A.* **1999**, *96*, 4330–4335. (b) Georgiadis, D.; Cuniassse, P.; Cotton, J.; Yiotakis, A.; Dive, V. Structural determinants of RXP4380, a potent and highly selective inhibitor of the angiotensin-converting enzyme C-domain. *Biochemistry* **2004**, *43*, 8048–8054.

- (14) Devel, L.; Rogakos, V.; David, A.; Makaritis, A.; Beau, F.; Cuniassse, P.; Yiotakis, A.; Dive, V. Development of selective inhibitors and substrate of matrix metalloproteinase-12. *J. Biol. Chem.* **2006**, *281*, 11152–11160.

- (15) Georgiadis, D.; Dive, V. Phosphinic peptides as potent inhibitors of zinc-metalloproteases. *Top. Curr. Chem.* **2014**, *360*, 1–38.
- (16) Yiotakis, A.; Georgiadis, D.; Matziari, M.; Makaritis, A.; Dive, V. Phosphinic peptides: Synthetic approaches and biochemical evaluation as Zn-metalloprotease inhibitors. *Curr. Org. Chem.* **2004**, *8*, 1135–1158.
- (17) (a) Jullien, N.; Makritis, A.; Georgiadis, D.; Beau, F.; Yiotakis, A.; Dive, V. Phosphinic tripeptides as dual angiotensin-converting enzyme C-domain and endothelin-converting enzyme-1 inhibitors. *J. Med. Chem.* **2010**, *53*, 208–220. (b) Masuyer, G.; Akif, M.; Czarny, B.; Beau, F.; Schwager, S. L. U.; Sturrock, E. D.; Isaac, R. E.; Dive, V.; Acharya, K. R. Crystal structures of highly specific phosphinic tripeptide enantiomers in complex with the angiotensin-I converting enzyme. *FEBS J.* **2014**, *281*, 943–956.
- (18) Mucha, A.; Drag, M.; Dalton, J. P.; Kafarski, P. Metallo-aminopeptidase inhibitors. *Biochimie* **2010**, *92*, 1509–1529.
- (19) (a) Chen, H.; Noble, F.; Mothé, A.; Meudal, H.; Coric, P.; Danascimento, S.; Roques, B. P.; George, P.; Fournié-Zaluski, M. C. Phosphinic derivatives as new dual enkephalin-degrading enzyme inhibitors: Synthesis, biological properties, and antinociceptive activities. *J. Med. Chem.* **2000**, *43*, 1398–1408. (b) Mucha, A.; Lämmerhofer, M.; Lindner, W.; Pawelczak, M.; Kafarski, P. Individual stereoisomers of phosphinic dipeptide inhibitor of leucine aminopeptidase. *Bioorg. Med. Chem. Lett.* **2008**, *18*, 1550–1554.
- (20) Makaritis, A.; Georgiadis, D.; Dive, V.; Yiotakis, A. Diastereoselective solution and multipin-based combinatorial array synthesis of a novel class of potent phosphinic metalloprotease inhibitors. *Chem. - Eur. J.* **2003**, *9*, 2079–2094.
- (21) (a) David, A.; Steer, D.; Bregant, S.; Devel, L.; Makaritis, A.; Beau, F.; Yiotakis, A.; Dive, V. Cross-linking yield variation of a potent matrix metalloproteinase photoaffinity probe and consequences for functional proteomics. *Angew. Chem., Int. Ed.* **2007**, *46*, 3275–3277. (b) Mores, A.; Matziari, M.; Beau, F.; Cuniasse, P.; Yiotakis, A.; Dive, V. Development of potent and selective phosphinic peptide inhibitors of angiotensin-converting enzyme 2. *J. Med. Chem.* **2008**, *51*, 2216–2226. (c) Marchant, D. J.; Bellac, C. L.; Moraes, T. J.; Wadsworth, S. J.; Dufour, A.; Butler, G. S.; Bilawchuk, L. M.; Hendry, R. G.; Robertson, A. G.; Cheung, C. T.; Ng, J.; Ang, L.; Luo, Z.; Heilbron, K.; Norris, M. J.; Duan, W.; Bucyk, T.; Karpov, A.; Devel, L.; Georgiadis, D.; Hegele, R. G.; Luo, H.; Granville, D. J.; Dive, V.; McManus, B. M.; Overall, C. M. A new transcriptional role for matrix metalloproteinase-12 in antiviral immunity. *Nat. Med.* **2014**, *20*, 493–502.
- (22) (a) Chen, H.; Noble, F.; Roques, B. P.; Fournié-Zaluski, M. C. Long lasting antinociceptive properties of enkephalin degrading enzyme (NEP and APN) inhibitor prodrugs. *J. Med. Chem.* **2001**, *44*, 3523–3530. (b) Matziari, M.; Dellis, D.; Dive, V.; Yiotakis, A.; Samios, J. Conformational and solvation studies via computer simulation of the novel large scale diastereoselectively synthesized phosphinic MMP inhibitor RXP03 diluted in selected solvents. *J. Phys. Chem. B* **2010**, *114*, 421–428.
- (23) Lämmerhofer, M.; Hebenstreit, D.; Gavioli, E.; Lindner, W.; Mucha, A.; Kafarski, P.; Wiczorek, P. High-performance liquid chromatographic enantiomer separation and determination of absolute configurations of phosphinic acid analogues of dipeptides and their  $\alpha$ -aminophosphinic acid precursors. *Tetrahedron: Asymmetry* **2003**, *14*, 2557–2565.
- (24) Baylis, E. K.; Campbell, C. D.; Dingwall, J. G. 1-Amino-alkylphosphonous acids. Part 1. Isosteres of the protein amino acids. *J. Chem. Soc., Perkin Trans. 1* **1984**, 2845–2853.
- (25) Kummer, D. A.; Chain, W. J.; Morales, M. R.; Quiroga, O.; Myers, A. G. Stereocontrolled alkylative construction of quaternary carbon centers. *J. Am. Chem. Soc.* **2008**, *130*, 13231–13233.
- (26) Georgiadis, D.; Matziari, M.; Vassiliou, S.; Dive, V.; Yiotakis, A. A convenient method to synthesize phosphinic peptides containing an aspartyl or glutamyl aminophosphinic acid. Use of the phenyl group as the carboxyl synthon. *Tetrahedron* **1999**, *55*, 14635–14648.
- (27) Christl, M.; Huisgen, R. 1,3-Dipolare Cycloadditionen, 74. Orientierungsphänomene bei cycloadditionen aliphatischer und aromatischer Nitroxide an  $\alpha,\beta$ -ungesättigte Carbonester. *Chem. Ber.* **1973**, *106*, 3345–3367.
- (28) Baldwin, J. E.; Adlington, R. M.; Birch, D. J.; Crawford, J. A.; Sweeney, J. B. Radical reactions in synthesis: carbon-carbon bond formation from 2-substituted allyl trialkyl stannanes. *J. Chem. Soc., Chem. Commun.* **1986**, 1339–1340.
- (29) Hin, B.; Majer, P.; Tsukamoto, T. Facile synthesis of  $\alpha$ -substituted acrylate esters. *J. Org. Chem.* **2002**, *67*, 7365–7368.
- (30) Hamilton, J. Y.; Sarlah, D.; Carreira, E. M. Iridium-catalyzed enantioselective allyl-alkene coupling. *J. Am. Chem. Soc.* **2014**, *136*, 3006–3009.
- (31) Devel, L.; Garcia, S.; Czarny, B.; Beau, F.; LaJeunesse, E.; Vera, L.; Georgiadis, D.; Stura, E.; Dive, V. Insights from selective non-phosphinic inhibitors of MMP-12 tailored to fit with an S1' loop canonical conformation. *J. Biol. Chem.* **2010**, *285*, 35900–35909.
- (32) Nguyen, T. T.; Chang, S.-C.; Evnouchidou, I.; York, I. A.; Zikos, C.; Rock, K. L.; Goldberg, A. L.; Stratikos, E.; Stern, L. J. Structural basis for antigenic peptide precursor processing by the endoplasmic reticulum aminopeptidase ERAP1. *Nat. Struct. Mol. Biol.* **2011**, *18*, 604–613.
- (33) (a) Andersson, H.; Demaegdt, H.; Vauquelin, G.; Lindeberg, G.; Karlén, A.; Hallberg, M.; Erdélyi, M.; Hallberg, A. Disulfide cyclized tripeptide analogues of angiotensin IV as potent and selective inhibitors of Insulin-Regulated Aminopeptidase (IRAP). *J. Med. Chem.* **2010**, *53*, 8059–8071. (b) Andersson, H.; Demaegdt, H.; Johnsson, A.; Vauquelin, G.; Lindeberg, G.; Hallberg, M.; Erdélyi, M.; Karlén, A.; Hallberg, A. Potent macrocyclic inhibitors of Insulin-Regulated Aminopeptidase (IRAP) by olefin ring-closing metathesis. *J. Med. Chem.* **2011**, *54*, 3779–3792.
- (34) Bukhaltsev, E.; Goldberg, I.; Cohen, R.; Vigalok, A. Tunable  $\pi$ -interactions in monomeric organozinc complexes: solution and solid-state studies. *Organometallics* **2007**, *26*, 4015–4020.
- (35) Papakyriakou, A.; Zervoudi, E.; Tsoukalidou, S.; Mauvais, F. X.; Sfyroera, G.; Mastellos, D. C.; van Endert, P.; Theodorakis, E. A.; Vourloumis, D.; Stratikos, E. 3,4-Diaminobenzoic acid derivatives as inhibitors of the oxytocinase subfamily of M1 aminopeptidases with immune-regulating properties. *J. Med. Chem.* **2015**, *58*, 1524–1543.
- (36) Morrison, R. A.; Singhvi, S. M.; Peterson, A. E.; Pocetti, D. A.; Migdalof, B. H. Relative contribution of the gut, liver, and lung to the first-pass hydrolysis (bioactivation) of orally administered 14C-fosinopril sodium in dogs. In vivo and in vitro studies. *Drug Metab. Dispos.* **1990**, *18*, 253–257.
- (37) Gottlieb, H. E.; Kotlyar, V.; Nudelman, A. NMR Chemical shifts of common laboratory solvents as trace impurities. *J. Org. Chem.* **1997**, *62*, 7512–7515.

Optimization and Structure-Activity  
Relationships of Phosphinic Pseudotriptide  
Inhibitors of Aminopeptidases that Generate  
Antigenic Peptides.

*Paraskevi Kokkala,<sup>†</sup> Anastasia Mpakali,<sup>‡</sup> Athanasios Papakyriakou,<sup>‡</sup> Ira Daskalaki,<sup>†</sup>  
Ioanna Petropoulou,<sup>†</sup> Sofia Kavalou,<sup>†</sup> Mirto Papathanasopoulou,<sup>†</sup> Stefanos Agrotis,<sup>†</sup>  
Theodora-Markisia Fonsou,<sup>†</sup> Efstratios Stratikos<sup>\*‡</sup> and Dimitris Georgiadis<sup>\*†</sup>*

<sup>†</sup>Department of Chemistry, Laboratory of Organic Chemistry, University of Athens,  
Panepistimiopolis, Zografou, 15771, Athens, Greece

<sup>‡</sup>National Center for Scientific Research ‘Demokritos’, Aghia Paraskevi Attikis, GR  
15310, Greece.

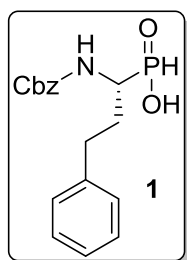
## SUPPORTING INFORMATION

### Table of contents

<b>1. Synthetic Methods and Characterizations</b>	<b>S3</b>
<b>Aminoacid derivatives</b>	<b>S3</b>
<b>Oxime derivatives</b>	<b>S6</b>
<b>2. RP-HPLC retention times and ES-MS data of inhibitors 6a-k, 13a-i, 14 and 22a-f</b>	<b>S7</b>
<b>3. Titration of T-cell responses versus BMDCs exposed to different amounts of soluble ovalbumin</b>	<b>S8</b>
<b>4. References</b>	<b>S9</b>



## 1. Synthetic Methods and Characterizations

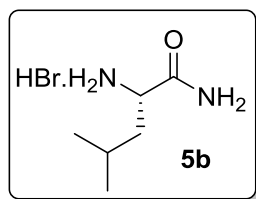


**((1R)-1-[[[(benzyloxy)carbonyl]amino]-3-phenylpropyl]phosphinic acid (1).** A racemic mixture of (1-[[[(benzyloxy)carbonyl]amino]-3-phenylpropyl]phosphinic acid (**rac-1**) (115 g, 345 mmol) prepared according to previously reported methods,<sup>1</sup> was suspended in abs. EtOH (980 mL) and the mixture was refluxed. After complete dissolution, (*S*)-(-)- $\alpha$ -methylbenzylamine (45 mL, 345 mmol) was added over a period of 10 min. After 15 min, the mixture was slowly cooled at room temperature

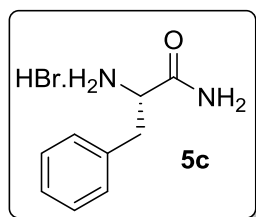
and then to 4 °C. After 4 days at this temperature (with occasional stirring), the white precipitate was filtrated and the solid was washed with cold EtOH (3  $\times$  100 mL) and Et<sub>2</sub>O (2  $\times$  100 mL). The solid was dried over P<sub>2</sub>O<sub>5</sub> and recrystallized by EtOH. After filtration, the solid was recrystallized once more to afford 33.8 g of the diastereoisomeric salt of **1** with (*S*)-(-)-amine ( $[\alpha]_D^{20} = -22.3$ ,  $c=1$ , EtOH). The salt was stirred with 4 M HCl during 3 h and the pure phosphinic acid **1** (24.7 g, 21%) ( $[\alpha]_D^{20} = -35.7$ ,  $c=1$ , EtOH) was isolated after filtration, washings with distilled water and drying in a desiccator over P<sub>2</sub>O<sub>5</sub>. A second batch of **1** (11.5 g, 10%) was obtained as follows: all filtrates from recrystallizations were concentrated, dried over P<sub>2</sub>O<sub>5</sub>, treated with 4 M HCl during 3 h, filtrated and washed with distilled water. After drying over P<sub>2</sub>O<sub>5</sub>, the solid (87 g, 261 mmol) was subjected to the same procedure as above, using (*R*)-(+)- $\alpha$ -methylbenzylamine. The filtrates obtained from the new round of recrystallizations were converted to the free acid (enriched to **1**) which was treated with (*S*)-(-)- $\alpha$ -methylbenzylamine as described above. The obtained spectral data were found identical to literature data.<sup>1b</sup>

### Aminoacid Derivatives:

Aminoacid derivatives **5a**, **5d** and **9e** were commercially available. D-Phe derivative **5k** was prepared according to the protocol employed for its enantiomer **5c**.

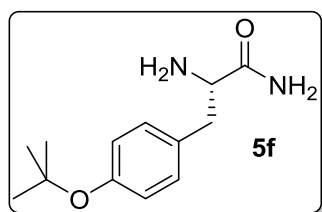


**(S)-2-amino-4-methylpentanamide hydrobromide (5b).** Cbz-(L)-Leu-OH (760 mg, 2.86 mmol) was converted to Cbz-(L)-Leu-NH<sub>2</sub> (501 mg, 66%) according to the two-step procedure (methylation and substitution of resulting methylester by aqueous ammonia) reported by Xu et al.<sup>2</sup> A solution of Cbz-(L)-Leu-NH<sub>2</sub> (496 mg, 1.88 mmol) in 33% HBr/AcOH (7.5 ml) was stirred at rt for 2 h. After removal of the volatiles, compound **5b** (334 mg, 84%) was obtained as a white solid after precipitation by EtOH. m.p. 238 – 240 °C;  $[\alpha]_D^{25} = +5.6^\circ$  ( $c = 0.5$ , H<sub>2</sub>O); <sup>1</sup>H NMR (200 MHz, D<sub>2</sub>O)  $\delta$  0.95 (d,  $J = 4.6$  Hz, 6H), 1.55 - 1.85 (m, 3H), 4.04 (t,  $J = 7$  Hz, 1H); <sup>13</sup>C NMR (50 MHz, D<sub>2</sub>O)  $\delta$  21.0, 22.0, 24.0, 39.9, 51.7, 172.9.



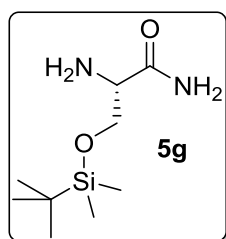
**(S)-2-amino-3-phenylpropanamide hydrobromide (5c).** Cbz-(L)-Phe-OH (887 mg, 2.96 mmol) was dissolved in AcOEt (10 mL) and 4-nitrophenol (620 mg, 4.45 mmol), DIPEA (129  $\mu$ L, 0.74 mmol) and EDC.HCl (843 mg, 4.4 mmol) were added. After stirring at rt for 4 h, AcOEt was evaporated *in vacuo* and the residue was diluted with Et<sub>2</sub>O (40 mL). The resulting solution was washed with 2 M HCl (2  $\times$  10

mL), 0.1 M NaOH (8 × 10 mL) and H<sub>2</sub>O (2 × 10 mL) and the organic phase was dried over Na<sub>2</sub>SO<sub>4</sub> and evaporated *in vacuo*. The white solid obtained after precipitation by light petroleum (628 mg) was dissolved in THF (9 mL), 25% aq. NH<sub>3</sub> (1.2 mL, 15 mmol) was slowly added at 0 °C and the resulting mixture was stirred at rt for 12 h. After evaporation of the volatiles, the residue was diluted with Et<sub>2</sub>O (40 mL) and the solution was washed with 1 M HCl (2 × 10 mL), H<sub>2</sub>O (1 × 10 mL), 0.1 M NaOH (9 × 10 mL) and H<sub>2</sub>O (2 × 10 mL). The organic phase was dried over Na<sub>2</sub>SO<sub>4</sub> and evaporated *in vacuo*. Cbz-(L)-Phe-NH<sub>2</sub> (400 mg, 45%) was obtained as a white solid after trituration of the residue with Et<sub>2</sub>O/AcOEt (1:3). <sup>1</sup>H NMR (200 MHz, DMSO-*d*<sub>6</sub>) δ 2.75 (dd, *J* = 10.6, 13.6 Hz, 1H), 3.02 (dd, *J* = 3.9, 13.7 Hz, 1H), 4.19 (dt, *J* = 3.9, 10.6 Hz, 1H), 4.95 (s, 2H), 7.09 (br s, 1H), 7.15 – 7.38 (m, 10H), 7.43 (d, *J* = 8.8 Hz, 1H), 7.50 (br s, 1H); <sup>13</sup>C NMR (50 MHz, DMSO-*d*<sub>6</sub>) δ 37.6, 56.1, 65.2, 126.3, 127.5, 127.7, 128.1, 128.3, 129.2, 137.1, 138.3, 155.9, 173.5. Cbz-(L)-Phe-NH<sub>2</sub> (400 mg, 1.34 mmol) was deprotected as described above for the synthesis of **5b**. Compound **5c** (301 mg, 92%) was obtained as a white solid after precipitation by Et<sub>2</sub>O. The obtained spectral data were found identical to literature data.<sup>3</sup>



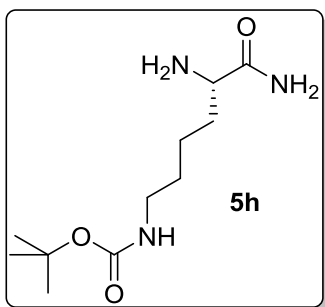
**(S)-2-amino-3-[4-(tert-butoxy)phenyl]propanamide (5f).**<sup>4</sup>

Commercially available HCl·H-(L)-Tyr(Bu<sup>t</sup>)-OMe (300 mg, 1.04 mmol) was suspended in water (1.5 mL), 25% aq. NH<sub>3</sub> (2.6 ml, 33 mmol) was added and the mixture was stirred for 72 hours. Extractions with DCM (4 × 10 mL) followed and the organic phase was dried over Na<sub>2</sub>SO<sub>4</sub> and evaporated *in vacuo* to afford amide **5f** as a white solid (190 mg, 78%). M.p. 121–124 °C; <sup>1</sup>H NMR (200 MHz, CD<sub>3</sub>OD) δ 1.29 (s, 9H), 2.73 (dd, 1H, *J* = 7.5, 13.5 Hz), 2.95 (dd, 1H, *J* = 6.1, 13.5 Hz), 3.51 (dd, 1H, *J* = 6.1, 7.5 Hz), 6.84 - 7.20 (m, 4H); <sup>13</sup>C NMR (50 MHz, CDCl<sub>3</sub>) δ 28.9, 40.3, 56.6, 78.5, 124.4, 129.7, 132.6, 154.2, 177.9; ES-MS *m/z*: calcd for [C<sub>13</sub>H<sub>20</sub>N<sub>2</sub>O<sub>2</sub> + H]<sup>+</sup> 237.3; found: 237.4.



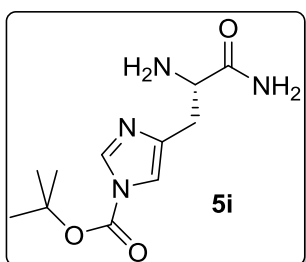
**(S)-2-amino-3-[(tert-butyldimethylsilyl)oxy]propanamide (5g).**

The hydroxyl group of Cbz-(L)-Ser-OH (1.0 g, 4.2 mmol) was protected with the TBS protecting group according to the protocol of Lu et al.<sup>5</sup> The resulting TBS-derivative Cbz-(L)-Ser(TBS)-OH was converted to the amide Cbz-(L)-Ser(TBS)-NH<sub>2</sub> by applying the two-step protocol used for the synthesis of **5c** described above. Cbz-(L)-Ser(TBS)-NH<sub>2</sub> was obtained as a white solid after trituration with Et<sub>2</sub>O/AcOEt (1:1) (585 mg, 40 % over three steps). M.p. 75 – 78 °C; [α]<sub>D</sub><sup>25</sup> = + 35.1° (c = 0.99, CHCl<sub>3</sub>); <sup>1</sup>H NMR (200 MHz, CDCl<sub>3</sub>) δ 0.08 & 0.09 (2 × s, 6H), 0.89 (s, 9H), 3.64 (dd, *J* = 7.5, 9.7 Hz, 1H), 4.06 (dd, *J* = 3.8, 9.7 Hz, 1H), 4.14 – 4.28 (m, 1H), 5.13 (s, 2H), 5.57 (br s, 1H), 5.70 (d, *J* = 4.9 Hz, 1H), 6.51 (br s, 1H), 7.30 – 7.40 (m, 5H); <sup>13</sup>C NMR (50 MHz, CD<sub>3</sub>OD) δ -5.3, 19.0, 26.3, 57.7, 64.5, 67.7, 79.3, 128.8, 128.9, 129.3, 137.7, 157.9, 174.9; ES-MS *m/z*: calcd for [C<sub>17</sub>H<sub>28</sub>N<sub>2</sub>O<sub>4</sub>Si + H]<sup>+</sup> 353.2; found: 353.2. A mixture of Cbz-(L)-Ser(TBS)-NH<sub>2</sub> (400 mg, 1.13 mmol) and Pd/C 10% (40 mg) in MeOH (5 mL) was stirred at rt for 3 h in a H<sub>2</sub> atmosphere. Then, the catalyst was removed by filtration through celite and the filtrates were concentrated to dryness affording **5g** (205 mg, 83%) as a white solid. The obtained spectral data were found identical to literature data.<sup>5</sup>



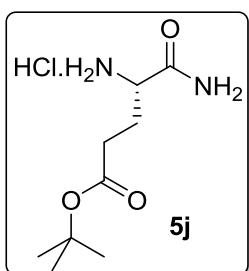
**tert-Butyl (S)-(5,6-diamino-6-oxohexyl)carbamate (5h).**

Commercially available Cbz-(L)-Lys(Boc)-OH (600 mg, 1.58 mmol) was converted to the amide Cbz-(L)-Lys(Boc)-NH<sub>2</sub> by applying the two-step protocol used for the synthesis of **5c** described above. Cbz-(L)-Lys(Boc)-NH<sub>2</sub> (420 mg, 70%) was obtained as a white solid and all spectral data were found identical to literature data.<sup>6</sup> Hydrogenolysis of Cbz-(L)-Lys(Boc)-NH<sub>2</sub> (416 mg, 1.1 mmol) according to the protocol used for the preparation of **5g** afforded **5h** (240 mg, 89%) as a white solid. <sup>1</sup>H NMR (200 MHz, D<sub>2</sub>O) δ 1.07 – 1.91 (m, 15H), 3.02 (t, *J* = 6.2 Hz, 2H), 3.47 – 3.75 (m, 1H); <sup>13</sup>C NMR (50 MHz, D<sub>2</sub>O) δ 21.8, 27.8, 28.8, 32.5, 39.7, 53.6, 80.9, 158.4, 177.0.



**tert-Butyl (S)-4-(2,3-diamino-3-oxopropyl)-1H-imidazole-1-carboxylate (5i).**

In a solution of commercially available Cbz-(L)-His-NH<sub>2</sub> (327 mg, 1.13 mmol) in DMF (4 mL), Boc<sub>2</sub>O (306 mg, 1.4 mmol) in DMF (0.4 mL) was slowly added at 0°C and the resulting mixture was stirred at rt for 24 h. Then, the mixture was diluted with H<sub>2</sub>O (20 mL) and AcOEt (30 mL). The aqueous phase was separated and the organic phase was extracted with 0.5 M HCl (1 × 10 mL) and H<sub>2</sub>O (5 × 10 mL). The organic phase was dried over Na<sub>2</sub>SO<sub>4</sub> and evaporated *in vacuo* to afford Cbz-(L)-His(Boc)-NH<sub>2</sub> (205 mg, 47%) as a white solid after precipitation by Et<sub>2</sub>O;<sup>7</sup> m.p 111 – 114 °C; [α]<sub>D</sub><sup>25</sup> = + 6.2° (c = 0.42, MeOH); <sup>1</sup>H NMR (200 MHz, CDCl<sub>3</sub>) δ 1.54 (s, 9H), 3.07 (dd, *J* = 7.5, 14.6 Hz, 1H), 3.32 (dd, *J* = 3.3, 14.6 Hz, 1H), 4.39 – 4.61 (m, 1H), 5.02 (s, 2H), 5.65 (br s, 1H), 6.49 (d, *J* = 7.3 Hz, 1H), 7.18 – 7.42 (m, 6H), 7.56 (br s, 1H), 8.58 (br s, 1H); <sup>13</sup>C NMR (50 MHz, CDCl<sub>3</sub>) δ 27.9, 30.3, 54.4, 67.0, 86.3, 115.2, 128.1, 128.6, 136.3, 136.8, 138.3, 146.6, 156.4, 173.8; ES-MS *m/z*: calcd for [C<sub>19</sub>H<sub>24</sub>N<sub>4</sub>O<sub>5</sub> + H]<sup>+</sup> 389.2; found: 389.3. Hydrogenolysis of Cbz-(L)-His(Boc)-NH<sub>2</sub> (200 mg, 0.51 mmol) according to the protocol used for the preparation of **5g** afforded **5i** (115 mg, 89%) as a white solid. <sup>1</sup>H NMR (200 MHz, CDCl<sub>3</sub>) δ 1.58 (s, 9H), 2.51 – 3.35 (m, 2H), 3.55 – 3.96 (m, 1H), 5.97 (br s, 1H), 7.18 (s, 1H), 7.35 (br s, 1H), 8.00 (s, 1H); <sup>13</sup>C NMR (50 MHz, CDCl<sub>3</sub>) δ 27.9, 32.9, 55.0, 85.7, 114.8, 136.9, 140.0, 147.0, 177.5; ES-MS *m/z*: calcd for [C<sub>11</sub>H<sub>18</sub>N<sub>4</sub>O<sub>3</sub> + H]<sup>+</sup> 255.2; found 255.3.



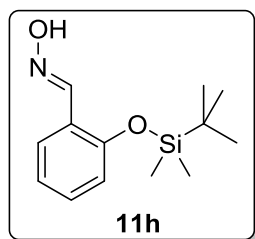
**tert-Butyl (S)-(5,6-diamino-6-oxohexyl)carbamate (5j).**

Commercially available Cbz-(L)-Glu(Bu<sup>t</sup>)-OH (600 mg, 1.78 mmol) was converted to the amide Cbz-(L)-Glu(Bu<sup>t</sup>)-NH<sub>2</sub> by applying the two-step protocol used for the synthesis of **5c** described above. Cbz-(L)-Glu(Bu<sup>t</sup>)-NH<sub>2</sub> (419 mg, 70%) was obtained as a white solid. M.p. 135 – 136 °C; [α]<sub>D</sub><sup>25</sup> = – 5.3° (c = 1, MeOH); <sup>1</sup>H NMR (200 MHz, CDCl<sub>3</sub>) δ 1.43 (s, 9H), 1.83 – 2.20 (m, 2H), 2.23 – 2.58 (m, 2H), 4.24 (dd, *J* = 7.8, 12.6 Hz, 1H), 5.55 (br s, 1H), 5.73 (d, *J* = 7.3 Hz, 1H), 6.38 (br s, 1H), 7.23 – 7.43 (m, 5H); <sup>13</sup>C NMR (50 MHz, CDCl<sub>3</sub>) δ 27.9, 28.1, 31.6, 54.0, 67.0, 80.9, 128.0, 128.2, 128.5, 136.2, 156.4, 172.7, 174.4; ES-MS *m/z*: calcd for [C<sub>17</sub>H<sub>24</sub>N<sub>2</sub>O<sub>5</sub> + H]<sup>+</sup> 337.2; found: 337.2. Hydrogenolysis of Cbz-(L)-Glu(Bu<sup>t</sup>)-NH<sub>2</sub> (395 mg, 1.17 mmol) according to the protocol used for the preparation of **5g** (with the addition of 5 drops of 2M HCl to the reaction mixture) afforded **5j** (249 mg, 89%) as a white solid. [α]<sub>D</sub><sup>25</sup> = + 16.6° (c = 0.5, H<sub>2</sub>O); <sup>1</sup>H NMR (200 MHz, D<sub>2</sub>O) δ 1.42 (s, 9H), 2.02 (q, *J* = 7.0 Hz, 2H), 2.42 (t, *J* = 7.2 Hz, 2H), 3.77 (m, 1H); <sup>13</sup>C NMR (50

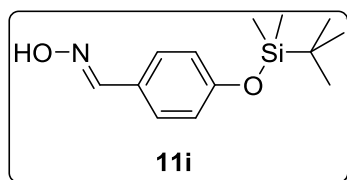
MHz, D<sub>2</sub>O)  $\delta$  27.3, 31.0, 52.8, 83.0, 174.1, 174.7; ES-MS m/z: calcd for [C<sub>9</sub>H<sub>18</sub>N<sub>2</sub>O<sub>3</sub> + H]<sup>+</sup> 203.1; found: 203.2.

### Oxime Derivatives:

**General procedure for conversion of aldehydes of type 10 to the corresponding oxime derivatives of type 11:** A solution of an aldehyde of type 10 (1mmol), hydroxylamine hydrochloride (97 mg, 1.4 mmol) and sodium acetate (164 mg, 2 mmol) in MeOH/H<sub>2</sub>O 3.5:1 was stirred at rt for 24 h. After the reaction was completed, the volatiles were removed by evaporation. The residue was diluted with Et<sub>2</sub>O (30 mL) and the organic phase was washed with H<sub>2</sub>O (3 x 10 mL), dried over anhydrous Na<sub>2</sub>SO<sub>4</sub> and evaporated *in vacuo*. The target oximes of type 11 were obtained (yields 85-95%) as mixtures of *E/Z* isomers of sufficient purity to be used in the next step without further purification. Physical and spectroscopic data were in agreement with literature reported data, for compounds 11a,<sup>8</sup> 11b-d,<sup>8a,9</sup> and 11e-g.<sup>10</sup> For the synthesis of oximes 11h and 11i, the above protocol was applied to TBS-protected aldehydes 10h and 10i, respectively, prepared according to literature procedures.<sup>11</sup>



**2-(*tert*-Butyldimethylsilyloxy)benzaldehyde oxime (11h).** <sup>1</sup>H NMR (200 MHz, CDCl<sub>3</sub>)  $\delta$  0.25 (s, 6H), 1.03 (s, 9H), 6.62 - 7.96 (m, 5H), 8.51 (s, 1H); <sup>13</sup>C NMR (50 MHz, CDCl<sub>3</sub>)  $\delta$  - 4.14, 18.5, 25.9, 119.7, 121.7, 123.1, 126.6, 131.3, 146.8; ES-MS m/z: calcd for [C<sub>13</sub>H<sub>21</sub>NO<sub>2</sub>Si + H]<sup>+</sup> 252.1; found: 252.2.



**4-(*tert*-Butyldimethylsilyloxy)benzaldehyde oxime (11i).** <sup>1</sup>H NMR (200 MHz, CDCl<sub>3</sub>)  $\delta$  0.22 (s, 6H), 0.99 (s, 1H, 9H), 6.68 - 7.13 (d, 2H), 7.30 - 7.59 (d, 2H), 8.11 (s, 1H); <sup>13</sup>C NMR (50 MHz, CDCl<sub>3</sub>)  $\delta$  - 4.26, 18.4, 25.8, 120.6, 128.6, 190.0; ES-MS m/z: calcd for [C<sub>13</sub>H<sub>21</sub>NO<sub>2</sub>Si + H]<sup>+</sup> 252.4; found: 252.2.

## 2. RP-HPLC retention times and ES-MS data of inhibitors 6a-k, 13a-i, 14 and 22a-f

Compound	t (min)	Gradient <sup>1</sup>	ES-MS ( <i>m/z</i> ) <sup>2</sup>		
			calcd for:		found
<b>6a</b>	13.3	t = 0 min (0% B), t = 25 min (100% B)	[C <sub>19</sub> H <sub>32</sub> N <sub>3</sub> O <sub>4</sub> P - H] <sup>-</sup>	396.2	396.2
<b>6b</b>	15.4	t = 0 min (0% B), t = 25 min (100% B)	[C <sub>22</sub> H <sub>38</sub> N <sub>3</sub> O <sub>4</sub> P - H] <sup>-</sup>	438.3	438.3
<b>6c</b>	16.8	t = 0 min (0% B), t = 25 min (100% B)	[C <sub>25</sub> H <sub>36</sub> N <sub>3</sub> O <sub>4</sub> P - H] <sup>-</sup>	472.2	472.1
<b>6d</b>	13.3	t = 0 min (0% B), t = 25 min (100% B)	[C <sub>21</sub> H <sub>34</sub> N <sub>3</sub> O <sub>4</sub> P - H] <sup>-</sup>	422.2	422.2
<b>6e</b>	16.1	t = 0 min (0% B), t = 25 min (100% B)	[C <sub>27</sub> H <sub>36</sub> N <sub>4</sub> O <sub>5</sub> P - H] <sup>-</sup>	511.3	511.4
<b>6f</b>	13.8	t = 0 min (0% B), t = 25 min (100% B)	[C <sub>25</sub> H <sub>36</sub> N <sub>3</sub> O <sub>5</sub> P + H] <sup>+</sup>	490.2	490.3
<b>6g</b>	12.6	t = 0 min (0% B), t = 25 min (100% B)	[C <sub>19</sub> H <sub>32</sub> N <sub>3</sub> O <sub>5</sub> P - H] <sup>-</sup>	412.2	412.3
<b>6h</b>	12.1	t = 0 min (0% B), t = 25 min (100% B)	[C <sub>22</sub> H <sub>39</sub> N <sub>4</sub> O <sub>4</sub> P + H] <sup>+</sup>	455.3	455.3
<b>6i</b>	13.4	t = 0 min (0% B), t = 25 min (100% B)	[C <sub>22</sub> H <sub>34</sub> N <sub>5</sub> O <sub>4</sub> P + H] <sup>+</sup>	464.2	464.3
<b>6j</b>	12.6	t = 0 min (0% B), t = 25 min (100% B)	[C <sub>21</sub> H <sub>34</sub> N <sub>3</sub> O <sub>6</sub> P - H] <sup>-</sup>	454.2	454.2
<b>6k</b>	17.3	t = 0 min (0% B), t = 25 min (100% B)	[C <sub>25</sub> H <sub>36</sub> N <sub>3</sub> O <sub>4</sub> P - H] <sup>-</sup>	472.2	472.1
<b>13a</b> <sup>3</sup>	11.3	t = 0 min (30% B), t = 25 min (100% B)	[C <sub>31</sub> H <sub>35</sub> N <sub>4</sub> O <sub>5</sub> P - H] <sup>-</sup>	573.2	573.3
<b>13b</b>	17.5	t = 0 min (15% B), t = 25 min (80% B)	[C <sub>32</sub> H <sub>37</sub> N <sub>4</sub> O <sub>6</sub> P - H] <sup>-</sup>	603.3	603.4
<b>13c</b>	17.2	t = 0 min (15% B), t = 25 min (80% B)	[C <sub>32</sub> H <sub>37</sub> N <sub>4</sub> O <sub>6</sub> P - H] <sup>-</sup>	603.3	603.3
<b>13d</b>	17.0	t = 0 min (15% B), t = 25 min (80% B)	[C <sub>32</sub> H <sub>37</sub> N <sub>4</sub> O <sub>6</sub> P - H] <sup>-</sup>	603.3	603.3
<b>13e</b>	18.3	t = 0 min (15% B), t = 25 min (80% B)	[C <sub>31</sub> H <sub>34</sub> ClN <sub>4</sub> O <sub>5</sub> P - H] <sup>-</sup>	607.2	607.3
<b>13f</b>	19.1	t = 0 min (15% B), t = 25 min (80% B)	[C <sub>31</sub> H <sub>34</sub> ClN <sub>4</sub> O <sub>5</sub> P - H] <sup>-</sup>	607.2	607.3
<b>13g</b>	19.0	t = 0 min (15% B), t = 25 min (80% B)	[C <sub>31</sub> H <sub>34</sub> ClN <sub>4</sub> O <sub>5</sub> P - H] <sup>-</sup>	607.2	607.4
<b>13h</b>	17.1	t = 0 min (15% B), t = 25 min (80% B)	[C <sub>31</sub> H <sub>35</sub> N <sub>4</sub> O <sub>6</sub> P - H] <sup>-</sup>	589.2	589.3
<b>13i</b>	14.0	t = 0 min (15% B), t = 25 min (80% B)	[C <sub>31</sub> H <sub>35</sub> N <sub>4</sub> O <sub>6</sub> P - H] <sup>-</sup>	589.2	589.3
<b>14</b>	14.6	t = 0 min (0% B), t = 25 min (100% B)	[C <sub>24</sub> H <sub>30</sub> N <sub>3</sub> O <sub>4</sub> P - H] <sup>-</sup>	454.2	454.2
<b>22a</b> <sup>4</sup>	21.0*	t = 0 min (30% B), t = 25 min (70% B)	[C <sub>32</sub> H <sub>44</sub> N <sub>3</sub> O <sub>4</sub> P + H] <sup>+</sup>	566.3	566.4
<b>22b</b> <sup>5</sup>	18.5*	t = 0 min (30% B), t = 25 min (70% B)	[C <sub>35</sub> H <sub>40</sub> N <sub>3</sub> O <sub>4</sub> P + H] <sup>+</sup>	598.3	598.3
<b>22c</b>	17.0**	t = 0 min (30% B), t = 25 min (70% B)	[C <sub>32</sub> H <sub>42</sub> N <sub>3</sub> O <sub>4</sub> P - H] <sup>-</sup>	562.3	562.3
<b>22d</b> <sup>6</sup>	21.8*	t = 0 min (40% B), t = 25 min (70% B)	[C <sub>40</sub> H <sub>42</sub> N <sub>3</sub> O <sub>4</sub> P + H] <sup>+</sup>	660.3	660.2
<b>22e</b>	15.4**	t = 0 min (40% B), t = 25 min (100% B)	[C <sub>37</sub> H <sub>44</sub> N <sub>3</sub> O <sub>4</sub> P - H] <sup>-</sup>	624.3	624.4
<b>22f</b>	19.7**	t = 0 min (40% B), t = 25 min (100% B)	[C <sub>37</sub> H <sub>42</sub> Cl <sub>2</sub> N <sub>3</sub> O <sub>4</sub> P - H] <sup>-</sup>	692.2	692.2

<sup>1</sup> Conditions: Hewlett-Packard 1100 model (C18-Cromasil-RP, 5 μm, UV/vis detector, flow: 0.5 mL/min, 254 and/or 280 nm detection). Buffers used: A buffer: 90% H<sub>2</sub>O with 0.1% TFA, 10% CH<sub>3</sub>CN; B buffer: 10% H<sub>2</sub>O with 0.09% TFA, 90% CH<sub>3</sub>CN.

<sup>2</sup> LC/MS analysis was performed to HPLC-purified isomers

<sup>3</sup> Retention time of its P<sub>1</sub>'-epimer, **13a'**, by using the same method: 12.3 min

<sup>4</sup> Retention time of its P<sub>1</sub>'-epimer, **22a'**, by using the same method: 22.1 min

<sup>5</sup> Retention time of its P<sub>1</sub>'-epimer, **22b'**, by using the same method: 19.5 min

<sup>6</sup> Retention time of its P<sub>1</sub>'-epimer, **22d'**, by using the same method: 23.9 min

### 3. Titration of T-cell responses versus BMDCs exposed to different amounts of soluble ovalbumin

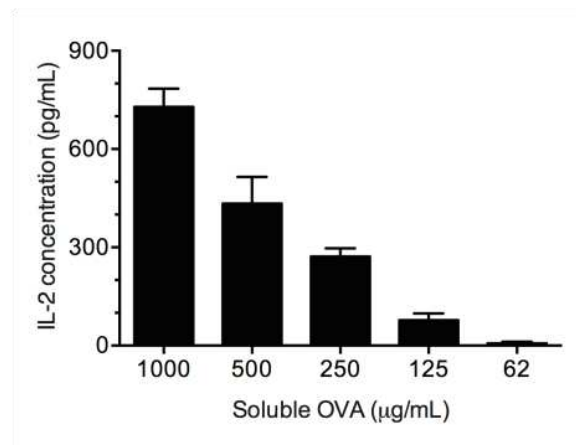


**Figure S1:** BMDCs isolated from wild-type mice were exposed to different concentrations of soluble ovalbumin, incubated for 6 hours, fixed and then mixed with CD8<sup>+</sup> T-cells isolated from the lymph nodes of Rag-1<sup>-/-</sup> C57Bl/6 OT-I mice. IL-2 secreted by the T-cells was measured by ELISA as described in the experimental methods section.

#### 4. REFERENCES

1. (a) Baylis, E. K.; Campbell, C. D.; Dingwall, J. G., 1-Aminoalkylphosphonous acids. Part 1. Isosteres of the protein amino acids. *J. Chem. Soc., Perkin Trans. 1* **1984**, 2845-2853; (b) Grembecka, J.; Mucha, A.; Cierpicki, T.; Kafarski, P., The most potent organophosphorus inhibitors of leucine aminopeptidase. Structure-based design, chemistry, and activity. *J. Med. Chem.* **2003**, *46* (13), 2641-2655.
2. Xu, Z.; DiCesare, J. C.; Baures, P. W., Parallel Synthesis of An Oligomeric Imidazole-4,5-dicarboxamide Library. *J. Comb. Chem.* **2010**, *12* (2), 248-254.
3. Moriguchi, T.; Yanagi, T.; Kunimori, M.; Wada, T.; Sekine, M., Synthesis and Properties of Aminoacylamido-AMP: Chemical Optimization for the Construction of an N-Acyl Phosphoramidate Linkage. *J. Org. Chem.* **2000**, *65* (24), 8229-8238.
4. Ager, D. J.; Prakash, I., Synthesis of aromatic amino acid amides. *Synth. Commun.* **1996**, *26* (20), 3865-3868.
5. Lu, J.-Y.; Riedrich, M.; Wojtas, K.; Arndt, H.-D., Assembly of the Nosiheptide A-Ring: A Fruitful Lesson. *Synthesis* **2013**, *45* (10), 1300-1311.
6. Routier, S.; Cotellet, N.; Catteau, J.-P.; Bernier, J.-L.; Waring, M. J.; Riou, J.-F.; Bailly, C., Salen-anthraquinone Conjugates. Synthesis, DNA-binding and cleaving properties, effects on topoisomerases and cytotoxicity. *Bioorg. Med. Chem.* **1996**, *4* (8), 1185-1196.
7. Bergeron, R. J.; Ludin, C.; Müller, R.; Smith, R. E.; Phanstiel IV, O., Development of a Hypusine Reagent for Peptide Synthesis. *J. Org. Chem.* **1997**, *62* (10), 3271-3284.
8. (a) Hou, Y.; Lu, S.; Liu, G., Iodine(III)-Mediated [3 + 2] cyclization for one-pot synthesis of benzo[d]isoxazole-4,7-diols in aqueous medium. *J. Org. Chem.* **2013**, *78* (17), 8386-8395; (b) Puerto Galvis, C. E.; Kouznetsov, V. V., An unexpected formation of the novel 7-oxa-2-azabicyclo[2.2.1]hept-5-ene skeleton during the reaction of furfurylamine with maleimides and their bioprospection using a zebrafish embryo model. *Org. Biomol. Chem.* **2013**, *11* (3), 407-411.
9. Patil, V. V.; Gayakwad, E. M.; Shankarling, G. S., Highly efficient and stable peracid for rapid and selective oxidation of aliphatic amines to oximes. *New J. Chem.* **2015**, *39* (8), 6677-6682.
10. Zhang, L.; Chen, H.; Zha, Z.; Wang, Z., Electrochemical tandem synthesis of oximes from alcohols using KNO<sub>3</sub> as the nitrogen source, mediated by tin microspheres in aqueous medium. *Chem. Commun.* **2012**, *48* (52), 6574-6576.
11. Schmidt, B.; Hölter, F.; Kelling, A.; Schilde, U., Pd-catalyzed arylation reactions with phenol diazonium salts: Application in the synthesis of diarylheptanoids. *J. Org. Chem.* **2011**, *76* (9), 3357-3365.

**Rab14<sup>+</sup> Endosomes Regulate Phagosome Maturation and MHC class I Cross-  
presentation by Dendritic Cells**

Loredana Saveanu<sup>1,2</sup>, Mirjana Weimershaus<sup>1,2</sup>, Joël Babdor<sup>1</sup>, Myriam Lawand<sup>1</sup>, Iri  
Evnouchidou<sup>1</sup>, Pablo Vargas<sup>3</sup>, Markus Zwick<sup>4</sup>, Thomas Brocker<sup>4</sup>, François-Xavier Mauvais<sup>1</sup>,  
Peter van Endert<sup>1\*</sup>

<sup>1</sup> Institut National de la Santé et de la Recherche Médicale, Unité 1151, Paris; Centre National  
de la Recherche Scientifique, Unité 8253, Paris; Université Paris Descartes, Sorbonne Paris  
Cité, Paris, 75015, France

<sup>2</sup> these authors contributed equally to the study

<sup>3</sup> Institut National de la Santé et de la Recherche Médicale, Unité 932; Institut Curie, Paris,  
75005, France

<sup>4</sup> Institute for Immunology, Ludwig Maximilian University, Munich, 80336, Germany

\* Corresponding author: [peter.van-endert@inserm.fr](mailto:peter.van-endert@inserm.fr); phone +33-1-44492563, fax +33-1-  
44495382



## SUMMARY

Phagocytosis of particulate material by myelomonocytic cells is followed by intracellular phagosome maturation that enables pathogen destruction and triggering of innate and adaptive immunity. In dendritic cells, master regulators of immune responses, phagosome maturation undergoes adaptations that regulate activation of endosomal innate immune receptors and limit destruction of internalized antigen, preserving it for cross-presentation to cytotoxic T cells. Here we show that dendritic cell phagosome maturation and cross-presentation are regulated by a class of endosomal vesicles related to adipocyte GLUT4 storage vesicles. Reduced abundance of these regulatory endosomes in cells lacking insulin-regulated aminopeptidase, or knockdown of Rab14 involved in their fusion with phagosomes, accelerate killing of phagocytosed pathogens, recruitment of lysosomal markers and proteases to, and acidification of phagosomes. The ensuing enhanced degradation of antigenic proteins compromises cross-presentation. Formation of regulatory endosomes requires the endoplasmic reticulum SNARE Sec22b, likely explaining the previously described acceleration of phagosome maturation upon Sec22b knockdown.

## INTRODUCTION

Dendritic cells (DCs) prime and orientate adaptive cellular immune responses in the context of innate immune signalling triggered by pathogen-associated molecular profiles (Steinman, 2012). Stimulation of antigen-specific adaptive immunity by DCs is intimately linked to their strong endocytic and phagocytic activity. Internalization of antigenic material is followed by intracellular proteolytic processing that results in production of peptides for loading of MHC molecules, which are exported to the cell surface for recognition by T lymphocytes. DCs excel in loading MHC class I molecules with peptides derived from internalized antigens, a process known as cross-presentation with a critical role in priming of cytotoxic CD8<sup>+</sup> T cell responses (Joffre et al., 2012).

The high efficiency of cross-presentation by DCs is thought to result from specific features of their endocytic vesicles. DC phagosomes fuse with the endoplasmic reticulum (ER) Golgi intermediate compartment (ERGIC) depending on the Soluble N-ethylmaleimide-sensitive factor Attachment protein Receptor (SNARE) Sec22b, thus acquiring ER proteins such as the transporters associated with antigen (TAP) that can provide peptides for loading of MHC class I molecules (Cebrian et al., 2011). However, since ER-phagosome fusion was first described in macrophages that cross-present poorly (Gagnon et al., 2002), it likely is necessary but not sufficient for efficient cross-presentation. Furthermore, results obtained with receptor-targeted protein antigens suggested that antigen trafficking to early endosomes, mediated for example by targeting to the mannose receptor (MR), enhances cross-presentation (Burgdorf et al., 2007; Cohn et al., 2013). However, the nature of these endosomes is poorly defined.

A reported hallmark feature of DCs with a critical role in cross-presentation is attenuated acidification. Phagosomes mature through a series of kiss-and-run interactions with intracellular compartments that result in progressive acidification, recruitment of hydrolases

and production of reactive oxygen species (Jutras and Desjardins, 2005). In DCs, acidification has been reported to be attenuated by recruitment of the NADPH oxidase NOX2 to early phagosomes and by delayed assembly of V-ATPase (Delamarre et al., 2005; Savina et al., 2006). Interestingly, phagosome acidification and maturation are accelerated in the absence of Sec22b (Cebrian et al., 2011). Since Sec22b knockdown also compromises recruitment of ER proteins to phagosomes, it is unclear whether accelerated phagosome maturation by itself affects cross-presentation.

We have recently described that insulin-regulated aminopeptidase (IRAP) removes N-terminal extensions from precursors of cross-presented MHC class I ligands (Saveanu et al., 2009). IRAP has been characterized mainly as a component of specific slowly recycling regulated endosomes found in adipocytes and muscle cells, which together with the glucose receptor GLUT4, their main cargo, are rapidly exported to the cell surface upon signalling by the insulin receptor (Keller, 2003). DCs lacking IRAP exhibited compromised cross-presentation, consistent with a role of IRAP as a trimming aminopeptidase for MHC class I ligands acting exclusively in cross-presentation (Saveanu et al., 2009).

We were intrigued by the fact that, in DCs, IRAP co-localizes strongly with the small GTPase Rab14. Rab14 has been implicated in “customization” of phagocytic vacuoles by pathogens which seek to inhibit vesicle maturation to acidic phagolysosomes equipped with active hydrolases (Capmany and Damiani, 2010; Kuijl et al., 2007; Kyei et al., 2006). Prompted by this context, we wondered whether the compartment containing IRAP affected physiologic phagosome maturation. Here we show that, in bone marrow-derived DCs (BM-DCs), a class of endosomes containing Rab14 and IRAP regulates phagosome maturation and thereby cross-presentation, and that the regulatory effect of Sec22b deficiency on phagosome maturation reflects the Sec22b requirement for formation of these endosomes.

## RESULTS

### **Reduced abundance of Rab14+ endosomes in IRAP-deficient BM-DCs**

Previous observations made in adipocytes suggested that formation or stability of GLUT4 storage vesicles (GSVs) is compromised in the absence of IRAP (Keller et al., 2002). To assess whether IRAP deficiency had a similar effect on DC endosomes, we examined the subcellular distribution of proteins showing extensive co-localization with IRAP. The small GTPase Rab14 and the SNARE syntaxin 6 (STX6) are markers of GSVs in adipocytes or muscle cells and label IRAP-positive endosomes in DCs (**Figure 1A**) (reviewed in Saveanu and van Endert, 2012). Because STX6 is involved in trafficking between endosomes and the Trans-Golgi Network (TGN) (Jung et al., 2012), it stains Golgi stacks but also endosomal vesicles where it co-localizes with IRAP. Analysis of IRAP-deficient DCs assuming similar shapes in micro-patterns (Faure-Andre et al., 2008) revealed a striking absence of endosomal STX6 staining whereas Golgi-type STX6 staining was unchanged; peripheral Rab14 staining was similarly absent in IRAP ko DCs (**Figure 1B**). In contrast, EEA1 and the mannose receptor (MR), known to target antigens to early endosomes for efficient cross-presentation (Burgdorf et al., 2007), displayed normal endosomal abundance and co-localization in IRAP ko DCs, whereas STX6 co-localization with both was strongly reduced (**Figure 1C**). We concluded that IRAP deficiency was associated with a selective decrease in STX6+ (Rab14+) endosomes whereas MR+ EEA1+ endosomes, previously suggested to be critical for cross-presentation, were not affected by it. Considering our results (see also below), we propose to refer to endosomal DC STX6+Rab14+ vesicles as “regulatory endosomes”. To further confirm the causal relationship between IRAP deficiency and the absence of STX6 endosomes, we reconstituted DCs with full-length IRAP. As expected, IRAP-transfected ko

DCs harboured peripheral STX6-positive vesicles in addition to Golgi vesicle staining seen in IRAP ko cells (**Figure 1D**).

Reconstitution of ko DCs also allowed us to confirm our previous conclusion that IRAP expression was required for efficient cross-presentation (Saveanu et al., 2009). Incubation of wt BM-DCs with an MR-targeted ovalbumin (OVA) fusion protein resulted in dose-dependent stimulation of OT-I CD8<sup>+</sup> T lymphocytes (**Figure 1E**). While IRAP-deficient BM-DCs exhibited a 60 per cent reduction in T cell stimulation, transfection with IRAP fully reconstituted OT-I T cell stimulation.

### **Accelerated phagosome maturation in IRAP ko DCs**

In DCs, phagosome acidification is attenuated and delayed relative to macrophages or neutrophils, presumably to protect phagocytised antigenic proteins from premature destruction by pH-dependent hydrolases (Amigorena and Savina, 2010). Given that Rab14 is known to be recruited by various pathogens to block or modulate maturation of phagosomes (Kuijl et al., 2007; Kyei et al., 2006), we wondered whether reduced abundance of IRAP+Rab14+STX6<sup>+</sup> endosomes might affect phagosome maturation.

We analysed the protein composition of purified latex bead phagosomes by immunoblot.

While IRAP ko phagosomes contained equal amounts of MHC class I molecules, we detected reduced amounts of EEA1 in early phagosomes, and increased amounts of the late endosome/lysosome markers LAMP1 and V-ATPase in late phagosomes (**Figure 2A**).

However, the abundance of two proteins presumably recruited from the ER through Sec22b-dependent ER-phagosome fusion (Cebrian et al., 2011), calnexin and TAP2, was unchanged in early and late vesicles. Increased and/or premature recruitment of the late endosome markers Rab7 and LAMP1 in IRAP ko DCs were also observed using flow cytometric analysis of crude latex bead phagosomes (**Figure 2B**). Accelerated loss of EEA1 and

acquisition of LAMP1 were confirmed in a quantitative analysis of phagosomes containing latex beads and yeast cells by confocal microscopy (**Figure 2C**). Yeast-containing IRAP ko vesicles showed increased early acquisition followed by accelerated subsequent loss of EEA1, possibly resulting from a specific accelerating effect of yeast-associated signals on phagosome interaction with early endosomes in IRAP ko DCs (**Figure 2C**). We concluded that IRAP deficiency resulted in accelerated acquisition of late endosome markers by phagosomes.

Phagosome maturation is associated with progressive acidification. Consistent with our analysis of phagosome protein composition, IRAP ko phagosomes acidified more rapidly (**Figure 2D**). Recently, proteins associated with the autophagy machinery such as LC3-II have been shown to be recruited to phagosomes containing ligands for innate Toll-like receptors (Sanjuan et al., 2007). Recruitment of autophagy-associated proteins accelerates phagosome maturation, killing of engulfed pathogens and antigen presentation by MHC class II molecules (Gutierrez et al., 2004; Lee et al., 2010). Consistent with previous reports, wt phagosomes containing inert beads showed very little staining for LC3 (**Figure 2E**). In contrast, IRAP ko phagosomes strongly recruited LC3. Interestingly, greatly increased LC3 staining was also observed in resting mouse embryonal fibroblasts (MEFs) (**Figure S1**), suggesting that mobilization of autophagy proteins was not limited to phagocytosis-related events.

Acidification and activation of proteases can limit availability of protein antigens for presentation by MHC molecules (Joffre et al., 2012). We analysed degradation of OVA and bovine serum albumin (BSA) coated on beads by flow cytometry analysis. Degradation of both proteins was more advanced in IRAP ko phagosomes after 20 min, while no difference was apparent after 60 min (**Figure 3A**). DC phagosomes are thought to function as MHC class I loading vesicles in which peptides derived by cytosolic degradation of phagocytised material

and re-imported by the TAP transporters assemble with MHC class I molecules (Guermónprez et al., 2003). We reasoned that accelerated phagosome maturation might also increase degradation of such peptides. To test this, we developed an assay monitoring TAP-dependent accumulation of a fluorescent peptide in phagosomes (**Figure S2A**). Peptide accumulation in vesicles obtained at 20 min after start of phagocytosis was not affected by IRAP deficiency (**Figure 3B**), consistent with normal amounts of TAP protein in purified IRAP ko phagosomes (**Figure 2A**). However, upon vesicle maturation for another 40 min, peptide accumulation increased in wt but decreased in IRAP ko phagosomes. This difference could be reversed by addition of protease inhibitors during the peptide transport assay (**Figure 3B**). In conclusion, IRAP ko phagosomes harboured increased protease activity acting both on phagocytised proteins and on TAP-imported antigenic peptides.

Phagosome maturation is the condition for destruction of ingested pathogens. We examined intracellular killing of phagocytised bacteria (*Pseudomonas aeruginosa*), fungus (*Aspergillus fumigatus* conidia) and yeast (*Saccharomyces cerevisiae*). IRAP deficiency did not affect the efficiency of pathogen uptake by BM-DCs (**Figure S2B,C**). All pathogens were killed more efficiently in IRAP ko BM-DCs (**Figure 3C**). We concluded that IRAP deficiency induces a complete array of phenotypic and functional alterations indicative of altered phagosome maturation, including accelerated acquisition of late endosome/lysosome proteins, acidification, recruitment of autophagy-associated LC-3II, protein degradation and pathogen killing. Therefore IRAP-containing vesicles control phagosome maturation.

### **IRAP peptidase activity is required for efficient cross-presentation but not formation of regulatory endosomes**

Stimuli promoting phagosome maturation can enhance antigen presentation by MHC class II but may compromise cross-presentation by MHC class I (Joffre et al., 2012). Considering this,

compromised cross-presentation by IRAP-deficient DCs could be due either to lack of antigenic peptide trimming by IRAP or to enhanced antigen destruction associated with accelerated phagosome maturation, or to both. Asking whether IRAP peptidase activity was involved in its effect on cross-presentation, we introduced an active site mutation expected to abolish peptidase activity into IRAP (Ye et al., 2007). Upon transfection into IRAP ko MEFs, the mutant was expressed at the same level as wt IRAP. As expected, immunoprecipitated mutant protein had no peptidase activity toward a fluorogenic peptidase substrate (**Figure 4A**). When IRAP-deficient DCs were transfected with inactive IRAP, the mutant protein was detected in peripheral vesicles where it co-localized with the markers highlighting regulatory endosomes, including STX6 and Rab14, but also with EEA1 and MR (**Figure 4B**). Thus inactive IRAP is sufficient to reconstitute formation and/or stability of DC regulatory endosomes, at least at steady state.

Is reconstitution of regulatory endosomes sufficient to normalize cross-presentation? We transfected IRAP ko DCs to express inactive IRAP together with GFP and tested GFP-positive cells for cross-presentation of OVA targeted to the MR. Inactive IRAP was unable to normalize cross-presentation, suggesting that IRAP's peptidase activity was mandatory for its role in this context (**Figure 4C**). Further evidence in support of this conclusion was obtained when wt DCs were incubated with OVA-carrying yeast cells after pre-incubation with a synthetic IRAP inhibitor (**Figure 4D**) (Nikolaou et al., 2013). IVDE inhibited cross-presentation by wt DCs by 30 per cent but had no effect on presentation by IRAP ko DCs. Note that the peptidase activity of IRAP purified from DCs pre-incubated with the inhibitor was reduced by only 50 per cent (**Figure S3**), consistent with partial reduction of cross-presentation.



## **Rab14 knockdown compromises regulatory endosome formation/stability and cross-presentation**

Our results so far demonstrated that DC regulatory endosomes depend for their formation and/or stability on IRAP and regulate phagosome maturation, and that IRAP's peptidase activity is required for cross-presentation. However, it remained unclear whether regulation of phagosome maturation by regulatory endosomes affected cross-presentation independent of IRAP's peptidase activity. We reasoned that knockdown of Rab14, which likely mediates fusion of regulatory endosomes with phagosomes, in wt DCs expressing active IRAP would be suitable to address this question. Lentiviral knockdown reduced Rab14 mRNA levels by about 75 per cent and protein levels to a similar or greater extent (**Figure 5A,B**). However, the cellular protein levels of IRAP and STX6 were unaltered upon Rab14 knockdown, as were those of TAP2 presumably recruited from the ER (**Figure 5B**), or those of MHC class I molecules on the DC surface (**Figure S4**).

BM-DCs transduced with Rab14 shRNA displayed features strikingly reminiscent of IRAP ko BM-DCs. While EEA1 and MR were normally present in endosome-like structures and co-localized like in control transduced cells, endosomal IRAP staining was essentially absent as was IRAP co-localization with EEA1 or MR (**Figure 5C**). DCs with low or absent Rab14 expression showed normal staining for STX6 in Golgi-type structures while endosomal STX6 staining and with it, STX6 co-localization with EEA1 were strongly reduced. Moreover, yeast-containing phagosomes in DCs lacking Rab14 rapidly lost EEA1 staining and became positive for LAMP1 (**Fig. 5D**). This was accompanied by enhanced killing of bacteria (**Fig. 5E**). Thus Rab14 knockdown resulted in production of DCs exhibiting accelerated phagosome maturation but expressing normal levels of active IRAP. This setting allowed us to examine whether control of phagosome maturation by regulatory endosomes affected cross-presentation without a potential confounding effect of absent epitope trimming by IRAP.

Rab14 knockdown compromised cross-presentation of MR-targeted OVA, reducing it to the level of presentation by IRAP-deficient DCs (**Fig. 5F**). However, Rab14 knockdown had no effect on presentation by IRAP ko DCs, consistent with a mechanistic overlap between IRAP and Rab14 function in cross-presentation. We concluded that both IRAP and Rab14 are required for normal formation and/or stability of DC regulatory endosomes and for normal phagosome maturation.

### **Aberrant Rab14 localization compromises cross-presentation**

Regulation of vesicle fusion by Rab proteins is controlled by GTP binding, hydrolysis to GDP and exchange against GTP which in turn is regulated by GTPase activating proteins and exchange factors, and which implicates effector proteins which all remain to be defined for Rab14 in DCs (Stenmark, 2009). Constitutively active or dominant negative mutants can mimic the GTP- and GDP-locked Rab states, respectively (Junutula et al., 2004). In macrophages containing mycobacteria, a constitutively active Rab14 mutant blocks phagosome maturation, whereas a dominant negative mutant inhibits phagosome fusion with early endosomes while increasing acidification (Kyei et al., 2006). We produced GFP fusion proteins comprising wt, constitutively active (Q70L) or dominant negative (S25N) Rab14 (Junutula et al., 2004) which upon nucleofection were over-expressed in BM-DCs. Expression of wt or mutant Rab14-GFP did not alter MHC class I expression significantly (**Figure S5A**). However, transfection of IRAP ko but not wt DCs with wt Rab14 increased expression of the co-stimulatory molecule CD80 reproducibly 1.5-fold (**Figure S5B**).

Wt Rab14-GFP transfected into wt BM-DCs co-localized strongly with IRAP and STX6 and weakly with LAMP1 and Sec22b (**Figure 6A,B**). Although this corresponded largely to the pattern observed for endogenous Rab14, we noticed a slight shift from STX6 to LAMP1 positive compartments. The same shift was more pronounced when IRAP ko cells were transfected (**Figure 6B**). Mis-localization from IRAP+STX6+ regulatory endosomes to a

LAMP1 compartment was substantially stronger for the constitutively active Rab14Q70L-GFP. In IRAP ko cells, this mutant was almost completely absent from STX6+ compartments indicating that it resided neither in Golgi nor in endosomal vesicles. Consistent with published data, the dominant negative variant Rab14S25N-GFP failed entirely to reach peripheral IRAP+ as well as LAMP1+ compartments and showed very strong co-localization with Sec22b, suggesting that it was blocked in the ERGIC or in the Golgi apparatus (Junutula et al., 2004). Within Golgi vesicles, Rab14S25N-GFP also localized to STX6 positive structures, whereas it was entirely absent from STX6 endosomes (**Figure 6A,B**). Expression of both Rab14 mutants diminished the total staining intensity for STX6 in the cellular periphery (**Figure 6C**), indicating that correct sub-cellular targeting of Rab14 contributed to formation or stability of regulatory endosomes.

We selected transfected cells for GFP expression (**Figure S5C**) and put them in contact with MR-targeted OVA and OT-I T cells (**Figure 6D**). Over-expression of wt Rab14 in wt BM-DCs resulted in a moderate increase in cross-presentation. In contrast, expression of both Rab14 mutants moderately decreased it relative to vector controls. Therefore correct intracellular location to STX6+ endosomes and/or physiologic cycles of GTP binding and hydrolysis by Rab14 are required for efficient cross-presentation. Surprisingly, transfection of IRAP ko DCs with wt Rab14 increased their cross-presentation capacity dramatically (five-fold), such that transfected IRAP ko cells presented more efficiently than equivalently transfected wt cells (**Figure 6D**). Highly efficient cross-presentation by IRAP ko DCs over-expressing may be related to up-regulation of co-stimulatory molecules (**Figure S5B**).

### **Sec22b knockdown abolishes formation of IRAP+ STX6+ regulatory endosomes**

Knockdown of the ERGIC SNARE Sec22b has previously been shown to induce accelerated phagosome maturation however the mechanism remained unclear (Cebrian et al., 2011).

Wondering whether there existed a mechanistic link between the roles of Sec22b and IRAP in DC biology, we used the lentiviral shRNA approach described by Cebrian et al to reduce Sec22b expression and examined the effect on endosomal compartments. Because in our hands the chosen sequence results in incomplete Sec22b knockdown the extent of which varied between individual cells, we measured the correlation between the staining intensities of Sec22b and other selected markers.

Sec22b did not alter total cellular TAP1 and LAMP1 staining, demonstrating the absence of global perturbations of the ER and late endosome/lysosome compartments (**Figure 7A**).

Sec22b staining correlated negatively with staining for the cis-Golgi marker GM130, consistent with perturbation of ER-Golgi trafficking by the knockdown. However, Sec22b knockdown had a dramatic effect on regulatory endosomes. Cells lacking Sec22b were devoid of IRAP staining and exhibited substantially reduced STX6 staining, establishing a strong and direct link between Sec22b and formation of regulatory endosomes. Although the distribution of STX6 between Golgi and endosome compartments was not statistically different, the effect of Sec22b knockdown was more pronounced in the latter (**Figure 7B**). We concluded that Sec22b is specifically required for formation of a class of endosomes containing IRAP and STX6 which regulate phagosome maturation in DCs.

## DISCUSSION

Our results highlight the critical role of a distinct endosomal compartment in regulation of phagosome maturation and MHC class I cross-presentation by DCs. This compartment carries a set of marker proteins (Rab14, STX6, IRAP) suggesting its close similarity to regulated slowly recycling storage vesicles described in adipocytes and muscle cells. These proteins place the compartment on a trafficking pathway between the TGN, early endosomes and the plasma membrane, enable it to fuse with phagosomes, and equip it for final proteolytic processing of MHC class I ligands. The nature of potential protein cargo stored in it, and the signals regulating its trafficking remain to be investigated.

Indirect evidence for an important role of an early endosomal compartment in cross-presentation has been obtained previously both for murine and human DCs. Thus different human DC subtypes cross-present with equal efficiency provided that antigen is delivered to early endosomes by targeting to receptors such as CD11c or CD40 (Cohn et al., 2013), which both also mediate highly efficient cross-presentation when targeted on murine DCs (Chatterjee et al., 2012). Moreover, antigen uptake by the murine MR results in optimized cross-presentation (Burgdorf et al., 2007). Viewed in the light of our results, these observations suggest that the cited receptors all traffic to Rab14+ endosomes, as demonstrated formally for the MR by us. Because IRAP ko DCs display normal formation of MR+ EEA1+ endosomes, and because cross-presentation of MR-targeted antigens is compromised in IRAP or Rab14-deficient DCs, our results suggest strongly that it is antigen and MR trafficking to the Rab14+IRAP+ compartment that mediates efficient cross-presentation.

The published phenotype resembling most closely our findings on IRAP-deficient DCs was obtained with DCs lacking Sec22b expression. Next to abolishing ER-phagosome fusion, Sec22b knockdown also accelerated phagosome maturation (Cebrian et al., 2011). However which of these two phenomena compromised cross-presentation was unclear, as was the

reason for accelerated phagosome maturation. Our results suggest strongly that the latter phenomenon results from the quasi disappearance of IRAP+ endosomes in cells lacking Sec22b expression. Moreover, since IRAP ko phagosomes express normal amounts of functional TAP complexes, fusion of ERGIC vesicles with phagosomes is unlikely to involve the Rab14+IRAP+ compartment. Consequently, Sec22b likely controls at least two pathways ending up with phagosome fusion that diverge upstream of regulatory endosomes.

The effect of Sec22b knockdown on MHC class I cross-presentation appears in a surprising new light considering its effect on the Rab14+IRAP+ compartment. Given that the quasi disappearance of that compartment upon Sec22b knockdown will alone compromise cross-presentation as shown in this study, it is formally impossible to determine the relative impact on cross-presentation of the two published effects of Sec22b knockdown: absent ERGIC-phagosome fusion and absent IRAP+ endosome-phagosome fusion. Although multiple studies including this one have confirmed the presence of functional TAP in DC phagosomes (Ackerman et al., 2003; Guermonprez et al., 2003; Houde et al., 2003), only a strategy that dissociates the two effects, i.e. that is suitable for specific exclusion of the TAP transporters from phagosomes while not interfering with phagosome maturation, will provide definite insight into their relative functional impact on cross-presentation.

Although the regulatory role of Rab14+ endosomes in DC phagosome maturation has not been recognized prior to this study, Rab14 recruitment has been described to be associated with “customization” of intracellular vacuoles and inclusions by pathogens. *Mycobacteria*, *Salmonella* and *Chlamydia* recruit Rab14 to their vacuoles and activate it to block phagosome maturation and promote pathogen survival, prompting Deretic et al to speculate that Rab14 might maintain early endosome identity physiologically, i.e. in non-infected cells (Kyei et al., 2006). We demonstrate that this is indeed the case, at least in DCs.

Published reports provide partly equivocal evidence on the function of Rab14. Thus both murine macrophage Rab14 and its 85% identical *Dictyostelium* analogue RabD promote homotypic phagosome fusion, but RabD also mediates fusion with late endosomes and homotypic lysosome fusion (Harris and Cardelli, 2002; Kyei et al., 2006). In murine macrophages, dominant negative Rab14S25N renders vacuoles permissive for fusion with late endosomes. Our observation that Rab14S25N localizes to the ERGIC is consistent with the latter finding and with the original characterization of the mutant (Junutula et al., 2004). However, strongly increased co-localization with LAMP1 of constitutively active Rab14Q70L in DCs and consequently compromised cross-presentation, while consistent with the mentioned trafficking profile of RabD, was a somewhat unexpected result given that this mutant blocks maturation of phagosomes containing killed mycobacteria. This possible discrepancy may point to differences between macrophages and DCs or be related to distinct Rab14 trafficking between steady state and phagocytosing cells.

How might Rab14+ endosomes modulate phagosome maturation? Among the three key proteins distinguishing these vesicles, two (Rab14 and STX6) mediate exchange between the TGN and early endosomes, while both STX6 and IRAP traffic between endosomes and the plasma membrane. In the case of pathogen-containing vacuoles, it has been speculated that exchange with the plasma membrane and the TGN may provide internalized nutrients and factors critical for pathogen survival such as sphingolipids for *Chlamydia* (Capmany and Damiani, 2010). Similar trafficking events may provide components required for cross-presentation to phagosomes; note that the adaptor AP-1 which labels an endosomal microdomain interconnecting early endosomes and the TGN was recently shown to be implicated in cross-presentation (Kulpa et al., 2013). An additional mechanistic lead was recently described by Junutula et al who identified Nischarin as Rab14 effector protein in *Salmonella*-infected cells (Kuijl et al., 2013). Being able to bind both Rab14 and Rab9, Nischarin may mediate an

alternative pathway of phagosome maturation resulting in Rab9 rather than Rab7-decorated lysosome-related vesicles. Because Rab9 mediates lysosome-TGN trafficking, this model would again suggest an important role of phagosome interaction with the TGN in cross-presentation.

Our discovery of a regulatory role of Rab14+ endosomes started with the investigation of IRAP-deficient DCs. How can IRAP regulate phagosome maturation? In adipocytes, IRAP deficiency results in a reduction of GLUT4 levels by 50 – 80% per cent, suggesting that IRAP may stabilize GLUT4 and/or GSVs (Keller et al., 2002). The fact that IRAP deficiency reduces endosomal Rab14 levels and vice versa may indicate stabilizing interactions between the two proteins. A stabilizing role of IRAP may also be related to the numerous protein interactions of its cytosolic tail which by binding to, among others, the cytoskeleton proteins vimentin and a formin homolog may anchor vesicles (Hirata et al., 2011; Tojo et al., 2003). In the context of cross-presentation, our previous results suggested that IRAP acted as trimming peptidase for MHC class I ligands (Saveanu et al., 2009). The fact that inactive IRAP does not reconstitute normal cross-presentation is consistent with this interpretation and suggests that IRAP acts at the same time as trimming enzyme and as stabilizer of Rab14+ endosomes, both of which contribute to efficient cross-presentation. However, we cannot rule out alternative explanations, for example that IRAP's enzymatic activity may be required in a trafficking step delivering IRAP to internalized antigens. Importantly, over-expression of wt Rab14 in IRAP ko DCs reconstitutes cross-presentation, demonstrating that neither IRAP's stabilizing nor its enzymatic activity are absolute requirements for cross-presentation. This finding highlights the important role of Rab14+ regulatory endosomes in optimizing DC phagosome maturation for stimulation of adaptive and innate immunity.



## EXPERIMENTAL PROCEDURES

### **Mice and cells**

Full information on animals and cells is provided in Supplemental Experimental Procedures.

### **Antibodies**

Details on the antibodies used are provided in the Supplemental Experimental Procedures.

### **Fluorescence microscopy**

Cell analysis by fluorescence microscopy was performed on day 7 BM-DCs plated on different supports including fibronectin-coated coverslips, micro-pattern slides for analysis of uniform cells (Faure-Andre et al., 2008) and IbiTreat channels (BioValley) for phagocytosis assays. Latex beads (Polysciences) or previously described (Saveanu and van Endert, 2013) *S. cerevisiae* cells expressing OVA attached to the cell wall were used in the latter assays. Cells were fixed, permeabilized and stained as described before (Saveanu et al., 2009). Images were acquired with a Leica SP8 confocal microscope or, where indicated, with a conventional Leica DMI 6000 microscope equipped with a piezoelectric-driven stage before processing by 3D deconvolution. Image analysis was performed using the IMARIScoloc module (IMARIS software, Bitplane AG) or with ImageJ; for details see Supplemental Experimental Procedures.

### **Cloning and plasmids**

Full-length IRAP cDNA was obtained from mouse splenocytes, amplified and modified by addition of a carboxyterminal HA tag. PCR-based mutagenesis was used to produce inactive IRAP in which the active site HELAH sequence was changed to HALAH. Wt and inactive IRAP were cloned into the expression plasmid pIRES2-GFP (Clontech). A Rab14 full-length clone was obtained from BM-DCs by RT-PCR and expressed as fluorescent fusion protein in pEGFP-C1 (Clontech). Mutagenesis was used to obtain the mutants Rab14S25N and Q70L. Cloning is described in detail in Supplemental Experimental Procedures.

### **Flow cytometry and sorting**

BM-DCs were incubated on ice with fluorochrome- or biotin-conjugated CD11b, CD11c and AF6-88.5 antibodies diluted in PBS with 2% FCS. APC/Cy7-streptavidin (Biolegend) was used as secondary reagent and 7-AAD (5  $\mu$ L/sample) to discriminate live and dead cells. BD Fortessa™ and FACS ARIA-II™ machines were used for cell analysis and sorting, respectively.

### **Cross-presentation assays**

Cross-presentation assays were performed on BM-DCs nucleofected on day 5 of culture with wt or mutant IRAP or Rab14 plasmids, or transduced with lentivirus-expressed shRNA. On day 7, Rab14-GFP transfected cells were sorted as live CD11b<sup>+</sup>CD11c<sup>+</sup> cells, while lentivirus-transduced cells were purified by Optiprep gradients. The cells were incubated with complexes of anti-MR and P3UO or P3UGAD fusion proteins, prepared as described before (Kratzer et al., 2010), and with OT-I T cells. T cell activation was read out as IL-2 secretion in duplicate wells by ELISA. Where applicable, the IVDE77 inhibitor was added 16 hr prior to phagocytosis and maintained during antigen uptake and processing. See Supplemental Experimental Procedures for additional detail.

### **Immunoblots**

Latex bead-containing phagosomes were prepared from BM-DCs by sucrose gradients according to published procedures (Desjardins et al., 1994). Briefly,  $1.5 \times 10^8$  BM-DCs were fed 0.5 mL deep-blue latex beads (Sigma). Cells were lysed mechanically, excess beads removed by FCS flotation and phagosomes purified via a sucrose gradient by ultracentrifugation. Phagosomes were finally lysed in 1% CHAPS, the protein concentration was measured with the Bradford reagent (BioRad), and the protein composition analyzed by immunoblots.

### **PhagoFACS and phagosomal pH**

PhagoFACS experiments and measurement of phagosomal pH were both performed using a modification of published protocols (Savina et al., 2010). Details of the modifications are described in Supplemental Experimental Procedures.

### **Phagosomal peptide transport assay**

Three micron latex beads (Polysciences) were coated by passive adsorption with 100 µg/mL rabbit immunoglobulin and incubated at a ratio of 3:1 for 20 min at 37°C for phagocytosis with BM-DCs. After elimination of free beads by FCS gradient, half of the preparation was incubated for another 40 min at 37°C to allow for maturation to “late phagosomes”. Then cells were disrupted mechanically in 220 mM sucrose, 3 mM imidazole, 1 mM DTT, 5 mM MgCl<sub>2</sub> and phagosomes pelleted after removal of nuclei. Phagosomes were pre-incubated during 5 min with 0.9 mM ATP, 2 mg/mL creatine kinase and 400 mM creatine phosphate and incubated for 15 min at 20°C or 4°C with 5 µM peptide RRYNAC(FITC)TEL (R9L-FITC) obtained at ~80% purity from Pepscan or Sigma-Genosys. Finally the phagosomes were washed with PBS, stained with 7.5 µg/ml CellMask Deep Red™ membrane stain (Invitrogen) for 30 min at 4°C and analysed for peptide accumulation by FACS.

### **Microbicidal activity in vitro**

*P. aeruginosa*, *S. cerevisiae* and *Aspergillus fumigatus* conidia were added to BM-DCs and incubated for 3, 6 or 5 hr (*Aspergillus*), respectively, before DC lysis, plating of the lysates and counting of colonies. To enhance attachment of conidia to DCs, cells were centrifuged with conidia for 30 min.

### **Peptidase activity assays**

IRAP was immunoprecipitated from lysates of IRAP ko mouse epithelial fibroblasts transfected 2 days before with wt or E465A mutant IRAP. Equivalent IRAP protein amounts were incubated for 15 min with a fluorogenic substrate with continuous measuring of the fluorescence signal at 460 nm. To measure the effect and cell penetration of the IVDE77

inhibitor, BM-DCs were pre-incubated for 16 hr with IVDE77 or solvent before lysis, immunoprecipitation of IRAP and measurement of peptidase activity using a fluorogenic substrate. See Supplemental Experimental Procedures for details.

### **Lentivirus production and infection**

Lentiviruses for knockdown of Rab14 and Sec22b were produced by transfection of HEK-293-FT with plasmids carrying specific sequences and a puromycin resistance gene together with packaging and envelope encoding plasmids. Virus-containing supernatants were concentrated and virus titers were determined by transduction of NIH3T3 fibroblasts followed by isolation of genomic DNA and determination of viral gene numbers by qPCR.

Bone marrow cells were transduced with lentiviruses at an MOI of 10 on day 3 of culture, followed by elimination of non-transduced cells by addition of puromycin on day 5.

Transduced cells were used on day 7-8 of culture. Details are described in Supplemental Experimental Procedures.

### **Statistical analysis**

Statistical analysis including regression analysis and unpaired t tests were performed using GraphPad Prism™ software.

## AUTHOR CONTRIBUTIONS

L.S., M.W. and F.-X.M. designed, performed and interpreted experiments. J.B., M.L. and I.E. performed and interpreted experiments. P.V. prepared micro-patterns. M.Z. and T.B. helped with production of lentiviruses. P.v.E. designed and interpreted experiments and wrote the paper.

## ACKNOWLEDGEMENTS

Supported by institutional grants from INSERM and Université Paris Descartes, by grant NT09\_522096 from the Agence Nationale de Recherche, and by a grant from Association de Recherche sur le Cancer for microscopy equipment. M.W. was supported by a PhD fellowship from the Boehringer Ingelheim Fonds, and I.E. by a grant from the Thyssen Foundation. We are grateful to Nicolas Goudin and Meriem Garfa-Traoré for assistance in confocal microscopy studies, to A. Nikolaou and P.M. Vanderheyden for the IVDE77 inhibitor, to A. Lennon-Dumenil for providing micropatterns.

## REFERENCES

- Ackerman, A.L., Kyritsis, C., Tampe, R., and Cresswell, P. (2003). Early phagosomes in dendritic cells form a cellular compartment sufficient for cross presentation of exogenous antigens. *Proc. Natl. Acad. Sci. U. S. A.* *100*, 12889-12894.
- Amigorena, S., and Savina, A. (2010). Intracellular mechanisms of antigen cross presentation in dendritic cells. *Curr. Opin. Immunol.* *22*, 109-117.
- Burgdorf, S., Kautz, A., Bohnert, V., Knolle, P.A., and Kurts, C. (2007). Distinct pathways of antigen uptake and intracellular routing in CD4 and CD8 T cell activation. *Science* *316*, 612-616.
- Capmany, A., and Damiani, M.T. (2010). Chlamydia trachomatis intercepts Golgi-derived sphingolipids through a Rab14-mediated transport required for bacterial development and replication. *PLoS One* *5*, e14084.
- Cebrian, I., Visentin, G., Blanchard, N., Jouve, M., Bobard, A., Moita, C., Enninga, J., Moita, L.F., Amigorena, S., and Savina, A. (2011). Sec22b regulates phagosomal maturation and antigen crosspresentation by dendritic cells. *Cell* *147*, 1355-1368.
- Chatterjee, B., Smed-Sorensen, A., Cohn, L., Chalouni, C., Vandlen, R., Lee, B.C., Widger, J., Keler, T., Delamarre, L., and Mellman, I. (2012). Internalization and endosomal degradation of receptor-bound antigens regulate the efficiency of cross presentation by human dendritic cells. *Blood* *120*, 2011-2020.
- Cohn, L., Chatterjee, B., Esselborn, F., Smed-Sorensen, A., Nakamura, N., Chalouni, C., Lee, B.C., Vandlen, R., Keler, T., Lauer, P., *et al.* (2013). Antigen delivery to early endosomes eliminates the superiority of human blood BDCA3+ dendritic cells at cross presentation. *J. Exp. Med.* *210*, 1049-1063.

Delamarre, L., Pack, M., Chang, H., Mellman, I., and Trombetta, E.S. (2005). Differential lysosomal proteolysis in antigen-presenting cells determines antigen fate. *Science* 307, 1630-1634.

Desjardins, M., Celis, J.E., van Meer, G., Dieplinger, H., Jahraus, A., Griffiths, G., and Huber, L.A. (1994). Molecular characterization of phagosomes. *J. Biol. Chem.* 269, 32194-32200.

Faure-Andre, G., Vargas, P., Yuseff, M.I., Heuze, M., Diaz, J., Lankar, D., Steri, V., Manry, J., Hugues, S., Vascotto, F., *et al.* (2008). Regulation of dendritic cell migration by CD74, the MHC class II-associated invariant chain. *Science* 322, 1705-1710.

Gagnon, E., Duclos, S., Rondeau, C., Chevet, E., Cameron, P.H., Steele-Mortimer, O., Paiement, J., Bergeron, J.J., and Desjardins, M. (2002). Endoplasmic reticulum-mediated phagocytosis is a mechanism of entry into macrophages. *Cell* 110, 119-131.

Guermonprez, P., Saveanu, L., Kleijmeer, M., Davoust, J., Van Endert, P., and Amigorena, S. (2003). ER-phagosome fusion defines an MHC class I cross-presentation compartment in dendritic cells. *Nature* 425, 397-402.

Gutierrez, M.G., Master, S.S., Singh, S.B., Taylor, G.A., Colombo, M.I., and Deretic, V. (2004). Autophagy is a defense mechanism inhibiting BCG and Mycobacterium tuberculosis survival in infected macrophages. *Cell* 119, 753-766.

Harris, E., and Cardelli, J. (2002). RabD, a Dictyostelium Rab14-related GTPase, regulates phagocytosis and homotypic phagosome and lysosome fusion. *J. Cell Sci.* 115, 3703-3713.

Hirata, Y., Hosaka, T., Iwata, T., Le, C.T., Jambaldorj, B., Teshigawara, K., Harada, N., Sakaue, H., Sakai, T., Yoshimoto, K., and Nakaya, Y. (2011). Vimentin binds IRAP and is involved in GLUT4 vesicle trafficking. *Biochem. Biophys. Res. Commun.* 405, 96-101.

Houde, M., Bertholet, S., Gagnon, E., Brunet, S., Goyette, G., Laplante, A., Princiotta, M.F., Thibault, P., Sacks, D., and Desjardins, M. (2003). Phagosomes are competent organelles for antigen cross-presentation. *Nature* 425, 402-406.

Joffre, O.P., Segura, E., Savina, A., and Amigorena, S. (2012). Cross-presentation by dendritic cells. *Nat. Rev. Immunol.* *12*, 557-569.

Jung, J.J., Inamdar, S.M., Tiwari, A., and Choudhury, A. (2012). Regulation of intracellular membrane trafficking and cell dynamics by syntaxin-6. *Biosci. Rep.* *32*, 383-391.

Junutula, J.R., De Maziere, A.M., Peden, A.A., Ervin, K.E., Advani, R.J., van Dijk, S.M., Klumperman, J., and Scheller, R.H. (2004). Rab14 is involved in membrane trafficking between the Golgi complex and endosomes. *Mol. Biol. Cell* *15*, 2218-2229.

Jutras, I., and Desjardins, M. (2005). Phagocytosis: at the crossroads of innate and adaptive immunity. *Annu. Rev. Cell Dev. Biol.* *21*, 511-527.

Keller, S.R. (2003). The insulin-regulated aminopeptidase: a companion and regulator of GLUT4. *Front. Biosci.* *8*, s410-420.

Keller, S.R., Davis, A.C., and Clairmont, K.B. (2002). Mice deficient in the insulin-regulated membrane aminopeptidase show substantial decreases in glucose transporter GLUT4 levels but maintain normal glucose homeostasis. *J Biol. Chem.* *277*, 17677-17686.

Kratzer, R., Mauvais, F.X., Burgevin, A., Barilleau, E., and van Endert, P. (2010). Fusion proteins for versatile antigen targeting to cell surface receptors reveal differential capacity to prime immune responses. *J. Immunol.* *184*, 6855-6864.

Kuijl, C., Pilli, M., Alahari, S.K., Janssen, H., Khoo, P.S., Ervin, K.E., Calero, M., Jonnalagadda, S., Scheller, R.H., Neefjes, J., and Junutula, J.R. (2013). Rac and Rab GTPases dual effector Nischarin regulates vesicle maturation to facilitate survival of intracellular bacteria. *Embo J.* *32*, 713-727.

Kuijl, C., Savage, N.D., Marsman, M., Tuin, A.W., Janssen, L., Egan, D.A., Ketema, M., van den Nieuwendijk, R., van den Eeden, S.J., Geluk, A., *et al.* (2007). Intracellular bacterial growth is controlled by a kinase network around PKB/AKT1. *Nature* *450*, 725-730.



Kulpa, D.A., Del Cid, N., Peterson, K.A., and Collins, K.L. (2013). Adaptor protein 1 promotes cross-presentation through the same tyrosine signal in major histocompatibility complex class I as that targeted by HIV-1. *J. Virol.* 87, 8085-8098.

Kyei, G.B., Vergne, I., Chua, J., Roberts, E., Harris, J., Junutula, J.R., and Deretic, V. (2006). Rab14 is critical for maintenance of Mycobacterium tuberculosis phagosome maturation arrest. *Embo J.* 25, 5250-5259.

Lee, H.K., Mattei, L.M., Steinberg, B.E., Alberts, P., Lee, Y.H., Chervonsky, A., Mizushima, N., Grinstein, S., and Iwasaki, A. (2010). In vivo requirement for Atg5 in antigen presentation by dendritic cells. *Immunity* 32, 227-239.

Nikolaou, A., Van den Eynde, I., Tourwe, D., Vauquelin, G., Toth, G., Mallareddy, J.R., Poglitsch, M., Van Ginderachter, J.A., and Vanderheyden, P.M. (2013). [3H]IVDE77, a novel radioligand with high affinity and selectivity for the insulin-regulated aminopeptidase. *Eur. J. Pharmacol.* 702, 93-102.

Sanjuan, M.A., Dillon, C.P., Tait, S.W., Moshiach, S., Dorsey, F., Connell, S., Komatsu, M., Tanaka, K., Cleveland, J.L., Withoff, S., and Green, D.R. (2007). Toll-like receptor signalling in macrophages links the autophagy pathway to phagocytosis. *Nature* 450, 1253-1257.

Saveanu, L., Carroll, O., Weimershaus, M., Guermonprez, P., Firat, E., Lindo, V., Greer, F., Davoust, J., Kratzer, R., Keller, S.R., *et al.* (2009). IRAP identifies an endosomal compartment required for MHC class I cross-presentation. *Science* 325, 213-217.

Saveanu, L., and van Endert, P. (2012). The role of insulin-regulated aminopeptidase in MHC class I antigen presentation. *Front. Immunol.* 3, 57.

Saveanu, L., and van Endert, P. (2013). Preparing antigens suitable for cross-presentation assays in vitro and in vivo. *Methods Mol. Biol.* 960, 389-400.

Savina, A., Jancic, C., Hugues, S., Guermonprez, P., Vargas, P., Moura, I.C., Lennon-Dumenil, A.M., Seabra, M.C., Raposo, G., and Amigorena, S. (2006). NOX2 controls

phagosomal pH to regulate antigen processing during crosspresentation by dendritic cells.

*Cell* 126, 205-218.

Savina, A., Vargas, P., Guermonprez, P., Lennon, A.M., and Amigorena, S. (2010).

Measuring pH, ROS production, maturation, and degradation in dendritic cell phagosomes using cytofluorometry-based assays. *Methods Mol. Biol.* 595, 383-402.

Steinman, R.M. (2012). Decisions about dendritic cells: past, present, and future. *Annu. Rev.*

*Immunol.* 30, 1-22.

Stenmark, H. (2009). Rab GTPases as coordinators of vesicle traffic. *Nat. Rev. Mol. Cell.*

*Biol.* 10, 513-525.

Tojo, H., Kaieda, I., Hattori, H., Katayama, N., Yoshimura, K., Kakimoto, S., Fujisawa, Y.,

Presman, E., Brooks, C.C., and Pilch, P.F. (2003). The Formin family protein, formin

homolog overexpressed in spleen, interacts with the insulin-responsive aminopeptidase and profilin IIa. *Mol. Endocrinol.* 17, 1216-1229.

Ye, S., Chai, S.Y., Lew, R.A., and Albiston, A.L. (2007). Insulin-regulated aminopeptidase:

analysis of peptide substrate and inhibitor binding to the catalytic domain. *Biol. Chem.* 388, 399-403.

## FIGURE LEGENDS

**Figure 1.** IRAP is required for normal steady-state levels of STX6<sup>+</sup> endosomes. In (**A**, **B** and **C**), wt or ko BM-DCs plated on fibronectin-coated micro-patterns were stained with the indicated marker combinations; nuclei were counter-stained with DAPI. Scale bars in this and all other figures correspond to 5  $\mu$ m. The plots in (**C**) show a cell-by-cell analysis of co-localisation (% of marker 1 colocalising with marker 2). \*\*\*,  $p < 0.001$ ;  $n > 15$  cells. (**D**) IRAP-deficient BM-DCs were transfected with HA-tagged full-length IRAP and stained for STX6 and HA. Dotted lines represent the contour of the cells. The intensity of the endosomal STX6 signal was estimated using ImageJ software. (**E**) Wt or IRAP BM-DCs were nucleofected with empty vector or HA-tagged IRAP. Sorted CD11c<sup>+</sup> CD11b<sup>+</sup> cells were incubated with pre-formed complexes formed between anti-MR and a fusion protein containing OVA. Activation of OVA-specific OT-I T cells was measured by IL-2 ELISA (mean  $\pm$  SEM). Result representative of 3 experiments.

**Figure 2.** Accelerated phagosome maturation in IRAP ko BM-DCs. (**A**) Latex bead phagosomes were isolated from wt or IRAP ko BM-DCs by sucrose gradients after a 20 min pulse (early) and after 120 min of chase (late) and analysed by immunoblot for the markers indicated. One of 3 or more experiments. CatD, cathepsin D. (**B**) Crude 20 min phagosomes were stained for LAMP1 and Rab7 and analysed by flow cytometry. One out of 10 (LAMP1) and 3 (Rab7) experiments. (**C**) BM-DCs were pulsed for 5 min with latex beads or *S. cerevisiae* cells, chased for the indicated periods and stained as indicated. Image analysis was performed with ImageJ software. (**D**) The fluorescence intensity of phagocytised latex beads conjugated to the pH-sensitive dye CFSE and the insensitive dye AF647 was monitored over time by flow cytometry. The ratio of CFSE to AF647 fluorescence was converted to pH values using a standard curve of beads in solutions of known pH. One of 3 similar

experiments. (E) BM-DCs were pulsed for 20 min with latex beads, and phagosomes analysed for LC3 staining by phagoFACS. The images to the right show BM-DCs pulsed with latex beads for 20 min. See also **Figure S1**.

**Figure 3.** Accelerated protein and peptide degradation and microbe killing in IRAP ko phagosomes. (A) Wt and IRAP ko BM-DCs were pulsed for 20 min with latex beads coupled to OVA or BSA and half of the cells were chased for 40 min. The cells were lysed and the beads were stained for BSA or Ovalbumin and analysed by flow cytometry. One out of 3 or more experiments. (B) Early and late phagosomes prepared from wt and IRAP ko BM-DCs were incubated for 15 min at 4°C or 20°C with peptide R9L-FITC followed by analysis of peptide accumulation by FACS; see also **Figure S2A**. (C) Wt and IRAP ko BM-DCs were allowed to phagocytose the indicated microbes and incubated for 3 hr (*Pseudomonas*), 5 hr (*Aspergillus fumigatus* conidia) or 6 hr (*S. cerevisiae*); see also **Figure S2B,C**. The microbe survival was determined as number of colony-forming units (cfu) in solid cultures. The numbers represent the means  $\pm$  SEM of 3 independent experiments and are expressed as per cent of survival in wt cells. \*  $p < 0.02$ , \*\*  $p < 0.002$ , \*\*\*  $p < 0.0001$

**Figure 4.** IRAP peptidase activity is required for efficient cross-presentation but not for formation of STX6 endosomes. (A) IRAP-deficient MEFs were transfected with full-length wt or mutant IRAP or mock-transfected (ctrl), followed by immunoprecipitation of IRAP 2 days later. The precipitates were analysed for IRAP content by immunoblot and for peptidase activity toward the fluorogenic Arg-AMC substrate, using mock-transfected cells as control. (B) IRAP-deficient BM-DCs were nucleofected with the plasmid pMAX-IRAP-E465A (lacking GFP) and analysed 36 hr later by confocal microscopy. (C) Wt or IRAP ko BM-DCs were nucleofected with empty pIRES2-GFP or the active site IRAP mutant E465A. Live GFP+ DCs were sorted and put in contact with complexes formed between MR antibodies and OVA fusion protein and with OT-I T cells. T cell stimulation was assessed by IL-2

ELISA. One of 3 experiments. **(D)** Wt and IRAP ko BM-DCs were incubated for 16 hr with 1  $\mu$ M IVDE77 or solvent before addition of OVA-yeast for 6 hr. Then cells were fixed, added to OT-I T cells for 24 hr, and T cell stimulation was assessed by IL-2 ELISA. Mean  $\pm$  S.E.M. values from 5 experiments are shown. See also **Figure S3**.

**Figure 5.** Rab14 knockdown in BM-DCs accelerates phagosome maturation and compromises cross-presentation. **(A)** Levels of Rab14 mRNA in transduced BM-DCs as measured by qRT-PCR. **(B)** BM-DCs were transduced with shNT, shSec22b or shRab14 lentiviruses and analysed for total cellular expression of the indicated proteins. One of 2 experiments. See also **Figure S4**. **(C)** BM-DCs transduced with shNT or shRab14 lentivirus were stained for the indicated markers and analysed by confocal microscopy for colocalisation. \*\*\*\*,  $p < 0.0001$ ; ns, not significant;  $n = 10$  cells. **(D)** BM-DCs transduced with shNT or shRab14 lentiviruses were pulsed with *S. cerevisiae* at 37°C for 5 min and incubated further at 37°C for the indicated periods of time before staining. The graphs to the right were obtained analysing at least 100 phagosomes for each time point. **(E)** Percent intracellular survival of *P. aeruginosa* in BM-DCs transduced with shRab14 relative to shNT lentivirus set at 100. Mean  $\pm$  S.E.M. of 3 experiments is shown. **(F)** Wt and IRAP ko BM-DCs were transduced with shNT or shRab14 lentiviruses and analysed for cross-presentation of MR-targeted OVA as in Figure 1**(E)** and 4**(D)** One of 3 experiments.

**Figure 6.** Rab14 mutants with aberrant subcellular location compromise STX6 endosomes and cross-presentation. **(A)** Wt and IRAP ko BM-DCs were nucleofected with plasmids encoding fusion proteins between eGFP and wt, dominant negative (S25N) and constitutively active (Q70L) Rab14. Thirty-six hours later, the cells were analysed by confocal microscopy. **(B)** Images as shown in **(A)** were used to compute the co-localization of wt and mutant Rab14. At least 5 cells per condition and marker were analysed using ImageJ software. \*\*\*\*,

p<0.0001; \*\*\*, p<0.001; \*\*, p<0.005. (C) Images as shown in (A) were used to measure intensity of endosomal STX6 staining in Rab14-transfected cells, using ImageJ.

(D) Cross-presentation by BM-DCs nucleofected with plasmids encoding Rab14-GFP fusion proteins was analysed like in Fig. 4(D). One of 4 experiments. See also **Figures S5A,B,C**.

**Figure 7.** Sec22b knockdown results in severe perturbation of IRAP+STX6+ endosomes. (A) BM-DCs were transduced with shNT or shSec22b lentiviruses, stained for Sec22b and analysed by confocal microscopy. The adjacent graphs show the correlation between the mean fluorescence intensities for Sec22b and for a second marker, each dot representing a different cell. (B) BM-DCs were transduced as in (A) and stained for Sec22b and STX6. The integrated density of STX6 staining was measured in the Golgi area and outside of it for each cell analysed. \*\*\*\*\*, p<0.0001; \*\*, p<0.001; n.s., not significant.

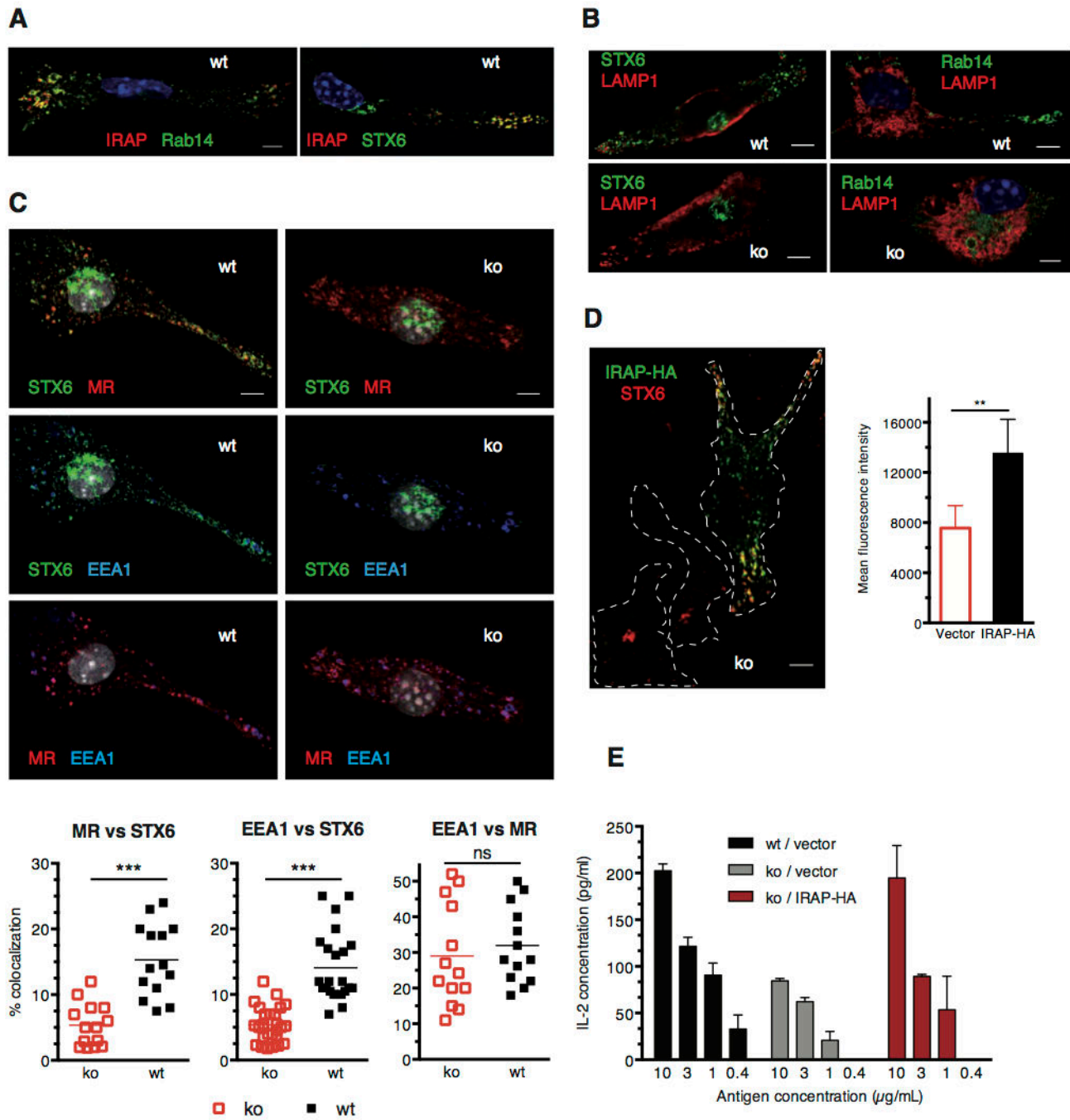
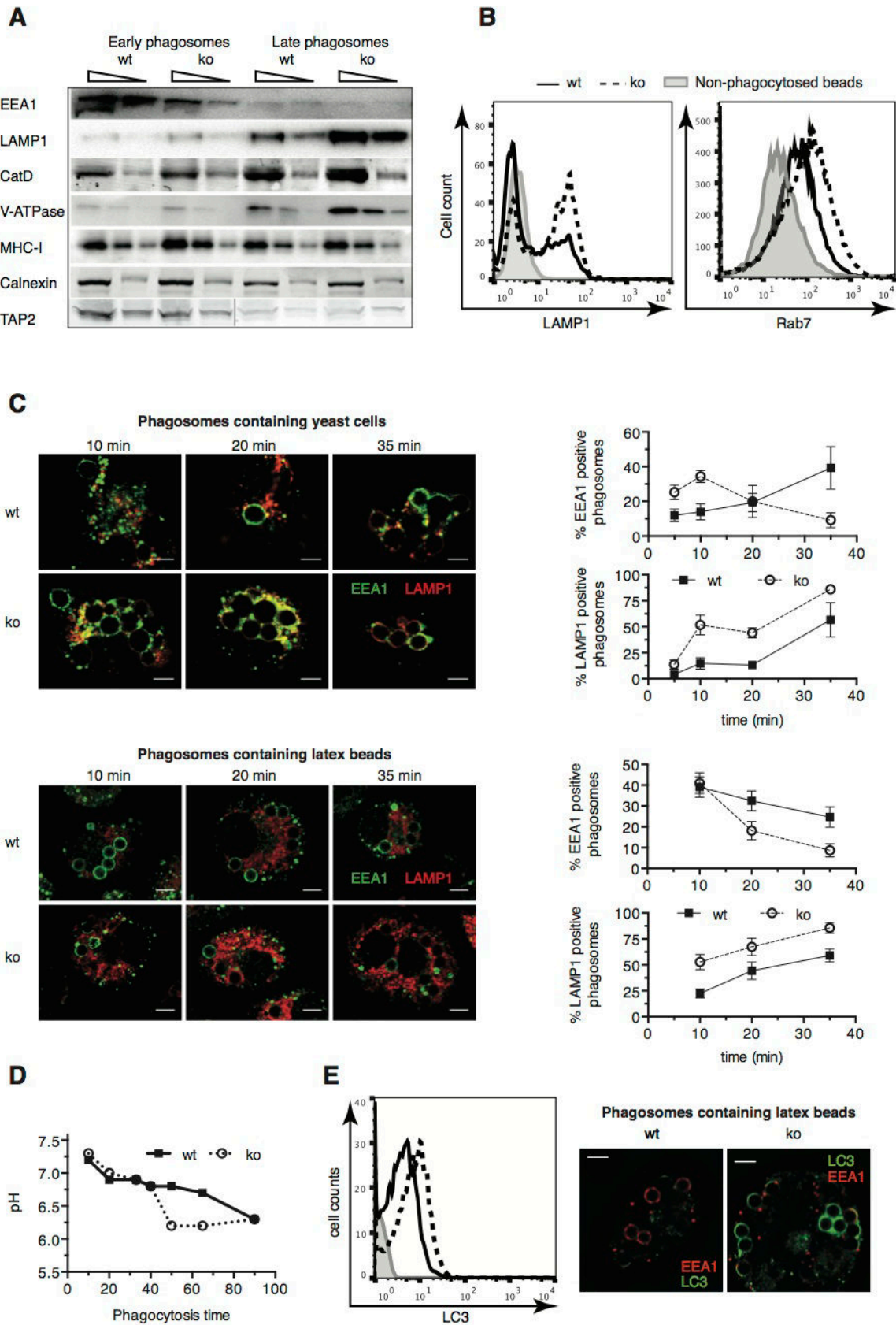
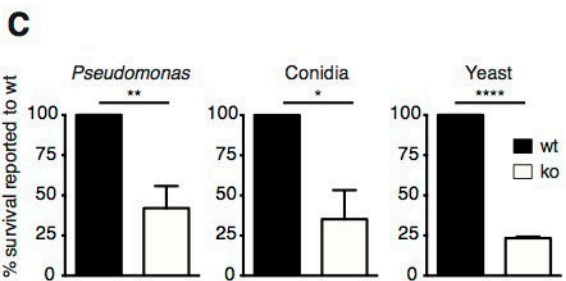
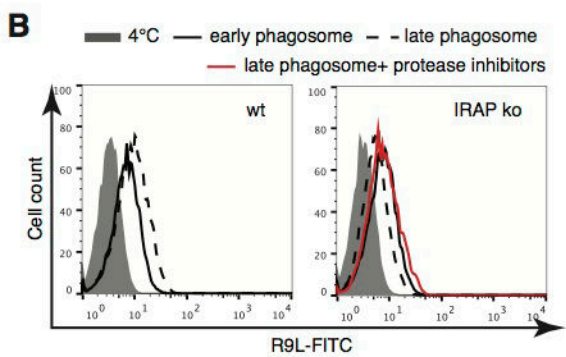
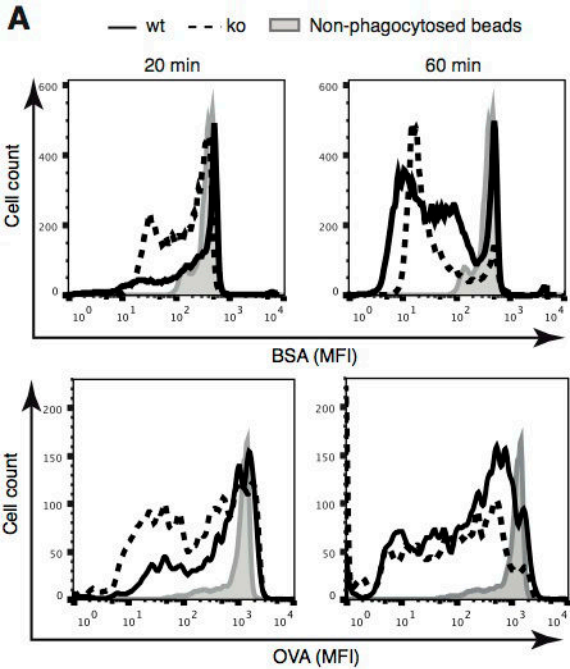


Figure 1

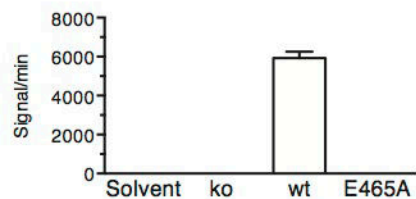
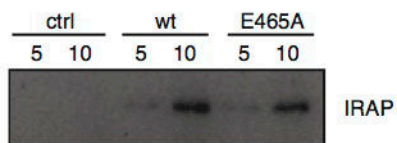
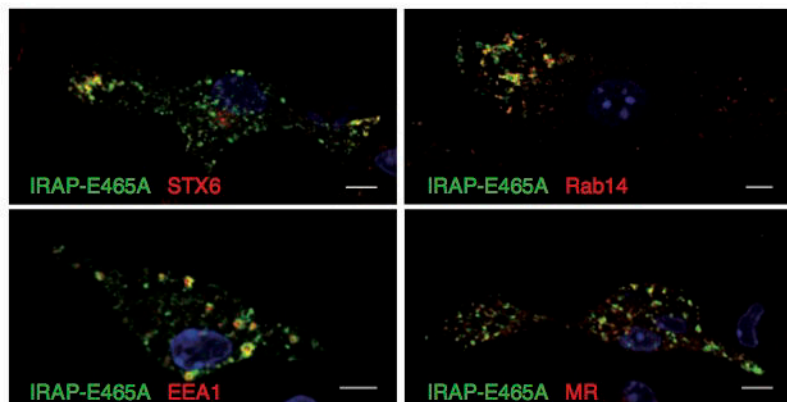
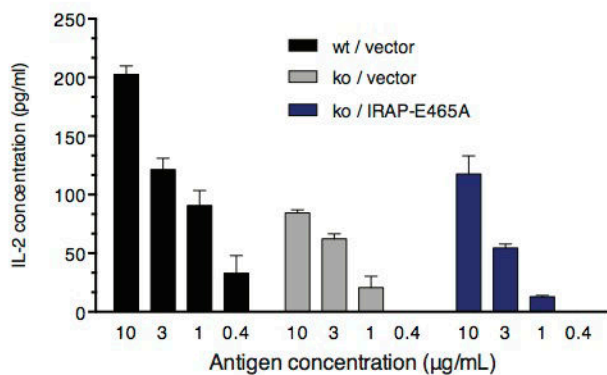
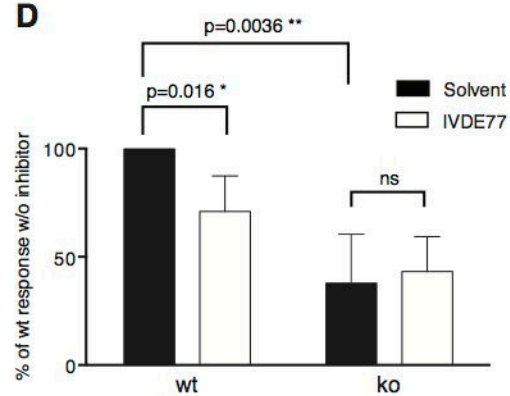






248

Figure 3

**A****B****C****D**

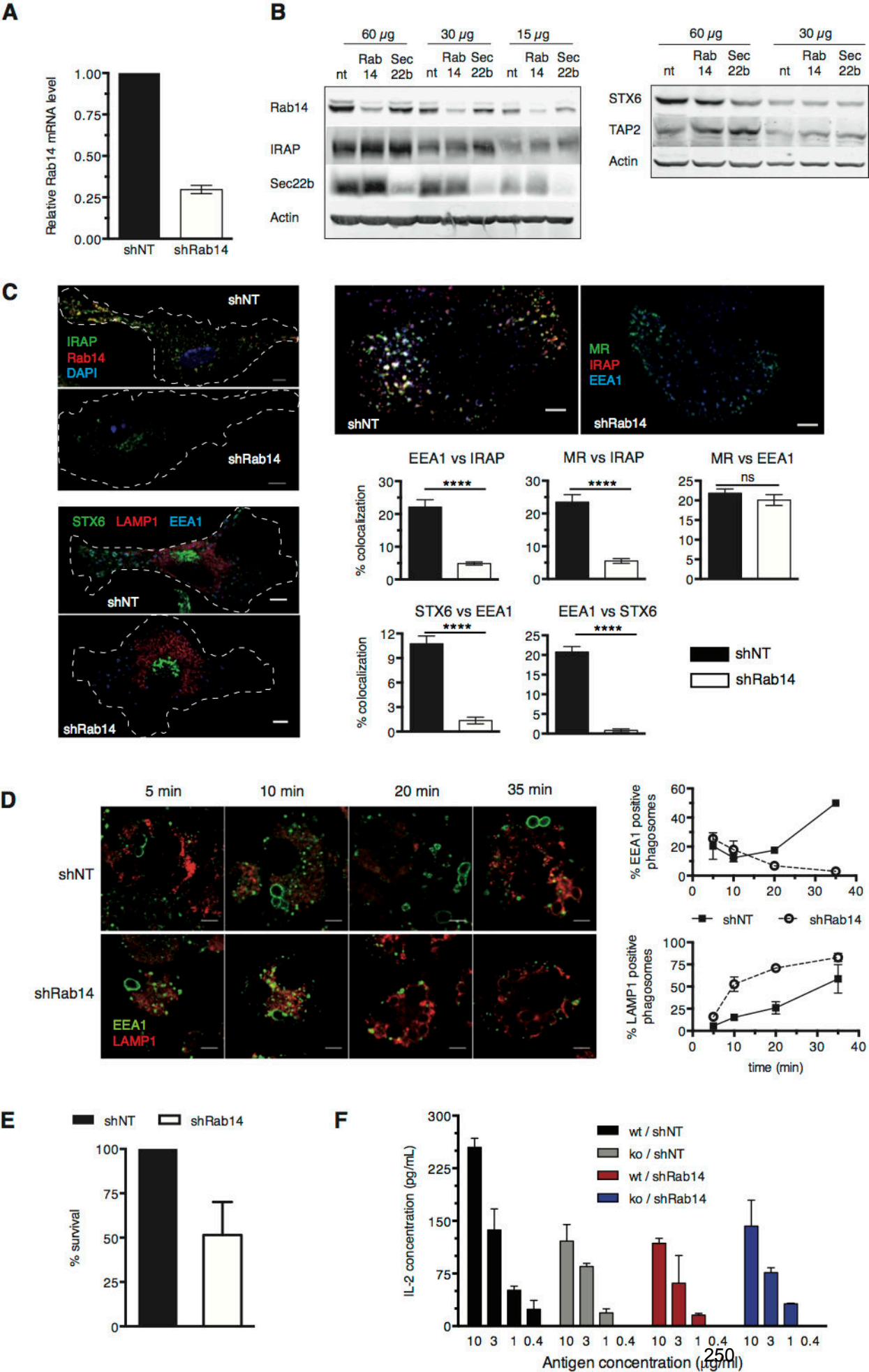
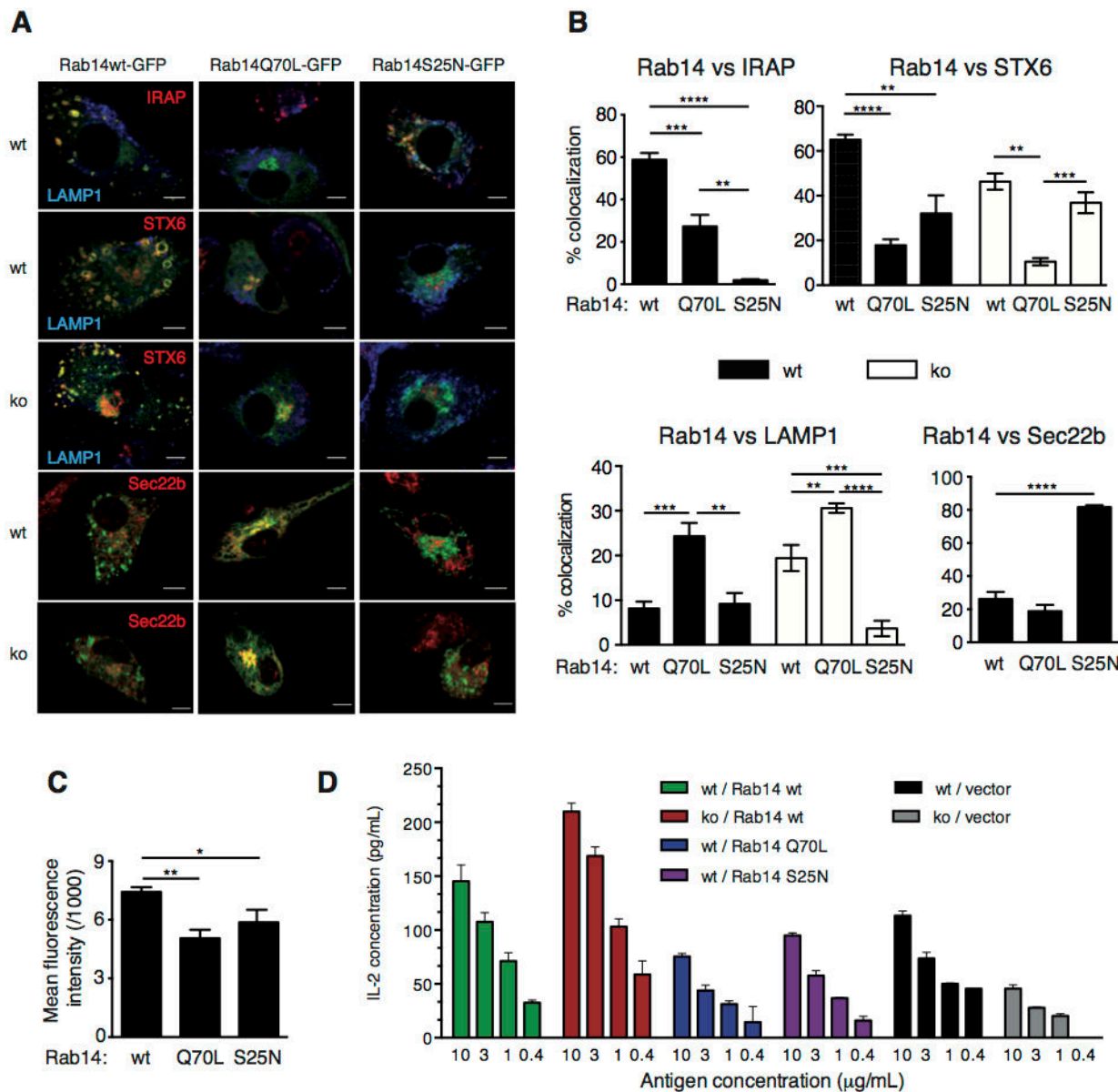
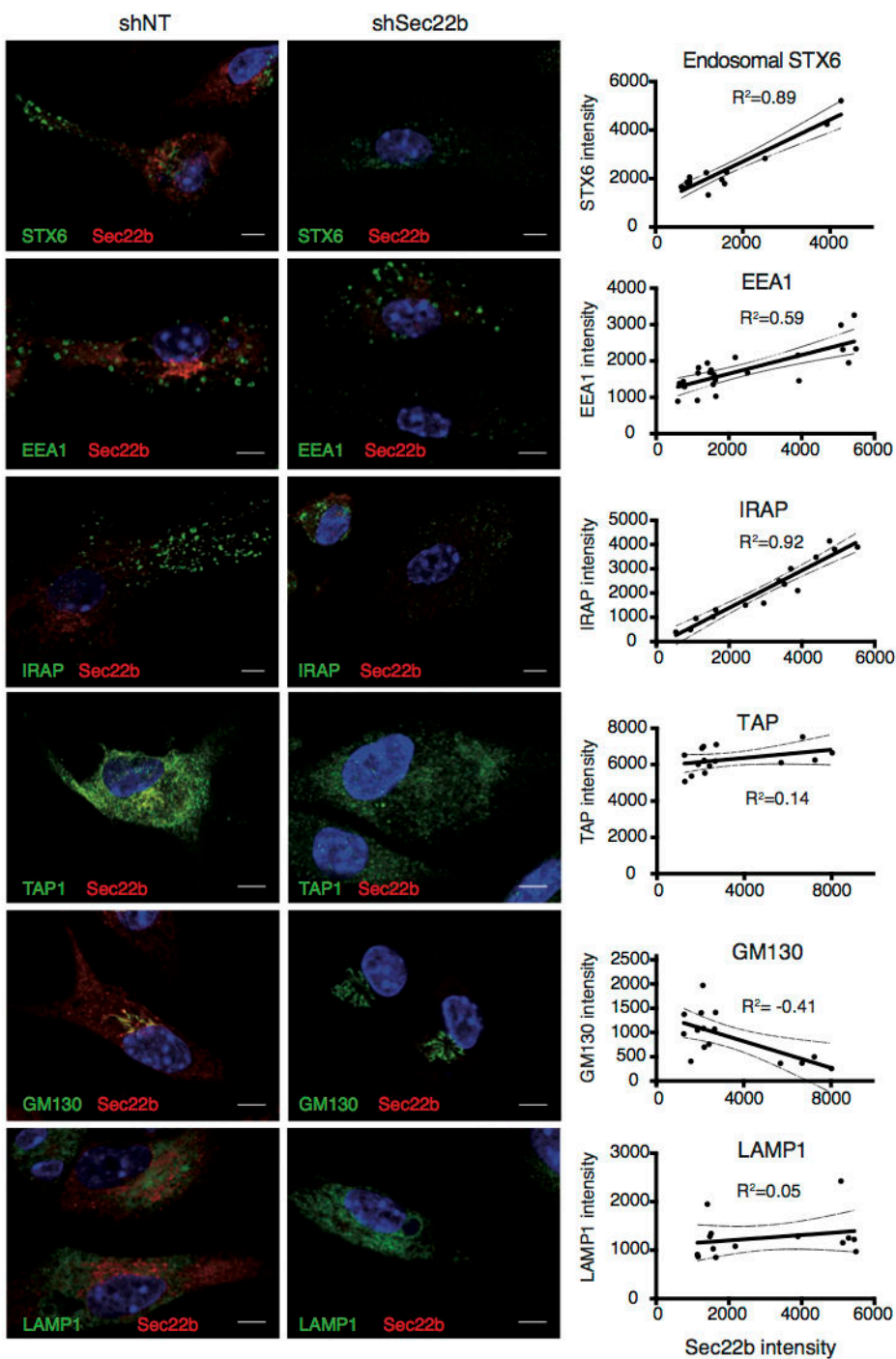
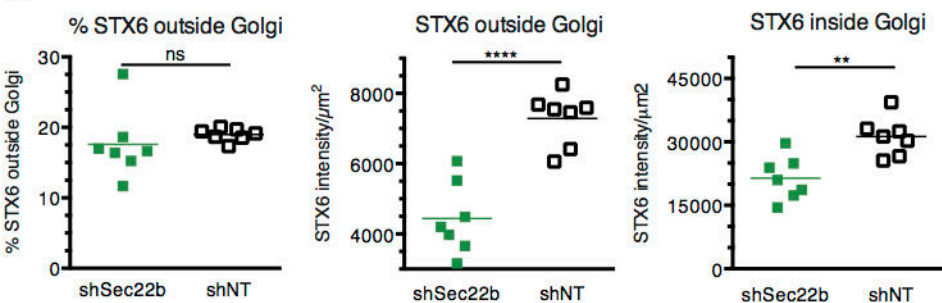


Figure 5



**A****B**

- Figure S1, related to Figure 2E, shows increased LC3 staining in non phagocytic MEF cells
- Figure S2, related to Figure 3, first shows that peptide accumulation in crude phagosomes is TAP-dependent; it furthermore demonstrates that the efficiency of microbe uptake by IRAP-deficient DCs is unaltered
- Figure S3, related to Figure 4, shows the peptidase activity of immunoaffinity-purified IRAP obtained from DCs incubated with the inhibitor IVDE77
- Figure S4, related to Figure 5, shows MHC class I expression in the presence of Rab14 knockdown
- Figure S5, related to Figure 6, shows expression of MHC class I and CD80 by DCs expressing Rab14 variants, as well as a sorting strategy for transfected cells
- Supplemental Experimental Procedures provide detailed information on the methods used, and are followed by three Supplemental References

**Rab14<sup>+</sup> Endosomes Regulate Phagosome Maturation and MHC class I Cross-presentation by Dendritic Cells**

Loredana Saveanu, Mirjana Weimershaus, Joël Babbdor, Myriam Lawand, Irimi Evnouchidou, Pablo Vargas, Markus Zwick, Thomas Brocker, François-Xavier Mauvais, Peter van Endert

Supplemental Figures 1 – 5

Supplemental Experimental Procedures

## SUPPLEMENTAL FIGURE LEGENDS

### **Figure S1, Related to Figure 2E. Increased autophagosome formation in IRAP ko MEFs**

(A) Wt and IRAP ko MEFs were plated on Ibitreat™ channels and stained for LAMP1 and LC3. Images were acquired on a Leica DMI 6000 microscope equipped with a piezoelectric-driven system and processed for 3D deconvolution. Scale bars represent 5 μm. A quantitative analysis is shown in (B). Statistical significance was analyzed using unpaired t test. \*\*\*, p=0.0001.

### **Figure S2, Related to Figure 3. TAP-dependent peptide accumulation in phagosomes, and quantification of microbe uptake by wt and IRAP-deficient BM-DCs**

(A) Wt or TAP ko BM-DCs were incubated for 20 min with rabbit-immunoglobulin-coated latex beads (early phagosomes), followed for half of the sample by a 40 min incubation at 37°C after removal of free beads (late phagosomes). Then crude phagosome were prepared, incubated in the presence of an ATP-regenerating system for 15 min at 4°C or 20°C with peptide R9L-FITC and analyzed using a cytometer. The figure shows the strategy for gating on membrane-enveloped beads and individual histograms for early and late phagosomes as well as control incubations at 4°C. (B) Wt and IRAP ko BM-DCs were incubated for 20 min with microbes (*Pseudomonas*, *Aspergillus fumigatus conidia* or *S. cerevisiae*), washed to remove non-phagocytized microbes, lysed and plated on solid cultures. The number of colony-forming units (CFU) in solid cultures was counted to estimate the phagocytic capacity. Three independent experiments for conidia and yeast and one experiment for *Pseudomonas*. (C) BM-DCs were pulsed for 20 min with CFSE labelled *S. cerevisiae* cells at 4°C or 37°C. Excess yeast cells were removed by FCS flotation and BM-DCs were analysed for CFSE fluorescence by flow cytometry.

### **Figure S3, Related to Figure 4D. Inhibitory effect of IVDE77 on IRAP**



BM-DCs were pre-incubated for 16 hr in the presence of 1  $\mu$ M IVDE77 or DMSO solvent before lysis and immunoprecipitation of IRAP followed by addition of Leu-AMC substrate for 30 min to measure peptidase activity. IRAP activity in the presence of IVDE77 is expressed as percent of activity in solvent only. The mean  $\pm$  SDEV of 6 experiments is shown. \*\*,  $p=0.0016$ .

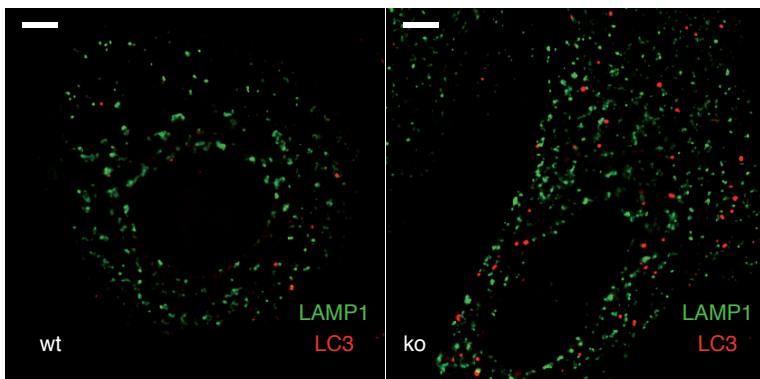
**Figure S4, Related to Figure 5. No effect of Rab14 knockdown on MHC class I expression by BM-DCs**

Live lentivirus-transduced and puromycin-selected BM-DCs were sorted as 7-AAD<sup>-</sup> CD11c<sup>+</sup>CD11b<sup>+</sup> cells before staining with conformational antibody AF6-88.5 to evaluate density of cell surface H-2K<sup>b</sup>. The numbers indicate mean fluorescence intensity. One of two experiments is shown.

**Figure S5, Related to Figure 6. Effect of expression of Rab14 variants on expression of MHC class I and CD80, and gating strategy for cell sorting of BM-DCs transfected with GFP-Rab14 variants**

In (A) and (B), live BM-DCs nucleofected with plasmids encoding wt and mutant Rab14-GFP fusion proteins were sorted as 7-AAD<sup>-</sup>GFP<sup>+</sup>CD11c<sup>+</sup>CD11b<sup>+</sup> cells before evaluation of cell surface density of H-2K<sup>b</sup> and CD80, respectively. Numbers indicate mean fluorescence intensity. One of two similar experiments is shown. In panel (C), after exclusion of doublets and dead cells by gating on the 7-AAD<sup>-</sup> population (not shown), transfected BM-DCs were selected as cells staining positive for both CD11b and CD11c (top panel). Among the CD11b<sup>+</sup>CD11c<sup>+</sup> cells, only the GFP<sup>+</sup> cells were sorted (bottom panel).

**A**



**B**

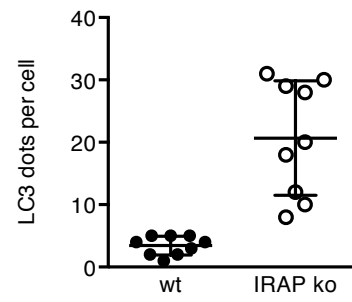


Figure S1

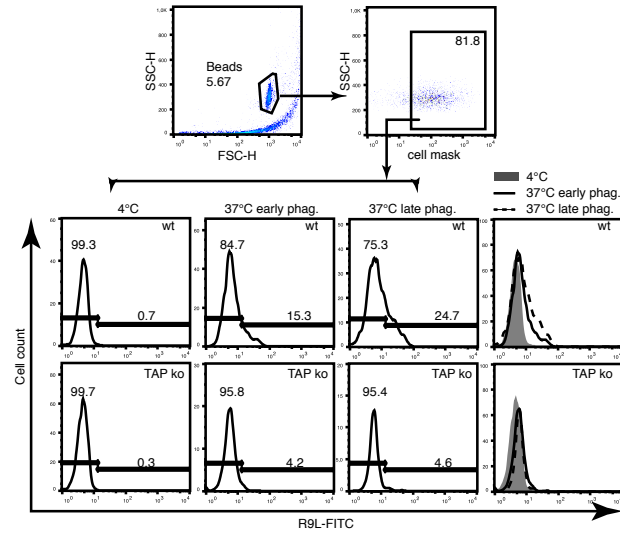
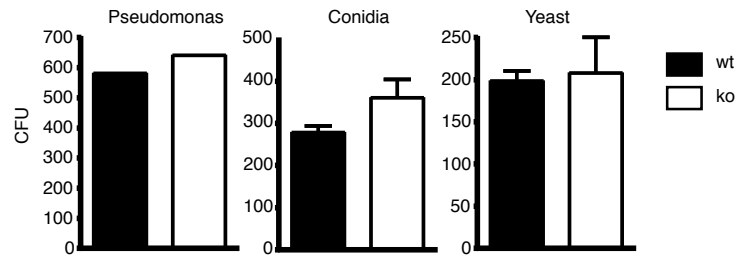
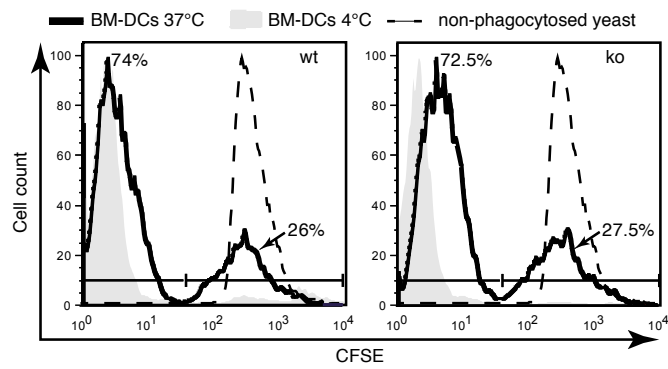
**A****B****C**

Figure S2

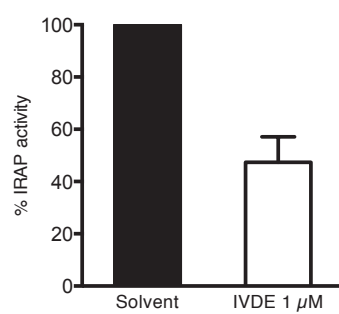


Figure S3

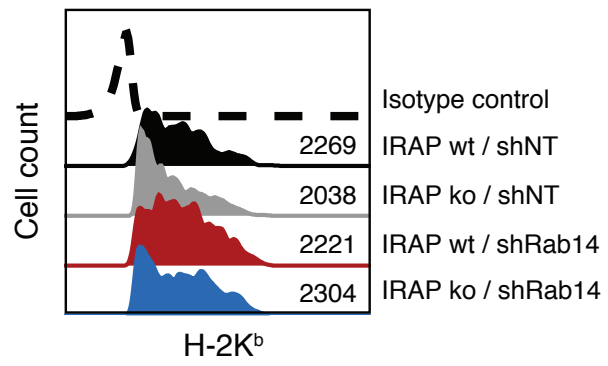


Figure S4

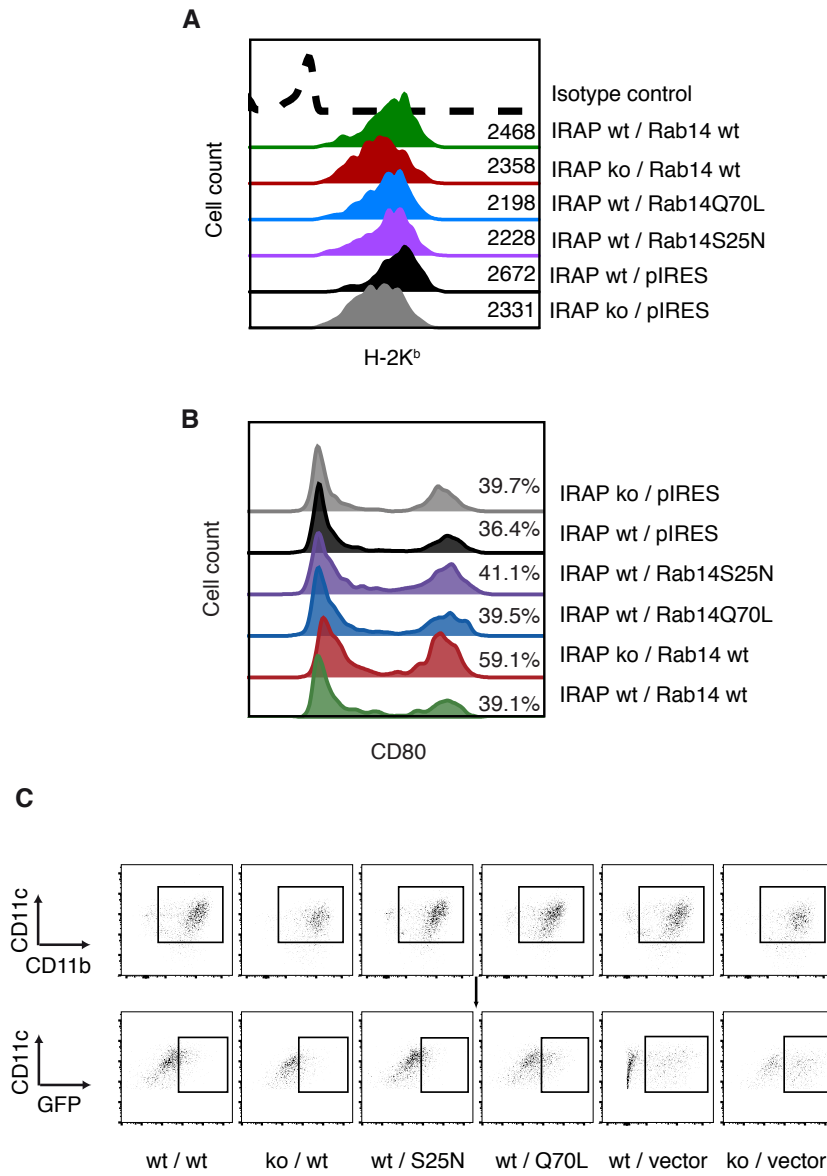


Figure S5

## SUPPLEMENTAL EXPERIMENTAL PROCEDURES

### **Mice and Cells**

Previously described IRAP ko mice on an Sv129 background obtained from S. Keller were back-crossed up to 10 times to C57BL/6 mice obtained from Janvier (St. Quentin-Fallavier, France). While for some experiments mice with a lower number of back-crosses were used, cross-presentation experiments were always performed with mice on an identical genetic background. Control mice were either mixed background or C57BL/6 mice bred in our facility, or C57BL/6 mice purchased from Janvier. RAG1-deficient OT-1 T cell receptor transgenic mice were obtained from Taconic (Germantown, NY), and bred in our animal facility. Animal experimentation was approved by the Comité d'éthique pour l'expérimentation animale Paris Descartes (n° P2.LS.156.10). Murine BM-DCs were produced *in vitro* by culturing cells extruded from large bones for 6 to 8 days in complete medium (IMDM complemented with 10%FCS, 2 mM glutamine, 100 U/mL penicillin, 100 µg/mL streptomycin, 50 µM β-mercaptoethanol supplemented with J558 supernatant containing 20 µg/mL GM-CSF). BM-DC differentiation and activation were checked by staining with CD11c and CD80 antibodies as described (Weimershaus and van Endert, 2013).

### **Fluorescence microscopy**

BM-DCs on day 7 were plated on fibronectin-coated 12 mm coverslips for 3 hr in complete medium at 37°C. The cells were fixed in 4% PFA for 20 min at RT, permeabilized in 0.2% saponin/0.2% BSA in PBS, quenched in 0.2 M glycine pH 7 and incubated with antibodies. Where indicated, cells were plated on micro-pattern slides and incubated at 37°C to allow for polarization. For phagocytosis assays, the BM-DCs were seeded on IbiTreat channels (BioValley) for 3 hr. Adherent cells were pulsed with latex beads (Polysciences) (dilution 1:100) or *S. cerevisiae* cells expressing OVA attached to the cell wall ( $2 \times 10^8$ /mL) in complete medium for 5 min at 37°C. The free particles were removed by washing with cold PBS and

cells were chased in complete medium. At the end of each chase period, the cells were fixed, permeabilized and stained.

Immunofluorescence images were acquired with a Leica SP8 confocal microscope using a 40x oil immersion objective. Alternatively and where indicated, images were acquired with a Leica DMI 6000 microscope equipped with a piezoelectric-driven stage and Optophotonics XF100-2 (FITC), XF102-2 (Texas Red) and XF06 (DAPI) filters, and processed for 3D deconvolution using Metamorph™ 6.3.7. Image analysis (colocalization and signal intensity) was performed using the IMARIScoloc module (IMARIS software, Bitplane AG) for cells polarized on micro-patterns and with ImageJ for other images.

### **Cloning of wt and mutant IRAP in pIRES2-eGFP**

A cDNA coding for IRAP truncated by the 79 aminoterminal amino acids and extended by a carboxyterminal HA tag was amplified from mouse spleen cDNA using the following primers: 5'-ACC GGT GCC ACC ATG CTA CTA GTA AAT CAG TCA C (AgeI site underlined) and 5'-GAG CTC CTA *GGC GTA GTC GGG CAC GTC GTA GGG GTA* TCC CGA CAG CCA CTG GGA GAG-3' (HA tag in italics, XhoI underlined). The PCR product was cloned in the pMAX-GFP vector (Lonza) between the AgeI and XhoI sites, thereby replacing the GFP cDNA and resulting in the plasmid pMAX-IRAP. The absence of errors was confirmed by sequencing. A cDNA encoding truncated inactive IRAP was obtained by the megaprimer method. A megaprimer of 235 bp was produced by PCR using pMAX-IRAP as template and the primers: 5'CT AAA ATC ATT GCT CAC GCA CTG GCA CAT CAG TGG-3' (mutated base underlined) and 5'-GAA GAC TGA ACA GAT GAT GAT ATT GGA TGA-3', the latter primer being located downstream of an EcoRI site in the IRAP cDNA. A second PCR product was obtained using the megaprimer and the sense primer 5'-ACC GGT GCC ACC ATG CTA CTA GTA AAT CAG TCA C (AgeI underlined). This PCR product was used to replace the fragment between the AgeI and EcoRI sites in pMAX-IRAP, creating



pMAX-IRAP E465A, followed by sequencing to confirm the mutation. To obtain plasmids encoding full-length IRAP, the first 650 bp of IRAP were amplified using the primers 5'-GCT AGC GCC ACC ATG GAG TCC TTT ACC AAT GA-3' (NheI underlined) and 5'-TTG AAA TAT TAT GTC CTG TGC TAT-3', using as template the cDNA clone MGC\_144171 (plasmid IMAGE\_40098425, obtained from Open Biosystems) corresponding to Genbank accession number BC120926.1. The N-terminal IRAP fragment was cloned in pCR Blunt (Invitrogen) and sequenced. The C-terminal fragments of wt and inactive IRAP were removed from the pMAX plasmids using EcoRV and XhoI and cloned together with the N-terminal fragment, excised using NheI and EcoRV, between the NheI and XhoI sites in pCDH-EF1alpha vector (System Biosciences). Finally, the full-length IRAP inserts were transferred from pCDH-EF1alpha into pIRES2-EGFP (Clontech) as NheI and XhoI fragments.

### **Antibodies**

The following antibodies were used in this study.

*Fluorescence microscopy:* immunoaffinity purified rabbit antibodies specific for the cytosolic IRAP domain (Keller et al., 1995); mouse monoclonal IRAP antibodies (a kind gift from M. Birnbaum, Univ. of Pennsylvania) (Garza and Birnbaum, 2000); goat polyclonal anti-EEA1 and anti-mouse TAP1 (both Santa Cruz Biotechnologies); rat anti-mouse LAMP1 clone 1D4B, mouse monoclonal anti-STX6, mouse monoclonal anti-GM130 (BD Pharmingen); rabbit polyclonal anti-STX6 (ProteinTech Group, Chicago); rat monoclonal anti-mouse mannose receptor, clone MR5D3 (AbD Serotec); rabbit polyclonal anti-Sec22b (Synaptic Systems); rabbit polyclonal anti-Rab14 (Sigma Aldrich); rat monoclonal anti-HA tag (Roche); rabbit polyclonal anti-LC3 (MBL). All secondary reagents were Alexa-coupled highly cross-adsorbed antibodies from Molecular Probes (Invitrogen).

*Immunoblotting:* in addition to antibodies also used for microscopy, the following antibodies were used for immunoblots: rabbit polyclonal anti-MHC-I (P8, a gift from H. Ploegh); rabbit

polyclonal anti-EEA1 (Abcam); rabbit polyclonal anti-TAP2 (a gift from J. Monaco); rabbit polyclonal anti-calnexin (Stressgen); rabbit polyclonal anti-V-ATPase subunit E and goat polyclonal anti-Cathepsin D (both Santa Cruz Biotechnologies).

*PhagoFACS assays:* (additional antibodies) rabbit polyclonal anti-OVA (Sigma Aldrich); mouse monoclonal anti-Rab7 (Abcam); rabbit polyclonal anti-BSA (Invitrogen).

*Flow cytometry and sorting:* (additional antibodies) rat anti-mouse CD11b/PE-Cy7 (clone M1/70; BD Biosciences); hamster anti-mouse CD11c/eFluor450 (clone N418; eBioscience); rat anti-H2-K<sup>b</sup> (clone AF6-88.5; Biolegend); mouse IgG2a isotype control (clone MOPC-173, Biolegend); 7-actinomycin D (7-AAD, BD Biosciences);

*ELISAs:* capture: rat anti-mouse IL-2 (clone JES6-1A12); detection: rat anti-mouse IL-2/Biotin (clone JES6-5H4; both BD Biosciences).

### **Image analysis**

Marker colocalization and signal intensity were evaluated using the IMARIScoloc module (IMARIS software, Bitplane AG) for cells polarized on micro-patterns and with Image J for other images. For each image, a stack of at least 10 planes was acquired and only non-saturated images were measured. A manual threshold was established for each channel before image analysis. Individual cells were delimited with the freehand selection tool and considered as region of interest (ROI) in ImageJ. For colocalization studies, all images were first translated to a binary image (black pixel intensity=0; white pixel intensity=1). The binary images for green and red channels were multiplied to create a mask that encompasses the pixels present in both channels. The areas of green pixels, red pixels and pixels of the mask were calculated using the plugin “measure stack” of ImageJ. The percentage of green pixels that colocalized with red pixels was calculated as the ratio: sum of area of pixels in the mask divided by sum of area of green pixels.

For measurement of endosomal STX6 intensity and Golgi STX6 intensity a z-projection of the stack image was performed using the sum projection method. On the z-projection image, two individual ROIs were delimited for each cell analyzed, one for the Golgi stacks and one for the cellular area outside Golgi. Measurements performed with ImageJ were limited to threshold and included ROI area, ROI mean fluorescence intensity and integrated density. The results were reported as mean of fluorescence or integrated density/area. Statistical analysis was performed with GraphPad Prism software using unpaired t-tests.

### **Cross-presentation assays**

$2 \times 10^6$  BM-DCs were transfected on day 5 of culture with 2  $\mu\text{g}$  of plasmids encoding wt or mutant forms of IRAP or Rab14 using the Amaxa (Lonza) nucleofection kit for mouse immature DCs and program Y-001. On day 7, the cells were stained with CD11b and CD11c antibodies for 20 min, sorted as 7-AAD<sup>-</sup>CD11b<sup>+</sup>CD11c<sup>+</sup>GFP<sup>+</sup> cells and seeded at a concentration of 15,000 to 20,000 cells/well into 96-well round bottom culture plates. Alternatively, when BM-DCs were transduced with non-targeted or Rab14 shRNAs, dead cells were removed from the culture by OptiPrep (Axis-Shield) density gradients the day before the assay. BM-DCs were then incubated with serial dilutions of pre-formed complexes of anti-MR and P3UO or P3UGAD fusion proteins. After 1 hr, CD8<sup>+</sup> T cells purified from lymph nodes of OT-I mice were added to the culture for 20 hr at a ratio T / BMDCs: 1.5 / 1. To assess T cell activation, IL-2 concentration in supernatants was measured by sandwich ELISA using Nunc Maxisorp plates, streptavidin/horse radish peroxidase (Thermo Scientific) and OptEIA TMB substrate (BD Biosciences). The signal obtained with P3UGAD control complexes was set as the background and subtracted from all O.D. values. Results represent the means of duplicate wells. Antigen presentation assays with the IVDE IRAP inhibitor were performed as previously described (Saveanu et al., 2009). BM-DCs were incubated for 16 hr with the inhibitor prior to phagocytosis of yeast cells and the drug was maintained during

antigen uptake and processing. After 6 hr, free antigen and inhibitor were washed off and the cells were fixed before adding OT-I cells.

### **PhagoFACS**

0.5 mg/mL OVA (Worthington) or ultrapure BSA (Sigma) were covalently coupled to 3  $\mu$ m latex aminobeads (Biovalley). BM-DCs were pulsed with beads for 10 min, the excess of non-phagocytized beads was removed by FCS flotation gradients and the phagosomes were allowed to mature for another 10 or 110 min unless stated otherwise. Finally, the cells were lysed in the presence of 0.5% NP-40, latex beads were recovered by differential centrifugation, stained with antibodies against the conjugated proteins and analyzed by FACS. For staining of maturation markers on the phagosome membrane, cells were lysed mechanically after phagocytosis in 250 mM sucrose, phagosomes enriched by FCS flotation, fixed and stained with the lipid marker CellMask (Invitrogen) and Rab7 or LAMP1 antibodies.

### **Phagosomal pH**

The pH-sensitive dye CFSE and the pH-insensitive dye AF647 were coupled to latex aminobeads (Polysciences) and added to DCs for phagocytosis. After removal of excess beads the decrease of the CFSE-emitted fluorescence intensity was measured over time by flow cytometry. The signal was corrected for non-specific dye degradation with the AF647 signal. PH values were obtained by plotting the CFSE mean fluorescence intensity values to a calibration curve that was obtained by lysing phagosomes containing fluorochrome-conjugated beads in 1% Tween-20 solutions of known pH.

### **Microbicidal activity in vitro**

BM-DCs were incubated with *P. aeruginosa* or *S. cerevisiae* for 3 hr at a microbe/DC ratio of 1. Then microbes were washed away and the DCs lysed in 0.1% Triton. The lysates were plated at different dilutions on yeast and bacterial culture plates, respectively, and colony formation was quantified after 18 hr of culture. For *Aspergillus fumigatus* conidia

phagocytosis, BM-DCs were incubated with conidia at a conidia/DC ratio of 2, in 24-well plates. The plates were centrifuged at 4°C for 30 min followed by extensive washing with cold PBS to remove free conidia. The number of conidia bound to BM-DCs membrane was identical for wt and IRAP-deficient cells. The BM-DCs were incubated for 5 hr at 37°C in complete medium. Finally the cells were lysed in 5 mM EDTA, 0.1% Tween 20 in H<sub>2</sub>O and the lysates were plated on agar plates. *Aspergillus fumigatus* colonies were counted 48 hr later.

### **Peptidase activity assays**

IRAP ko mouse epithelial fibroblasts were transfected with wt IRAP or the E465A mutant by electroporation. Two days later, 2x10<sup>6</sup> surviving cells were lysed in 1% Triton, and IRAP was immunoprecipitated with specific mouse antibodies immobilized on Sepharose 4B beads. Half of the beads was resuspended in gel loading buffer and analyzed by immunoblot for IRAP content. The other half was used to prepare triplicate samples and incubated for 15 min with 50 μM Arg-AMC with continuous measuring of the fluorescence signal at 460 nm using a Mithras™ fluorometer (Berthold). To measure the effect of the IVDE77 IRAP inhibitor, BM-DCs on day 6 were incubated for 16 hr in complete medium supplemented with 1 μM IVDE77 or 0.1% DMSO, lysed in 1% Tween-20 in the presence of protease inhibitors and incubated for 2 hr with 20 μL protein G Sepharose previously associated with 5 μg murine IRAP antibodies. The beads were incubated for 30 min with 500 μM Leu-AMC at 37°C, and fluorescence was measured on a Versafluor fluorometer (Bio-Rad).

### **Lentivirus production and infection**

The plasmids pLK0.1-puro carrying shRNA sequences specific for Rab14 (TRCN0000089375) and Sec22b (TRCN0000115089, also used by Cebrian et al.) and a puromycin resistance gene were purchased from Open Biosystems. The control pLK0.1 plasmid carrying a non-targeting shRNA sequence (SHC002H) was purchased from Sigma Aldrich. The pLK0.1 plasmids were co-transfected with the packaging plasmids

pCMVDelta8.2 and the envelope plasmid pMD2G into HEK-293-FT cells via calcium chloride transfection. Five hr post-transfection the buffer was exchanged for complete DMEM and virus-containing supernatant was collected 24, 36 and 72 hr post-transfection. The supernatants were concentrated in Centricon 70 devices (Millipore). To determine virus titers, NIH3T3 fibroblasts were transduced with several dilutions of viral supernatants. Two days later, cells were harvested, genomic DNA was isolated, and the viral gene *fugw* was amplified by qPCR, and copy numbers were determined by plotting the obtained signal against dilutions of a *fugw*-encoding plasmid amplified in the same experiment.

Red cell-depleted bone marrow cells on day 3 of culture in the presence of GM-CSF were put in contact with lentiviral supernatants at an MOI of 10 supplemented with 8 mg/mL polybrene and centrifuged for 100 min at 32°C. Subsequently, supernatants were washed off and replaced by BM-DC culture medium. Non-transduced cells were depleted by addition of 5 µg/mL puromycin on day 5. Transduced cells were used on day 7-8 of culture. The efficiency of knockdown was confirmed by immunoblot and qPCR.

### **Wild-type and mutated Rab14-GFP cloning in pEGFP-C1**

Complementary DNA encoding full-length murine Rab14 was PCR-amplified from BM-DCs using the following primers: 5'-AGA TCT GCA ACT GCA CCG TAC AAC TAC T-3' (BglII site underlined) and 5'-GAA TTC CTA GCA GCC ACA GCC TTC TCT-3' (EcoRI site underlined) and cloned into pEGFP-C1 (Clontech). Mutagenesis was performed by the megaprimer method. The megaprimer for the mutation Rab14S25N was obtained by PCR using the primers: 5'-G ATG AAG CAA GCA *ATT TTT TCC TAC TCC CAT ATC CCC*-3' (mutated bases in italics) and 5'-AGA TCT GCA ACT GCA CCG TAC AAC TAC T-3' primer (BglII site underlined). This megaprimer (91 bp) was used in combination with the primer 5'-GAA TTC CTA GCA GCC ACA GCC TTC TCT-3' (EcoRI site underlined) to obtain full-length Rab14S25N lacking an ATG initiation codon that was cloned in pEGFP-C1

between BglIII and EcoRI. The megaprimer for Rab14Q70L was obtained by PCR using the primers 5'-C CGC TCT GAA CCG CTC CAG CCC TGC TGT ATC CC-3' (mutated base in italics) and 5'-AGA TCT GCA ACT GCA CCG TAC AAC TAC T-3' (BglIII site underlined). The megaprimer obtained (229 bp) was used in combination with the primer 5'-GAA TTC CTA GCA GCC ACA GCC TTC TCT-3' (EcoRI site underlined) to obtain full length Rab14Q70L lacking an ATG that was cloned in pEGFP-C1 between BglIII and EcoRI.

#### **qRT-PCR for IRAP and Rab14**

Total RNA was prepared with RNeasy mini kit (Qiagen). Complementary DNA was obtained using the IMPROM II reverse transcription system (Promega) with random hexamers and 1 µg of total RNA. Quantitative PCR was performed with the SyberGreen method using MESA FAST qPCR SYBR MasterMix (Eurogentec) and the following primers:

GAPDH FW 5'-TGGCAAAGTGGAGATTGTTGCC-3'

GAPDH RV 5'- AAGATGGTGATGGGCTTCCCG-3'

HPRT1 FW 5'-AGCTACTGTAATGATCAGTCAACG-3'

HPRT1 RV 5'-AGAGGTCCTTTTCACCAGCA-3'

ACTIN B FW 5'-AGGTGACAGCATTGCTTCTG-3'

ACTIN B RV 5'-GCTGCCTCAACACCTCAAC-3'

IRAP FW 5'-GCGAGAGCTTCGGTCAGCCT-3'

IRAP RV 5'- TCGGTTCTCGCTCCCACCTTGA-3'

Rab14 FW 5'-TGCCACCATGGCAACTGCAC-3'

Rab14 RV 5'- CGCTCCTGCCCTGCTCTATCC-3'

#### SUPPLEMENTAL REFERENCES

Garza, L.A., and Birnbaum, M.J. (2000). Insulin-responsive aminopeptidase trafficking in 3T3-L1 adipocytes. *J. Biol. Chem.* *275*, 2560-2567.

Keller, S.R., Scott, H.M., Mastick, C.C., Aebersold, R., and Lienhard, G.E. (1995). Cloning and characterization of a novel insulin-regulated membrane aminopeptidase from Glut4 vesicles. *J. Biol. Chem.* *270*, 23612-23618.

Weimershaus, M., and van Endert, P. (2013). Preparation of dendritic cells by in vitro cultures. *Methods Mol. Biol.* *960*, 351-357.



## IRAP endosomes restrict TLR9 activation and signaling

Joel Babbor<sup>1,2,3&</sup>, Delphine Descamps<sup>1,2,3,4&</sup>, Adiko Assi Aimé Cézaire<sup>9,10</sup>, Mira Tohmé<sup>1,2,3,5</sup>,  
Sophia Maschalidi<sup>1,2,3</sup>, Luiz Vasconcellos<sup>1,2,3</sup>, Mariacristina De Luca<sup>9,10</sup>, Francois-Xavier  
Mauvais<sup>1,2,3</sup>, Meriem Garfa-Traore<sup>1,2,3</sup>, Melanie M. Brinkmann<sup>8</sup>, Michel Chignard<sup>6,7</sup>,  
Bénédicte Manoury<sup>1,2,3\*</sup>, Loredana Saveanu<sup>9,10\*</sup>

1. Institut National de la Santé et de la Recherche Médicale, Unité 1151, Paris, 75015, France
2. Centre National de la Recherche Scientifique, Unité 8253, Paris, 75015, France
3. Université Paris Descartes, Sorbonne Paris Cité, Faculté de médecine Paris Descartes, 75015 Paris, France
4. VIM, INRA, Université Paris-Saclay, 78350, Jouy-en-Josas, France.
5. Institut National de la Santé et de la Recherche Médicale, Unité 932, Institut Curie, 75005, Paris, France
6. Institut National de la Santé et de la Recherche Médicale, UMR S 938, CDR Saint-Antoine, Paris, France
7. Sorbonne Université, UPMC Univ Paris 06, UMR S 938, CDR Saint-Antoine, Paris, France
8. Helmholtz Centre for Infection Research, 38124 Braunschweig, Germany
9. Institut National de la Santé et de la Recherche Médicale, Unité UMR 1149, Centre de Recherche sur l'Inflammation, Paris, France
10. Université Paris Diderot, Faculté de Médecine Xavier Bichat, Paris, France

& These authors contributed equally to this work

\* Corresponding authors

### \* Corresponding author:

Loredana Saveanu, INSERM, Unité 1149, Faculté de Médecine Bichat, 16 rue Henri Huchard, 75018, Paris cedex 18, France

Bénédicte Manoury INSERM, Unité 1151, Hôpital Necker-Enfants malades, 149 rue de Sèvres, 75743 Paris cedex 15, France

Emails: [loredana.saveanu@inserm.fr](mailto:loredana.saveanu@inserm.fr), [benedicte.manoury@inserm.fr](mailto:benedicte.manoury@inserm.fr)

## **Abstract**

Retention of intracellular TLRs in the endoplasmic reticulum prevents their untimely activation under basal conditions. Under stimulation, activation of TLRs is correlated with relocalization to endosomal compartments through pathways that are different for the various intracellular TLRs. We identified IRAP (insulin responsive aminopeptidase) as a transmembrane component and stabilizer of the endosomal compartment in which TLR9 is transported under cell stimulation. The endosome stabilization effect of IRAP could be explained by the interaction of the cytosolic domain of IRAP with the actin nucleation factor FHOD4, which can anchor vesicles to the actin network. Cells lacking this anchoring, in the absence of IRAP, redistributed intracellular TLR9, which accumulated in its partially cleaved form in lysosomes even in basal conditions. The lysosomal localization of TLR9 was responsible for the uncontrolled, lethal inflammatory response of IRAP-deficient mice to TLR9 ligands during model infections.

Innate and adaptive immune responses depend on the ability of toll-like receptors (TLRs) to discriminate between different classes of microbial products and initiate specific signaling cascades. While microbial products with no equivalent in mammalian cells, such as the components of the bacterial wall, are recognized by surface TLRs (1, 2, 4, 5 and 6), pathogen derived nucleic acids are bound by intracellular TLRs (3, 7, 8 and 9). Recognition of nucleic acids by intracellular TLRs has an intrinsic potential to trigger autoimmune diseases through interaction with self nucleic acids<sup>1</sup>. To avoid inappropriate activation, nucleic acid dependent TLR signaling does not occur in basal conditions, because the receptors are located in the endoplasmic reticulum (ER) and translocate to endocytic vesicles only after cell stimulation. In addition to the transfer into the endocytic pathway, a second step leading to activation of endosomal TLRs is their partial proteolysis by an array of different proteases, specific for each TLR<sup>2-8</sup>.

Although all intracellular TLRs reside in the ER and require the chaperone Unc93b for their transfer to endosomes<sup>9,10</sup>, the trafficking pathways that move the receptors into the endocytic pathway show considerable variation among intracellular TLRs<sup>4,11,12</sup>. For example, the TLR7/Unc93b complex traffics from Golgi stacks directly to endosomes using the clathrin adaptor AP4, while the TLR9/Unc93b complex is directed to the cell surface and joins the endosomes via AP2-mediated clathrin-dependent endocytosis<sup>12</sup>.

The complexity of endosomal TLR trafficking is rendered possible by the diversity and plasticity of the endocytic system. This system includes the early endosomes that fuse to generate the sorting endosome. From there, cargos are directed to different organelles, such as Rab4<sup>+</sup> fast recycling endosomes, Rab11<sup>+</sup> slow recycling endosomes, the trans Golgi network (TGN) or to lysosomes. Next to these universal routes of endosome trafficking, specialized cells, such as dendritic cells (DCs), display particular, albeit poorly characterized endosomal populations that affect TLR function, such as the VAMP3<sup>+</sup> vesicles, which are involved in TLR9 trafficking<sup>13</sup>.

A particular and abundant endocytic population present in DCs, not yet investigated in the context of TLR signaling, is the slow recycling endosomes. They are characterized by the presence of aminopeptidase IRAP (Insulin Responsive AminoPeptidase), a type II transmembrane protein that has the enzymatic site located inside the vesicles and a domain of 110 amino-acids located on the cytosolic side of the membrane. We have previously demonstrated that in DCs, IRAP<sup>+</sup> vesicles are rapidly recruited to DC phagosomes, where the

enzymatic activity of IRAP is involved in antigen processing during MHC-I cross presentation<sup>14,15</sup>.

In addition to DCs, IRAP<sup>+</sup> endosomes have been extensively studied in adipocytes, where they are called Glut4 storage vesicles (GSVs) and are rapidly transported to the cell surface under insulin stimulation. After the fusion of the endosomes with the cell membrane, Glut4 remains at the cell surface to facilitate glucose uptake, while IRAP is rapidly internalized<sup>16</sup>. Thus, both in adipocytes and in DCs, IRAP displays a complex trafficking, sensitive to external regulation by insulin or phagocytic receptors activation. The regulated trafficking of IRAP depends on the cytosolic domain of the enzyme, which has been shown to interact with several proteins involved in vesicles formation or in cytoskeleton remodeling, such as the golgin p115<sup>17</sup>, vimentin<sup>18</sup> and FHOS (formin homologue overexpressed in the spleen, also called FHOD1)<sup>19</sup>. Whether these proteins and their interaction with the cytosolic domain of IRAP play a role in the complex trafficking of IRAP and IRAP<sup>+</sup> endosomes is not known. Such a role could depend on known features of the IRAP interacting partners: the golgin p115 is a tethering factor involved in vesicle trafficking between ER and Golgi stacks, while vimentin and the formin FHOD1 are two cytoskeleton factors. Vimentin forms intermediate filaments, the cytoskeleton component that is important for anchoring intracellular organelles in a cell, while the formins catalyze actin polymerization and are involved in the interaction of intracellular vesicles with the actin cytoskeleton<sup>20</sup>.

Considering the dynamic and potentially regulated nature of IRAP<sup>+</sup> endosomes, we wondered if IRAP plays a role in endosomal TLR trafficking and activation. We report here that a specific step in TLR9 trafficking requires IRAP. The absence of IRAP resulted in localization of TLR9 to lysosomes in unstimulated cells and led to a dramatic increase in TLR9 signaling *in vitro* and *in vivo*. These effects can be explained by the potential role of IRAP as an intermediate in anchoring the TLR9 endosomes to the actin cytoskeleton, which would limit TLR9-driven inflammatory responses. These findings provide a mechanistic explanation to the link between IRAP mutations and autoimmune disorders implicating TLR9<sup>21</sup> and identify new factors and cellular pathways involved in TLR9 activation.

## RESULTS

### IRAP deletion selectively increases the TLR9 response

While TLR4 is activated both at cell surface and in endosomal vesicles, TLR3 and TLR9 are activated exclusively in endocytic vesicles<sup>22</sup>. To investigate the involvement of IRAP in the

activation of these endosomal TLRs, we stimulated wild type (wt) and IRAP-deficient bone marrow derived dendritic cells (BM-DCs) with ligands specific for TLR3 (polyIC), TLR4 (LPS), and TLR9 (CpG-B) and measured the production of the pro-inflammatory cytokines IL-6, IL-12p40 and TNF- $\alpha$ . While IRAP deletion did not affect TLR3- and TLR4-dependent pro-inflammatory cytokine production, it enhanced pro-inflammatory cytokine production driven by TLR9 activation (**Fig. 1a**). These results suggest that IRAP affects the NF- $\kappa$ B pathway downstream of TLR9. Since the second pathway of TLR9 signaling involves IRF-7 and leads to type I IFN production, we wondered whether IRAP deletion affected type I IFN secretion. We measured IFN- $\beta$  production by wt and IRAP-deficient BM-DCs stimulated with TLR3, 4 and 9 ligands (**Fig. 1b**). IRAP deletion significantly increased only TLR9-driven IFN- $\beta$  production but not IFN- $\beta$  production by TLR3 and TLR4. Thus, IRAP controls the amplitude of both pro-inflammatory cytokine and type I IFN production in a TLR9-dependent manner in BM-DCs.

We then wondered whether the hypersensitivity of IRAP-deficient cells to TLR9 ligands was restricted to BM-DCs, which correspond to monocyte-derived inflammatory DCs, or if it also occurred in other cell types. To address this question, we purified conventional DCs (cDCs) and plasmacytoid DCs (pDCs) from the spleen. When incubated with CpG, IRAP-deficient spleen cDCs (**Fig. 1c**) and pDCs (**Fig. 1d**) produced significantly higher amounts of pro-inflammatory cytokines and INF- $\alpha$  than their wt counterparts. These results demonstrated that IRAP expression was required to prevent exacerbated inflammatory cytokine production in response to TLR9 activation in all tested DC subsets.

At least two mechanisms might account for the increased TLR9 response in IRAP-deficient DCs. IRAP<sup>+</sup> vesicles, which are storage compartments sensitive to regulation by cell-specific stimulation in adipocytes, could store pro-inflammatory cytokines and control their trafficking and secretion. Alternatively, IRAP<sup>+</sup> endosomes could directly control TLR9 activation. We then analyzed the intracellular localization of pro-inflammatory cytokines in wt and IRAP-deficient cells. While both IL-6 and IL-12 could not be detected in unstimulated cells, incubation with CpG resulted in staining for IL-6 and IL-12 in intracellular structures with a morphology indicative of Golgi stacks but devoid of IRAP staining (**Supplementary Fig. 1a**). The staining for the cis-Golgi matrix protein GM130, consistent with previous reports, confirmed IL-6 localization in Golgi stacks (**Supplementary Fig. 1b**)<sup>23</sup>.

Thus IRAP<sup>+</sup> endosomes are unlikely to be implicated in trafficking or secretion of IL-6 or IL-12(p40) and are most likely controlling TLR9 trafficking and/or signaling. To further support

this hypothesis, we measured cytokine messenger RNA (mRNA) levels. At the steady state, no pro-inflammatory cytokine mRNAs were detected in wt and IRAP-deficient BM-DCs (**Fig. 1e**) and pDCs (**Fig. 1f**). However, upon CpG but not LPS stimulation, DCs lacking IRAP expressed significantly higher levels of pro-inflammatory cytokine mRNAs than wt DCs (**Fig. 1e-f**).

The increase in cytokines, both at the mRNA and protein level, in IRAP deficient cells following TLR9 stimulation should be the result of an increased TLR9 signaling. To investigate TLR9 signaling we tested the association of the MyD88 adaptor with the transcription factors NF- $\kappa$ B and IRF7. The proximity ligation assay (Duolink), which detects protein complexes in situ <sup>24</sup>, demonstrated a significantly increased association of MyD88 with NF- $\kappa$ B (**Supplementary Fig. 2a**) and of MyD88 with IRF7 (**Supplementary Fig. 2b**) in IRAP-deficient, as compared with wt cells. These results indicate that signaling downstream of TLR9 is enhanced in IRAP deficient DCs.

### **IRAP-deficient mice display a hyper-inflammatory phenotype driven by TLR9 activation**

Our *in vitro* data demonstrated the regulation of TLR9 signaling by IRAP. We next addressed the question whether IRAP-deficient mice display increased TLR9 signaling. To test this, we measured the level of IL-6 in the serum of wt and IRAP-deficient mice 2 h after intravenous injection of PBS, CpG-B or LPS. While wt and IRAP-deficient animals responded identically to PBS and LPS injection, TLR9 stimulation led to higher levels of IL-6 in the serum of mice lacking IRAP than in wt animals (**Fig. 2a**).

We wondered if the observed exacerbated pro-inflammatory TLR9 signaling might affect the innate immune response during a bacterial infection. *Pseudomonas aeruginosa* (*P. aeruginosa*) is an opportunistic Gram-negative bacterium that activates several TLRs including TLR9 on alveolar macrophages (AM) and epithelial cells <sup>25</sup>. TLR9-deficient mice were recently shown to be resistant to *P. aeruginosa* infection, suggesting that TLR9 signaling can have deleterious effects in this model <sup>26</sup>. In order to test whether the TLR9-dependent hyper-activation observed in IRAP-deficient mice could affect survival upon bacterial pulmonary infection, we intranasally inoculated IRAP-deficient and wt mice with 10<sup>6</sup> cfu of *P. aeruginosa* and monitored them for survival. At least 36% of wt mice survived during the two weeks of observation, while all IRAP-deficient mice died within 72 h after infection (**Fig. 2b**). We investigated the correlation between mice survival and the inflammatory response monitored in the lungs 24 h post-infection. In infected IRAP-deficient

mice, broncho-alveolar lavage (BAL) fluid contained higher levels of KC, IL-6, TNF- $\alpha$  and IL-1 $\beta$  than in wt mice (**Fig. 2c**). Since AMs are the first innate immune cells to encounter bacteria in the lungs, we isolated AM and tested their cytokine production upon TLR9 and TLR4 stimulation *in vitro*. While a response was barely detectable in AM isolated from wt mice, IRAP-deficient AMs secreted substantial higher amounts of all pro-inflammatory cytokines tested upon CpG stimulation (**Fig. 2d**) in comparison to wt mice. In contrast, IRAP deficiency did not alter IL-6 and TNF- $\alpha$  secretion upon LPS stimulation, indicating that the hyper-inflammatory phenotype produced was restricted to TLR9 (**Fig. 2d**).

To control for a potential difference between the two mouse strains in their ability to clear bacteria from the lungs, we measured the pulmonary bacterial load and found it to be identical in IRAP-deficient and wt mice (**Fig. 2e**). Consistent with an identical ability of both strains to clear bacteria, *P. aeruginosa* infection led to a similar accumulation of neutrophils and macrophages/monocytes in the airways of both groups (**Supplementary Fig. 3a**). In addition, myeloperoxidase activity that mirrors neutrophil degranulation was similar in BALs from both wt and IRAP-deficient mice (**Supplementary Fig. 3b**). Altogether, these experiments suggest that following *P. aeruginosa* infection, IRAP-deficient mice died earlier probably because of an excessive inflammatory response driven by TLR9 hyper-stimulation.

### **Increased processing and aberrant trafficking of TLR9 in the absence of IRAP**

Our *in vitro* and *in vivo* data demonstrated that IRAP deletion led to hyper-production of pro-inflammatory cytokines and uncontrolled inflammation upon TLR9 activation. Since TLR9 signaling is tightly linked to its intracellular trafficking<sup>13,27,28</sup>, we wondered if IRAP deletion could disturb the trafficking of TLR9. Therefore, we investigated the intracellular localization of TLR9 in IRAP-deficient BM-DCs by imaging TLR9 fused to GFP. As expected, in basal conditions, TLR9 showed a reticular staining and was not found in the lysosomes of wt cells. In cells stimulated with CpG for 2 h, TLR9 was recruited to LAMP<sup>+</sup> vesicles (**Fig. 3a-b**). In contrast, in IRAP-deficient BM-DCs, TLR9 was found in lysosomes even in the absence of CpG stimulation (**Fig. 3a-b**). The presence of TLR9 in the LAMP<sup>+</sup> compartment correlates with proteolytic generation of a highly active C-terminal fragment of the receptor in DCs and macrophages<sup>2,3,7,8,29</sup>. In agreement with lysosomal localization of TLR9 in unstimulated IRAP-deficient cells, we found that in IRAP-deficient, but not in wt primary mouse embryonic fibroblasts transfected with TLR9-GFP and UNC93B-cherry, the majority of immunoprecipitated TLR9-GFP runs at 100 kDa, a molecular weight corresponding to the active, processed C-terminal fragment (75kD) fused to GFP (27kD) (**Fig. 3c**). Thus, in the

absence of IRAP, TLR9 is targeted to lysosomes where it is cleaved even without stimulation. To ensure that the lysosomal expression of TLR9 in IRAP-deficient cells was not the consequence of TLR9-GFP expression by nucleofection, we investigated the localization of endogenous TLR9 when the expression of IRAP was silenced by shRNA. Since specific antibodies suitable for visualizing TLR9 are not available, we used TLR9-GFP transgenic mice<sup>30</sup>. We analyzed the receptor localization in BM-DCs derived from these mice upon shRNA-mediated knockdown of IRAP. The shRNA construct led to complete depletion of IRAP protein (**Fig. 3d**), which correlated with lysosomal targeting of TLR9 in steady-state conditions (**Fig. 3e**). Thus, TLR9 requires IRAP for regulation of its trafficking.

To monitor whether TLR9 was the only endosomal TLR dependent on IRAP for its trafficking, we tested the localization of TLR3. Previously published data have revealed significant differences between the regulation of TLR9 and TLR3 trafficking and activation<sup>4,31</sup>. As expected from the functional assays of TLR stimulation (**Fig. 1a-b**), intracellular localization of TLR3 was not affected by IRAP deletion (**Supplementary Fig. 4**). This result suggests that IRAP affects specifically TLR9 intracellular trafficking.

### **TLR9 is transported to IRAP vesicles upon stimulation**

The lysosomal localization of TLR9 in IRAP-deficient cells indicated that IRAP is involved at least in one step of TLR9 trafficking. Known TLR9 trafficking intermediates include ER localization in basal conditions and early VAMP3<sup>+</sup> endosomes and late LAMP<sup>+</sup> endosomes under CpG stimulation<sup>13</sup>. Since IRAP does not colocalize with LAMP or ER markers<sup>14,15</sup>, we wondered if its localization overlaps with the SNARE protein VAMP3. We analyzed VAMP3-GFP expression in BM-DCs by confocal microscopy and found that about 65% (+/- 5%) of IRAP colocalized with VAMP3-GFP (**Supplementary Fig. 5a**). Moreover, VAMP3-GFP colocalized with the small GTPase Rab14 and the Q-SNARE Syntaxin 6 (Stx6) (**Supplementary Fig. 5b-c**), two additional markers of IRAP<sup>+</sup> vesicles in DCs<sup>14,15</sup>.

The reported colocalization of TLR9 with VAMP3 and our results showing a significant colocalization of VAMP3 and IRAP led us to test the potential colocalization of IRAP and TLR9. Under basal conditions, neither TLR9-GFP nor TLR3-HA, used as a control, colocalized with IRAP in BM-DCs (**Fig. 4a-b**). Stimulation of BM-DCs for 20 min with CpG or polyIC was followed by localization of TLR9, but not TLR3, in IRAP<sup>+</sup> vesicles (**Fig. 4a-c**). **These results show that under cell stimulation by CpG, TLR9 is localized to IRAP<sup>+</sup> vesicles and indicate that the transient co-localization of the receptor with IRAP is required to limit TLR9 activation.**



### **IRAP enzymatic activity is not involved in TLR9 activation**

Our results showed that TLR9 translocates to IRAP<sup>+</sup> vesicles upon CpG stimulation and that proper regulation of TLR9 signaling required IRAP. Since IRAP is an aminopeptidase, we wondered if the enzymatic activity of IRAP was involved in the control of TLR9 activation. To investigate this possibility, we tested the effect of an inactive form of IRAP on TLR9 activation. IRAP, similar to all M1 aminopeptidases, has a Zn<sup>2+</sup> atom in the active site<sup>32</sup> and contains the canonical zinc-binding amino acid motif HELAH, which is essential for the enzymatic activity. A form of IRAP in which the HELAH sequence was changed into HALAH (E465A substitution) co-localizes as well as the wild-type protein with Stx6, a SNARE of IRAP<sup>+</sup> vesicles<sup>14,15</sup> (Fig. 5a). Both the wt and mutated form of IRAP were well expressed, as shown by immunoblotting with anti-IRAP antibodies (Fig. 5b) but the mutated form was enzymatically inactive (Fig. 5c). When we reconstituted IRAP-deficient BM-DCs with wild-type IRAP (Fig. 5d) or enzymatically inactive IRAP (Fig. 5d), pro-inflammatory cytokine production upon CpG stimulation was similar to wt cells. These results demonstrated that the enzymatic activity of IRAP is not involved in the control of TLR9 activation.

### **IRAP interacts with the FHOD family of formins**

Since IRAP activity was not required for the control of TLR9 activation, we reasoned that IRAP could contribute to TLR9 trafficking by interacting with proteins involved in vesicular trafficking. Two cytoskeleton factors have been previously identified to interact with the cytosolic domain of IRAP: vimentin<sup>18</sup> and FHOD1 (formin homology domain-containing proteins; synonym: FHOS-formin homologue overexpressed in the spleen)<sup>19</sup>. Vimentin forms intermediate filaments, the cytoskeleton component that is important for anchoring intracellular organelles<sup>33</sup>. FHOD formins are proteins essential for actin polymerization and are involved in anchoring vesicles to the actin cytoskeleton<sup>20</sup>. Thus, vimentin and formins could play a role in the control of IRAP-mediated trafficking of TLR9. Duolink and co-immunoprecipitation experiments in fibroblasts and in DCs failed to show a robust interaction between IRAP and vimentin (data not shown), which implies that the IRAP-vimentin interaction that has been demonstrated in adipocytes<sup>18</sup> might be specific to that cell type.

To investigate the FHOD1-IRAP interaction in DCs, we analyzed the expression of FHOD1 in different cell types as reported in the gene expression database of the ImmGen<sup>34</sup> consortium (Fig. 6a). The mRNA expression data recovered from ImmGen (<https://www.immgen.org/Databrowserpage.swf>) show that while FHOD1 expression is

restricted to a subset of macrophages, FHOD4, a formin from the same family, has a wider distribution and higher expression levels in monocytes and DCs. Thus, we expressed FHOD4 as a GFP fusion protein and demonstrated by reciprocal co-immunoprecipitation that IRAP interacts with FHOD4 (**Fig. 6b**). We confirmed IRAP-FHOD4 interaction by the proximity ligation assay (Duolink), an alternative method used to investigate protein interaction *in situ*<sup>24</sup> (**Fig. 6c**). Confocal microscopy showed that FHOD4 could be recruited to IRAP<sup>+</sup> vesicles, together with a vesicular actin coat labeled by phalloidin (**Fig. 6d**). These results suggested that FHOD4 could anchor IRAP<sup>+</sup> vesicles to the actin cytoskeleton.

### **FHOD4 inactivation, similar to IRAP deficiency, increases TLR9 activation**

To investigate if FHOD4-IRAP interaction was involved in the control of TLR9 activation in DCs, we knocked-down FHOD4 expression using lentiviral transduction of shRNA in BM-DCs from TLR9-GFP transgenic mice. The mRNA of FHOD4 was reproducibly reduced by 85% ( $\pm$  10%) in the cells transduced with the shRNA targeting FHOD4 (**Fig. 7a**). In the absence of FHOD4, 40% ( $\pm$  5%) of the endogenous TLR9-GFP was found in the cleaved form, without CpG stimulation of the cells (**Fig. 7b**). In concordance with the increased basal processing of TLR9-GFP, the GFP-fused TLR9 was found in lysosomes in FHOD4 depleted cells (**Fig. 7c**). Thus, TLR9 trafficking and processing was affected by FHOD4 depletion in an identical manner as by IRAP deletion (**Fig. 3**). Considering the impact of FHOD4 depletion on the receptor localization, we expected to have an increased TLR9-driven inflammatory response in FHOD4 depleted BM-DCs. When incubated with CpG, FHOD4 depleted cells (wt-shFHOD4) secreted significantly more pro-inflammatory cytokines than the cells transduced with a non-targeting shRNA (wt-shNT) (**Fig. 7d**). Similarly to IRAP-deficient cells, the FHOD4 depleted cells displayed an exacerbated inflammatory response exclusively to TLR9 ligands, and not to TLR4 or TLR3 ligands (**Fig. 7d**). Altogether these results suggest that IRAP, via its interaction with FHOD4, anchors the TLR9 containing vesicles to the actin cytoskeleton, slowing their transport to lysosomes.

## **DISCUSSION**

The capacity of intracellular TLRs to recognize host nucleic acids is a risk for auto-immunity. For example, inappropriate activation of endosomal TLRs by self DNA has a major role in the systematic inflammation that occurs in systemic lupus erythematosus, arthritis and psoriasis<sup>35</sup>. To avoid hyper-activation of TLRs, their encounter with the ligands and ability to signal must be tightly regulated. First, exposure to ligands is restricted through the retention

of TLRs in the ER in basal conditions<sup>22</sup> and second, downstream signaling depends on the partial proteolysis of TLRs that occurs in the endosomes<sup>2-4,8,36</sup>. Although these two steps apply to all intracellular TLRs, recent in-depth studies show that the trafficking routes used by distinct endosomal TLRs to reach the endocytic pathway are different<sup>4,12</sup>. TLR9, like other TLRs, exits ER by interacting with Unc93b<sup>22</sup>. Unlike other TLRs, the TLR9-Unc93b complex reaches the cell surface and is later internalized into a poorly characterized endosomal compartment through AP-2 mediated endocytosis<sup>12</sup>.

In this study we identified IRAP as a regulator of TLR9 intracellular trafficking and *in vivo* activation of the receptor. IRAP deficiency led to TLR9 localization in lysosomes, where TLR9 is cleaved into its active C-ter form in the absence of CpG ligand. We observed this aberrant TLR9 trafficking and processing not only for TLR9-GFP expressed in IRAP-deficient cells by transfection, but also for TLR9-GFP expressed from its chromosomal locus in TLR9-GFP knock-in cells, when IRAP was down regulated by shRNA. Lysosomal localization of TLR9 in IRAP-deficient cells led to an uncontrolled inflammatory response to TLR9 ligands, which culminated with animal death during a model bacterial infection. Altogether, our results show that IRAP is required to avoid excessive TLR9-driven inflammatory responses. In view of these results, it is conceivable that IRAP plays a role in human autoimmune pathologies through its effects on TLR9 signaling. The recent identification of a genetic association between psoriasis, one of the autoimmune disorders implicating TLR9 activation, and a nonsense mutation in the LNPEP gene encoding IRAP is consistent with this hypothesis<sup>21</sup>.

The new role of IRAP and our co-localization experiments define a TLR9 endosomal compartment that is described by the presence of Rab14 and Stx6 (**Supplementary Fig.6**) and partially overlaps with VAMP3<sup>+</sup> vesicles. VAMP3 and TLR9 have been shown to co-localize in an intermediate step of the route that TLR9 follows towards lysosomes and which depends on the AP-3 adaptor<sup>13</sup>. Our data suggest that IRAP delays the movement of TLR9 towards lysosomes, with important functional consequences. To understand how IRAP could mechanistically affect the dynamics of the TLR9 endosomal compartment, we tested which protein-protein interactions could interfere with endosomal motility. Considering that the cytosolic tail of IRAP was shown to interact with two cytoskeleton components, an actin nucleation factor, the formin FHOD1<sup>19</sup> and the intermediate filament vimentin<sup>18</sup>, we hypothesized that these interactions ensure the anchoring of IRAP and the associated TLR9 endosomes to cytoskeleton. Whereas the interaction of IRAP with vimentin might be specific

to adipocytes, as it was not detectable in DCs (experiments not shown), we found that IRAP binds to FHOD1 (not shown) and FHOD4 formins.

Formins are major actin nucleation factors that drive the assembly of actin monomers into filamentous structures and remain associated with the barbed end during filament elongation<sup>37</sup>. A knock-down of FHOD4 had effects similar to IRAP deletion on TLR9 trafficking and the cellular response to CpG. These results suggest that by promoting actin assembly on endosomes, FHOD4 prevents the transfer of endosomes to microtubules, delaying their retrograde transport towards lysosomes, as reported for the formin mDia1<sup>38</sup>. Actin polymerization around the endosomal vesicles containing TLR9 ligands has been shown to be also driven by the other key actin nucleation factor, Arp2/3, and to be essential in limiting TLR9 signaling<sup>39</sup>. Interestingly, both, FHOD4 and Arp2/3 are activated by the same small GTPase of Rho family, Cdc42<sup>37</sup>, suggesting that these two actin-remodeling factors might cooperate in the regulation of TLR9 signaling, like they cooperate in phagocytic cup formation<sup>40</sup>. The intervention of FHOD4 in interaction with IRAP for modulating TLR9 function has major implications for potential links between extracellular stimuli, such as cytokines and the ability of TLR9 to respond to its ligands. It has been previously reported that TLR responses can be inhibited by extracellular stimuli such as cytokines<sup>41</sup> or integrin ligation<sup>42,43</sup>. Since Cdc42 activation occurs downstream integrin, receptor tyrosine kinase or G-protein-coupled receptors signaling<sup>44</sup>, it could affect actin polymerization and the anchoring of TLR9<sup>+</sup> vesicles by IRAP. Thus, the anchoring of TLR9 vesicles to actin cytoskeleton could be essential in modulating TLR9 dependent cellular responses to the environment.

## **ACKNOWLEDGEMENTS**

We are grateful to N. Goudin and S. Benadda for advice on analysis and quantification of confocal microscopy images, to S. Keller for anti-IRAP rabbit antibodies and mice and to F. Benvenuti, F. Perez and S. Blystone for plasmid vectors. This work received financial support from the French “Agence Nationale de Recherche”, ANR for CytoEndoStor project to L.S., ANR 2010 MIDI 008 01 project to B. M. and ANR post-doctoral support to D. D. We thank the Foundation “ARC pour la Recherche sur le cancer” for the acquisition of Leica SP8 confocal microscope and for the financial support to J.B.

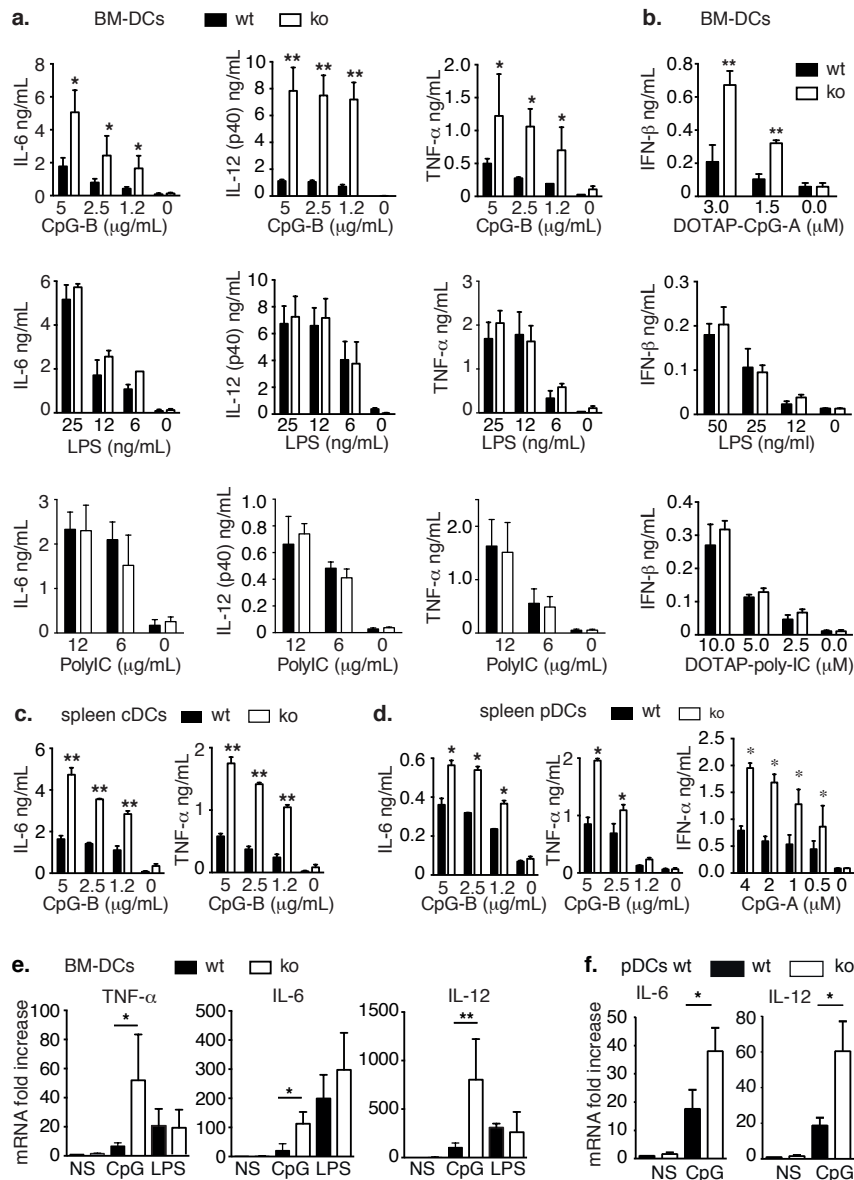


Figure 1 Babdor et al.

### Figure 1. IRAP deletion selectively increases TLR9 response

(a) Wt and IRAP-deficient BM-DCs were stimulated with different TLR ligands for 16 h and the secretion of IL-6, IL-12(p40) and TNF- $\alpha$  in supernatants was measured by ELISA (n=10 experiments, mean  $\pm$  SEM, \* p<0.05, \*\* p<0.01). (b) Wt and IRAP-deficient BM-DCs were incubated for 16 h with TLR ligands and IFN- $\beta$  was measured by ELISA (n=3 experiments, \*\*p<0.01). (c-d) Splenic cDCs (c) or pDCs (d) from wt and IRAP-deficient mice were isolated by cell sorting (c) or anti-PDCA-1 magnetic beads (d), incubated overnight with CpG-B or CpG-A and cytokine secretion was measured by ELISA (n=2 experiments, \*\*p<0.001). (e) Wt and IRAP-deficient BM-DCs were incubated for 3 h with CpG-B or LPS and mRNA for TNF- $\alpha$ , IL-6 and IL-12 was quantified by RT-PCR using as reporters GAPDH and HPRT1. NS= non-stimulated cells. (n= 4 experiments, data are represented as means  $\pm$  SEM, \* p<0.05, \*\* p<0.01). (f) mRNA for IL-6 and IL-12 from wt and IRAP-deficient splenic pDCs, stimulated or not (NS) with CpG-B, was measured by RT-PCR using the same reporter genes as in (e) (n= 3 experiments, means  $\pm$  SEM, \* p<0.05). See also **Supplementary Fig. 1 and 2**.

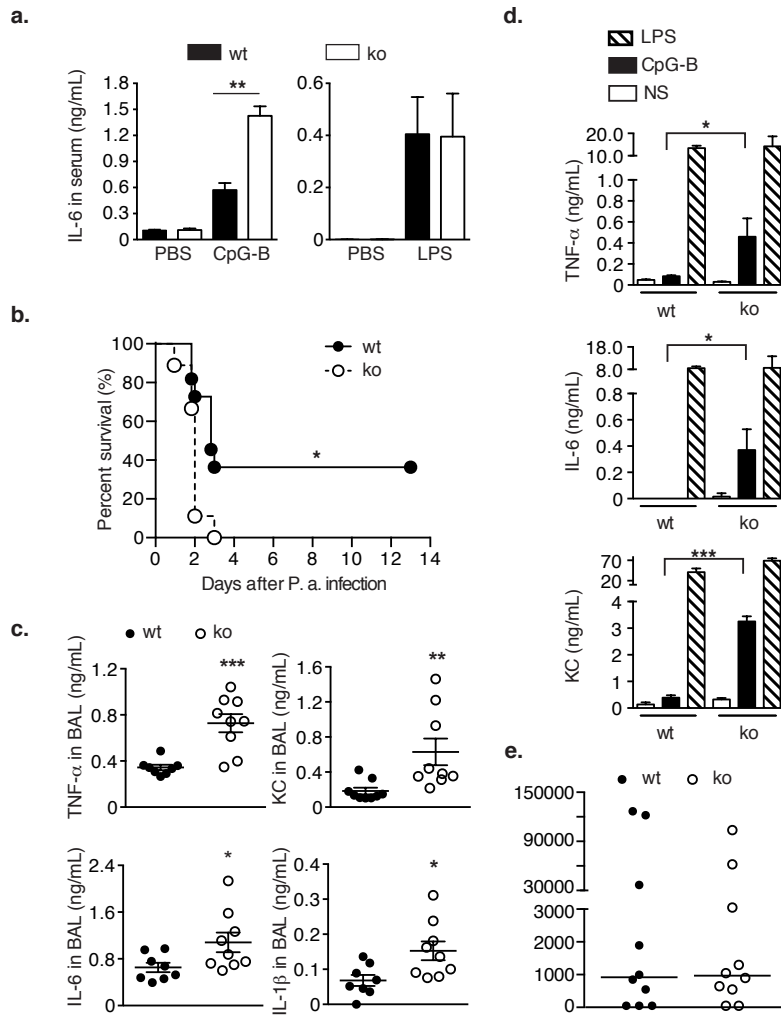


Figure 2. Babdor et al.

## Figure 2. IRAP-deficient mice display a hyper-inflammatory phenotype driven by TLR9 activation

(a) IL-6 production was measured in serum of wt or IRAP-deficient mice 2 h after i.v. injection of CpG-B (left panel) or LPS (right panel) (n=9 animals, mean  $\pm$  SEM, \*\* p<0.01). (b) Wt and IRAP deficient mice (n=9-11 in each group), were inoculated intranasally with *P. Aeruginosa* at  $10^6$  cfu/mouse. Animal survival was determined up to 7 days post-infection (n=3 independent experiments, \* p<0.05). (c) Broncho-alveolar lavage (BAL) fluid levels of KC, IL-6, TNF- $\alpha$  and IL-1 $\beta$  in wt and IRAP-deficient mice 24 h after intranasal inoculation of *P. Aeruginosa* ( $10^6$  cfu/mice) (n=9 animals, 3 independent experiments, mean  $\pm$  SEM \* p<0.05, \*\* p<0.01, \*\*\* p<0.001). (d) TNF- $\alpha$ , KC and IL-6 secretion in supernatants of non-stimulated (NS), CpG-B- or LPS-stimulated wt or IRAP-deficient alveolar macrophages (2 independent experiments, mean  $\pm$  SEM, \* p<0.05, \*\*\* p<0.001). (e) Twenty-four hours post-infection, bacterial load was determined in lungs from wt and IRAP-deficient mice. (n=9 animals; graphs show mean  $\pm$  SEM of 2 independent experiments). See also **Supplementary Fig. 3**.

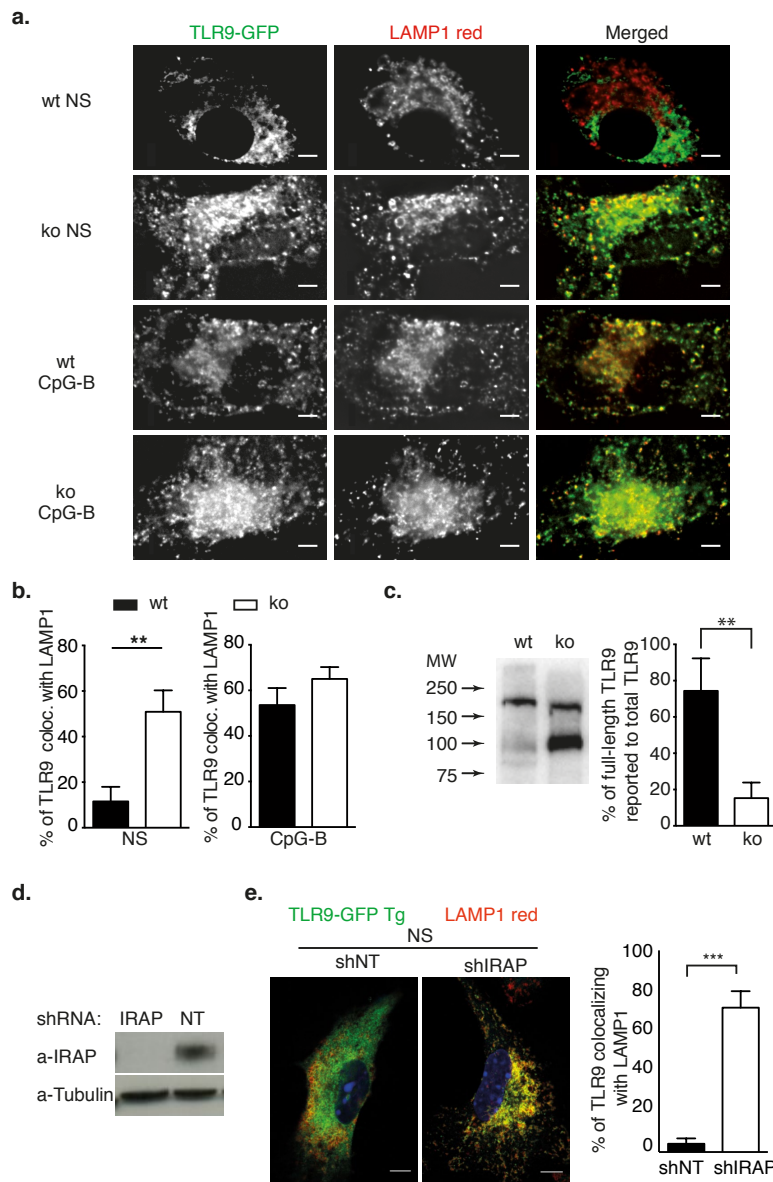


Figure 3. Babdor et al.

**Figure 3. Increased processing and aberrant trafficking of TLR9 in the absence of IRAP**  
**(a)** IRAP-deficient and wt BM-DCs were transfected with TLR9-GFP by nucleofection and 48 h later stimulated or not with CpG-B for 2 h. The cells were fixed and stained with specific antibodies for LAMP1. **(b)** Quantification of TLR9-GFP/LAMP1 co-localization in the experiments shown in the **(c)** Wt and IRAP-deficient fibroblasts expressing TLR9-GFP and Unc93b-Cherry were lysed in 1% NP-40 and TLR9-GFP was immunoprecipitated with anti-GFP antibodies and analyzed by anti-GFP immunoblot. One experiment out of three is shown. The graph represents the quantification of GFP immunoblots from the three independent experiments. **(d-e)** BM-DCs from TLR9-GFP transgenic mice were transduced with a lentivirus coding for an shRNA against IRAP or a non-targeting shRNA (shNT). The efficiency of IRAP knock-down was verified by immunoblotting with anti-IRAP specific antibodies **(d)**. Unstimulated cells were stained with an anti-LAMP1 antibody and endogenous TLR9-GFP co-localization with LAMP1 was analyzed by confocal microscopy **(e)**. Quantification of co-localization were done using Image J Software **(c, e)** n=10 cells from

2 independent experiments. Statistical analysis was performed with Student t test (\*\*p<0.01; \*\*\*p<0.001). See also **Supplementary Fig. 4**.



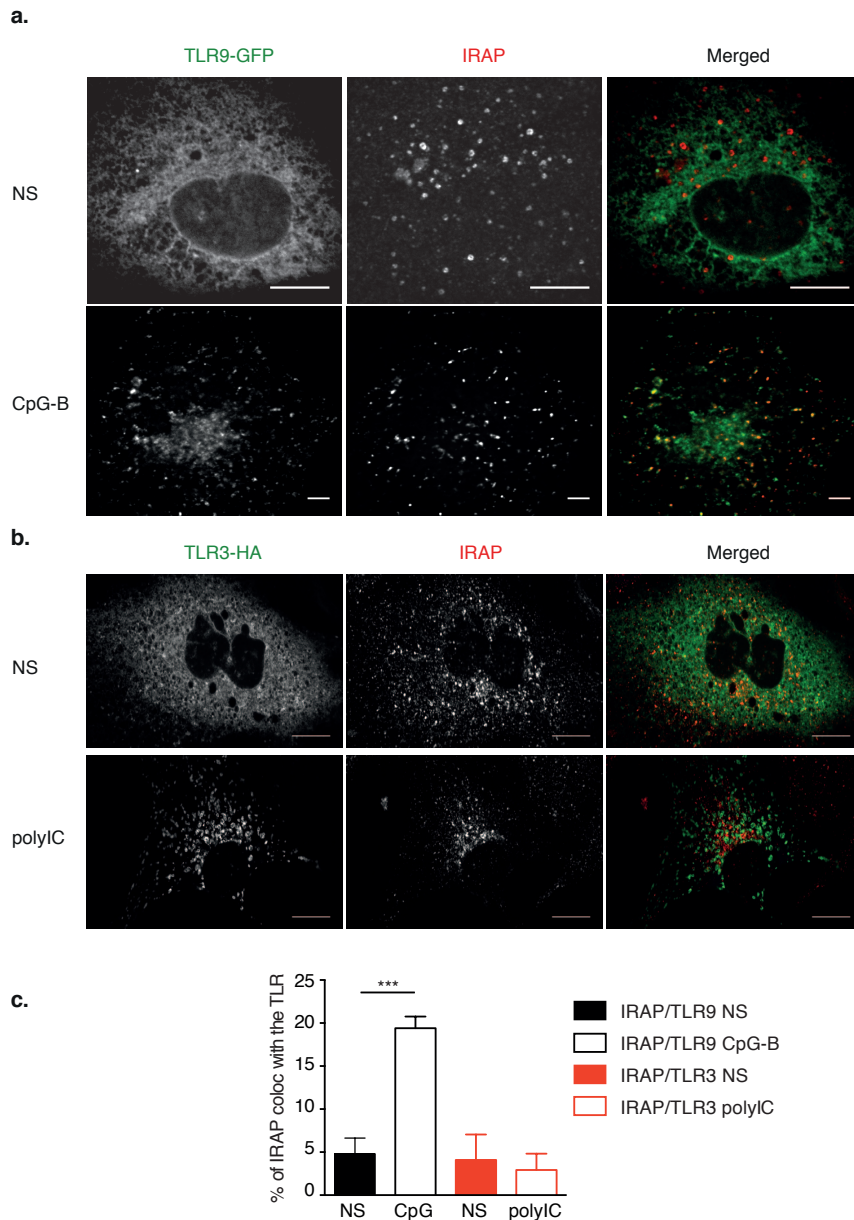


Figure 4 Babdor et al.

### Figure 4. TLR9 traffics to IRAP<sup>+</sup> vesicles upon stimulation

(a) Wt BM-DCs were transfected with TLR9-GFP by nucleofection. Two days later the cells were stimulated or not (NS) with CpG-B for 20 min, fixed and stained with antibodies against IRAP. (b) Wt BM-DCs were transfected with TLR3-HA by nucleofection. Two days later the cells were stimulated or not (NS) with polyIC for 20 min, fixed and stained with antibodies against IRAP. (c) Quantification of TLR9/IRAP and TLR3/IRAP co-localization, n=10 cells from the experiments shown in (a) and (b) using the Image J Software. Statistical analysis was performed with Student t test (\*\*\*)p<0.001). See also **Supplementary Fig. 5**.

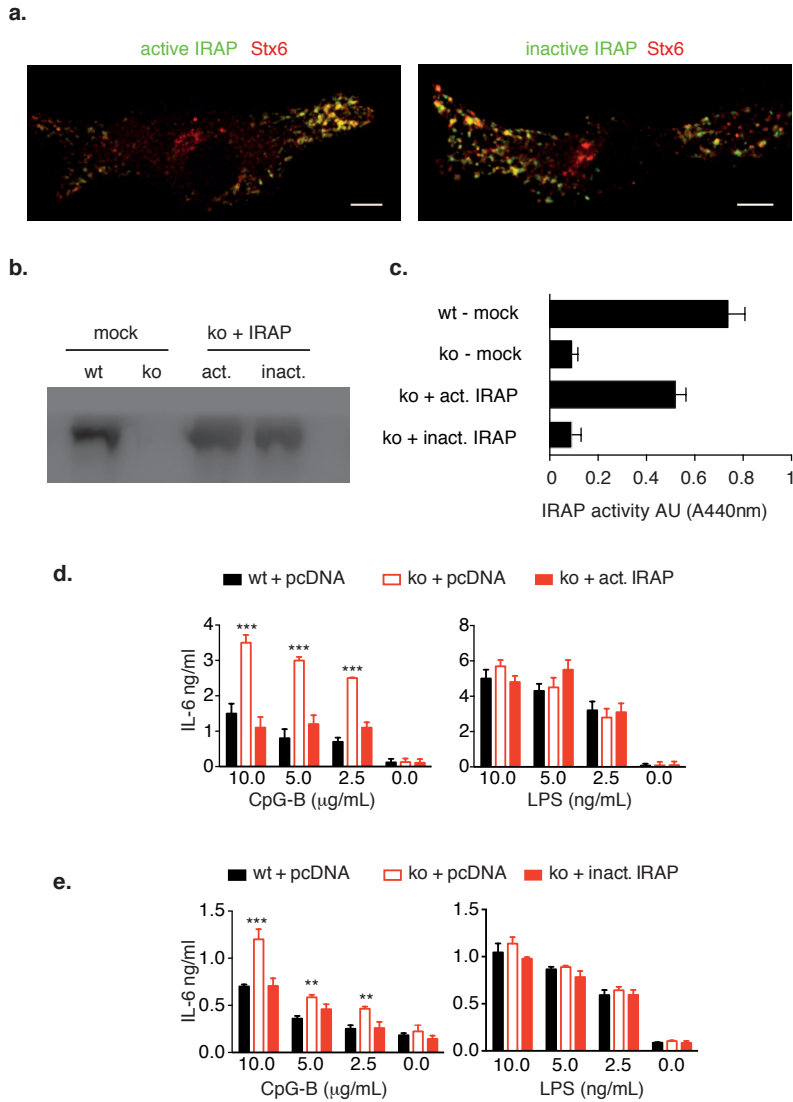


Figure 5. Babdor et al

**Figure 5. IRAP enzymatic activity is not involved in TLR9 activation**

(a) IRAP-deficient BM-DCs reconstituted with active or inactive IRAP-HA by nucleofection were seeded on fibronectin-coated slides and stained with anti-Stx6 and anti-HA specific antibodies. (b) IRAP-deficient fibroblasts were transfected by electroporation with active or inactive IRAP and 36 h later, IRAP expression was analyzed by immunoblotting with anti-IRAP antibodies. (c) IRAP was immunoprecipitated with anti-IRAP antibodies from the fibroblasts transfected as in (b) and the aminopeptidase activity was tested by incubation of the beads with the colorimetric substrate Leu-AMC (2 independent experiments). (d-e) IRAP-deficient BM-DCs reconstituted with active (d) or inactive (e) IRAP were stimulated with TLR ligands for 16 h and IL-6 secretion was measured by ELISA (two (d) or 3 (e) independent experiments, mean  $\pm$  SEM, \*\* $p$ <0.01, \*\*\* $p$ <0.001).

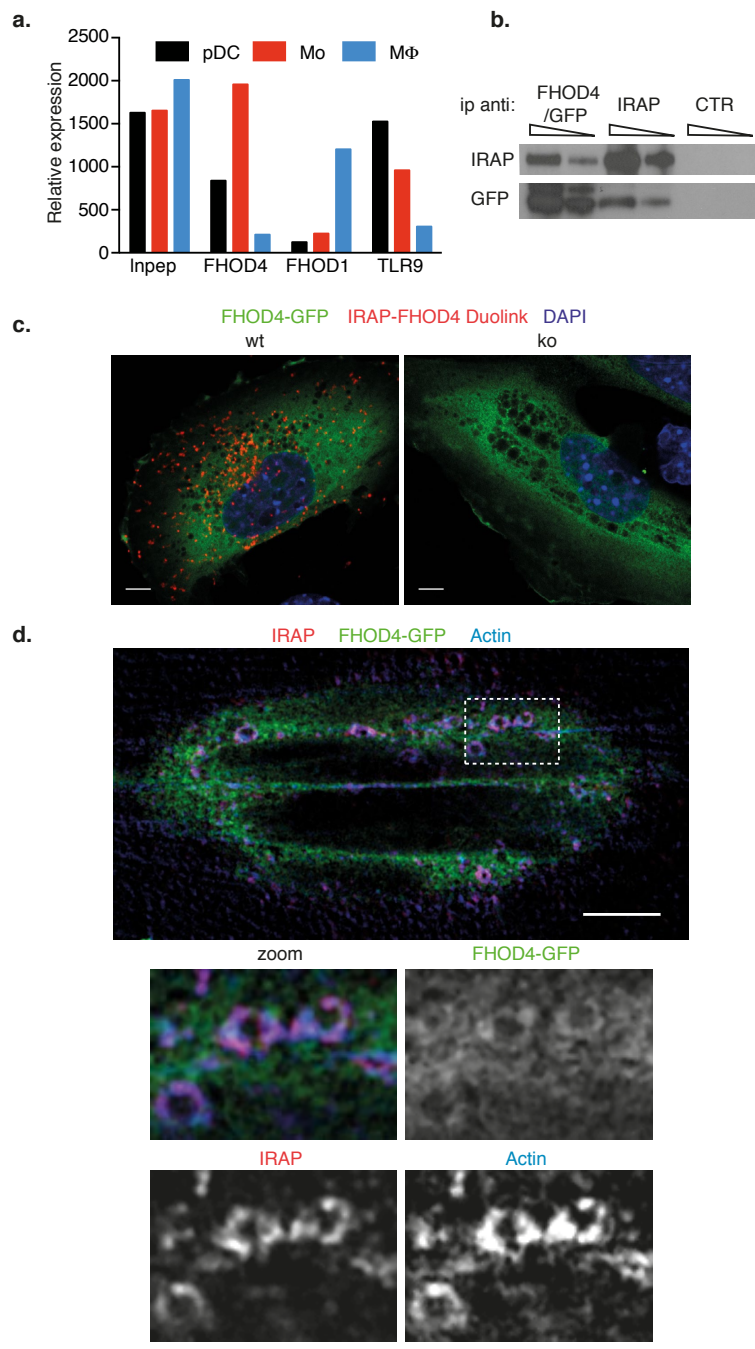


Figure 6 Babdor et al.

### Figure 6. IRAP interacts with the FHOD family of formins

(a) IRAP, FHOD4, FHOD4 and TLR9 mRNA expression data were recovered from immgen (<https://www.immgen.org/Databrowserpage.swf>) for pDCs (pDCs\_8+\_sp sub-type), Monocytes (Mo\_C6+\_II+\_Bl type) and Macrophages (MF\_RP\_Sp type). (b) Wt fibroblasts were transfected by electroporation with a plasmid expressing FHOD4-GFP. Thirty-six hours later IRAP and FHOD4 were immunoprecipitated with anti-IRAP and anti-GFP respectively and the precipitates were split in two and analyzed by immunoblot as indicated. (c) Wt and IRAP-deficient fibroblasts were transfected as in (a) and a Duolink assays for detection of IRAP/FHOD4 interaction was performed with antibodies against IRAP and GFP. (d) Wt fibroblasts expressing FHOD4-GFP were fixed and stained with phalloidin and anti-IRAP antibodies.

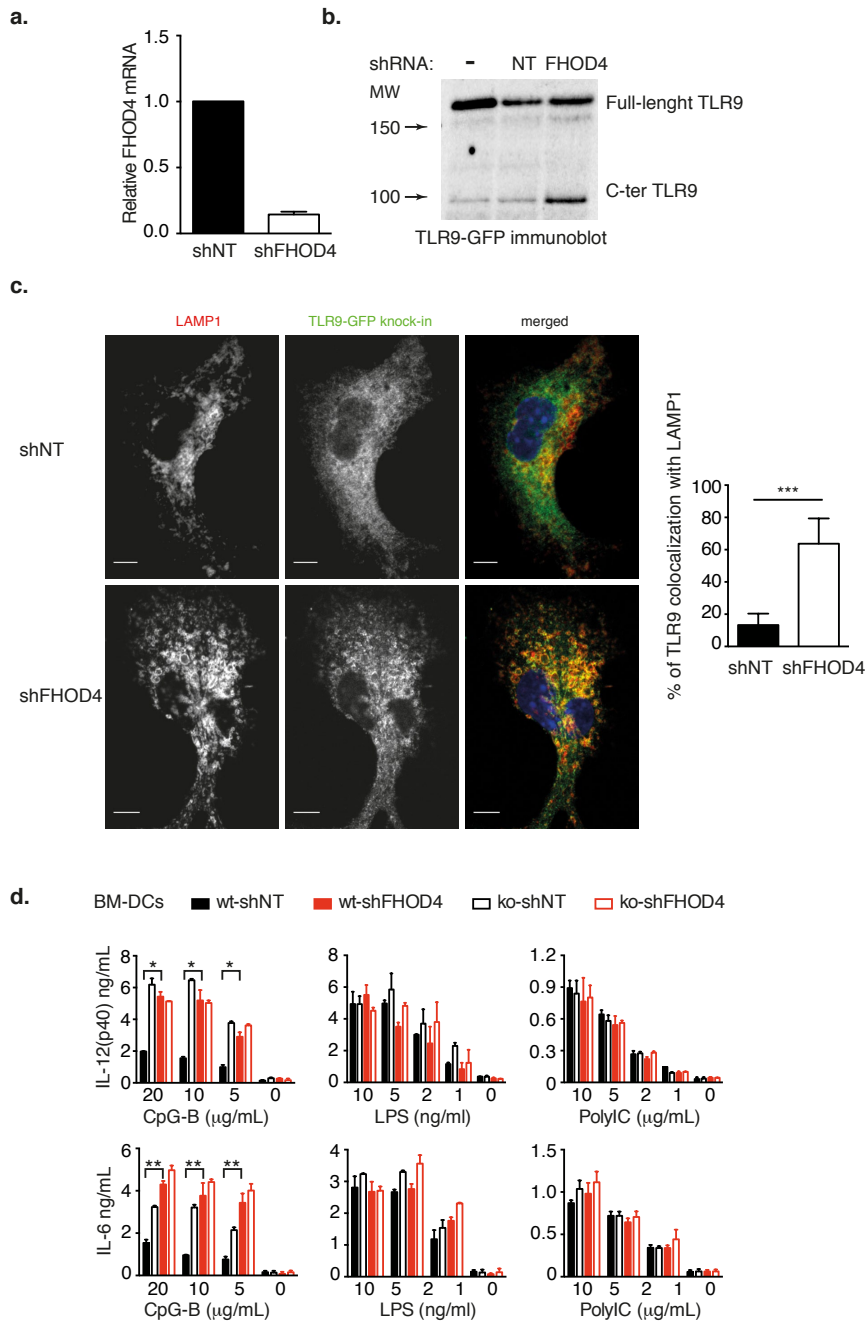


Figure7 Babbdor et al.

**Figure 7. FHOD4 inactivation, similar to IRAP deficiency, increases TLR9 activation**

BM-DCs from TLR9-GFP transgenic mice were transduced with a lentivirus coding for a shRNA against FHOD4 (shFHOD4) or a non-targeting shRNA (shNT). (a) The efficiency of FHOD4 knock-down was analyzed by quantitative RT-PCR using HPRT1, Actin B and GAPDH as internal control. (b) Endogenous TLR9-GFP processing in unstimulated cells was analyzed by immunoblot with anti-GFP antibodies. Control corresponds to untransduced wt BMDCs. (c) Endogenous TLR9-GFP localization in steady state conditions was analyzed by confocal microscopy using an anti-LAMP1 antibody. The graph represents the quantification of TLR9-GFP/Lamp1 colocalization (2 experiments, n=10 cells, \*\*\*p<0.001). (d) Wt and IRAP-deficient BMDCs were transduced with shNT (non-targeting) and shFHOD4 lentiviruses and stimulated with different TLR ligands for 6 h. The secretion of IL-6 and IL-

12(p40) in supernatants was measured by ELISA (n=3 experiments, mean  $\pm$  SEM, \*\*p<0.01, \*p<0.05)

## References

- 1 Lee, B. L. & Barton, G. M. Trafficking of endosomal Toll-like receptors. *Trends in cell biology* 24, 360-369, doi:10.1016/j.tcb.2013.12.002 (2014).
- 2 Asagiri, M. *et al.* Cathepsin K-dependent toll-like receptor 9 signaling revealed in experimental arthritis. *Science* 319, 624-627, doi:10.1126/science.1150110 (2008).
- 3 Ewald, S. E. *et al.* Nucleic acid recognition by Toll-like receptors is coupled to stepwise processing by cathepsins and asparagine endopeptidase. *J Exp Med* 208, 643-651, doi:10.1084/jem.20100682 (2011).
- 4 Garcia-Cattaneo, A. *et al.* Cleavage of Toll-like receptor 3 by cathepsins B and H is essential for signaling. *Proc Natl Acad Sci U S A* 109, 9053-9058, doi:10.1073/pnas.1115091109 (2012).
- 5 Hipp, M. M. *et al.* Processing of human toll-like receptor 7 by furin-like proprotein convertases is required for its accumulation and activity in endosomes. *Immunity* 39, 711-721, doi:10.1016/j.immuni.2013.09.004 (2013).
- 6 Maschalidi, S. *et al.* Asparagine endopeptidase controls anti-influenza virus immune responses through TLR7 activation. *PLoS Pathog* 8, e1002841, doi:10.1371/journal.ppat.1002841 (2012).
- 7 Park, B. *et al.* Proteolytic cleavage in an endolysosomal compartment is required for activation of Toll-like receptor 9. *Nat Immunol* 9, 1407-1414, doi:10.1038/ni.1669 (2008).
- 8 Sepulveda, F. E. *et al.* Critical role for asparagine endopeptidase in endocytic Toll-like receptor signaling in dendritic cells. *Immunity* 31, 737-748, doi:10.1016/j.immuni.2009.09.013 (2009).
- 9 Latz, E. *et al.* TLR9 signals after translocating from the ER to CpG DNA in the lysosome. *Nat Immunol* 5, 190-198, doi:10.1038/ni1028 (2004).
- 10 Leifer, C. A. *et al.* TLR9 is localized in the endoplasmic reticulum prior to stimulation. *J Immunol* 173, 1179-1183 (2004).
- 11 Fukui, R. *et al.* Unc93B1 restricts systemic lethal inflammation by orchestrating Toll-like receptor 7 and 9 trafficking. *Immunity* 35, 69-81, doi:10.1016/j.immuni.2011.05.010 (2011).
- 12 Lee, B. L. *et al.* UNC93B1 mediates differential trafficking of endosomal TLRs. *Elife* 2, e00291, doi:10.7554/eLife.00291 (2013).
- 13 Sasai, M., Linehan, M. M. & Iwasaki, A. Bifurcation of Toll-like receptor 9 signaling by adaptor protein 3. *Science* 329, 1530-1534, doi:10.1126/science.1187029 (2010).
- 14 Saveanu, L. *et al.* IRAP identifies an endosomal compartment required for MHC class I cross-presentation. *Science* 325, 213-217, doi:10.1126/science.1172845 (2009).
- 15 Weimershaus, M. *et al.* Conventional dendritic cells require IRAP-Rab14 endosomes for efficient cross-presentation. *J Immunol* 188, 1840-1846, doi:10.4049/jimmunol.1101504 (2012).
- 16 Keller, S. R., Scott, H. M., Mastick, C. C., Aebersold, R. & Lienhard, G. E. Cloning and characterization of a novel insulin-regulated membrane aminopeptidase from GLUT4 vesicles. *J Biol Chem* 270, 23612-23618 (1995).
- 17 Hosaka, T. *et al.* p115 Interacts with the GLUT4 vesicle protein, IRAP, and plays a critical role in insulin-stimulated GLUT4 translocation. *Mol Biol Cell* 16, 2882-2890, doi:10.1091/mbc.E05-01-0072 (2005).
- 18 Hirata, Y. *et al.* Vimentin binds IRAP and is involved in GLUT4 vesicle trafficking. *Biochem Biophys Res Commun* 405, 96-101, doi:10.1016/j.bbrc.2010.12.134 (2011).

- 19 Tojo, H. *et al.* The Formin family protein, formin homolog overexpressed in spleen, interacts with the insulin-responsive aminopeptidase and profilin IIa. *Mol Endocrinol* 17, 1216-1229, doi:10.1210/me.2003-0056 (2003).
- 20 Goode, B. L. & Eck, M. J. Mechanism and function of formins in the control of actin assembly. *Annu Rev Biochem* 76, 593-627, doi:10.1146/annurev.biochem.75.103004.142647 (2007).
- 21 Cheng, H. *et al.* Identification of a missense variant in LNPEP that confers psoriasis risk. *J Invest Dermatol* 134, 359-365, doi:10.1038/jid.2013.317 (2014).
- 22 Brinkmann, M. M. *et al.* The interaction between the ER membrane protein UNC93B and TLR3, 7, and 9 is crucial for TLR signaling. *J Cell Biol* 177, 265-275, doi:10.1083/jcb.200612056 (2007).
- 23 Stow, J. L., Low, P. C., Offenhauser, C. & Sangermani, D. Cytokine secretion in macrophages and other cells: pathways and mediators. *Immunobiology* 214, 601-612, doi:10.1016/j.imbio.2008.11.005 (2009).
- 24 Leuchowius, K. J., Weibrecht, I. & Soderberg, O. In situ proximity ligation assay for microscopy and flow cytometry. *Curr Protoc Cytom* Chapter 9, Unit 9 36, doi:10.1002/0471142956.cy0936s56 (2011).
- 25 Greene, C. M. *et al.* TLR-induced inflammation in cystic fibrosis and non-cystic fibrosis airway epithelial cells. *J Immunol* 174, 1638-1646 (2005).
- 26 Benmohamed, F. *et al.* Toll-Like Receptor 9 Deficiency Protects Mice against *Pseudomonas aeruginosa* Lung Infection. *PLoS One* 9, e90466, doi:10.1371/journal.pone.0090466 (2014).
- 27 Guiducci, C. *et al.* Properties regulating the nature of the plasmacytoid dendritic cell response to Toll-like receptor 9 activation. *J Exp Med* 203, 1999-2008, doi:10.1084/jem.20060401 (2006).
- 28 Honda, K. *et al.* IRF-7 is the master regulator of type-I interferon-dependent immune responses. *Nature* 434, 772-777, doi:10.1038/nature03464 (2005).
- 29 Onji, M. *et al.* An essential role for the N-terminal fragment of Toll-like receptor 9 in DNA sensing. *Nat Commun* 4, 1949, doi:10.1038/ncomms2949 (2013).
- 30 Avalos, A. M. *et al.* Cell-specific TLR9 trafficking in primary APCs of transgenic TLR9-GFP mice. *J Immunol* 190, 695-702, doi:10.4049/jimmunol.1202342 (2013).
- 31 Fukui, R. *et al.* Unc93B1 biases Toll-like receptor responses to nucleic acid in dendritic cells toward DNA- but against RNA-sensing. *J Exp Med* 206, 1339-1350, doi:10.1084/jem.20082316 (2009).
- 32 Saveanu, L. & van Endert, P. The role of insulin-regulated aminopeptidase in MHC class I antigen presentation. *Front Immunol* 3, 57, doi:10.3389/fimmu.2012.00057 (2012).
- 33 Kim, S. & Coulombe, P. A. Intermediate filament scaffolds fulfill mechanical, organizational, and signaling functions in the cytoplasm. *Genes Dev* 21, 1581-1597, doi:10.1101/gad.1552107 (2007).
- 34 Heng, T. S. & Painter, M. W. The Immunological Genome Project: networks of gene expression in immune cells. *Nat Immunol* 9, 1091-1094, doi:10.1038/ni1008-1091 (2008).
- 35 Rifkin, I. R., Leadbetter, E. A., Busconi, L., Viglianti, G. & Marshak-Rothstein, A. Toll-like receptors, endogenous ligands, and systemic autoimmune disease. *Immunological reviews* 204, 27-42, doi:10.1111/j.0105-2896.2005.00239.x (2005).
- 36 Descamps, D. *et al.* Toll-like receptor 5 (TLR5), IL-1beta secretion, and asparagine endopeptidase are critical factors for alveolar macrophage phagocytosis and bacterial killing. *Proc Natl Acad Sci U S A* 109, 1619-1624, doi:10.1073/pnas.1108464109 (2012).

- 37 Kuhn, S. & Geyer, M. Formins as effector proteins of Rho GTPases. *Small GTPases* 5, e29513, doi:10.4161/sgtp.29513 (2014).
- 38 Fernandez-Borja, M., Janssen, L., Verwoerd, D., Hordijk, P. & Neefjes, J. RhoB regulates endosome transport by promoting actin assembly on endosomal membranes through Dia1. *Journal of cell science* 118, 2661-2670, doi:10.1242/jcs.02384 (2005).
- 39 Prete, F. *et al.* Wiskott-Aldrich syndrome protein-mediated actin dynamics control type-I interferon production in plasmacytoid dendritic cells. *J Exp Med* 210, 355-374, doi:10.1084/jem.20120363 (2013).
- 40 Seth, A., Otomo, C. & Rosen, M. K. Autoinhibition regulates cellular localization and actin assembly activity of the diaphanous-related formins FRLalpha and mDia1. *J Cell Biol* 174, 701-713, doi:10.1083/jcb.200605006 (2006).
- 41 Wimmer, N. *et al.* Lymphotoxin beta receptor activation on macrophages induces cross-tolerance to TLR4 and TLR9 ligands. *J Immunol* 188, 3426-3433, doi:10.4049/jimmunol.1103324 (2012).
- 42 Acharya, M. *et al.* alphav Integrins combine with LC3 and atg5 to regulate Toll-like receptor signalling in B cells. *Nat Commun* 7, 10917, doi:10.1038/ncomms10917 (2016).
- 43 Han, C. *et al.* Integrin CD11b negatively regulates TLR-triggered inflammatory responses by activating Syk and promoting degradation of MyD88 and TRIF via Cbl-b. *Nat Immunol* 11, 734-742, doi:10.1038/ni.1908 (2010).
- 44 Etienne-Manneville, S. Cdc42--the centre of polarity. *Journal of cell science* 117, 1291-1300, doi:10.1242/jcs.01115 (2004).



## **METHODS ONLINE**

### **Mice**

IRAP-deficient mice on the Sv129 background were obtained from S. Keller (Univ. of Virginia) and back-crossed 9 times to C57Bl/6 mice obtained from Janvier (St. Quentin-Fallavier, France). Mice were bred in a specific pathogen free facility and animal experiments were approved by the Comité d'éthique pour l'expérimentation animale Paris Descartes (n° P2.LS.156.10).

### **Preparation of BM-DCs, MEFs, AM, spleen pDCs and cDCs**

BM-DCs were generated from wt and IRAP-deficient mice by a 7-day culture of BM precursors in IMDM supplemented with 10% FCS, 2 mM L-glutamine, 50 mM  $\beta$ -mercaptoethanol and 20 ng/mL GM-CSF. Cell differentiation was assessed by FACS staining using anti-CD11c and CD11b antibodies (BD, Biosciences). MEFs were generated by trypsin dissociation of 13.5 days embryos and repetitive passages in DMEM medium containing 10% FCS, 2 mM L-glutamine, 100 U/mL penicillin and 100 mg/mL streptomycin. The immortalized cells were used between passage 25 and 35.

Mouse AMs were isolated after lungs rinsing with PBS as described elsewhere <sup>1</sup>. The cells were plated in complete RPMI medium supplemented with 2 mM L-glutamine and 5% inactivated FCS for 24 h to allow AM adhesion <sup>2</sup>. AMs were then used for TLR stimulation assays.

Spleens from wt and IRAP-deficient mice were digested with 500  $\mu$ g/mL Liberase DL Research grade (Roche Diagnostics, Meylan, France) and 50 ng/mL DNase I recombinant (Roche Diagnostics) in PBS. DCs were pre-enriched from splenocytes by a very-low density gradient. Briefly, splenocytes were resuspended in 5 mL of PBS containing 5 mM EDTA, 5% FCS and 18% Optiprep (Axis-Shield PoC AS) and were loaded between 5mL IMDM containing 5mM EDTA, 5% FCS and 25% Optiprep (bottom layer) and 2 mL of IMDM medium (top layer). After 20 minutes of centrifugation without break at room temperature and 580 x g, the low-density fraction was collected at the interface between IMDM and 18% Optiprep. The cells were immunostained with the following antibodies: CD11b (M1/70) and GR-1 (RB6-8C5), both from BD Biosciences (Le Pont de Claix, France); CD11c (N418), CD127 (A7R34), NK1.1 (PK136), TCR Beta (H57-597), all from eBioscience (Paris, France); PDCA-1 (129-C1), CD169 (3D6.112) and F4/80 (BM8), all from BioLegend (Ozyme, Saint Quentin Yvelines, France). After exclusion of doublets, dead cells (gating on 7-Actinomycin D 7-AAD- cells) as well as B cells (CD19<sup>+</sup>), NK cells (NK1.1<sup>+</sup>) and T lymphocytes (TCR-

b<sup>+</sup>), all grouped in a “dump-channel”, pDCs (dump<sup>-</sup>, CD11b<sup>low</sup>, CD11c<sup>int</sup>, GR-1<sup>high</sup>, PDCA-1<sup>+</sup>) and cDCs (CD11b<sup>+/+</sup>CD11c<sup>high</sup>GR-1<sup>low/neg</sup>CD169<sup>neg</sup>) were sorted on a BD FACS ARIA-II with 95% purity. Alternatively, for quantitative RT-PCRs experiments, splenic pDCs were isolated with anti-mPDCA-1 magnetic beads (Miltenyi Biotech SAS Paris, France).

### **Cell stimulation and cytokine detection**

Wt and IRAP-deficient BM-DCs, *ex-vivo* isolated splenic cDCs, pDCs and MΦs were plated in 96-well plates and treated with the indicated concentration of different compounds for 6 h or 20 h. Cytokine secretion was measured in culture supernatants with commercial (IL-6, IL-12/23(p40), TNFα, eBiosciences; type I IFN, PBL Interferon Source) ELISA kits. CpG-A (CpG ODN 1585 [5'-ggG GTC AAC GTT Gag ggg gg-3']) and Imiquimod were from Invivogen (Toulouse, France), CpG-B ([5'-tga ctg tga acg ttc gag atg a-3']) was produced by TriLink Biotechnologies (Tebu-Bio, Le Perray en Yvelines, France), LPS was from Sigma-Aldrich (Lyon, France). For mRNA measurements by qRT-PCR, the cells were incubated with the different TLR ligands for 3 h. CpG-A complexes with DOTAP (Roche Diagnostics) were obtained by incubation at room temperature for 15 min.

### ***In vivo* injection with TLR ligands and *Pseudomonas Aeruginosa* (PA) infection**

WT and IRAP-deficient mice were injected i.v. with 10 μg of CpG, 1 μg of LPS or PBS alone. Blood was collected 2 h after injection and serum was obtained by centrifugation after overnight incubation at 4°C.

*Pseudomonas aeruginosa* strain PAK (obtained from S. Lory, Harvard Medical School, Boston, MA) was prepared as previously described<sup>2</sup>. Briefly, a mid-log phase culture of PAK was centrifuged at 3.000 x g, the bacterial pellet was washed once in PBS and resuspended in PBS at the indicated concentration by measuring the OD at 600 nm. The inoculum was verified by serial dilutions plated on LB agar to determine the number of colony-forming unit (CFU). WT and IRAP-deficient mice were infected intra-nasally with 1x10<sup>6</sup> CFU of PAK. Twenty-four hours after infection, the mice were sacrificed and BALs were obtained by rinsing with PBS using a blunted needle inserted into trachea. Commercial ELISA assays were used to measure IL-6, TNF-α (eBiosciences), KC and IL-1β (R&D Systems, Lille, France).

### **Quantitative RT-PCR**

Total RNA was extracted from  $1 \times 10^6$  BM-DCs or  $0.5 \times 10^6$  pDCs with the RNeasy kit (Qiagen, Courtaboeuf, France) according to the manufacturer's instructions. One  $\mu\text{g}$  of total RNA was reverse transcribed into cDNA with the IMPROM-II Reverse Transcription System (Promega, Lyon, France) using random hexamers. Quantitative PCR was performed with MESA FAST qPCR SYBR (Eurogentec) MasterMix using the 7900 real-time PCR instrument from Applied Biosystem. The sequences of qRT-PCRs primers are described in supplemental information.

The following primers were used to detect the pro-inflammatory cytokines, FHOD4 and the house keeping mRNAs:

IL-6 FW : 5'-CACTCCCAACAGACCAGAGG -3'

IL-6 RV : 5'-GGTACTCCAGAAGACCAGAGG-3'

IL-12-p40 FW : 5'-GAGACTCTGAGCCACTCACA-3'

Il-12-p40 RV : 5'-GAGAGTCAGGGGAACTGCTA-3'

TNF $\alpha$  FW : 5'-TAGCCCACGTCGTAGCAAA-3'

TNF $\alpha$  RV : 5'-GATAGCAAATCGGCTGACGG-3'

GAPDH FW : 5'-TGGCAAAGTGGAGATTGTTGCC-3'

GAPDH RV : 5'-AAGATGGTGATGGGCTTCCCG-3'

HPRT1 FW : 5'-AGCTACTGTAATGATCAGTCAACG-3'

HPRT1 RV : 5'-AGAGGTCCTTTTCACCAGCA-3'

ACTIN-B FW : 5'-AGGTGACAGCATTGCTTCTG-3'

ACTIN-B RV : 5'-GCTGCCTCAACACCTCAAC-3'

FHOD4 FW: 5'-CATCTGTGCCCAAAGTCGC-3'

FHOD4 RV: 5'-GAAGCCGGACTGGTAGTTCA-3'

### **Plasmid constructs and cell transfection**

TLR9-GFP plasmid was used as previously described<sup>3</sup>. Mouse UNC93B1 cDNA (Invivogen) was amplified with the following primers forward 5'-GCGGCTAGCATGGAGGTGGAGCCTC-3' and reverse 5'-GGCGCTAGCCCCTGCTCCTCAGGCC-3' (underlined NheI) and fused to N terminus of mcherry (pmCherry plasmid was a kindly gift from F. Perez, Institut Curie, Paris). The pEGFP-VAMP3 and pCDNA3.1-FHOD4 were generous gifts from F. Benvenuto and Scott Blystone, respectively. pUno-TLR3-HA plasmid was purchased from Invivogen.

For expression of fluorescent fusion proteins,  $4 \times 10^6$  MEF were electroporated with 15  $\mu\text{g}$  of plasmids in 200  $\mu\text{L}$  of PBS containing 10 mM Hepes using the GenePulser electroporator (250 kV, 900 mF, Biorad, Marnes-la-Coquette, France). Two million BM-DCs were

transfected on day 6 with 1.5 µg of plasmids coding for GFP-tagged VAMP3 or TLR9 with the AMAXA kit (Lonza, Germany). Thirty-six to 48 h after transfection, the cells were used for immunofluorescence studies or immunoblot.

### **Immunoprecipitations and Immunoblots**

GFP-tagged TLR9 and GFP-FHODs proteins were immunoprecipitated with GFP turbo A beads (ChromoTek, Bayern, Germany) and IRAP was immunoprecipitated with the rabbit anti-IRAP antibody kindly provided by Susanna Keller. The GFP-fusion proteins were detected on PVDF membranes with a monoclonal mouse antibody against GFP (clones 7.1 and 13.1, Roche Diagnostics). IRAP was detected on immunoblots either with the rabbit antibody provided by S. Keller, or with the mouse monoclonal antibody (3E1) from Cell Signaling Technology.

### **Mutagenesis and aminopeptidase activity of IRAP**

The cDNA coding for full-length IRAP was amplified from the clone 40098425 (accession: BC120925) purchased from Dharmacon and subsequently cloned into pIRES2-EGFP (Clontech) between NheI and XhoI. The inactive form of IRAP was produced by mutagenesis with the megaprimer method <sup>4</sup> and cloned into pIRES2-EGFP. The sequence of mutagenic primer was CT AAA ATC ATT GCT CAC GCA CTG GCA CAT CAG TGG, in which the mutated base is underlined. IRAP-deficient fibroblasts were transfected by electroporation with wt or mutated form of IRAP, lysed in 50 mM Tris, 150mM NaCl and 1% NP-40. IRAP was immunoprecipitated with anti-IRAP antibodies and the aminopeptidase activity on the beads was measured as previously published <sup>5</sup>.

### **Immunofluorescence microscopy**

BM-DCs or MEFs were seeded on IBItreat µ-channels (IBIDI, BioValley, Marne La Vallée, France) or fibronectin-coated slides for 6 or 16 h, respectively. Cells were fixed with 4% PFA and permeabilized with 0.2% saponin in PBS containing 0.2% BSA and stained in the same buffer. Primary antibodies used were: rat anti-LAMP1 (BD Bioscience), rabbit anti-Rab14 (Sigma Aldrich), rabbit anti-Stx6 (ProteinTech), rabbit anti-IRAP (a generous gift from S. Keller, Virginia University, USA), mouse monoclonal anti-GM130 (BD Biosciences), anti-IL-12(p40) (capture antibody from ELISA Ready-set-Go! Kit) and rabbit anti-IL-6 antibody (AbDSerotec, Colmar, France). Secondary antibodies coupled with Alexa fluorochromes were from Molecular Probes (Life Technologies, Saint Aubin, France). Images were acquired on a

Leica SP8 confocal microscope or, where specified, on a Leica DMI 6000 microscope equipped with a piezoelectric-driven stage and Optophotonics XF100-2 (FITC), XF102-2 (Texas Red) and XF06 (DAPI) filters. Image treatment and analysis were performed with Image J software.

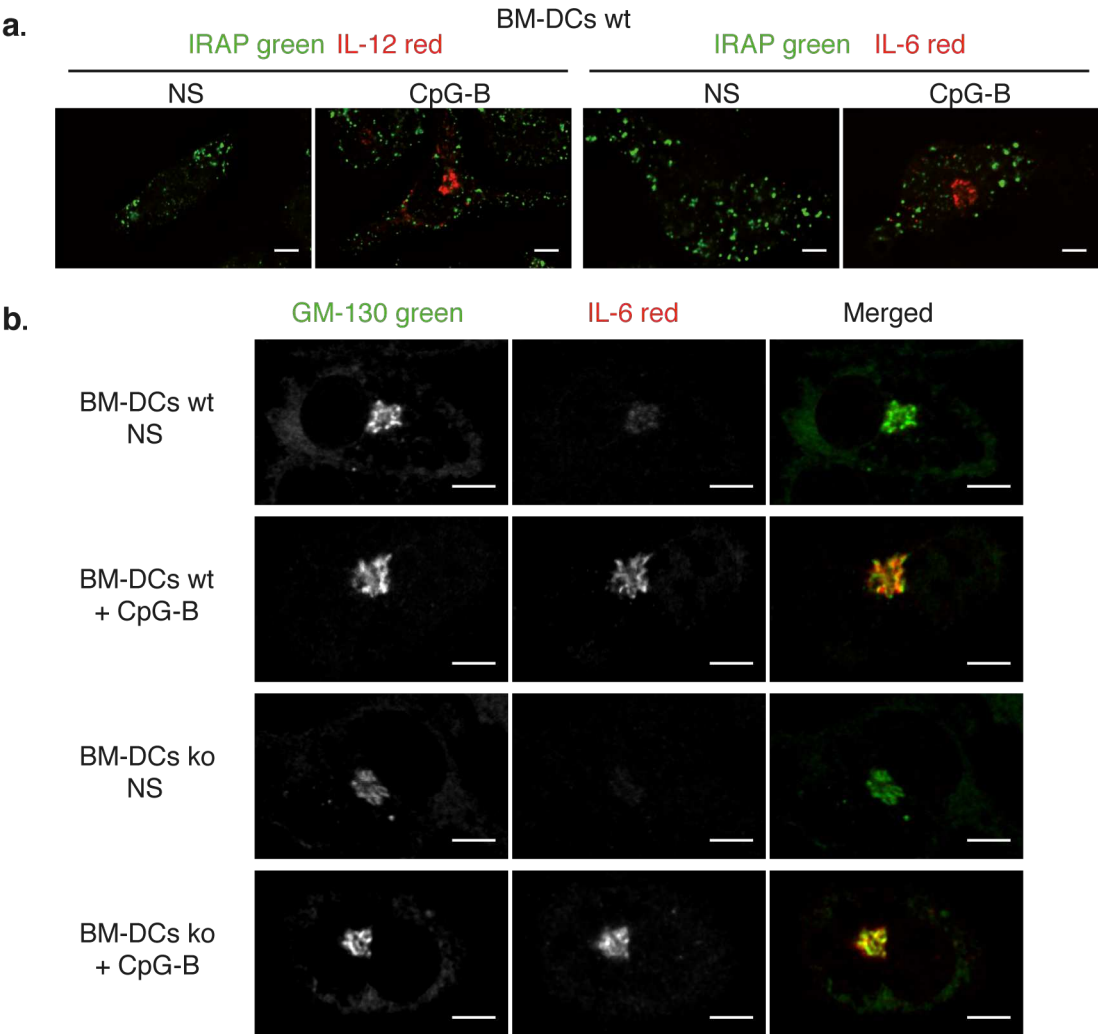
### **Proximity ligation assay (Duolink)**

Duolink™ (OLINK Bioscience) was performed according to the manufacturer's instructions. Briefly, the cells were grown on fibronectin-coated coverslips, fixed for 10 min in 2% paraformaldehyde at 37°C, permeabilized in PBS, 0.05% saponin, 0.2% BSA for 10 min and blocked with 3% BSA in PBS. Primary antibodies used were mouse anti-GFP (Roche Diagnostics), rabbit anti-IRAP, mouse anti-MyD88 (Abcam), rabbit anti-NF-κB (RelA C20 from Santa Cruz) and mouse anti-IRF7 (Abcam). After washing the cells, PLA probes were added, followed by hybridization, ligation, and amplification for 90 min at 37°C. Nuclear DNA (DAPI labeling) and protein interactions were visualized after incubation with the detection solution. Fluorescence signal was acquired on a Leica SP8 confocal microscope.

### **Lentiviral shRNA knock-down of FHOD4 and IRAP**

The pLK0.1-puromycin plasmids coding for IRAP specific shRNA (TRCN0000031113) and FHOD4 specific shRNA (TRCN0000120520) and a non-targeting shRNA (shNT) were purchased from Sigma Aldrich. The lentiviral particles were produced according to the protocol published by Tiscornia G. *et al*<sup>6</sup>. BM precursor cells were seeded in 96 wells plate at 10<sup>5</sup> cells per well. They were transduced on the second day of differentiation using the MOI of 10, in the presence of 8 µg/mL polybrene. Following 2 h centrifugation at 37°C and 950xg, the lentiviral mix was replaced with BM-DCs differentiation medium. On day 5 of differentiation, the non-transduced cells were eliminated by puromycin (5µg/mL) selection for 48 h. The cells were analyzed between day 7 and 9 of differentiation.

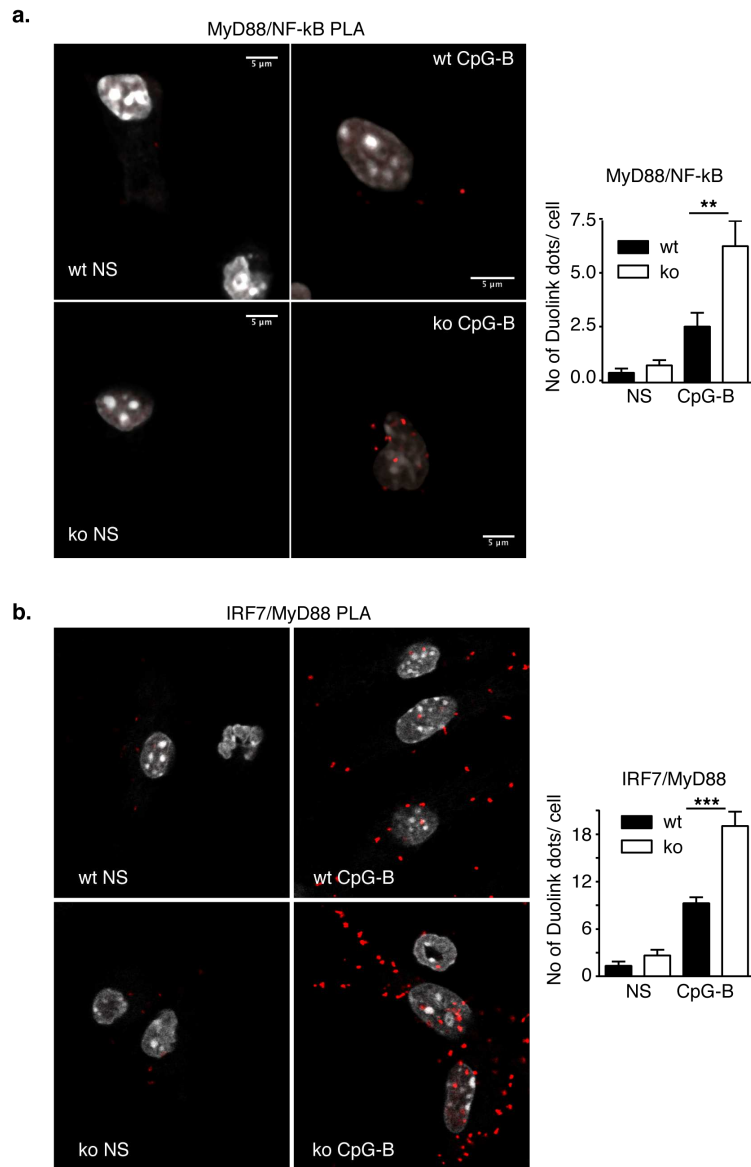
**SUPPLEMENTARY FIGURES**



Supplementary Figure 1 Babdor et al.

**Supplementary Figure 1. Pro-inflammatory cytokines trafficking is intact in BM-DCs lacking IRAP**

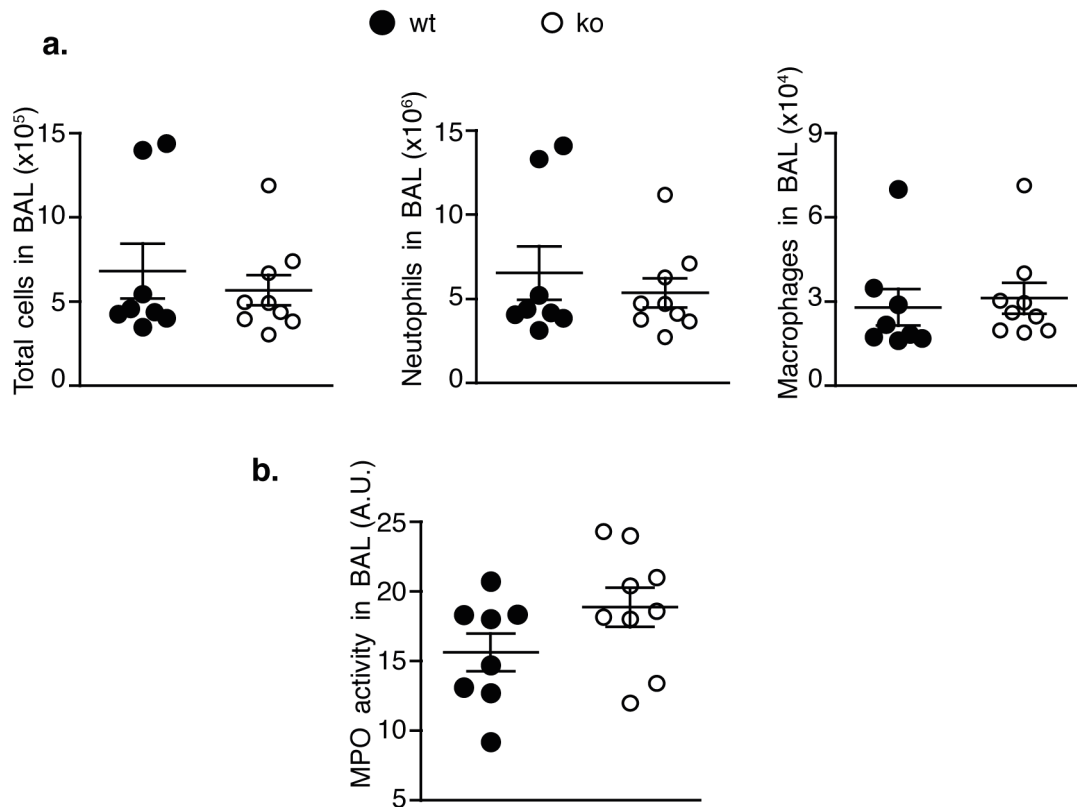
Immunofluorescence microscopy of BM-DCs from wt or IRAP deficient mice stimulated or not (NS) with CpG-B and stained for IRAP and IL-6 or IL-12 (a), and IRAP and GM-130 (b) using specific antibodies. One experiment representative out of three is shown.



Supplementary Figure 2. Babdor et al.

### Supplementary Figure 2. Increased TLR9 signaling in IRAP-deficient DCs

PLA for detection of NF- $\kappa$ B/MyD88 (**a**) or MyD88/IRF7 (**b**) proximity was performed with specific antibodies against MyD88, NF- $\kappa$ B and IRF7. The graphs show the quantification of MyD88 interaction with NF- $\kappa$ B (**a**) or IRF7 (**b**) by PLA. A minimum of 30 cells was analyzed in each condition. (n=3 experiments, means  $\pm$  SD, \*\* p<0.01, \*\*\*p<0.001). Statistical analysis was performed with Student t test.

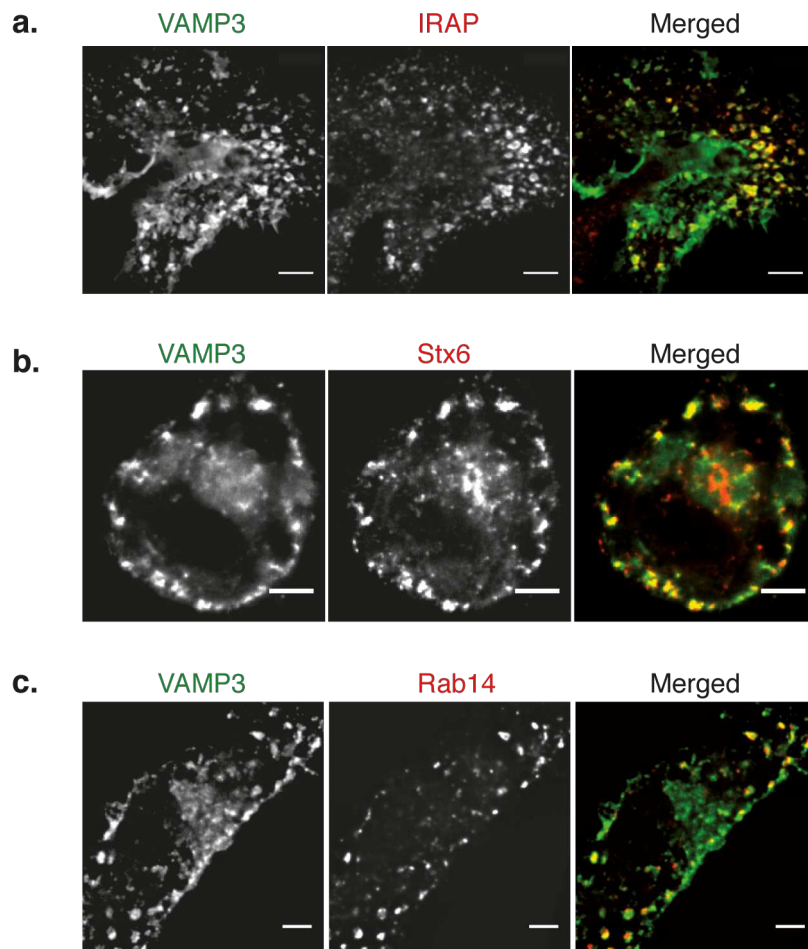


Supplementary Figure 3. Babdor et al.

**Supplementary Figure 3. The innate inflammatory infiltrate of *Pseudomonas aeruginosa*-infected lungs is not altered by the absence of IRAP.**

(a) The presence of macrophages/monocytes ( $CD11b^+/GR-1^{Int}$ ) and neutrophils ( $CD11b^+/GR-1^{high}$ ) was analyzed by flow cytometry of single cell suspensions in BAL fluids from wt and IRAP deficient mice 24 h post infection (n=12 animals; graphs show mean  $\pm$  SEM of two independent experiments). (b) Myeloperoxidase (MPO) activity (lower left panel) was measured in BAL fluids from wt and IRAP deficient mice 24 h post infection (n=8 animals; graphs show mean  $\pm$  SEM of two independent experiments).

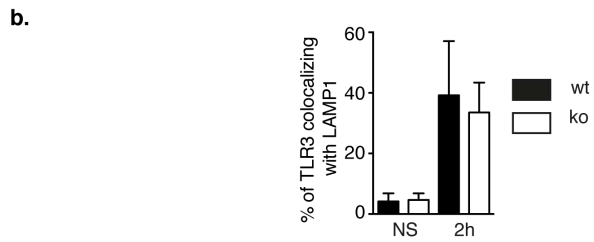
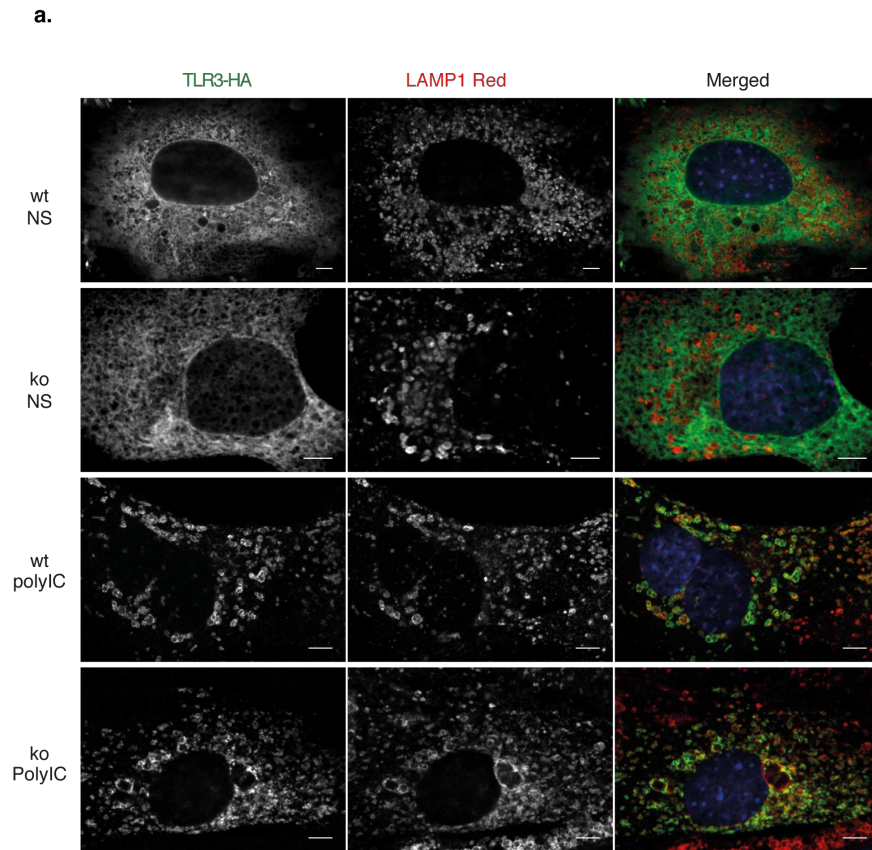




Supplementary Figure 4 Babdor et al.

#### Supplementary Figure 4. Normal TLR3 trafficking in cells lacking IRAP

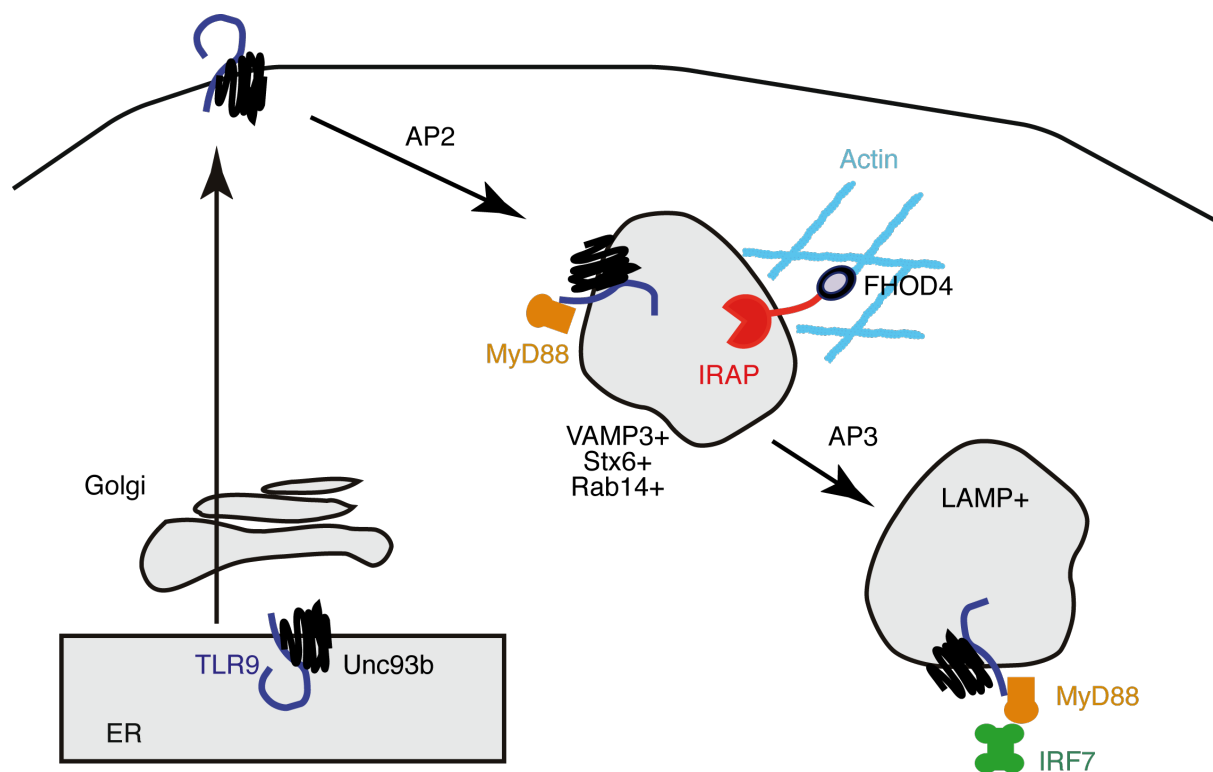
(a) Wt and IRAP deficient fibroblasts expressing TLR3-HA were stimulated or not (NS) with 12  $\mu$ g/ml polyIC for 2 h, fixed and stained with monoclonal antibodies specific for LAMP1 and HA-tag. (b) Quantification of TLR3-HA and LAMP1 co-localization in the experiment shown in (a) using Image J Software (n=10 cells from 2 independent experiments).



Supplementary Figure 5 Babbdor et al.

**Supplementary Figure 5. VAMP3 is a component of IRAP vesicles**

Wt BM-DCs were transfected with VAMP3-GFP by nucleofection. Two days later, the cells were stained with the antibodies specific for IRAP (a), STX6 (b) or Rab14 (c) and analyzed by confocal microscopy.



Supplementary Figure 6\_ Babbdor et al.

**Supplementary Figure 6. Integration of literature data and our results for a model of TLR9 trafficking.**

Under basal conditions, TLR9 is retained in the ER. Upon cell stimulation, the TLR9/Unc93b complex traffics to cell surface and is internalized via AP2 and clathrin mediated endocytosis<sup>7</sup>. Once intracellular, TLR9 reaches IRAP<sup>+</sup> vesicles that contain Rab14 and Stx6 and overlap with VAMP3 vesicles. The sorting of TLR9 from VAMP3<sup>+</sup> vesicles is dependent on the clathrin adaptor AP3<sup>8</sup> and allows TLR9 transport, probably via microtubules<sup>9</sup>, to lysosomes, from where it can signal via both, MyD88 and IRFs. Actin polymerization around early endosomal compartments delays TLR9 transport to lysosomes<sup>10</sup>. IRAP interaction with the actin nucleator FHOD4 anchors TLR9 endosomes to the actin network, blocking its transport towards lysosomes and limiting TLR9 activation.

- 1 Goncalves de Moraes, V. L., Singer, M., Vargaftig, B. B. & Chignard, M. Effects of rolipram on cyclic AMP levels in alveolar macrophages and lipopolysaccharide-induced inflammation in mouse lung. *Br J Pharmacol* **123**, 631-636, doi:10.1038/sj.bjp.0701649 (1998).
- 2 Descamps, D. *et al.* Toll-like receptor 5 (TLR5), IL-1beta secretion, and asparagine endopeptidase are critical factors for alveolar macrophage phagocytosis and bacterial killing. *Proc Natl Acad Sci U S A* **109**, 1619-1624, doi:10.1073/pnas.1108464109 (2012).
- 3 Sepulveda, F. E. *et al.* Critical role for asparagine endopeptidase in endocytic Toll-like receptor signaling in dendritic cells. *Immunity* **31**, 737-748, doi:10.1016/j.immuni.2009.09.013 (2009).
- 4 Vander Kooi, C. W. Megaprimer method for mutagenesis of DNA. *Methods Enzymol* **529**, 259-269, doi:10.1016/b978-0-12-418687-3.00021-5 (2013).
- 5 Saveanu, L. *et al.* Concerted peptide trimming by human ERAP1 and ERAP2 aminopeptidase complexes in the endoplasmic reticulum. *Nat Immunol* **6**, 689-697, doi:10.1038/ni1208 (2005).
- 6 Tiscornia, G., Singer, O. & Verma, I. M. Production and purification of lentiviral vectors. *Nat Protoc* **1**, 241-245, doi:10.1038/nprot.2006.37 (2006).
- 7 Lee, B. L. *et al.* UNC93B1 mediates differential trafficking of endosomal TLRs. *Elife* **2**, e00291, doi:10.7554/eLife.00291 (2013).
- 8 Sasai, M., Linehan, M. M. & Iwasaki, A. Bifurcation of Toll-like receptor 9 signaling by adaptor protein 3. *Science* **329**, 1530-1534, doi:10.1126/science.1187029 (2010).
- 9 Seth, A., Otomo, C. & Rosen, M. K. Autoinhibition regulates cellular localization and actin assembly activity of the diaphanous-related formins FRLalpha and mDia1. *J Cell Biol* **174**, 701-713, doi:10.1083/jcb.200605006 (2006).
- 10 Prete, F. *et al.* Wiskott-Aldrich syndrome protein-mediated actin dynamics control type-I interferon production in plasmacytoid dendritic cells. *J Exp Med* **210**, 355-374, doi:10.1084/jem.20120363 (2013).



REVIEW

# Beta cell antigens in type 1 diabetes: triggers in pathogenesis and therapeutic targets [version 1; referees: 3 approved]

François-Xavier Mauvais<sup>1-3</sup>, Julien Diana<sup>1-3</sup>, Peter van Endert<sup>1-3</sup>

<sup>1</sup>Institut National de la Santé et de la Recherche Médical, Unité 1151, Paris, 75015, France

<sup>2</sup>Centre National de la Recherche Scientifique, UMR8253, Paris, 75015, France

<sup>3</sup>Université Paris Descartes, Sorbonne Paris Cité, Paris, 75015, France

**v1** First published: 22 Apr 2016, 5(F1000 Faculty Rev):728 (doi: 10.12688/f1000research.7411.1)

Latest published: 22 Apr 2016, 5(F1000 Faculty Rev):728 (doi: 10.12688/f1000research.7411.1)

**Abstract**

Research focusing on type 1 diabetes (T1D) autoantigens aims to explore our understanding of these beta cell proteins in order to design assays for monitoring the pathogenic autoimmune response, as well as safe and efficient therapies preventing or stopping it. In this review, we will discuss progress made in the last 5 years with respect to mechanistic understanding, diagnostic monitoring, and therapeutic modulation of the autoantigen-specific cellular immune response in T1D. Some technical progress in monitoring tools has been made; however, the potential of recent technologies for highly multiplexed exploration of human cellular immune responses remains to be exploited in T1D research, as it may be the key to the identification of surrogate markers of disease progression that are still wanting. Detailed analysis of autoantigen recognition by T cells suggests an important role of non-conventional antigen presentation and processing in beta cell-directed autoimmunity, but the impact of this in human T1D has been little explored. Finally, therapeutic administration of autoantigens to T1D patients has produced disappointing results. The application of novel modes of autoantigen administration, careful translation of mechanistic understanding obtained in preclinical studies and *in vitro* with human cells, and combination therapies including CD3 antibodies may help to make autoantigen-based immunotherapy for T1D a success story in the future.



This article is included in the **F1000 Faculty Reviews** channel.

**Open Peer Review**

Referee Status:

	Invited Referees		
	1	2	3
<b>version 1</b> published 22 Apr 2016			

F1000 Faculty Reviews are commissioned from members of the prestigious F1000 Faculty. In order to make these reviews as comprehensive and accessible as possible, peer review takes place before publication; the referees are listed below, but their reports are not formally published.

- 1 **Mario Ehlers**, Immune Tolerance Network USA
- 2 **Massimo Pietropaolo**, Baylor College of Medicine USA
- 3 **Kathryn M. Haskins**, University of Colorado School of Medicine at Denver USA, National Jewish Health USA

**Discuss this article**

Comments (0)

**Corresponding author:** Peter van Endert ([peter.van-endert@inserm.fr](mailto:peter.van-endert@inserm.fr))

**How to cite this article:** Mauvais FX, Diana J and van Endert P. **Beta cell antigens in type 1 diabetes: triggers in pathogenesis and therapeutic targets [version 1; referees: 3 approved]** *F1000Research* 2016, 5(F1000 Faculty Rev):728 (doi: [10.12688/f1000research.7411.1](https://doi.org/10.12688/f1000research.7411.1))

**Copyright:** © 2016 Mauvais FX *et al.* This is an open access article distributed under the terms of the [Creative Commons Attribution Licence](#), which permits unrestricted use, distribution, and reproduction in any medium, provided the original work is properly cited.

**Grant information:** Work in the authors' laboratory is supported by grants from Fondation pour la Recherche Médicale (DEQ20130326539) and Idex Sorbonne Paris Cité to PvE, by a grant from Aide aux Jeunes Diabétiques to FXM and PvE, and by grants from EFSD-Lilly and from the Juvenile Diabetes Research Foundation (47-2013-524 and 2-SRA-2015-73) to JD.

*The funders had no role in study design, data collection and analysis, decision to publish, or preparation of the manuscript.*

**Competing interests:** The authors declare that they have no competing interests.

**First published:** 22 Apr 2016, 5(F1000 Faculty Rev):728 (doi: [10.12688/f1000research.7411.1](https://doi.org/10.12688/f1000research.7411.1))

## Introduction and context

The key role in type 1 diabetes (T1D) of T lymphocytes recognizing self-antigens expressed by insulin-producing beta cells in pancreatic islets is amply documented and beyond reasonable doubt. As discussed in detail in many excellent reviews (see, for example, 1–4), a large number of such autoantigens, generally also recognized by autoantibodies, have been identified and are targeted by CD8+ and CD4+ T cells that may contribute to beta cell destruction but can also have a regulatory, protective role. (Pre-)proinsulin ([P]PI), glutamic acid decarboxylase (GAD), the tyrosine phosphatase IA-2, and the zinc transporter ZnT8 play a particularly prominent role and are recognized by autoantibodies detected in routine clinical laboratory assays (see 5,6 for a discussion of the role of B lymphocytes and autoantibodies in T1D). Given that autoantigens provide specificity to the autoimmune pathology in T1D, major efforts in the scientific field have been devoted, on the one hand, to developing assays for monitoring pathogenic T cell responses against them and, on the other hand, to designing therapeutic strategies specifically silencing such responses.

This short review will take a look at the progress towards the development of diagnostic and therapeutic approaches focusing on T cell autoantigens in the last 5 years. Reviewing the pertinent literature, we will propose three general conclusions. With regard to diagnostic tools, we believe that the number of beta cell proteins and major histocompatibility complex (MHC)-restricted epitopes thereof, as well as the performance of tetramers for the detection of cognate T cells, now provides an increasingly promising basis for monitoring autoreactive T cells. However, as recently argued by Odegard *et al.*, assays for antigen-specific cells are still not robust enough for routine use in clinical trials, particularly multicenter trials<sup>7</sup>. In this context, we will argue that, first, the information obtained in current analyses of such cells is insufficient so that the methods are in need of complementation and, second, that T cell analysis in human T1D should not be limited to self-reactive cells. Concerning autoantigen-based immunotherapy, we agree with Greenbaum and colleagues<sup>8</sup> and believe that the general failure of published recent trials calls for more research in preclinical models and *in vitro* with human cells, which should precede small proof-of-concept trials. This being said, occasional discordance between results in the nonobese diabetic (NOD) model and human T1D (e.g. concerning the effect of interleukin [IL]-2 in combination with rapamycin<sup>9</sup>), and poor reproducibility of some other results in the NOD model<sup>10</sup>, calls for caution when translating preclinical results to human T1D. Finally, we will argue that important gaps in our understanding of processing, presentation, and T cell recognition of beta cell antigens may have to be addressed to design efficient autoantigen-based immunotherapies.

## T cell epitopes and tetramers

Next to the simple and efficient enzyme-linked immunosorbent spot (ELISpot) assays, tetramers have become standard and increasingly sophisticated tools for detecting both CD8+ and CD4+ autoreactive T cells. Production of these reagents requires identification of MHC-restricted epitopes, the number of which is still increasing. Thus, using mass spectrometric analysis of human leukocyte antigen (HLA) class I eluates<sup>11</sup>, or prediction algorithm-assisted analysis of PI degradation products produced by the proteasome<sup>12</sup>, new epitopes presented by four HLA class I alleles, including the

disease-associated A\*24 and recognized preferentially by patient CD8+ T cells, could be identified. Using the technology of combinatorial labeling of identical tetramers with different sets of multiple fluorochromes, Roep and colleagues developed a tetramer “kit” able to detect T cells specific for multiple dominant autoreactive epitopes simultaneously<sup>13</sup>. Such kits will be useful where small blood volumes must be analyzed, especially when studying pediatric samples, although even with recent approaches it will be difficult to obtain satisfactory results with blood volumes of significantly less than 20 mL, which realistically can be obtained in trials involving young children. Interestingly, investigators led by von Herrath succeeded in using HLA class I tetramers to analyze pancreatic islets from T1D patients<sup>14</sup>. Somewhat astonishingly, on average no more than two to nine CD8+ T cells, the dominant lymphocyte type in islet infiltrates, were present per islet; tetramer staining revealed recognition of one or multiple antigens by these cells.

Tetramers have also provided interesting insight into insulin B<sub>9-23</sub>-specific CD4+ T cell responses restricted by the strongly T1D-associated allele HLA-DQ8 (DQB1\*03:02). T cells with this specificity were found in six out of 16 patients and recognized denatured but not native antigen. The authors speculate that the disulfide bridges in native insulin might inhibit processing by myeloid cells, perhaps suggesting special processing pathways overcoming this inhibition in pancreatic islets (see also below)<sup>15</sup>. DQ8-restricted CD4+ T cells recognizing PI (C peptide in this case) were also found in islet infiltrates of a T1D patient and among blood lymphocytes of several T1D patients<sup>16</sup>. Interestingly, in both studies, autoreactive DQ8-restricted T cells were exclusively found in patients, an unusual feature given that autoimmunity generally leads to amplification and activation but not *de novo* appearance of autoreactive cells, which are also present in healthy individuals. As recently reviewed by Ehlers and Rigby<sup>17</sup>, it is well documented that self-reactive T cells tend to have a naïve phenotype in healthy individuals but a memory phenotype in subjects with T1D.

ZnT8 has also joined the ranks of CD4+ T cell-recognized autoantigens in human T1D. T1D patients responded to a larger number of ZnT8 epitopes with greater proliferative responses<sup>18</sup>; moreover, ZnT8-specific CD4+ T cells were skewed towards T helper 1 (Th1) cells in T1D patients, while Th2 and IL-10-producing cells were prevalent in healthy adults<sup>19</sup>. We have found that ZnT8 is a major autoantigen for CD8+ T cells in pediatric diabetes<sup>20</sup>; as transfer of ZnT8-specific human CD8+ T cells can induce diabetes in HLA-humanized mice, such cells may play an important role in the human pathology<sup>21</sup>.

Because tetramer detection of human CD4+ T cells recognizing islet cell antigens generally requires their prior expansion, methods for quantitative assessment of such cells in untouched lymphocytes could be of substantial interest. Eugster and colleagues analyzed sequences of 1650 T cell receptors (TCRs), obtained from six patients, recognizing the dominant DR4-restricted epitope GAD 557I and then used next-generation sequencing to determine the frequency of individual TCR sequences among patient CD4+ cells, which was found to rank from <0.00001 to 1.6%<sup>22</sup>. Disappointingly, there were almost as many different TCR sequences as T cell clones, suggesting that specific TCR-targeted therapies have little chance of success.

## Novel insights on frequency and expression signatures of self-reactive T cells

While the vast majority of research efforts concerning autoreactive T cells has focused on detecting and enumerating such cells, possibly combined with limited functional analyses, recent studies suggest that exploration of adaptive autoimmunity should go beyond this step and aim to perform in-depth characterization of phenotypic and functional properties. One critical finding is the abundance of the self-reactive T cell repertoire in healthy individuals and the surprisingly limited purging of it during thymic education. Yu and colleagues found that T cells recognizing male antigens were only threefold more abundant in females than in males, with full cytotoxic potential and equivalent tetramer staining intensity for cells from male and female donors. Moreover, the frequency range of self-reactive cells was similar to that of cells recognizing foreign antigens<sup>23</sup>. As an example, the frequency of T cells recognizing a dominant insulin epitope (B<sub>10-18</sub>) was 1 in 10<sup>4</sup>, with only a 2.66-fold increase in T1D patients. Similar findings were reported by Maeda *et al.* for T cells recognizing Melan-A<sup>24</sup>. However, in both studies, self-reactive CD8+ T cells were anergic when challenged with antigen, reflected in distinct gene expression profiles including low Bcl-2 expression and up-regulation of CTLA-4. Interestingly, anergic self-reactive CD8+ T cells may not only indicate the absence of auto-aggressive responses in healthy individuals but also play a beneficial role in patients with ongoing autoimmunity, since such cells increase in frequency upon treatment with CD3 antibodies<sup>25</sup>.

Another study suggested that not only is looking at gene expression profiles of self-reactive cells more informative than counting cells but also screening for self-reactivity can sometimes be omitted when searching for gene expression profiles with prognostic value in organ-specific autoimmune diseases. McKinney and associates compared gene expression by single CD8+ T cells from patients with chronic infections and patients with autoimmune diseases and found a profile indicative of T cell exhaustion with good clinical outcome in the latter but poor outcome and response to therapy in the former setting<sup>26</sup>. A single surrogate marker, the anti-apoptotic transcription factor KAT2B, correlated with progression to disease in children at risk of T1D and with triggering of autoimmunity in the NOD model. Thus, one might say that one of the most interesting surrogate markers of progression to T1D described so far was identified while ignoring the antigenic specificity of the CD8+ T cells examined. Why a surprisingly large number of peripheral blood T cells would express a signature indicating progressive disease is unclear; however, this may be related to systemic immune and metabolic alterations in pre-diabetic children, such as a type 1 interferon (IFN) transcription signature<sup>27</sup> and altered lipid and amino acid metabolism<sup>28</sup>. Whatever the reason for the findings of McKinney *et al.*, they indicate that the search for surrogate markers of disease progression or immunotherapeutic effects in T1D should not be limited to self-reactive T cells or, to be more precise, should not be limited to cells detectable with tetramers. This is not only because systemic effects of a type 1 IFN signature and of metabolic perturbation might produce surrogate markers in non-autoreactive cells but also because many autoreactive cells are likely to escape detection due to the frequently low affinity of self-reactive T cells. This was impressively demonstrated by Sabatino and colleagues, who used a novel method (micropipette adhesion

frequency assay) to show that low-affinity, tetramer-undetectable but fully functionally competent T cells outnumbered tetramer-detectable cells in both an anti-viral and an autoimmune response<sup>29</sup>. In conclusion, recent technological advances, in particular single cell technology, have opened up new avenues for the identification of surrogate markers of T1D risk, rate of progression, and response to immunotherapy. These technologies should now be applied to the analysis of different immune cell populations from T1D patients including, but not limited to, self-reactive T lymphocytes.

## Are self-reactive T cell responses unique?

Results obtained in the last 5 years have provided more evidence for some unique features preferentially found in self-reactive T cell responses. One of them is the unusual interaction among TCR, peptide, and MHC molecule resulting in weak avidity. Lamont and colleagues identified a self-peptide (an epitope in the insulin A chain) lacking the C-terminal anchor residue and thus extending the list of self-epitopes filling MHC peptide-binding sites only partially, a feature thought to facilitate escape from thymic negative selection<sup>30</sup>. Bulek and colleagues found another mechanism resulting in “ultra-weak” TCR-pMHC interaction (studying presentation of PPI<sub>15-24</sub> by HLA-A2), in which an extremely peptide-centric TCR-pMHC interaction limited TCR-MHC interactions to a “light touch” unlikely to be sufficient for negative selection<sup>31</sup>. Post-translational epitope modification in the periphery (in this case by transglutaminase) is another mechanism allowing epitopes to escape negative selection and has recently been suggested to be implicated in the autoantigenicity of a chromogranin A epitope (one of the epitopes filling the peptide binding site partially) recognized by the popular BDC2.5 CD4+ T cells<sup>32</sup>. Similarly, citrullination of the GRP78 protein specifically in the NOD beta cells induces the translocation of this chaperone from the endoplasmic reticulum to the plasma membrane and generates a novel autoantigen recognized by effector T cells<sup>33</sup>.

An additional mechanism contributing to escape from thymic deletion is the phenomenon of type B CD4+ T cells. This type of T cell, identified first and studied in depth by Unanue’s group, recognizes cognate peptides exogenously added to antigen-presenting cells (APCs), but not peptides produced within APCs from native antigen (at least when peptide loading occurs in standard H-2M-equipped intracellular compartments)<sup>34</sup>. In the NOD model, Mohan and colleagues found that the majority of islet-infiltrating CD4+ T cells recognizing insulin B<sub>9-23</sub> were of type B. Having previously shown that type B clones transferred diabetes, the group demonstrated that a mouse expressing the transgenic type B TCR 8F10 on a RAG knockout background developed T1D with faster kinetics than an analogous mouse expressing a standard type A TCR (recognizing both exogenous and APC-processed peptide)<sup>35</sup>. Interestingly, diabetes was also triggered by 8F10 cells in mice lacking pancreatic lymph nodes, suggesting that stimulation of type B T cells can occur directly in islets, bypassing for unknown reasons the requirement for priming by APCs migrating to lymph nodes documented for other T cells recognizing islet antigens. Presumably, dendritic cells (DCs) reaching into islet vessels attract such cells<sup>36</sup>; whether direct expression of MHC class II by beta cells, recently confirmed to occur in the NOD model, plays a role in recruiting type B T cells, or any autoreactive CD4+ T cells, into islets remains to be determined<sup>37</sup>.



### Insulin recognition by CD4+ T cells

Insulin is arguably the “number one” autoantigen in the NOD model of T1D, not only because of its expression restricted to beta cells, the association of its genetic polymorphism with disease risk, and the role of its recognition in initial triggering of the autoimmune response<sup>38</sup> but also because the structural basis of its recognition by CD4+ T cells is well understood and provides more evidence for the key role of unusual TCR-pMHC interactions in T1D. The insulin B chain fragment 9–23 has long been known as the key self-epitope recognized by murine and human CD4+ T cells. Examining the interaction of this peptide with the murine MHC class II molecule I-A<sup>g7</sup>, Stadinski and colleagues identified four possible “binding registers” of which number 1 and 2 were most efficient<sup>39</sup>. Surprisingly, four different T cell clones examined recognized register 3, the least efficient register due to a conflict between the p9 peptide residue and the p9 binding site pocket. The authors proposed that particularly poor autoantigen presentation underlies the predisposing effect of some MHC class II alleles in T1D and postulated that only the very high insulin concentrations in islets allow for the formation of MHC complexes with poor ligands, consistent with a model proposed by Unanue and colleagues<sup>40</sup>. Given that activation of many T cells recognizing register 3 can be ameliorated by removing a glutamic acid in p8 (residue B<sub>21</sub>), the authors speculated that an islet-specific processing (i.e. proteolytic) event might remove this residue, thus creating a “cryptic” epitope absent during thymic T cell selection<sup>41</sup>.

A similar study by Unanue’s group agreed that I-A<sup>g7</sup> can bind B<sub>9-23</sub> in multiple registers; however, the authors did not find any T cells recognizing register 3<sup>42</sup>. Standard type A T cells recognized the efficient register 1, but type B cells dominating responses upon immunization with B<sub>9-23</sub> reacted with register 2 presented poorly by I-A<sup>g7</sup>.

Because I-A<sup>g7</sup>-restricted CD4+ T cell responses to B<sub>10-23</sub> trigger islet cell autoimmunity, studying specific responses in non-autoimmune mice expressing I-A<sup>g7</sup> might reveal insight into the regulatory mechanisms that protect against T1D. Pauken and colleagues found specific T cells both in NOD mice and in C57BL/6 mice expressing I-A<sup>g7</sup><sup>43</sup>. Interestingly, in the pancreatic lymph nodes of young NOD mice, i.e. in early pre-diabetes, the majority of these cells were anergic or expressed Foxp3 and IFN- $\gamma$  expression was limited to intra-islet cells. However, in non-autoimmune B6/I-A<sup>g7</sup> mice, B<sub>10-23</sub> reactive cells remained naïve, suggesting that they did not encounter antigen. Therefore, islet insults or inflammation in the NOD mouse are likely to precede priming of key autoreactive CD4+ T cells.

Collectively, the molecular and functional characterization of autoreactive T cells from patients and in the NOD model raises a number of intriguing questions. How common is “ultra-weak” TCR/pHLA interaction in human T1D, and what are the mechanisms underlying low-avidity interactions? Can the micropipette adhesion assay reveal an additional autoreactive repertoire in human T1D? Are type B CD4+ T cells as critical in humans as they are in the NOD model? Finally, are there specific processing/proteolytic events producing “cryptic” epitopes in pancreatic islets?

### Antigen-based immunotherapy trials in patients

Given encouraging results of prior preclinical or human pilot studies, hopes had been raised that antigen-based immunotherapy might provide a safe and efficient strategy to prevent or even cure human T1D. Unfortunately, the trials concluded in recent years have almost completely failed to provide any evidence of clinical efficacy. Treatment starting with nasally applied insulin at T1D onset of 52 adult patients not requiring exogenous insulin had no effect on C peptide levels or progression to dependence on exogenous insulin<sup>44</sup>, thereby repeating a previous failure of a trial of oral insulin. Immunization of 12 patients with newly diagnosed T1D with insulin B chain in incomplete Freund’s adjuvant induced robust insulin-specific adaptive responses, but a clinical effect was not noted<sup>45</sup>. Two independent and relatively large trials in which patients were injected within 3 months of disease onset with GAD and alum adjuvant also showed no effect on C peptide levels or insulin requirement<sup>46,47</sup>. However, as has been commented on by others<sup>48</sup>, the regimens used in the GAD trials differed in numerous parameters (dose, route of injection, timing relative to disease onset, and use of alum adjuvant) from those tested in preclinical experiments, making trial failure appear less surprising. The single glimpse of hope published derives from a trial in which a PI-encoding plasmid was injected for 12 weeks after disease onset<sup>49</sup>. One of the regimens resulted in a transient increase of C peptide levels by 15% (vs. -10% for placebo) at 15 weeks after start of treatment. The authors also noted a decrease in CD8+ T cells specific for one peptide/HLA combination, although it was not clear whether this decrease was related to the transient clinical response.

Globally, it is safe to say that antigen-based therapy is far from having met expectations and that new avenues must be explored to produce more encouraging results. Presently, immunomodulatory approaches, particularly CD3 antibodies, remain the “gold standard” with respect to efficacy<sup>50,51</sup>, although transient EBV reactivation by anti-CD3 dosing schemes with the best clinical efficacy has been a source of concern<sup>52</sup>. Only short-term treatment with CD3 antibodies has been able to suppress the rise in insulin requirement over a period of 48 months<sup>53</sup>. Others better placed than we are have made recommendations on how to make progress, which we wish to reiterate here<sup>8,48,54</sup>. The need for better biomarkers has been formulated repeatedly but remains as urgent as ever. More research on the natural history of T1D, including the issues formulated above, is required to design more efficient therapies. *In vitro* studies with human samples, and large-scale in-depth characterization of the autoimmune response as outlined above, should be performed. The focus should be on preventing T1D onset. Small pilot studies based on rigorous hypothesis testing in the preclinical model and including mechanistic outcome studies should be preferred to large studies as performed in the past. Novel therapeutic strategies developed in the NOD model may also point the way to more efficient antigen-based immune intervention.

### Novel strategies for antigen-based immune therapy of T1D

The last few years have seen a wealth of novel ideas on how to treat or prevent T1D, most of them developed and tested in the NOD model. One of these uses targeting of complete autoantigens to

specific APC receptors to induce regulatory responses. Targeting of self or non-self proteins to the DC asialoglycoprotein receptor induces suppressive T regulatory type 1 (Tr1) cells secreting large amounts of IL-10 but little tumor necrosis factor- $\alpha$ , IFN- $\gamma$ , and IL-2, which are all produced upon targeting of the same proteins to Dectin-1, DC-SIGN, or Lox1<sup>55</sup>. Interestingly, the approach also works in cynomolgus macaques; however, its efficacy in a pre-existing autoimmune setting has not been tested. Another approach uses *Lactococcus lactis* engineered to secrete PI and IL-10; in combination with low-dose parenteral anti-CD3, oral administration of these bacteria to freshly diabetic mice can induce lasting remission of T1D, possibly due to the induction of PI-specific regulatory T cells found in the intestinal mucosa and in islets<sup>56</sup>.

Various other recent strategies use self-epitopes to attenuate the autoimmune response. Injection of 10-week-old mice with a lentivirus, driving exclusive expression of B<sub>9-23</sub> in hepatocytes due to a microRNA sequence, induces peptide-specific CD8+ T cells and regulatory T cells and halts the progression of T1D; combining the virus with low-dose anti-CD3 may induce remission of T1D<sup>57</sup>. Administration of a super-agonist variant of B<sub>9-23</sub> with strongly enhanced stimulatory capacity provides complete protection from T1D if this peptide is delivered in subimmunogenic doses via an osmotic pump, starting at a young age, or via a DEC205-targeted fusion antibody. The protective effect was reflected in an increase of Foxp3+ T cells and a decrease in IFN- $\gamma$  and IL-17 production. However, the necessity of administration during very early pre-diabetes and of determining the precise subimmunogenic dose will complicate the practical application of this strategy<sup>58</sup>. Others have proposed using TCR-like antibodies blocking or deleting specific autoreactive T cell populations<sup>59,60</sup>, or to produce tetramers targeting presumably pathogenic T cells and eliminating them by inducing apoptosis or by directly killing them through tetramer conjugation with saponin<sup>61,62</sup>. Some of these approaches can reduce the number of the targeted T cells significantly *in vivo* and delay or reduce onset of T1D. Determining biomarker profiles of patients prior to antigen-based immunotherapy may be key for the success of such treatments.

Probably the most exciting novel approach was reported during the drafting of this article by the group of Santamaria<sup>63</sup>. This group had previously demonstrated protection from spontaneous diabetes in the NOD model upon stimulation and expansion of autoantigen-experienced CD8+ T cells by nanoparticles coated with cognate MHC-class I/peptide complexes<sup>64</sup>. Applying this approach to stimulating CD4+ T cells by nanoparticles coated with MHC class II/peptide complexes, the group could now show that the novel strategy can not only prevent and revert T1D in the NOD model but also attenuate autoimmune inflammation in rodent models of collagen-induced autoimmune arthritis and in experimental autoimmune encephalomyelitis. Remarkably, the approach even works when T cells recognizing subdominant epitopes are targeted. Applied to patients, this would obviate the need for identifying dominant or triggering epitopes and T cell populations, thereby removing one of the major obstacles to epitope-based immunotherapy in the outbred human population. The strategy seems to work by converting Th1 memory cells to Tr1 cells producing IL-10 and transforming growth factor- $\beta$ , which in turn induce the differentiation of cognate regulatory B lymphocytes producing IL-10. Expanded Tr1 and regulatory B lymphocytes then suppress autoimmunity in a synergistic

manner, presumably both by direct effects on effector T cells and by suppressing the pro-inflammatory action of cognate APCs<sup>63</sup>. A limitation of the strategy is the need to maintain bi-weekly treatment, since about half of NOD mice relapse with disease upon interruption of treatment.

### Concluding remarks

The period reviewed in this article has witnessed significant progress in the mechanistic understanding of autoantigen recognition and the development of some novel tools for monitoring the cellular autoimmune response in T1D. However, much remains to be learned with respect to the phenotype and function of pathogenic and protective human T cells, and surrogate markers of disease progression and response to therapy are still urgently needed. Moreover, the initial events activating autoreactive T cells and subsequent factors, both genetic and environmental, resulting in expansion rather than silencing of such cells remain poorly understood. The very recent finding that islet-infiltrating CD4+ T cells both in the NOD model and in T1D patients can recognize covalently linked hybrids of PI peptides with other beta cell peptides highlights the need to better understand the peculiar antigen processing environment in the islet organ<sup>65</sup>. This important finding may also suggest that the antigens used in previous trials of antigen-specific immunotherapy may not have been optimal. We anticipate that the application of recent technologies to highly multiplexed analysis of gene and protein expression by single human cells will make an important contribution to identifying surrogate markers and advancing our mechanistic understanding of human T1D. Recent results also suggest that simple oral or parenteral administration of autoantigens may stand little chance in achieving remission of human T1D. Given that CD3 antibodies so far have produced the most promising results, combining antigen administration with anti-CD3 has become a preferred option for many in the field. The future will show whether novel approaches such as those cited above can obviate the need for broadly immunomodulatory components in combination therapies or enhance their therapeutic efficacy.

### Abbreviations

APC, antigen-presenting cell; DC, dendritic cell; ELISpot, enzyme-linked immunosorbent spot; GAD, glutamic acid decarboxylase; HLA, human leukocyte antigen; IFN, interferon; IL, interleukin; MHC, major histocompatibility complex; NOD, nonobese diabetic; (P)PI, (pre-)proinsulin; T1D, type 1 diabetes; TCR, T cell receptor; Tr1, T regulatory type 1.

### Competing interests

The authors declare that they have no competing interests.

### Grant information

Work in the authors' laboratory is supported by grants from *Fondation pour la Recherche Médicale* (DEQ20130326539) and *Idex Sorbonne Paris Cité* to PvE, by a grant from *Aide aux Jeunes Diabétiques* to FXM and PvE, and by grants from EFSD-Lilly and from the Juvenile Diabetes Research Foundation (47-2013-524 and 2-SRA-2015-73) to JD.

*The funders had no role in study design, data collection and analysis, decision to publish, or preparation of the manuscript.*

## References



1. **F** Stadinski B, Kappler J, Eisenbarth GS: **Molecular targeting of islet autoantigens.** *Immunity.* 2010; **32**(4): 446–456.  
[PubMed Abstract](#) | [Publisher Full Text](#) | [F1000 Recommendation](#)
2. **F** Babad J, Gelliebter A, DiLorenzo TP: **T-cell autoantigens in the non-obese diabetic mouse model of autoimmune diabetes.** *Immunology.* 2010; **131**(4): 459–465.  
[PubMed Abstract](#) | [Publisher Full Text](#) | [Free Full Text](#) | [F1000 Recommendation](#)
3. Wenzlau JM, Frisch LM, Gardner TJ, *et al.*: **Novel antigens in type 1 diabetes: the importance of ZnT8.** *Curr Diab Rep.* 2009; **9**(2): 105–112.  
[PubMed Abstract](#) | [Publisher Full Text](#)
4. **F** Unanue ER: **Antigen presentation in the autoimmune diabetes of the NOD mouse.** *Annu Rev Immunol.* 2014; **32**: 579–608.  
[PubMed Abstract](#) | [Publisher Full Text](#) | [F1000 Recommendation](#)
5. Hinman RM, Cambier JC: **Role of B lymphocytes in the pathogenesis of type 1 diabetes.** *Curr Diab Rep.* 2014; **14**(11): 543.  
[PubMed Abstract](#) | [Publisher Full Text](#)
6. Tooley JE, Herold KC: **Biomarkers in type 1 diabetes: application to the clinical trial setting.** *Curr Opin Endocrinol Diabetes Obes.* 2014; **21**(4): 287–292.  
[PubMed Abstract](#) | [Publisher Full Text](#) | [Free Full Text](#)
7. Odegard JM, Nepom GT, Wambre E: **Biomarkers for antigen immunotherapy in allergy and type 1 diabetes.** *Clin Immunol.* 2015; **161**(1): 44–50.  
[PubMed Abstract](#) | [Publisher Full Text](#) | [Free Full Text](#)
8. Greenbaum CJ, Schatz DA, Haller MJ, *et al.*: **Through the fog: recent clinical trials to preserve  $\beta$ -cell function in type 1 diabetes.** *Diabetes.* 2012; **61**(6): 1323–1330.  
[PubMed Abstract](#) | [Publisher Full Text](#) | [Free Full Text](#)
9. **F** Long SA, Rieck M, Sanda S, *et al.*: **Rapamycin/IL-2 combination therapy in patients with type 1 diabetes augments Tregs yet transiently impairs  $\beta$ -cell function.** *Diabetes.* 2012; **61**(9): 2340–2348.  
[PubMed Abstract](#) | [Publisher Full Text](#) | [Free Full Text](#) | [F1000 Recommendation](#)
10. Sarikonda G, Sachithanantham S, Manenkova Y, *et al.*: **Transient B-cell depletion with anti-CD20 in combination with proinsulin DNA vaccine or oral insulin: immunologic effects and efficacy in NOD mice.** *PLoS one.* 2013; **8**(2): e54712.  
[PubMed Abstract](#) | [Publisher Full Text](#) | [Free Full Text](#)
11. Kronenberg D, Knight RR, Estorninho M, *et al.*: **Circulating proinsulin signal peptide-specific CD8 T cells restricted by the susceptibility molecule HLA-A24 are expanded at onset of type 1 diabetes and kill  $\beta$ -cells.** *Diabetes.* 2012; **61**(7): 1752–1759.  
[PubMed Abstract](#) | [Publisher Full Text](#) | [Free Full Text](#)
12. Unger WW, Velthuis J, Abreu JR, *et al.*: **Discovery of low-affinity proinsulin epitopes and detection of autoreactive CD8 T-cells using combinatorial MHC multimers.** *J Autoimmun.* 2011; **37**(3): 151–159.  
[PubMed Abstract](#) | [Publisher Full Text](#)
13. **F** Velthuis JH, Unger WW, Abreu JR, *et al.*: **Simultaneous detection of circulating autoreactive CD8<sup>+</sup> T-cells specific for different islet cell-associated epitopes using combinatorial MHC multimers.** *Diabetes.* 2010; **59**(7): 1721–1730.  
[PubMed Abstract](#) | [Publisher Full Text](#) | [Free Full Text](#) | [F1000 Recommendation](#)
14. **F** Coppieters KT, Dotta F, Amirian N, *et al.*: **Demonstration of islet-autoreactive CD8 T cells in insulinitis lesions from recent onset and long-term type 1 diabetes patients.** *J Exp Med.* 2012; **209**(1): 51–60.  
[PubMed Abstract](#) | [Publisher Full Text](#) | [Free Full Text](#) | [F1000 Recommendation](#)
15. **F** Yang J, Chow IT, Sosinowski T, *et al.*: **Autoreactive T cells specific for insulin B:11-23 recognize a low-affinity peptide register in human subjects with autoimmune diabetes.** *Proc Natl Acad Sci U S A.* 2014; **111**(41): 14840–14845.  
[PubMed Abstract](#) | [Publisher Full Text](#) | [Free Full Text](#) | [F1000 Recommendation](#)
16. **F** Pathiraja V, Kuehlich JP, Campbell PD, *et al.*: **Proinsulin-specific, HLA-DQ8, and HLA-DQ8-transdimer-restricted CD4<sup>+</sup> T cells infiltrate islets in type 1 diabetes.** *Diabetes.* 2015; **64**(1): 172–182.  
[PubMed Abstract](#) | [Publisher Full Text](#) | [F1000 Recommendation](#)
17. Ehlers MR, Rigby MR: **Targeting memory T cells in type 1 diabetes.** *Curr Diab Rep.* 2015; **15**(11): 84.  
[PubMed Abstract](#) | [Publisher Full Text](#)
18. Dang M, Rockell J, Wagner R, *et al.*: **Human type 1 diabetes is associated with T cell autoimmunity to zinc transporter 8.** *J Immunol.* 2011; **186**(10): 6056–6063.  
[PubMed Abstract](#) | [Publisher Full Text](#) | [Free Full Text](#)
19. Chujo D, Foucat E, Nguyen TS, *et al.*: **ZnT8-Specific CD4<sup>+</sup> T cells display distinct cytokine expression profiles between type 1 diabetes patients and healthy adults.** *PLoS One.* 2013; **8**(2): e55595.  
[PubMed Abstract](#) | [Publisher Full Text](#) | [Free Full Text](#)
20. Éné E, Kratzer R, Amoux JB, *et al.*: **ZnT8 is a major CD8<sup>+</sup> T cell-recognized autoantigen in pediatric type 1 diabetes.** *Diabetes.* 2012; **61**(7): 1779–1784.  
[PubMed Abstract](#) | [Publisher Full Text](#) | [Free Full Text](#)
21. Li S, Li H, Chen B, *et al.*: **Identification of novel HLA-A 0201-restricted cytotoxic T lymphocyte epitopes from Zinc Transporter 8.** *Vaccine.* 2013; **31**(12): 1610–1615.  
[PubMed Abstract](#) | [Publisher Full Text](#)
22. **F** Eugster A, Lindner A, Catani M, *et al.*: **High diversity in the TCR repertoire of GAD65 autoantigen-specific human CD4<sup>+</sup> T cells.** *J Immunol.* 2015; **194**(6): 2531–2538.  
[PubMed Abstract](#) | [Publisher Full Text](#) | [F1000 Recommendation](#)
23. Yu W, Jiang N, Ebert PJ, *et al.*: **Clonal Deletion Prunes but Does Not Eliminate Self-Specific  $\alpha\beta$  CD8<sup>+</sup> T Lymphocytes.** *Immunity.* 2015; **42**(5): 929–941.  
[PubMed Abstract](#) | [Publisher Full Text](#) | [Free Full Text](#)
24. Maeda Y, Nishikawa H, Sugiyama D, *et al.*: **Detection of self-reactive CD8<sup>+</sup> T cells with an anergic phenotype in healthy individuals.** *Science.* 2014; **346**(6216): 1536–1540.  
[PubMed Abstract](#) | [Publisher Full Text](#)
25. **F** Tooley JE, Vudattu N, Choi J, *et al.*: **Changes in T-cell subsets identify responders to FcR-nonbinding anti-CD3 mAb (teplizumab) in patients with type 1 diabetes.** *Eur J Immunol.* 2016; **46**(1): 230–241.  
[PubMed Abstract](#) | [Publisher Full Text](#) | [F1000 Recommendation](#)
26. **F** McKinney EF, Lee JC, Jayne DR, *et al.*: **T-cell exhaustion, co-stimulation and clinical outcome in autoimmunity and infection.** *Nature.* 2015; **523**(7562): 612–616.  
[PubMed Abstract](#) | [Publisher Full Text](#) | [Free Full Text](#) | [F1000 Recommendation](#)
27. **F** Ferreira RC, Guo H, Coulson RM, *et al.*: **A type I interferon transcriptional signature precedes autoimmunity in children genetically at risk for type 1 diabetes.** *Diabetes.* 2014; **63**(7): 2538–2550.  
[PubMed Abstract](#) | [Publisher Full Text](#) | [Free Full Text](#) | [F1000 Recommendation](#)
28. **F** Oresic M, Simell S, Sysi-Aho M, *et al.*: **Dysregulation of lipid and amino acid metabolism precedes islet autoimmunity in children who later progress to type 1 diabetes.** *J Exp Med.* 2008; **205**(13): 2975–2984.  
[PubMed Abstract](#) | [Publisher Full Text](#) | [Free Full Text](#) | [F1000 Recommendation](#)
29. **F** Sabatino JJ Jr, Huang J, Zhu C, *et al.*: **High prevalence of low affinity peptide-MHC II tetramer-negative effectors during polyclonal CD4<sup>+</sup> T cell responses.** *J Exp Med.* 2011; **208**(1): 81–90.  
[PubMed Abstract](#) | [Publisher Full Text](#) | [Free Full Text](#) | [F1000 Recommendation](#)
30. **F** Lamont D, Mukherjee G, Kumar PR, *et al.*: **Compensatory mechanisms allow undersized anchor-deficient class I MHC ligands to mediate pathogenic autoreactive T cell responses.** *J Immunol.* 2014; **193**(5): 2135–2146.  
[PubMed Abstract](#) | [Publisher Full Text](#) | [Free Full Text](#) | [F1000 Recommendation](#)
31. **F** Bulek AM, Cole DK, Skowera A, *et al.*: **Structural basis for the killing of human beta cells by CD8<sup>+</sup> T cells in type 1 diabetes.** *Nat Immunol.* 2012; **13**(3): 283–289.  
[PubMed Abstract](#) | [Publisher Full Text](#) | [Free Full Text](#) | [F1000 Recommendation](#)
32. Delong T, Baker RL, He J, *et al.*: **Diabetogenic T-cell clones recognize an altered peptide of chromogranin A.** *Diabetes.* 2012; **61**(12): 3239–3246.  
[PubMed Abstract](#) | [Publisher Full Text](#) | [Free Full Text](#)
33. **F** Rondas D, Crèvecoeur I, D'Hertog W, *et al.*: **Citrullinated glucose-regulated protein 78 is an autoantigen in type 1 diabetes.** *Diabetes.* 2015; **64**(2): 573–586.  
[PubMed Abstract](#) | [Publisher Full Text](#) | [F1000 Recommendation](#)
34. **F** Mohan JF, Unanue ER: **Unconventional recognition of peptides by T cells and the implications for autoimmunity.** *Nat Rev Immunol.* 2012; **12**(10): 721–728.  
[PubMed Abstract](#) | [Publisher Full Text](#) | [F1000 Recommendation](#)
35. **F** Mohan JF, Calderon B, Anderson MS, *et al.*: **Pathogenic CD4<sup>+</sup> T cells recognizing an unstable peptide of insulin are directly recruited into islets bypassing local lymph nodes.** *J Exp Med.* 2013; **210**(11): 2403–2414.  
[PubMed Abstract](#) | [Publisher Full Text](#) | [Free Full Text](#) | [F1000 Recommendation](#)
36. **F** Calderon B, Carrero JA, Miller MJ, *et al.*: **Cellular and molecular events in the localization of diabetogenic T cells to islets of Langerhans.** *Proc Natl Acad Sci U S A.* 2011; **108**(4): 1561–1566.  
[PubMed Abstract](#) | [Publisher Full Text](#) | [Free Full Text](#) | [F1000 Recommendation](#)
37. Zhao Y, Scott NA, Quah HS, *et al.*: **Mouse pancreatic beta cells express MHC class II and stimulate CD4<sup>+</sup> T cells to proliferate.** *Eur J Immunol.* 2015; **45**(9): 2494–2503.  
[PubMed Abstract](#) | [Publisher Full Text](#)
38. **F** Nakayama M, Abiru N, Moriyama H, *et al.*: **Prime role for an insulin epitope in the development of type 1 diabetes in NOD mice.** *Nature.* 2005; **435**(7039): 220–223.  
[PubMed Abstract](#) | [Publisher Full Text](#) | [Free Full Text](#) | [F1000 Recommendation](#)
39. **F** Stadinski BD, Zhang L, Crawford F, *et al.*: **Diabetogenic T cells recognize insulin bound to IA<sup>g</sup> in an unexpected, weakly binding register.** *Proc Natl Acad Sci U S A.* 2010; **107**(24): 10978–10983.  
[PubMed Abstract](#) | [Publisher Full Text](#) | [Free Full Text](#) | [F1000 Recommendation](#)
40. Suri A, Levisetti MG, Unanue ER: **Do the peptide-binding properties of diabetogenic class II molecules explain autoreactivity?** *Curr Opin Immunol.* 2008; **20**(1): 105–110.  
[PubMed Abstract](#) | [Publisher Full Text](#) | [Free Full Text](#)
41. Crawford F, Stadinski B, Jin N, *et al.*: **Specificity and detection of insulin-reactive CD4<sup>+</sup> T cells in type 1 diabetes in the nonobese diabetic (NOD) mouse.** *Proc Natl Acad Sci U S A.* 2011; **108**(40): 16729–16734.  
[PubMed Abstract](#) | [Publisher Full Text](#) | [Free Full Text](#)
42. **F** Mohan JF, Petzold SJ, Unanue ER: **Register shifting of an insulin peptide-MHC**

- complex allows diabetogenic T cells to escape thymic deletion. *J Exp Med*. 2011; **208**(12): 2375–2383.  
[PubMed Abstract](#) | [Publisher Full Text](#) | [Free Full Text](#) | [F1000 Recommendation](#)
43. **F** Pauken KE, Linehan JL, Spanier JA, *et al.*: Cutting edge: type 1 diabetes occurs despite robust anergy among endogenous insulin-specific CD4<sup>+</sup> T cells in NOD mice. *J Immunol*. 2013; **191**(10): 4913–4917.  
[PubMed Abstract](#) | [Publisher Full Text](#) | [Free Full Text](#) | [F1000 Recommendation](#)
44. **F** Fourlanos S, Perry C, Gellert SA, *et al.*: Evidence that nasal insulin induces immune tolerance to insulin in adults with autoimmune diabetes. *Diabetes*. 2011; **60**(4): 1237–1245.  
[PubMed Abstract](#) | [Publisher Full Text](#) | [Free Full Text](#) | [F1000 Recommendation](#)
45. **F** Orban T, Farkas K, Jalahej H, *et al.*: Autoantigen-specific regulatory T cells induced in patients with type 1 diabetes mellitus by insulin B-chain immunotherapy. *J Autoimmun*. 2010; **34**(4): 408–415.  
[PubMed Abstract](#) | [Publisher Full Text](#) | [Free Full Text](#) | [F1000 Recommendation](#)
46. **F** Ludvigsson J, Krisky D, Casas R, *et al.*: GAD65 antigen therapy in recently diagnosed type 1 diabetes mellitus. *N Engl J Med*. 2012; **366**(5): 433–442.  
[PubMed Abstract](#) | [Publisher Full Text](#) | [F1000 Recommendation](#)
47. **F** Wherrett DK, Bundy B, Becker DJ, *et al.*: Antigen-based therapy with glutamic acid decarboxylase (GAD) vaccine in patients with recent-onset type 1 diabetes: a randomised double-blind trial. *Lancet*. 2011; **378**(9788): 319–327.  
[PubMed Abstract](#) | [Publisher Full Text](#) | [Free Full Text](#) | [F1000 Recommendation](#)
48. Tooley JE, Waldron-Lynch F, Herold KC: New and future immunomodulatory therapy in type 1 diabetes. *Trends Mol Med*. 2012; **18**(3): 173–181.  
[PubMed Abstract](#) | [Publisher Full Text](#) | [Free Full Text](#)
49. **F** Roep BO, Solvason N, Gottlieb PA, *et al.*: Plasmid-encoded proinsulin preserves C-peptide while specifically reducing proinsulin-specific CD8<sup>+</sup> T cells in type 1 diabetes. *Sci Transl Med*. 2013; **5**(191): 191ra82.  
[PubMed Abstract](#) | [Publisher Full Text](#) | [Free Full Text](#) | [F1000 Recommendation](#)
50. **F** Hagopian W, Ferry RJ Jr, Sherry N, *et al.*: Teplizumab preserves C-peptide in recent-onset type 1 diabetes: two-year results from the randomized, placebo-controlled Protégé trial. *Diabetes*. 2013; **62**(11): 3901–3908.  
[PubMed Abstract](#) | [Publisher Full Text](#) | [Free Full Text](#) | [F1000 Recommendation](#)
51. Herold KC, Gitelman SE, Ehlers MR, *et al.*: Teplizumab (anti-CD3 mAb) treatment preserves C-peptide responses in patients with new-onset type 1 diabetes in a randomized controlled trial: metabolic and immunologic features at baseline identify a subgroup of responders. *Diabetes*. 2013; **62**(11): 3766–3774.  
[PubMed Abstract](#) | [Publisher Full Text](#) | [Free Full Text](#)
52. Keymeulen B, Candon S, Fafi-Kremer S, *et al.*: Transient Epstein-Barr virus reactivation in CD3 monoclonal antibody-treated patients. *Blood*. 2010; **115**(6): 1145–1155.  
[PubMed Abstract](#) | [Publisher Full Text](#)
53. Keymeulen B, Walter M, Mathieu C, *et al.*: Four-year metabolic outcome of a randomised controlled CD3-antibody trial in recent-onset type 1 diabetic patients depends on their age and baseline residual beta cell mass. *Diabetologia*. 2010; **53**(4): 614–623.  
[PubMed Abstract](#) | [Publisher Full Text](#)
54. Matthews JB, Staeva TP, Bernstein PL, *et al.*: Developing combination immunotherapies for type 1 diabetes: recommendations from the ITN-JDRF Type 1 Diabetes Combination Therapy Assessment Group. *Clin Exp Immunol*. 2010; **160**(2): 176–184.  
[PubMed Abstract](#) | [Publisher Full Text](#) | [Free Full Text](#)
55. **F** Li D, Romain G, Flamar AL, *et al.*: Targeting self- and foreign antigens to dendritic cells via DC-ASGPR generates IL-10-producing suppressive CD4<sup>+</sup> T cells. *J Exp Med*. 2012; **209**(1): 109–121.  
[PubMed Abstract](#) | [Publisher Full Text](#) | [Free Full Text](#) | [F1000 Recommendation](#)
56. **F** Takiishi T, Korf H, van Belle TL, *et al.*: Reversal of autoimmune diabetes by restoration of antigen-specific tolerance using genetically modified *Lactococcus lactis* in mice. *J Clin Invest*. 2012; **122**(5): 1717–1725.  
[PubMed Abstract](#) | [Publisher Full Text](#) | [Free Full Text](#) | [F1000 Recommendation](#)
57. **F** Akbarpour M, Goudy KS, Cantore A, *et al.*: Insulin B chain 9-23 gene transfer to hepatocytes protects from type 1 diabetes by inducing Ag-specific FoxP3<sup>+</sup> T<sub>reg</sub> cells. *Sci Transl Med*. 2015; **7**(289): 289ra81.  
[PubMed Abstract](#) | [Publisher Full Text](#) | [F1000 Recommendation](#)
58. **F** Daniel C, Weigmann B, Bronson R, *et al.*: Prevention of type 1 diabetes in mice by tolerogenic vaccination with a strong agonist insulin mimotope. *J Exp Med*. 2011; **208**(7): 1501–1510.  
[PubMed Abstract](#) | [Publisher Full Text](#) | [Free Full Text](#) | [F1000 Recommendation](#)
59. **F** Dahan R, Gebe JA, Preisinger A, *et al.*: Antigen-specific immunomodulation for type 1 diabetes by novel recombinant antibodies directed against diabetes-associated auto-reactive T cell epitope. *J Autoimmun*. 2013; **47**: 83–93.  
[PubMed Abstract](#) | [Publisher Full Text](#) | [F1000 Recommendation](#)
60. **F** Zhang L, Crawford F, Yu L, *et al.*: Monoclonal antibody blocking the recognition of an insulin peptide-MHC complex modulates type 1 diabetes. *Proc Natl Acad Sci U S A*. 2014; **111**(7): 2656–2661.  
[PubMed Abstract](#) | [Publisher Full Text](#) | [Free Full Text](#) | [F1000 Recommendation](#)
61. **F** Samanta D, Mukherjee G, Ramagopal UA, *et al.*: Structural and functional characterization of a single-chain peptide-MHC molecule that modulates both naive and activated CD8<sup>+</sup> T cells. *Proc Natl Acad Sci U S A*. 2011; **108**(33): 13682–13687.  
[PubMed Abstract](#) | [Publisher Full Text](#) | [Free Full Text](#) | [F1000 Recommendation](#)
62. **F** Vincent BG, Young EF, Buntzman AS, *et al.*: Toxin-coupled MHC class I tetramers can specifically ablate autoreactive CD8<sup>+</sup> T cells and delay diabetes in nonobese diabetic mice. *J Immunol*. 2010; **184**(8): 4196–4204.  
[PubMed Abstract](#) | [Publisher Full Text](#) | [Free Full Text](#) | [F1000 Recommendation](#)
63. **F** Clemente-Casares X, Blanco J, Ambalavanan P, *et al.*: Expanding antigen-specific regulatory networks to treat autoimmunity. *Nature*. 2016; **530**(7591): 434–440.  
[PubMed Abstract](#) | [Publisher Full Text](#) | [F1000 Recommendation](#)
64. **F** Tsai S, Shamel A, Yamanouchi J, *et al.*: Reversal of autoimmunity by boosting memory-like autoregulatory T cells. *Immunity*. 2010; **32**(4): 568–580.  
[PubMed Abstract](#) | [Publisher Full Text](#) | [F1000 Recommendation](#)
65. **F** Delong T, Wiles TA, Baker RL, *et al.*: Pathogenic CD4<sup>+</sup> T cells in type 1 diabetes recognize epitopes formed by peptide fusion. *Science*. 2016; **351**(6274): 711–714.  
[PubMed Abstract](#) | [Publisher Full Text](#) | [F1000 Recommendation](#)

## Open Peer Review

Current Referee Status:



---

### Editorial Note on the Review Process

**F1000 Faculty Reviews** are commissioned from members of the prestigious **F1000 Faculty** and are edited as a service to readers. In order to make these reviews as comprehensive and accessible as possible, the referees provide input before publication and only the final, revised version is published. The referees who approved the final version are listed with their names and affiliations but without their reports on earlier versions (any comments will already have been addressed in the published version).

---

### The referees who approved this article are:

#### Version 1

- 1 Kathryn M. Haskins**, <sup>1,2</sup> <sup>1</sup> Department of Immunology and Microbiology, University of Colorado School of Medicine at Denver, Aurora, Colorado, 80045, USA  
<sup>2</sup> Department of Biomedical Research, National Jewish Health, Denver, Colorado, USA  
**Competing Interests:** No competing interests were disclosed.
- 2 Massimo Pietropaolo**, Division of Diabetes, Endocrinology and Metabolism, McNair Medical Institute, Baylor College of Medicine, Houston, Texas, USA  
**Competing Interests:** No competing interests were disclosed.
- 3 Mario Ehlers**, Immune Tolerance Network, San Francisco, California, USA  
**Competing Interests:** No competing interests were disclosed.



## A unique CD8<sup>+</sup> T lymphocyte signature in pediatric type 1 diabetes



Yamina Hamel <sup>a, b, c, 1</sup>, François-Xavier Mauvais <sup>a, b, c, 1</sup>, Hang-Phuong Pham <sup>d, e</sup>,  
 Roland Kratzer <sup>a, b, c</sup>, Christophe Marchi <sup>a, b, c</sup>, Émilie Barilleau <sup>a, b, c</sup>,  
 Emmanuelle Waeckel-Enée <sup>a, b, c</sup>, Jean-Baptiste Arnoux <sup>b, f</sup>, Agnès Hartemann <sup>g, h</sup>,  
 Corinne Cordier <sup>i, j</sup>, Jerome Mégret <sup>i, j</sup>, Benedita Rocha <sup>a, b, c</sup>, Pascale de Lonlay <sup>b, f, k</sup>,  
 Jacques Beltrand <sup>b, l</sup>, Adrien Six <sup>d, e</sup>, Jean-Jacques Robert <sup>b, l</sup>, Peter van Endert <sup>a, b, c, \*</sup>

<sup>a</sup> Institut National de la Santé et de la Recherche Médicale, Unité 1151, 75015 Paris, France

<sup>b</sup> Université Paris Descartes, Sorbonne Paris Cité, Faculté de médecine, 75015 Paris, France

<sup>c</sup> Centre National de la Recherche Scientifique, UMR8253, 75015 Paris, France

<sup>d</sup> Sorbonne Universités, UPMC Université Paris 6, 75015 Paris, France

<sup>e</sup> Institut National de la Santé et de la Recherche Médicale, UMRS 959, Immunology-Immunopathology-Immunotherapy (i3), 75013 Paris, France

<sup>f</sup> Centre de référence des Maladies Héritaires du Métabolisme, Hôpital Necker, Assistance Publique-Hôpitaux de Paris, 75015 Paris, France

<sup>g</sup> Université Pierre & Marie Curie, IHU ICAN, 75013 Paris, France

<sup>h</sup> Service de Diabétologie, Hôpital de la Pitié-Salpêtrière, Assistance Publique-Hôpitaux de Paris, 75013 Paris, France

<sup>i</sup> Institut National de la Santé et de la Recherche Médicale, US24, 75015 Paris, France

<sup>j</sup> Centre National de la Recherche Scientifique, UMS3633, 75015 Paris, France

<sup>k</sup> Institut Imagine, Institut National de la Santé et de la Recherche Médicale, Unité 1163, 75015 Paris, France

<sup>l</sup> Endocrinologie, Gynécologie et Diabétologie Pédiatrique, Hôpital Necker, Assistance Publique-Hôpitaux de Paris, 75015 Paris, France

### ARTICLE INFO

#### Article history:

Received 20 October 2015

Received in revised form

1 June 2016

Accepted 8 June 2016

Available online 16 June 2016

#### Keywords:

CD8<sup>+</sup> T lymphocyte

Gene expression profile

Protein expression signature

Single cell PCR

Type 1 diabetes

### ABSTRACT

Human type 1 diabetes results from a destructive auto-reactive immune response in which CD8<sup>+</sup> T lymphocytes play a critical role. Given the intense ongoing efforts to develop immune intervention to prevent and/or cure the disease, biomarkers suitable for prediction of disease risk and progress, as well as for monitoring of immunotherapy are required. We undertook separate multi-parameter analyses of single naïve and activated/memory CD8<sup>+</sup> T lymphocytes from pediatric and adult patients, with the objective of identifying cellular profiles associated with onset of type 1 diabetes. We observe global perturbations in gene and protein expression and in the abundance of T cell populations characterizing pediatric but not adult patients, relative to age-matched healthy individuals. Pediatric diabetes is associated with a unique population of CD8<sup>+</sup> T lymphocytes co-expressing effector (perforin, granzyme B) and regulatory (transforming growth factor  $\beta$ , interleukin-10 receptor) molecules. This population persists after metabolic normalization and is especially abundant in children with high titers of auto-antibodies to glutamic acid decarboxylase and with elevated HbA1c values. These findings highlight striking differences between pediatric and adult type 1 diabetes, indicate prolonged large-scale perturbations in the CD8<sup>+</sup> T cell compartment in the former, and suggest that CD8<sup>+</sup>CD45RA<sup>-</sup> T cells co-expressing effector and regulatory factors are of interest as biomarkers in pediatric type 1 diabetes.

© 2016 Elsevier Ltd. All rights reserved.

### 1. Introduction

The critical role of CD8<sup>+</sup> T lymphocytes, the dominant immune cell population in pancreatic islet infiltrates in type 1 diabetes (T1D)

\* Corresponding author. INSERM U1151, Hôpital Necker, 149 rue de Sèvres, 75015 Paris, France.

E-mail address: [peter.van-endert@inserm.fr](mailto:peter.van-endert@inserm.fr) (P. van Endert).

<sup>1</sup> These authors contributed equally to this work.

<http://dx.doi.org/10.1016/j.jaut.2016.06.003>

0896-8411/© 2016 Elsevier Ltd. All rights reserved.

patients, both in the initial and in the final destructive phase of autoimmune beta cell attack T1D is amply documented [1–3]. Consequently assays characterizing CD8<sup>+</sup> T cells could reveal important information and provide biomarkers of disease risk, progression and response to immunotherapy. However, insight on the CD8<sup>+</sup> T cell response in human type 1 diabetes is largely limited to the demonstration of autoreactive T lymphocytes secreting interferon (IFN)- $\gamma$  or granzyme (Gzm) B at disease onset [4]. Others and we have provided evidence for the presence among peripheral

blood mononuclear cells (PBMCs) of newly diagnosed T1D patients of small numbers of CD8<sup>+</sup> T cells [5–7] producing IFN- $\gamma$  upon recognition of beta cell antigens. However, both cells precipitating autoimmunity and others protecting from it can produce IFN- $\gamma$  [8], so that the significance of these cells is unclear. High-resolution analysis of gene and protein expression by lymphocytes has recently been shown to be informative for prediction of both normal [9] and pathological [10] (auto-)immune responses and appears as a promising approach to biomarker development, especially when selected cell populations are analyzed to avoid the confounding effects of bulk leucocyte examination.

Because CD8<sup>+</sup> T cells recognizing epitopes derived from beta cell antigens may contribute to destruction of insulin-producing cells, various previous reports studied secretion of key cytokines such as IFN- $\gamma$  by such cells, using tetramers to identify them. One study examined gene expression by small numbers of single tetramer-reactive CD8<sup>+</sup> T cells but did not identify an expression profile associated with T1D [11]. We reasoned that analysis of bulk CD8<sup>+</sup> T cells might be equally or more relevant when searching for signatures associated with T1D. Increasing evidence suggests the existence of systemic immune perturbation in T1D. Examining gene expression in whole blood or bulk lymphocytes of T1D patients, several groups observed a type I IFN signature resembling an innate response to viral infection [12–15]. The pro-inflammatory effects on normal lymphocytes of serum from T1D patients [16,17] and the detection of an altered balance of lipids and amino acids in the blood of pre-diabetic children [18] are further evidence for systemic perturbations in T1D.

Further support for analyzing bulk cells rather than tetramer-identified cells recognizing known self-epitopes comes from a recent study comparing CD8<sup>+</sup> T lymphocyte gene expression profiles in chronic infection and autoimmunity [19]. These authors reported that a signature indicating bulk CD8<sup>+</sup> T cell exhaustion predicted favorable long-term outcome in autoimmune vasculitis, lupus and inflammatory bowel disease. Conversely, expression of an anti-apoptotic transcriptional co-activator was associated with development of several autoimmune pathologies and indicative of progression to T1D in children at high risk of disease. Moreover, transcriptional profiling of CD8<sup>+</sup> lymphocytes has prognostic value in systemic lupus erythematosus and vasculitis [20]. Examining bulk CD8<sup>+</sup> T cells also has practical advantages because it does not require identification of T cell epitopes and tetramer production, is not limited to patients carrying specific HLA class I alleles, and allows for examining larger cell numbers when only small blood volumes are available i.e. in pediatric T1D. Prompted by these considerations and by the encouraging recent results, we analyzed gene and protein expression by single CD8<sup>+</sup> lymphocytes from pediatric and adult T1D patients and report an expression signature associated specifically with pediatric T1D.

## 2. Materials and methods

### 2.1. Patients

All patients were included in the study within one month from diagnosis of T1D and were positive for one or more autoantibodies (auto-Abs) with specificity for GAD65, IA-2, islet cell Abs (ICA) or ZnT8. Patients aged 18 years or more were assigned to the adult-onset group and younger patients to the juvenile-onset group. Adult patients were followed in the Endocrinology and Diabetology department of the Pitié-Salpêtrière Hospital and juvenile patients in the Pediatric Endocrinology and Diabetology department of the Necker Hospital or in the Pediatric Departments of the Antoine Bécère (Clamart, France) and Ambroise Paré Hospitals (Boulogne-Billancourt, France). The patients were on no other medication than

insulin treatment. Detailed information on the patients is in [Supplementary Table 1](#).

### 2.2. Controls

Control individuals for the adult-onset group were healthy donors with no personal or family history of autoimmune disorders including T1D, free of infectious diseases and not taking immunosuppressive medication. Control individuals for the pediatric group met these criteria and in addition had to be more than 2 years old and have a minimum weight of 18 kg. The maximum blood volume drawn from children was 0.8 ml per kg of body weight. All control individuals enrolled were followed-up in the Metabolic Disorders Department of the Necker Hospital and presented various metabolic disorders detailed in [Supplementary Table 2](#). Sera from all control individuals were tested to confirm absence of T1D auto-Abs.

### 2.3. Study approval

Ethics approval for pediatric and adult type 1 diabetes patients and adult control individuals was obtained from the *Comité d'Évaluation éthique* of INSERM (IRB0000388, FWA00005381; approval of 2 June 2005 extended January 9, 2007), whereas ethics approval pediatric control patients was obtained from the *Comité de Protection des Personnes "Ile de France II"* (Protocol JJR-2009–01). All patients and healthy donors, or both parents of pediatric subjects provided written informed consent. Blood samples were taken during scheduled clinical laboratory monitoring.

### 2.4. Antibodies

Monoclonal mouse Abs with the following specificities and labeled with the indicated fluorochromes were used (all Abs from BD Biosciences, Le Pont de Claix France, unless indicated otherwise). For sorting of single CD8<sup>+</sup> T cells: CD8/fluorescein isothiocyanate (FITC) (clone B9.11); CD14/phycoerythrin (PE) (clone M5E2); CD19/PE (clone SJ25C1); CD16/PE (clone 3G8); CD56/PE (clone B159); CD45RA/Pacific Blue (clone HI100; eBioscience, Paris, France). For multi-parametric analysis of CD8<sup>+</sup> T cells from pediatric T1D patients: CCR7/Brilliant Violet 421 (clone 150503); CD4/PE (clone RPA-T4); CD8/V500 (clone RPA-T8); CD14/PE (clone M5E2); CD16/PE (clone 3G8); CD19/PE (clone SJ25C1); CD45RA/PE-CF594 (clone HI100); CD56/PE (clone B159); CDw210a/biotin (clone 3F9; AbD Serotec/Bio-Rad, Colmar, France); Gzm A/Peridinin chlorophyll protein (PerCP)-cyanin (Cy)5.5 (clone CB9; Biolegend, Ozyme, Saint Quentin Yvelines, France); Gzm B/alexa fluor (AF) 700 (clone GB11); LAP (transforming growth factor (TGF)- $\beta$ 1)/PE-Cy7 (clone TW4-2F8; Biolegend); Perforin (PRF)/FITC (clone  $\delta$ G9); RANTES (regulated on activation, normal T cell expressed and secreted)/AF 647 (clone VL1; Biolegend); AF 647 Mouse IgG2b,  $\kappa$  isotype control (clone MPC-11; Biolegend); FITC Mouse IgG1,  $\kappa$  isotype control (anti-dansyl); PerCP/Cy5.5 Mouse IgG1,  $\kappa$  isotype control (clone MOPC-21; Biolegend); PE/Cy7 Mouse IgG1,  $\kappa$  isotype control (clone MOPC-21; Biolegend); AF 700 Mouse IgG1,  $\kappa$  isotype control (clone MOPC-21); Brilliant Violet 421 Mouse IgG2a,  $\kappa$  isotype control (clone G155-178); biotin Rat IgG2a Negative/Isotype control (anti-Dinitrophenyl Hapten; AbD Serotec/Bio-Rad). Additional information concerning Abs and cell staining is in [Supplementary Table 3](#).

### 2.5. Lymphocyte preparation

PBMCs were isolated by Ficoll-isopaque density gradient centrifugation, frozen in 90% pooled human AB Serum and 10% dimethyl sulfoxide and stored in liquid nitrogen until use. Cells were thawed rapidly in pre-warmed RPMI 1640 medium.

## 2.6. Sorting of single CD8<sup>+</sup> T lymphocytes

PBMCs ( $3 \times 10^6$ ) were simultaneously incubated for 30 min on ice with Abs of the following specificities diluted in 100  $\mu$ L FACS buffer (PBS supplemented with 2% fetal bovine serum): CD8/FITC; CD45RA/Pacific Blue; CD4/PE, CD14/PE, CD16/PE and CD19/PE (dump gate). After being washed twice, cells were re-suspended in 500  $\mu$ L of PBS with 2% fetal bovine serum containing 7-aminocoumarinyl D (BD Biosciences) to label dead cells. Live CD8<sup>+</sup>CD45RA<sup>+</sup> or CD8<sup>+</sup>CD45RA<sup>-</sup> T cells were sorted using a FACS ARIA-ITM machine (BD Biosciences). Cells were collected in individual PCR tubes containing 5  $\mu$ L of PBS-Diethylpyrocarbonate 0.1% and stored at  $-80^\circ\text{C}$  until use.

## 2.7. Multi-parametric qualitative reverse transcription (RT)-PCR

This method has previously been described [21,22]. In this study, primers for interleukin (IL)-10, programmed cell death-1 and macrophage inflammatory protein (MIP)1- $\alpha$  genes were not included because very few cells were found positive. Gene expression was considered only for cells expressing CD3 $\epsilon$  mRNA to eliminate potential contamination by natural killer (NK)-T cells. Multi-parametric PCR was performed using SYBR Green PCR Master Mix (Eurogentec, Angers, France) and AmpliTaq Gold polymerase (Applied Biosystems/Life Technologies). PCR products were analyzed with reference to the predicted melting temperature by measuring dissociation curves alongside positive controls, using SDS2.4 software and Applied Biosystems 7900 equipment. Products with melting temperatures identical to the control sample and corresponding to the predicted value were immediately considered positive. PCR products displaying a melting temperature differing by  $\geq 0.7^\circ\text{C}$  from the control were verified by electrophoretic separation in 2% agarose gels. Products migrating like the control sample were considered positive.

## 2.8. Identification of lymphocyte sub-populations

To identify CD8<sup>+</sup> T cell subsets based on gene expression, we used agglomerative hierarchical clustering to build dendrograms showing successively aggregated clusters. We used Jaccard's distance and Ward's strategy as criteria to select clusters to be aggregated. The number of subsets was chosen by cutting the tree at an appropriate level to form clusters as homogeneous as possible. To check the stability of each sub-population, the data was re-sampled 1000 times using the bootstrap technique [23] as developed by Hennig [24]. For each bootstrap, a hierarchical classification was performed from which the same number of clusters was deduced as compared to the original dataset. Then, the method developed by Hennig [24] was applied to determine the mean Jaccard similarities across bootstrap datasets as an estimate of cluster stability. Highly stable clusters should yield average Jaccard similarities of 0.85 and above. Clusters with average Jaccard similarities below 0.5 were merged. This process was repeated several times for increasing cluster numbers ( $k = 2$  to 10) in order to determine the optimal cluster number (N). In order to group patient and control cells in classes and to identify a set of most discriminant genes, random forest models [25] were trained on adult and child datasets separately. Each random forest model was run with 1000 trees. In addition to the out-of-bag error, classification accuracy was assessed using the confusion matrix through 10-fold and leave-one-out cross-validation processes.

## 2.9. Multi-parametric flow cytometry analysis

PBMCs ( $2 \times 10^6/\text{mL}$ ) were incubated in a  $37^\circ\text{C}$ , 5% CO<sub>2</sub> incubator

for 20 h with 10  $\mu\text{g}/\text{mL}$  of brefeldin A (Sigma Aldrich) in RPMI-1640 medium supplemented with 10% human pooled serum, L-glutamine and Penicillin/Streptomycin (Gibco). After extensive washing,  $2 \times 10^6$  cells were incubated for 40 min on ice with Abs with the following specificities, diluted in 100  $\mu$ L FACS buffer: CD4/PE, CD14/PE, CD16/PE, CD19/PE (dump gate); CD8/V500; CD45RA/PE-CF594; CCR7/Brilliant Violet 421; LAP (TGF- $\beta$ 1)/PE-Cy7; CDw210a/biotin. After washing twice, cells were incubated with Streptavidin/allophycocyanin-Cy7 (Biolegend) for 15 min on ice. After permeabilization and fixation by incubating cells with 200  $\mu$ L of Cytofix/Cytoperm (BD Biosciences), cells were stained for 30 min on ice to detect the following additional proteins: Gzm A/PerCP-Cy5.5; Gzm B/AF 700; PRF/FITC; and RANTES/AF 647. Finally fluorescent events were recorded on a BD LSR Fortessa analyzer. Post-acquisition analysis was performed using the FlowJo X version 10.0.7 software (TreeStar). To verify the specificity of cell staining and validate the gating strategy, the Fluorescence Minus One method was employed, based on the parallel use of adequate isotype controls coupled to the following fluorochromes: biotin (+streptavidin/allophycocyanin-Cy7), FITC, PE-Cy7, Brilliant Violet 421, PerCP-Cy5.5, AF 647 and AF 700.

## 2.10. Statistical and bioinformatics analysis

The common approach that consists in the transformation into cell percentages for each individual is inappropriate for detecting differentially expressed genes due to the unequal variance of data; over-representation of a gene in only one individual biases the estimation of truly differential expression [26]. Thus, we used SAMseq, an RNA-seq based method, to test for the differential expression between two biological groups [27]. SAMseq is a non-parametric method based on average Wilcoxon's statistics through a resampling procedure. The false discovery rate for each gene is computed using a permutation-based scheme of samples.

To determine whether the relative prevalence of populations defined by bioinformatics was altered and to analyze protein expression in patients vs. controls, two-sided Student t-tests were used. The sample size for the protein analysis was selected by using a power analysis with  $\alpha = 0.05$  (type 1 error);  $\beta = 0.2$  (type 2 error) and a two-sided test; the expected effect size was guided by gene expression analysis. The Pearson coefficient was calculated to test the correlation between auto-Ab titers, HbA1c and protein expression levels. The threshold for statistical significance was set to  $\alpha = 0.05$  (type 1 error). All analyses were performed using R software and the following additional packages: fpc v2.1-9 for cluster stability assessment; randomForest v4.6-10 for random forest models; caret v6.0-37 for cross-validation of random forest models; Heatplus v2.10-0 for heatmap plotting. These packages as well as R are available at <http://www.r-project.org> and <http://www.bioconductor.org>.

## 3. Results

### 3.1. Gene expression by bulk CD8<sup>+</sup> T cells from T1D patients

We examined gene expression by single CD8<sup>+</sup> T lymphocytes obtained (with one exception) within one week of diagnosis of T1D (Supplementary Table 1). In order to homogenize the experimental conditions for cells obtained with different delays between blood drawing and laboratory analysis, we analyzed cryopreserved cells, an approach designed to eventually allow us examining cells from a wide range of biobanks. The cells were sorted as CD8<sup>+</sup>CD45RA<sup>+</sup> (naïve cells and memory cells re-expressing CD45RA) and CD8<sup>+</sup>CD45RA<sup>-</sup> (effector and central memory cells) [28] (Supplementary Fig. 1). Considering age-dependent lymphocyte



development, and evidence for a distinct impact of genetic predisposition in pediatric as compared to adult T1D [29,30], we analyzed separately groups of 10–12 juvenile (median age 9, 10 for controls) and adult (median age 28, 30 for controls) patients together with an equivalent number of age-matched controls (Supplementary Table 2). For each donor, an average of 30–50 CD45RA<sup>+</sup> and CD45RA<sup>-</sup> cells were analyzed, amounting to a total of 1595 CD45RA<sup>+</sup> and 1738 CD45RA<sup>-</sup> cells. Each individual cell was scored for absent or present expression of 13 genes related to effector function (Supplementary Table 4): Gzm A and B [31,32], PRF, IFN- $\gamma$ , tumor necrosis factor (TNF)- $\alpha$ , Fas-L, RANTES, MIP-1 $\beta$ ; survival and differentiation: IL-2, IL-7 receptor (IL-7R), killer cell lectin-like receptor subfamily G (KLRG1); homing: CCR7; and regulation: TGF- $\beta$ , IL-10R. Differences were tested for statistical significance using an approach (SAMseq) designed for comparing gene expression at the level of each individual, thus taking into account inter-individual variation. Statistical evaluation was limited to genes positive in  $\geq 10\%$  of cells for patients and/or controls in each analysis.

Applying these criteria, gene expression by the CD45RA<sup>+</sup> and CD45RA<sup>-</sup> subpopulations of CD8<sup>+</sup> lymphocytes from adult patients and controls did not show any significant difference (Table 1). In striking contrast, gene expression by CD8<sup>+</sup> lymphocytes from pediatric subjects differed greatly between patients and controls. CD45RA<sup>+</sup> cells from pediatric patients displayed significant down-regulation of Gzm A and RANTES. Striking and wide-ranging differences were observed for pediatric CD45RA<sup>-</sup> cells. Gzm A was strongly down-regulated while expression of KLRG1, CCR7 and IL-7R was moderately decreased. In contrast, PRF and TGF- $\beta$  were

strongly up-regulated while RANTES showed moderate up-regulation. The percentage of pediatric CD45RA-cells expressing Gzm B and IL-10R was strongly increased although this was not statistically significant because of strong inter-individual variation. Collectively examination of individual gene expression demonstrated no changes in adult patients but massive perturbation in activated/memory CD8<sup>+</sup> cells from juvenile patients, including the surprising findings of i) combined up-regulation of effector genes (PRF, Gzm B and RANTES) and genes usually associated with regulation (TGF- $\beta$ , IL-10R) [33–35], and ii) dissociation of Gzm A and B expression.

We also compared gene expression between the adult and pediatric groups of patients and between the adult and pediatric control groups (Table 2). Consistent with strongly divergent gene expression profiles in pediatric T1D for CD45RA<sup>-</sup> cells, this comparison revealed significant differences for a large group of genes most of which were strongly dysregulated in pediatric but not adult patients; this group included PRF, RANTES, TGF- $\beta$ , IL-10R and IL-7R. Another smaller group included genes (CCR7, Gzm A, KLRG1) showing significantly altered expression in the pediatric patient group when compared to age-matched controls, but not between T1D patients of different age. Importantly, juvenile control individuals harbored less CD45RA<sup>+</sup> and CD45RA<sup>-</sup> cells expressing PRF than adult controls. This underscores the significance of our observation that juvenile CD45RA-cells express more PRF than both age-matched controls and adult T1D patients.

### 3.2. Identification of sub-populations among single CD8<sup>+</sup>CD45RA<sup>+</sup> T cells

At variance with classical PCR on bulk cells, single cell PCR

**Table 1**

Percentage (Standard Deviation, SD) of gene expression by single CD45RA<sup>+</sup> and CD45RA<sup>-</sup> CD8<sup>+</sup> T cells from peripheral blood of patients with adult onset and juvenile onset T1D in comparison with controls.

	CD8 <sup>+</sup> CD45RA <sup>+</sup> T cells			CD8 <sup>+</sup> CD45RA <sup>-</sup> T cells		
	Patients <sup>a</sup>	Controls <sup>b</sup>	FDR <sup>c</sup>	Patients <sup>a</sup>	Controls <sup>b</sup>	FDR
<b>Adult onset</b>						
Gzm A	15.3 (12.2)	22.3 (26.0)	1	35.1 (24.7)	46.3 (35.1)	1
Gzm B	5.5 (9.4)	11.3 (19.9)	0.36	13.8 (14.1)	14.3 (23.0)	0.36
PRF	9.9 (10.5)	20.3 (15.7)	0.24	25.0 (12.3)	34.8 (19.2)	0.42
IL-2	7.3 (19.7)	7.3 (13.0)	– <sup>d</sup>	8.0 (15.2)	4.6 (4.2)	–
IFN- $\gamma$	14.7 (22.7)	14.1 (19.8)	0.58	16.2 (16.7)	16.7 (29.1)	0.36
TGF- $\beta$	32.3 (17.0)	32.7 (13.0)	0.58	50.7 (22.7)	46.0 (24.5)	0.55
FASL	1.4 (3.7)	4.6 (5.3)	–	2.2 (2.2)	2.8 (5.1)	–
KLRG1	0.9 (1.5)	7.0 (9.5)	–	5.5 (10.2)	14.9 (17.6)	0.42
IL-10R	18.1 (16.6)	31.6 (18.7)	0.24	40.0 (17.2)	51.0 (24.8)	0.42
IL-7R	74.0 (22.1)	75.5 (27.5)	0.58	82.8 (10.7)	82.8 (14.5)	1
CCR7	36.5 (18.9)	40.7 (29.1)	0.58	14.6 (11.3)	22.1 (23.3)	1
RANTES	13.8 (11.4)	25.7 (23.4)	0.24	48.7 (16.7)	45.8 (32.7)	1
MIP-1 $\beta$	7.5 (8.6)	6.3 (5.6)	–	12.3 (8.0)	11.0 (9.2)	0.36
<b>Juvenile onset</b>						
Gzm A	<b>13.5 (19.5)</b>	<b>21.6 (16.5)</b>	<b>0<sup>e</sup></b>	<b>42.7 (24.2)</b>	<b>63.8 (25.0)</b>	<b>0</b>
Gzm B	14.0 (22.4)	6.6 (8.5)	0.48	21.7 (15.5)	11.6 (9.7)	0.12
PRF	6.2 (6.3)	10.1 (8.3)	0.22	<b>43.5 (20.3)</b>	<b>17.9 (10.9)</b>	<b>0</b>
IL-2	1.8 (2.5)	2.7 (3.5)	–	1.5 (2.0)	4.1 (3.3)	–
IFN- $\gamma$	10.4 (19.5)	8.1 (4.7)	0.22	19.2 (14.7)	9.3 (6.1)	0.12
TGF- $\beta$	28.0 (17.9)	23.9 (10.9)	1	<b>74.4 (12.2)</b>	<b>35.4 (11.1)</b>	<b>0</b>
FASL	4.2 (9.6)	5.7 (6.4)	–	5.2 (8.9)	8.7 (13.3)	–
KLRG1	1.3 (2.9)	6.9 (6.4)	–	<b>5.5 (7.5)</b>	<b>13.6 (12.7)</b>	<b>0</b>
IL-10R	32.4 (17.2)	20.5 (9.1)	0.22	55.7 (15.7)	37.7 (11.8)	0.16
IL-7R	88.9 (15.3)	76.3 (18.3)	1	<b>61.4 (16.8)</b>	<b>73.2 (15.7)</b>	<b>0</b>
CCR7	54.9 (20.7)	40.0 (17.7)	0.22	<b>11.6 (9.3)</b>	<b>16.3 (13.4)</b>	<b>0</b>
RANTES	<b>8.7 (6.9)</b>	<b>18.4 (13.8)</b>	<b>0</b>	<b>68.7 (12.2)</b>	<b>62.6 (14.4)</b>	<b>0</b>
MIP-1 $\beta$	3.1 (7.3)	4.2 (4.2)	–	13.2 (8.5)	8.6 (6.3)	0.16

<sup>a</sup> N = 10 for adult patients and N = 12 for pediatric patients.

<sup>b</sup> N = 12 for adult controls and N = 10 for pediatric controls.

<sup>c</sup> False discovery rate in SAMseq test.

<sup>d</sup> FDR not calculated since < 10% of cells positive.

<sup>e</sup> **Bold:** FDR < 0.05 in SAMseq test.

**Table 2**

Percentages (SD) of gene expression by single CD45RA<sup>+</sup> and CD45RA<sup>-</sup> CD8<sup>+</sup> T cells from patients with adult vs. juvenile onset of T1D, and from adult vs. juvenile control individuals.

	CD8 <sup>+</sup> CD45RA <sup>+</sup> T cells			CD8 <sup>+</sup> CD45RA <sup>-</sup> T cells		
	Adult	Juvenile	FDR <sup>a</sup>	Adult	Juvenile	FDR
<b>Patients</b>						
Gzm A	15.3 (12.2)	13.5 (19.5)	0.53	35.1 (24.7)	42.7 (24.2)	1
Gzm B	5.5 (9.4)	14.0 (22.4)	0.67	13.8 (14.1)	21.7 (15.5)	0.09
PRF	9.9 (10.5)	6.2 (6.3)	0.67	<b>25.0 (12.3)</b>	<b>43.5 (20.3)</b>	<b>0</b>
IL-2	7.3 (19.7)	1.8 (2.5)	– <sup>b</sup>	8.0 (15.2)	1.5 (2.0)	–
IFN- $\gamma$	14.7 (22.7)	10.4 (19.5)	0.53	16.2 (16.7)	19.2 (14.7)	1
TGF- $\beta$	32.3 (17.0)	28.0 (17.9)	0.53	<b>50.7 (22.7)</b>	<b>74.4 (12.2)</b>	<b>0</b>
FASL	1.4 (3.7)	4.2 (9.6)	–	2.2 (2.2)	5.2 (8.9)	–
KLRG1	0.9 (1.5)	1.3 (2.9)	–	5.5 (10.2)	5.5 (7.5)	1
IL-10R	<b>18.1 (16.6)</b>	<b>32.4 (17.2)</b>	<b>0<sup>c</sup></b>	<b>40.0 (17.2)</b>	<b>55.7 (15.7)</b>	<b>0</b>
IL-7R	74.0 (22.1)	88.9 (15.3)	1	<b>82.8 (10.7)</b>	<b>61.4 (16.8)</b>	<b>0</b>
CCR7	36.5 (18.9)	54.9 (20.7)	0.67	14.6 (11.3)	11.6 (9.3)	1
RANTES	13.8 (11.4)	8.7 (6.9)	0.53	<b>48.7 (16.7)</b>	<b>68.7 (12.2)</b>	<b>0</b>
MIP-1 $\beta$	7.5 (8.6)	3.1 (7.3)	–	12.3 (8.0)	13.2 (8.5)	1
<b>Controls</b>						
Gzm A	22.3 (26.0)	21.6 (16.5)	0.67	46.3 (35.1)	63.8 (25.0)	0.12
Gzm B	11.3 (19.9)	6.6 (8.5)	1	14.3 (23.0)	11.6 (9.7)	0.58
PRF	<b>20.3 (15.7)</b>	<b>10.1 (8.3)</b>	<b>0</b>	<b>34.8 (19.2)</b>	<b>17.9 (10.9)</b>	<b>0</b>
IL-2	7.3 (13.0)	2.7 (3.5)	–	4.6 (4.2)	4.1 (3.3)	–
IFN- $\gamma$	14.1 (19.8)	8.1 (4.7)	0.67	16.7 (29.1)	9.3 (6.1)	0.58
TGF- $\beta$	32.7 (13.0)	23.9 (10.9)	1	46.0 (24.5)	35.4 (11.1)	0.18
FASL	4.6 (5.3)	5.7 (6.4)	–	2.8 (5.1)	8.7 (13.3)	–
KLRG1	7.0 (9.5)	6.9 (6.4)	–	14.9 (17.6)	13.6 (12.7)	0.58
IL-10R	31.6 (18.7)	20.5 (9.1)	1	51.0 (24.8)	37.7 (11.8)	0.18
IL-7R	75.5 (27.5)	76.3 (18.3)	0.67	82.8 (14.5)	73.2 (15.7)	0.18
CCR7	40.7 (29.1)	40.0 (17.7)	0.67	22.1 (23.3)	16.3 (13.4)	1
RANTES	25.7 (23.4)	18.4 (13.8)	0.67	45.8 (32.7)	62.6 (14.4)	0.12
MIP-1 $\beta$	6.3 (5.6)	4.2 (4.2)	–	11.0 (9.2)	8.6 (6.3)	0.42

<sup>a</sup> False discovery rate in SAMseq test.

<sup>b</sup> FDR not calculated since < 10% of cells positive.

<sup>c</sup> **Bold:** FDR < 0.05 in SAMseq test.

allows for identifying combinations of genes expressed by individual cells and thereby defining functional lymphocyte populations. As detailed in the Materials and Methods section, we performed a Jaccard similarity-based analysis, as described in Refs. [24], in order to determine the most stable cell clusters that can be deduced from the hierarchical clustering of patient and control CD8<sup>+</sup>CD45RA<sup>+</sup> single cell PCR data. Four populations could be identified with the best cluster coherence (Fig. 1A, B). These included presumably naïve populations expressing the IL-7R alone (P1) or with CCR7 (P2), a population with additional expression of genes linked to regulation (IL-10R and TGF-β; P4) and a population expressing all of these plus effector molecules such as Gzm A and B, PRF, IFN-γ and RANTES (P3).

Although patient and control CD8<sup>+</sup>CD45RA<sup>+</sup> cells harbored similar proportions of the four populations (Fig. 1A), gene expression within them showed some significant differences (Fig. 1C). Most notably, IL-10R expression in the adult “regulatory” population (P4) was strongly reduced. Other smaller differences concerned the IL-7R and a set of genes in the pediatric P3 consistent with the global tendencies discussed above (Table 1), such as down-regulation of Gzm A and RANTES. In a random forest analysis, IL-7R, CCR7, Gzm A and IL-10R had significant discriminatory power between pediatric patients and controls, while only expression of the IL-10R discriminated adult patients significantly (Fig. 1D).

### 3.3. Identification of sub-populations among single CD8<sup>+</sup>CD45RA<sup>-</sup> T cells

Applying the same clustering analysis as in the previous paragraph, three stable populations were identified among single CD8<sup>+</sup>CD45RA<sup>-</sup> effector/memory cells (Fig. 2A, B). P2 expressed a small number of genes such as KLRG1, Gzm A and RANTES while P3 expressed genes associated with regulation (IL-10R and TGF-β), similar to P4 among CD45RA<sup>+</sup> cells, together with RANTES and Gzm A. The third and dominant population (P1) similarly expressed genes linked to regulation however together with genes encoding the effector molecules Gzm B, PRF, IFN-γ and MIP-1β. Comparison of adult patients and controls showed equal abundance of the populations (Fig. 2A) but somewhat different expression within them, including strong down-regulation of IL-10R in P1, as well as altered expression of CCR7 and TGF-β in P3 (Fig. 2C).

In striking contrast to adult patients, CD8<sup>+</sup>CD45RA<sup>-</sup> cells from pediatric patients showed strong alterations in population abundance, with a strong increase of P1 expressing a complex set of genes at the expense of the transcriptionally little active P2 (Fig. 2A). Furthermore, gene expression within the populations was significantly altered, including strongly reduced expression of Gzm A in all populations, increased expression of TGF-β in P1 and P3 and IL-10R in P1, in which PRF also was over-expressed (Fig. 2C). TGF-β but also Gzm A and PRF discriminated strongly between pediatric patients and controls, while CCR7, IL-10R and Gzm A had moderate discriminatory power among adult subjects (Fig. 2D). Thus, biostatistical analysis revealed strong homeostatic perturbation among activated/effector CD8<sup>+</sup> T cells at onset of pediatric but not adult T1D, combined with significantly altered expression of genes associated with effector as well as regulatory functions.

### 3.4. Longitudinal analysis of CD8<sup>+</sup> T cell subpopulations

Altered gene expression by CD8<sup>+</sup> lymphocytes could reflect systemic effects of inflammatory or infectious events but also the metabolic perturbation at onset of T1D. In the latter case, the perturbations were expected to vanish after start of insulin therapy. We could monitor gene expression by CD45RA<sup>-</sup> T cells over a

period of three months in four pediatric patients. At disease onset, the profile of gene expression by this subgroup of patients largely reflected that of the complete group of juvenile patients, with strong up-regulation of PRF, TGF-β and IL-10R contrasting with down-regulation of Gzm A; in addition, CCR7 and RANTES showed limited dysregulation (Table 3). While expression of the latter genes normalized by day 10, PRF, TGF-β and IL-10R remained strongly up-regulated 3 months after diagnosis. Thus immune perturbation independent of hyperglycemia, possibly linked to destruction of remaining beta cells by CD8<sup>+</sup> T cells, continues after onset of pediatric T1D.

### 3.5. Protein expression by CD8<sup>+</sup> T cells from pediatric T1D patients

Finally, to verify whether altered gene expression resulted in altered protein profiles, we analyzed lymphocytes obtained at diagnosis of T1D from an independent group of 25 pediatric patients with an equal number of controls. We set up a flow cytometry protocol allowing for simultaneous analysis of un-stimulated CD8<sup>+</sup> T cells for seven parameters (Supplementary Fig. 2 and Supplementary Table 3). CD8<sup>+</sup>CD45RA<sup>+</sup> cells displayed significantly reduced expression of Gzm A and RANTES combined with increased expression of CCR7 (Fig. 3A), consistent with gene expression. Analysis of protein expression by CD8<sup>+</sup>CD45RA<sup>-</sup> cells produced results entirely consistent with gene expression data (Table 1) and showed significant down-regulation of Gzm A and significant up-regulation of IL-10R, TGF-β, Gzm B and PRF (Fig. 3A). Importantly, searching for the populations identified by cluster analysis of gene expression (Fig. 2A), we confirmed significantly reduced abundance of Gzm A<sup>+</sup> Gzm B<sup>+</sup> cells (Fig. 3B). At the same time, the abundance of IL-10R<sup>+</sup> TGF-β<sup>+</sup> cells was increased, as was that of cells co-expressing effector and regulatory proteins, including cells expressing Gzm B, PRF, IL-10R and TGF-β simultaneously (Fig. 3B). Importantly, the frequency of cells expressing TGF-β, or co-expressing TGF-β and IL-10R, correlated strongly with the titer of autoantibodies to GAD (Fig. 3C). The frequency of the latter population also correlated with the level of HbA1c.

## 4. Discussion

This study has revealed two key findings. The first is the existence of a CD8<sup>+</sup> T cell expression signature at the onset of pediatric but not adult T1D. Importantly, we validated the signature observed at the level of gene expression by analyzing protein expression in an independent group of pediatric patients, using age-matched control individuals. The discrepancy related to the patients' age points to important differences in the immunologic and metabolic pathogenesis of adult and pediatric T1D [36]. The second finding is the increased and prolonged emergence of unusual memory/effector CD8<sup>+</sup> lymphocytes in pediatric patients that simultaneously express molecules associated with cytotoxic effector functions (PRF, Gzm B) together with others associated with regulation (IL-10R, TGF-β). The increased abundance of this population is evident at multiple levels: when comparing the proportion of pediatric CD8<sup>+</sup>CD45RA<sup>-</sup> cells individual genes (Table 1), when analyzing sub-populations among these cells (Fig. 2A), when analyzing gene expression by these subpopulations (Fig. 2C), and in multi-parameter flow cytometric analysis of protein expression (Fig. 3). The significance of this CD8<sup>+</sup>CD45RA<sup>-</sup> T cell population in the pathogenesis of T1D is indicated by the correlation between its abundance and key auto-immune and metabolic parameters.

Our observation of a CD8<sup>+</sup> T cell signature present exclusively in pediatric patients is consistent with previous reports suggesting age-related heterogeneity in the immunological presentation of

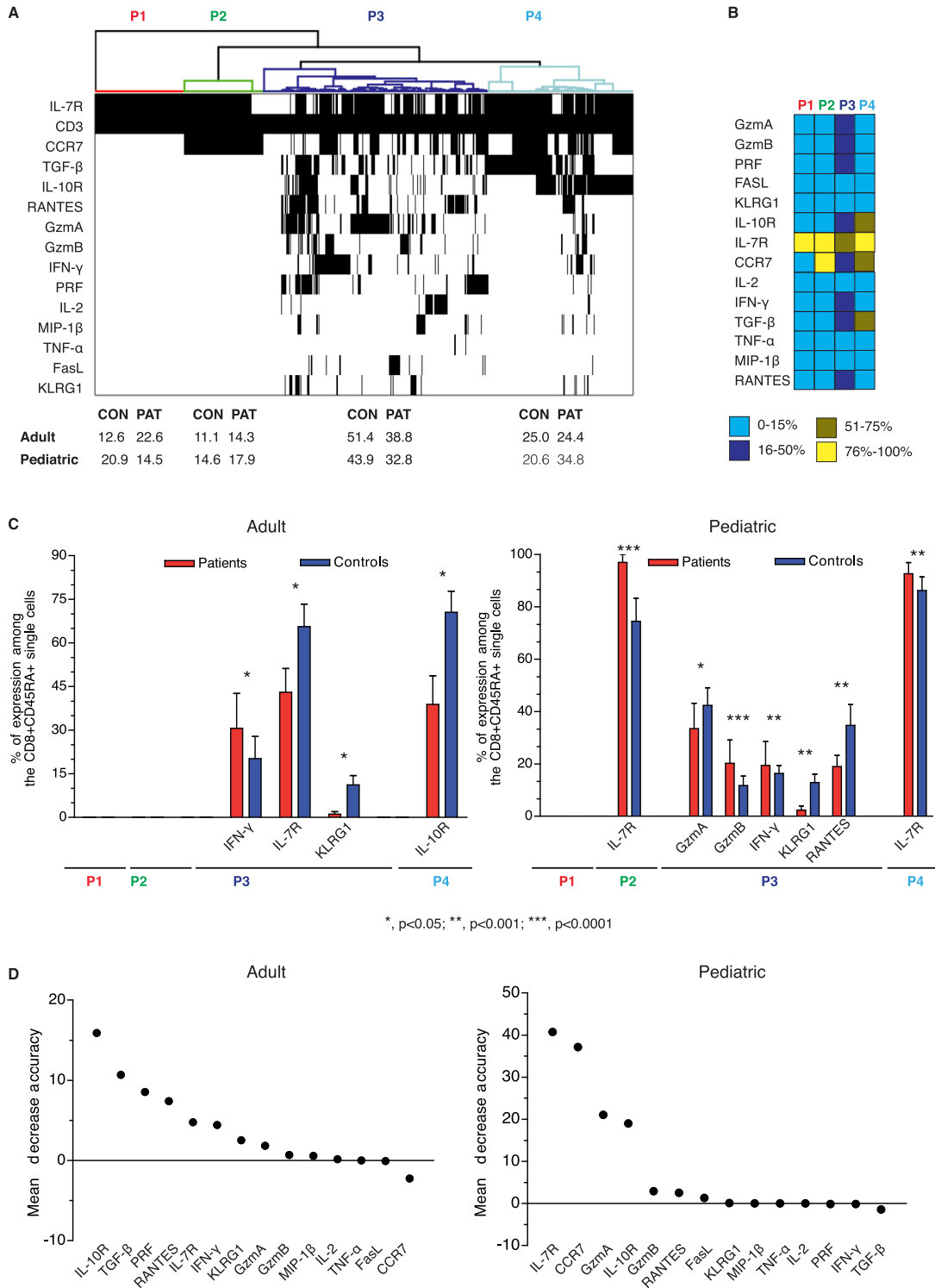


**Fig. 1. CD45RA<sup>+</sup>CD8<sup>+</sup> T lymphocyte sub-populations and their gene expression profiles.** (A) Data generated by single-cell RT-PCR analysis of CD45RA<sup>+</sup>CD8<sup>+</sup> T cells from T1D patients and controls was pooled to generate a dendrogram showing successively aggregated clusters of genes. Lymphocyte sub-populations were delimited by selection for highly stable clusters present in both patients and controls. The numbers below the dendrogram represent the percentage of cells belonging to each population among cells from adult and pediatric controls (CON) and patients (PAT). (B) The heat map shows the gene expression signature of the lymphocyte sub-populations represented as the percentage of single cells expressing each mRNA. (C) The histograms represent the percentage of positive cells in the sub-populations identified in (A) for those genes displaying significantly different expression in the patient vs. control sub-population. *P*-values were determined using Mann-Whitney tests and corrected by the Benjamini-Hochberg method. (D) Each gene was tested for its power to discriminate patients from controls by determining the mean decrease in discriminatory accuracy in a random forest model.

T1D. Thus patients aged <15 years display a higher frequency of high-risk HLA-DR alleles, higher titers of islet cell antibodies and

greater insulin dependence at diagnosis [29]. A negative association between patient age and titers of autoantibodies to insulin and IA-2

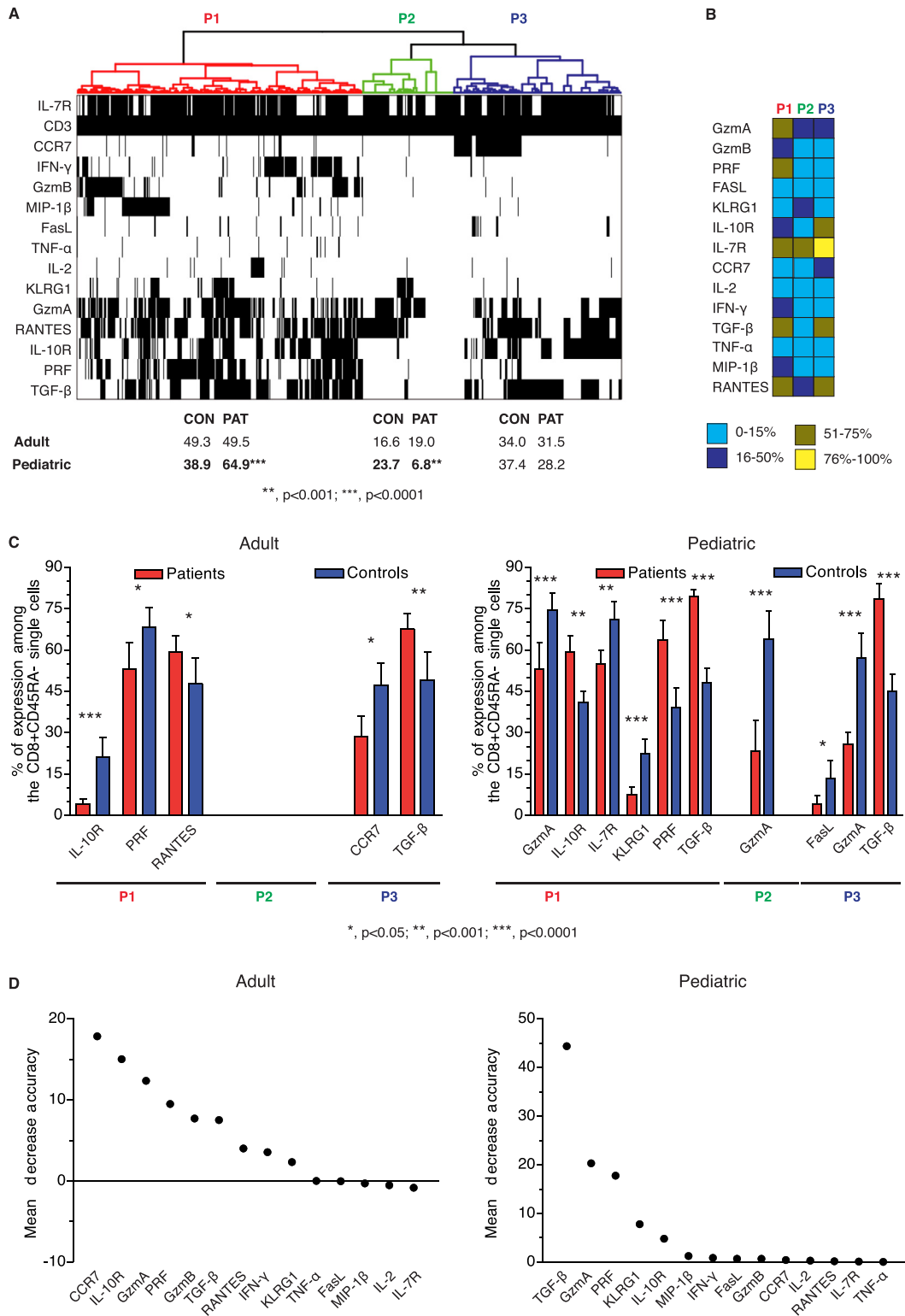


**Fig. 2. CD45RA<sup>-</sup>CD8<sup>+</sup> T lymphocyte sub-populations and their gene expression profiles.** Data for CD45RA<sup>-</sup> activated/memory CD8<sup>+</sup> T cells are represented in the same manner as for CD45<sup>+</sup> cells in Fig. 1. (A) Dendrogram showing the three stable sub-populations identified. (B) Heat map indicating gene expression in the sub-populations. (C) Histograms showing genes differentially expressed in the sub-populations of patients vs. controls. *P*-values were determined using Mann-Whitney tests and corrected by the Benjamini-Hochberg method. (D) Random forest evaluation of the capacity of individual genes to discriminate patient and control cells.

was found in another study [37], and a third study reported an association between a high-risk HLA-DQ allele and insulin

autoantibodies exclusively in patients aged <10 years [38]. Thus, pediatric T1D develops on a background of stronger genetic

**Table 3**

Longitudinal monitoring of gene expression, expressed as percent positive (SD), by single CD8<sup>+</sup>CD45RA<sup>-</sup> lymphocytes from four pediatric patients (patients DP08, DP09, DP11, DP12 in [Supplementary Table 1](#)). Control values are taken from [Table 1](#).

% Positive	Controls	Day 0	FDR <sup>a</sup>	Day 10	FDR	Day 30	FDR	Day 90	FDR
Gzm A	63.8 (25.0)	<b>41.8 (5.2)</b>	<b>0<sup>b</sup></b>	56.1 (3.7)	0.47	<b>64.4 (13.8)</b>	<b>0.04</b>	60.2 (5.6)	0.21
Gzm B	11.6 (9.7)	<b>21.1 (27.9)</b>	<b>0</b>	15.8 (0.0)	0.19	30.3 (8.1)	0.06	11.4 (16.9)	0.13
PRF	17.9 (10.9)	<b>51.7 (9.3)</b>	<b>0</b>	<b>39.9 (2.7)</b>	<b>0</b>	<b>51.2 (9.1)</b>	<b>0</b>	<b>48.9 (13.0)</b>	<b>0</b>
TGF-β	35.4 (11.1)	<b>76.8 (21.6)</b>	<b>0</b>	57.9 (20.8)	0.19	<b>68.9 (32.1)</b>	<b>0</b>	<b>52.5 (15.7)</b>	<b>0</b>
IL-10R	37.7 (11.8)	<b>61.7 (13.7)</b>	<b>0</b>	<b>59.1 (10.0)</b>	<b>0</b>	<b>65.8 (18.4)</b>	<b>0</b>	<b>51.7 (18.0)</b>	<b>0</b>
CCR7	16.3 (13.4)	<b>8.1 (14.0)</b>	<b>0</b>	12.9 (18.0)	0.47	<b>5.4 (13.8)</b>	<b>0.04</b>	6.7 (18.3)	0.08
IL-7R	73.2 (15.7)	73.3 (5.4)	0.47	<b>68.6 (8.4)</b>	<b>0</b>	73.9 (10.7)	0.08	<b>57.2 (15.5)</b>	<b>0.04</b>
RANTES	62.6 (14.4)	<b>64.4 (6.3)</b>	<b>0</b>	60.5 (8.4)	0.47	77.3 (14.2)	0.09	55.7 (8.1)	1

<sup>a</sup> False discovery rate in SAMseq test.

<sup>b</sup> **Bold:** FDR <0.05 in SAMseq test.

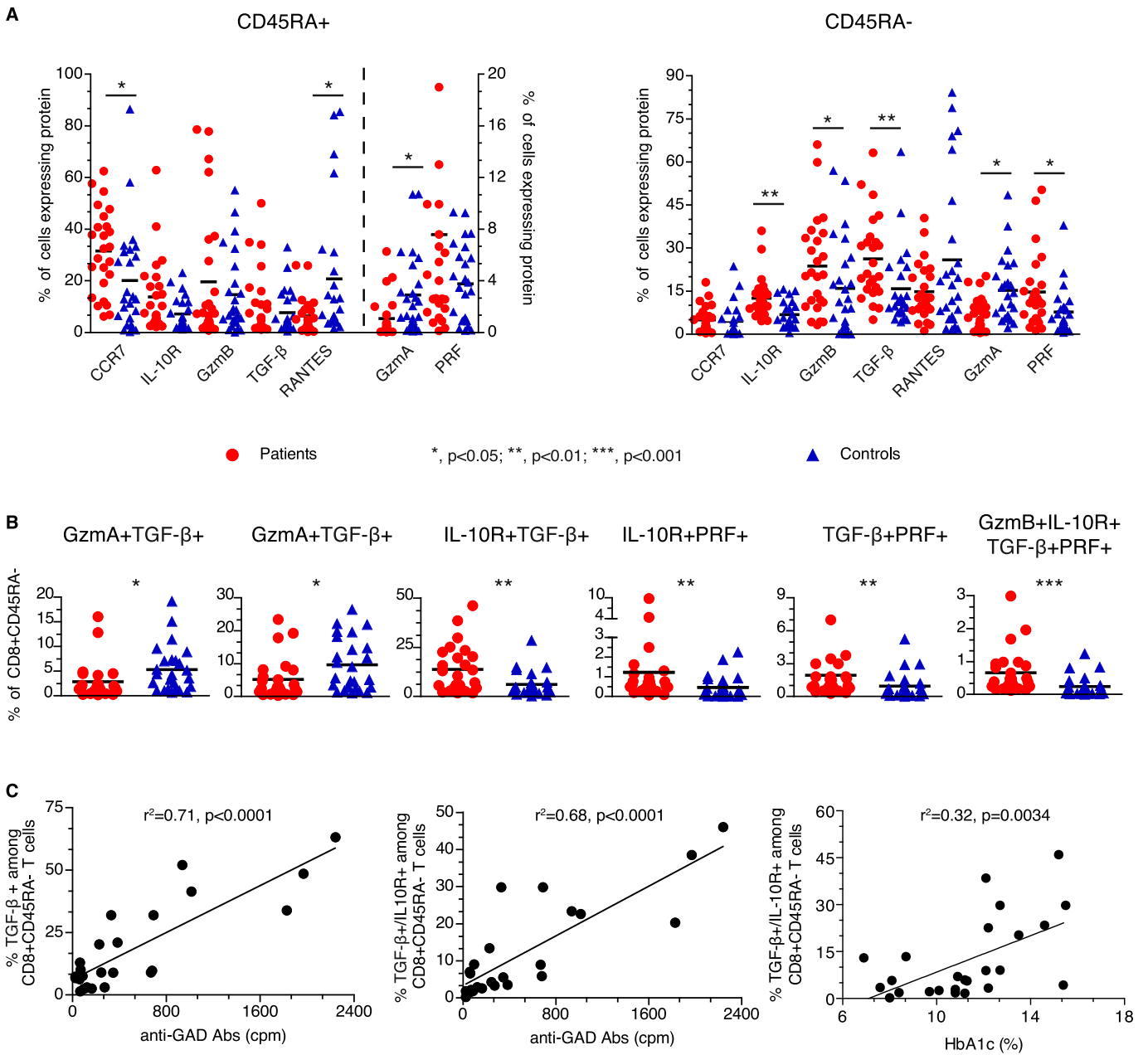


**Fig. 3. Protein expression signature in CD8<sup>+</sup> T lymphocytes from juvenile-onset type 1 diabetes patients.** PBMCs from 25 juvenile-onset patients and 25 age-matched control individuals were analyzed by multi-parametric flow cytometry. **(A)** Percentage of bulk CD8<sup>+</sup>CD45RA<sup>+</sup> and CD8<sup>+</sup>CD45RA<sup>-</sup> cells expressing each of the seven parameters analyzed. Each dot represents one individual. *P*-values were determined using the Wilcoxon test and adjusted by the Benjamini-Hochberg method. **(B)** Frequency among CD8<sup>+</sup>CD45RA<sup>-</sup> cells of cells co-expressing the proteins indicated in the titles. **(C)** Correlation between titers of autoantibodies to GAD, blood level of HbA1c and abundance of CD8<sup>+</sup> T cell subpopulations as indicated on the y-axis.

predisposition resulting in a more aggressive autoimmune response, as indicated by higher titers of autoantibodies. Our findings suggest that this more aggressive response involves CD8<sup>+</sup>CD45RA<sup>-</sup> T cells.

Because we chose not to restrict our analysis to T cells recognized by HLA class I tetramers, we do not know what proportion of the CD8<sup>+</sup>CD45RA<sup>-</sup> cells carrying the expression signature recognizes islet cell peptides. This signature is carried by significant numbers of T cells that exceed the numbers usually recognized by individual islet peptide-HLA tetramers [39]. For example, in pediatric patients, about 25% of CD8<sup>+</sup>CD45RA<sup>-</sup> T cells shift from the naïve populations 2 and 3 to the activated heterogeneous population 1 (Fig. 2). In the FACS analysis, many pediatric patients harbor double-digit percentages of IL-10R<sup>+</sup>/TGF-β<sup>+</sup> CD8<sup>+</sup>CD45RA<sup>-</sup> T cells (Fig. 3B). It is possible that these relatively elevated numbers reflect metabolic and/or inflammatory perturbation associated with T1D onset; the latter could be related to the systemic type I IFN signature already present in pre-diabetic children [12]. However, it is also conceivable that tetramer studies underestimate the number of islet-reactive CD8<sup>+</sup> T cells. Application of novel technologies such as Major Histo-Compatibility class I dodecamers [40] or micropipette adhesion [41] has revealed that the number of self-reactive T cells is much larger than previously assumed based on conventional tetramers. Whatever the antigenic specificity of the T cells carrying the expression signature, our results demonstrate that analysis of gene and protein expression by bulk memory/activated CD8<sup>+</sup> T cells uncovers a signature associated with onset of pediatric T1D. Importantly the abundance of T cells co-expressing the signature proteins TGF-β and IL-10R correlates strongly with GAD autoantibody titers which in turn correlate with disease risk [42], as well as with HbA1c levels. Therefore the presence of these T cells reflects key metabolic and auto-immune parameters of T1D, indicating a positive association with the pathogenesis of the disease.

While the finding of increased PRF and Gzm B expression at T1D onset is less surprising in an auto-aggressive setting, strong up-regulation of TGF-β and IL-10R was unexpected. Both TGF-β and IL-10 can be secreted by regulatory CD8<sup>+</sup> T cells that suppress anti-tumor and anti-infectious responses as well as autoimmune responses, for example in a murine model of multiple sclerosis or in human systemic lupus erythematosus [33,43–45]. Moreover, TGF-β directly inhibits CD8<sup>+</sup> T cell cytotoxicity and cytokine secretion [46]. Therefore, the cells co-expressing effector with regulatory functions might have a suppressive function, for example by eliminating cells presenting islet antigens. The abundance of such cells in pediatric patients and specifically in those with high GAD auto-Ab titers and elevated HbA1c could then be viewed as an attempt of counteracting an especially aggressive autoimmune response, consistent for example with the finding that lymphocytes from siblings of T1D patient with a high diabetes risk showed more robust expression of genes associate with regulation than lymphocytes from siblings with low risk [16]. This phenomenon might also be due to the boosting effect of pathogenic T cells on regulatory T cells, as observed in the model of the non-obese diabetic mouse [47].

However, other functions more consistent with a direct auto-aggressive role of the cells co-expressing regulatory and effector proteins are conceivable. TGF-β can promote the growth and survival of memory/activated CD8<sup>+</sup> T cells [34,48], and IL-10 can paradoxically enhance the cytotoxic activity of tumor-specific CD8<sup>+</sup> T cells [49]. Moreover, in a murine model where CD8<sup>+</sup> T cells recognizing a viral antigen cause T1D with slow onset, TGF-β promoted accumulation and activation of autoreactive cells in islets [50].

The striking dissociation of Gzm A and Gzm B expression among pediatric CD8<sup>+</sup> cells is another surprising observation awaiting

future functional studies. In conclusion, while our report highlights the specific emergence of unusual CD8<sup>+</sup> T cells in pediatric T1D, additional studies are required to establish their function and potential autoreactivity. It will be critical to examine the possible correlation of these cells with the likelihood and imminence of disease in individuals at risk of T1D, and to monitor the effect of therapeutic immune intervention on it. Depending on the results of such studies, the CD8<sup>+</sup> lymphocyte signature may represent a biomarker exploitable for early diagnostic and stratification of T1D as well as monitoring of disease progress and response to immunotherapy.

## Competing interests

The authors have no competing financial interests.

## Acknowledgements

We thank Cecile Vuong and Cindy Guillaume for help in single cell PCR work. Funding: supported by institutional grants from INSERM and grants from the European Union through DIAPREPP (DIABETES type 1 Prediction Early Pathogenesis and Prevention, [www.diaprepp.eu](http://www.diaprepp.eu); HEALTH-F2-2008-202013) to PvE, from AJD (L'Aide aux jeunes Diabétiques, Paris, France) to PvE and FXM and from La Fondation pour la Recherche Médicale (DEQ20130326539) to PvE, and by a grant from ARC (Association pour la Recherche sur le Cancer, grant no 7869, Villejuif, France) to the cytometry platform of INSERM US24. The single cell PCR method is covered by European patent 0208593 registered by *Institut Necker*.

## Appendix A. Supplementary data

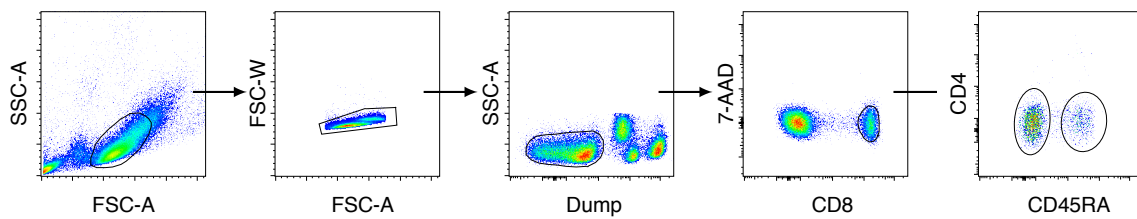
Supplementary data related to this article can be found at <http://dx.doi.org/10.1016/j.jaut.2016.06.003>.

## References

- [1] P. Santamaria, The long and winding road to understanding and conquering type 1 diabetes, *Immunity* 32 (2010) 437–445.
- [2] K.T. Coppieters, F. Dotta, N. Amirian, P.D. Campbell, T.W. Kay, M.A. Atkinson, et al., Demonstration of islet-autoreactive CD8 T cells in insulinitic lesions from recent onset and long-term type 1 diabetes patients, *J. Exp. Med.* 209 (2012) 51–60.
- [3] R.S. Liblau, F.S. Wong, L.T. Mars, P. Santamaria, Autoreactive CD8 T cells in organ-specific autoimmunity: emerging targets for therapeutic intervention, *Immunity* 17 (2002) 1–6.
- [4] M. Knip, H. Siljander, Autoimmune mechanisms in type 1 diabetes, *Autoimmun. Rev.* 7 (2008) 550–557.
- [5] T.P. Di Lorenzo, M. Peakman, B.O. Roep, Translational mini-review series on type 1 diabetes: systematic analysis of T cell epitopes in autoimmune diabetes, *Clin. Exp. Immunol.* 148 (2007) 1–16.
- [6] E. Enee, R. Kratzer, J.B. Arnoux, E. Barilleau, Y. Hamel, C. Marchi, et al., ZnT8 is a major CD8<sup>+</sup> T cell-recognized autoantigen in pediatric type 1 diabetes, *Diabetes* 61 (2012) 1779–1784.
- [7] B.O. Roep, M. Peakman, Diabetogenic T lymphocytes in human type 1 diabetes, *Curr. Opin. Immunol.* 23 (2011) 746–753.
- [8] S. Tsai, A. Shameli, J. Yamanouchi, X. Clemente-Casares, J. Wang, P. Serra, et al., Reversal of autoimmunity by boosting memory-like autoregulatory T cells, *Immunity* 32 (2010) 568–580.
- [9] J.S. Tsang, P.L. Schwartzberg, Y. Kotliarov, A. Biancotto, Z. Xie, R.N. Germain, et al., Global analyses of human immune variation reveal baseline predictors of postvaccination responses, *Cell* 157 (2014) 499–513.
- [10] V. Pascual, D. Chaussabel, J. Banachereau, A genomic approach to human autoimmune diseases, *Annu. Rev. Immunol.* 28 (2010) 535–571.
- [11] S. Luce, F. Lemonnier, J.P. Briand, J. Coste, N. Lahlou, S. Muller, et al., Single insulin-specific CD8<sup>+</sup> T cells show characteristic gene expression profiles in human type 1 diabetes, *Diabetes* 60 (2011) 3289–3299.
- [12] R.C. Ferreira, H. Guo, R.M. Coulson, D.J. Smyth, M.L. Pekalski, O.S. Burren, et al., A type I interferon transcriptional signature precedes autoimmunity in children genetically at risk for type 1 diabetes, *Diabetes* 63 (2014) 2538–2550.
- [13] M. Heinig, E. Petretto, C. Wallace, L. Bottolo, M. Rotival, H. Lu, et al., A trans-acting locus regulates an anti-viral expression network and type 1 diabetes risk, *Nature* 467 (2010) 460–464.

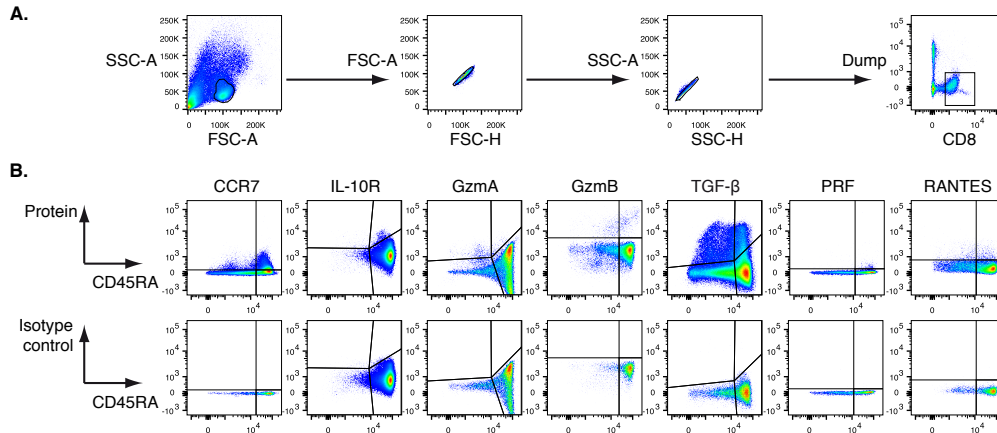
- [14] H. Kallionpää, L.L. Elo, E. Laajala, J. Mykkanen, I. Ricano-Ponce, M. Vaarma, et al., Innate immune activity is detected prior to seroconversion in children with HLA-conferred type 1 diabetes susceptibility, *Diabetes* 63 (2014) 2402–2414.
- [15] X. Wang, S. Jia, R. Geoffrey, R. Alemzadeh, S. Ghosh, M.J. Hessner, Identification of a molecular signature in human type 1 diabetes mellitus using serum and functional genomics, *J. Immunol.* 180 (2008) 1929–1937.
- [16] Y.G. Chen, S.M. Cabrera, S. Jia, M.L. Kaldunski, J. Kramer, S. Cheong, et al., Molecular signatures differentiate immune states in type 1 diabetic families, *Diabetes* 63 (2014) 3960–3973.
- [17] Q. Zhang, T.L. Fillmore, A.A. Schepmoes, T.R. Clauss, M.A. Gritsenko, P.W. Mueller, et al., Serum proteomics reveals systemic dysregulation of innate immunity in type 1 diabetes, *J. Exp. Med.* 210 (2013) 191–203.
- [18] M. Oresic, S. Simell, M. Sysi-Aho, K. Nanto-Salonen, T. Seppanen-Laakso, V. Parikka, et al., Dysregulation of lipid and amino acid metabolism precedes islet autoimmunity in children who later progress to type 1 diabetes, *J. Exp. Med.* 205 (2008) 2975–2984.
- [19] E.F. McKinney, J.C. Lee, D.R. Jayne, P.A. Lyons, K.G. Smith, T-cell exhaustion, costimulation and clinical outcome in autoimmunity and infection, *Nature* 523 (2015) 612–616.
- [20] E.F. McKinney, P.A. Lyons, E.J. Carr, J.L. Hollis, D.R. Jayne, L.C. Willcocks, et al., A CD8+ T cell transcription signature predicts prognosis in autoimmune disease, *Nat. Med.* 16 (2010) 586–591, 1p following 91.
- [21] A. Peixoto, M. Monteiro, B. Rocha, H. Veiga-Fernandes, Quantification of multiple gene expression in individual cells, *Genome Res.* 14 (2004) 1938–1947.
- [22] M. Monteiro, C. Evaristo, A. Legrand, A. Nicoletti, B. Rocha, Cartography of gene expression in CD8 single cells: novel CCR7- subsets suggest differentiation independent of CD45RA expression, *Blood* 109 (2007) 2863–2870.
- [23] B. Efron, Bootstrap methods: another look at the jackknife, *Ann. Stat.* 7 (1979) 1–26.
- [24] C. Hennig, Cluster-wise assessment of cluster stability, *Comput. Stat. Data An.* 52 (2007) 258–271.
- [25] L. Breiman, Random forests, *Mach. Learn.* 45 (2001) 5–32.
- [26] J.H. Bullard, E. Purdom, K.D. Hansen, S. Dudoit, Evaluation of statistical methods for normalization and differential expression in mRNA-Seq experiments, *BMC Bioinforma.* 11 (2010) 94.
- [27] J. Li, R. Tibshirani, Finding consistent patterns: a nonparametric approach for identifying differential expression in RNA-Seq data, *Stat. Methods Med. Res.* 22 (2013) 519–536.
- [28] T. Willinger, T. Freeman, H. Hasegawa, A.J. McMichael, M.F. Callan, Molecular signatures distinguish human central memory from effector memory CD8 T cell subsets, *J. Immunol.* 175 (2005) 5895–5903.
- [29] S. Caillat-Zucman, H.J. Garchon, J. Timsit, R. Assan, C. Boitard, I. Djilali-Saiah, et al., Age-dependent HLA genetic heterogeneity of type 1 insulin-dependent diabetes mellitus, *J. Clin. Investig.* 90 (1992) 2242–2250.
- [30] E. Sabbah, K. Savola, T. Ebeling, P. Kulmala, P. Vahasalo, J. Ilonen, et al., Genetic, autoimmune, and clinical characteristics of childhood- and adult-onset type 1 diabetes, *Diabetes Care* 23 (2000) 1326–1332.
- [31] J. Lieberman, Granzyme A activates another way to die, *Immunol. Rev.* 235 (2010) 93–104.
- [32] H.E. Thomas, J.A. Trapani, T.W. Kay, The role of perforin and granzymes in diabetes, *Cell Death Diff.* 17 (2010) 577–585.
- [33] M.L. Chen, B.S. Yan, D. Kozoriz, H.L. Weiner, Novel CD8+ Treg suppress EAE by TGF-beta- and IFN-gamma-dependent mechanisms, *Eur. J. Immunol.* 39 (2009) 3423–3435.
- [34] S.A. Oh, M.O. Li, TGF-beta: guardian of T cell function, *J. Immunol.* 191 (2013) 3973–3979.
- [35] K.W. Moore, R. de Waal Malefyt, R.L. Coffman, A. O'Garra, Interleukin-10 and the interleukin-10 receptor, *Annu. Rev. Immunol.* 19 (2001) 683–765.
- [36] P. Kulmala, K. Savola, H. Reijonen, R. Veijola, P. Vahasalo, J. Karjalainen, et al., Genetic markers, humoral autoimmunity, and prediction of type 1 diabetes in siblings of affected children, Childhood Diabetes in Finland Study Group, *Diabetes* 49 (2000) 48–58.
- [37] J. Graham, W.A. Hagopian, I. Kockum, L.S. Li, C.B. Sanjeevi, R.M. Lowe, et al., Genetic effects on age-dependent onset and islet cell autoantibody markers in type 1 diabetes, *Diabetes* 51 (2002) 1346–1355.
- [38] C.L. Vandewalle, T. Decraene, F.C. Schuit, I.H. De Leeuw, D.G. Pipeleers, F.K. Gorus, Insulin autoantibodies and high titre islet cell antibodies are preferentially associated with the HLA DQA1\*0301-DQB1\*0302 haplotype at clinical type 1 (insulin-dependent) diabetes mellitus before age 10 years, but not at onset between age 10 and 40 years, The Belgian Diabetes Registry, *Diabetologia* 36 (1993) 1155–1162.
- [39] J.H. Velthuis, W.W. Unger, J.R. Abreu, G. Duinkerken, K. Franken, M. Peakman, et al., Simultaneous detection of circulating autoreactive CD8+ T-cells specific for different islet cell-associated epitopes using combinatorial MHC multimers, *Diabetes* 59 (2010) 1721–1730.
- [40] J. Huang, X. Zeng, N. Sigal, P.J. Lund, L.F. Su, H. Huang, et al., Detection, phenotyping, and quantification of antigen-specific T cells using a peptide-MHC dodecamer, *Proc. Natl. Acad. Sci. U. S. A.* 113 (2016) E1890–E1897.
- [41] J.J. Sabatino Jr., J. Huang, C. Zhu, B.D. Evavold, High prevalence of low affinity peptide-MHC II tetramer-negative effectors during polyclonal CD4+ T cell responses, *J. Exp. Med.* 208 (2011) 81–90.
- [42] T. Orban, J.M. Sosenko, D. Cuthbertson, J.P. Krischer, J.S. Skyler, R. Jackson, et al., Pancreatic islet autoantibodies as predictors of type 1 diabetes in the diabetes prevention trial-type 1, *Diabetes Care* 32 (2009) 2269–2274.
- [43] S. Harfouch, M. Guiguet, M.A. Valantin, A. Samri, Z. Ouazene, L. Slama, et al., Lack of TGF-beta production by hepatitis C virus-specific T cells during HCV acute phase is associated with HCV clearance in HIV coinfection, *J. Hepatol.* 56 (2012) 1259–1268.
- [44] A.G. Jarnicki, J. Lysaght, S. Todryk, K.H. Mills, Suppression of antitumor immunity by IL-10 and TGF-beta-producing T cells infiltrating the growing tumor: influence of tumor environment on the induction of CD4+ and CD8+ regulatory T cells, *J. Immunol.* 177 (2006) 896–904.
- [45] L. Zhang, A.M. Bertucci, R. Ramsey-Goldman, R.K. Burt, S.K. Datta, Regulatory T cell (Treg) subsets return in patients with refractory lupus following stem cell transplantation, and TGF-beta-producing CD8+ Treg cells are associated with immunological remission of lupus, *J. Immunol.* 183 (2009) 6346–6358.
- [46] L. Gorelik, R.A. Flavell, Transforming growth factor-beta in T-cell biology, *Nat. Rev. Immunol.* 2 (2002) 46–53.
- [47] Y. Grinberg-Bleyer, D. Saadoun, A. Baeyens, F. Billiard, J.D. Goldstein, S. Gregoire, et al., Pathogenic T cells have a paradoxical protective effect in murine autoimmune diabetes by boosting Tregs, *J. Clin. Investig.* 120 (2010) 4558–4568.
- [48] J.H. Kehrl, L.M. Wakefield, A.B. Roberts, S. Jakowlew, M. Alvarez-Mon, R. Derynck, et al., Pillars article: production of transforming growth factor beta by human T lymphocytes and its potential role in the regulation of T cell growth, *J. Exp. Med.* 163 (1986) 1037–1050, *J. Immunol.* 2014;192:2939–52.
- [49] J.B. Mumm, M. Oft, Pegylated IL-10 induces cancer immunity: the surprising role of IL-10 as a potent inducer of IFN-gamma-mediated CD8(+) T cell cytotoxicity, *BioEssays News Rev. Mol. Cell. Dev. Biol.* 35 (2013) 623–631.
- [50] C.M. Filippi, A.E. Juedes, J.E. Oldham, E. Ling, L. Togher, Y. Peng, et al., Transforming growth factor-beta suppresses the activation of CD8+ T-cells when naive but promotes their survival and function once antigen experienced: a two-faced impact on autoimmunity, *Diabetes* 57 (2008) 2684–2692.

## Supplementary Data



**Supplementary Figure 1.** Sorting of single  $CD8^+CD45RA^+$  and  $CD8^+CD45RA^-$  T cells for analysis by RT-PCR. Single lymphocytes were selected using successive gates for FSC-A/SSC-A and FSC-W/FSC-A, followed by selection of viable cells negative for the “dump-channel” (CD14-, CD16-, CD56-, CD19-PE) and for 7-AAD, and subdivision in the  $CD45RA^+$  and  $CD45RA^-$  subsets.





**Supplementary Figure 2. Gating strategy and thresholds used for multi-parametric flow cytometry. (A)** Successive dot plots represent the gating strategy used to identify CD8<sup>+</sup> T cells: after exclusion of doublets, contaminating cells (B cells, monocytes, CD4<sup>+</sup> T cells, NK cells and NK-T cells) were excluded by gating on cells positive for CD8 and negative for CD4, CD14, CD16, CD19 and CD56, all stained in the dump channel. **(B)** Staining observed with fluorochrome-conjugated antibodies specific for CCR7, IL-10R, Gzm A, Gzm B, TGF-β, PRF and RANTES was compared with fluorochrome-conjugated isotype controls. The thresholds of positivity for a given protein were delineated using the Fluorescence Minus One method.

**Supplementary Table 1. Characteristics of T1D patients**

Subject code	Sex	Age (years)	Days after diagnosis	GAD Abs (>90 cpm*)	IA-2 Abs (>55 cpm*)	ICA Abs (titer)	ZnT8 Abs (>150 cpm*)	HbA1c (%)
<b>Subjects included in the gene expression analysis</b>								
DA.01	M	21	5	<b>2488</b>	22	N/A	N/A	9.6
DA.02	F	20	4	<b>166</b>	37	N/A	N/A	15.1
DA.03	M	28	2	<b>149</b>	27	N/A	N/A	15.0
DA.04	M	26	3	<b>584</b>	-	N/A	-	9.4
DA.05	M	29	6	72	<b>78</b>	N/A	N/A	8.1
DA.06	M	61	1	<b>112</b>	6	N/A	N/A	13.1
DA.07	F	46	4	1050	-	N/A	N/A	11.5
DA.08	M	23	5	<b>2765</b>	<b>199</b>	-	103	9.5
DA.09	F	61	2	<b>3614</b>	<b>5182</b>	N/A	N/A	12.1
DA.10	F	21	0	<b>123</b>	20	N/A	38	14.2
DP.01	F	5	3	<b>2075</b>	<b>4010</b>	+ (>1/8)	N/A	11.8
DP.02	M	3	2	<b>478</b>	<b>972</b>	+ (>1/8)	N/A	9.2
DP.03	M	6	1	<b>157</b>	<b>2232</b>	+ (>1/8)	N/A	14.2
DP.04	F	14	1	<b>514</b>	<b>2184</b>	+ (>1/8)	N/A	7.4
DP.05	F	2	0	<b>372</b>	<b>3399</b>	+ (1/4)	N/A	10.5
DP.06	F	12	0	<b>872</b>	1118	+ (1/8)	N/A	14.1
DP.07	F	3	1	<b>872</b>	19	-	N/A	8.3
DP.08	F	10	0	<b>206</b>	<b>2339</b>	+ (>1/8)	<b>747</b>	9.8
DP.09	F	3	0	<b>112</b>	44	+ (1/4)	<b>51</b>	7.5
DP.10	F	10	29	<b>184</b>	<b>2823</b>	+ (>1/8)	58	14.2
DP.11	M	9	0	<b>890</b>	<b>3134</b>	+ (>1/8)	<b>549</b>	13.4
DP.12	F	9	9	<b>693</b>	<b>3358</b>	+ (>1/8)	139	12.2
<b>Subjects included in the protein expression analysis</b>								
DP.14	M	5	6	<b>122</b>	<b>4606</b>	+ (>1/8)	<b>1326</b>	10.8
DP.15	F	13	4	<b>163</b>	<b>242</b>	+ (1/4)	<b>2351</b>	10.1
DP.16	M	8	0	69	<b>2057</b>	+ (1/4)	60	12.1
DP.17	M	15	0	<b>329</b>	<b>5634</b>	+ (>1/8)	96	12.7
DP.18	F	6	0	<b>244</b>	<b>3410</b>	+ (1/4)	90	6.9
DP.19	F	11	1	<b>2241</b>	20	+ (1/4)	<b>178</b>	15.2
DP.20	F	10	1	<b>273</b>	<b>3369</b>	+ (>1/8)	<b>975</b>	12.2
DP.21	F	4	0	<b>691</b>	<b>4626</b>	+ (>1/8)	56	15.5
DP.22	M	9	3	25	21	+ (>1/8)	<b>1581</b>	9.7
DP.23	F	9	1	<b>1827</b>	<b>5558</b>	+ (>1/8)	<b>1313</b>	13.5
DP.24	M	15	1	<b>96</b>	<b>320</b>	+ (1/8)	80	12.7
DP.25	M	10	4	86	<b>422</b>	-	129	8.6
DP.26	M	9	0	63	<b>4245</b>	+ (>1/8)	110	12.2
DP.27	F	8	2	<b>384</b>	<b>1696</b>	+ (>1/8)	<b>1370</b>	7.6
DP.28	M	9	4	<b>227</b>	<b>2680</b>	+ (>1/8)	67	8.7
DP.29	M	9	0	<b>679</b>	<b>5078</b>	+ (>1/8)	131	11.2
DP.30	M	7	0	<b>1969</b>	<b>6801</b>	+ (>1/8)	<b>4248</b>	12.1
DP.31	F	5	0	<b>669</b>	8	-	25	10.8
DP.32	F	12	0	25	<b>328</b>	+ (>1/8)	<b>890</b>	9.7
DP.33	M	5	0	66	1	+ (>1/8)	<b>780</b>	11.2
DP.34	M	4	0	<b>1013</b>	55	+ (1/4)	54	15.4
DP.35	F	13	1	NA	5	+ (>1/8)	<b>1842</b>	8.1
DP.36	M	8	0	60	<b>5072</b>	+ (>1/8)	11	10.9
DP.37	M	9	1	<b>936</b>	NA	+ (>1/8)	N/A	14.6
DP.38	F	4	0	<b>347</b>	NA	+ (>1/8)	10	11.3

DA: Non Diabetic Adult patient; DP: Diabetic Pediatric patient; Abs: antibodies; N/A: Not Analyzed; \*, threshold of positivity.

**Supplementary Table 2. Characteristics of control subjects**

Subject code	Sex	Age	Diagnosis	Medications
<b>Subjects included in the molecular analysis</b>				
NDA.01	F	30	N/A	None
NDA.02	M	35	N/A	None
NDA.03	F	26	N/A	None
NDA.04	M	38	N/A	None
NDA.05	M	30	N/A	None
NDA.06	F	32	N/A	None
NDA.07	F	29	N/A	None
NDA.08	F	39	N/A	None
NDA.09	M	25	N/A	None
NDA.10	M	30	N/A	None
NDA.11	F	30	N/A	None
NDA.12	M	38	N/A	None
NDP.01	M	9	Osteogenesis imperfecta	Pamidronate
NDP.02	F	17	Progressive multi-focal encephalopathy	Vigabatrin
NDP.03	F	16	Growth hormone deficiency	Growth hormone
NDP.04	M	7	Citrullinemia, type 1	Sodium benzoate, arginine
NDP.05	M	10	Glycogen storage disease, type 1	Cornstarch
NDP.06	M	12	Osteogenesis imperfecta	Pamidronate
NDP.07	F	15	Leucinosi-mapple syrup disease	Amino acids
NDP.08	M	6	Ornithine Transcarbamylase deficiency	Sodium benzoate, citrulline
NDP.09	M	14	Posttraumatic epilepsy	valproic acid
NDP.10	F	5	Fasting test	None
<b>Subjects included in the protein analysis</b>				
NDP.11	M	5	Ornithine Transcarbamylase deficiency	Sodium benzoate, citrulline
NDP.12	M	16	Hypophysis adenoma	Growth hormone
NDP.13	M	12	Osteogenesis imperfecta	Pamidronate
NDP.14	M	8	Ornithine Transcarbamylase deficiency	Sodium benzoate, citrulline
NDP.15	M	14	Medullary cysts	None
NDP.16	F	8	Idiopathic generalized dystonia	None
NDP.17	M	9	Osteogenesis imperfecta	Pamidronate
NDP.18	F	10	Growth hormone deficiency	Growth hormone
NDP.19	F	6	Hyperketotic hypoglycemia	None
NDP.20	F	7	Carbamoyl Phosphate Synthetase 1 deficiency	Sodium benzoate, citrulline
NDP.21	F	6	Citrullinemia, type 1	Sodium benzoate, arginine
NDP.22	M	9	Carbamoyl Phosphate Synthetase 1 deficiency	Sodium benzoate, citrulline
NDP.23	M	9	Arginase deficiency	Sodium benzoate
NDP.24	M	7	Hyperinsulinism	Cornstarch/Proglucem
NDP.25	M	8	Osteogenesis imperfecta	Pamidronate
NDP.26	F	12	Growth hormone deficiency	Growth hormone
NDP.27	F	8	Fructose-1-6-bisphosphatase deficiency	Fructose-free diet
NDP.28	M	5	Glycogen storage disease, type 3	Cornstarch
NDP.29	M	10	Osteogenesis imperfecta	Pamidronate
NDP30	M	8	Osteogenesis imperfecta	Pamidronate
NDP.31	F	4	Pyruvate Dehydrogenase Complex deficiency	Thiamine, ketogenic diet
NDP.32	F	12	Ornithine Transcarbamylase deficiency	Sodium benzoate, citrulline
NDP.33	M	4	Idiopathic mental disability	None

NDP.34	F	6	Ornithine Transcarbamylase deficiency	Sodium benzoate, citrulline
NDP.35	F	12	Citrullinemia, type 1	Sodium benzoate, arginine

---

NDA: Non Diabetic Adult subject; NDP: Non Diabetic Pediatric patient; N/A, not applicable.

**Supplementary Table 3.** Characteristics and working dilution for antibodies used for cell sorting or analysis.

Antibody	Fluorochrome	Clone or specificity	Species / Isotype	Company	Dilution ( $\mu\text{L}/100 \mu\text{L}$ )
CCR-7	Brilliant Violet 421	150503	Mouse IgG2a, $\kappa$	BD Biosciences	5
CD4	PE	RPA-T4	Mouse IgG1, $\kappa$	BD Biosciences	20
CD8	FITC	RPA-T8	Mouse IgG1, $\kappa$	BD Biosciences	10
CD8	V500	RPA-T8	Mouse IgG1, $\kappa$	BD Biosciences	5
CD14	PE	M5E2	Mouse IgG2a, $\kappa$	BD Biosciences	8
CD16	PE	3G8	Mouse IgG1, $\kappa$	BD Biosciences	8
CD19	PE	SJ25C1	Mouse IgG1, $\kappa$	BD Biosciences	8
CD45RA	Pacific Blue	HI100	Mouse IgG2b, $\kappa$	eBioscience	10
CD45RA	PE-CF594	HI100	Mouse IgG2b, $\kappa$	BD Biosciences	3
CD56	PE	B159	Mouse IgG1, $\kappa$	BD Biosciences	8
CDw210a	Biotin	3F9	Rat IgG2a	AbD Serotec	10
Granzyme A	PerCP-Cy5.5	CB9	Mouse IgG1, $\kappa$	Biolegend	5
Granzyme B	Alexa Fluor 700	GB11	Mouse IgG1, $\kappa$	Biolegend	5
LAP(TGF- $\beta$ 1)	PE/Cy7	TW4-2F8	Mouse IgG1, $\kappa$	Biolegend	5
Perforin	FITC	$\delta$ G8	Mouse IgG1, $\kappa$	BD Biosciences	20
RANTES	Alexa Fluor 647	VL1	Mouse IgG2b, $\kappa$	Biolegend	5
Isotype ctrl	Alexa Fluor 647	MPC-11	Mouse IgG2b, $\kappa$	Biolegend	5
Isotype ctrl	Alexa Fluor 700	MOPC-21	Mouse IgG1, $\kappa$	BD Biosciences	5
Isotype ctrl	Biotin	dNTP Hapten	Rat IgG2a	AbD Serotec	10
Isotype ctrl	Brilliant Violet 421	G155-178	Mouse IgG2a, $\kappa$	BD Biosciences	5
Isotype ctrl	FITC	Anti-dansyl	Mouse IgG1, $\kappa$	BD Biosciences	20
Isotype ctrl	PE/Cy7	MOPC-21	Mouse IgG1, $\kappa$	Biolegend	5
Isotype ctrl	PerCP/Cy5.5	MOPC-21	Mouse IgG1, $\kappa$	Biolegend	5

Isotype ctrl: isotype control; dNTP: dinitrophenol.

**Supplementary Table 4.** Gene expression by single CD45RA<sup>+</sup> and CD45RA<sup>-</sup> CD8<sup>+</sup> T cells from peripheral blood of patients with adult-onset and juvenile-onset T1D in comparison with controls

	CD8 <sup>+</sup> CD45RA <sup>+</sup> T cells					CD8 <sup>+</sup> CD45RA <sup>-</sup> T cells				
	Patients <sup>a</sup>		Controls <sup>b</sup>		FDR <sup>e</sup>	Patients		Controls		FDR
	Pos. <sup>c</sup>	Neg. <sup>d</sup>	Pos.	Neg.		Pos.	Neg.	Pos.	Neg.	
<b>ADULT ONSET</b>										
GzmA	52	257	82	331	1	215	292	195	226	1
GzmB	23	286	38	375	0.36	100	407	57	364	0.36
PRF <sup>c</sup>	30	279	79	334	0.24	149	358	143	278	0.42
IL-2	28	281	33	380	- <sup>e</sup>	30	477	21	400	-
IFN- $\gamma$	47	262	52	361	0.58	86	421	71	350	0.36
TGF- $\beta$	112	197	132	281	0.58	242	265	185	236	0.55
FASL	3	306	16	397	-	13	494	11	410	-
KLRG1	3	306	30	383	-	53	454	66	355	0.42
IL-10R	64	245	124	289	0.24	188	319	209	212	0.42
IL-7R	232	77	315	98	0.58	431	76	357	64	1
CCR7	118	191	175	238	0.58	63	444	86	335	1
RANTES	45	264	98	315	0.24	275	232	193	228	1
MIP-1 $\beta$	22	287	25	388	-	74	433	48	373	0.36
<b>JUVENILE ONSET</b>										
<b>GzmA</b>	<b>43</b>	<b>349</b>	<b>117</b>	<b>364</b>	<b>0</b>	<b>156</b>	<b>226</b>	<b>288</b>	<b>140</b>	<b>0</b>
<b>GzmB</b>	57	335	37	444	0.48		305			
						77		51	377	0.12
<b>PRF</b>	22	370	52	429	0.22	<b>171</b>	<b>211</b>	<b>80</b>	<b>348</b>	<b>0</b>
IL-2	7	385	14	467	-	6	376	16	412	-
IFN- $\gamma$	52	340	41	440	0.22					
						71	311	42	386	0.12
<b>TGF-<math>\beta</math></b>	102	290	126	355	1	<b>285</b>	<b>97</b>	<b>146</b>	<b>282</b>	<b>0</b>
FASL	12	380	32	449	-	19	363	37	391	-
<b>KLRG1</b>	6	386	38	443	-	<b>18</b>	<b>364</b>	<b>62</b>	<b>366</b>	<b>0</b>
<b>IL-10R</b>	124	268	106	375	0.22					
						205	177	165	263	0.16
<b>IL-7R</b>	354	38	358	123	1	<b>242</b>	<b>140</b>	<b>316</b>	<b>112</b>	<b>0</b>
<b>CCR7</b>	219	173	209	272	0.22	<b>44</b>	<b>338</b>	<b>71</b>	<b>357</b>	<b>0</b>
<b>RANTES</b>	<b>32</b>	<b>360</b>	<b>97</b>	<b>384</b>	<b>0</b>	<b>262</b>	<b>120</b>	<b>276</b>	<b>152</b>	<b>0</b>
MIP-1 $\beta$	9	383	24	457	-	54	328	39	389	0.16

<sup>a</sup> N=10 for adult patients and N=12 for pediatric patients. <sup>b</sup> N=12 for adult controls and N=10 for pediatric controls. <sup>c</sup> Pos., number of cells expressing the gene. <sup>d</sup> Neg., number of cells not expressing the gene. <sup>e</sup> False discovery rate in SAMseq test. **bold**: FDR < 0.05 in SAMseq test.

Highly efficient cross-priming of CD8<sup>+</sup> T cells by splenic CD169<sup>+</sup> macrophages employing a unique endosomal processing pathway. **Mauvais FX**, Hamel Y, Garfa-Traore M, Diana J, van Endert P. **(manuscript in preparation, not submitted)**

**Highly efficient cross-priming of CD8+ T cells by splenic CD169+ macrophages employing a unique endosomal processing pathway.**

**Mauvais FX<sup>1,2,3</sup>, Hamel Y<sup>3,4</sup>, Garfa-Traore M<sup>5</sup>, Diana J<sup>1,2,3</sup>, van Endert P<sup>1,2,3\*</sup>.**

1. Institut National de la Santé et de la Recherche Médicale, Unité 1151, Paris, 75015, France

2. Centre National de la Recherche Scientifique, Unité 8253, Paris, 75015, France

3. Université Paris Descartes, Sorbonne Paris Cité, Faculté de médecine Paris Descartes, 75015 Paris, France

4. Institut National de la Santé et de la Recherche Médicale, Unité 1163, Paris, 75015, France

5. Cell Imaging Platform, INSERM US24 Centre National de la Recherche Scientifique Unité Mixte de Service 3633, Structure Fédérative de Recherche Necker, Paris, France

\* Corresponding author

\* Corresponding author

Peter van Endert INSERM, Unité 1151, Hôpital Necker-Enfants malades, 149 rue de Sèvres, 75743 Paris cedex 15, France

Email: [peter.van-endert@inserm.fr](mailto:peter.van-endert@inserm.fr)



## **ABSTRACT.**

Splenic CD169<sup>+</sup> metallophilic marginal zone macrophages are strategically located for uptake of soluble and particulate blood-borne antigens. However, their role in T cell priming is commonly considered limited to antigen capture and transfer to adjacent dendritic cells. To critically evaluate this concept, we developed a novel protocol allowing for the first time to purify these cells and examine their function *in vitro*. Purified CD169<sup>+</sup> macrophages are clearly distinct from dendritic cells by size and morphology and by expression of key genes and of a vast panel of surface receptors. In contrast to current concepts, we demonstrate that purified CD169<sup>+</sup> macrophages cross-present receptor-targeted antigen as well as CD8<sup>+</sup> DCs, and soluble and particulate antigen with greater efficacy. Consistent with this, antigen targeting to CD169<sup>+</sup> and DEC205 *in vivo* induce T cell proliferation with equivalent efficiency. However, quality of cross-priming by CD169<sup>+</sup> macrophages is better than conventional cDC1s, with a higher proportion of poly-functional effector and memory CD8<sup>+</sup> T cell subsets. Intravital two-photon live imaging of splenic marginal sinuses reveals rapid T cell arrest on CD169<sup>+</sup> metallophilic macrophages upon antigen targeting. We also examined the intracellular cross-presentation pathway employed by CD169<sup>+</sup> macrophages. Although, in the case of dendritic cells, strictly endosomal (“vacuolar”) cross-presentation is considered inefficient, we find that, in CD169<sup>+</sup> macrophages, endosomal processing and presentation of internalized antigen is highly efficient, possibly due to a unique MHC class I recycling pathway. Thus, CD169<sup>+</sup> metallophilic macrophages, together with cDC1s, belong to a small group of professional antigen cross-presenting cells capable of generating robust CD8<sup>+</sup> T cell responses.

Dendritic cells and macrophages are both components of the mononuclear phagocyte system and contribute to tissue homeostasis, to initiate and regulate inflammation and to initiate or modulate adaptive immune responses (Geissmann, Gordon et al. 2010). Dendritic cells are the only professional antigen-presenting cells capable of generating a protective immunity against microbial pathogens and tumors, especially because they are specialized in the presentation of exogenous antigens to CD4<sup>+</sup> and CD8<sup>+</sup> T lymphocytes through both the MHC-II and the MHC-I molecules, the latter process being referred to as antigen cross-presentation (Joffre, Segura et al. 2012). While most of the molecular mechanisms remain probably elusive, several reports have characterized key features of dendritic cells that regulate antigen cross-presentation.

In this context, several reports have identified different pathways of cross-presentation that differ in the site of antigen processing into MHC-I ligands as well as presumably in the site of peptide loading onto MHC-I molecules (Joffre, Segura et al. 2012). In the cytosolic pathway, antigenic material are actively exported (Zehner, Marschall et al. 2015) from the endosome or the phagosome to the cytosol for a digestion by the proteasome complex (van Endert 2016); proteasome products may get access to the endoplasmic reticulum by the transporter associated antigen protein (TAP) for further processing by the ER-aminopeptidases and loading into MHC-I molecules (Joffre, Segura et al. 2012), or may return by an active retro-transport back to the phagosome (Ackerman, Giodini et al. 2006, Cebrian, Visentin et al. 2011) or endosome for additional processing by the insulin-related aminopeptidase (IRAP) and loading into MHC-I molecules. In the vacuolar pathway, antigenic material exclusively resides within the endocytic pathway to be degraded by endosomal and lysosomal proteases (Joffre, Segura et al. 2012), including cathepsin S (Shen, Sigal et al. 2004) and peptide loading onto MHC-I occurs in endosomes or phagosomes. Despite the presence of several pathways, cross-presenting dendritic cells preferentially employ the cytosolic pathway (Mant,

Chinnery et al. 2012) to generate antigenic peptides and have developed specific characteristics to prevent premature degradation by lysosomal proteases of antigenic material: the phagosomal pH is less acidic and the lysosomal protease content less important than other phagocytes (Savina, Peres et al. 2009); the phagosomal maturation is slower in dendritic cells presumably because of an important communication between the ER-Golgi intermediate compartment (ERGIC) and the maturing phagosomes (Cebrian, Visentin et al. 2011) as well as the particular regulation of the lysosomal fusion machinery (Alloatti, Kotsias et al. 2015).

The functional dichotomy between dendritic cells and macrophages for antigen presentation has recently been challenged by the characterization of a group of tissue-resident macrophages within the secondary lymphoid organs characterized by their high expression of the CD169 antigen (den Haan and Kraal 2012, Gray and Cyster 2012), their unique location and functional properties: the subcapsular sinus macrophages in the lymph nodes and the metallophilic marginal zone macrophages in the spleen are strategically distributed in a transitional area, the subcapsular zone and the marginal sinus, where they are in direct contact with lymph-borne and blood-borne antigens, respectively (den Haan and Kraal 2012, Gray and Cyster 2012). Consistent with a role in orchestrating immunity, subcapsular sinus macrophages prevent the systemic dissemination of infections by trapping lethal pathogens (Iannacone, Moseman et al. 2010, Moseman, Iannacone et al. 2012), massively activate the inflammasome complex to enhance adaptive immunity triggered by dendritic cells (Sagoo, Garcia et al. 2016), participate in the generation of robust humoral responses (Junt, Moseman et al. 2007, Phan, Grigorova et al. 2007). Unexpectedly, recent reports have demonstrated a direct role of a subset of CD169+ subcapsular sinus macrophage population in generating cytotoxic lymphocytes by cross-presenting dead-cell tumor antigens, thereby promoting the control of tumor growth, with a marginal role of dendritic cells (Asano, Nabeyama et al. 2011). Supporting their role in antigen processing and presentation to

cognate lymphocytes, subcapsular sinus macrophages are capable of presenting exogenous lipid antigens more efficiently than dendritic cells (Barral, Polzella et al. 2010) and are equipped with a low content of endosomal and lysosomal proteases (Phan, Green et al. 2009), one of the hallmarks of cross-presenting dendritic cells (Joffre, Segura et al. 2012).

In the spleen, the metallophilic marginal zone macrophages display similar features and they promote the tolerogenic clearance of cell debris (Miyake, Asano et al. 2007, McGaha, Chen et al. 2011) and the generation of robust humoral responses by activating T follicular helper cells and marginal zone B cells (Karlsson, Guinamard et al. 2003, You, Myers et al. 2011, Arnon, Horton et al. 2013, Veninga, Borg et al. 2015). They can also regulate antiviral adaptive immunity by keeping trapped intact antigens promoting their presentation to cognate CD8<sup>+</sup> T cells, through the initiation of type I interferon responses (Honke, Shaabani et al. 2012, Shaabani, Khairnar et al. 2016). However, their contribution in directly processing and presenting exogenous antigens to cognate lymphocytes is controversial. On the one hand, metallophilic macrophages are also efficient in activating invariant NK-T cells by presenting exogenous lipid antigens (Kawasaki, Vela et al. 2013). On the other hand, at variance with subcapsular sinus macrophages, metallophilic macrophages may act as a platform to transfer trapped antigens to cross-presenting cDC1 dendritic cells (Backer, Schwandt et al. 2010). However, due to technical limitations the isolation of metallophilic marginal zone macrophages has never been achieved so that their precise phenotype and functions including antigen presentation to T cells remain largely elusive (den Haan and Kraal 2012).

Here, we identify an important non-redundant contribution for splenic CD169<sup>+</sup> metallophilic marginal zone macrophages in the cross-presentation of antigenic material to cognate CD8<sup>+</sup> T cells. We propose an original and reproducible strategy to isolate with a high purity splenic CD169<sup>+</sup> cells. We find that these cells display a macrophage signature regarding their morphology, their gene-expression and protein-expression profiles. Analyzing their functional

properties, we find that CD169<sup>+</sup> macrophages can directly cross-present *in vitro* and *in vivo* antigens more efficiently than cDC1s, by forming long-standing and stable contacts with cognate CD8<sup>+</sup> T lymphocytes resulting in the generation of robust effector and memory responses with correlates of protective immunity. Unexpectedly and strikingly contrasting with cDC1s, CD169<sup>+</sup> macrophages exclusively use the vacuolar pathway to generate MHC-I ligands, and the molecules that recycle back from the plasma membrane as the sole source of MHC-I.

## **RESULTS.**

### **Splenic CD169<sup>+</sup> cells display a morphologic, protein and gene macrophage signature.**

The critical barrier to study the function of splenic CD169<sup>+</sup> macrophages resides in the fact that all the classical strategies to purify them have failed, with the exception of capture by laser microdissection (Honke, Shaabani et al. 2012) that do not allow for further functional analysis. This has been explained by the scarcity of the macrophages, by denaturation of surface antigens due to the enzymatic digestion and by the presence of cell contaminants (den Haan and Kraal 2012, Gray, Friend et al. 2012). Consequently, most of the studies trying to decipher their functions have used depletion strategies for dendritic cells and macrophages, which lack of specificity in addition to alter the anatomical distribution of other cell populations. However, the most recent technologies have not been tested for solving this technical problem.

We therefore focused on a novel purification and strategy and by combining pre-enrichment in phagocytes by density gradients and multiplex cell conventional flow cytometry as well as imaging flow cytometry, we succeeded in identifying a population of CD169<sup>+</sup> cells (**Fig. 1a**). After exclusion of doublets and depletion of remaining B cells and dead cells, this population was characterized by the lack of GR-1 expression, thereby excluding the fact detected CD169<sup>+</sup> cells are monocytes, and high expression of CD11b. Importantly, further gating steps

allowed for the successive identification of MHC-II<sup>int</sup> and F4/80<sup>bright</sup> RPMs that were also CD11b<sup>low</sup> (data not shown) and CD11c<sup>low/int</sup> (**Fig. S1a**). Among the remaining fraction of cells, conventional dendritic cells were easily identified as CD11c<sup>bright</sup>MHC-II<sup>high</sup> cells, and could be as expected divided into both cDC1 (CD24<sup>high</sup>CD11<sup>low</sup>) and cDC2 (CD24<sup>low</sup>CD11b<sup>high</sup>) subsets. By applying an overlapping panel of antibodies and the same gating strategy, we could identify by imaging flow cytometry the same populations of phagocytes (**Fig S1b**). The use of alternative panels, in which CD24 was replaced by XCR1 or CD8 $\alpha$ , resulted in the same successful identification of the main phagocyte subsets. Thus, **we have succeeded in the identification of a CD169-expressing cell population, with a very low number of pre-gating steps, a prerequisite for recovering high numbers of cells by cell sorting strategies.** Because innate-like lymphoid cells have been reported to be high contaminants in lymph node subcapsular macrophage preparations (Gray, Friend et al. 2012), we looked at but failed to evidence any co-expression of CCR7 and CD127 in the splenic CD169+ cells by conventional flow cytometry or by imaging flow cytometry (data not shown).

Examination of a large panel of surface pattern-recognition receptors by multiplex flow cytometry revealed that CD169+ cells like RPMs, expressed high levels of Dectin-1, Dectin-2, TLR2, TLR4, consistent with a macrophage (Davies, Jenkins et al. 2013) rather than dendritic cell population (**Fig. 1b**). Consistent with a macrophage signature, CD169+ cells were strikingly bigger and more auto-fluorescent than cDC1s, cDC2s or pDCs and they exhibited a high expression of CD64 and mer-tyrosine kinase (merTK), that were recently shown by high-dimensional analysis to discriminate tissue-resident macrophage populations from dendritic cells (Gautier, Shay et al. 2012), under homeostatic conditions (**Fig. 1b**). Also supporting their macrophage nature, we could not detect any significant expression of CLEC9A or 33D1 among the identified CD169+ cells, two markers broadly and selectively expressed by cDC1 and cDC2 dendritic cell subsets (Dudziak, Kamphorst et al. 2007, Hanc,

Fujii et al. 2015), respectively (**Fig. S1a**), as well as a total lack of expression of XCR1 (Yamazaki, Sugiyama et al. 2013) or Langerin (Takahara, Omatsu et al. 2002) (data not shown). Signing striking with RPMs, CD169<sup>+</sup> cells expressed higher levels of CD11b as well as CD11c (**Fig. S1a**) and MHC-II (data not shown).

Gene expression analysis on macrophage and dendritic cell populations has allowed for a robust identification of transcription factors associated to their ontogeny and/or maintenance. However, such factors have not been identified for splenic CD169<sup>+</sup> macrophages, with the exception of the *nr1h3* gene that encodes for the liver receptors LXR $\alpha$  that was found to be crucial for both populations of marginal zone macrophages (N, Guillen et al. 2013). Therefore, we chose to test macrophage and dendritic cell populations delineated by our gating strategy for quantitative gene expression of this marker as well as of genes encoding transcription factors required for dendritic cell development and maintenance (Guilliams, Ginhoux et al. 2014). Performing qPCR analysis on splenic phagocytes sorted by flow cytometry with a purity > 98%, we observed a high expression of both *siglec-1* and *nr1h3* genes only in CD169<sup>+</sup> cells. Surprisingly, while cDC1 and cDC2 subsets were found to expressed the highest number of *zbtb46* gene copies, as expected, we observed a selective expression of *batf3* in CD169<sup>+</sup> cells and conventional dendritic cells in similar quantities. Thus, we tested whether *batf3* and other signals promoting the development of some or all cDC subsets were also required for CD169<sup>+</sup> cell development. If so, this result would make us classify identified CD169<sup>+</sup> cell population as a cDC population, according to a recent classification based on ontogeny. However, CD169<sup>+</sup> cells were identified using our flow cytometry procedure with normal proportions (**Fig. 1d. and 1e.**) and phenotypes (data not shown) in the spleen of Flt3 and Flt3-ligand ko mice. Similar results were observed when examining the spleen of *batf3* ko mice, yet the global intensity level of the CD169 staining was reproducibly found to be lower than wt mice (**Fig. 1d and 1e.**).

Finally, we found that sorted CD169<sup>+</sup> cells allowed to rest for 2h exhibited a macrophage-like morphology (**Fig. 1f**). Similar findings were observed in unsorted splenic phagocytes analyzed by imaging flow cytometry, with striking differences in terms of morphology of between CD169<sup>+</sup> cells and cDC1 subset, including a bigger size and granular intracytoplasmic elements in CD169<sup>+</sup> cells. Taken together, we have designed a novel procedure for the identification of splenic CD169<sup>+</sup> cells, by the combination of density gradient and multiplex flow cytometry. The relatively low number of pre-gating steps together with the scarcity of potential contaminant cells including other macrophage populations and dendritic cell subsets, ensure the success of our strategy to collect high number of CD169<sup>+</sup> cells as well as other population of interest. By a careful examination of morphology and the profile of protein- and gene-expression of the CD169<sup>+</sup> cells relatively to other splenic phagocytes, **we have demonstrated that CD169<sup>+</sup> cells exhibit a macrophage signature according to a recently proposed classification** (Guilliams, Ginhoux et al. 2014). We have also **verified the reliability of our strategy by succeeding in reproducing our results by imaging flow cytometry and by identifying CD169<sup>+</sup> macrophages in normal proportions in the spleen of animals that lack of dendritic cell subsets.**

**CD169<sup>+</sup> macrophages cross-present *in vitro* and *in vivo* exogenous phagocytic and endocytic antigens more efficiently than cDC1 and cDC2 dendritic cell subsets.**

Having established a powerful strategy to purify splenic CD169<sup>+</sup> macrophages that allows for phenotypic and functional comparisons with other phagocytes, we next wondered whether CD169<sup>+</sup> macrophages can efficiently cross-present antigenic material to cognate CD8<sup>+</sup> T lymphocytes *in vitro* and *in vivo*. Examination of antigen uptake *in vitro*, a prerequisite for cross-presentation (Joffre, Segura et al. 2012), revealed that CD169<sup>+</sup> macrophages internalized endocytosed the fluorescent model antigen ovalbumin (OVA), with a similar efficacy to what observed for purified dendritic cells or RPMs (**Fig. 2a**). Similar findings



were observed with fluorescent dextrans (not shown). In the context of phagocytosed antigens, CD169<sup>+</sup> macrophages and RPMs were at least as efficient for internalizing irradiated fluorescent cell debris than cDC1s and far much superior than cDC2s and pDCs (**Fig. S2a**). Similarly, fluorescent irradiated yeast cells were internalized by CD169<sup>+</sup> macrophages, RPMs, cDC2s and to a lesser extent by cDC1s (data not shown). Wondering whether these results could extend *in vivo*, we evaluated the uptake of fluorescent OVA, irradiated-fluorescent apoptotic cells, which are more relevant than fluorescent dextrans. While the uptake of fluorescent dead cells mostly overlapped the results collected *in vitro*, we found striking differences for soluble OVA. In fact, consistent with a potential direct role in antigen presentation, we observed that CD169<sup>+</sup> macrophages and red pulp macrophages were significantly more efficient than cDC1s in capturing circulating soluble protein. As previously observed by others, we could not find any significant internalization of fluorescent OVA by other dendritic cell populations (Pooley, Heath et al. 2001). More surprisingly when examining whether the distribution of antigen might vary with time, we found a detectable fluorescent signal up to 4 days after immunization in CD169<sup>+</sup> macrophages but not in other phagocytes, suggesting that CD169<sup>+</sup> macrophages can keep antigens in their intact form for a long time, confirming recent findings (Veninga, Borg et al. 2015).

Having verified that CD169<sup>+</sup> macrophages could efficiently internalize antigenic material, we then investigated whether they are capable of cross-presentation to naïve CD8<sup>+</sup> T cells. We pulsed sorted splenic phagocyte subsets with various forms of the model antigen OVA and tested their ability to activate OT-I T cells, a transgenic CD8<sup>+</sup> T cell, which specifically recognize the OVA SIINFEKL peptide presented by H2-Kb molecules. Comparing the capacity of splenic phagocytes at a fixed dose of antigen (500 µg/mL soluble OVA and soluble endograde OVA; 5 µg/mL of an OVA fusion protein complexed to an anti-CD11c antibody; a 5:1 ratio of OVA-yeast cells: antigen-presenting cell), we unexpectedly found

than CD169<sup>+</sup> macrophages were at least as efficient as cDC1 and cDC2 dendritic cell subsets in cross-presenting OVA. Thus, cross-presentation of soluble OVA by CD169<sup>+</sup> macrophages was a 170% and a 300% more efficient than cDC1s and cDC2s in activating naïve OT-I T cell, respectively (**Fig. 2c.**). This effect was observed at other amounts of antigens and when the incubation was prolonged up to 16h (Fig S2b.) and was not explained by endotoxin contamination of soluble OVA, since replacing soluble OVA by endograde OVA did not result in significant modifications in the rank of efficacy (**Fig. 2c.**). Highly efficient antigen cross-presentation by CD169<sup>+</sup> macrophages also extended to receptor-mediated endocytosed antigens, since targeting OVA to CD11c, a receptor expressed by both cDC subsets and to a lesser extent by CD169<sup>+</sup> macrophages (**Fig. S1a**) resulted in a OT-I activation with an equivalent efficiency by cDC1s and CD169<sup>+</sup> macrophages. Again, this effect persisted at different amounts of antigens as well as with longer times of incubation with antigen (**Fig. S2c** and data not shown). Finally, we observed that cDC2s cross-presented more efficiently OVA-yeast cells than cDC1s, as already published by several groups including ours (Backer, van Leeuwen et al. 2008, Weimershaus, Maschalidi et al. 2012). Surprisingly, we observed that CD169<sup>+</sup> macrophages were about two-fold more efficient than cDC2s for this phagocytosed antigen. These results could not be explained by a higher ability of presenting peptides to naïve OT-I cells, since we did not observe any significant difference for the activation of transgenic CD8<sup>+</sup> T cells by synthetic S8L presentation by CD169<sup>+</sup> macrophages and dendritic cells (data not shown).

Wondering whether these results might extend *in vivo*, we choose to force the routing of OVA selectively to the CD169<sup>+</sup> macrophages or to the cDC1s, by targeting the fusion protein P3U-OVA (1µg/ mouse) to either CD169 or to DEC-205, respectively. We evaluated the proliferation of fluorescently-labeled OT-I T cells adoptively transferred into C57Bl/6 mice prior to i.v. This resulted in the activation and subsequent proliferation of OT-I T cells (**Fig.**

**2d left**), as previously reported (Backer, Schwandt et al. 2010), yet we observed a significant degree of proliferation when antigen was targeted to CD169 (**Fig. 2d, middle**). We next tested whether the persistence of a pool of intact antigen within the CD169+ macrophages may result in prolonged activation of antigen-specific T cells. Supporting this hypothesis, we observed a significant activation of naïve OT-I T cells transferred into mice up to four days after immunization, when the antigen was targeted to CD169+ macrophages and not cDC1s (**Fig. 2d**).

The group of J.M. den Haan has suggested that CD169+ macrophage generate efficient cytotoxic CD8+ responses by acting as a platform for transferring antigens to cross-presenting dendritic cells (Backer, Schwandt et al. 2010). Although we have demonstrated that CD169+ macrophages *per se* are clearly capable of efficient cross-presentation to CD8+ cells *in vitro* and that they can efficiently uptake antigenic material *in vivo*, we could not exclude that such surprising findings did not extend *in vivo*, the efficient cross-priming observed with CD169 antigen targeting being the consequence of a long-lasting distribution of captured antigens to cross-presenting dendritic cells. In our effort to eliminate such a possibility, we decided to visualize whether or not OT-I T cells could form long-lasting and stable contact with antigen-bearing CD169+ macrophages, a prerequisite for a productive cross-priming in the lymph nodes (Moreau, Lemaitre et al. 2012, Moreau, Lemaitre et al. 2015). By two-photon live imaging of the marginal zone, we could visualize after labeling with fluorescent specific antibodies both CD169+ marginal zone macrophages and dendritic cells (defined as CD11c<sup>high</sup> cells). Unexpectedly, after i.v. antigen targeting to CD169+ macrophages, but not cDC1s, we could observe an increasing number of long-lasting (>15 min), and stable contacts over time after immunization (**Fig. 2e**). Trying to dissect the nature of contacts between OT-I cells and CD169+ macrophages or dendritic cells, we first analyzed over time the velocity profile of OT-I T cells after targeting to CD169 or to DEC-205. We observed a similar decrease in T

cell motility with time after antigen targeting to DEC-205 or CD169, with a high numbers of cells exhibiting “synapse-like” (Moreau, Lemaitre et al. 2012, Moreau, Lemaitre et al. 2015) behaviors (velocity < 3µm/min) in both cases. Importantly, antigen targeting to metallophilic macrophages resulted in a significantly high number of contacts between OT-I T cells and CD169+ macrophages, compared to antigen targeting to cDC1 population (**Fig. 2e, supplementary movies**). This observation persisted over a period of time of at least 16hrs post-immunization, thereby supporting a direct role for CD169+ macrophages for the cross-priming of OT-I T cells (data not shown). Altogether, our results suggest that CD169+ macrophages can cross-present endocytosed and phagocytosed antigens *in vitro* more efficiently than cDC1s and cDC2s and cross-present endocytosed antigens at least as efficiently as cDC1s, by forming long-standing and stable contacts with OT-I cells.

#### **Cross-presentation by CD169+ macrophages generate protective immunity.**

Having established that CD169+ macrophages belong to a small group of phagocytes capable of efficient cross-presentation *in vitro* and *in vivo*, we next wondered whether the activation of antigen specific CD8+ T cells might result in productive priming, or in cross-tolerance, as previously reported for dendritic cells under homeostatic conditions (Joffre, Segura et al. 2012). To gain some insight, we started by analyzing the quality of antigen specific cells from the endogenous repertoire after an immunization by OVA targeted to CD169+ macrophages or cDC1s. By determining by flow cytometry the frequency and the poly-functionality of IFN-γ producing cells (**Fig. 3a**) upon *ex vivo* re-stimulation by the cognate peptide as the reflect of the presence of effector antigen-specific CD8+ T cells, we observed that although antigen targeting to metallophilic macrophages resulted in an efficient priming of antigen-specific CD8+ T cells, the presence of a maturation stimulus such as an agonistic anti-CD40 antibody CD8 T cells enhanced the quality of cross-priming by diversifying the cytokines secreted by effector cells, as this is the case for cDC1s (**Fig. 3b**). Interestingly, the presence of

an inflammatory stimulus such as lipopolysaccharides resulted in the generation of a significantly higher number of poly-functional effector cells by CD169+ macrophages **(Fig.3b)**.

When analyzing the quality of the pool of activated OT-I T cells adoptively transferred one day prior to immunization, we observed that antigen targeting to metallophilic macrophages resulted in the generation of a significantly higher proportion of poly-functional effectors CD8+ T cells during the primary response **(Fig. 3c and S3a)** and a higher proportion of memory CD8+ T cells 30 days post-immunization **(Fig. 3d left)**, yet no differences in terms of effector functions could be observed with mice immunized with OVA targeted to DEC-205 **(Fig. 3d, right)**, after the administration of an antigenic boost for 7 days. These observations were consistent with the significantly higher ratio of Eomes/T-bet, the lower level of Blimp-1 expression, together with a higher proportion of memory-precursor cells (MPECS) (Chang, Wherry et al. 2014), observed 12 days after antigen targeting to metallophilic macrophages **(Fig. 3e S3b and S3c)**. Collectively, our results support that cross-priming of CD8+ T cells by splenic CD169+ macrophages generate correlates of protective immunity, as assessed by the high number of poly-functional antigen specific CD8+ T cells and the development of memory T cells.

#### **CD169+ macrophages degrade antigenic material by the vacuolar pathway.**

To generate MHC-ligands, dendritic cells can use the cytosolic pathway, in which after export to the cytosol and a digestion by the proteasome, the antigens are further degraded by aminopeptidases that reside in the ER, ERAP1 (Blanchard, Gonzalez et al. 2008), and in Rab14+ regulatory endosomes, a cell compartment recently identified to be crucial for antigen cross-presentation by the trimming activity of the insulin-responsive aminopeptidase IRAP that is selectively found in the endocytic pathway (Saveanu, Carroll et al. 2009, Weimershaus, Maschalidi et al. 2012) as well as by controlling the phagosomal maturation (Weimershaus,

Maschalidi et al. 2012). Whatever the final route of antigenic material, antigenic peptides either enter into the ER or back into endosomes/phagosomes by active transport, with an important role for TAP (Joffre, Segura et al. 2012). By contrast, in the vacuolar pathway, antigenic material is dependent on lysosomal proteases (Joffre, Segura et al. 2012).

Prompted by this context, we first tried to examine the content in antigen-processing molecules in splenic phagocytes by imaging flow cytometry. Among the key results, we found that splenic metallophilic macrophages expressed regular levels of ERAP1 and IRAP, lower levels of TAP1 than cDC1s but similar than cDC2s and higher levels of Lamp-2 (**Fig. 4a**). By imaging flow cytometry, we observed that metallophilic macrophages exhibited a similar composition in the Rab14+ compartment than cDC1s, with no detectable co-localization of Rab14+ and Lamp1 in CD169+ macrophages compared to cDC2s (**Fig. 4b and Fig. S4a**).

Due to the highly efficient cross-presentation by CD169+ macrophages we initially suspected they would use exclusively the cytosolic pathway, a feature of cross-presenting dendritic cells (Joffre, Segura et al. 2012). However, incubating OVA together with a proteasome inhibitor such as MG-132 or Epoxomicin did not result in a inhibition of cross-presentation by CD169+ macrophages, strikingly contrasting with cDC1s. Conversely, we found that cross-presentation of OVA by CD169+ macrophages was decreased by a broad inhibition of endosomal and lysosomal proteases using leupeptin or a more selective inhibition of cathepsins using z-FA-fmk, in a dose-dependent manner (**Fig. 4c**). Consistent with these findings, absence of IRAP activity by the use of IRAP ko sorted cells (**Fig. 4d**) or of a specific inhibitor (Kokkala, Mpakali et al. 2016) did not affect cross-presentation by CD169+ macrophages *in vitro* (data not shown) or by immunizing mice *in vivo* with P3U-OVA targeted to CD169. (**Fig. 4f**). Complicating the picture, we observed a drastic inhibition of cross-presentation by CD169+ macrophages *in vitro* and *in vivo* in TAP ko and ERAP ko

cells (**Fig. 4d, 4e, 4f**). Indeed, because the generation of MHC-I ligands by CD169+ macrophages is proteasome-insensitive and dependent on lysosomal proteases, it is unlikely that both TAP and ERAP would contribute in degrading antigenic material. Therefore, we reasoned that these two proteins might have at least an indirect role in controlling the routing of MHC-I for peptide loading, as suggested for TAP by a recent report from our group (Merzougui, Kratzer et al. 2011). Consistent with this, we observed a full restoration of cross-presentation by CD169+ macrophages (**Fig. 4g**), but not by cDC1s, following the recovery of physiological MHC-I levels by pre-incubating phagocytes at low temperature (**Fig. S4b** and data not shown for ERAP ko).

Collectively our examination of the mechanisms promoting the generation of antigenic peptides by **cross-presenting CD169+ macrophages has revealed that they exclusively use the vacuolar pathway and especially the cathepsin S to degrade antigenic material**. We found that antigen cross-presentation by CD169+ macrophages is **not dependent on proteasome inhibition, on TAP transport, or on aminoterminal trimming by ERAP or IRAP**. These results strikingly contrast with what observed with cross-presenting cDC1s.

**The source of MHC-I for cross-presentation is the pool of recycling molecules.**

As directly supported by the fact that the restoration of physiological levels of surface MHC-I results in the recovery of efficient cross-presentation by CD169+ macrophages at least *in vitro*, peptide loading onto MHC-I molecules is another critical step in antigen cross-presentation. In dendritic cells, both the source and the route of MHC-I contributing to cross-presentation remains still elusive, yet they are thought to come from the plasma membrane, by recycling back to the endocytic pathway, from the pool of neosynthesized MHC-I exiting from the ER (Joffre, Segura et al. 2012). Prompted by this context, we first examined the profile of basal expression and of rate of endocytosis of MHC-I molecules in the different phagocyte populations. We found that CD169+ macrophages exhibited the highest level of

MHC-I molecules at the surface (**Fig. 5a**), despite a comparable level of total MHC-I molecules (data not shown). Moreover, this was associated to a significantly lower rate of MHC-I endocytosis as compared to other phagocytes, suggesting that MHC-I molecules are more stable in metallophilic macrophages and/or the quality control machinery is less permissive (**Fig. 5b**). Supporting this hypothesis, MHC-I levels at the surface of CD169+ macrophages was fully restored in TAP ko and ERAP ko mice by a 16h incubation at 26°C, whereas only a partial restoration was observed with cDC1s (**Fig. 5c and S4b**).

Trying to gain additional insight, we studied the consequences of inhibiting the anterograde protein transport or the recycling of some endosome populations on surface levels of the different phagocytes. Blocking the provision of neosynthesized MHC-I molecules by incubating cells with brefeldin A did not affect the levels of surface MHC-I in metallophilic macrophages but resulted in a significant and drastic reduction in dendritic cell populations, resulting in reduced cross-presentation by cDCs. By contrast, blocking the provision of recycling molecules by primaquine resulted in the accumulation of MHC-I molecules at the surface of wt macrophages, but not dendritic cells and prevented the restoration of MHC-I molecules and of cross-presentation at the surface in TAP ko macrophages. **Altogether, these results suggest that MHC-I molecules are more stable and that internalized MHC-I trafficking is critically dependent on a pool of recycling molecules sensitive to primaquine in CD169+ macrophages.**

## **DISCUSSION.**

Splenic metallophilic macrophages are strategically located in the marginal sinus where they are in direct contact with blood-borne antigens. However, for technical limitations, their precise functions, notably in antigen presentation, remain elusive. Proposed roles include a platform for antigen transfer to cross-presenting dendritic cells (Backer, Schwandt et al. 2010). Our strategy designed for characterizing CD169+ cells has allowed us to confirm they



belong to macrophage lineage and more surprisingly to a small group of professional antigen-presenting cells capable of highly efficient cross-priming of CD8<sup>+</sup> lymphocytes, resulting in the generation of a pool poly-functional effector and memory cytotoxic T cells. Contrary to cross-presenting dendritic cells, CD169<sup>+</sup> macrophages exclusively generate MHC-I ligands by the vacuolar pathway and we have identified they use a unique MHC-I trafficking to supply in MHC-I for cross-presentation.

Antigen cross-presentation by CD169<sup>+</sup> macrophages has been observed in the lymph nodes. Indeed, a subset of CD11c<sup>+</sup> subcapsular sinus macrophages cross-presents dead-tumor cell associated antigens, resulting in the generation of protective immunity (Asano, Nabeyama et al. 2011). Our findings suggest that this ability extends to their spleen counterpart, the metallophilic marginal zone macrophages. Whether the CD11c<sup>+</sup> subcapsular sinus cells are macrophages or dendritic cells is a subject of controversy, since a significant expression of *zbtb46* has been observed (Meredith, Liu et al. 2012, Satpathy, Kc et al. 2012). In the context of our study in the spleen, CD169<sup>+</sup> cells display a morphologic and a profile of protein and gene expression compatible with a macrophage signature, thereby excluding the presence of contaminant dendritic cells in the preparation. Importantly, our strategy allows for the discrimination of metallophilic macrophages from marginal zone macrophages, which is considered to be another critical barrier in unraveling the role of the phagocytes residing in the splenic marginal zone.

By live imaging of the spleen, we have directly visualized direct interactions between CD169<sup>+</sup> macrophages and cognate antigen specific CD8<sup>+</sup> T cells after antigen targeting to metallophilic macrophages: they form long-standing and stable contacts with CD169<sup>+</sup> macrophages through a synapse-like interaction. Although we did not provide any clue about whether these contact result in productive activation of cognate T cells or whether they interact with antigen-bearing cells, such T cell behaviors have been associated with efficient

priming of CD8+ T cells, at least in the lymph nodes (Hugues, Fetler et al. 2004, Bousso 2008, Moreau, Lemaitre et al. 2012, Moreau, Lemaitre et al. 2015). This strikingly contrasts with the conclusions raised by the group of J.M den Haan, who proposes that metallophilic macrophages act as a platform for antigen transfer to cross-presenting cDC1s, due to the loss of cross-priming *in vivo* of cytotoxic T cells by immunization with an antigen targeted to CD169 after the depletion of CD11c+ cells (Backer, Schwandt et al. 2010). We provide some explanation for their observation, since CD169+ cells express significant levels of CD11c, yet inferior to cDC1 and cDC2 subsets, consistent with previous reports (Kawasaki, Vela et al. 2013).

Examination of mechanisms regulating antigen cross-presentation has been mainly achieved in dendritic cells and has led to the identification of hallmarks of cross-presentation, and include a low lysosomal protease content, a more alkaline pH (Jancic, Savina et al. 2007, Mantegazza, Savina et al. 2008, Savina, Peres et al. 2009), a slow endosomal/phagosomal maturation process (Cebrian, Visentin et al. 2011), the presence of Rab14+IRAP+ regulatory endosomes, an efficient phagosome-to-cytosol export (Zehner, Marschall et al. 2015) and the preferential use of the cytosolic pathway (Joffre, Segura et al. 2012, Mant, Chinnery et al. 2012). Similar to cross-presenting dendritic cells, splenic metallophilic macrophages are poorly degradative as assessed by the long-term detection of intact antigens *ex vivo* and despite a relatively high levels of lysosomal content. By contrast, splenic metallophilic macrophages do not excel in phagosome-to-cytosol export and do not use the Rab14+IRAP+ regulatory endosomes to modulate cross-presentation, yet this compartment is found in CD169+ splenic macrophages. More surprisingly is the selective use of vacuolar pathway, that has been already observed for a limited set of antigens in dendritic cells and that is considered to be 10-fold less efficient than the proteasome-sensitive cytosolic pathway (Mant, Chinnery et al. 2012). These contradictory findings strongly suggest the mechanisms

regulating antigen processing, and mainly the endocytic pathway, strikingly differ between cDC1s and CD169+ metallophilic macrophages. Our combined strategy eliminates undesired contaminants in phagocyte preparations and provides a versatile tool to test whether CD169+ lymph node macrophage populations are also capable of antigen cross-presentation, and if so do they also use unique mechanisms for antigen processing, as suggested by their molecular equipment (Phan, Green et al. 2009).

The source of MHC-I molecules that supply for peptide loading remains elusive in cross-presenting dendritic cells, yet some indirect evidence suggests that ER, ERGIC, ERC and plasma membrane are candidates. While we do not visualize directly the intracellular trafficking of MHC-I to cross-presentation compartments in macrophages and dendritic cells, we observe that metallophilic macrophages express the highest levels of MHC-I among the splenic phagocytes and together with the complete restoration of MHC-I levels at the surface of TAP ko cells incubated at low temperature, these results suggest a more permissive quality control in macrophages. The unique behavior of MHC-I expression in metallophilic macrophages after exposure to brefeldin A or primaquine strongly support the central role of a post-ERGIC endosome recycling compartment in the physiologic maintenance of MHC-I levels at the surface, yet the relevance of these findings are not necessary applicable to MHC-I molecules supplied for cross-presentation in CD169+ macrophages. A pool of Rab11a recycling endosomes has been recently identified as the source of MHC-I molecules for TLR-dependent cross-presentation and this compartment is likely a good candidate for the regulation of MHC-I trafficking in metallophilic macrophages (Nair-Gupta, Baccarini et al. 2014).

Finally, our novel strategy for preparing pure phagocyte populations may be used for high-throughput analysis of gene and protein-expression profiles by recent technological tools, such as single-cell mRNA sequencing and/or mass cytometry, with the objective of

determining what specific factors regulate CD169+ macrophage development, maintenance and functions in the secondary lymphoid organs (Ginhoux, Schultze et al. 2016, Guilliams, Dutertre et al. 2016).

The small group of antigen cross-presenting cells has incorporated a new candidate phagocyte population, the metallophilic macrophages that use a unique endocytic pathway to prevent premature degradation of MHC-I ligands and to regulate MHC-I molecules expression and intracellular routing.

## EXPERIMENTAL METHODS

### **Mice.**

C57Bl/6 mice were purchased from Janvier (St. Quentin-Fallavier, France). Ly5.1 C57Bl/6 mice and TAP1-deficient mice (Van Kaer, Ashton-Rickardt et al. 1992) were obtained from Jackson Laboratories (Sacramento, CA) and Ly5.2 RAG-1 deficient OT-I transgenic mice (Hogquist et al, 1994; Mombaerts et al, 1992) were obtained from Taconic (Germantown, NY), and bred in our animal facility. Previously described ERAP ko (Hammer, Gonzalez et al. 2007) and IRAP ko (Keller, Scott et al. 1995, Weimershaus, Maschalidi et al. 2012) mice on a Sv129 background were back-crossed up to 10 times to C57BL/6 mice obtained from Janvier. Control mice were C57Bl/6 mice bred in our facility. Batf3 ko mice, Flt3 and Flt3-L ko mice were a gift from C. Kurts and G. Darrasse-Jeze, respectively. Animal experimentation was approved by the Comité d'éthique pour l'expérimentation animale Paris Descartes (n° P2.LS.156.10).

### **Antibodies.**

Flow cytometry. The following fluorescently-labeled anti-mouse antibodies were from Miltenyi Biotech (Paris, France): CD64 (REA286), CD169 (REA197), CD207 (caa8 28H10), CLEC9A (7H11) TLR2 (REA109), TLR4 (MTS510), Dectin-1 (REA154), Dectin-2 (KV6E7), MerTK (REA477). The following fluorescently-labeled antibodies were from Biolegend (Ozyme): CD11c (N418), CD19 (6D5), F4/80 (BM8), CD8a (53-6.7), CD169 (3D6.112), GR-1 (RB6-8C5), XCR1 (ZET), MHC-II (M5/114.15.2), DC Marker (33D1), H-2Kb (AF6-88.5), PDCA-1 (129C1), T-bet (4B10), Blimp-1 (5E7) and KLRG-1 (2F1). The following fluorescently-labeled antibodies were purchased from BD Biosciences (Le Pont de Claix, France): CD11b (M1/70), CD8a (53-6.7), CD45.2 (104), CD24 (M1/69), CD11c

(N418) and. The following antibodies were from eBioscience (Paris, France): TcR- $\beta$  (H57-597), CD40 (1C10), EOMES (Dan11mag), CD127 (A7R34), NK1.1 (PK136). MHC-I (B8.24-3), an antibody against H2-Kb recognizing non conformational determinants and was a kind gift from F. Lemonnier (Institut Pasteur, Paris France).

Imaging flow cytometry. In addition to the antibodies used for flow cytometry, polyclonal anti-Rab14 (Sigma-Aldrich), anti-mouse Lamp-2 (M3/84, BD Biosciences), anti-mouse TAP1 (M-18), polyclonal anti-ERAP1 (Proteintech, Manchester, UK), mouse monoclonal IRAP antibody (a kind gift from M. Birnbaum, University of Pennsylvania) were used. All secondary reagents were Alexa-coupled highly cross-adsorbed antibodies from Molecular Probes (Invitrogen).

ELISA. For the detection and quantification of IL-2 secreted into culture supernatants a rat anti-mouse IL-2 (clone JES6-1A12) was used for capture and a rat anti-mouse IL-2/Biotin (clone JES6-5H4) for detection, both from BD Biosciences.

Formation of immune complexes. We used rat anti-mouse DEC205 purified from hybridoma (clone NLDC-145, American Type Culture Collection) and purified rat anti-mouse CD169 (clone 3D6.112, AbD Serotec/Bio-Rad, Puccheim, Germany) for preparing immune complexes with fusion proteins.

## **Reagents**

Epoxomicin, MG-132, Z-FA-fmk were from Enzo Life Sciences (Villeurbanne, France) and primaquin was purchased from Sigma-Aldrich. Synthetic peptide SIINFEKL or S8L (OVA<sub>257-264</sub>), corresponding to the H-2Kb restricted CTL epitope of Ovalbumin (OVA), and TSYKFESV used as a negative control, both > 90% pure, were purchased from Schafer (Copenhagen, Denmark). Soluble OVA and soluble endograde OVA were from Worthington

Biochemical Corporation (Lakewood, NJ), and Bovine Serum Albumin (BSA) from Sigma-Aldrich (Cergy-Pontoise, France). Recombinant *Saccharomyces cerevisiae* cells expressing full length OVA were prepared as previously described (Saveanu and van Endert 2013) and were a kind gift from C. Saveanu (Institut Pasteur). IMDM medium was from Sigma-Aldrich (Cergy-Pontoise, France). Lipopolysaccharide from *E. coli* O55:B5 ultrapure was purchased from InvivoGen (Toulouse, France).

### **Flow cytometry and sorting of spleen and lymph node phagocytes.**

Spleens from wt and ko mice were digested with 500 µg/mL Liberase DL Research grade (Roche Diagnostics, Meylan, France) and 50 ng/mL DNase-I recombinant (Roche Diagnostics) diluted in PBS. Dendritic cells and macrophages were pre-enriched from splenocytes by a very-low density gradient. Briefly, splenocytes were re-suspended in 5.2 mL of IMDM containing 5 mM EDTA, 5% FCS and 18% Optiprep (Axis-Shield PoC AS) and were loaded between 4 mL PBS medium containing 5 mM EDTA, 5% FCS and 25% Optiprep (bottom layer) and 1.8 mL of PBS (top layer). After 20 minutes of 580x g centrifugation without break at 20°C the low-density fraction was collected at the interface between PBS and 18% Optiprep. The cells were immunostained with fluorescent antibodies diluted in saline solution 2% FCS 2 mM EDTA on ice and 7-Actinomycin D (7-AAD, BD Biosciences) was added prior analysis on BD FACS LSR Fortessa or cell sorting on BD FACS ARIA-II cell sorter. After exclusion of doublets, dead cells (gating on 7-AAD- cells) as well as B cells (CD19+), NK cells (NK1.1+) and T lymphocytes (TCR-β+), all grouped in a “dump-channel”, phagocytes were identified as following based on their phenotype: pDCs (dump-, CD11blow, CD11cint, GR-1high, PDCA-1+), cDC1s (CD24+CD11b-CD11c<sup>high</sup>GR-1<sup>low/neg</sup>CD169<sup>low/neg</sup>), cDC2s (CD24-CD11b+CD11c<sup>high</sup>GR-1<sup>low/neg</sup>CD169<sup>neg</sup>), CD169+ macrophages (CD24<sup>low</sup>CD11b<sup>high</sup>GR-1<sup>low/neg</sup>CD169<sup>high</sup>F4/80<sup>high</sup>CD11c<sup>int</sup>MHC-II<sup>int</sup>), and red pulp

macrophages (CD11b<sup>low</sup>, CD169<sup>low/neg</sup>, GR-1<sup>low</sup>, PDCA-1-, CD11c-, MHC-II<sup>int</sup>). Post-sort purity was typically 93-99% depending on the cell population.

#### **qPCR analysis on sorted phagocytes.**

mRNA was extracted from  $3.10^4$  to  $5.10^4$  sorted phagocytes by using with the Dynabeads mRNA DIRECT Purification micro kit from Ambion (Thermo-Fisher Scientific, Villebon-sur-Yvette, France) and following the manufacturer's instructions. Recovered total RNA was reverse transcribed into cDNA with the IMPROM-II Reverse Transcription System (Promega, Lyon, France) using random hexamers. Quantitative PCR was performed with MESA FAST qPCR SYBR (Eurogentec) MasterMix using the 7900 real-time PCR instrument from Applied Biosystem. The sequences of qRT-PCRs primers used for batf3, nr1h3, siglec-1 and zbtb46 are described in supplemental information.

#### **Antigen uptake by phagocytes *in vitro* and *ex vivo*.**

*In vitro antigen uptake.* Molecular weight 40-KDa FITC-dextran, and OVA protein labeled with Alexa Fluor 647 were purchased from Thermo-Fisher Scientific (Villebon-sur-Yvette, France). *Saccharomyces cerevisiae* yeast cells and C57Bl/6 splenocytes were labeled with 10  $\mu$ M CellTracker Orange CMRA (Thermo-Fisher Scientific) dye prior to irradiation of cells (80 Gy). After enrichment with phagocyte subsets by density gradient, cells were incubated at 37°C or 4°C as a control sample, with the different model antigens for various periods of time. At the end of incubation, cells were washed with cold PBS before staining for identifying phagocyte populations in a saline solution containing 2% SVF and 0.01% NaN<sub>3</sub>. Cells were analyzed by flow cytometry.

*Ex vivo antigen uptake.* For *ex vivo* antigen uptake, antigens were injected i.v. and were allowed for internalization for various periods of time. Splenocytes were prepared as



previously described and enriched with phagocytes before staining and analysis by flow cytometry.

### **Cross-presentation assays**

Cross-presentation assays were performed on sorted phagocyte populations from spleen or lymph nodes. Fifteen thousand phagocytes per culture well were incubated for 8h or 16h with the following forms of OVA, prepared as described before: soluble OVA or BSA, yeast cells expressing or not OVA (OVA-yeast cells) at their surface, irradiated-C57Bl/6 splenocytes previously loaded with OVA or BSA and complexes of anti-MR and P3U-OVA or P3U-GAD fusion proteins. Phagocytes were fixed in 0.0008% glutaraldehyde for 30s, neutralized by the addition of 0.2 M glycine in PBS, washed twice in PBS, re-suspended in medium before the addition of 65,000 OT-I T cells purified from lymph nodes per well for 16h to 20h. When inhibitors were used for cross-presentation assays, a pre-incubation with the given inhibitor was performed for 30min to 45min before adding the antigen with the inhibitor for another 8h or 16h. Presentation of synthetic peptide S8L was tested routinely in all assays by pulsing phagocytes with  $10^{-8}$  to  $10^{-15}$  M peptide for 2 h followed by phagocyte fixation, neutralization, washing and suspension in medium and addition of T cells as described above. Pre-fixed phagocytes were treated with glutaraldehyde in the same manner before antigen addition. To assess the activation of OT-I T cells, we detected and quantified the IL-2 secreted into culture supernatant by ELISA, as described elsewhere (Merzougui, Kratzer et al. 2011), using Maxisorp ELISA plates (Nunc, Roskilde, Denmark), Pierce High Sensitivity streptavidin-horseradish peroxidase (Thermo-fisher Scientific), TMB substrate reagent (OptEIA™, BD Biosciences). The absorbance at 450 nm was read using a Mithras LB940 reader (Berthold Technologies, Thoiry, France). The results of antigen presentation experiments represent the means of triplicate wells obtained after pooling at least four independent experiments.

### ***In vivo* T cell proliferation assay.**

For adoptive transfer tests using OT-I T cells,  $0.5-1.0 \times 10^6$  lymph node cells from Ly5.2 RAG ko OT-I mice were labeled with 10  $\mu$ M Violet Proliferation Dye. Violet Proliferation Dye-labeled lymph node cells were injected i.v. into recipient mice, followed 24 h later by i.v. injection of antigens. Cross-presented antigens were complexes of anti-DEC-205 or anti-CD169 and P3U-OVA or P3U-GAD fusion proteins. The amount of fusion protein per mouse was 1  $\mu$ g for targeting to the DEC-205 and CD169. Three days after antigen injection, spleens were removed, and proliferation measured in CD8<sup>+</sup> cells identified using V $\beta$ - specific antibodies, as described (Kratzer, Mauvais et al. 2010). In some experiments, complexes of anti-DEC-205 or anti-CD169 and P3U-OVA or P3U-GAD fusion proteins were injected at different times prior to the adoptive transfers of OT-I T cells. The division index of transferred cells was calculated following a published method (Kratzer, Mauvais et al. 2010).

### **Cross-priming of endogenous CD8<sup>+</sup> T cells and of transferred OT-I T cells.**

*Endogenous CD8<sup>+</sup> T cells.* Complexes of anti-DEC-205 or anti-CD169 and P3U-OVA or P3U-GAD (1  $\mu$ g of fusion protein per animal) fusion proteins were injected i.v. alone or in the presence of 25  $\mu$ g of anti-CD40 or 10  $\mu$ g of LPS injected i.p. Ten to fourteen days later (peak response) or 30 days later (contraction phase) or 7 days after a novel immunization of mice with the same antigen and/or cocktail of adjuvants at day 30 to 45 post-immunization,  $10^6$  of splenocytes of immunized mice were re-stimulated with  $5 \cdot 10^{-6}$  M of synthetic S8L or TSV peptides (negative control) or with Phorbol 12-myristate 13-acetate and ionomycin (Sigma-Aldrich) as positive control for 6h in the presence of cocktail enzyme inhibitor for the last 4.5hrs. After fixation and permeabilization using the BD Cytotfix/Cytoperm solution (BD Biosciences) of re-stimulated cells, cells were stained for CD8, V $\beta$ 5.1/V $\beta$ 5.2, CD19 and IL-2, IFN- $\gamma$ , TNF- $\alpha$  and analyzed by flow cytometry.

OT-I T cells. Immunizations were performed as described for endogenous CD8+ T cells, with the following exception: 0.5-1.0 OT-I T cells were transferred the day before immunization into Ly5.1 C57Bl/6 recipient mice; concentrations of synthetic peptides were  $10^{-6}$  M; CD45.2 antibody was used instead of V $\beta$ 5.1/V $\beta$ 5.2. In parallel, phenotype of OT-I T cells was analyzed by staining splenocytes from immunized mice without any stimulation, by staining the cells with CD45.2, CD19, CD8a, CD127, KLRG-1, CCR-7 and CD62L, followed by fixation and permeabilization using the Cell Signaling Buffer Set A (Miltenyi Biotech) and intracellular staining with T-bet, Blimp-1 and EOMES and analysis by flow cytometry.

### **Intravital multiphoton imaging of the spleen.**

Imaging was performed 2 to 4 hr after T cell adoptive transfer. Recipient mice were anesthetized by intraperitoneal injection of with a mixture of 10ml/kg saline solution containing xylazine (1 mg/ml) and ketamine (5 mg/ml) and maintenance doses of intramuscular injections of 5ml/kg of xylazine (1 mg/ml) and ketamine (5 mg/ml) were given every 45 min. The spleen was surgically exposed by a skin incision performed below the costal margin in the left flank, with a typical open window of 1 cm in the peritoneum. A careful attention was given to preserve the vessels in the hilum from damaging. The spleen was then irrigated by a heated saline solution and placed on a custom-heated stage preserving blood irrigation. A coverslip, onto which is glued a heated metal ring, was placed on top of the spleen, and the ring was filled with pre-warmed saline solution to immerse a 20x/0.95 objective (Olympus). The mouse was placed on a Biotherm stage warmer at 37°C (Thermo-Scientific) for the duration of the imaging. For detection of metallophilic macrophages, VioBright-FITC anti-mouse CD169 (REA197) was injected i.v. up to 30 min before imaging. Two-photon imaging was performed with a TriM Scope II bi-photon equipped with an inverted motorized intravital stage (LaVision Biotech). Excitation was provided by a 690-

1020 nm MaiTai HP pulsed laser (Spectra-Physics, Stahnsdorf, Germany). Emitted fluorescence was split with 4 PMTs passed through 400/480, 510/545, 575/630 and 660/700 nm bandpass filters. For imaging, areas of the spleen showing clear evidence of T cell accumulation were selected. Typically, images from 3–5 z planes spaced 3–5  $\mu\text{m}$  apart were collected every 30 s for up to 1 hr. The full longitudinal extent of the spleen was surveyed in each animal at depths of 50–80  $\mu\text{m}$  and typically 3 to 5 marginal sinuses presenting significant numbers of CD169+ cells were observed. Videos were made and analyzed with ImageJ and Fiji (NIH, USA). To track cells and to measure velocities, we used the ICY software (Institut Pasteur, Paris, France). At least two independent sets of experiments were performed.

### **Imaging flow cytometry**

For imaging flow cytometry, after enrichment with phagocyte subsets by density gradient, cells were stained with the following antibodies: CD8a, F4/80, CD19, CD11c, CD169 (3D6.112), GR-1. Cells were fixed, permeabilized using the BD Cytofix/Cytoperm solution (BD Biosciences) and stained again with the following antibodies: Rab14, Lamp1, IRAP. All samples were analyzed using an ImageStreamX Mk II imaging flow cytometer (Amnis), followed by IDEAS analysis software (v. 6.1, Amnis). The 60x magnification objective was used and at least 1,000 events of interest were collected from the final gating step to ensure robust statistical analysis. The gating strategy used is depicted in the supplementary figure. We used the bright detail similarity R3 feature to evaluate the degree of co-localization between the markers of interest. Single stains samples run in the same conditions as the samples of interest were used to generate compensation matrices in the IDEAS analysis software. Additional controls included the use of an isotype control for the intracellular staining. Two independent sets of experiments were performed.

### **MHC-I expression and receptor-mediated endocytosis**

For MHC-I expression, cells were stained in a PBS SVF 2% and NaN<sub>3</sub> 0.01% to avoid further internalization of MHC-I (B8.24-3). For MHC-I endocytosis, splenocytes enriched with phagocytes were incubated for 20 min with Fc-Block (BD Pharmingen) before labeling for 30 minutes at 4°C with biotinylated anti-H-2Kb (AF6-88.5). After two washes in cold PBS, samples were shifted to 37°C or 4°C for various periods of time in IMDM medium. At the end of incubation, cells were washed in PBS NaN<sub>3</sub> 0.01% and stained with streptavidin/FITC at 4°C in PBS SVF NaN<sub>3</sub>, then examined by flow cytometry. Percentage of endocytosis for a given population was calculated as following % endocytosis = 100 x [(Geometric mean fluorescence intensity (MFI) of fluorescent protein in control population incubated at 4°C - Geometric MFI of fluorescent protein in population incubated at 37°C) / Geometric MFI of fluorescent protein in control population incubated at 4°C]. All experiments were performed at least three times using triplicates

### **Statistical analysis**

Statistical analysis including Mann-Withney U test, one-way ANOVA and two-way ANOVA tests were performed using GraphPad Prism™ software.

## FIGURE LEGENDS.

**Figure 1. Splenic CD169+ cells belong to macrophage lineage.** (a) the hierarchical gating strategy to identify and purify CD169+ cells and other phagocytes after enzymatic digestion and density gradient is depicted. (b) expression of macrophage-related receptors by CD169+ cells and other splenic phagocytes by multiplex flow cytometry. (c) qPCR analysis of the expression of macrophage-related genes (*siglec-1*, *nr1h3*) and dendritic cell-related genes (*batf3*, *zbtb46*); the histograms represent the mean of three independent experiments. (d) Examination of the presence of CD169+ cells in *Batf3*, *Flt3* and *Flt-3L* ko mice. (e) quantification of CD169+ cells in the spleen of wt and *Batf3*, *Flt3* and *Flt3-L* ko mice. (f) Typical confocal image of a sorted CD169+ cell allowed to adhere for 2h. All experiments have been performed at least three times, except for (e), two times.

**Figure 2. Splenic CD169+ macrophages belong to the small group of professional antigen cross-presenting cells.** (a) splenic CD169+ macrophages and other splenic phagocytes were allowed to endocytose OVA-AF647 *in vitro* at 4°C (negative control) or 37°C and the rate of active uptake was expressed as the ratio of fluorescence observed at 37°C to 4°C. (b) 100 µg of OVA-AF647 was injected i.v. to C57Bl/6 mice and uptake was determined after 2hrs by flow cytometry. (c) Cell sorted splenic phagocytes were pulsed with soluble OVA (top left) or endograde soluble OVA (top right), or with an OVA fusion protein targeted to CD11c, or with OVA-yeast cells, before the addition of OT-I cells. Activation of transgenic CD8+ T cells was assessed by measuring IL-2 secretion by ELISA. The histograms represent the mean of at least four independent experiments pooled together (d). One million of OT-I cells labeled with Violet Proliferation Dye 450 were injected before the immunization of mice with an OVA fusion protein (1 µg) i.v. targeted to either DEC-205 (cDC1 subset), or CD169 and proliferation of transgenic CD8+ T cells was analyzed *ex vivo*

on day 3 post-immunization by studying the dilution of Violet Proliferation Dye 450 (left and middle). In some experiments, mice were immunized before the injection of OT-I cells at different periods of time (right panel); the histograms represent the mean of 6-10 individual mice per condition (e) The formation of stable contacts between OT-I cells and CD169<sup>+</sup> macrophages were visualized *in vivo* by two-photon live imaging of the spleen of mice immunized i.v. with an OVA fusion protein (1 µg) targeted to CD169. Representative two-photon images of one T cell of interest prior to immunization and at various time points after immunization. (f) during *in vivo* imaging, the velocity of splenic OT-I T cells after antigen targeting to DEC-205 or CD169 was calculated by analyzing time-lapse movies of 15-20 min every 45 min (left and middle); in addition, was quantified the proportion of OT-I cells in contact with CD169<sup>+</sup> macrophages depending on the receptor targeted (right). For statistical analysis, comparisons were made relative to CD169<sup>+</sup> macrophages and two-way Anova (c) or Mann-Whitney U (d and f)) tests were used; \* p<0.05, \*\*, p<0.01 (a), (b), (d), (e) and (f) are representative of three independent experiments, whereas panels in (c) are representative of at least five independent experiments.

**Figure 3. Cross-priming by CD169<sup>+</sup> macrophages generates robust effector and memory CD8<sup>+</sup> T cell immunity in the presence of adjuvants.** (a) and (b) C57Bl/6 mice were immunized i.v. by an OVA protein (1 µg) targeted to DEC-205 or CD169 alone or together with an agonistic anti-CD40 antibody or with LPS as adjuvants. The quality of the antigen-specific effector CD8<sup>+</sup> T cells primed was read out as the secretion of IFN-γ, IL-2 and TNF-α by flow cytometry, after a short-term re-stimulation with the synthetic peptide S8L *ex vivo* on day 12. (a) The dot plots depict a representative IFN-γ as well as IL-2 and TNF-α secretion by endogenous antigen specific CD8<sup>+</sup> T cells primed by an OVA protein targeted to CD169 (top) or by a GAD protein targeted to the same receptor. (b) The

proportion of effector cells was calculated as the number of IFN- $\gamma$  positive cells for 10,000 CD8<sup>+</sup> T cells; to assess their poly-functionality, the percentage of endogenous CD8<sup>+</sup> T cells capable of multi-cytokine secretion was determined. (c), (d) and (e) Similar to (a) and (b), the quality of OT-I cell priming by CD169<sup>+</sup> macrophages was evaluated by flow cytometry by determining the proportion of OT-I cells in the spleen as well as the percentage of effector cells on day 12 (c) or on day 45 after a boost of 7 days (d). (e), the expression of transcription factors Blimp-1, Eomes and T-bet was analyzed by flow cytometry on OT-I cells 12 days post-immunization, as well as the percentages of short-lived effector cells (SLECs) and memory-precursor effector cells (MPECs). Histograms represent one representative experiment, for which 5-6 individual mice per condition were used. For statistical analysis, two-way Anova (b) or Mann-Whitney U (c, d and e) tests were used; \*  $p < 0.05$ , \*\*,  $p < 0.01$ . (a), (b), (c) are representative of three independent experiments, whereas (d) and (e) are representative of two independent experiments.

**Figure 4. CD169<sup>+</sup> macrophages process antigenic material exclusively through an endocytic pathway.** (a) Quantitative expression of ERAP, IRAP, TAP and Lamp2 proteins, as evaluated by imaging flow cytometry and IDEAS software. (b) Representative staining of Rab14, IRAP and co-localization between Rab14 and Lamp1 and Rab14 and IRAP, as determined by the Bright Detail Similarity R3 feature in IDEAS software, with a co-localization defined as a Pearson coefficient  $> 1.5$ . Scale bar 7  $\mu\text{m}$ . (c) sorted splenic phagocytes were incubated for 6h with soluble OVA together with the proteasome inhibitors epoxomicin or MG132 or to lysosomal protease inhibitors leupeptin or z-FA-fmk and then added to OT-I T cells. Activation of transgenic T cells was quantified by IL-2 ELISA. Splenic phagocytes sorted from ERAP or IRAP ko mice (d) or TAP ko mouse (e) were incubated with soluble OVA and cross-presentation was quantified by dosing the secretion of IL-2 by



ELISA. (f) Cross-presentation *in vivo* by CD169+ macrophages and cDC1s in ERAP, IRAP and TAP ko mice of an OVA fusion protein targeted to a specific receptor was evaluated by flow cytometry by calculation the division index of OT-I precursors; the histograms represent the mean of 8-10 individual mice per condition. (g) Similar to (d) and (e) but sorted splenic phagocytes were incubated at 37°C or 26° for 12hr before antigen pulse and addition of transgenic T cells. For (c), (d) and (e), the histograms represent the mean of at least four independent experiments pooled together. For statistical analysis two-way Anova (c, d f and g) or mann-withney U (e) tests were used; \* p<0.05, \*\*, p<0.01. All images and plots are representative of two experiments for (a) and (b) and at least 5 independent experiments for (c), (d), (e), (f) and (g).

**Figure 5. A pool of recycling endosomes but not the protein neosynthesis supply MHC-I molecules for antigen cross-presentation by CD169+ macrophages.** (a) Levels of expression of surface MHC-I on splenic phagocytes were examined by flow cytometry using the non-conformative clone B8.24-3. (b) Percentage of internalization of MHC-I in CD169+ macrophages and cDC1s after labeling the cell surface at 4°C with biotinylated anti-H-2Kb (AF6-88.5), shifted to 37°C for different times, and evaluated at different times by FACS for remaining biotinylated surface H-2Kb. (c) and (d) Surface expression of MHC-I (B8.24-3, left and middle) and cross-presentation (right) of soluble cDC1s in the presence of brefeldin (c) or primaquine (d) for 12hrs were assessed in wt and TAP ko CD169+ macrophages. The histograms represent the mean of a pool of at least 4 independent experiments. All the tested conditions for MHC-I expression were compared to the condition “wt 37°C” and for cross-presentation assays to “DMSO”; \* p<0.05, \*\* p<0.01, \*\*\* p<0.001 (one-way Anova or mann-whitney U tests). All the experiments have been performed independently at least three times.

## REFERENCES.

- Ackerman, A. L., A. Giodini and P. Cresswell (2006). "A role for the endoplasmic reticulum protein retrotranslocation machinery during crosspresentation by dendritic cells." *Immunity* **25**(4): 607-617.
- Alloatti, A., F. Kotsias, A. M. Pauwels, J. M. Carpier, M. Jouve, E. Timmerman, L. Pace, P. Vargas, M. Maurin, U. Gehrman, L. Joannas, O. I. Vivar, A. M. Lennon-Dumenil, A. Savina, K. Gevaert, R. Beyaert, E. Hoffmann and S. Amigorena (2015). "Toll-like Receptor 4 Engagement on Dendritic Cells Restrains Phago-Lysosome Fusion and Promotes Cross-Presentation of Antigens." *Immunity* **43**(6): 1087-1100.
- Arnon, T. I., R. M. Horton, I. L. Grigorova and J. G. Cyster (2013). "Visualization of splenic marginal zone B-cell shuttling and follicular B-cell egress." *Nature* **493**(7434): 684-688.
- Asano, K., A. Nabeyama, Y. Miyake, C. H. Qiu, A. Kurita, M. Tomura, O. Kanagawa, S. Fujii and M. Tanaka (2011). "CD169-positive macrophages dominate antitumor immunity by crosspresenting dead cell-associated antigens." *Immunity* **34**(1): 85-95.
- Backer, R., T. Schwandt, M. Greuter, M. Oosting, F. Jungerkes, T. Tuting, L. Boon, T. O'Toole, G. Kraal, A. Limmer and J. M. den Haan (2010). "Effective collaboration between marginal metallophilic macrophages and CD8+ dendritic cells in the generation of cytotoxic T cells." *Proc Natl Acad Sci U S A* **107**(1): 216-221.
- Backer, R., F. van Leeuwen, G. Kraal and J. M. den Haan (2008). "CD8- dendritic cells preferentially cross-present *Saccharomyces cerevisiae* antigens." *Eur J Immunol* **38**(2): 370-380.
- Barral, P., P. Polzella, A. Bruckbauer, N. van Rooijen, G. S. Besra, V. Cerundolo and F. D. Batista (2010). "CD169(+) macrophages present lipid antigens to mediate early activation of iNKT cells in lymph nodes." *Nat Immunol* **11**(4): 303-312.
- Blanchard, N., F. Gonzalez, M. Schaeffer, N. T. Joncker, T. Cheng, A. J. Shastri, E. A. Robey and N. Shastri (2008). "Immunodominant, protective response to the parasite *Toxoplasma gondii* requires antigen processing in the endoplasmic reticulum." *Nat Immunol* **9**(8): 937-944.
- Bousso, P. (2008). "T-cell activation by dendritic cells in the lymph node: lessons from the movies." *Nat Rev Immunol* **8**(9): 675-684.
- Cebrian, I., G. Visentin, N. Blanchard, M. Jouve, A. Bobard, C. Moita, J. Enninga, L. F. Moita, S. Amigorena and A. Savina (2011). "Sec22b regulates phagosomal maturation and antigen crosspresentation by dendritic cells." *Cell* **147**(6): 1355-1368.
- Chang, J. T., E. J. Wherry and A. W. Goldrath (2014). "Molecular regulation of effector and memory T cell differentiation." *Nat Immunol* **15**(12): 1104-1115.
- Davies, L. C., S. J. Jenkins, J. E. Allen and P. R. Taylor (2013). "Tissue-resident macrophages." *Nat Immunol* **14**(10): 986-995.

den Haan, J. M. and G. Kraal (2012). "Innate immune functions of macrophage subpopulations in the spleen." J Innate Immun **4**(5-6): 437-445.

Dudziak, D., A. O. Kamphorst, G. F. Heidkamp, V. R. Buchholz, C. Trumfheller, S. Yamazaki, C. Cheong, K. Liu, H. W. Lee, C. G. Park, R. M. Steinman and M. C. Nussenzweig (2007). "Differential antigen processing by dendritic cell subsets in vivo." Science **315**(5808): 107-111.

Gautier, E. L., T. Shay, J. Miller, M. Greter, C. Jakubzick, S. Ivanov, J. Helft, A. Chow, K. G. Elpek, S. Gordonov, A. R. Mazloom, A. Ma'ayan, W. J. Chua, T. H. Hansen, S. J. Turley, M. Merad, G. J. Randolph and C. Immunological Genome (2012). "Gene-expression profiles and transcriptional regulatory pathways that underlie the identity and diversity of mouse tissue macrophages." Nat Immunol **13**(11): 1118-1128.

Geissmann, F., S. Gordon, D. A. Hume, A. M. Mowat and G. J. Randolph (2010). "Unravelling mononuclear phagocyte heterogeneity." Nat Rev Immunol **10**(6): 453-460.

Ginhoux, F., J. L. Schultze, P. J. Murray, J. Ochando and S. K. Biswas (2016). "New insights into the multidimensional concept of macrophage ontogeny, activation and function." Nat Immunol **17**(1): 34-40.

Gray, E. E. and J. G. Cyster (2012). "Lymph node macrophages." J Innate Immun **4**(5-6): 424-436.

Gray, E. E., S. Friend, K. Suzuki, T. G. Phan and J. G. Cyster (2012). "Subcapsular sinus macrophage fragmentation and CD169+ bleb acquisition by closely associated IL-17-committed innate-like lymphocytes." PLoS One **7**(6): e38258.

Guilliams, M., C. A. Dutertre, C. L. Scott, N. McGovern, D. Sichien, S. Chakarov, S. Van Gassen, J. Chen, M. Poidinger, S. De Prijck, S. J. Tavernier, I. Low, S. E. Irac, C. N. Mattar, H. R. Sumatoh, G. H. Low, T. J. Chung, D. K. Chan, K. K. Tan, T. L. Hon, E. Fossum, B. Bogen, M. Choolani, J. K. Chan, A. Larbi, H. Luche, S. Henri, Y. Saeys, E. W. Newell, B. N. Lambrecht, B. Malissen and F. Ginhoux (2016). "Unsupervised High-Dimensional Analysis Aligns Dendritic Cells across Tissues and Species." Immunity **45**(3): 669-684.

Guilliams, M., F. Ginhoux, C. Jakubzick, S. H. Naik, N. Onai, B. U. Schraml, E. Segura, R. Tussiwand and S. Yona (2014). "Dendritic cells, monocytes and macrophages: a unified nomenclature based on ontogeny." Nat Rev Immunol **14**(8): 571-578.

Hammer, G. E., F. Gonzalez, E. James, H. Nolla and N. Shastri (2007). "In the absence of aminopeptidase ERAAP, MHC class I molecules present many unstable and highly immunogenic peptides." Nat Immunol **8**(1): 101-108.

Hanc, P., T. Fujii, S. Iborra, Y. Yamada, J. Huotari, O. Schulz, S. Ahrens, S. Kjaer, M. Way, D. Sancho, K. Namba and C. Reis e Sousa (2015). "Structure of the Complex of F-Actin and DNGR-1, a C-Type Lectin Receptor Involved in Dendritic Cell Cross-Presentation of Dead Cell-Associated Antigens." Immunity **42**(5): 839-849.

Honke, N., N. Shaabani, G. Cadeddu, U. R. Sorg, D. E. Zhang, M. Trilling, K. Klingel, M. Sauter, R. Kandolf, N. Gailus, N. van Rooijen, C. Burkart, S. E. Baldus, M. Grusdat, M. Lohning, H. Hengel, K. Pfeffer, M. Tanaka, D. Haussinger, M. Recher, P. A. Lang and K. S.

Lang (2012). "Enforced viral replication activates adaptive immunity and is essential for the control of a cytopathic virus." Nat Immunol **13**(1): 51-57.

Hugues, S., L. Fetler, L. Bonifaz, J. Helft, F. Amblard and S. Amigorena (2004). "Distinct T cell dynamics in lymph nodes during the induction of tolerance and immunity." Nat Immunol **5**(12): 1235-1242.

Iannacone, M., E. A. Moseman, E. Tonti, L. Bosurgi, T. Junt, S. E. Henrickson, S. P. Whelan, L. G. Guidotti and U. H. von Andrian (2010). "Subcapsular sinus macrophages prevent CNS invasion on peripheral infection with a neurotropic virus." Nature **465**(7301): 1079-1083.

Jancic, C., A. Savina, C. Wasmeier, T. Tolmachova, J. El-Benna, P. M. Dang, S. Pascolo, M. A. Gougerot-Pocidallo, G. Raposo, M. C. Seabra and S. Amigorena (2007). "Rab27a regulates phagosomal pH and NADPH oxidase recruitment to dendritic cell phagosomes." Nat Cell Biol **9**(4): 367-378.

Joffre, O. P., E. Segura, A. Savina and S. Amigorena (2012). "Cross-presentation by dendritic cells." Nat Rev Immunol **12**(8): 557-569.

Junt, T., E. A. Moseman, M. Iannacone, S. Massberg, P. A. Lang, M. Boes, K. Fink, S. E. Henrickson, D. M. Shayakhmetov, N. C. Di Paolo, N. van Rooijen, T. R. Mempel, S. P. Whelan and U. H. von Andrian (2007). "Subcapsular sinus macrophages in lymph nodes clear lymph-borne viruses and present them to antiviral B cells." Nature **450**(7166): 110-114.

Karlsson, M. C., R. Guinamard, S. Bolland, M. Sankala, R. M. Steinman and J. V. Ravetch (2003). "Macrophages control the retention and trafficking of B lymphocytes in the splenic marginal zone." J Exp Med **198**(2): 333-340.

Kawasaki, N., J. L. Vela, C. M. Nycholat, C. Rademacher, A. Khurana, N. van Rooijen, P. R. Crocker, M. Kronenberg and J. C. Paulson (2013). "Targeted delivery of lipid antigen to macrophages via the CD169/sialoadhesin endocytic pathway induces robust invariant natural killer T cell activation." Proc Natl Acad Sci U S A **110**(19): 7826-7831.

Keller, S. R., H. M. Scott, C. C. Mastick, R. Aebersold and G. E. Lienhard (1995). "Cloning and characterization of a novel insulin-regulated membrane aminopeptidase from Glut4 vesicles." J Biol Chem **270**(40): 23612-23618.

Kokkala, P., A. Mpakali, F. X. Mauvais, A. Papakyriakou, I. Daskalaki, I. Petropoulou, S. Kavvalou, M. Papanthanasopoulou, S. Agrotis, T. M. Fonsou, P. van Endert, E. Stratikos and D. Georgiadis (2016). "Optimization and Structure-Activity Relationships of Phosphinic Pseudotriptide Inhibitors of Aminopeptidases That Generate Antigenic Peptides." J Med Chem.

Kratzer, R., F. X. Mauvais, A. Burgevin, E. Barilleau and P. van Endert (2010). "Fusion proteins for versatile antigen targeting to cell surface receptors reveal differential capacity to prime immune responses." J Immunol **184**(12): 6855-6864.

Mant, A., F. Chinnery, T. Elliott and A. P. Williams (2012). "The pathway of cross-presentation is influenced by the particle size of phagocytosed antigen." Immunology **136**(2): 163-175.

- Mantegazza, A. R., A. Savina, M. Vermeulen, L. Perez, J. Geffner, O. Hermine, S. D. Rosenzweig, F. Faure and S. Amigorena (2008). "NADPH oxidase controls phagosomal pH and antigen cross-presentation in human dendritic cells." Blood **112**(12): 4712-4722.
- McGaha, T. L., Y. Chen, B. Ravishankar, N. van Rooijen and M. C. Karlsson (2011). "Marginal zone macrophages suppress innate and adaptive immunity to apoptotic cells in the spleen." Blood **117**(20): 5403-5412.
- Meredith, M. M., K. Liu, G. Darrasse-Jeze, A. O. Kamphorst, H. A. Schreiber, P. Guermonprez, J. Idoyaga, C. Cheong, K. H. Yao, R. E. Niec and M. C. Nussenzweig (2012). "Expression of the zinc finger transcription factor zDC (Zbtb46, Btd4) defines the classical dendritic cell lineage." J Exp Med **209**(6): 1153-1165.
- Merzougui, N., R. Kratzer, L. Saveanu and P. van Endert (2011). "A proteasome-dependent, TAP-independent pathway for cross-presentation of phagocytosed antigen." EMBO Rep **12**(12): 1257-1264.
- Miyake, Y., K. Asano, H. Kaise, M. Uemura, M. Nakayama and M. Tanaka (2007). "Critical role of macrophages in the marginal zone in the suppression of immune responses to apoptotic cell-associated antigens." J Clin Invest **117**(8): 2268-2278.
- Moreau, H. D., F. Lemaitre, K. R. Garrod, Z. Garcia, A. M. Lennon-Dumenil and P. Bousso (2015). "Signal strength regulates antigen-mediated T-cell deceleration by distinct mechanisms to promote local exploration or arrest." Proc Natl Acad Sci U S A **112**(39): 12151-12156.
- Moreau, H. D., F. Lemaitre, E. Terriac, G. Azar, M. Piel, A. M. Lennon-Dumenil and P. Bousso (2012). "Dynamic in situ cytometry uncovers T cell receptor signaling during immunological synapses and kinapses in vivo." Immunity **37**(2): 351-363.
- Moseman, E. A., M. Iannaccone, L. Bosurgi, E. Tonti, N. Chevrier, A. Tumanov, Y. X. Fu, N. Hacohen and U. H. von Andrian (2012). "B cell maintenance of subcapsular sinus macrophages protects against a fatal viral infection independent of adaptive immunity." Immunity **36**(3): 415-426.
- N, A. G., J. A. Guillen, G. Gallardo, M. Diaz, J. V. de la Rosa, I. H. Hernandez, M. Casanova-Acebes, F. Lopez, C. Tabraue, S. Beceiro, C. Hong, P. C. Lara, M. Andujar, S. Arai, T. Miyazaki, S. Li, A. L. Corbi, P. Tontonoz, A. Hidalgo and A. Castrillo (2013). "The nuclear receptor LXRalpha controls the functional specialization of splenic macrophages." Nat Immunol **14**(8): 831-839.
- Nair-Gupta, P., A. Baccarini, N. Tung, F. Seyffer, O. Florey, Y. Huang, M. Banerjee, M. Overholtzer, P. A. Roche, R. Tampe, B. D. Brown, D. Amsen, S. W. Whiteheart and J. M. Blander (2014). "TLR signals induce phagosomal MHC-I delivery from the endosomal recycling compartment to allow cross-presentation." Cell **158**(3): 506-521.
- Phan, T. G., J. A. Green, E. E. Gray, Y. Xu and J. G. Cyster (2009). "Immune complex relay by subcapsular sinus macrophages and noncognate B cells drives antibody affinity maturation." Nat Immunol **10**(7): 786-793.

- Phan, T. G., I. Grigorova, T. Okada and J. G. Cyster (2007). "Subcapsular encounter and complement-dependent transport of immune complexes by lymph node B cells." Nat Immunol **8**(9): 992-1000.
- Pooley, J. L., W. R. Heath and K. Shortman (2001). "Cutting edge: intravenous soluble antigen is presented to CD4 T cells by CD8- dendritic cells, but cross-presented to CD8 T cells by CD8+ dendritic cells." J Immunol **166**(9): 5327-5330.
- Sagoo, P., Z. Garcia, B. Breart, F. Lemaitre, D. Michonneau, M. L. Albert, Y. Levy and P. Bousso (2016). "In vivo imaging of inflammasome activation reveals a subcapsular macrophage burst response that mobilizes innate and adaptive immunity." Nat Med **22**(1): 64-71.
- Satpathy, A. T., W. Kc, J. C. Albring, B. T. Edelson, N. M. Kretzer, D. Bhattacharya, T. L. Murphy and K. M. Murphy (2012). "Zbtb46 expression distinguishes classical dendritic cells and their committed progenitors from other immune lineages." J Exp Med **209**(6): 1135-1152.
- Saveanu, L., O. Carroll, M. Weimershaus, P. Guermonprez, E. Firat, V. Lindo, F. Greer, J. Davoust, R. Kratzer, S. R. Keller, G. Niedermann and P. van Endert (2009). "IRAP identifies an endosomal compartment required for MHC class I cross-presentation." Science **325**(5937): 213-217.
- Saveanu, L. and P. van Endert (2013). "Preparing antigens suitable for cross-presentation assays in vitro and in vivo." Methods Mol Biol **960**: 389-400.
- Savina, A., A. Peres, I. Cebrian, N. Carmo, C. Moita, N. Hacohen, L. F. Moita and S. Amigorena (2009). "The small GTPase Rac2 controls phagosomal alkalization and antigen crosspresentation selectively in CD8(+) dendritic cells." Immunity **30**(4): 544-555.
- Shaabani, N., V. Khairnar, V. Duhan, F. Zhou, R. F. Tur, D. Haussinger, M. Recher, A. V. Tumanov, C. Hardt, D. Pinschewer, U. Christen, P. A. Lang, N. Honke and K. S. Lang (2016). "Two separate mechanisms of enforced viral replication balance innate and adaptive immune activation." J Autoimmun **67**: 82-89.
- Shen, L., L. J. Sigal, M. Boes and K. L. Rock (2004). "Important role of cathepsin S in generating peptides for TAP-independent MHC class I crosspresentation in vivo." Immunity **21**(2): 155-165.
- Takahara, K., Y. Omatsu, Y. Yashima, Y. Maeda, S. Tanaka, T. Iyoda, B. E. Clausen, K. Matsubara, J. Letterio, R. M. Steinman, Y. Matsuda and K. Inaba (2002). "Identification and expression of mouse Langerin (CD207) in dendritic cells." Int Immunol **14**(5): 433-444.
- van Endert, P. (2016). "Intracellular recycling and cross-presentation by MHC class I molecules." Immunol Rev **272**(1): 80-96.
- Van Kaer, L., P. G. Ashton-Rickardt, H. L. Ploegh and S. Tonegawa (1992). "TAP1 mutant mice are deficient in antigen presentation, surface class I molecules, and CD4-8+ T cells." Cell **71**(7): 1205-1214.
- Veninga, H., E. G. Borg, K. Vreeman, P. R. Taylor, H. Kalay, Y. van Kooyk, G. Kraal, L. Martinez-Pomares and J. M. den Haan (2015). "Antigen targeting reveals splenic CD169+

macrophages as promoters of germinal center B-cell responses." Eur J Immunol **45**(3): 747-757.

Weimershaus, M., S. Maschalidi, F. Sepulveda, B. Manoury, P. van Endert and L. Saveanu (2012). "Conventional dendritic cells require IRAP-Rab14 endosomes for efficient cross-presentation." J Immunol **188**(4): 1840-1846.

Yamazaki, C., M. Sugiyama, T. Ohta, H. Hemmi, E. Hamada, I. Sasaki, Y. Fukuda, T. Yano, M. Nobuoka, T. Hirashima, A. Iizuka, K. Sato, T. Tanaka, K. Hoshino and T. Kaisho (2013). "Critical roles of a dendritic cell subset expressing a chemokine receptor, XCR1." J Immunol **190**(12): 6071-6082.

You, Y., R. C. Myers, L. Freeberg, J. Foote, J. F. Kearney, L. B. Justement and R. H. Carter (2011). "Marginal zone B cells regulate antigen capture by marginal zone macrophages." J Immunol **186**(4): 2172-2181.

Zehner, M., A. L. Marschall, E. Bos, J. G. Schloetel, C. Kreer, D. Fehrenschild, A. Limmer, F. Ossendorp, T. Lang, A. J. Koster, S. Dubel and S. Burgdorf (2015). "The translocon protein Sec61 mediates antigen transport from endosomes in the cytosol for cross-presentation to CD8(+) T cells." Immunity **42**(5): 850-863.

## SUPPLEMENTARY FIGURE LEGENDS.

**Figure S1 (related to Fig. 1). Splenic CD169+ cells are not a dendritic cell subset.** (a) the expression of CLEC9A and 33D1 was examined by flow cytometry using specific antibodies (colored histograms) and isotype controls (black histograms), as was the expression of CD11c (right panel). One replicate out of five is shown from one of the three independent experiments performed. (b) by using a similar antibody cocktail than for conventional flow cytometry, CD169+ cells and other phagocytes were identified by imaging flow cytometry: after gating on focused cells (not shown), doublets were excluded from the analysis before gating on the different phagocyte populations. (c) Morphology of phagocyte population was visualized through the use of the brightfield channel, and a small gallery of images of CD169+ cells and cDC1s is depicted. One experiment out of two is shown.

**Figure S2 (related to Fig.2). Splenic CD169+ macrophages belong to the small group of professional antigen cross-presenting cells.** (a) irradiated fluorescent apoptotic splenocytes were incubated for two hours with splenic phagocytes at 37°C to allow for their phagocytosis or at 4°C as a negative control. Then, the cells were stained for flow cytometry analysis. One out of three independent experiments is shown (n=5 samples per condition) (b) serial dilutions of soluble OVA were incubated for 4h or 16h with splenic phagocytes before the addition of OT-I T cells and the quantification of IL-2 secreted by ELISA. (c) and (d) Similarly, splenic phagocytes were incubated with serial dilution of P3U-OVA complexed to anti-CD11c antibody (c) or of OVA-yeast cells (d). Graphs represent mean +/- SEM of 5 independent experiments.

**Figure S3 (related to Fig.3). Examination of the effector functions of effector and memory OT-I T cells cross-primed by CD169+ macrophages or cDC1s.** (a) Splenocytes purified from immunized mice that had been transferred with OT-I transgenic T cells were re-stimulated *ex vivo* with cognate peptide or an irrelevant peptide as a negative control and



stained with CD19, CD8, CD45.2, IFN- $\gamma$ , TNF- $\alpha$ , and IL-2 before analysis by flow cytometry (b) and (c), splenocytes from immunized mice were stained without any re-stimulation for CD45.2, CD19, CD8, KLRG-1, CD127, Blimp-1, Eomes and T-bet before analysis by flow cytometry. (b) After gating on OT-I T cells (CD19<sup>-</sup>, CD8a<sup>+</sup> and CD45.2<sup>+</sup>), MPECs and SLECs were identified as CD127<sup>high</sup>KLRG-1<sup>low</sup> and CD127<sup>low</sup>KLRG-1<sup>high</sup> OT-I T cells, respectively. (c) The expression of the transcription factors Blimp-1, Eomes and T-bet was assessed by flow cytometry and the presence of a specific staining was checked by comparing the MFI calculated for isotype controls (black histograms) and for specific antibodies (red histograms). One representative out of three independent experiments is shown.

**Figure S4 (related to Fig.4 and Fig.5). Molecular antigen-processing equipment of CD169+ macrophages or cDC1s.** (a) The presence of significant levels of IRAP in CD169+ macrophages was confirmed by comparing the mean pixel intensity of IRAP wt and IRAP ko cells stained with the mouse anti-IRAP antibody. One out of two experiments is shown. (b) Restoration of MHC-I (clone B8.24-3) expression at the surface by a low temperature incubation of TAP ko and ERAP ko (not shown) splenic phagocytes. One representative out of five independent experiments is shown. (c) Consequences of the incubation with inhibitors on antigen uptake by phagocytes were examined by incubating fluorescent antigens with phagocytes together with the inhibitor, prior to staining for analysis by flow cytometry. (d) Contribution of protein synthesis for cross-presentation of antigens by CD169+ macrophages and cDC1 and cDC2 dendritic cell subsets was assessed by incubating sorted phagocytes with the antigen in the presence of increasing doses of cycloheximide, before addition to OT-I T cells and quantification of cross-presentations. Pool of the means of four independent experiments is represented by the histograms.

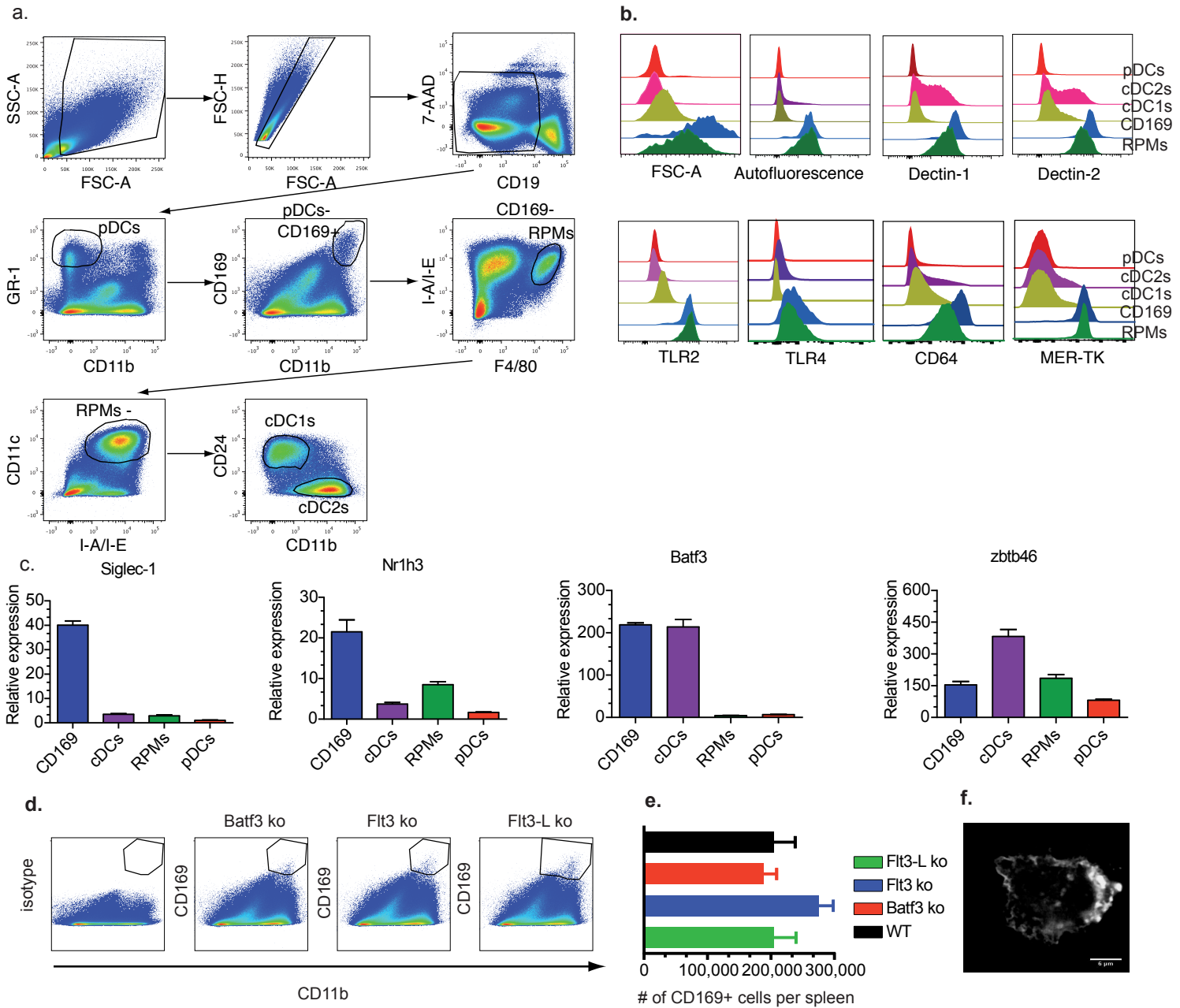


Figure 1. Mauvais et al.

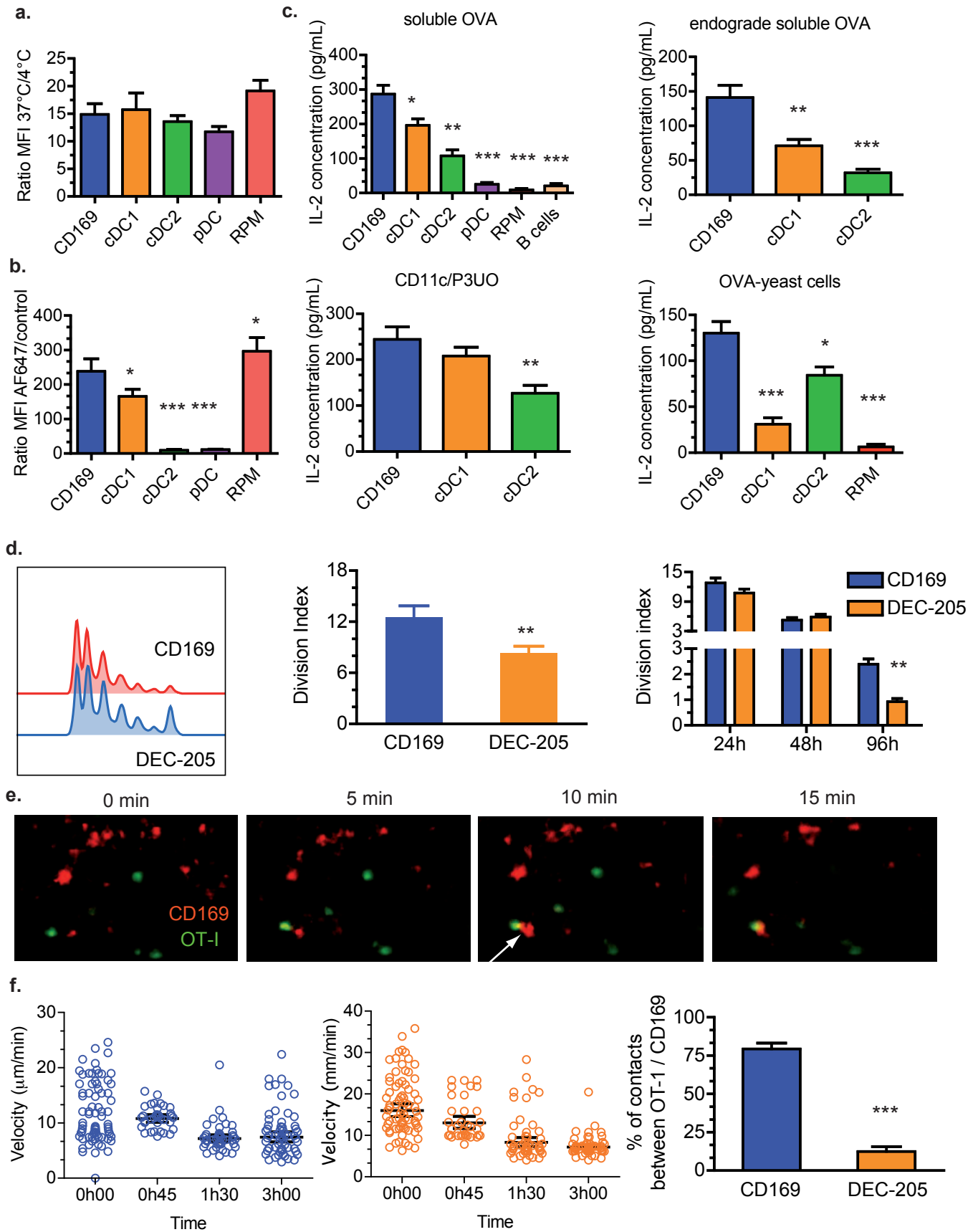
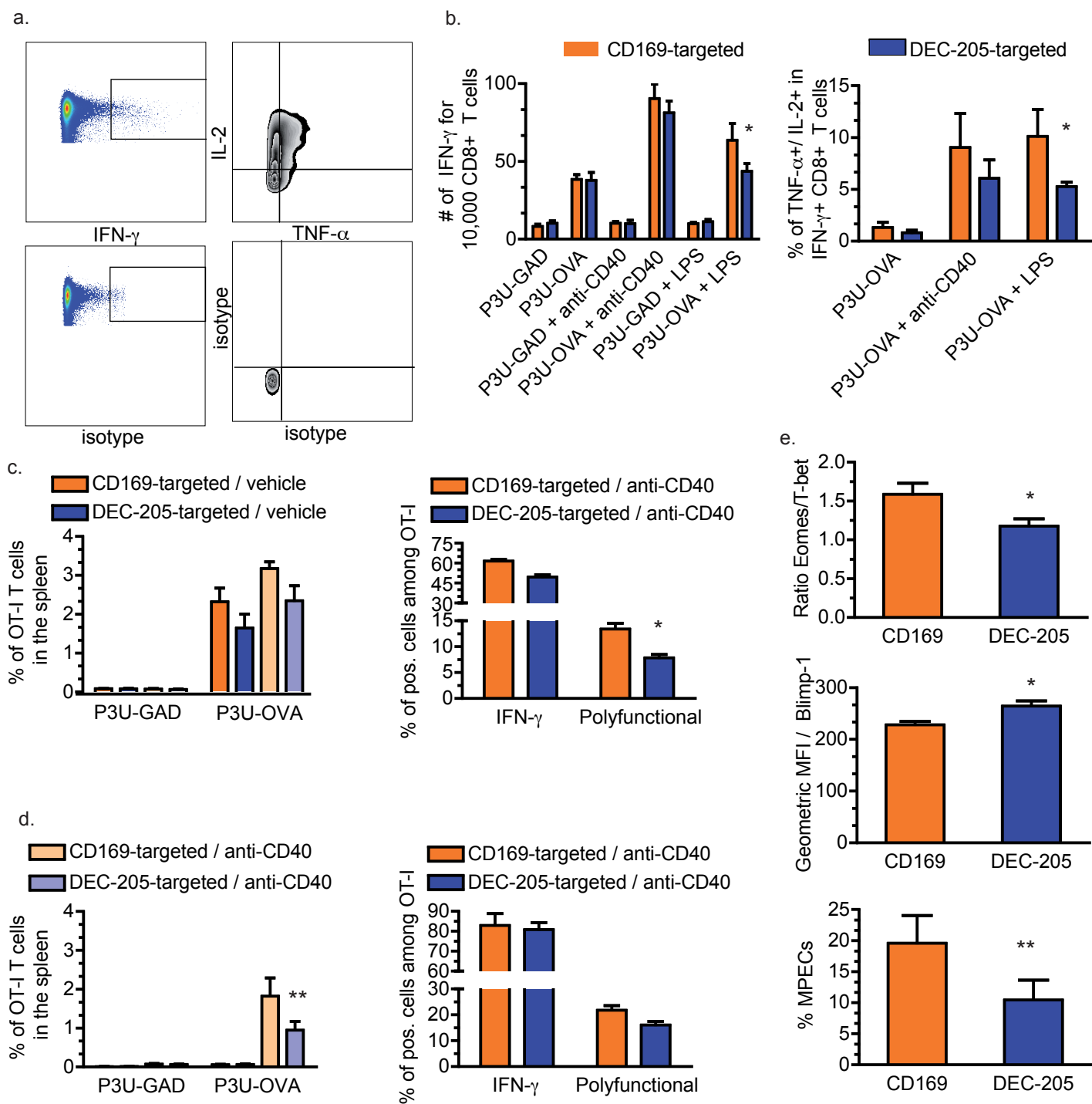


Figure 2. Mauvais et al.



**Figure 3. Mauvais et al.**

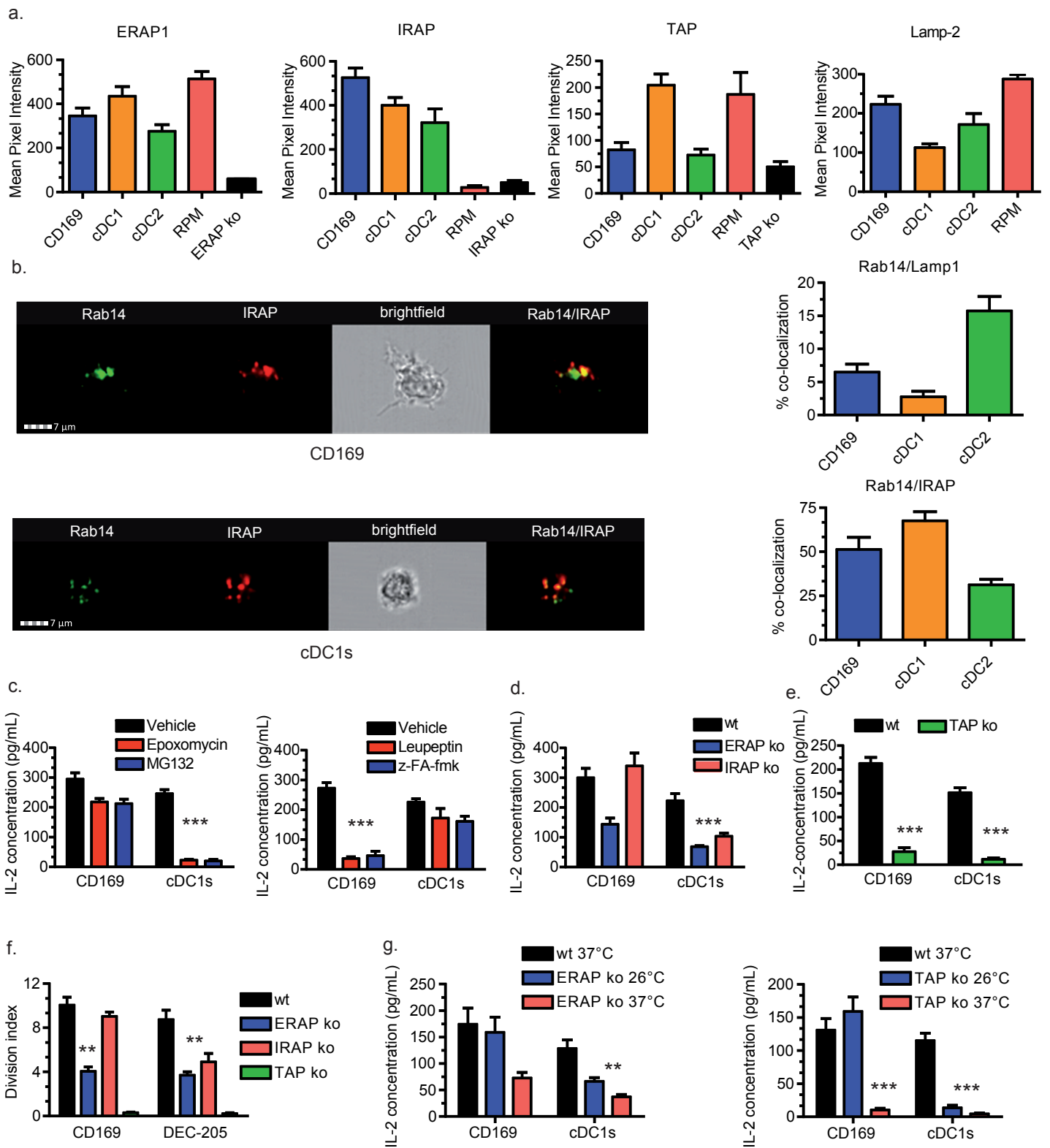


Figure 4. Mauvais et al.

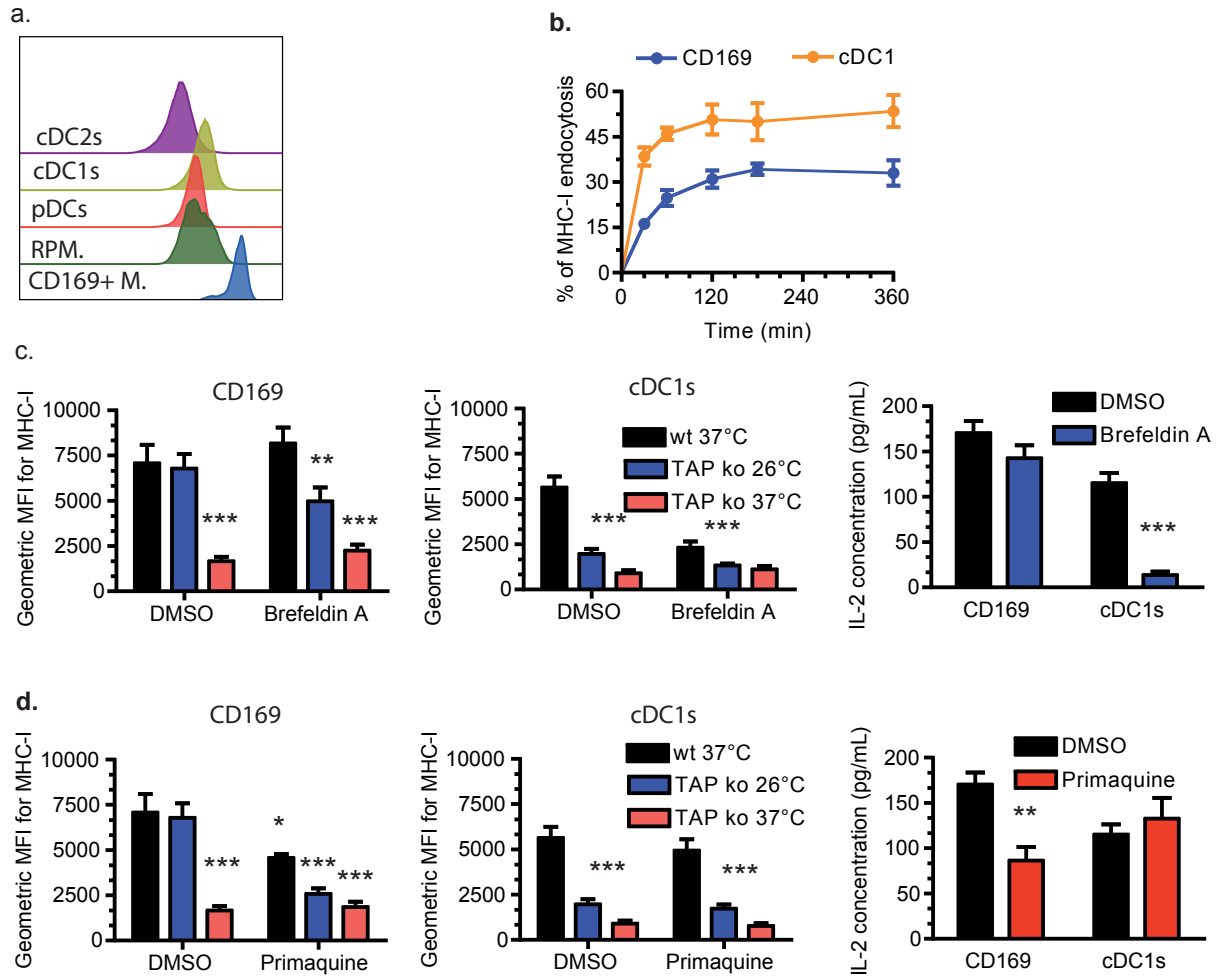
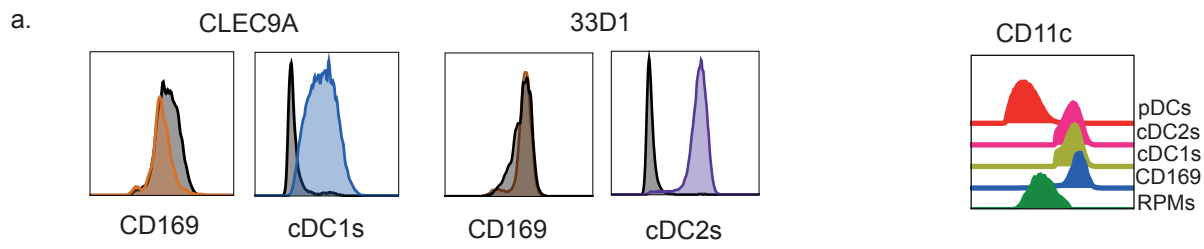
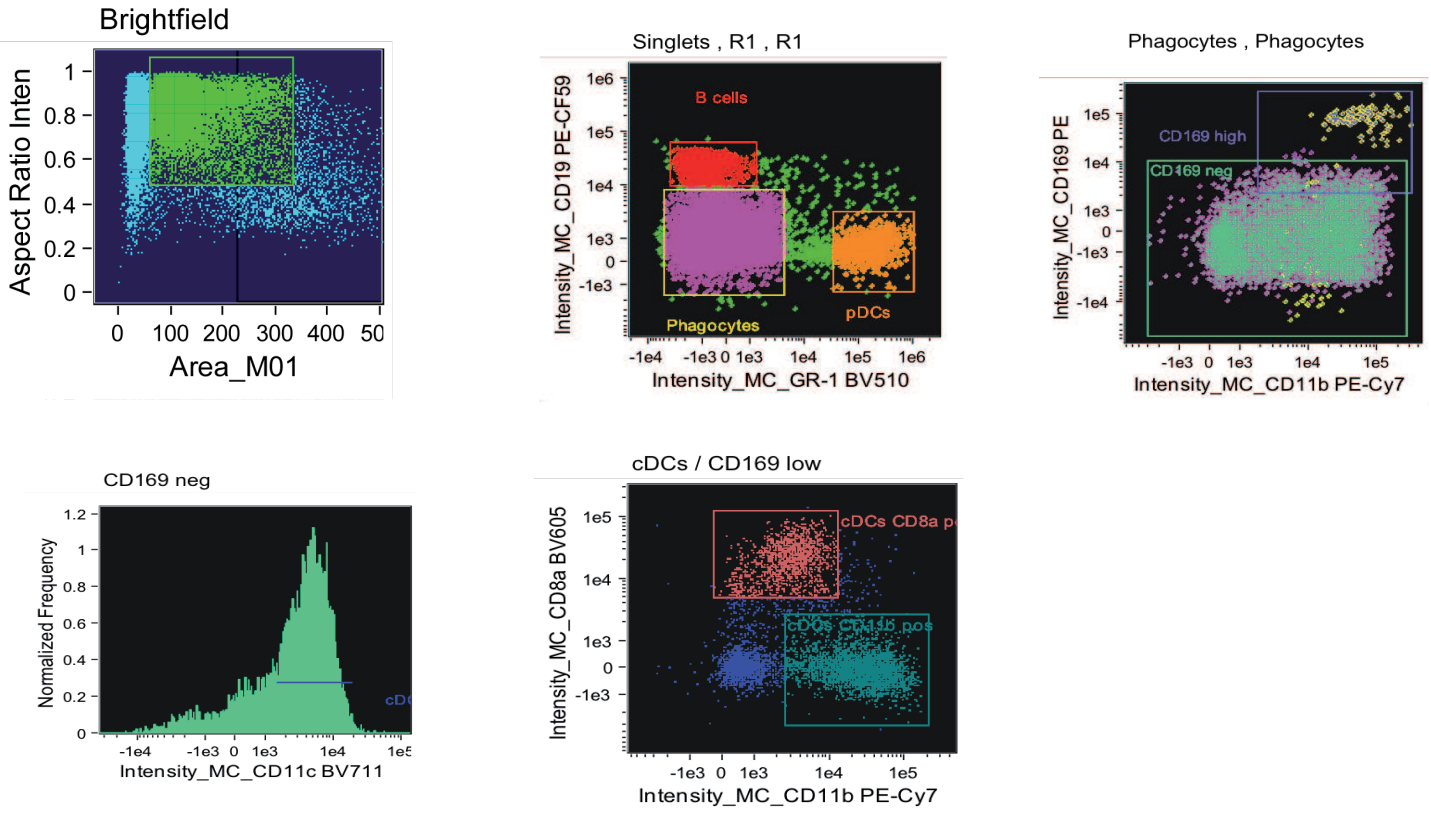


Figure 5. Mauvais et al.



b.



c.

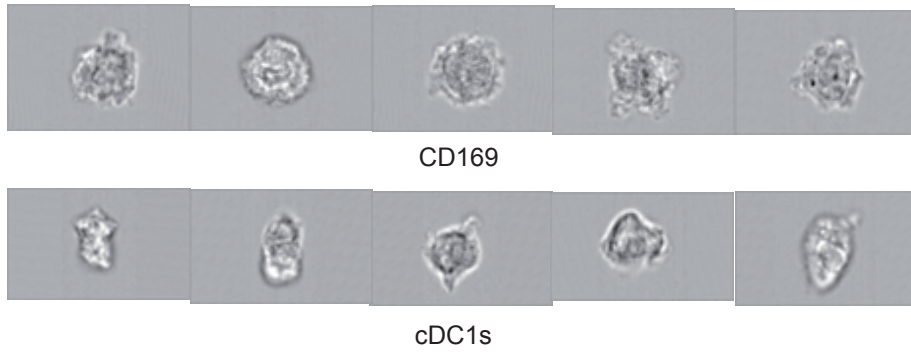


Figure S1. Mauvais et al.

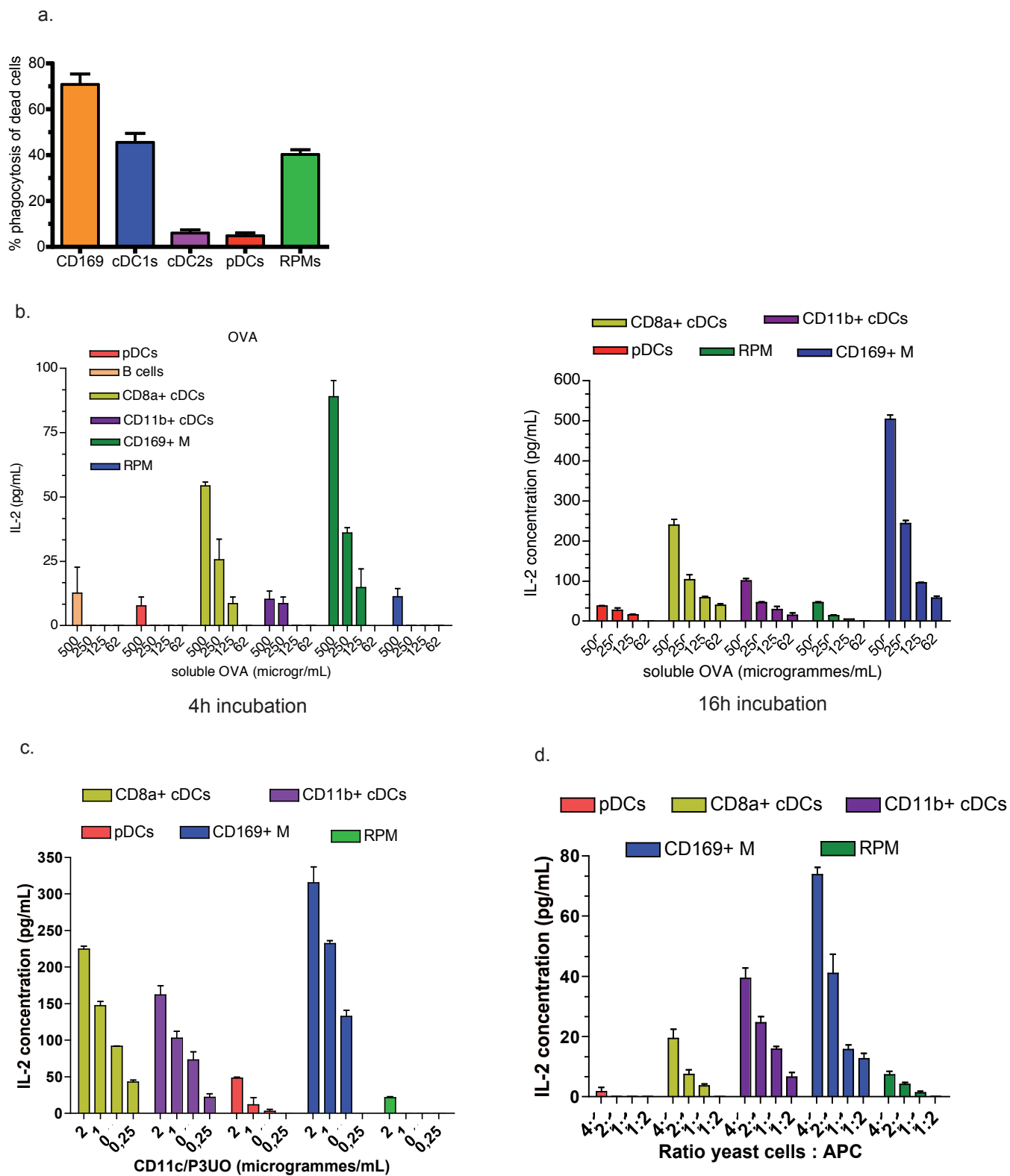


Figure S2. Mauvais et al.



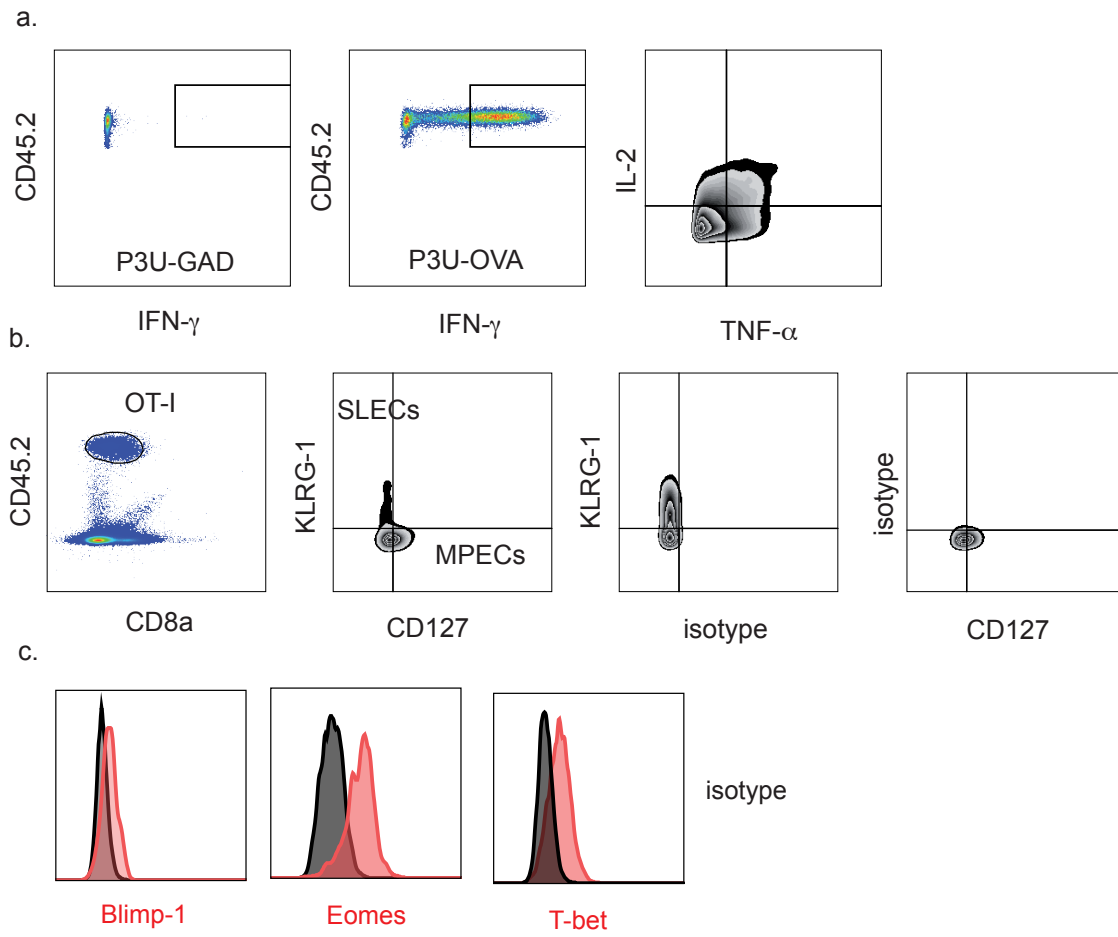


Figure S3. Mauvais et al.

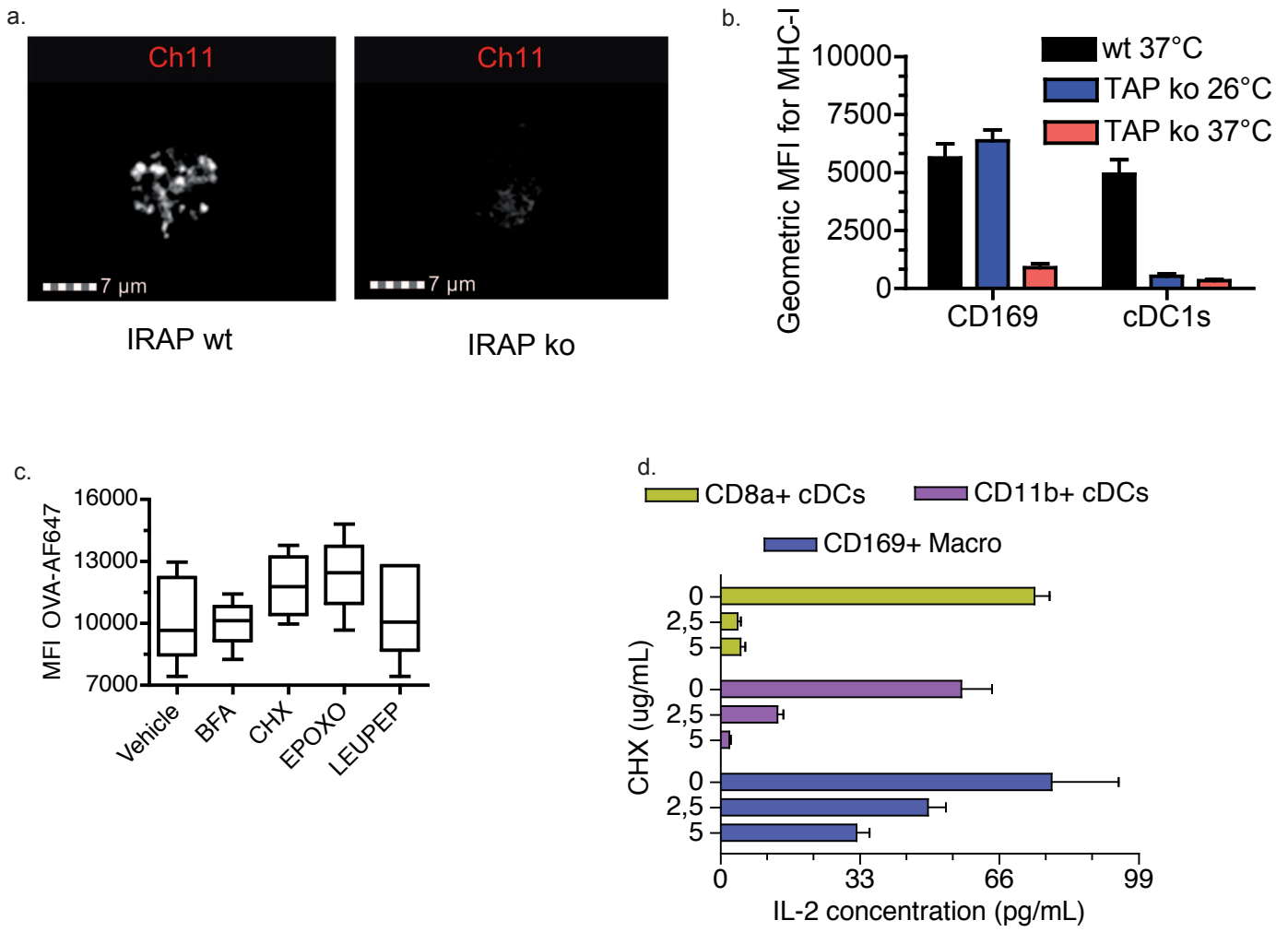


Figure S4. Mauvais et al.

## CONCLUSION AND DISCUSSION

---

### PART I - CONCLUSIONS

Despite their unique location in a transitional area placing them in direct contact with circulating antigenic material, splenic CD169<sup>+</sup> marginal zone macrophages have been suggested to activate adaptive immune responses by transferring in an intact form trapped antigens to cDC1 dendritic cells, the latter being responsible for antigen cross-presentation to CD8<sup>+</sup> T cells (Backer, Schwandt et al. 2010). In the main work I was implicated in, I have collected strong evidence that place the CD169<sup>+</sup> metallophilic marginal zone macrophages together with cDC1s, in a small group of professional antigen presenting cells capable of highly efficient cross-priming. The exclusive use of the vacuolar pathway to generate antigenic peptides from both phagocytic and endocytic antigens as well as the marginal role of the Rab14<sup>+</sup> endosomes in this process and the particular MHC-I trafficking in this macrophage population are other surprising results. My additional contribution to other studies has allowed me to participate in the identification of molecules capable of modulating antigen cross-presentation by inhibiting the activity of the ERAP and IRAP aminopeptidases in dendritic cells; to elucidate the molecular mechanisms regulating the formation, the distribution and the functions of the Rab14<sup>+</sup>IRAP<sup>+</sup> regulatory endosomes, which regulate the innate and adaptive immune responses by controlling TLR-9 trafficking and activation and the phagosomal maturation. These mechanisms are dependent on cytoskeleton remodeling and involve interactions with formins and kinesin/dynein proteins, respectively. Finally, we have identified a signature in the bulk (not necessary autoreactive) CD8<sup>+</sup> T cell responses associated with juvenile recent-onset type 1 diabetes by multiplex single-cell qPCR and flow cytometry analysis. Besides the validation of the interest of single-cell technologies in the context of human autoimmune settings, this study supports the power of single-cell technologies in analyzing heterogeneous immune cell populations to decipher their functions, their phenotype, their state of differentiation, or their origin. Based on these results, I will now address and discuss several questions that may have future implications in our understanding on how immune responses are regulated.

## PART II - DISCUSSION

### **Chapter 1. Do splenic CD169<sup>+</sup> cells belong to the dendritic cell or macrophage lineage?**

The CD169 antigen has been invariably associated to macrophage subpopulations in the lymphoid organs, including the spleen and the lymph nodes (den Haan and Kraal 2012, Gray and Cyster 2012), yet some expression has been detected under inflammatory conditions on human monocytes and dendritic cells. However, strategies developed to isolate CD169<sup>+</sup> macrophages in the spleen have remained unsuccessful, presumably because of the scarcity of the cells or the digestion of several surface epitopes including the CD169 antigen by cocktail enzyme digestion. The flow cytometry-based strategy I have designed and tested allows us to purify with limited contaminant cells live CD169<sup>+</sup> cells compatible for further phenotypic and functional analysis. This contrasts with the unique published technique study that has succeeded, by laser microdissection, in purifying CD169<sup>+</sup> metallophilic macrophages, that only permits gene expression analysis (Honke, Shaabani et al. 2012). Our panel for analysis of gene and protein expression by CD169<sup>+</sup> splenic cells has allowed us to suggest that the identified population is close to a macrophage-lineage, notably because of the significant expression of Mer-TK and CD64 (Gautier, Chow et al. 2012). Furthermore, this cell population was distinguishable at the protein level from the other macrophage populations including outer marginal zone macrophages or red pulp macrophages and from cDC1 and cDC2 conventional dendritic cells and from plasmacytoid dendritic cells; no contaminant cells (Gray, Friend et al. 2012) could be observed either by flow cytometry or by imaging flow cytometry. Reinforcing our findings, we still detected our CD169<sup>+</sup> population in the spleen of *Batf3*<sup>-/-</sup> mice as well as *flt3*<sup>-/-</sup> and *flt3-L*<sup>-/-</sup> mice that selectively lack of specific dendritic cell populations. However, regarding their functions, CD169<sup>+</sup> cells are close to the dendritic cell-lineage, since they are capable of efficient cross-presentation, a functional hallmark of dendritic cells (Joffre, Segura et al. 2012). Consequently, a morphological analysis as well as gene expression analysis the most recent technics including bulk or single-cell RNA sequencing or single-cell qPCR on a selective set of genes of splenic and lymph node CD169<sup>+</sup> cells (Ginhoux, Schultze et al. 2016), in comparison with other macrophage and dendritic cell populations, will be required to further dissect the lineage of spleen CD169<sup>+</sup> cells identified by our strategy. In this context, our recent study on recent-onset type 1 diabetes patients has allowed us to familiarize with the technical requirements and limitations. Contrasting with the model of CD169<sup>+</sup> macrophages as an antigen transfer platform to the cDC1 subset proposed by the group of J. den Haan (Backer, Schwandt et al.

2010), we have visualized directly by live multiphoton microscopy stable contacts between antigen specific CD8<sup>+</sup> T lymphocytes and CD169<sup>+</sup> macrophages but not CD11c<sup>+</sup> dendritic cells when the antigen is routed to this population. Although promising, these findings should be reinforced by testing whether these contacts result in productive signals, for instance by observing an intracellular accumulation of calcium in the cognate T cells that interact with macrophages (Moreau, Lemaitre et al. 2012, Moreau, Lemaitre et al. 2015). In addition, a broader picture of the entire spleen rather than a small number of marginal sinuses analyzed would be appreciated to formally exclude the presence of contacts over time between dendritic cells and cognate CD8<sup>+</sup> T cells when the antigen is targeted to the metallophilic macrophages. In this context, the use of the light sheet fluorescence microscopy technology would give precious clues about the global picture of the actors responsible for CD8<sup>+</sup> T lymphocyte priming in our model (Abe, Ozga et al. 2016). Also, the study of the type of contacts *in vitro* would help in predicting if they promote either productive or unproductive signals (Moreau, Lemaitre et al. 2012, Moreau, Lemaitre et al. 2015).

## **Chapter 2. What renders the vacuolar cross-presentation pathway uniquely efficient in the metallophilic marginal zone macrophages?**

We have demonstrated that splenic CD169<sup>+</sup> macrophages are endowed with a highly efficient antigen cross-presentation capacity *in vitro* and *in vivo*. Importantly, this key finding extends to all the antigen forms tested including endocytosed and phagocytosed OVA. This intriguing result is supported by a recent study published by the group of M. Tanaka, which demonstrated a direct cross-presentation by the lymph node counterparts of a dead-cell associated antigen (Asano, Nabeyama et al. 2011), yet the precise lineage of the identified population is controversial. Mechanistic exploration has allowed to identify that contrary to cDC1s (Joffre, Segura et al. 2012), CD169<sup>+</sup> macrophages do not employ the cytosolic pathway to generate MHC-I ligands, as assessed by the lack of antigen transfer to the cytosol, the total insensitivity of cross-presentation to proteasome inhibitors, to IRAP deficiency and to ERAP and TAP deficiencies, when surface MHC-I levels are restored to their physiological levels by a low temperature pre-incubation. By contrast, while the aforementioned treatments did not trigger significant changes in cDC1s, inhibition of endolysosomal proteases or of cathepsin S resulted in the dose-dependent inhibition of cross-presentation, suggesting that CD169<sup>+</sup> macrophages generate MHC-I ligands by the selective use of the vacuolar pathway (Kurotaki, Tamura et al. 2007). While the vacuolar pathway has been reported to contribute to the generation of MHC-I antigenic peptides for several antigens including the model antigen

OVA (Shen, Sigal et al. 2004, Kurotaki, Tamura et al. 2007), it is thought to be less efficient than the cytosolic pathway, as assessed by its preferential use by the cross-presenting cDC1 subset and other studies. Importantly, an efficient vacuolar antigen cross-presentation pathway has been reported in the context of memory CD8<sup>+</sup> T cell priming by human plasmacytoid dendritic cells (Di Pucchio, Chatterjee et al. 2008) or in cell types capable of both cytosolic and vacuolar pathways (Mant, Chinnery et al. 2012), however its role has been considered as marginal. If MHC class I ligands can indeed be generated with similar efficiency and independently by two different intracellular pathways and by different phagocytes, it remains unclear whether this creates redundancy or alternatively whether each pathway associated with each type of phagocytes fulfills specific and distinct biological functions. One answer might be that the peptide repertoires generated by the use of these two different pathways are not identical but partly overlapping. This assessment is supported by a recent report from the group of T. Brocker that showed that in the absence of dendritic cells, CD169<sup>+</sup> spleen macrophages can generate efficient CTL responses by direct endogenous antigen presentation and therefore complement the repertoire of peptides presented by cross-presenting cDCs, which is biased to MHC-I ligands with strong affinity (Bernhard, Ried et al. 2015). However, further examination is required to test the relevance of this study in the context of antigens cross-presented by the CD169<sup>+</sup> macrophages. An important insight might be provided by determining and comparing the peptide repertoire presented by CD169<sup>+</sup> macrophages and cDC1 cells, yet such analysis would be difficult even exploiting the high sensitivity of the most recent mass spectrometry analytic tools, due to the low number of CD169<sup>+</sup> cells purified per spleen. Another critical factor in the generation of antigenic peptides are the source and the trafficking of MHC-I within the antigen presenting cell. In the context of CD169<sup>+</sup> macrophages, we have found that the source of MHC-I molecules for cross-presentation is the recycling pool of MHC-I molecules and not the *de novo* synthesized pool of MHC-I molecules. This finding is in agreement with the available literature on the cells capable of antigen cross-presentation by the vacuolar pathway (Adiko, Babdor et al. 2015). Additional and more surprising results are the high basal level of surface MHC-I molecules in CD169<sup>+</sup> macrophages together with the rapid and complete restoration of MHC-I at the cell surface of not only TAP but also ERAP deficient CD169<sup>+</sup> macrophages at low temperature. Collectively these results suggest that MHC-I molecules are more stable in CD169<sup>+</sup> macrophages than in dendritic cells. Although this may again reflect differences in the peptide repertoire, it is likely that MHC-I trafficking is unique in splenic CD169<sup>+</sup> macrophages. Among the candidate explanations, it is possible that MHC-I recycling in

CD169<sup>+</sup> macrophages involves a fast-recycling endosome compartment as described previously for plasmacytoid dendritic cells (Di Pucchio, Chatterjee et al. 2008); the quality control machinery might additionally be more permissive in CD169<sup>+</sup> macrophages than in dendritic cells. Further examination to address these hypotheses is consequently required and should include the dynamic visualization of the endosomal and lysosomal distribution of MHC-I molecules after endocytosis. Although in theory possible by confocal imaging, such investigations would benefit from the recent new imaging technologies including the imaging flow cytometry that allow for multiplex analysis of such biological processes, including a comparison between various cell types in the same time. We have used this technique to monitor the phagosome maturation over time in bone marrow-derived dendritic cells transduced with various shRNA to silence the expression of proteins, so that the technical limitations and requirements are well known to me. Analyzing the contribution of the tyrosine residue motif in the cytoplasmic MHC-I tail in its trafficking will be of particular interest since it is thought to regulate MHC-I endocytosis and routing to a recycling endosome compartment, at least in some dendritic cell populations (Lizee, Basha et al. 2003).

Both antigen uptake and presentation are also positively influenced by external signals such as inflammatory signals. In addition to the higher expression of co-stimulatory molecules, accumulating evidence from the groups of J.M. Blander, R. Medzhitov and S. Amigorena suggest that exposure to TLR ligands modulate antigen presentation by various mechanisms: by promoting the phagocytosis of pathogens (Blander and Medzhitov 2004), by delivering MHC-I molecules from a recycling endosome compartment to maturing phagosomes containing TLR-ligands (Nair-Gupta, Baccarini et al. 2014) or by delaying the fusion between the maturing phagosomes and lysosomes (Alloatti, Kotsias et al. 2015). Whether such mechanisms are involved in antigen cross-presentation by CD169<sup>+</sup> macrophages upon inflammatory conditions should be tested, as antigen cross-presentation is expected to be more active in an inflammatory environment.

### **Chapter 3. What is the role of the Rab14<sup>+</sup> regulatory endosomes in CD169<sup>+</sup> macrophages?**

In one of the projects presented above, we have identified a crucial role for the small GTPase Rab14 in the regulation of a specific regulatory endosome compartment that regulates antigen presentation by delaying phagosome maturation in bone marrow-derived dendritic cells, thereby preventing the premature degradation of MHC-I ligands. To do this, the regulatory endosome compartment fuses with the early phagosome or endosome, in a mechanism

dependent on the kinesin protein KIF16b and on dynein proteins. Two previous studies from our group have already documented the contribution of this endosome compartment in the regulation of the cross-presentation of antigen that are routed to the cytosolic pathway in mouse splenic cDC1s, and the role of the aminopeptidase IRAP that is located specifically in this compartment (Saveanu, Carroll et al. 2009, Weimershaus, Maschalidi et al. 2012). Interestingly, inflammatory stimuli activate kinesin-mediated tubulin transport of this compartment. This original study sheds light on a novel mechanism involving early endosomes as regulators of antigen cross-presentation, complementary to the recent reports by the groups of J.M. Blander and S. Amigorena. However, although present in splenic CD169+ macrophages, this compartment, at least under homeostatic conditions, is not required for optimizing antigen cross-presentation as assessed by the lack of inhibition in IRAP<sup>-/-</sup> and by the use of specific inhibitors or IRAP during antigen presentation assays (data not shown). This is in agreement with the two published reports from our group, since IRAP and/or the Rab14+ storage endosomes have been shown to play a role in the cytosolic pathway and not the vacuolar pathway (Saveanu, Carroll et al. 2009, Weimershaus, Maschalidi et al. 2012). Whether the Rab14+ endosomes exert a role in adaptive immune responses triggered by CD169+ macrophages upon inflammation remains to be determined. Despite the lack of role for the Rab14+ storage endosomes in regulating phagosomal/endosomal maturation, the endolysosomal system of splenic CD169+ macrophages is probably a low-degradative compartment. Indirect evidence supports this hypothesis: intravenous injection of soluble OVA resulted in its long-term (intact) detection in CD169+ macrophages but not dendritic cell subsets, as observed in our study and by another group (Veninga, Borg et al. 2015); the lymph node counterpart of CD169+ macrophages has been shown to have low protease content (Phan, Green et al. 2009). Taken together, both the use of the vacuolar pathway and the absence of regulation of phagosome maturation by the Rab14+ storage endosomes suggest that the cell biology of the endocytic pathway contributing to antigen cross-presentation is different in CD169+ macrophages and dendritic cells. To gain additional insight, the characterization of the endosome compartment responsible for antigen degradation and peptide loading onto MHC-I will be an important objective.

The regulatory endosomes may also play an alternative role, such as the regulation of innate immunity. Indeed, in the context of another study conducted by a current member of our team together with a former member, we have identified a role for the regulatory endosomes in regulating TLR-9 trafficking and signaling through the endocytic pathway, in a formin-dependent manner. Absence of regulatory endosomes induced by the lack of IRAP expression



in dendritic cells resulted in a hyper-inflammatory phenotype both *in vitro* and *in vivo*. Interestingly, unpublished personal results suggest a similar role of the Rab14 storage endosomes in the CD169<sup>+</sup> macrophages, since upon exposure to a synthetic TLR-9 ligand IRAP<sup>-/-</sup> CD169<sup>+</sup> macrophages significantly produced higher levels of inflammatory cytokines and type I IFNs. This observation is of particular interest since in addition to the role of inflammatory molecules such as IL-12 to promote antigen presentation or to attract inflammatory cells (Valenzuela, Schmidt et al. 2002), type-I IFN signaling has been recently shown to be required to trap some pathogens in the metallophilic marginal zone macrophages by the group of K.S. Lang (Honke, Shaabani et al. 2012, Honke, Shaabani et al. 2013, Shaabani, Khairnar et al. 2016). Therefore, the Rab14<sup>+</sup> storage endosomes could help splenic CD169<sup>+</sup> macrophages to act as a reservoir for pathogens that depend on TLR-9 signaling.

#### **Chapter 4. What is the functional relevance of the cross-presentation by CD169<sup>+</sup> macrophages *in vivo*?**

Assessing the impact of cross-presentation by CD169<sup>+</sup> metallophilic macrophages and its contribution during adaptive immune responses is a crucial question. By using an antigen targeting system previously elaborated in the laboratory, we started to address these questions by targeting a model antigen to either the cDC1 subset (DEC-205<sup>+</sup>) or to metallophilic marginal zone macrophages (CD169<sup>+</sup>). Consistent with the published literature on tumor antigens (Asano, Nabeyama et al. 2011), we observed an efficient cross-priming of CD8<sup>+</sup> T cells by CD169<sup>+</sup> macrophages *in vivo*, both in quantity and in quality. The most striking difference with the cross-priming of CD8<sup>+</sup> T cells by cDC1s was the higher proportion of MPECs, resulting in higher memory responses during antigen recall. As discussed before, further analysis will be required to completely rule out any antigen transfer to dendritic cell populations in our system, even if stable contacts between naïve T cells and macrophages but not dendritic cells were observed by live imaging after antigen targeting to CD169. Depletion of dendritic cells by conditional ablation or/and the use of animals deficient for transcription factors might be a simple way to check the persistence of a cross-priming by CD169<sup>+</sup> splenic macrophages; however, these models have several limitations that complicate the interpretation of such experiments, including the modification in spleen architecture, the presence of compensatory mechanisms or of undesired side effects that might affect T cell functions. An alternative strategy could be the generation of transgenic mice that do not express any MHC-I molecules selectively in cDC1 and/or cDC2 dendritic cell subsets but normal levels in CD169<sup>+</sup> macrophages.

For the same reasons, it would be difficult to test the contribution of cross-priming by CD169<sup>+</sup> macrophages *in vivo*, in infectious or tumor settings, by using mice depleted for dendritic cell populations since this may result in variations in pathogen load and/or distribution. Again generating mice with dendritic cells lacking MHC-I expression could solve the problem. An indirect approach might also be proposed, using a vaccine-like strategy, for instance by transferring primed T cells after antigen targeting to CD169 or DEC205 in wild-type animal or mice depleted from conventional dendritic cell subsets into naïve hosts that will be infected or that will receive a tumor injection.

## BIBLIOGRAPHY

- Abe, J., A. J. Ozga, J. Swoger, J. Sharpe, J. Ripoll and J. V. Stein (2016). "Light sheet fluorescence microscopy for in situ cell interaction analysis in mouse lymph nodes." *J Immunol Methods* **431**: 1-10.
- Abele, R. and R. Tampe (2011). "The TAP translocation machinery in adaptive immunity and viral escape mechanisms." *Essays Biochem* **50**(1): 249-264.
- Accapezzato, D., V. Visco, V. Francavilla, C. Molette, T. Donato, M. Paroli, M. U. Mondelli, M. Doria, M. R. Torrasi and V. Barnaba (2005). "Chloroquine enhances human CD8+ T cell responses against soluble antigens in vivo." *J Exp Med* **202**(6): 817-828.
- Ackerman, A. L., A. Giodini and P. Cresswell (2006). "A role for the endoplasmic reticulum protein retrotranslocation machinery during crosspresentation by dendritic cells." *Immunity* **25**(4): 607-617.
- Adiko, A. C., J. Babdor, E. Gutierrez-Martinez, P. Guermonprez and L. Saveanu (2015). "Intracellular Transport Routes for MHC I and Their Relevance for Antigen Cross-Presentation." *Front Immunol* **6**: 335.
- Aghaeepour, N., G. Finak, C. A. P. C. Flow, D. Consortium, H. Hoos, T. R. Mosmann, R. Brinkman, R. Gottardo and R. H. Scheuermann (2013). "Critical assessment of automated flow cytometry data analysis techniques." *Nat Methods* **10**(3): 228-238.
- Ahmed, R. and D. Gray (1996). "Immunological memory and protective immunity: understanding their relation." *Science* **272**(5258): 54-60.
- Alba, R., A. C. Bradshaw, L. Coughlan, L. Denby, R. A. McDonald, S. N. Waddington, S. M. Buckley, J. A. Greig, A. L. Parker, A. M. Miller, H. Wang, A. Lieber, N. van Rooijen, J. H. McVey, S. A. Nicklin and A. H. Baker (2010). "Biodistribution and retargeting of FX-binding ablated adenovirus serotype 5 vectors." *Blood* **116**(15): 2656-2664.
- Aldhamen, Y. A., Y. Pepelyayeva, D. P. Rastall, S. S. Seregin, E. Zervoudi, D. Koumantou, C. F. Aylsworth, D. Quiroga, S. Godbehere, D. Georgiadis, E. Stratikos and A. Amalfitano (2015). "Autoimmune disease-associated variants of extracellular endoplasmic reticulum aminopeptidase 1 induce altered innate immune responses by human immune cells." *J Innate Immun* **7**(3): 275-289.
- Allen, C. D., T. Okada, H. L. Tang and J. G. Cyster (2007). "Imaging of germinal center selection events during affinity maturation." *Science* **315**(5811): 528-531.
- Alloatti, A., F. Kotsias, A. M. Pauwels, J. M. Carpiere, M. Jouve, E. Timmerman, L. Pace, P. Vargas, M. Maurin, U. Gehrman, L. Joannas, O. I. Vivar, A. M. Lennon-Dumenil, A. Savina, K. Gevaert, R. Beyaert, E. Hoffmann and S. Amigorena (2015). "Toll-like Receptor 4 Engagement on Dendritic Cells Restrains Phago-Lysosome Fusion and Promotes Cross-Presentation of Antigens." *Immunity* **43**(6): 1087-1100.
- Amsen, D., C. G. Spilianakis and R. A. Flavell (2009). "How are T(H)1 and T(H)2 effector cells made?" *Curr Opin Immunol* **21**(2): 153-160.
- Anbazzhagan, K., I. Duroux-Richard, C. Jorgensen and F. Apparailly (2014). "Transcriptomic network support distinct roles of classical and non-classical monocytes in human." *Int Rev Immunol* **33**(6): 470-489.
- Angelo, M., S. C. Bendall, R. Finck, M. B. Hale, C. Hitzman, A. D. Borowsky, R. M. Levenson, J. B. Lowe, S. D. Liu, S. Zhao, Y. Natkunam and G. P. Nolan (2014). "Multiplexed ion beam imaging of human breast tumors." *Nat Med* **20**(4): 436-442.
- Angelosanto, J. M., S. D. Blackburn, A. Crawford and E. J. Wherry (2012). "Progressive loss of memory T cell potential and commitment to exhaustion during chronic viral infection." *J Virol* **86**(15): 8161-8170.

Arnon, T. I., R. M. Horton, I. L. Grigorova and J. G. Cyster (2013). "Visualization of splenic marginal zone B-cell shuttling and follicular B-cell egress." *Nature* **493**(7434): 684-688.

Arora, P., A. Baena, K. O. Yu, N. K. Saini, S. S. Kharkwal, M. F. Goldberg, S. Kunnath-Velayudhan, L. J. Carreno, M. M. Venkataswamy, J. Kim, E. Lazar-Molnar, G. Lauvau, Y. T. Chang, Z. Liu, R. Bittman, A. Al-Shamkhani, L. R. Cox, P. J. Jervis, N. Veerapen, G. S. Besra and S. A. Porcelli (2014). "A single subset of dendritic cells controls the cytokine bias of natural killer T cell responses to diverse glycolipid antigens." *Immunity* **40**(1): 105-116.

Arredouani, M., Z. Yang, Y. Ning, G. Qin, R. Soininen, K. Tryggvason and L. Kobzik (2004). "The scavenger receptor MARCO is required for lung defense against pneumococcal pneumonia and inhaled particles." *J Exp Med* **200**(2): 267-272.

Arsenio, J., B. Kakaradov, P. J. Metz, S. H. Kim, G. W. Yeo and J. T. Chang (2014). "Early specification of CD8+ T lymphocyte fates during adaptive immunity revealed by single-cell gene-expression analyses." *Nat Immunol* **15**(4): 365-372.

Asano, K., A. Nabeyama, Y. Miyake, C. H. Qiu, A. Kurita, M. Tomura, O. Kanagawa, S. Fujii and M. Tanaka (2011). "CD169-positive macrophages dominate antitumor immunity by crosspresenting dead cell-associated antigens." *Immunity* **34**(1): 85-95.

Asano, K., N. Takahashi, M. Ushiki, M. Monya, F. Aihara, E. Kuboki, S. Moriyama, M. Iida, H. Kitamura, C. H. Qiu, T. Watanabe and M. Tanaka (2015). "Intestinal CD169(+) macrophages initiate mucosal inflammation by secreting CCL8 that recruits inflammatory monocytes." *Nat Commun* **6**: 7802.

Asperti-Boursin, F., E. Real, G. Bismuth, A. Trautmann and E. Donnadieu (2007). "CCR7 ligands control basal T cell motility within lymph node slices in a phosphoinositide 3-kinase-independent manner." *J Exp Med* **204**(5): 1167-1179.

Aspord, C., C. Leloup, S. Reche and J. Plumaz (2014). "pDCs efficiently process synthetic long peptides to induce functional virus- and tumour-specific T-cell responses." *Eur J Immunol* **44**(10): 2880-2892.

Ato, M., H. Nakano, T. Kakiuchi and P. M. Kaye (2004). "Localization of marginal zone macrophages is regulated by C-C chemokine ligands 21/19." *J Immunol* **173**(8): 4815-4820.

Auffray, C., D. Fogg, M. Garfa, G. Elain, O. Join-Lambert, S. Kayal, S. Sarnacki, A. Cumano, G. Lauvau and F. Geissmann (2007). "Monitoring of blood vessels and tissues by a population of monocytes with patrolling behavior." *Science* **317**(5838): 666-670.

Backer, R., T. Schwandt, M. Greuter, M. Oosting, F. Jungerkes, T. Tuting, L. Boon, T. O'Toole, G. Kraal, A. Limmer and J. M. den Haan (2010). "Effective collaboration between marginal metallophilic macrophages and CD8+ dendritic cells in the generation of cytotoxic T cells." *Proc Natl Acad Sci U S A* **107**(1): 216-221.

Backer, R., F. van Leeuwen, G. Kraal and J. M. den Haan (2008). "CD8- dendritic cells preferentially cross-present *Saccharomyces cerevisiae* antigens." *Eur J Immunol* **38**(2): 370-380.

Banchereau, R., S. Hong, B. Cantarel, N. Baldwin, J. Baisch, M. Edens, A. M. Cepika, P. Acs, J. Turner, E. Anguiano, P. Vinod, S. Kahn, G. Obermoser, D. Blankenship, E. Wakeland, L. Nassi, A. Gotte, M. Punaro, Y. J. Liu, J. Banchereau, J. Rossello-Urgell, T. Wright and V. Pascual (2016). "Personalized Immunomonitoring Uncovers Molecular Networks that Stratify Lupus Patients." *Cell* **165**(3): 551-565.

Banerjee, A., S. M. Gordon, A. M. Intlekofer, M. A. Paley, E. C. Mooney, T. Lindsten, E. J. Wherry and S. L. Reiner (2010). "Cutting edge: The transcription factor eomesodermin enables CD8+ T cells to compete for the memory cell niche." *J Immunol* **185**(9): 4988-4992.

Barral, P., P. Polzella, A. Bruckbauer, N. van Rooijen, G. S. Besra, V. Cerundolo and F. D. Batista (2010). "CD169(+) macrophages present lipid antigens to mediate early activation of iNKT cells in lymph nodes." *Nat Immunol* **11**(4): 303-312.

Basha, G., K. Omilusik, A. Chavez-Steenbock, A. T. Reinicke, N. Lack, K. B. Choi and W. A. Jefferies (2012). "A CD74-dependent MHC class I endolysosomal cross-presentation pathway." Nat Immunol **13**(3): 237-245.

Becher, B., A. Schlitzer, J. Chen, F. Mair, H. R. Sumatoh, K. W. Teng, D. Low, C. Ruedl, P. Riccardi-Castagnoli, M. Poidinger, M. Greter, F. Ginhoux and E. W. Newell (2014). "High-dimensional analysis of the murine myeloid cell system." Nat Immunol **15**(12): 1181-1189.

Beck, H., G. Schwarz, C. J. Schroter, M. Deeg, D. Baier, S. Stevanovic, E. Weber, C. Driessen and H. Kalbacher (2001). "Cathepsin S and an asparagine-specific endoprotease dominate the proteolytic processing of human myelin basic protein in vitro." Eur J Immunol **31**(12): 3726-3736.

Bellone, M., G. Iezzi, P. Rovere, G. Galati, A. Ronchetti, M. P. Protti, J. Davoust, C. Rugarli and A. A. Manfredi (1997). "Processing of engulfed apoptotic bodies yields T cell epitopes." J Immunol **159**(11): 5391-5399.

Bendall, S. C., K. L. Davis, A. D. Amir el, M. D. Tadmor, E. F. Simonds, T. J. Chen, D. K. Shenfeld, G. P. Nolan and D. Pe'er (2014). "Single-cell trajectory detection uncovers progression and regulatory coordination in human B cell development." Cell **157**(3): 714-725.

Benvenuti, F. (2016). "The Dendritic Cell Synapse: A Life Dedicated to T Cell Activation." Front Immunol **7**: 70.

Bergman, C. M., C. B. Marta, M. Maric, S. E. Pfeiffer, P. Cresswell and N. H. Ruddle (2012). "A switch in pathogenic mechanism in myelin oligodendrocyte glycoprotein-induced experimental autoimmune encephalomyelitis in IFN-gamma-inducible lysosomal thiol reductase-free mice." J Immunol **188**(12): 6001-6009.

Bernhard, C. A., C. Ried, S. Kochanek and T. Brocker (2015). "CD169+ macrophages are sufficient for priming of CTLs with specificities left out by cross-priming dendritic cells." Proc Natl Acad Sci U S A **112**(17): 5461-5466.

Bertholet, S., R. Goldszmid, A. Morrot, A. Debrabant, F. Afrin, C. Collazo-Custodio, M. Houde, M. Desjardins, A. Sher and D. Sacks (2006). "Leishmania antigens are presented to CD8+ T cells by a transporter associated with antigen processing-independent pathway in vitro and in vivo." J Immunol **177**(6): 3525-3533.

Blackburn, S. D., A. Crawford, H. Shin, A. Polley, G. J. Freeman and E. J. Wherry (2010). "Tissue-specific differences in PD-1 and PD-L1 expression during chronic viral infection: implications for CD8 T-cell exhaustion." J Virol **84**(4): 2078-2089.

Blackburn, S. D., H. Shin, W. N. Haining, T. Zou, C. J. Workman, A. Polley, M. R. Betts, G. J. Freeman, D. A. Vignali and E. J. Wherry (2009). "Coregulation of CD8+ T cell exhaustion by multiple inhibitory receptors during chronic viral infection." Nat Immunol **10**(1): 29-37.

Blanchard, N., F. Gonzalez, M. Schaeffer, N. T. Joncker, T. Cheng, A. J. Shastri, E. A. Robey and N. Shastri (2008). "Immunodominant, protective response to the parasite *Toxoplasma gondii* requires antigen processing in the endoplasmic reticulum." Nat Immunol **9**(8): 937-944.

Blanchard, N., T. Kanaseki, H. Escobar, F. Delebecque, N. A. Nagarajan, E. Reyes-Vargas, D. K. Crockett, D. H. Raulet, J. C. Delgado and N. Shastri (2010). "Endoplasmic reticulum aminopeptidase associated with antigen processing defines the composition and structure of MHC class I peptide repertoire in normal and virus-infected cells." J Immunol **184**(6): 3033-3042.

Blander, J. M. and R. Medzhitov (2004). "Regulation of phagosome maturation by signals from toll-like receptors." Science **304**(5673): 1014-1018.

Blasi, T., H. Hennig, H. D. Summers, F. J. Theis, J. Cerveira, J. O. Patterson, D. Davies, A. Filby, A. E. Carpenter and P. Rees (2016). "Label-free cell cycle analysis for high-throughput imaging flow cytometry." Nat Commun **7**: 10256.

- Bonifaz, L., D. Bonnyay, K. Mahnke, M. Rivera, M. C. Nussenzweig and R. M. Steinman (2002). "Efficient targeting of protein antigen to the dendritic cell receptor DEC-205 in the steady state leads to antigen presentation on major histocompatibility complex class I products and peripheral CD8+ T cell tolerance." J Exp Med **196**(12): 1627-1638.
- Bonifaz, L. C., D. P. Bonnyay, A. Charalambous, D. I. Darguste, S. Fujii, H. Soares, M. K. Brimnes, B. Moltedo, T. M. Moran and R. M. Steinman (2004). "In vivo targeting of antigens to maturing dendritic cells via the DEC-205 receptor improves T cell vaccination." J Exp Med **199**(6): 815-824.
- Borges da Silva, H., R. Fonseca, R. M. Pereira, A. Cassado Ados, J. M. Alvarez and M. R. D'Imperio Lima (2015). "Splenic Macrophage Subsets and Their Function during Blood-Borne Infections." Front Immunol **6**: 480.
- Bousso, P. (2008). "T-cell activation by dendritic cells in the lymph node: lessons from the movies." Nat Rev Immunol **8**(9): 675-684.
- Bousso, P. and E. Robey (2003). "Dynamics of CD8+ T cell priming by dendritic cells in intact lymph nodes." Nat Immunol **4**(6): 579-585.
- Bozzacco, L., C. Trumpfheller, F. P. Siegal, S. Mehandru, M. Markowitz, M. Carrington, M. C. Nussenzweig, A. G. Piperno and R. M. Steinman (2007). "DEC-205 receptor on dendritic cells mediates presentation of HIV gag protein to CD8+ T cells in a spectrum of human MHC I haplotypes." Proc Natl Acad Sci U S A **104**(4): 1289-1294.
- Brede, C., M. Friedrich, A. L. Jordan-Garrote, S. S. Riedel, C. A. Bauerlein, K. G. Heinze, T. Bopp, S. Schulz, A. Mottok, C. Kiesel, K. Mattenheimer, M. Ritz, V. von Krosigk, A. Rosenwald, H. Einsele, R. S. Negrin, G. S. Harms and A. Beilhack (2012). "Mapping immune processes in intact tissues at cellular resolution." J Clin Invest **122**(12): 4439-4446.
- Breton, G., J. Lee, Y. J. Zhou, J. J. Schreiber, T. Keler, S. Puhr, N. Anandasabapathy, S. Schlesinger, M. Caskey, K. Liu and M. C. Nussenzweig (2015). "Circulating precursors of human CD1c+ and CD141+ dendritic cells." J Exp Med **212**(3): 401-413.
- Brooks, D. G., D. B. McGavern and M. B. Oldstone (2006). "Reprogramming of antiviral T cells prevents inactivation and restores T cell activity during persistent viral infection." J Clin Invest **116**(6): 1675-1685.
- Brooks, D. G., M. J. Trifilo, K. H. Edelmann, L. Teyton, D. B. McGavern and M. B. Oldstone (2006). "Interleukin-10 determines viral clearance or persistence in vivo." Nat Med **12**(11): 1301-1309.
- Bucks, C. M., J. A. Norton, A. C. Boesteanu, Y. M. Mueller and P. D. Katsikis (2009). "Chronic antigen stimulation alone is sufficient to drive CD8+ T cell exhaustion." J Immunol **182**(11): 6697-6708.
- Burgdorf, S., V. Lukacs-Kornek and C. Kurts (2006). "The mannose receptor mediates uptake of soluble but not of cell-associated antigen for cross-presentation." J Immunol **176**(11): 6770-6776.
- Burgdorf, S., C. Scholz, A. Kautz, R. Tampe and C. Kurts (2008). "Spatial and mechanistic separation of cross-presentation and endogenous antigen presentation." Nat Immunol **9**(5): 558-566.
- Burgdorf, S., V. Schuette, V. Semmling, K. Hochheiser, V. Lukacs-Kornek, P. A. Knolle and C. Kurts (2010). "Steady-state cross-presentation of OVA is mannose receptor-dependent but inhibitable by collagen fragments." Proc Natl Acad Sci U S A **107**(13): E48-49; author reply E50-41.
- Burster, T., A. Beck, E. Tolosa, V. Marin-Esteban, O. Rotzschke, K. Falk, A. Lautwein, M. Reich, J. Brandenburg, G. Schwarz, H. Wiendl, A. Melms, R. Lehmann, S. Stevanovic, H. Kalbacher and C. Driessen (2004). "Cathepsin G, and not the asparagine-specific endoprotease, controls the processing of myelin basic protein in lysosomes from human B lymphocytes." J Immunol **172**(9): 5495-5503.
- Campi, G., R. Varma and M. L. Dustin (2005). "Actin and agonist MHC-peptide complex-dependent T cell receptor microclusters as scaffolds for signaling." J Exp Med **202**(8): 1031-1036.

- Cannarile, M. A., N. A. Lind, R. Rivera, A. D. Sheridan, K. A. Camfield, B. B. Wu, K. P. Cheung, Z. Ding and A. W. Goldrath (2006). "Transcriptional regulator Id2 mediates CD8+ T cell immunity." Nat Immunol **7**(12): 1317-1325.
- Cannons, J. L., H. Qi, K. T. Lu, M. Dutta, J. Gomez-Rodriguez, J. Cheng, E. K. Wakeland, R. N. Germain and P. L. Schwartzberg (2010). "Optimal germinal center responses require a multistage T cell:B cell adhesion process involving integrins, SLAM-associated protein, and CD84." Immunity **32**(2): 253-265.
- Canton, J., D. Schlam, C. Breuer, M. Gutschow, M. Glogauer and S. Grinstein (2016). "Calcium-sensing receptors signal constitutive macropinocytosis and facilitate the uptake of NOD2 ligands in macrophages." Nat Commun **7**: 11284.
- Carlin, L. M., E. G. Stamatiades, C. Auffray, R. N. Hanna, L. Glover, G. Vizcay-Barrena, C. C. Hedrick, H. T. Cook, S. Diebold and F. Geissmann (2013). "Nr4a1-dependent Ly6C(low) monocytes monitor endothelial cells and orchestrate their disposal." Cell **153**(2): 362-375.
- Caron, E. and A. Hall (1998). "Identification of two distinct mechanisms of phagocytosis controlled by different Rho GTPases." Science **282**(5394): 1717-1721.
- Castellino, F., A. Y. Huang, G. Altan-Bonnet, S. Stoll, C. Scheinecker and R. N. Germain (2006). "Chemokines enhance immunity by guiding naive CD8+ T cells to sites of CD4+ T cell-dendritic cell interaction." Nature **440**(7086): 890-895.
- Caza, T. and S. Landas (2015). "Functional and Phenotypic Plasticity of CD4(+) T Cell Subsets." Biomed Res Int **2015**: 521957.
- Cebrian, I., G. Visentin, N. Blanchard, M. Jouve, A. Bobard, C. Moita, J. Enninga, L. F. Moita, S. Amigorena and A. Savina (2011). "Sec22b regulates phagosomal maturation and antigen crosspresentation by dendritic cells." Cell **147**(6): 1355-1368.
- Cella, M., D. Jarrossay, F. Facchetti, O. Alebardi, H. Nakajima, A. Lanzavecchia and M. Colonna (1999). "Plasmacytoid monocytes migrate to inflamed lymph nodes and produce large amounts of type I interferon." Nat Med **5**(8): 919-923.
- Celli, S., M. L. Albert and P. Bousso (2011). "Visualizing the innate and adaptive immune responses underlying allograft rejection by two-photon microscopy." Nat Med **17**(6): 744-749.
- Celli, S., F. Lemaitre and P. Bousso (2007). "Real-time manipulation of T cell-dendritic cell interactions in vivo reveals the importance of prolonged contacts for CD4+ T cell activation." Immunity **27**(4): 625-634.
- Cerveira, J., J. Begum, R. Di Marco Barros, A. G. van der Veen and A. Filby (2015). "An imaging flow cytometry-based approach to measuring the spatiotemporal calcium mobilisation in activated T cells." J Immunol Methods **423**: 120-130.
- Chang, J. T., M. L. Ciocca, I. Kinjyo, V. R. Palanivel, C. E. McClurkin, C. S. Dejong, E. C. Mooney, J. S. Kim, N. C. Steinle, J. Oliaro, C. C. Yin, B. I. Florea, H. S. Overkleeft, L. J. Berg, S. M. Russell, G. A. Koretzky, M. S. Jordan and S. L. Reiner (2011). "Asymmetric proteasome segregation as a mechanism for unequal partitioning of the transcription factor T-bet during T lymphocyte division." Immunity **34**(4): 492-504.
- Chang, J. T., V. R. Palanivel, I. Kinjyo, F. Schambach, A. M. Intlekofer, A. Banerjee, S. A. Longworth, K. E. Vinup, P. Mrass, J. Oliaro, N. Killeen, J. S. Orange, S. M. Russell, W. Weninger and S. L. Reiner (2007). "Asymmetric T lymphocyte division in the initiation of adaptive immune responses." Science **315**(5819): 1687-1691.
- Chang, J. T., E. J. Wherry and A. W. Goldrath (2014). "Molecular regulation of effector and memory T cell differentiation." Nat Immunol **15**(12): 1104-1115.

Chang, S. C., F. Momburg, N. Bhutani and A. L. Goldberg (2005). "The ER aminopeptidase, ERAP1, trims precursors to lengths of MHC class I peptides by a "molecular ruler" mechanism." Proc Natl Acad Sci U S A **102**(47): 17107-17112.

Chapman, D. C. and D. B. Williams (2010). "ER quality control in the biogenesis of MHC class I molecules." Semin Cell Dev Biol **21**(5): 512-519.

Chatterjee, B., A. Smed-Sorensen, L. Cohn, C. Chalouni, R. Vandlen, B. C. Lee, J. Widger, T. Keler, L. Delamarre and I. Mellman (2012). "Internalization and endosomal degradation of receptor-bound antigens regulate the efficiency of cross presentation by human dendritic cells." Blood **120**(10): 2011-2020.

Chattopadhyay, P. K. and M. Roederer (2012). "Cytometry: today's technology and tomorrow's horizons." Methods **57**(3): 251-258.

Chefalo, P. J., A. G. Grandea, 3rd, L. Van Kaer and C. V. Harding (2003). "Tapasin<sup>-/-</sup> and TAP1<sup>-/-</sup> macrophages are deficient in vacuolar alternate class I MHC (MHC-I) processing due to decreased MHC-I stability at phagolysosomal pH." J Immunol **170**(12): 5825-5833.

Chen, H., M. C. Lau, M. T. Wong, E. W. Newell, M. Poidinger and J. Chen (2016). "Cytokit: A Bioconductor Package for an Integrated Mass Cytometry Data Analysis Pipeline." PLoS Comput Biol **12**(9): e1005112.

Chen, M. and M. Bouvier (2007). "Analysis of interactions in a tapasin/class I complex provides a mechanism for peptide selection." EMBO J **26**(6): 1681-1690.

Cheong, C., I. Matos, J. H. Choi, D. B. Dandamudi, E. Shrestha, M. P. Longhi, K. L. Jeffrey, R. M. Anthony, C. Kluger, G. Nchinda, H. Koh, A. Rodriguez, J. Idoyaga, M. Pack, K. Velinzon, C. G. Park and R. M. Steinman (2010). "Microbial stimulation fully differentiates monocytes to DC-SIGN/CD209(+) dendritic cells for immune T cell areas." Cell **143**(3): 416-429.

Chester, C. and H. T. Maecker (2015). "Algorithmic Tools for Mining High-Dimensional Cytometry Data." J Immunol **195**(3): 773-779.

Chi, H. (2012). "Regulation and function of mTOR signalling in T cell fate decisions." Nat Rev Immunol **12**(5): 325-338.

Chiu, I., D. M. Davis and J. L. Strominger (1999). "Trafficking of spontaneously endocytosed MHC proteins." Proc Natl Acad Sci U S A **96**(24): 13944-13949.

Choudhuri, K., J. Llodra, E. W. Roth, J. Tsai, S. Gordo, K. W. Wucherpfennig, L. C. Kam, D. L. Stokes and M. L. Dustin (2014). "Polarized release of T-cell-receptor-enriched microvesicles at the immunological synapse." Nature **507**(7490): 118-123.

Chu, C. C., N. Ali, P. Karagiannis, P. Di Meglio, A. Skowera, L. Napolitano, G. Barinaga, K. Gryns, E. Sharif-Paghaleh, S. N. Karagiannis, M. Peakman, G. Lombardi and F. O. Nestle (2012). "Resident CD141 (BDCA3)+ dendritic cells in human skin produce IL-10 and induce regulatory T cells that suppress skin inflammation." J Exp Med **209**(5): 935-945.

Ciechanover, A. (2005). "Proteolysis: from the lysosome to ubiquitin and the proteasome." Nat Rev Mol Cell Biol **6**(1): 79-87.

Cisse, B., M. L. Caton, M. Lehner, T. Maeda, S. Scheu, R. Locksley, D. Holmberg, C. Zweier, N. S. den Hollander, S. G. Kant, W. Holter, A. Rauch, Y. Zhuang and B. Reizis (2008). "Transcription factor E2-2 is an essential and specific regulator of plasmacytoid dendritic cell development." Cell **135**(1): 37-48.

Coelho, F. M., D. Natale, S. F. Soriano, M. Hons, J. Swoger, J. Mayer, R. Danuser, E. Scandella, M. Pieczyk, H. G. Zerwes, T. Junt, A. W. Sailer, B. Ludewig, J. Sharpe, M. T. Figge and J. V. Stein (2013). "Naive B-cell trafficking is



shaped by local chemokine availability and LFA-1-independent stromal interactions." *Blood* **121**(20): 4101-4109.

Cohn, L., B. Chatterjee, F. Esselborn, A. Smed-Sorensen, N. Nakamura, C. Chalouni, B. C. Lee, R. Vandlen, T. Keler, P. Lauer, D. Brockstedt, I. Mellman and L. Delamarre (2013). "Antigen delivery to early endosomes eliminates the superiority of human blood BDCA3+ dendritic cells at cross presentation." *J Exp Med* **210**(5): 1049-1063.

Comrie, W. A., A. Babich and J. K. Burkhardt (2015). "F-actin flow drives affinity maturation and spatial organization of LFA-1 at the immunological synapse." *J Cell Biol* **208**(4): 475-491.

Crites, T. J., K. Padhan, J. Muller, M. Krosggaard, P. R. Gudla, S. J. Lockett and R. Varma (2014). "TCR Microclusters pre-exist and contain molecules necessary for TCR signal transduction." *J Immunol* **193**(1): 56-67.

Crocker, P. R. and S. Gordon (1985). "Isolation and characterization of resident stromal macrophages and hematopoietic cell clusters from mouse bone marrow." *J Exp Med* **162**(3): 993-1014.

Crocker, P. R., S. Mucklow, V. Bouckson, A. McWilliam, A. C. Willis, S. Gordon, G. Milon, S. Kelm and P. Bradfield (1994). "Sialoadhesin, a macrophage sialic acid binding receptor for haemopoietic cells with 17 immunoglobulin-like domains." *EMBO J* **13**(19): 4490-4503.

Crocker, P. R., M. Vinson, S. Kelm and K. Drickamer (1999). "Molecular analysis of sialoside binding to sialoadhesin by NMR and site-directed mutagenesis." *Biochem J* **341 ( Pt 2)**: 355-361.

Croft, N. P., S. A. Smith, Y. C. Wong, C. T. Tan, N. L. Dudek, I. E. Flesch, L. C. Lin, D. C. Tschärke and A. W. Purcell (2013). "Kinetics of antigen expression and epitope presentation during virus infection." *PLoS Pathog* **9**(1): e1003129.

Crotzer, V. L., J. D. Matute, A. A. Arias, H. Zhao, L. A. Quilliam, M. C. Dinauer and J. S. Blum (2012). "Cutting edge: NADPH oxidase modulates MHC class II antigen presentation by B cells." *J Immunol* **189**(8): 3800-3804.

Cui, W., Y. Liu, J. S. Weinstein, J. Craft and S. M. Kaech (2011). "An interleukin-21-interleukin-10-STAT3 pathway is critical for functional maturation of memory CD8+ T cells." *Immunity* **35**(5): 792-805.

Curtsinger, J. M. and M. F. Mescher (2010). "Inflammatory cytokines as a third signal for T cell activation." *Curr Opin Immunol* **22**(3): 333-340.

Day, P. M., F. Esquivel, J. Lukszo, J. R. Bennink and J. W. Yewdell (1995). "Effect of TAP on the generation and intracellular trafficking of peptide-receptive major histocompatibility complex class I molecules." *Immunity* **2**(2): 137-147.

DeKosky, B. J., G. C. Ippolito, R. P. Deschner, J. J. Lavinder, Y. Wine, B. M. Rawlings, N. Varadarajan, C. Giesecke, T. Dorner, S. F. Andrews, P. C. Wilson, S. P. Hunicke-Smith, C. G. Willson, A. D. Ellington and G. Georgiou (2013). "High-throughput sequencing of the paired human immunoglobulin heavy and light chain repertoire." *Nat Biotechnol* **31**(2): 166-169.

Del Val, M., S. Lazaro, M. Ramos and L. C. Anton (2013). "Are membrane proteins favored over cytosolic proteins in TAP-independent processing pathways?" *Mol Immunol* **55**(2): 117-119.

den Haan, J. M. and M. J. Bevan (2002). "Constitutive versus activation-dependent cross-presentation of immune complexes by CD8(+) and CD8(-) dendritic cells in vivo." *J Exp Med* **196**(6): 817-827.

den Haan, J. M. and G. Kraal (2012). "Innate immune functions of macrophage subpopulations in the spleen." *J Innate Immun* **4**(5-6): 437-445.

Denzin, L. K. and P. Cresswell (1995). "HLA-DM induces CLIP dissociation from MHC class II alpha beta dimers and facilitates peptide loading." *Cell* **82**(1): 155-165.

Di Pucchio, T., B. Chatterjee, A. Smed-Sorensen, S. Clayton, A. Palazzo, M. Montes, Y. Xue, I. Mellman, J. Banchereau and J. E. Connolly (2008). "Direct proteasome-independent cross-presentation of viral antigen by plasmacytoid dendritic cells on major histocompatibility complex class I." Nat Immunol **9**(5): 551-557.

Dick, T. P. and P. Cresswell (2002). "Thiol oxidation and reduction in major histocompatibility complex class I-restricted antigen processing and presentation." Methods Enzymol **348**: 49-54.

Dickinson, R. E., H. Griffin, V. Bigley, L. N. Reynard, R. Hussain, M. Haniffa, J. H. Lakey, T. Rahman, X. N. Wang, N. McGovern, S. Pagan, S. Cookson, D. McDonald, I. Chua, J. Wallis, A. Cant, M. Wright, B. Keavney, P. F. Chinnery, J. Loughlin, S. Hambleton, M. Santibanez-Koref and M. Collin (2011). "Exome sequencing identifies GATA-2 mutation as the cause of dendritic cell, monocyte, B and NK lymphoid deficiency." Blood **118**(10): 2656-2658.

DiLillo, D. J., M. Horikawa and T. F. Tedder (2011). "B-lymphocyte effector functions in health and disease." Immunol Res **49**(1-3): 281-292.

Dixon, L. J., M. Barnes, H. Tang, M. T. Pritchard and L. E. Nagy (2013). "Kupffer cells in the liver." Compr Physiol **3**(2): 785-797.

Drickamer, K. and M. E. Taylor (2015). "Recent insights into structures and functions of C-type lectins in the immune system." Curr Opin Struct Biol **34**: 26-34.

Ducreux, J., P. R. Crocker and R. Vanbever (2009). "Analysis of sialoadhesin expression on mouse alveolar macrophages." Immunol Lett **124**(2): 77-80.

Dudziak, D., A. O. Kamphorst, G. F. Heidkamp, V. R. Buchholz, C. Trumpfheller, S. Yamazaki, C. Cheong, K. Liu, H. W. Lee, C. G. Park, R. M. Steinman and M. C. Nussenzweig (2007). "Differential antigen processing by dendritic cell subsets in vivo." Science **315**(5808): 107-111.

Duhan, V., V. Khairnar, S. K. Friedrich, F. Zhou, A. Gassa, N. Honke, N. Shaabani, N. Gailus, L. Botezatu, C. Khandanpour, U. Dittmer, D. Haussinger, M. Recher, C. Hardt, P. A. Lang and K. S. Lang (2016). "Virus-specific antibodies allow viral replication in the marginal zone, thereby promoting CD8(+) T-cell priming and viral control." Sci Rep **6**: 19191.

Durand, M. and E. Segura (2015). "The known unknowns of the human dendritic cell network." Front Immunol **6**: 129.

Dzhagalov, I. L., K. G. Chen, P. Herzmark and E. A. Robey (2013). "Elimination of self-reactive T cells in the thymus: a timeline for negative selection." PLoS Biol **11**(5): e1001566.

Dzionek, A., A. Fuchs, P. Schmidt, S. Cremer, M. Zysk, S. Miltenyi, D. W. Buck and J. Schmitz (2000). "BDCA-2, BDCA-3, and BDCA-4: three markers for distinct subsets of dendritic cells in human peripheral blood." J Immunol **165**(11): 6037-6046.

Eberl, G., J. P. Di Santo and E. Vivier (2015). "The brave new world of innate lymphoid cells." Nat Immunol **16**(1): 1-5.

Eickhoff, S., A. Brewitz, M. Y. Gerner, F. Klauschen, K. Komander, H. Hemmi, N. Garbi, T. Kaisho, R. N. Germain and W. Kastenmuller (2015). "Robust Anti-viral Immunity Requires Multiple Distinct T Cell-Dendritic Cell Interactions." Cell **162**(6): 1322-1337.

Ejrnaes, M., C. M. Filippi, M. M. Martinic, E. M. Ling, L. M. Togher, S. Crotty and M. G. von Herrath (2006). "Resolution of a chronic viral infection after interleukin-10 receptor blockade." J Exp Med **203**(11): 2461-2472.

Ellis, S. D., E. R. Carthy and C. A. Notley (2014). "Advances on regulatory T cells from the 15th International Congress of Immunology." Expert Rev Clin Immunol **10**(2): 203-205.

Elmore, M. R., A. R. Najafi, M. A. Koike, N. N. Dagher, E. E. Spangenberg, R. A. Rice, M. Kitazawa, B. Matusow, H. Nguyen, B. L. West and K. N. Green (2014). "Colony-stimulating factor 1 receptor signaling is necessary for microglia viability, unmasking a microglia progenitor cell in the adult brain." *Neuron* **82**(2): 380-397.

Elomaa, O., M. Kangas, C. Sahlberg, J. Tuukkanen, R. Sormunen, A. Liakka, I. Thesleff, G. Kraal and K. Tryggvason (1995). "Cloning of a novel bacteria-binding receptor structurally related to scavenger receptors and expressed in a subset of macrophages." *Cell* **80**(4): 603-609.

Eloranta, M. L. and G. V. Alm (1999). "Splenic marginal metallophilic macrophages and marginal zone macrophages are the major interferon-alpha/beta producers in mice upon intravenous challenge with herpes simplex virus." *Scand J Immunol* **49**(4): 391-394.

Epelman, S., K. J. Lavine, A. E. Beaudin, D. K. Sojka, J. A. Carrero, B. Calderon, T. Brija, E. L. Gautier, S. Ivanov, A. T. Satpathy, J. D. Schilling, R. Schwendener, I. Sergin, B. Razani, E. C. Forsberg, W. M. Yokoyama, E. R. Unanue, M. Colonna, G. J. Randolph and D. L. Mann (2014). "Embryonic and adult-derived resident cardiac macrophages are maintained through distinct mechanisms at steady state and during inflammation." *Immunity* **40**(1): 91-104.

Evnochidou, I., M. Weimershaus, L. Saveanu and P. van Endert (2014). "ERAP1-ERAP2 dimerization increases peptide-trimming efficiency." *J Immunol* **193**(2): 901-908.

Farber, D. L. (1998). "Differential TCR signaling and the generation of memory T cells." *J Immunol* **160**(2): 535-539.

Farfan-Arribas, D. J., L. J. Stern and K. L. Rock (2012). "Using intein catalysis to probe the origin of major histocompatibility complex class I-presented peptides." *Proc Natl Acad Sci U S A* **109**(42): 16998-17003.

Farrell, H. E., N. Davis-Poynter, K. Bruce, C. Lawler, L. Dolken, M. Mach and P. G. Stevenson (2015). "Lymph Node Macrophages Restrict Murine Cytomegalovirus Dissemination." *J Virol* **89**(14): 7147-7158.

Faure-Andre, G., P. Vargas, M. I. Yuseff, M. Heuze, J. Diaz, D. Lankar, V. Steri, J. Manry, S. Hugues, F. Vascotto, J. Boulanger, G. Raposo, M. R. Bono, M. Roseblatt, M. Piel and A. M. Lennon-Dumenil (2008). "Regulation of dendritic cell migration by CD74, the MHC class II-associated invariant chain." *Science* **322**(5908): 1705-1710.

Feng, Y., N. Zhang, K. M. Jacobs, W. Jiang, L. V. Yang, Z. Li, J. Zhang, J. Q. Lu and X. H. Hu (2014). "Polarization imaging and classification of Jurkat T and Ramos B cells using a flow cytometer." *Cytometry A* **85**(9): 817-826.

Fernandez, R. and H. Maecker (2015). "Cytokine-stimulated Phosphoflow of PBMC Using CyTOF Mass Cytometry." *Bio Protoc* **5**(11).

Fernandez, R. and H. Maecker (2015). "Cytokine-Stimulated Phosphoflow of Whole Blood Using CyTOF Mass Cytometry." *Bio Protoc* **5**(11).

Ferreira, R. C., H. Guo, R. M. Coulson, D. J. Smyth, M. L. Pekalski, O. S. Burren, A. J. Cutler, J. D. Doecke, S. Flint, E. F. McKinney, P. A. Lyons, K. G. Smith, P. Achenbach, A. Beyerlein, D. B. Dunger, D. G. Clayton, L. S. Wicker, J. A. Todd, E. Bonifacio, C. Wallace and A. G. Ziegler (2014). "A type I interferon transcriptional signature precedes autoimmunity in children genetically at risk for type 1 diabetes." *Diabetes* **63**(7): 2538-2550.

Fillatreau, S. (2016). "Regulatory roles of B cells in infectious diseases." *Clin Exp Rheumatol* **34**(4 Suppl 98): 1-5.

Finak, G., A. McDavid, P. Chattopadhyay, M. Dominguez, S. De Rosa, M. Roederer and R. Gottardo (2014). "Mixture models for single-cell assays with applications to vaccine studies." *Biostatistics* **15**(1): 87-101.

Fiorentino, D. F., M. W. Bond and T. R. Mosmann (1989). "Two types of mouse T helper cell. IV. Th2 clones secrete a factor that inhibits cytokine production by Th1 clones." *J Exp Med* **170**(6): 2081-2095.

- Firat, E., L. Saveanu, P. Aichele, P. Staeheli, J. Huai, S. Gaedicke, A. Nil, G. Besin, B. Kanzler, P. van Endert and G. Niedermann (2007). "The role of endoplasmic reticulum-associated aminopeptidase 1 in immunity to infection and in cross-presentation." *J Immunol* **178**(4): 2241-2248.
- Flatz, L., R. Roychoudhuri, M. Honda, A. Filali-Mouhim, J. P. Goulet, N. Kettaf, M. Lin, M. Roederer, E. K. Haddad, R. P. Sekaly and G. J. Nabel (2011). "Single-cell gene-expression profiling reveals qualitatively distinct CD8 T cells elicited by different gene-based vaccines." *Proc Natl Acad Sci U S A* **108**(14): 5724-5729.
- Forbes, L. R. and A. Haczku (2010). "SP-D and regulation of the pulmonary innate immune system in allergic airway changes." *Clin Exp Allergy* **40**(4): 547-562.
- Frederico, B., B. Chao, C. Lawler, J. S. May and P. G. Stevenson (2015). "Subcapsular sinus macrophages limit acute gammaherpesvirus dissemination." *J Gen Virol* **96**(8): 2314-2327.
- Freeman, S. D., S. Kelm, E. K. Barber and P. R. Crocker (1995). "Characterization of CD33 as a new member of the sialoadhesin family of cellular interaction molecules." *Blood* **85**(8): 2005-2012.
- Frei, A. P., F. A. Bava, E. R. Zunder, E. W. Hsieh, S. Y. Chen, G. P. Nolan and P. F. Gherardini (2016). "Highly multiplexed simultaneous detection of RNAs and proteins in single cells." *Nat Methods* **13**(3): 269-275.
- Freitas, A. A. and B. Rocha (2000). "Population biology of lymphocytes: the flight for survival." *Annu Rev Immunol* **18**: 83-111.
- Fruci, D., P. Romania, V. D'Alicandro and F. Locatelli (2014). "Endoplasmic reticulum aminopeptidase 1 function and its pathogenic role in regulating innate and adaptive immunity in cancer and major histocompatibility complex class I-associated autoimmune diseases." *Tissue Antigens* **84**(2): 177-186.
- Fukui, Y., T. Ishimoto, M. Utsuyama, T. Gytoku, T. Koga, K. Nakao, K. Hirokawa, M. Katsuki and T. Sasazuki (1997). "Positive and negative CD4+ thymocyte selection by a single MHC class II/peptide ligand affected by its expression level in the thymus." *Immunity* **6**(4): 401-410.
- Futamara, K., M. Sekino, A. Hata, R. Ikebuchi, Y. Nakanishi, G. Egawa, K. Kabashima, T. Watanabe, M. Furuki and M. Tomura (2015). "Novel full-spectral flow cytometry with multiple spectrally-adjacent fluorescent proteins and fluorochromes and visualization of in vivo cellular movement." *Cytometry A* **87**(9): 830-842.
- Gagnon, E., S. Duclos, C. Rondeau, E. Chevet, P. H. Cameron, O. Steele-Mortimer, J. Paiement, J. J. Bergeron and M. Desjardins (2002). "Endoplasmic reticulum-mediated phagocytosis is a mechanism of entry into macrophages." *Cell* **110**(1): 119-131.
- Galvez, T., J. Gilleron, M. Zerial and G. A. O'Sullivan (2012). "SnapShot: Mammalian Rab proteins in endocytic trafficking." *Cell* **151**(1): 234-234 e232.
- Ganz, T. (2012). "Macrophages and systemic iron homeostasis." *J Innate Immun* **4**(5-6): 446-453.
- Gao, B., R. Adhikari, M. Howarth, K. Nakamura, M. C. Gold, A. B. Hill, R. Knee, M. Michalak and T. Elliott (2002). "Assembly and antigen presenting function of MHC class I molecules in cells lacking the ER chaperone calreticulin." *Immunity* **16**(1): 99-109.
- Garbi, N., G. Hammerling and S. Tanaka (2007). "Interaction of ERp57 and tapasin in the generation of MHC class I-peptide complexes." *Curr Opin Immunol* **19**(1): 99-105.
- Garcia, Z., F. Lemaitre, N. van Rooijen, M. L. Albert, Y. Levy, O. Schwartz and P. Bousso (2012). "Subcapsular sinus macrophages promote NK cell accumulation and activation in response to lymph-borne viral particles." *Blood* **120**(24): 4744-4750.

- Garcia, Z., E. Pradelli, S. Celli, H. Beuneu, A. Simon and P. Bousso (2007). "Competition for antigen determines the stability of T cell-dendritic cell interactions during clonal expansion." Proc Natl Acad Sci U S A **104**(11): 4553-4558.
- Garulli, B., G. Di Mario, E. Sciaraffia, D. Accapezzato, V. Barnaba and M. R. Castrucci (2013). "Enhancement of T cell-mediated immune responses to whole inactivated influenza virus by chloroquine treatment in vivo." Vaccine **31**(13): 1717-1724.
- Gaudilliere, B., G. K. Fragiadakis, R. V. Bruggner, M. Nicolau, R. Finck, M. Tingle, J. Silva, E. A. Ganio, C. G. Yeh, W. J. Maloney, J. I. Huddleston, S. B. Goodman, M. M. Davis, S. C. Bendall, W. J. Fantl, M. S. Angst and G. P. Nolan (2014). "Clinical recovery from surgery correlates with single-cell immune signatures." Sci Transl Med **6**(255): 255ra131.
- Gautier, E. L., A. Chow, R. Spanbroek, G. Marcelin, M. Greter, C. Jakubzick, M. Bogunovic, M. Leboeuf, N. van Rooijen, A. J. Habenicht, M. Merad and G. J. Randolph (2012). "Systemic analysis of PPARgamma in mouse macrophage populations reveals marked diversity in expression with critical roles in resolution of inflammation and airway immunity." J Immunol **189**(5): 2614-2624.
- Gautier, E. L., S. Ivanov, P. Lesnik and G. J. Randolph (2013). "Local apoptosis mediates clearance of macrophages from resolving inflammation in mice." Blood **122**(15): 2714-2722.
- Geijtenbeek, T. B., P. C. Groot, M. A. Nolte, S. J. van Vliet, S. T. Gangaram-Panday, G. C. van Duijnhoven, G. Kraal, A. J. van Oosterhout and Y. van Kooyk (2002). "Marginal zone macrophages express a murine homologue of DC-SIGN that captures blood-borne antigens in vivo." Blood **100**(8): 2908-2916.
- Geissmann, F., S. Gordon, D. A. Hume, A. M. Mowat and G. J. Randolph (2010). "Unravelling mononuclear phagocyte heterogeneity." Nat Rev Immunol **10**(6): 453-460.
- Gerner, M. Y., W. Kastentmuller, I. Ifrim, J. Kabat and R. N. Germain (2012). "Histo-cytometry: a method for highly multiplex quantitative tissue imaging analysis applied to dendritic cell subset microanatomy in lymph nodes." Immunity **37**(2): 364-376.
- Gerner, M. Y., P. Torabi-Parizi and R. N. Germain (2015). "Strategically localized dendritic cells promote rapid T cell responses to lymph-borne particulate antigens." Immunity **42**(1): 172-185.
- Gett, A. V., F. Sallusto, A. Lanzavecchia and J. Geginat (2003). "T cell fitness determined by signal strength." Nat Immunol **4**(4): 355-360.
- GeurtsvanKessel, C. H., M. A. Willart, L. S. van Rijt, F. Muskens, M. Kool, C. Baas, K. Thielemans, C. Bennett, B. E. Clausen, H. C. Hoogsteden, A. D. Osterhaus, G. F. Rimmelzwaan and B. N. Lambrecht (2008). "Clearance of influenza virus from the lung depends on migratory langerin+CD11b- but not plasmacytoid dendritic cells." J Exp Med **205**(7): 1621-1634.
- Giesen, C., H. A. Wang, D. Schapiro, N. Zivanovic, A. Jacobs, B. Hattendorf, P. J. Schuffler, D. Grolimund, J. M. Buhmann, S. Brandt, Z. Varga, P. J. Wild, D. Gunther and B. Bodenmiller (2014). "Highly multiplexed imaging of tumor tissues with subcellular resolution by mass cytometry." Nat Methods **11**(4): 417-422.
- Gil-Torregrosa, B. C., A. M. Lennon-Dumenil, B. Kessler, P. Guermonprez, H. L. Ploegh, D. Fruci, P. van Endert and S. Amigorena (2004). "Control of cross-presentation during dendritic cell maturation." Eur J Immunol **34**(2): 398-407.
- Ginhoux, F., M. Greter, M. Leboeuf, S. Nandi, P. See, S. Gokhan, M. F. Mehler, S. J. Conway, L. G. Ng, E. R. Stanley, I. M. Samokhvalov and M. Merad (2010). "Fate mapping analysis reveals that adult microglia derive from primitive macrophages." Science **330**(6005): 841-845.
- Ginhoux, F. and S. Jung (2014). "Monocytes and macrophages: developmental pathways and tissue homeostasis." Nat Rev Immunol **14**(6): 392-404.

Ginhoux, F., J. L. Schultze, P. J. Murray, J. Ochando and S. K. Biswas (2016). "New insights into the multidimensional concept of macrophage ontogeny, activation and function." Nat Immunol **17**(1): 34-40.

Goldberg, A. L. (2007). "Functions of the proteasome: from protein degradation and immune surveillance to cancer therapy." Biochem Soc Trans **35**(Pt 1): 12-17.

Goldmann, T., P. Wieghofer, M. J. Jordao, F. Prutek, N. Hagemeyer, K. Frenzel, L. Amann, O. Staszewski, K. Kierdorf, M. Krueger, G. Locatelli, H. Hochgerner, R. Zeiser, S. Epelman, F. Geissmann, J. Priller, F. M. Rossi, I. Bechmann, M. Kerschensteiner, S. Linnarsson, S. Jung and M. Prinz (2016). "Origin, fate and dynamics of macrophages at central nervous system interfaces." Nat Immunol **17**(7): 797-805.

Goldszmid, R. S., I. Coppens, A. Lev, P. Caspar, I. Mellman and A. Sher (2009). "Host ER-parasitophorous vacuole interaction provides a route of entry for antigen cross-presentation in *Toxoplasma gondii*-infected dendritic cells." J Exp Med **206**(2): 399-410.

Gollwitzer, E. S., S. Saglani, A. Trompette, K. Yadava, R. Sherburn, K. D. McCoy, L. P. Nicod, C. M. Lloyd and B. J. Marsland (2014). "Lung microbiota promotes tolerance to allergens in neonates via PD-L1." Nat Med **20**(6): 642-647.

Gomez Perdiguero, E., K. Klapproth, C. Schulz, K. Busch, E. Azzoni, L. Crozet, H. Garner, C. Trouillet, M. F. de Bruijn, F. Geissmann and H. R. Rodewald (2015). "Tissue-resident macrophages originate from yolk-sac-derived erythro-myeloid progenitors." Nature **518**(7540): 547-551.

Goritzka, M., S. Makris, F. Kausar, L. R. Durant, C. Pereira, Y. Kumagai, F. J. Culley, M. Mack, S. Akira and C. Johansson (2015). "Alveolar macrophage-derived type I interferons orchestrate innate immunity to RSV through recruitment of antiviral monocytes." J Exp Med **212**(5): 699-714.

Grajales-Reyes, G. E., A. Iwata, J. Albring, X. Wu, R. Tussiwand, W. Kc, N. M. Kretzer, C. G. Briseno, V. Durai, P. Bagadia, M. Haldar, J. Schonheit, F. Rosenbauer, T. L. Murphy and K. M. Murphy (2015). "Batf3 maintains autoactivation of Irf8 for commitment of a CD8alpha(+) conventional DC clonogenic progenitor." Nat Immunol **16**(7): 708-717.

Grakoui, A., S. K. Bromley, C. Sumen, M. M. Davis, A. S. Shaw, P. M. Allen and M. L. Dustin (1999). "The immunological synapse: a molecular machine controlling T cell activation." Science **285**(5425): 221-227.

Grande, A. G., 3rd, T. N. Golovina, S. E. Hamilton, V. Sriram, T. Spies, R. R. Brutkiewicz, J. T. Harty, L. C. Eisenlohr and L. Van Kaer (2000). "Impaired assembly yet normal trafficking of MHC class I molecules in Tapasin mutant mice." Immunity **13**(2): 213-222.

Granucci, F., E. Ferrero, M. Foti, D. Aggujaro, K. Vettoreto and P. Ricciardi-Castagnoli (1999). "Early events in dendritic cell maturation induced by LPS." Microbes Infect **1**(13): 1079-1084.

Gray, E. E. and J. G. Cyster (2012). "Lymph node macrophages." J Innate Immun **4**(5-6): 424-436.

Gray, E. E., S. Friend, K. Suzuki, T. G. Phan and J. G. Cyster (2012). "Subcapsular sinus macrophage fragmentation and CD169+ bleb acquisition by closely associated IL-17-committed innate-like lymphocytes." PLoS One **7**(6): e38258.

Greenwald, R. J., Y. E. Latchman and A. H. Sharpe (2002). "Negative co-receptors on lymphocytes." Curr Opin Immunol **14**(3): 391-396.

Greter, M., I. Lelios, P. Pelczar, G. Hoeffel, J. Price, M. Leboeuf, T. M. Kundig, K. Frei, F. Ginhoux, M. Merad and B. Becher (2012). "Stroma-derived interleukin-34 controls the development and maintenance of langerhans cells and the maintenance of microglia." Immunity **37**(6): 1050-1060.

Griffin, F. M., Jr., C. Bianco and S. C. Silverstein (1975). "Characterization of the macrophage receptor for complement and demonstration of its functional independence from the receptor for the Fc portion of immunoglobulin G." J Exp Med **141**(6): 1269-1277.

Griffiths, G. M., A. Tsun and J. C. Stinchcombe (2010). "The immunological synapse: a focal point for endocytosis and exocytosis." J Cell Biol **189**(3): 399-406.

Gubler, B., S. Daniel, E. A. Armandola, J. Hammer, S. Caillat-Zucman and P. M. van Endert (1998). "Substrate selection by transporters associated with antigen processing occurs during peptide binding to TAP." Mol Immunol **35**(8): 427-433.

Guermonprez, P., L. Saveanu, M. Kleijmeer, J. Davoust, P. Van Endert and S. Amigorena (2003). "ER-phagosome fusion defines an MHC class I cross-presentation compartment in dendritic cells." Nature **425**(6956): 397-402.

Guillerme, J. B., N. Boisgerault, D. Roulois, J. Menager, C. Combredet, F. Tangy, J. F. Fonteneau and M. Gregoire (2013). "Measles virus vaccine-infected tumor cells induce tumor antigen cross-presentation by human plasmacytoid dendritic cells." Clin Cancer Res **19**(5): 1147-1158.

Guilliams, M., I. De Kleer, S. Henri, S. Post, L. Vanhoutte, S. De Prijck, K. Deswarte, B. Malissen, H. Hammad and B. N. Lambrecht (2013). "Alveolar macrophages develop from fetal monocytes that differentiate into long-lived cells in the first week of life via GM-CSF." J Exp Med **210**(10): 1977-1992.

Guilliams, M., C. A. Dutertre, C. L. Scott, N. McGovern, D. Sichien, S. Chakarov, S. Van Gassen, J. Chen, M. Poidinger, S. De Prijck, S. J. Tavernier, I. Low, S. E. Irac, C. N. Mattar, H. R. Sumatoh, G. H. Low, T. J. Chung, D. K. Chan, K. K. Tan, T. L. Hon, E. Fossum, B. Bogen, M. Choolani, J. K. Chan, A. Larbi, H. Luche, S. Henri, Y. Saeys, E. W. Newell, B. N. Lambrecht, B. Malissen and F. Ginhoux (2016). "Unsupervised High-Dimensional Analysis Aligns Dendritic Cells across Tissues and Species." Immunity **45**(3): 669-684.

Guilliams, M., F. Ginhoux, C. Jakubzick, S. H. Naik, N. Onai, B. U. Schraml, E. Segura, R. Tussiwand and S. Yona (2014). "Dendritic cells, monocytes and macrophages: a unified nomenclature based on ontogeny." Nat Rev Immunol **14**(8): 571-578.

Guilliams, M., B. N. Lambrecht and H. Hammad (2013). "Division of labor between lung dendritic cells and macrophages in the defense against pulmonary infections." Mucosal Immunol **6**(3): 464-473.

Guilliams, M. and B. Malissen (2015). "A Death Notice for In-Vitro-Generated GM-CSF Dendritic Cells?" Immunity **42**(6): 988-990.

Guttman-Yassky, E., M. A. Lowes, J. Fuentes-Duculan, J. Whynot, I. Novitskaya, I. Cardinale, A. Haider, A. Khatcherian, J. A. Carucci, R. Bergman and J. G. Krueger (2007). "Major differences in inflammatory dendritic cells and their products distinguish atopic dermatitis from psoriasis." J Allergy Clin Immunol **119**(5): 1210-1217.

Hambleton, S., S. Salem, J. Bustamante, V. Bigley, S. Boisson-Dupuis, J. Azevedo, A. Fortin, M. Haniffa, L. Ceron-Gutierrez, C. M. Bacon, G. Menon, C. Trouillet, D. McDonald, P. Carey, F. Ginhoux, L. Alsina, T. J. Zumwalt, X. F. Kong, D. Kumararatne, K. Butler, M. Hubeau, J. Feinberg, S. Al-Muhsen, A. Cant, L. Abel, D. Chaussabel, R. Doffinger, E. Talesnik, A. Grumach, A. Duarte, K. Abarca, D. Moraes-Vasconcelos, D. Burk, A. Berghuis, F. Geissmann, M. Collin, J. L. Casanova and P. Gros (2011). "IRF8 mutations and human dendritic-cell immunodeficiency." N Engl J Med **365**(2): 127-138.

Hammer, G. E., F. Gonzalez, E. James, H. Nolla and N. Shastri (2007). "In the absence of aminopeptidase ERAAP, MHC class I molecules present many unstable and highly immunogenic peptides." Nat Immunol **8**(1): 101-108.

Han, A., E. W. Newell, J. Glanville, N. Fernandez-Becker, C. Khosla, Y. H. Chien and M. M. Davis (2013). "Dietary gluten triggers concomitant activation of CD4+ and CD8+ alpha beta T cells and gamma delta T cells in celiac disease." Proc Natl Acad Sci U S A **110**(32): 13073-13078.

Hanayama, R., M. Tanaka, K. Miyasaka, K. Aozasa, M. Koike, Y. Uchiyama and S. Nagata (2004). "Autoimmune disease and impaired uptake of apoptotic cells in MFG-E8-deficient mice." Science **304**(5674): 1147-1150.

Hanc, P., T. Fujii, S. Iborra, Y. Yamada, J. Huotari, O. Schulz, S. Ahrens, S. Kjaer, M. Way, D. Sancho, K. Namba and C. Reis e Sousa (2015). "Structure of the Complex of F-Actin and DNCR-1, a C-Type Lectin Receptor Involved in Dendritic Cell Cross-Presentation of Dead Cell-Associated Antigens." Immunity **42**(5): 839-849.

Haniffa, M., F. Ginhoux, X. N. Wang, V. Bigley, M. Abel, I. Dimmick, S. Bullock, M. Grisotto, T. Booth, P. Taub, C. Hilkens, M. Merad and M. Collin (2009). "Differential rates of replacement of human dermal dendritic cells and macrophages during hematopoietic stem cell transplantation." J Exp Med **206**(2): 371-385.

Haniffa, M., A. Shin, V. Bigley, N. McGovern, P. Teo, P. See, P. S. Wasan, X. N. Wang, F. Malinarich, B. Malleret, A. Larbi, P. Tan, H. Zhao, M. Poidinger, S. Pagan, S. Cookson, R. Dickinson, I. Dimmick, R. F. Jarrett, L. Renia, J. Tam, C. Song, J. Connolly, J. K. Chan, A. Gehring, A. Bertoletti, M. Collin and F. Ginhoux (2012). "Human tissues contain CD141hi cross-presenting dendritic cells with functional homology to mouse CD103+ nonlymphoid dendritic cells." Immunity **37**(1): 60-73.

Hanna, R. N., L. M. Carlin, H. G. Hubbeling, D. Nackiewicz, A. M. Green, J. A. Punt, F. Geissmann and C. C. Hedrick (2011). "The transcription factor NR4A1 (Nur77) controls bone marrow differentiation and the survival of Ly6C- monocytes." Nat Immunol **12**(8): 778-785.

Hanna, R. N., C. Cekic, D. Sag, R. Tacke, G. D. Thomas, H. Nowyhed, E. Herrley, N. Rasquinha, S. McArdle, R. Wu, E. Peluso, D. Metzger, H. Ichinose, I. Shaked, G. Chodaczek, S. K. Biswas and C. C. Hedrick (2015). "Patrolling monocytes control tumor metastasis to the lung." Science **350**(6263): 985-990.

Hartnell, A., J. Steel, H. Turley, M. Jones, D. G. Jackson and P. R. Crocker (2001). "Characterization of human sialoadhesin, a sialic acid binding receptor expressed by resident and inflammatory macrophage populations." Blood **97**(1): 288-296.

Harwood, N. E. and F. D. Batista (2009). "The antigen expressway: follicular conduits carry antigen to B cells." Immunity **30**(2): 177-179.

Hashimoto-Tane, A. and T. Saito (2016). "Dynamic Regulation of TCR-Microclusters and the Microsynapse for T Cell Activation." Front Immunol **7**: 255.

Heikema, A. P., M. P. Bergman, H. Richards, P. R. Crocker, M. Gilbert, J. N. Samsom, W. J. van Wamel, H. P. Endtz and A. van Belkum (2010). "Characterization of the specific interaction between sialoadhesin and sialylated *Campylobacter jejuni* lipooligosaccharides." Infect Immun **78**(7): 3237-3246.

Heikema, A. P., R. I. Koning, S. Duarte dos Santos Rico, H. Rempel, B. C. Jacobs, H. P. Endtz, W. J. van Wamel and J. N. Samsom (2013). "Enhanced, sialoadhesin-dependent uptake of Guillain-Barre syndrome-associated *Campylobacter jejuni* strains by human macrophages." Infect Immun **81**(6): 2095-2103.

Helft, J., J. Bottcher, P. Chakravarty, S. Zelenay, J. Huotari, B. U. Schraml, D. Goubau and C. Reis e Sousa (2015). "GM-CSF Mouse Bone Marrow Cultures Comprise a Heterogeneous Population of CD11c(+)MHCII(+) Macrophages and Dendritic Cells." Immunity **42**(6): 1197-1211.

Helft, J., J. P. Bottcher, P. Chakravarty, S. Zelenay, J. Huotari, B. U. Schraml, D. Goubau and E. S. C. Reis (2016). "Alive but Confused: Heterogeneity of CD11c(+) MHC Class II(+) Cells in GM-CSF Mouse Bone Marrow Cultures." Immunity **44**(1): 3-4.

Helft, J., B. Manicassamy, P. Guernonprez, D. Hashimoto, A. Silvin, J. Agudo, B. D. Brown, M. Schmolke, J. C. Miller, M. Leboeuf, K. M. Murphy, A. Garcia-Sastre and M. Merad (2012). "Cross-presenting CD103+ dendritic cells are protected from influenza virus infection." J Clin Invest **122**(11): 4037-4047.

Hennies, C. M., M. A. Lehn and E. M. Janssen (2015). "Quantitating MHC class II trafficking in primary dendritic cells using imaging flow cytometry." J Immunol Methods **423**: 18-28.



Henrickson, S. E., T. R. Mempel, I. B. Mazo, B. Liu, M. N. Artyomov, H. Zheng, A. Peixoto, M. P. Flynn, B. Senman, T. Junt, H. C. Wong, A. K. Chakraborty and U. H. von Andrian (2008). "T cell sensing of antigen dose governs interactive behavior with dendritic cells and sets a threshold for T cell activation." Nat Immunol **9**(3): 282-291.

Herold, S., N. M. Gabrielli and I. Vadasz (2013). "Novel concepts of acute lung injury and alveolar-capillary barrier dysfunction." Am J Physiol Lung Cell Mol Physiol **305**(10): L665-681.

Hettinger, J., D. M. Richards, J. Hansson, M. M. Barra, A. C. Joschko, J. Krijgsveld and M. Feuerer (2013). "Origin of monocytes and macrophages in a committed progenitor." Nat Immunol **14**(8): 821-830.

Hickman, H. D., K. Takeda, C. N. Skon, F. R. Murray, S. E. Hensley, J. Loomis, G. N. Barber, J. R. Bennink and J. W. Yewdell (2008). "Direct priming of antiviral CD8+ T cells in the peripheral interfollicular region of lymph nodes." Nat Immunol **9**(2): 155-165.

Hiemstra, I. H., M. R. Beijer, H. Veninga, K. Vrijland, E. G. Borg, B. J. Olivier, R. E. Mebius, G. Kraal and J. M. den Haan (2014). "The identification and developmental requirements of colonic CD169(+) macrophages." Immunology **142**(2): 269-278.

Hildner, K., B. T. Edelson, W. E. Purtha, M. Diamond, H. Matsushita, M. Kohyama, B. Calderon, B. U. Schraml, E. R. Unanue, M. S. Diamond, R. D. Schreiber, T. L. Murphy and K. M. Murphy (2008). "Batf3 deficiency reveals a critical role for CD8alpha+ dendritic cells in cytotoxic T cell immunity." Science **322**(5904): 1097-1100.

Hilgendorf, I., L. M. Gerhardt, T. C. Tan, C. Winter, T. A. Holderried, B. G. Chousterman, Y. Iwamoto, R. Liao, A. Zirlik, M. Scherer-Crosbie, C. C. Hedrick, P. Libby, M. Nahrendorf, R. Weissleder and F. K. Swirski (2014). "Ly-6Chigh monocytes depend on Nr4a1 to balance both inflammatory and reparative phases in the infarcted myocardium." Circ Res **114**(10): 1611-1622.

Ho, I. C., T. S. Tai and S. Y. Pai (2009). "GATA3 and the T-cell lineage: essential functions before and after T-helper-2-cell differentiation." Nat Rev Immunol **9**(2): 125-135.

Hoeffel, G., A. C. Ripoche, D. Matheoud, M. Nascimbeni, N. Escriou, P. Lebon, F. Heshmati, J. G. Guillet, M. Gannage, S. Caillat-Zucman, N. Casartelli, O. Schwartz, H. De la Salle, D. Hanau, A. Hosmalin and C. Maranon (2007). "Antigen crosspresentation by human plasmacytoid dendritic cells." Immunity **27**(3): 481-492.

Hoeffel, G., Y. Wang, M. Greter, P. See, P. Teo, B. Malleret, M. Leboeuf, D. Low, G. Oller, F. Almeida, S. H. Choy, M. Grisotto, L. Renia, S. J. Conway, E. R. Stanley, J. K. Chan, L. G. Ng, I. M. Samokhvalov, M. Merad and F. Ginhoux (2012). "Adult Langerhans cells derive predominantly from embryonic fetal liver monocytes with a minor contribution of yolk sac-derived macrophages." J Exp Med **209**(6): 1167-1181.

Hoepfner, S., F. Severin, A. Cabezas, B. Habermann, A. Runge, D. Gillyooly, H. Stenmark and M. Zerial (2005). "Modulation of receptor recycling and degradation by the endosomal kinesin KIF16B." Cell **121**(3): 437-450.

Honke, N., N. Shaabani, G. Cadeddu, U. R. Sorg, D. E. Zhang, M. Trilling, K. Klingel, M. Sauter, R. Kandolf, N. Gailus, N. van Rooijen, C. Burkart, S. E. Baldus, M. Grusdat, M. Lohning, H. Hengel, K. Pfeffer, M. Tanaka, D. Haussinger, M. Recher, P. A. Lang and K. S. Lang (2012). "Enforced viral replication activates adaptive immunity and is essential for the control of a cytopathic virus." Nat Immunol **13**(1): 51-57.

Honke, N., N. Shaabani, K. Merches, A. Gassa, A. Kraft, K. Ehrhardt, D. Haussinger, M. Lohning, U. Dittmer, H. Hengel, M. Recher, P. A. Lang and K. S. Lang (2016). "Immunoactivation induced by chronic viral infection inhibits viral replication and drives immunosuppression through sustained IFN-I responses." Eur J Immunol **46**(2): 372-380.

Honke, N., N. Shaabani, D. E. Zhang, G. Iliakis, H. C. Xu, D. Haussinger, M. Recher, M. Lohning, P. A. Lang and K. S. Lang (2013). "Usp18 driven enforced viral replication in dendritic cells contributes to break of immunological tolerance in autoimmune diabetes." PLoS Pathog **9**(10): e1003650.

Hu, Y. S., H. Cang and B. F. Lillemeier (2016). "Superresolution imaging reveals nanometer- and micrometer-scale spatial distributions of T-cell receptors in lymph nodes." Proc Natl Acad Sci U S A **113**(26): 7201-7206.

Hugues, S., A. Boissonnas, S. Amigorena and L. Fetler (2006). "The dynamics of dendritic cell-T cell interactions in priming and tolerance." Curr Opin Immunol **18**(4): 491-495.

Hugues, S., L. Fetler, L. Bonifaz, J. Helft, F. Amblard and S. Amigorena (2004). "Distinct T cell dynamics in lymph nodes during the induction of tolerance and immunity." Nat Immunol **5**(12): 1235-1242.

Hulpke, S. and R. Tampe (2013). "The MHC I loading complex: a multitasking machinery in adaptive immunity." Trends Biochem Sci **38**(8): 412-420.

Huntington, N. D., S. Carpentier, E. Vivier and G. T. Belz (2016). "Innate lymphoid cells: parallel checkpoints and coordinate interactions with T cells." Curr Opin Immunol **38**: 86-93.

Huotari, J. and A. Helenius (2011). "Endosome maturation." EMBO J **30**(17): 3481-3500.

Huppa, J. B., M. Axmann, M. A. Mortelmaier, B. F. Lillemeier, E. W. Newell, M. Brameshuber, L. O. Klein, G. J. Schutz and M. M. Davis (2010). "TCR-peptide-MHC interactions in situ show accelerated kinetics and increased affinity." Nature **463**(7283): 963-967.

Huppa, J. B., M. Gleimer, C. Sumen and M. M. Davis (2003). "Continuous T cell receptor signaling required for synapse maintenance and full effector potential." Nat Immunol **4**(8): 749-755.

Hurley, J. H. and H. Stenmark (2011). "Molecular mechanisms of ubiquitin-dependent membrane traffic." Annu Rev Biophys **40**: 119-142.

Huse, M., B. F. Lillemeier, M. S. Kuhns, D. S. Chen and M. M. Davis (2006). "T cells use two directionally distinct pathways for cytokine secretion." Nat Immunol **7**(3): 247-255.

Huysamen, C., J. A. Willment, K. M. Dennehy and G. D. Brown (2008). "CLEC9A is a novel activation C-type lectin-like receptor expressed on BDCA3+ dendritic cells and a subset of monocytes." J Biol Chem **283**(24): 16693-16701.

Iannacone, M., E. A. Moseman, E. Tonti, L. Bosurgi, T. Junt, S. E. Henrickson, S. P. Whelan, L. G. Guidotti and U. H. von Andrian (2010). "Subcapsular sinus macrophages prevent CNS invasion on peripheral infection with a neurotropic virus." Nature **465**(7301): 1079-1083.

Iezzi, G., K. Karjalainen and A. Lanzavecchia (1998). "The duration of antigenic stimulation determines the fate of naive and effector T cells." Immunity **8**(1): 89-95.

Intlekofer, A. M., N. Takemoto, E. J. Wherry, S. A. Longworth, J. T. Northrup, V. R. Palanivel, A. C. Mullen, C. R. Gasink, S. M. Kaech, J. D. Miller, L. Gapin, K. Ryan, A. P. Russ, T. Lindsten, J. S. Orange, A. W. Goldrath, R. Ahmed and S. L. Reiner (2005). "Effector and memory CD8+ T cell fate coupled by T-bet and eomesodermin." Nat Immunol **6**(12): 1236-1244.

Irish, J. M. and D. B. Doxie (2014). "High-dimensional single-cell cancer biology." Curr Top Microbiol Immunol **377**: 1-21.

Iwasaki, A. and R. Medzhitov (2015). "Control of adaptive immunity by the innate immune system." Nat Immunol **16**(4): 343-353.

Izquierdo-Useros, N., M. Lorizate, P. J. McLaren, A. Telenti, H. G. Krausslich and J. Martinez-Picado (2014). "HIV-1 capture and transmission by dendritic cells: the role of viral glycolipids and the cellular receptor Siglec-1." PLoS Pathog **10**(7): e1004146.

Izquierdo-Useros, N., M. Lorizate, M. C. Puertas, M. T. Rodriguez-Plata, N. Zangger, E. Erikson, M. Pino, I. Erkizia, B. Glass, B. Clotet, O. T. Keppler, A. Telenti, H. G. Krausslich and J. Martinez-Picado (2012). "Siglec-1 is a novel dendritic cell receptor that mediates HIV-1 trans-infection through recognition of viral membrane gangliosides." *PLoS Biol* **10**(12): e1001448.

Jaitin, D. A., E. Kenigsberg, H. Keren-Shaul, N. Elefant, F. Paul, I. Zaretsky, A. Mildner, N. Cohen, S. Jung, A. Tanay and I. Amit (2014). "Massively parallel single-cell RNA-seq for marker-free decomposition of tissues into cell types." *Science* **343**(6172): 776-779.

Jancic, C., A. Savina, C. Wasmeier, T. Tolmachova, J. El-Benna, P. M. Dang, S. Pascolo, M. A. Gougerot-Pocidalò, G. Raposo, M. C. Seabra and S. Amigorena (2007). "Rab27a regulates phagosomal pH and NADPH oxidase recruitment to dendritic cell phagosomes." *Nat Cell Biol* **9**(4): 367-378.

Janssen, E. M., N. M. Droin, E. E. Lemmens, M. J. Pinkoski, S. J. Bensinger, B. D. Ehst, T. S. Griffith, D. R. Green and S. P. Schoenberger (2005). "CD4+ T-cell help controls CD8+ T-cell memory via TRAIL-mediated activation-induced cell death." *Nature* **434**(7029): 88-93.

Joffre, O. P., E. Segura, A. Savina and S. Amigorena (2012). "Cross-presentation by dendritic cells." *Nat Rev Immunol* **12**(8): 557-569.

Johansson, J., A. Karlsson, J. Bylund and A. Welin (2015). "Phagocyte interactions with Mycobacterium tuberculosis--Simultaneous analysis of phagocytosis, phagosome maturation and intracellular replication by imaging flow cytometry." *J Immunol Methods* **427**: 73-84.

Johnston, R. J., A. C. Poholek, D. DiToro, I. Yusuf, D. Eto, B. Barnett, A. L. Dent, J. Craft and S. Crotty (2009). "Bcl6 and Blimp-1 are reciprocal and antagonistic regulators of T follicular helper cell differentiation." *Science* **325**(5943): 1006-1010.

Jordens, I., M. Fernandez-Borja, M. Marsman, S. Dusseljee, L. Janssen, J. Calafat, H. Janssen, R. Wubbolts and J. Neefjes (2001). "The Rab7 effector protein RILP controls lysosomal transport by inducing the recruitment of dynein-dynactin motors." *Curr Biol* **11**(21): 1680-1685.

Junt, T., E. A. Moseman, M. Iannaccone, S. Massberg, P. A. Lang, M. Boes, K. Fink, S. E. Henrickson, D. M. Shayakhmetov, N. C. Di Paolo, N. van Rooijen, T. R. Mempel, S. P. Whelan and U. H. von Andrian (2007). "Subcapsular sinus macrophages in lymph nodes clear lymph-borne viruses and present them to antiviral B cells." *Nature* **450**(7166): 110-114.

Jusforgues-Saklani, H., M. Uhl, N. Blachere, F. Lemaitre, O. Lantz, P. Bousso, D. Braun, J. J. Moon and M. L. Albert (2008). "Antigen persistence is required for dendritic cell licensing and CD8+ T cell cross-priming." *J Immunol* **181**(5): 3067-3076.

Kabanova, A., F. Sanseviero, V. Candi, A. Gamberucci, A. Gozzetti, G. Campoccia, M. Bocchia and C. T. Baldari (2016). "Human Cytotoxic T Lymphocytes Form Dysfunctional Immune Synapses with B Cells Characterized by Non-Polarized Lytic Granule Release." *Cell Rep* **15**(10): 2313.

Kaech, S. M., S. Hemby, E. Kersh and R. Ahmed (2002). "Molecular and functional profiling of memory CD8 T cell differentiation." *Cell* **111**(6): 837-851.

Kaech, S. M. and E. J. Wherry (2007). "Heterogeneity and cell-fate decisions in effector and memory CD8+ T cell differentiation during viral infection." *Immunity* **27**(3): 393-405.

Kamphorst, A. O., P. Guermonprez, D. Dudziak and M. C. Nussenzweig (2010). "Route of antigen uptake differentially impacts presentation by dendritic cells and activated monocytes." *J Immunol* **185**(6): 3426-3435.

Kang, Y. S., Y. Do, H. K. Lee, S. H. Park, C. Cheong, R. M. Lynch, J. M. Loeffler, R. M. Steinman and C. G. Park (2006). "A dominant complement fixation pathway for pneumococcal polysaccharides initiated by SIGN-R1 interacting with C1q." *Cell* **125**(1): 47-58.

Kang, Y. S., J. Y. Kim, S. A. Bruening, M. Pack, A. Charalambous, A. Pritsker, T. M. Moran, J. M. Loeffler, R. M. Steinman and C. G. Park (2004). "The C-type lectin SIGN-R1 mediates uptake of the capsular polysaccharide of *Streptococcus pneumoniae* in the marginal zone of mouse spleen." Proc Natl Acad Sci U S A **101**(1): 215-220.

Kang, Y. S., S. Yamazaki, T. Iyoda, M. Pack, S. A. Bruening, J. Y. Kim, K. Takahara, K. Inaba, R. M. Steinman and C. G. Park (2003). "SIGN-R1, a novel C-type lectin expressed by marginal zone macrophages in spleen, mediates uptake of the polysaccharide dextran." Int Immunol **15**(2): 177-186.

Karlsson, M. C., R. Guinamard, S. Bolland, M. Sankala, R. M. Steinman and J. V. Ravetch (2003). "Macrophages control the retention and trafficking of B lymphocytes in the splenic marginal zone." J Exp Med **198**(2): 333-340.

Kastenmuller, W., G. Gasteiger, N. Subramanian, T. Sparwasser, D. H. Busch, Y. Belkaid, I. Drexler and R. N. Germain (2011). "Regulatory T cells selectively control CD8<sup>+</sup> T cell effector pool size via IL-2 restriction." J Immunol **187**(6): 3186-3197.

Kawai, T. and S. Akira (2010). "The role of pattern-recognition receptors in innate immunity: update on Toll-like receptors." Nat Immunol **11**(5): 373-384.

Kawasaki, N., J. L. Vela, C. M. Nycholat, C. Rademacher, A. Khurana, N. van Rooijen, P. R. Crocker, M. Kronenberg and J. C. Paulson (2013). "Targeted delivery of lipid antigen to macrophages via the CD169/sialoadhesin endocytic pathway induces robust invariant natural killer T cell activation." Proc Natl Acad Sci U S A **110**(19): 7826-7831.

Kelm, S., R. Schauer, J. C. Manuguerra, H. J. Gross and P. R. Crocker (1994). "Modifications of cell surface sialic acids modulate cell adhesion mediated by sialoadhesin and CD22." Glycoconj J **11**(6): 576-585.

Kerrigan, A. M. and G. D. Brown (2009). "C-type lectins and phagocytosis." Immunobiology **214**(7): 562-575.

Kierdorf, K., D. Erny, T. Goldmann, V. Sander, C. Schulz, E. G. Perdiguero, P. Wieghofer, A. Heinrich, P. Riemke, C. Holscher, D. N. Muller, B. Luckow, T. Brocker, K. Debowski, G. Fritz, G. Opdenakker, A. Diefenbach, K. Biber, M. Heikenwalder, F. Geissmann, F. Rosenbauer and M. Prinz (2013). "Microglia emerge from erythromyeloid precursors via Pu.1- and Irf8-dependent pathways." Nat Neurosci **16**(3): 273-280.

Kim, E. Y., L. Lynch, P. J. Brennan, N. R. Cohen and M. B. Brenner (2015). "The transcriptional programs of iNKT cells." Semin Immunol **27**(1): 26-32.

Kim, H. M., B. S. Park, J. I. Kim, S. E. Kim, J. Lee, S. C. Oh, P. Enkhbayar, N. Matsushima, H. Lee, O. J. Yoo and J. O. Lee (2007). "Crystal structure of the TLR4-MD-2 complex with bound endotoxin antagonist Eritoran." Cell **130**(5): 906-917.

King, C. (2009). "New insights into the differentiation and function of T follicular helper cells." Nat Rev Immunol **9**(11): 757-766.

King, C. G., S. Koehli, B. Hausmann, M. Schmalzer, D. Zehn and E. Palmer (2012). "T cell affinity regulates asymmetric division, effector cell differentiation, and tissue pathology." Immunity **37**(4): 709-720.

Kisselev, A. F., T. N. Akopian, K. M. Woo and A. L. Goldberg (1999). "The sizes of peptides generated from protein by mammalian 26 and 20 S proteasomes. Implications for understanding the degradative mechanism and antigen presentation." J Biol Chem **274**(6): 3363-3371.

Klaas, M. and P. R. Crocker (2012). "Sialoadhesin in recognition of self and non-self." Semin Immunopathol **34**(3): 353-364.

Klaas, M., C. Oetke, L. E. Lewis, L. P. Erwig, A. P. Heikema, A. Easton, H. J. Willison and P. R. Crocker (2012). "Sialoadhesin promotes rapid proinflammatory and type I IFN responses to a sialylated pathogen, *Campylobacter jejuni*." J Immunol **189**(5): 2414-2422.

- Kleijmeer, M., G. Ramm, D. Schuurhuis, J. Griffith, M. Rescigno, P. Ricciardi-Castagnoli, A. Y. Rudensky, F. Ossendorp, C. J. Melief, W. Stoorvogel and H. J. Geuze (2001). "Reorganization of multivesicular bodies regulates MHC class II antigen presentation by dendritic cells." J Cell Biol **155**(1): 53-63.
- Kmiec, Z. (2001). "Cooperation of liver cells in health and disease." Adv Anat Embryol Cell Biol **161**: III-XIII, 1-151.
- Koike, M., H. Nakanishi, P. Saftig, J. Ezaki, K. Isahara, Y. Ohsawa, W. Schulz-Schaeffer, T. Watanabe, S. Waguri, S. Kametaka, M. Shibata, K. Yamamoto, E. Kominami, C. Peters, K. von Figura and Y. Uchiyama (2000). "Cathepsin D deficiency induces lysosomal storage with ceroid lipofuscin in mouse CNS neurons." J Neurosci **20**(18): 6898-6906.
- Kong, K. F., T. Yokosuka, A. J. Canonigo-Balancio, N. Isakov, T. Saito and A. Altman (2011). "A motif in the V3 domain of the kinase PKC-theta determines its localization in the immunological synapse and functions in T cells via association with CD28." Nat Immunol **12**(11): 1105-1112.
- Kool, M., C. Geurtsvankessel, F. Muskens, F. B. Madeira, M. van Nimwegen, H. Kuipers, K. Thielemans, H. C. Hoogsteden, H. Hammad and B. N. Lambrecht (2011). "Facilitated antigen uptake and timed exposure to TLR ligands dictate the antigen presenting potential of plasmacytoid DCs." J Leukoc Biol **90**(6): 1177-1190.
- Koppel, E. A., M. Litjens, V. C. van den Berg, Y. van Kooyk and T. B. Geijtenbeek (2008). "Interaction of SIGNR1 expressed by marginal zone macrophages with marginal zone B cells is essential to early IgM responses against *Streptococcus pneumoniae*." Mol Immunol **45**(10): 2881-2887.
- Korn, T., E. Bettelli, M. Oukka and V. K. Kuchroo (2009). "IL-17 and Th17 Cells." Annu Rev Immunol **27**: 485-517.
- Kovacsovic-Bankowski, M. and K. L. Rock (1995). "A phagosome-to-cytosol pathway for exogenous antigens presented on MHC class I molecules." Science **267**(5195): 243-246.
- Kratzer, R., F. X. Mauvais, A. Burgevin, E. Barilleau and P. van Endert (2010). "Fusion proteins for versatile antigen targeting to cell surface receptors reveal differential capacity to prime immune responses." J Immunol **184**(12): 6855-6864.
- Kristiansen, M., J. H. Graversen, C. Jacobsen, O. Sonne, H. J. Hoffman, S. K. Law and S. K. Moestrup (2001). "Identification of the haemoglobin scavenger receptor." Nature **409**(6817): 198-201.
- Kropshofer, H., A. B. Vogt, G. Moldenhauer, J. Hammer, J. S. Blum and G. J. Hammerling (1996). "Editing of the HLA-DR-peptide repertoire by HLA-DM." EMBO J **15**(22): 6144-6154.
- Kruger, E. and P. M. Kloetzel (2012). "Immunoproteasomes at the interface of innate and adaptive immune responses: two faces of one enzyme." Curr Opin Immunol **24**(1): 77-83.
- Krummel, M. F., M. D. Sjaastad, C. Wulfig and M. M. Davis (2000). "Differential clustering of CD4 and CD3zeta during T cell recognition." Science **289**(5483): 1349-1352.
- Krutzik, P. O., J. M. Crane, M. R. Clutter and G. P. Nolan (2008). "High-content single-cell drug screening with phosphospecific flow cytometry." Nat Chem Biol **4**(2): 132-142.
- Kulpa, D. A., N. Del Cid, K. A. Peterson and K. L. Collins (2013). "Adaptor protein 1 promotes cross-presentation through the same tyrosine signal in major histocompatibility complex class I as that targeted by HIV-1." J Virol **87**(14): 8085-8098.
- Kumagai, Y., H. Kumar, S. Koyama, T. Kawai, O. Takeuchi and S. Akira (2009). "Cutting Edge: TLR-Dependent viral recognition along with type I IFN positive feedback signaling masks the requirement of viral replication for IFN- $\alpha$  production in plasmacytoid dendritic cells." J Immunol **182**(7): 3960-3964.

Kurotaki, T., Y. Tamura, G. Ueda, J. Oura, G. Kutomi, Y. Hirohashi, H. Sahara, T. Torigoe, H. Hiratsuka, H. Sunakawa, K. Hirata and N. Sato (2007). "Efficient cross-presentation by heat shock protein 90-peptide complex-loaded dendritic cells via an endosomal pathway." J Immunol **179**(3): 1803-1813.

Lafourcade, C., K. Sobo, S. Kieffer-Jaquinod, J. Garin and F. G. van der Goot (2008). "Regulation of the V-ATPase along the endocytic pathway occurs through reversible subunit association and membrane localization." PLoS One **3**(7): e2758.

Landsverk, O. J., O. Bakke and T. F. Gregers (2009). "MHC II and the endocytic pathway: regulation by invariant chain." Scand J Immunol **70**(3): 184-193.

Langlet, C., S. Tamoutounour, S. Henri, H. Luche, L. Ardouin, C. Gregoire, B. Malissen and M. Guilliams (2012). "CD64 expression distinguishes monocyte-derived and conventional dendritic cells and reveals their distinct role during intramuscular immunization." J Immunol **188**(4): 1751-1760.

Lautwein, A., T. Burster, A. M. Lennon-Dumenil, H. S. Overkleeft, E. Weber, H. Kalbacher and C. Driessen (2002). "Inflammatory stimuli recruit cathepsin activity to late endosomal compartments in human dendritic cells." Eur J Immunol **32**(12): 3348-3357.

Lautwein, A., M. Kraus, M. Reich, T. Burster, J. Brandenburg, H. S. Overkleeft, G. Schwarz, W. Kammer, E. Weber, H. Kalbacher, A. Nordheim and C. Driessen (2004). "Human B lymphoblastoid cells contain distinct patterns of cathepsin activity in endocytic compartments and regulate MHC class II transport in a cathepsin S-independent manner." J Leukoc Biol **75**(5): 844-855.

Lauvau, G., M. Boutet, T. M. Williams, S. S. Chin and L. Chorro (2016). "Memory CD8(+) T Cells: Innate-Like Sensors and Orchestrators of Protection." Trends Immunol **37**(6): 375-385.

Lavin, Y., D. Winter, R. Blecher-Gonen, E. David, H. Keren-Shaul, M. Merad, S. Jung and I. Amit (2014). "Tissue-resident macrophage enhancer landscapes are shaped by the local microenvironment." Cell **159**(6): 1312-1326.

Lawand, M., A. Abramova, V. Manceau, S. Springer and P. van Endert (2016). "TAP-Dependent and -Independent Peptide Import into Dendritic Cell Phagosomes." J Immunol.

LeBien, T. W. and T. F. Tedder (2008). "B lymphocytes: how they develop and function." Blood **112**(5): 1570-1580.

Lee, G. R., S. T. Kim, C. G. Spilianakis, P. E. Fields and R. A. Flavell (2006). "T helper cell differentiation: regulation by cis elements and epigenetics." Immunity **24**(4): 369-379.

Lee, J., G. Breton, T. Y. Oliveira, Y. J. Zhou, A. Aljoufi, S. Pühr, M. J. Cameron, R. P. Sekaly, M. C. Nussenzweig and K. Liu (2015). "Restricted dendritic cell and monocyte progenitors in human cord blood and bone marrow." J Exp Med **212**(3): 385-399.

Lee, J. C., P. A. Lyons, E. F. McKinney, J. M. Sowerby, E. J. Carr, F. Bredin, H. M. Rickman, H. Ratlamwala, A. Hatton, T. F. Rayner, M. Parkes and K. G. Smith (2011). "Gene expression profiling of CD8+ T cells predicts prognosis in patients with Crohn disease and ulcerative colitis." J Clin Invest **121**(10): 4170-4179.

Lee, K. H., A. D. Holdorf, M. L. Dustin, A. C. Chan, P. M. Allen and A. S. Shaw (2002). "T cell receptor signaling precedes immunological synapse formation." Science **295**(5559): 1539-1542.

Lee, Y. K., R. Mukasa, R. D. Hatton and C. T. Weaver (2009). "Developmental plasticity of Th17 and Treg cells." Curr Opin Immunol **21**(3): 274-280.

Lefrancois, L. and J. J. Obar (2010). "Once a killer, always a killer: from cytotoxic T cell to memory cell." Immunol Rev **235**(1): 206-218.

Lennon-Dumenil, A. M., A. H. Bakker, R. Maehr, E. Fiebiger, H. S. Overkleeft, M. Roseblatt, H. L. Ploegh and C. Lagaudriere-Gesbert (2002). "Analysis of protease activity in live antigen presenting cells shows regulation of the phagosomal proteolytic contents during dendritic cell activation." J Exp Med **196**(4): 529-540.

Lennon-Dumenil, A. M., A. H. Bakker, P. Wolf-Bryant, H. L. Ploegh and C. Lagaudriere-Gesbert (2002). "A closer look at proteolysis and MHC-class-II-restricted antigen presentation." Curr Opin Immunol **14**(1): 15-21.

Leong, M. L. and E. W. Newell (2015). "Multiplexed Peptide-MHC Tetramer Staining with Mass Cytometry." Methods Mol Biol **1346**: 115-131.

Levin, R., S. Grinstein and J. Canton (2016). "The life cycle of phagosomes: formation, maturation, and resolution." Immunol Rev **273**(1): 156-179.

Li, M., G. M. Davey, R. M. Sutherland, C. Kurts, A. M. Lew, C. Hirst, F. R. Carbone and W. R. Heath (2001). "Cell-associated ovalbumin is cross-presented much more efficiently than soluble ovalbumin in vivo." J Immunol **166**(10): 6099-6103.

Liang, Y., M. Cucchetti, R. Roncagalli, T. Yokosuka, A. Malzac, E. Bertosio, J. Imbert, I. J. Nijman, M. Suchanek, T. Saito, C. Wulfiging, B. Malissen and M. Malissen (2013). "The lymphoid lineage-specific actin-uncapping protein Rltpr is essential for costimulation via CD28 and the development of regulatory T cells." Nat Immunol **14**(8): 858-866.

Lin, M. L., Y. Zhan, A. I. Proietto, S. Prato, L. Wu, W. R. Heath, J. A. Villadangos and A. M. Lew (2008). "Selective suicide of cross-presenting CD8+ dendritic cells by cytochrome c injection shows functional heterogeneity within this subset." Proc Natl Acad Sci U S A **105**(8): 3029-3034.

Liu, J. and J. I. Shapiro (2003). "Endocytosis and signal transduction: basic science update." Biol Res Nurs **5**(2): 117-128.

Liu, Z., M. Y. Gerner, N. Van Panhuys, A. G. Levine, A. Y. Rudensky and R. N. Germain (2015). "Immune homeostasis enforced by co-localized effector and regulatory T cells." Nature **528**(7581): 225-230.

Lizee, G., G. Basha, J. Tiong, J. P. Julien, M. Tian, K. E. Biron and W. A. Jefferies (2003). "Control of dendritic cell cross-presentation by the major histocompatibility complex class I cytoplasmic domain." Nat Immunol **4**(11): 1065-1073.

Lutz, M. B., K. Inaba, G. Schuler and N. Romani (2016). "Still Alive and Kicking: In-Vitro-Generated GM-CSF Dendritic Cells!" Immunity **44**(1): 1-2.

Luzio, J. P., P. R. Pryor and N. A. Bright (2007). "Lysosomes: fusion and function." Nat Rev Mol Cell Biol **8**(8): 622-632.

Ma, C., R. Fan, H. Ahmad, Q. Shi, B. Comin-Anduix, T. Chodon, R. C. Koya, C. C. Liu, G. A. Kwong, C. G. Radu, A. Ribas and J. R. Heath (2011). "A clinical microchip for evaluation of single immune cells reveals high functional heterogeneity in phenotypically similar T cells." Nat Med **17**(6): 738-743.

Mackay, F., G. R. Majeau, P. Lawton, P. S. Hochman and J. L. Browning (1997). "Lymphotoxin but not tumor necrosis factor functions to maintain splenic architecture and humoral responsiveness in adult mice." Eur J Immunol **27**(8): 2033-2042.

Mahoney, K. M., P. D. Rennert and G. J. Freeman (2015). "Combination cancer immunotherapy and new immunomodulatory targets." Nat Rev Drug Discov **14**(8): 561-584.

Makedonas, G., N. Hutnick, D. Haney, A. C. Amick, J. Gardner, G. Cosma, A. R. Hersperger, D. Dolfi, E. J. Wherry, G. Ferrari and M. R. Betts (2010). "Perforin and IL-2 upregulation define qualitative differences among highly functional virus-specific human CD8 T cells." PLoS Pathog **6**(3): e1000798.

- Manoury, B. (2011). "TLR9 regulation by proteolysis: a friend or a foe." *Eur J Immunol* **41**(8): 2142-2144.
- Manoury, B., E. W. Hewitt, N. Morrice, P. M. Dando, A. J. Barrett and C. Watts (1998). "An asparaginyl endopeptidase processes a microbial antigen for class II MHC presentation." *Nature* **396**(6712): 695-699.
- Mant, A., F. Chinnery, T. Elliott and A. P. Williams (2012). "The pathway of cross-presentation is influenced by the particle size of phagocytosed antigen." *Immunology* **136**(2): 163-175.
- Mantegazza, A. R., A. L. Zajac, A. Twelvetrees, E. L. Holzbaur, S. Amigorena and M. S. Marks (2014). "TLR-dependent phagosome tubulation in dendritic cells promotes phagosome cross-talk to optimize MHC-II antigen presentation." *Proc Natl Acad Sci U S A* **111**(43): 15508-15513.
- Maric, M., B. Arunachalam, U. T. Phan, C. Dong, W. S. Garrett, K. S. Cannon, C. Alfonso, L. Karlsson, R. A. Flavell and P. Cresswell (2001). "Defective antigen processing in GILT-free mice." *Science* **294**(5545): 1361-1365.
- Markey, K. A., K. H. Gartlan, R. D. Kuns, K. P. MacDonald and G. R. Hill (2015). "Imaging the immunological synapse between dendritic cells and T cells." *J Immunol Methods* **423**: 40-44.
- Martinez-Picado, J., P. J. McLaren, I. Erkizia, M. P. Martin, S. Benet, M. Rotger, J. Dalmau, D. Ouchi, S. M. Wolinsky, S. Penugonda, H. F. Gunthard, J. Fellay, M. Carrington, N. Izquierdo-Useros and A. Telenti (2016). "Identification of Siglec-1 null individuals infected with HIV-1." *Nat Commun* **7**: 12412.
- Matsumoto, M., Y. X. Fu, H. Molina and D. D. Chaplin (1997). "Lymphotoxin-alpha-deficient and TNF receptor-I-deficient mice define developmental and functional characteristics of germinal centers." *Immunol Rev* **156**: 137-144.
- Matthews, S. P., I. Werber, J. Deussing, C. Peters, T. Reinheckel and C. Watts (2010). "Distinct protease requirements for antigen presentation in vitro and in vivo." *J Immunol* **184**(5): 2423-2431.
- Mayer, J., J. Swoger, A. J. Ozga, J. V. Stein and J. Sharpe (2012). "Quantitative measurements in 3-dimensional datasets of mouse lymph nodes resolve organ-wide functional dependencies." *Comput Math Methods Med* **2012**: 128431.
- McCord, L. A., W. G. Liang, E. Dowdell, V. Kalas, R. J. Hoey, A. Koide, S. Koide and W. J. Tang (2013). "Conformational states and recognition of amyloidogenic peptides of human insulin-degrading enzyme." *Proc Natl Acad Sci U S A* **110**(34): 13827-13832.
- McGaha, T. L., Y. Chen, B. Ravishankar, N. van Rooijen and M. C. Karlsson (2011). "Marginal zone macrophages suppress innate and adaptive immunity to apoptotic cells in the spleen." *Blood* **117**(20): 5403-5412.
- McGovern, N., A. Schlitzer, M. Gunawan, L. Jardine, A. Shin, E. Poyner, K. Green, R. Dickinson, X. N. Wang, D. Low, K. Best, S. Covins, P. Milne, S. Pagan, K. Aljefri, M. Windebank, D. Miranda-Saavedra, A. Larbi, P. S. Wasan, K. Duan, M. Poidinger, V. Bigley, F. Ginhoux, M. Collin and M. Haniffa (2014). "Human dermal CD14(+) cells are a transient population of monocyte-derived macrophages." *Immunity* **41**(3): 465-477.
- McKinney, E. F., P. A. Lyons, E. J. Carr, J. L. Hollis, D. R. Jayne, L. C. Willcocks, M. Koukoulaki, A. Brazma, V. Jovanovic, D. M. Kemeny, A. J. Pollard, P. A. Macary, A. N. Chaudhry and K. G. Smith (2010). "A CD8+ T cell transcription signature predicts prognosis in autoimmune disease." *Nat Med* **16**(5): 586-591, 581p following 591.
- Mempel, T. R., S. E. Henrickson and U. H. Von Andrian (2004). "T-cell priming by dendritic cells in lymph nodes occurs in three distinct phases." *Nature* **427**(6970): 154-159.
- Merad, M., P. Sathe, J. Helft, J. Miller and A. Mortha (2013). "The dendritic cell lineage: ontogeny and function of dendritic cells and their subsets in the steady state and the inflamed setting." *Annu Rev Immunol* **31**: 563-604.



Meredith, M. M., K. Liu, G. Darrasse-Jeze, A. O. Kamphorst, H. A. Schreiber, P. Guermonprez, J. Idoyaga, C. Cheong, K. H. Yao, R. E. Niec and M. C. Nussenzweig (2012). "Expression of the zinc finger transcription factor zDC (Zbtb46, Btbd4) defines the classical dendritic cell lineage." J Exp Med **209**(6): 1153-1165.

Merzougui, N., R. Kratzer, L. Saveanu and P. van Endert (2011). "A proteasome-dependent, TAP-independent pathway for cross-presentation of phagocytosed antigen." EMBO Rep **12**(12): 1257-1264.

Michaud, J. P., M. A. Bellavance, P. Prefontaine and S. Rivest (2013). "Real-time in vivo imaging reveals the ability of monocytes to clear vascular amyloid beta." Cell Rep **5**(3): 646-653.

Miller, J. C., B. D. Brown, T. Shay, E. L. Gautier, V. Jojic, A. Cohain, G. Pandey, M. Leboeuf, K. G. Elpek, J. Helft, D. Hashimoto, A. Chow, J. Price, M. Greter, M. Bogunovic, A. Bellemare-Pelletier, P. S. Frenette, G. J. Randolph, S. J. Turley, M. Merad and C. Immunological Genome (2012). "Deciphering the transcriptional network of the dendritic cell lineage." Nat Immunol **13**(9): 888-899.

Miller, M. J., A. S. Hejazi, S. H. Wei, M. D. Cahalan and I. Parker (2004). "T cell repertoire scanning is promoted by dynamic dendritic cell behavior and random T cell motility in the lymph node." Proc Natl Acad Sci U S A **101**(4): 998-1003.

Miller, M. J., O. Safrina, I. Parker and M. D. Cahalan (2004). "Imaging the single cell dynamics of CD4+ T cell activation by dendritic cells in lymph nodes." J Exp Med **200**(7): 847-856.

Miller, M. J., S. H. Wei, I. Parker and M. D. Cahalan (2002). "Two-photon imaging of lymphocyte motility and antigen response in intact lymph node." Science **296**(5574): 1869-1873.

Mingueneau, M., S. Boudaoud, S. Haskett, T. L. Reynolds, G. Nocturne, E. Norton, X. Zhang, M. Constant, D. Park, W. Wang, T. Lazure, C. Le Pajolec, A. Ergun and X. Mariette (2016). "Cytometry by time-of-flight immunophenotyping identifies a blood Sjogren's signature correlating with disease activity and glandular inflammation." J Allergy Clin Immunol **137**(6): 1809-1821 e1812.

Mingueneau, M., S. Krishnaswamy, M. H. Spitzer, S. C. Bendall, E. L. Stone, S. M. Hedrick, D. Pe'er, D. Mathis, G. P. Nolan and C. Benoist (2014). "Single-cell mass cytometry of TCR signaling: amplification of small initial differences results in low ERK activation in NOD mice." Proc Natl Acad Sci U S A **111**(46): 16466-16471.

Miyake, Y., K. Asano, H. Kaise, M. Uemura, M. Nakayama and M. Tanaka (2007). "Critical role of macrophages in the marginal zone in the suppression of immune responses to apoptotic cell-associated antigens." J Clin Invest **117**(8): 2268-2278.

Molawi, K., Y. Wolf, P. K. Kandalla, J. Favret, N. Hagemeyer, K. Frenzel, A. R. Pinto, K. Klapproth, S. Henri, B. Malissen, H. R. Rodewald, N. A. Rosenthal, M. Bajenoff, M. Prinz, S. Jung and M. H. Sieweke (2014). "Progressive replacement of embryo-derived cardiac macrophages with age." J Exp Med **211**(11): 2151-2158.

Momburg, F. and P. Tan (2002). "Tapasin-the keystone of the loading complex optimizing peptide binding by MHC class I molecules in the endoplasmic reticulum." Mol Immunol **39**(3-4): 217-233.

Monteiro, V. G., C. S. Lobato, A. R. Silva, D. V. Medina, M. A. de Oliveira, S. H. Seabra, W. de Souza and R. A. DaMatta (2005). "Increased association of Trypanosoma cruzi with sialoadhesin positive mice macrophages." Parasitol Res **97**(5): 380-385.

Moreau, H. D., F. Lemaitre, K. R. Garrod, Z. Garcia, A. M. Lennon-Dumenil and P. Bousso (2015). "Signal strength regulates antigen-mediated T-cell deceleration by distinct mechanisms to promote local exploration or arrest." Proc Natl Acad Sci U S A **112**(39): 12151-12156.

Moreau, H. D., F. Lemaitre, E. Terriac, G. Azar, M. Piel, A. M. Lennon-Dumenil and P. Bousso (2012). "Dynamic in situ cytometry uncovers T cell receptor signaling during immunological synapses and kinapses in vivo." Immunity **37**(2): 351-363.

Morris, D. G., X. Huang, N. Kaminski, Y. Wang, S. D. Shapiro, G. Dolganov, A. Glick and D. Sheppard (2003). "Loss of integrin alpha(v)beta6-mediated TGF-beta activation causes Mmp12-dependent emphysema." Nature **422**(6928): 169-173.

Moseman, E. A., M. Iannacone, L. Bosurgi, E. Tonti, N. Chevrier, A. Tumanov, Y. X. Fu, N. Hacohen and U. H. von Andrian (2012). "B cell maintenance of subcapsular sinus macrophages protects against a fatal viral infection independent of adaptive immunity." Immunity **36**(3): 415-426.

Moss, C. X., J. A. Villadangos and C. Watts (2005). "Destructive potential of the aspartyl protease cathepsin D in MHC class II-restricted antigen processing." Eur J Immunol **35**(12): 3442-3451.

Mouries, J., G. Moron, G. Schlecht, N. Escriou, G. Dadaglio and C. Leclerc (2008). "Plasmacytoid dendritic cells efficiently cross-prime naive T cells in vivo after TLR activation." Blood **112**(9): 3713-3722.

Mucklow, S., S. Gordon and P. R. Crocker (1997). "Characterization of the mouse sialoadhesin gene, Sn." Mamm Genome **8**(12): 934-937.

Murphy, K. M. and S. L. Reiner (2002). "The lineage decisions of helper T cells." Nat Rev Immunol **2**(12): 933-944.

N, A. G., J. A. Guillen, G. Gallardo, M. Diaz, J. V. de la Rosa, I. H. Hernandez, M. Casanova-Acebes, F. Lopez, C. Tabraue, S. Beceiro, C. Hong, P. C. Lara, M. Andujar, S. Arai, T. Miyazaki, S. Li, A. L. Corbi, P. Tontonoz, A. Hidalgo and A. Castrillo (2013). "The nuclear receptor LXRalpha controls the functional specialization of splenic macrophages." Nat Immunol **14**(8): 831-839.

Nagasawa, M., H. Schmidlin, M. G. Hazekamp, R. Schotte and B. Blom (2008). "Development of human plasmacytoid dendritic cells depends on the combined action of the basic helix-loop-helix factor E2-2 and the Ets factor Spi-B." Eur J Immunol **38**(9): 2389-2400.

Nair-Gupta, P., A. Baccharini, N. Tung, F. Seyffer, O. Florey, Y. Huang, M. Banerjee, M. Overholtzer, P. A. Roche, R. Tampe, B. D. Brown, D. Amsen, S. W. Whiteheart and J. M. Blander (2014). "TLR signals induce phagosomal MHC-I delivery from the endosomal recycling compartment to allow cross-presentation." Cell **158**(3): 506-521.

Nakagawa, T., W. Roth, P. Wong, A. Nelson, A. Farr, J. Deussing, J. A. Villadangos, H. Ploegh, C. Peters and A. Y. Rudensky (1998). "Cathepsin L: critical role in li degradation and CD4 T cell selection in the thymus." Science **280**(5362): 450-453.

Nakamura, A., R. Ebina-Shibuya, A. Itoh-Nakadai, A. Muto, H. Shima, D. Saigusa, J. Aoki, M. Ebina, T. Nukiwa and K. Igarashi (2013). "Transcription repressor Bach2 is required for pulmonary surfactant homeostasis and alveolar macrophage function." J Exp Med **210**(11): 2191-2204.

Newell, E. W. and M. M. Davis (2014). "Beyond model antigens: high-dimensional methods for the analysis of antigen-specific T cells." Nat Biotechnol **32**(2): 149-157.

Newell, E. W., N. Sigal, S. C. Bendall, G. P. Nolan and M. M. Davis (2012). "Cytometry by time-of-flight shows combinatorial cytokine expression and virus-specific cell niches within a continuum of CD8+ T cell phenotypes." Immunity **36**(1): 142-152.

Niedergang, F., V. Di Bartolo and A. Alcover (2016). "Comparative Anatomy of Phagocytic and Immunological Synapses." Front Immunol **7**: 18.

Nilsson, I., H. Ohvo-Rekila, J. P. Slotte, A. E. Johnson and G. von Heijne (2001). "Inhibition of protein translocation across the endoplasmic reticulum membrane by sterols." J Biol Chem **276**(45): 41748-41754.

Nolte, M. A., R. Arens, M. Kraus, M. H. van Oers, G. Kraal, R. A. van Lier and R. E. Mebius (2004). "B cells are crucial for both development and maintenance of the splenic marginal zone." J Immunol **172**(6): 3620-3627.

- Norbury, C. C., B. J. Chambers, A. R. Prescott, H. G. Ljunggren and C. Watts (1997). "Constitutive macropinocytosis allows TAP-dependent major histocompatibility complex class I presentation of exogenous soluble antigen by bone marrow-derived dendritic cells." *Eur J Immunol* **27**(1): 280-288.
- Norbury, C. C., L. J. Hewlett, A. R. Prescott, N. Shastri and C. Watts (1995). "Class I MHC presentation of exogenous soluble antigen via macropinocytosis in bone marrow macrophages." *Immunity* **3**(6): 783-791.
- Norbury, C. C., D. Malide, J. S. Gibbs, J. R. Bennink and J. W. Yewdell (2002). "Visualizing priming of virus-specific CD8+ T cells by infected dendritic cells in vivo." *Nat Immunol* **3**(3): 265-271.
- Nunes, P., N. Demaurex and M. C. Dinayer (2013). "Regulation of the NADPH oxidase and associated ion fluxes during phagocytosis." *Traffic* **14**(11): 1118-1131.
- Nurieva, R. I., Y. Chung, G. J. Martinez, X. O. Yang, S. Tanaka, T. D. Matskevitch, Y. H. Wang and C. Dong (2009). "Bcl6 mediates the development of T follicular helper cells." *Science* **325**(5943): 1001-1005.
- Oehen, S., B. Odermatt, U. Karrer, H. Hengartner, R. Zinkernagel and C. Lopez-Macias (2002). "Marginal zone macrophages and immune responses against viruses." *J Immunol* **169**(3): 1453-1458.
- Oetke, C., M. C. Vinson, C. Jones and P. R. Crocker (2006). "Sialoadhesin-deficient mice exhibit subtle changes in B- and T-cell populations and reduced immunoglobulin M levels." *Mol Cell Biol* **26**(4): 1549-1557.
- Ohya, T., M. Miaczynska, U. Coskun, B. Lommer, A. Runge, D. Drechsel, Y. Kalaidzidis and M. Zerial (2009). "Reconstitution of Rab- and SNARE-dependent membrane fusion by synthetic endosomes." *Nature* **459**(7250): 1091-1097.
- Oliveira, C. C., M. Sluijter, B. Querido, F. Ossendorp, S. H. van der Burg and T. van Hall (2014). "Dominant contribution of the proteasome and metalloproteinases to TAP-independent MHC-I peptide repertoire." *Mol Immunol* **62**(1): 129-136.
- Pack, M., C. Trumppheller, D. Thomas, C. G. Park, A. Granelli-Piperno, C. Munz and R. M. Steinman (2008). "DEC-205/CD205+ dendritic cells are abundant in the white pulp of the human spleen, including the border region between the red and white pulp." *Immunology* **123**(3): 438-446.
- Paolicelli, R. C., G. Bolasco, F. Pagani, L. Maggi, M. Scianni, P. Panzanelli, M. Giustetto, T. A. Ferreira, E. Guiducci, L. Dumas, D. Ragozzino and C. T. Gross (2011). "Synaptic pruning by microglia is necessary for normal brain development." *Science* **333**(6048): 1456-1458.
- Papamichail, M., S. A. Perez, A. D. Gritzapis and C. N. Baxevanis (2004). "Natural killer lymphocytes: biology, development, and function." *Cancer Immunol Immunother* **53**(3): 176-186.
- Parish, I. A., H. D. Marshall, M. M. Staron, P. A. Lang, A. Brustle, J. H. Chen, W. Cui, Y. C. Tsui, C. Perry, B. J. Laidlaw, P. S. Ohashi, C. T. Weaver and S. M. Kaech (2014). "Chronic viral infection promotes sustained Th1-derived immunoregulatory IL-10 via BLIMP-1." *J Clin Invest* **124**(8): 3455-3468.
- Parmentier, N., V. Stroobant, D. Colau, P. de Diesbach, S. Morel, J. Chapiro, P. van Endert and B. J. Van den Eynde (2010). "Production of an antigenic peptide by insulin-degrading enzyme." *Nat Immunol* **11**(5): 449-454.
- Paul, F., Y. Arkin, A. Giladi, D. A. Jaitin, E. Kenigsberg, H. Keren-Shaul, D. Winter, D. Lara-Astiaso, M. Gury, A. Weiner, E. David, N. Cohen, F. K. Lauridsen, S. Haas, A. Schlitzer, A. Mildner, F. Ginhoux, S. Jung, A. Trumpp, B. T. Porse, A. Tanay and I. Amit (2015). "Transcriptional Heterogeneity and Lineage Commitment in Myeloid Progenitors." *Cell* **163**(7): 1663-1677.
- Pearce, E. L., A. C. Mullen, G. A. Martins, C. M. Krawczyk, A. S. Hutchins, V. P. Zediak, M. Banica, C. B. DiCioccio, D. A. Gross, C. A. Mao, H. Shen, N. Cereb, S. Y. Yang, T. Lindsten, J. Rossant, C. A. Hunter and S. L. Reiner (2003). "Control of effector CD8+ T cell function by the transcription factor Eomesodermin." *Science* **302**(5647): 1041-1043.

Pentcheva-Hoang, T., J. G. Egen, K. Wojnoonski and J. P. Allison (2004). "B7-1 and B7-2 selectively recruit CTLA-4 and CD28 to the immunological synapse." *Immunity* **21**(3): 401-413.

Peplowska, K., D. F. Markgraf, C. W. Ostrowicz, G. Bange and C. Ungermann (2007). "The CORVET tethering complex interacts with the yeast Rab5 homolog Vps21 and is involved in endo-lysosomal biogenesis." *Dev Cell* **12**(5): 739-750.

Pepper, M., A. J. Pagan, B. Z. Igyarto, J. J. Taylor and M. K. Jenkins (2011). "Opposing signals from the Bcl6 transcription factor and the interleukin-2 receptor generate T helper 1 central and effector memory cells." *Immunity* **35**(4): 583-595.

Peters, P. J., J. J. Neefjes, V. Oorschot, H. L. Ploegh and H. J. Geuze (1991). "Segregation of MHC class II molecules from MHC class I molecules in the Golgi complex for transport to lysosomal compartments." *Nature* **349**(6311): 669-676.

Pfeifer, J. D., M. J. Wick, R. L. Roberts, K. Findlay, S. J. Normark and C. V. Harding (1993). "Phagocytic processing of bacterial antigens for class I MHC presentation to T cells." *Nature* **361**(6410): 359-362.

Phan, T. G., J. A. Green, E. E. Gray, Y. Xu and J. G. Cyster (2009). "Immune complex relay by subcapsular sinus macrophages and noncognate B cells drives antibody affinity maturation." *Nat Immunol* **10**(7): 786-793.

Phan, T. G., I. Grigorova, T. Okada and J. G. Cyster (2007). "Subcapsular encounter and complement-dependent transport of immune complexes by lymph node B cells." *Nat Immunol* **8**(9): 992-1000.

Picard, C., W. Al-Herz, A. Bousfiha, J. L. Casanova, T. Chatila, M. E. Conley, C. Cunningham-Rundles, A. Etzioni, S. M. Holland, C. Klein, S. Nonoyama, H. D. Ochs, E. Oksenhendler, J. M. Puck, K. E. Sullivan, M. L. Tang, J. L. Franco and H. B. Gaspar (2015). "Primary Immunodeficiency Diseases: an Update on the Classification from the International Union of Immunological Societies Expert Committee for Primary Immunodeficiency 2015." *J Clin Immunol* **35**(8): 696-726.

Pickert, G., C. Neufert, M. Leppkes, Y. Zheng, N. Wittkopf, M. Warntjen, H. A. Lehr, S. Hirth, B. Weigmann, S. Wirtz, W. Ouyang, M. F. Neurath and C. Becker (2009). "STAT3 links IL-22 signaling in intestinal epithelial cells to mucosal wound healing." *J Exp Med* **206**(7): 1465-1472.

Pino, M., I. Erkizia, S. Benet, E. Erikson, M. T. Fernandez-Figueras, D. Guerrero, J. Dalmau, D. Ouchi, A. Rausell, A. Ciuffi, O. T. Keppler, A. Telenti, H. G. Krausslich, J. Martinez-Picado and N. Izquierdo-Useros (2015). "HIV-1 immune activation induces Siglec-1 expression and enhances viral trans-infection in blood and tissue myeloid cells." *Retrovirology* **12**: 37.

Pluger, E. B., M. Boes, C. Alfonso, C. J. Schroter, H. Kalbacher, H. L. Ploegh and C. Driessen (2002). "Specific role for cathepsin S in the generation of antigenic peptides in vivo." *Eur J Immunol* **32**(2): 467-476.

Plumlee, C. R., J. J. Obar, S. L. Colpitts, E. R. Jellison, W. N. Haining, L. Lefrancois and K. M. Khanna (2015). "Early Effector CD8 T Cells Display Plasticity in Populating the Short-Lived Effector and Memory-Precursor Pools Following Bacterial or Viral Infection." *Sci Rep* **5**: 12264.

Pooley, J. L., W. R. Heath and K. Shortman (2001). "Cutting edge: intravenous soluble antigen is presented to CD4 T cells by CD8- dendritic cells, but cross-presented to CD8 T cells by CD8+ dendritic cells." *J Immunol* **166**(9): 5327-5330.

Porichis, F., M. G. Hart, M. Griesbeck, H. L. Everett, M. Hassan, A. E. Baxter, M. Lindqvist, S. M. Miller, D. Z. Soghoian, D. G. Kavanagh, S. Reynolds, B. Norris, S. K. Mordecai, Q. Nguyen, C. Lai and D. E. Kaufmann (2014). "High-throughput detection of miRNAs and gene-specific mRNA at the single-cell level by flow cytometry." *Nat Commun* **5**: 5641.

Poteryaev, D., S. Datta, K. Ackema, M. Zerial and A. Spang (2010). "Identification of the switch in early-to-late endosome transition." *Cell* **141**(3): 497-508.

Prabagar, M. G., Y. Do, S. Ryu, J. Y. Park, H. J. Choi, W. S. Choi, T. J. Yun, J. Moon, I. S. Choi, K. Ko, K. Ko, C. Young Shin, C. Cheong and Y. S. Kang (2013). "SIGN-R1, a C-type lectin, enhances apoptotic cell clearance through the complement deposition pathway by interacting with C1q in the spleen." *Cell Death Differ* **20**(4): 535-545.

Prinz, M. and J. Priller (2014). "Microglia and brain macrophages in the molecular age: from origin to neuropsychiatric disease." *Nat Rev Neurosci* **15**(5): 300-312.

Probst, H. C., K. Tschannen, B. Odermatt, R. Schwendener, R. M. Zinkernagel and M. Van Den Broek (2005). "Histological analysis of CD11c-DTR/GFP mice after in vivo depletion of dendritic cells." *Clin Exp Immunol* **141**(3): 398-404.

Proietto, A. I., D. Mittag, A. W. Roberts, N. Sprigg and L. Wu (2012). "The equivalents of human blood and spleen dendritic cell subtypes can be generated in vitro from human CD34(+) stem cells in the presence of fms-like tyrosine kinase 3 ligand and thrombopoietin." *Cell Mol Immunol* **9**(6): 446-454.

Prokopec, K. E., A. M. Georgoudaki, S. Sohn, F. Wermeling, H. Gronlund, E. Lindh, M. C. Carroll and M. C. Karlsson (2016). "Cutting Edge: Marginal Zone Macrophages Regulate Antigen Transport by B Cells to the Follicle in the Spleen via CD21." *J Immunol* **197**(6): 2063-2068.

Pucci, F., C. Garris, C. P. Lai, A. Newton, C. Pfirschke, C. Engblom, D. Alvarez, M. Sprachman, C. Evavold, A. Magnuson, U. H. von Andrian, K. Glatz, X. O. Breakefield, T. R. Mempel, R. Weissleder and M. J. Pittet (2016). "SCS macrophages suppress melanoma by restricting tumor-derived vesicle-B cell interactions." *Science* **352**(6282): 242-246.

Pulendran, B., J. Banachereau, S. Burkeholder, E. Kraus, E. Guinet, C. Chalouni, D. Caron, C. Maliszewski, J. Davoust, J. Fay and K. Palucka (2000). "Flt3-ligand and granulocyte colony-stimulating factor mobilize distinct human dendritic cell subsets in vivo." *J Immunol* **165**(1): 566-572.

Puryear, W. B., H. Akiyama, S. D. Geer, N. P. Ramirez, X. Yu, B. M. Reinhard and S. Gummuru (2013). "Interferon-inducible mechanism of dendritic cell-mediated HIV-1 dissemination is dependent on Siglec-1/CD169." *PLoS Pathog* **9**(4): e1003291.

Qi, H., J. L. Cannons, F. Klauschen, P. L. Schwartzberg and R. N. Germain (2008). "SAP-controlled T-B cell interactions underlie germinal centre formation." *Nature* **455**(7214): 764-769.

Qi, H., J. G. Egen, A. Y. Huang and R. N. Germain (2006). "Extrafollicular activation of lymph node B cells by antigen-bearing dendritic cells." *Science* **312**(5780): 1672-1676.

Qiu, P., E. F. Simonds, S. C. Bendall, K. D. Gibbs, Jr., R. V. Bruggner, M. D. Linderman, K. Sachs, G. P. Nolan and S. K. Plevritis (2011). "Extracting a cellular hierarchy from high-dimensional cytometry data with SPADE." *Nat Biotechnol* **29**(10): 886-891.

Quigley, M., F. Pereyra, B. Nilsson, F. Porichis, C. Fonseca, Q. Eichbaum, B. Julg, J. L. Jesneck, K. Brosnahan, S. Imam, K. Russell, I. Toth, A. Piechocka-Trocha, D. Dolfi, J. Angelosanto, A. Crawford, H. Shin, D. S. Kwon, J. Zupkosky, L. Francisco, G. J. Freeman, E. J. Wherry, D. E. Kaufmann, B. D. Walker, B. Ebert and W. N. Haining (2010). "Transcriptional analysis of HIV-specific CD8+ T cells shows that PD-1 inhibits T cell function by upregulating BATF." *Nat Med* **16**(10): 1147-1151.

Racanelli, V. and B. Rehermann (2006). "The liver as an immunological organ." *Hepatology* **43**(2 Suppl 1): S54-62.

Radtke, A. J., W. Kastenmuller, D. A. Espinosa, M. Y. Gerner, S. W. Tse, P. Sinnis, R. N. Germain, F. P. Zavala and I. A. Cockburn (2015). "Lymph-node resident CD8alpha+ dendritic cells capture antigens from migratory malaria sporozoites and induce CD8+ T cell responses." *PLoS Pathog* **11**(2): e1004637.

Ravishankar, B., H. Liu, R. Shinde, P. Chandler, B. Baban, M. Tanaka, D. H. Munn, A. L. Mellor, M. C. Karlsson and T. L. McGaha (2012). "Tolerance to apoptotic cells is regulated by indoleamine 2,3-dioxygenase." Proc Natl Acad Sci U S A **109**(10): 3909-3914.

Ravishankar, B., H. Liu, R. Shinde, K. Chaudhary, W. Xiao, J. Bradley, M. Koritzinsky, M. P. Madaio and T. L. McGaha (2015). "The amino acid sensor GCN2 inhibits inflammatory responses to apoptotic cells promoting tolerance and suppressing systemic autoimmunity." Proc Natl Acad Sci U S A **112**(34): 10774-10779.

Ravishankar, B., R. Shinde, H. Liu, K. Chaudhary, J. Bradley, H. P. Lemos, P. Chandler, M. Tanaka, D. H. Munn, A. L. Mellor and T. L. McGaha (2014). "Marginal zone CD169+ macrophages coordinate apoptotic cell-driven cellular recruitment and tolerance." Proc Natl Acad Sci U S A **111**(11): 4215-4220.

Reid, P. A. and C. Watts (1990). "Cycling of cell-surface MHC glycoproteins through primaquine-sensitive intracellular compartments." Nature **346**(6285): 655-657.

Reits, E., J. Neijssen, C. Herberths, W. Benckhuijsen, L. Janssen, J. W. Drijfhout and J. Neefjes (2004). "A major role for TPP1 in trimming proteasomal degradation products for MHC class I antigen presentation." Immunity **20**(4): 495-506.

Reits, E. A., J. C. Vos, M. Gromme and J. Neefjes (2000). "The major substrates for TAP in vivo are derived from newly synthesized proteins." Nature **404**(6779): 774-778.

Rempel, H., C. Calosing, B. Sun and L. Pulliam (2008). "Sialoadhesin expressed on IFN-induced monocytes binds HIV-1 and enhances infectivity." PLoS One **3**(4): e1967.

Riese, R. J. and H. A. Chapman (2000). "Cathepsins and compartmentalization in antigen presentation." Curr Opin Immunol **12**(1): 107-113.

Rissin, D. M., C. W. Kan, L. Song, A. J. Rivnak, M. W. Fishburn, Q. Shao, T. Piech, E. P. Ferrell, R. E. Meyer, T. G. Campbell, D. R. Fournier and D. C. Duffy (2013). "Multiplexed single molecule immunoassays." Lab Chip **13**(15): 2902-2911.

Rivnak, A. J., D. M. Rissin, C. W. Kan, L. Song, M. W. Fishburn, T. Piech, T. G. Campbell, D. R. DuPont, M. Gardel, S. Sullivan, B. A. Pink, C. G. Cabrera, D. R. Fournier and D. C. Duffy (2015). "A fully-automated, six-plex single molecule immunoassay for measuring cytokines in blood." J Immunol Methods **424**: 20-27.

Robbins, S. H., T. Walzer, D. Dembele, C. Thibault, A. Defays, G. Bessou, H. Xu, E. Vivier, M. Sellars, P. Pierre, F. R. Sharp, S. Chan, P. Kastner and M. Dalod (2008). "Novel insights into the relationships between dendritic cell subsets in human and mouse revealed by genome-wide expression profiling." Genome Biol **9**(1): R17.

Roberts, R. L., M. A. Barbieri, J. Ullrich and P. D. Stahl (2000). "Dynamics of rab5 activation in endocytosis and phagocytosis." J Leukoc Biol **68**(5): 627-632.

Rocha, N. and J. Neefjes (2008). "MHC class II molecules on the move for successful antigen presentation." EMBO J **27**(1): 1-5.

Rock, K. L., D. J. Farfan-Arribas, J. D. Colbert and A. L. Goldberg (2014). "Re-examining class-I presentation and the DRiP hypothesis." Trends Immunol **35**(4): 144-152.

Rock, K. L. and A. L. Goldberg (1999). "Degradation of cell proteins and the generation of MHC class I-presented peptides." Annu Rev Immunol **17**: 739-779.

Rock, K. L., C. Gramm, L. Rothstein, K. Clark, R. Stein, L. Dick, D. Hwang and A. L. Goldberg (1994). "Inhibitors of the proteasome block the degradation of most cell proteins and the generation of peptides presented on MHC class I molecules." Cell **78**(5): 761-771.

Rodriguez, A., A. Regnault, M. Kleijmeer, P. Ricciardi-Castagnoli and S. Amigorena (1999). "Selective transport of internalized antigens to the cytosol for MHC class I presentation in dendritic cells." Nat Cell Biol **1**(6): 362-368.

Roeth, J. F., M. Williams, M. R. Kasper, T. M. Filzen and K. L. Collins (2004). "HIV-1 Nef disrupts MHC-I trafficking by recruiting AP-1 to the MHC-I cytoplasmic tail." J Cell Biol **167**(5): 903-913.

Rose, T., A. Grutzkau, H. Hirsland, D. Huscher, C. Dahnrich, A. Dzionek, T. Ozimkowski, W. Schlumberger, P. Enghard, A. Radbruch, G. Riemekasten, G. R. Burmester, F. Hiepe and R. Biesen (2013). "IFNalpha and its response proteins, IP-10 and SIGLEC-1, are biomarkers of disease activity in systemic lupus erythematosus." Ann Rheum Dis **72**(10): 1639-1645.

Rosenblum, M. D., S. S. Way and A. K. Abbas (2016). "Regulatory T cell memory." Nat Rev Immunol **16**(2): 90-101.

Rotta, G., E. W. Edwards, S. Sangaletti, C. Bennett, S. Ronzoni, M. P. Colombo, R. M. Steinman, G. J. Randolph and M. Rescigno (2003). "Lipopolysaccharide or whole bacteria block the conversion of inflammatory monocytes into dendritic cells in vivo." J Exp Med **198**(8): 1253-1263.

Roy, S. and C. Mandal (2016). "Leishmania donovani Utilize Sialic Acids for Binding and Phagocytosis in the Macrophages through Selective Utilization of Siglecs and Impair the Innate Immune Arm." PLoS Negl Trop Dis **10**(8): e0004904.

Sagoo, P., Z. Garcia, B. Breart, F. Lemaitre, D. Michonneau, M. L. Albert, Y. Levy and P. Bousso (2016). "In vivo imaging of inflammasome activation reveals a subcapsular macrophage burst response that mobilizes innate and adaptive immunity." Nat Med **22**(1): 64-71.

Sallusto, F. and A. Lanzavecchia (2001). "Exploring pathways for memory T cell generation." J Clin Invest **108**(6): 805-806.

Samie, M. and P. Cresswell (2015). "The transcription factor TFEB acts as a molecular switch that regulates exogenous antigen-presentation pathways." Nat Immunol **16**(7): 729-736.

Sandler, N. G., S. E. Bosinger, J. D. Estes, R. T. Zhu, G. K. Tharp, E. Boritz, D. Levin, S. Wijeyesinghe, K. N. Makamdop, G. Q. del Prete, B. J. Hill, J. K. Timmer, E. Reiss, G. Yarden, S. Darko, E. Contijoch, J. P. Todd, G. Silvestri, M. Nason, R. B. Norgren, Jr., B. F. Keele, S. Rao, J. A. Langer, J. D. Lifson, G. Schreiber and D. C. Douek (2014). "Type I interferon responses in rhesus macaques prevent SIV infection and slow disease progression." Nature **511**(7511): 601-605.

Sapoznikov, A., J. A. Fischer, T. Zaft, R. Krauthgamer, A. Dzionek and S. Jung (2007). "Organ-dependent in vivo priming of naive CD4+, but not CD8+, T cells by plasmacytoid dendritic cells." J Exp Med **204**(8): 1923-1933.

Sardiello, M., M. Palmieri, A. di Ronza, D. L. Medina, M. Valenza, V. A. Gennarino, C. Di Malta, F. Donaudo, V. Embrione, R. S. Polishchuk, S. Banfi, G. Parenti, E. Cattaneo and A. Ballabio (2009). "A gene network regulating lysosomal biogenesis and function." Science **325**(5939): 473-477.

Saric, T., S. C. Chang, A. Hattori, I. A. York, S. Markant, K. L. Rock, M. Tsujimoto and A. L. Goldberg (2002). "An IFN-gamma-induced aminopeptidase in the ER, ERAP1, trims precursors to MHC class I-presented peptides." Nat Immunol **3**(12): 1169-1176.

Satpathy, A. T., W. Kc, J. C. Albring, B. T. Edelson, N. M. Kretzer, D. Bhattacharya, T. L. Murphy and K. M. Murphy (2012). "Zbtb46 expression distinguishes classical dendritic cells and their committed progenitors from other immune lineages." J Exp Med **209**(6): 1135-1152.

Saveanu, L., O. Carroll, V. Lindo, M. Del Val, D. Lopez, Y. Lepelletier, F. Greer, L. Schomburg, D. Fruci, G. Niedermann and P. M. van Endert (2005). "Concerted peptide trimming by human ERAP1 and ERAP2 aminopeptidase complexes in the endoplasmic reticulum." Nat Immunol **6**(7): 689-697.

Saveanu, L., O. Carroll, M. Weimershaus, P. Guermonprez, E. Firat, V. Lindo, F. Greer, J. Davoust, R. Kratzer, S. R. Keller, G. Niedermann and P. van Endert (2009). "IRAP identifies an endosomal compartment required for MHC class I cross-presentation." Science **325**(5937): 213-217.

Saveanu, L., D. Fruci and P. van Endert (2002). "Beyond the proteasome: trimming, degradation and generation of MHC class I ligands by auxiliary proteases." Mol Immunol **39**(3-4): 203-215.

Schafer, D. P., E. K. Lehrman, A. G. Kautzman, R. Koyama, A. R. Mardinly, R. Yamasaki, R. M. Ransohoff, M. E. Greenberg, B. A. Barres and B. Stevens (2012). "Microglia sculpt postnatal neural circuits in an activity and complement-dependent manner." Neuron **74**(4): 691-705.

Schenkel, J. M. and D. Masopust (2014). "Tissue-resident memory T cells." Immunity **41**(6): 886-897.

Schmidt, J. H., S. Pietkiewicz, M. Naumann and I. N. Lavrik (2015). "Quantification of CD95-induced apoptosis and NF-kappaB activation at the single cell level." J Immunol Methods **423**: 12-17.

Scholer, A., S. Hugues, A. Boissonnas, L. Fetler and S. Amigorena (2008). "Intercellular adhesion molecule-1-dependent stable interactions between T cells and dendritic cells determine CD8+ T cell memory." Immunity **28**(2): 258-270.

Schreibelt, G., L. J. Klinkenberg, L. J. Cruz, P. J. Tacken, J. Tel, M. Kreutz, G. J. Adema, G. D. Brown, C. G. Figdor and I. J. de Vries (2012). "The C-type lectin receptor CLEC9A mediates antigen uptake and (cross-)presentation by human blood BDCA3+ myeloid dendritic cells." Blood **119**(10): 2284-2292.

Schrum, A. G. and L. A. Turka (2002). "The proliferative capacity of individual naive CD4(+) T cells is amplified by prolonged T cell antigen receptor triggering." J Exp Med **196**(6): 793-803.

Schulz, C., E. Gomez Perdiguero, L. Chorro, H. Szabo-Rogers, N. Cagnard, K. Kierdorf, M. Prinz, B. Wu, S. E. Jacobsen, J. W. Pollard, J. Frampton, K. J. Liu and F. Geissmann (2012). "A lineage of myeloid cells independent of Myb and hematopoietic stem cells." Science **336**(6077): 86-90.

Schulz, O. and C. Reis e Sousa (2002). "Cross-presentation of cell-associated antigens by CD8alpha+ dendritic cells is attributable to their ability to internalize dead cells." Immunology **107**(2): 183-189.

Scott, C. C., F. Vacca and J. Gruenberg (2014). "Endosome maturation, transport and functions." Semin Cell Dev Biol **31**: 2-10.

Scott, C. L., B. Soen, L. Martens, N. Skrypek, W. Saelens, J. Taminau, G. Blancke, G. Van Isterdael, D. Huylebroeck, J. Haigh, Y. Saeys, M. Guilliams, B. N. Lambrecht and G. Bercx (2016). "The transcription factor Zeb2 regulates development of conventional and plasmacytoid DCs by repressing Id2." J Exp Med **213**(6): 897-911.

Scott, C. L., F. Zheng, P. De Baetselier, L. Martens, Y. Saeys, S. De Prijck, S. Lippens, C. Abels, S. Schoonooghe, G. Raes, N. Devoogdt, B. N. Lambrecht, A. Beschinn and M. Guilliams (2016). "Bone marrow-derived monocytes give rise to self-renewing and fully differentiated Kupffer cells." Nat Commun **7**: 10321.

Seder, R. A., P. A. Darrah and M. Roederer (2008). "T-cell quality in memory and protection: implications for vaccine design." Nat Rev Immunol **8**(4): 247-258.

Segura, E., M. Durand and S. Amigorena (2013). "Similar antigen cross-presentation capacity and phagocytic functions in all freshly isolated human lymphoid organ-resident dendritic cells." J Exp Med **210**(5): 1035-1047.

Segura, E., M. Touzot, A. Bohineust, A. Cappuccio, G. Chiocchia, A. Hosmalin, M. Dalod, V. Soumelis and S. Amigorena (2013). "Human inflammatory dendritic cells induce Th17 cell differentiation." Immunity **38**(2): 336-348.



Seifert, U., C. Maranon, A. Shmueli, J. F. Desoutter, L. Wesoloski, K. Janek, P. Henklein, S. Diescher, M. Andrieu, H. de la Salle, T. Weinschenk, H. Schild, D. Laderach, A. Galy, G. Haas, P. M. Kloetzel, Y. Reiss and A. Hosmalin (2003). "An essential role for tripeptidyl peptidase in the generation of an MHC class I epitope." Nat Immunol **4**(4): 375-379.

Sepulveda, F. E., S. Maschalidi, R. Colisson, L. Heslop, C. Ghirelli, E. Sakka, A. M. Lennon-Dumenil, S. Amigorena, L. Cabanie and B. Manoury (2009). "Critical role for asparagine endopeptidase in endocytic Toll-like receptor signaling in dendritic cells." Immunity **31**(5): 737-748.

Serwold, T., F. Gonzalez, J. Kim, R. Jacob and N. Shastri (2002). "ERAAP customizes peptides for MHC class I molecules in the endoplasmic reticulum." Nature **419**(6906): 480-483.

Seyerl, M., S. Kirchberger, O. Majdic, J. Seipelt, C. Jindra, C. Schrauf and J. Stockl (2010). "Human rhinoviruses induce IL-35-producing Treg via induction of B7-H1 (CD274) and sialoadhesin (CD169) on DC." Eur J Immunol **40**(2): 321-329.

Shaabani, N., V. Khairnar, V. Duhan, F. Zhou, R. F. Tur, D. Haussinger, M. Recher, A. V. Tumanov, C. Hardt, D. Pinschewer, U. Christen, P. A. Lang, N. Honke and K. S. Lang (2016). "Two separate mechanisms of enforced viral replication balance innate and adaptive immune activation." J Autoimmun **67**: 82-89.

Shalek, A. K., R. Satija, X. Adiconis, R. S. Gertner, J. T. Gaublomme, R. Raychowdhury, S. Schwartz, N. Yosef, C. Malboeuf, D. Lu, J. J. Trombetta, D. Gennert, A. Gnirke, A. Goren, N. Hacohen, J. Z. Levin, H. Park and A. Regev (2013). "Single-cell transcriptomics reveals bimodality in expression and splicing in immune cells." Nature **498**(7453): 236-240.

Shalek, A. K., R. Satija, J. Shuga, J. J. Trombetta, D. Gennert, D. Lu, P. Chen, R. S. Gertner, J. T. Gaublomme, N. Yosef, S. Schwartz, B. Fowler, S. Weaver, J. Wang, X. Wang, R. Ding, R. Raychowdhury, N. Friedman, N. Hacohen, H. Park, A. P. May and A. Regev (2014). "Single-cell RNA-seq reveals dynamic paracrine control of cellular variation." Nature **510**(7505): 363-369.

Shapiro, E., T. Biezuner and S. Linnarsson (2013). "Single-cell sequencing-based technologies will revolutionize whole-organism science." Nat Rev Genet **14**(9): 618-630.

Shen, L., L. J. Sigal, M. Boes and K. L. Rock (2004). "Important role of cathepsin S in generating peptides for TAP-independent MHC class I crosspresentation in vivo." Immunity **21**(2): 155-165.

Sheng, J., C. Ruedl and K. Karjalainen (2015). "Most Tissue-Resident Macrophages Except Microglia Are Derived from Fetal Hematopoietic Stem Cells." Immunity **43**(2): 382-393.

Shi, G. P., J. A. Villadangos, G. Dranoff, C. Small, L. Gu, K. J. Haley, R. Riese, H. L. Ploegh and H. A. Chapman (1999). "Cathepsin S required for normal MHC class II peptide loading and germinal center development." Immunity **10**(2): 197-206.

Shin, H., S. D. Blackburn, A. M. Intlekofer, C. Kao, J. M. Angelosanto, S. L. Reiner and E. J. Wherry (2009). "A role for the transcriptional repressor Blimp-1 in CD8(+) T cell exhaustion during chronic viral infection." Immunity **31**(2): 309-320.

Siegel, F. P., N. Kadowaki, M. Shodell, P. A. Fitzgerald-Bocarsly, K. Shah, S. Ho, S. Antonenko and Y. J. Liu (1999). "The nature of the principal type 1 interferon-producing cells in human blood." Science **284**(5421): 1835-1837.

Sieker, F., T. P. Straatsma, S. Springer and M. Zacharias (2008). "Differential tapasin dependence of MHC class I molecules correlates with conformational changes upon peptide dissociation: a molecular dynamics simulation study." Mol Immunol **45**(14): 3714-3722.

Sierra, A., J. M. Encinas, J. J. Deudero, J. H. Chancey, G. Enikolopov, L. S. Overstreet-Wadiche, S. E. Tsirka and M. Maletic-Savatic (2010). "Microglia shape adult hippocampal neurogenesis through apoptosis-coupled phagocytosis." Cell Stem Cell **7**(4): 483-495.

- Skokos, D., G. Shakhar, R. Varma, J. C. Waite, T. O. Cameron, R. L. Lindquist, T. Schwickert, M. C. Nussenzweig and M. L. Dustin (2007). "Peptide-MHC potency governs dynamic interactions between T cells and dendritic cells in lymph nodes." Nat Immunol **8**(8): 835-844.
- Snelgrove, R. J., J. Goulding, A. M. Didierlaurent, D. Lyonga, S. Vekaria, L. Edwards, E. Gwyer, J. D. Sedgwick, A. N. Barclay and T. Hussell (2008). "A critical function for CD200 in lung immune homeostasis and the severity of influenza infection." Nat Immunol **9**(9): 1074-1083.
- Spits, H., D. Artis, M. Colonna, A. Diefenbach, J. P. Di Santo, G. Eberl, S. Koyasu, R. M. Locksley, A. N. McKenzie, R. E. Mebius, F. Powrie and E. Vivier (2013). "Innate lymphoid cells--a proposal for uniform nomenclature." Nat Rev Immunol **13**(2): 145-149.
- Spitzer, M. H. and G. P. Nolan (2016). "Mass Cytometry: Single Cells, Many Features." Cell **165**(4): 780-791.
- Steinman, R. M. and Z. A. Cohn (1973). "Identification of a novel cell type in peripheral lymphoid organs of mice. I. Morphology, quantitation, tissue distribution." J Exp Med **137**(5): 1142-1162.
- Stemberger, C., K. M. Huster, M. Koffler, F. Anderl, M. Schiemann, H. Wagner and D. H. Busch (2007). "A single naive CD8+ T cell precursor can develop into diverse effector and memory subsets." Immunity **27**(6): 985-997.
- Stinchcombe, J. C., G. Bossi, S. Booth and G. M. Griffiths (2001). "The immunological synapse of CTL contains a secretory domain and membrane bridges." Immunity **15**(5): 751-761.
- Stinchcombe, J. C., E. Majorovits, G. Bossi, S. Fuller and G. M. Griffiths (2006). "Centrosome polarization delivers secretory granules to the immunological synapse." Nature **443**(7110): 462-465.
- Stoll, S., J. Delon, T. M. Brotz and R. N. Germain (2002). "Dynamic imaging of T cell-dendritic cell interactions in lymph nodes." Science **296**(5574): 1873-1876.
- Stratikos, E. (2014). "Modulating antigen processing for cancer immunotherapy." Oncoimmunology **3**(1): e27568.
- Stratikos, E. (2014). "Regulating adaptive immune responses using small molecule modulators of aminopeptidases that process antigenic peptides." Curr Opin Chem Biol **23**: 1-7.
- Stratikos, E., A. Stamogiannos, E. Zervoudi and D. Fruci (2014). "A role for naturally occurring alleles of endoplasmic reticulum aminopeptidases in tumor immunity and cancer pre-disposition." Front Oncol **4**: 363.
- Stritesky, G. L., S. C. Jameson and K. A. Hogquist (2012). "Selection of self-reactive T cells in the thymus." Annu Rev Immunol **30**: 95-114.
- Suan, D., A. Nguyen, I. Moran, K. Bourne, J. R. Hermes, M. Arshi, H. R. Hampton, M. Tomura, Y. Miwa, A. D. Kelleher, W. Kaplan, E. K. Deenick, S. G. Tangye, R. Brink, T. Chtanova and T. G. Phan (2015). "T follicular helper cells have distinct modes of migration and molecular signatures in naive and memory immune responses." Immunity **42**(4): 704-718.
- Sundrud, M. S., S. M. Grill, D. Ni, K. Nagata, S. S. Alkan, A. Subramaniam and D. Unutmaz (2003). "Genetic reprogramming of primary human T cells reveals functional plasticity in Th cell differentiation." J Immunol **171**(7): 3542-3549.
- Sung, J. H., H. Zhang, E. A. Moseman, D. Alvarez, M. Iannacone, S. E. Henrickson, J. C. de la Torre, J. R. Groom, A. D. Luster and U. H. von Andrian (2012). "Chemokine guidance of central memory T cells is critical for antiviral recall responses in lymph nodes." Cell **150**(6): 1249-1263.
- Susaki, E. A., K. Tainaka, D. Perrin, H. Yukinaga, A. Kuno and H. R. Ueda (2015). "Advanced CUBIC protocols for whole-brain and whole-body clearing and imaging." Nat Protoc **10**(11): 1709-1727.

- Suzuki, K., I. Grigorova, T. G. Phan, L. M. Kelly and J. G. Cyster (2009). "Visualizing B cell capture of cognate antigen from follicular dendritic cells." J Exp Med **206**(7): 1485-1493.
- Swaidani, S., K. Bulek, Z. Kang, M. F. Gulen, C. Liu, W. Yin, A. Abbadi, M. Aronica and X. Li (2011). "T cell-derived Act1 is necessary for IL-25-mediated Th2 responses and allergic airway inflammation." J Immunol **187**(6): 3155-3164.
- Szabo, S. J., S. T. Kim, G. L. Costa, X. Zhang, C. G. Fathman and L. H. Glimcher (2000). "A novel transcription factor, T-bet, directs Th1 lineage commitment." Cell **100**(6): 655-669.
- Takahama, Y., K. Takada, S. Murata and K. Tanaka (2012). "beta5t-containing thymoproteasome: specific expression in thymic cortical epithelial cells and role in positive selection of CD8+ T cells." Curr Opin Immunol **24**(1): 92-98.
- Tang, F., C. Barbacioru, Y. Wang, E. Nordman, C. Lee, N. Xu, X. Wang, J. Bodeau, B. B. Tuch, A. Siddiqui, K. Lao and M. A. Surani (2009). "mRNA-Seq whole-transcriptome analysis of a single cell." Nat Methods **6**(5): 377-382.
- Tang, J., N. van Panhuys, W. Kastentmuller and R. N. Germain (2013). "The future of immunomaging--deeper, bigger, more precise, and definitively more colorful." Eur J Immunol **43**(6): 1407-1412.
- Tate, M. D., D. L. Pickett, N. van Rooijen, A. G. Brooks and P. C. Reading (2010). "Critical role of airway macrophages in modulating disease severity during influenza virus infection of mice." J Virol **84**(15): 7569-7580.
- Tel, J., G. Schreibelt, S. P. Sittig, T. S. Mathan, S. I. Buschow, L. J. Cruz, A. J. Lambeck, C. G. Figdor and I. J. de Vries (2013). "Human plasmacytoid dendritic cells efficiently cross-present exogenous Ags to CD8+ T cells despite lower Ag uptake than myeloid dendritic cell subsets." Blood **121**(3): 459-467.
- Thacker, R. I. and E. M. Janssen (2012). "Cross-presentation of cell-associated antigens by mouse splenic dendritic cell populations." Front Immunol **3**: 41.
- Thomas, G., R. Tacke, C. C. Hedrick and R. N. Hanna (2015). "Nonclassical patrolling monocyte function in the vasculature." Arterioscler Thromb Vasc Biol **35**(6): 1306-1316.
- Tinoco, R., V. Alcalde, Y. Yang, K. Sauer and E. I. Zuniga (2009). "Cell-intrinsic transforming growth factor-beta signaling mediates virus-specific CD8+ T cell deletion and viral persistence in vivo." Immunity **31**(1): 145-157.
- Tomori, O. (2011). "From smallpox eradication to the future of global health: innovations, application and lessons for future eradication and control initiatives." Vaccine **29 Suppl 4**: D145-148.
- Touret, N., P. Paroutis, M. Terebiznik, R. E. Harrison, S. Trombetta, M. Pypaert, A. Chow, A. Jiang, J. Shaw, C. Yip, H. P. Moore, N. van der Wel, D. Houben, P. J. Peters, C. de Chastellier, I. Mellman and S. Grinstein (2005). "Quantitative and dynamic assessment of the contribution of the ER to phagosome formation." Cell **123**(1): 157-170.
- Travis, J. (2009). "Origins. On the origin of the immune system." Science **324**(5927): 580-582.
- Trombetta, E. S., M. Ebersold, W. Garrett, M. Pypaert and I. Mellman (2003). "Activation of lysosomal function during dendritic cell maturation." Science **299**(5611): 1400-1403.
- Tube, N. J., A. J. Pagan, J. J. Taylor, R. W. Nelson, J. L. Linehan, J. M. Ertelt, E. S. Huseby, S. S. Way and M. K. Jenkins (2013). "Single naive CD4+ T cells from a diverse repertoire produce different effector cell types during infection." Cell **153**(4): 785-796.
- Tussiwand, R. and E. L. Gautier (2015). "Transcriptional Regulation of Mononuclear Phagocyte Development." Front Immunol **6**: 533.

- Vakkila, J., R. A. DeMarco and M. T. Lotze (2004). "Imaging analysis of STAT1 and NF-kappaB translocation in dendritic cells at the single cell level." J Immunol Methods **294**(1-2): 123-134.
- Valenzuela, J., C. Schmidt and M. Mescher (2002). "The roles of IL-12 in providing a third signal for clonal expansion of naive CD8 T cells." J Immunol **169**(12): 6842-6849.
- Vallentin, B., V. Barlogis, C. Piperoglou, S. Cypowyj, N. Zucchini, M. Chene, F. Navarro, C. Farnarier, E. Vivier and F. Vely (2015). "Innate Lymphoid Cells in Cancer." Cancer Immunol Res **3**(10): 1109-1114.
- van de Laar, L., W. Saelens, S. De Prijck, L. Martens, C. L. Scott, G. Van Isterdael, E. Hoffmann, R. Beyaert, Y. Saeys, B. N. Lambrecht and M. Guilliams (2016). "Yolk Sac Macrophages, Fetal Liver, and Adult Monocytes Can Colonize an Empty Niche and Develop into Functional Tissue-Resident Macrophages." Immunity **44**(4): 755-768.
- van der Kuyl, A. C., R. van den Burg, F. Zorgdrager, F. Groot, B. Berkhout and M. Cornelissen (2007). "Sialoadhesin (CD169) expression in CD14+ cells is upregulated early after HIV-1 infection and increases during disease progression." PLoS One **2**(2): e257.
- van der Laan, L. J., M. Kangas, E. A. Dopp, E. Broug-Holub, O. Elomaa, K. Tryggvason and G. Kraal (1997). "Macrophage scavenger receptor MARCO: in vitro and in vivo regulation and involvement in the anti-bacterial host defense." Immunol Lett **57**(1-3): 203-208.
- van Endert, P. (2016). "Intracellular recycling and cross-presentation by MHC class I molecules." Immunol Rev **272**(1): 80-96.
- van Furth, R., Z. A. Cohn, J. G. Hirsch, J. H. Humphrey, W. G. Spector and H. L. Langevoort (1972). "[Mononuclear phagocytic system: new classification of macrophages, monocytes and of their cell line]." Bull World Health Organ **47**(5): 651-658.
- Van Kaer, L., P. G. Ashton-Rickardt, H. L. Ploegh and S. Tonegawa (1992). "TAP1 mutant mice are deficient in antigen presentation, surface class I molecules, and CD4-8+ T cells." Cell **71**(7): 1205-1214.
- van Kasteren, S. I. and H. S. Overkleeft (2014). "Endo-lysosomal proteases in antigen presentation." Curr Opin Chem Biol **23**: 8-15.
- van Leeuwen, E. M., J. Sprent and C. D. Surh (2009). "Generation and maintenance of memory CD4(+) T Cells." Curr Opin Immunol **21**(2): 167-172.
- Varma, R., G. Campi, T. Yokosuka, T. Saito and M. L. Dustin (2006). "T cell receptor-proximal signals are sustained in peripheral microclusters and terminated in the central supramolecular activation cluster." Immunity **25**(1): 117-127.
- Veldhoen, M., C. Uytendhove, J. van Snick, H. Helmbj, A. Westendorf, J. Buer, B. Martin, C. Wilhelm and B. Stockinger (2008). "Transforming growth factor-beta 'reprograms' the differentiation of T helper 2 cells and promotes an interleukin 9-producing subset." Nat Immunol **9**(12): 1341-1346.
- Veninga, H., E. G. Borg, K. Vreeman, P. R. Taylor, H. Kalay, Y. van Kooyk, G. Kraal, L. Martinez-Pomares and J. M. den Haan (2015). "Antigen targeting reveals splenic CD169+ macrophages as promoters of germinal center B-cell responses." Eur J Immunol **45**(3): 747-757.
- Vieira, O. V., R. J. Botelho, L. Rameh, S. M. Brachmann, T. Matsuo, H. W. Davidson, A. Schreiber, J. M. Backer, L. C. Cantley and S. Grinstein (2001). "Distinct roles of class I and class III phosphatidylinositol 3-kinases in phagosome formation and maturation." J Cell Biol **155**(1): 19-25.
- Vigneron, N. and B. J. Van den Eynde (2012). "Proteasome subtypes and the processing of tumor antigens: increasing antigenic diversity." Curr Opin Immunol **24**(1): 84-91.
- Virgin, H. W., E. J. Wherry and R. Ahmed (2009). "Redefining chronic viral infection." Cell **138**(1): 30-50.

- Vivier, E., S. A. van de Pavert, M. D. Cooper and G. T. Belz (2016). "The evolution of innate lymphoid cells." Nat Immunol **17**(7): 790-794.
- Wake, H., A. J. Moorhouse and J. Nabekura (2011). "Functions of microglia in the central nervous system--beyond the immune response." Neuron Glia Biol **7**(1): 47-53.
- Wang, Y., K. J. Szretter, W. Vermi, S. Gilfillan, C. Rossini, M. Cella, A. D. Barrow, M. S. Diamond and M. Colonna (2012). "IL-34 is a tissue-restricted ligand of CSF1R required for the development of Langerhans cells and microglia." Nat Immunol **13**(8): 753-760.
- Watchmaker, P. B., K. Lahl, M. Lee, D. Baumjohann, J. Morton, S. J. Kim, R. Zeng, A. Dent, K. M. Ansel, B. Diamond, H. Hadeiba and E. C. Butcher (2014). "Comparative transcriptional and functional profiling defines conserved programs of intestinal DC differentiation in humans and mice." Nat Immunol **15**(1): 98-108.
- Watts, C. (1997). "Capture and processing of exogenous antigens for presentation on MHC molecules." Annu Rev Immunol **15**: 821-850.
- Watts, C. (2004). "The exogenous pathway for antigen presentation on major histocompatibility complex class II and CD1 molecules." Nat Immunol **5**(7): 685-692.
- Wearsch, P. A., D. R. Peaper and P. Cresswell (2011). "Essential glycan-dependent interactions optimize MHC class I peptide loading." Proc Natl Acad Sci U S A **108**(12): 4950-4955.
- Wei, S. H., O. Safrina, Y. Yu, K. R. Garrod, M. D. Cahalan and I. Parker (2007). "Ca<sup>2+</sup> signals in CD4<sup>+</sup> T cells during early contacts with antigen-bearing dendritic cells in lymph node." J Immunol **179**(3): 1586-1594.
- Weimershaus, M., S. Maschalidi, F. Sepulveda, B. Manoury, P. van Endert and L. Saveanu (2012). "Conventional dendritic cells require IRAP-Rab14 endosomes for efficient cross-presentation." J Immunol **188**(4): 1840-1846.
- Weimershaus, M. and P. van Endert (2013). "Preparation of dendritic cells by in vitro cultures." Methods Mol Biol **960**: 351-357.
- West, M. A., R. P. Wallin, S. P. Matthews, H. G. Svensson, R. Zaru, H. G. Ljunggren, A. R. Prescott and C. Watts (2004). "Enhanced dendritic cell antigen capture via toll-like receptor-induced actin remodeling." Science **305**(5687): 1153-1157.
- Wherry, E. J. and R. Ahmed (2004). "Memory CD8 T-cell differentiation during viral infection." J Virol **78**(11): 5535-5545.
- Willekens, F. L., J. M. Werre, J. K. Kruijt, B. Roerdinkholder-Stoelwinder, Y. A. Groenen-Dopp, A. G. van den Bos, G. J. Bosman and T. J. van Berkel (2005). "Liver Kupffer cells rapidly remove red blood cell-derived vesicles from the circulation by scavenger receptors." Blood **105**(5): 2141-2145.
- Williams, M. A. and M. J. Bevan (2004). "Shortening the infectious period does not alter expansion of CD8 T cells but diminishes their capacity to differentiate into memory cells." J Immunol **173**(11): 6694-6702.
- Williams, M. A. and M. J. Bevan (2007). "Effector and memory CTL differentiation." Annu Rev Immunol **25**: 171-192.
- Wilson, C. B., E. Rowell and M. Sekimata (2009). "Epigenetic control of T-helper-cell differentiation." Nat Rev Immunol **9**(2): 91-105.
- Winkelmann, E. R., D. G. Widman, J. Xia, A. J. Johnson, N. van Rooijen, P. W. Mason, N. Bourne and G. N. Milligan (2014). "Subcapsular sinus macrophages limit dissemination of West Nile virus particles after inoculation but are not essential for the development of West Nile virus-specific T cell responses." Virology **450-451**: 278-289.

Wong, M. T., D. E. Ong, F. S. Lim, K. W. Teng, N. McGovern, S. Narayanan, W. Q. Ho, D. Cerny, H. K. Tan, R. Anicete, B. K. Tan, T. K. Lim, C. Y. Chan, P. C. Cheow, S. Y. Lee, A. Takano, E. H. Tan, J. K. Tam, E. Y. Tan, J. K. Chan, K. Fink, A. Bertolotti, F. Ginhoux, M. A. Curotto de Lafaille and E. W. Newell (2016). "A High-Dimensional Atlas of Human T Cell Diversity Reveals Tissue-Specific Trafficking and Cytokine Signatures." *Immunity* **45**(2): 442-456.

Wynn, T. A. and K. M. Vannella (2016). "Macrophages in Tissue Repair, Regeneration, and Fibrosis." *Immunity* **44**(3): 450-462.

Xin, A., F. Masson, Y. Liao, S. Preston, T. Guan, R. Gloury, M. Olshansky, J. X. Lin, P. Li, T. P. Speed, G. K. Smyth, M. Ernst, W. J. Leonard, M. Pellegrini, S. M. Kaech, S. L. Nutt, W. Shi, G. T. Belz and A. Kallies (2016). "A molecular threshold for effector CD8(+) T cell differentiation controlled by transcription factors Blimp-1 and T-bet." *Nat Immunol* **17**(4): 422-432.

Xiong, Y. S., Y. Cheng, Q. S. Lin, A. L. Wu, J. Yu, C. Li, Y. Sun, R. Q. Zhong and L. J. Wu (2014). "Increased expression of Siglec-1 on peripheral blood monocytes and its role in mononuclear cell reactivity to autoantigen in rheumatoid arthritis." *Rheumatology (Oxford)* **53**(2): 250-259.

Xu, H. C., J. Huang, V. Khairnar, V. Duhan, A. A. Pandyra, M. Grusdat, P. Shinde, D. R. Mcllwain, S. K. Maney, J. Gommerman, M. Lohning, P. S. Ohashi, T. W. Mak, K. Pieper, H. Sic, M. Speletas, H. Eibel, C. F. Ware, A. V. Tumanov, A. A. Kruglov, S. A. Nedospasov, D. Haussinger, M. Recher, K. S. Lang and P. A. Lang (2015). "Deficiency of the B cell-activating factor receptor results in limited CD169+ macrophage function during viral infection." *J Virol* **89**(9): 4748-4759.

Yang, X. O., B. P. Pappu, R. Nurieva, A. Akimzhanov, H. S. Kang, Y. Chung, L. Ma, B. Shah, A. D. Panopoulos, K. S. Schluns, S. S. Watowich, Q. Tian, A. M. Jetten and C. Dong (2008). "T helper 17 lineage differentiation is programmed by orphan nuclear receptors ROR alpha and ROR gamma." *Immunity* **28**(1): 29-39.

Yao, Y., R. Liu, M. S. Shin, M. Trentalange, H. Allore, A. Nassar, I. Kang, J. S. Pober and R. R. Montgomery (2014). "CyTOF supports efficient detection of immune cell subsets from small samples." *J Immunol Methods* **415**: 1-5.

Yewdell, J. W. (2011). "DRiPs solidify: progress in understanding endogenous MHC class I antigen processing." *Trends Immunol* **32**(11): 548-558.

Yokosuka, T., W. Kobayashi, K. Sakata-Sogawa, M. Takamatsu, A. Hashimoto-Tane, M. L. Dustin, M. Tokunaga and T. Saito (2008). "Spatiotemporal regulation of T cell costimulation by TCR-CD28 microclusters and protein kinase C theta translocation." *Immunity* **29**(4): 589-601.

Yokosuka, T., K. Sakata-Sogawa, W. Kobayashi, M. Hiroshima, A. Hashimoto-Tane, M. Tokunaga, M. L. Dustin and T. Saito (2005). "Newly generated T cell receptor microclusters initiate and sustain T cell activation by recruitment of Zap70 and SLP-76." *Nat Immunol* **6**(12): 1253-1262.

Yokosuka, T., M. Takamatsu, W. Kobayashi-Imanishi, A. Hashimoto-Tane, M. Azuma and T. Saito (2012). "Programmed cell death 1 forms negative costimulatory microclusters that directly inhibit T cell receptor signaling by recruiting phosphatase SHP2." *J Exp Med* **209**(6): 1201-1217.

York, M. R., T. Nagai, A. J. Mangini, R. Lemaire, J. M. van Seventer and R. Lafyatis (2007). "A macrophage marker, Siglec-1, is increased on circulating monocytes in patients with systemic sclerosis and induced by type I interferons and toll-like receptor agonists." *Arthritis Rheum* **56**(3): 1010-1020.

You, Y., R. C. Myers, L. Freeberg, J. Foote, J. F. Kearney, L. B. Justement and R. H. Carter (2011). "Marginal zone B cells regulate antigen capture by marginal zone macrophages." *J Immunol* **186**(4): 2172-2181.

Yu, X., S. Vasiljevic, D. A. Mitchell, M. Crispin and C. N. Scanlan (2013). "Dissecting the molecular mechanism of IVlg therapy: the interaction between serum IgG and DC-SIGN is independent of antibody glycoform or Fc domain." *J Mol Biol* **425**(8): 1253-1258.

Yuan, J., S. Gnjatic, H. Li, S. Powel, H. F. Gallardo, E. Ritter, G. Y. Ku, A. A. Jungbluth, N. H. Segal, T. S. Rasalan, G. Manukian, Y. Xu, R. A. Roman, S. L. Terzulli, M. Heywood, E. Pogoriler, G. Ritter, L. J. Old, J. P. Allison and J. D. Wolchok (2008). "CTLA-4 blockade enhances polyfunctional NY-ESO-1 specific T cell responses in metastatic melanoma patients with clinical benefit." Proc Natl Acad Sci U S A **105**(51): 20410-20415.

Zavasnik-Bergant, T. and B. Turk (2007). "Cysteine proteases: destruction ability versus immunomodulation capacity in immune cells." Biol Chem **388**(11): 1141-1149.

Zediak, V. P., J. B. Johnnidis, E. J. Wherry and S. L. Berger (2011). "Cutting edge: persistently open chromatin at effector gene loci in resting memory CD8+ T cells independent of transcriptional status." J Immunol **186**(5): 2705-2709.

Zehner, M., A. L. Marschall, E. Bos, J. G. Schloetel, C. Kreer, D. Fehrenschild, A. Limmer, F. Ossendorp, T. Lang, A. J. Koster, S. Dubel and S. Burgdorf (2015). "The translocon protein Sec61 mediates antigen transport from endosomes in the cytosol for cross-presentation to CD8(+) T cells." Immunity **42**(5): 850-863.

Zervoudi, E., E. Saridakis, J. R. Birtley, S. S. Seregin, E. Reeves, P. Kokkala, Y. A. Aldhamen, A. Amalfitano, I. M. Mavridis, E. James, D. Georgiadis and E. Stratikos (2013). "Rationally designed inhibitor targeting antigen-trimming aminopeptidases enhances antigen presentation and cytotoxic T-cell responses." Proc Natl Acad Sci U S A **110**(49): 19890-19895.

Zhan, Y., R. C. Paolicelli, F. Sforzini, L. Weinhard, G. Bolasco, F. Pagani, A. L. Vyssotski, A. Bifone, A. Gozzi, D. Ragazzino and C. T. Gross (2014). "Deficient neuron-microglia signaling results in impaired functional brain connectivity and social behavior." Nat Neurosci **17**(3): 400-406.

Zhang, J. G., P. E. Czabotar, A. N. Policheni, I. Caminschi, S. S. Wan, S. Kitsoulis, K. M. Tullett, A. Y. Robin, R. Brammananth, M. F. van Delft, J. Lu, L. A. O'Reilly, E. C. Josefsson, B. T. Kile, W. J. Chin, J. D. Mintern, M. A. Olshina, W. Wong, J. Baum, M. D. Wright, D. C. Huang, N. Mohandas, R. L. Coppel, P. M. Colman, N. A. Nicola, K. Shortman and M. H. Lahoud (2012). "The dendritic cell receptor Clec9A binds damaged cells via exposed actin filaments." Immunity **36**(4): 646-657.

Zhang, W., P. A. Wearsch, Y. Zhu, R. M. Leonhardt and P. Cresswell (2011). "A role for UDP-glucose glycoprotein glucosyltransferase in expression and quality control of MHC class I molecules." Proc Natl Acad Sci U S A **108**(12): 4956-4961.

Zhu, J., H. Yamane and W. E. Paul (2010). "Differentiation of effector CD4 T cell populations (\*)." Annu Rev Immunol **28**: 445-489.

Zinkernagel, R. M., M. F. Bachmann, T. M. Kundig, S. Oehen, H. Pirchet and H. Hengartner (1996). "On immunological memory." Annu Rev Immunol **14**: 333-367.